McGill University

Doctoral Thesis

Purinergic Mechanotransduction in Bone

Author:
Nicholas Mikolajewicz

Supervisor:
Dr. Svetlana V Komarova

A thesis submitted to McGill University in partial fulfillment of the requirements for the degree of Doctor of Philosophy

McGill University

Faculty of Dentistry

Montréal, Québec

December 2018

Acknowledgements

First and foremost, I want to thank my supervisor **Dr. Svetlana V. Komarova**. It has been a privilege to work with her, and I could not have wished for a better mentor. Throughout the course of our many discussions and meetings, Dr. Komarova has diligently guided my academic journey, providing me with endless opportunities and support – Your influence and dedication are the cornerstone to my success.

Next, I would like to extend my gratitude to the many present and past members of the **Komarova Lab**. Special thanks to **Dr. Gula Sadvakassova** for starting me on this path when she first recruited me as an undergraduate trainee in the Summer of 2013, and for your consistent readiness to teach and help, no matter the circumstance. **Dr. Kerstin Tiedemann** for her kindness, compassion and ever-present support. To **Dr. Iris Boraschi-Diaz** for treating me like her little brother. To **Dr. Josephine Tauer** for your positivity, enthusiasm, and work ethic – I have learned considerably from your example. To **Mariya Stavnichuk** for your friendship, patience and collaboration – somehow, we managed to create and teach a course together. To **Turney McKee**, who was the first person I met when I moved to Montreal to begin my studies, thank you for *always* being there, I'll never forget those days in 1023 and 3579. To all my undergraduate trainees, particularly **Ali Mohammed**, **Sequoia Crooks**, **Owen Dunkley** and **Janet Tang**, for your help in teaching me to become a better mentor, as well as your perseverance and hard work. To everyone else that has been in and out of the lab, thank you for making it a wonderful place.

A big thanks to my advisory committee members **Dr. Monzur Murshed**, **Dr. Bettina Willie** and **Dr. Luda Diatchenko** for their thoughtful discussions and feedback. Dr. Murshed for sharing cell lines and protocols, as well providing much needed reassurance when working with CRIPSR/Cas9. Dr. Willie for expanding my scope of interest and enabling my work in an *in vivo* setting. Dr. Diatchenko for constructive discussions and a unique perspective.

Thank you to all my collaborators for working with me to expand the breadth of my research. **Dr. Willie** and **Dr. Elizabeth Zimmerman** for helping me to validate my *in vitro* findings *in vivo*, and a special thanks to **Catherine Julien** and **Maximilian Rummler** who helped me with loading experiments. **Laurent Mackay** and **Dr. Anmar Khadra** for introducing me to signal processing

and helping me get a jump start on mathematical modelling to complement my experimental work. **Martin Morris** for teaching me to find exactly what I need amongst the endless sea of literature out there. **Simon Sehayek** and **Dr. Paul Wiseman** for helping me with diffusion modeling in the remaining months of my project. Thanks to the support from the technical staff at the RI-MUHC Molecular Imaging Platform (McGill University) for helping me with confocal imaging. Thanks to the St. Arnaud Lab for letting me walk away with their luminometer for hours at a time. Thanks to technicians in the animal facility, including **Mia Esser**, for going the extra mile when I needed it.

A special thanks to coffee and the Shriner's hospitality staff, particularly **Ignace**, who helped keep me caffeinated and fed.

I would like to acknowledge those that have funded my work, namely Natural Sciences and Engineering Research Council, Canadian Institutes for Health Research, Faculty of Dentistry (McGill University) and le Réseau de Recherche en Santé Buccodentaire et Osseuse (RSBO). Also, a big thanks to **Maria Palumbo** who has been persistent in her administrative support, always ensuring I remained up to date and never fell behind.

Lastly, I would not have gotten this far without the loving support of **Tatiana Sanchez** and my **Mom**, **Brother** and **Grandma**, who have supported me since the beginning. My mom who has always taught me that "if there is a will, there is a way", and has supported me in every way imaginable, words cannot convey that gratitude I feel.

Table of Contents

Appendix

List of Figures and Tables

Chapter 7 (pages 263-289)

Chapter 8 (pages 290-310)

A6. Chapter 7 supplemental figures and tables

Abbreviations

Abbreviation	Description
95% CI	95% confidence interval
A_{base}	Absolute basal extracellular ATP
A_{cell}	Absolute intracellular ATP content
A_{mech}	Absolute amount of mechanically-stimulated ATP release
ABC	ATP-binding cassette
Ado	Adenosine
ADP	Adenosine diphosphate
ADPKD	Autosomal dominant polycystic kidney disease
AFM	Atomic force microscopy
AJ	Adherent junction
ALP	Alkaline phosphatase
Alveolar	Alveolar type II epithelial cells
AMP	Adenosine monophosphate
Aq. Hum	Aqueous humour
ARPKD	Autosomal recessive polycystic kidney disease
Astro.	Astrocyte
ATP	Adenosine triphosphate
AUC	Area under curve
BM	Bone marrow
BM-OB	Bone marrow-derived primary osteoblasts
BMD	Bone mineral density
BMP	Bone morphogen protein
BMU	Basic multicellular unit
C2-OB	BMP2-transfected C2C12 osteoblastic cells
$[Ca^{2+}]_i$	Cytosolic free calcium
$[Ca^{2+}]_e$	Extracellular calcium

Abbreviation	Description
Cav-1	Caveolin-1
CB-OB	Compact bone-derived primary osteoblasts
CD	Collecting duct
CFTR	cystic fibrosis transmembrane conductance regulator
cGMP	Cyclic guanosine monophosphate
Chol.	Cholesterol
COX	Cyclooxygenase
Cx	Connexins
D	Diffusion coefficient
Dlx5	Distal-less homeobox 5
DMD	Duchenne muscular dystrophy
EC	Extracellular
ECM	Extracellular matrix
eN	ecto-5'-nucleotidase, CD73
Endo.	Endothelial cells
eNOS	Endothelial NOS
Epi.	Epithelial cells
ER	endoplasmic reticulum
FA	Focal adhesion
FDA	Food and Drug Administration
Fibro.	Fibroblasts
FSS	Fluid shear stress
FWHM	Full-width half max
Gd^{3+}	Gadolinium
Glomer.	Glomerular
GPCR	G-protein coupled receptor
GPI	glycosylphosphatidylinositol
HPLC	High-performance liquid chromatography
IC	Intracellular

Abbreviation	Description
IGF	Insulin-like growth factor
iNOS	Inducible NOS
JNK	cJun NH2-terminal protein kinase
Kin.	kinases
LPA	Lysophosphatidic acid
MAC	Maxi-anion channel
MAPK	Mitogen-activated protein kinase
mTs	microtubules
M-CSF	Macrophage-colony stimulating factor
MMP	Matrix metalloproteinase
MPR	Multi-peak response
MSAR	Mechanically-stimulated ATP release
MSC	Mesenchymal stem cells
nNOS	Neuronal NOS
NO	Nitric oxide
NOS	Nitric oxide synthase
NPP	ecto-nucleotide pyrophosphatase/phosphodiesterases
NTPDase	ectonucleoside triphosphate diphophohydrolases
OA	Osteoarthritis
OPG	Osteoprotegerin
Osx	Osterix
Panc. Epi.	Pancreatic epithelia
P2R	Purinergic receptors
p38 MAPK	P38 mitogen-activated protein kinase
PG	Prostaglandin
PGE_2	Prostaglandin E_2
PGT	Prostaglandin transporter
PKA	Protein kinase A
PKC	Protein kinase C

Abbreviation	Description
PKD	Protein kinase D
PKG	Protein kinase G
PLC	Phospholipase C
P_i	Inorganic phosphate
PP_i	pyrophosphate
PPH	Primary pulmonary hypertension
PTH	Parathyroid hormone
PTHrp	PTH-related protein
Pul. Art.	Pulmonary artery
Px	Pannexins
RA	Rheumatoid arthritis
RANK	Receptor activator of nuclear factor kappa-B
RANKL	RANK ligand
RBC	Red blood cells
Resp. epi.	Respiratory (airway) epithelia
R_{mech}	Relative amount of mechanically-stimulated ATP release
Runx2	Runt-related transcription factor 2
RVD	Regulatory volume decrease
SCI	Spinal cord injury
S.M.	Smooth muscle
SNP	Single nucleotide polymorphism
t_{half}	Time to half-max ATP release
TNAP	tissue nonspecific alkaline phosphatase
Trab. Mesh.	Trabecular meshwork cells
TR	Transient response
TRP	Transient receptor potential
TV	Total-variational
Um.	Umbilical
VDAC	Voltage-dependent anion channel

Abbreviation	Description
VNUT	Vesicular nucleotide transporter
VRAC	Volume-regulated anion channels
VSCC	Voltage sensitive calcium channels
Wnt	Wingless-related integration site

Abstract

Athletes' skeletons get stronger with training, while bones weaken in people who cannot move or in astronauts experiencing weightlessness. These changes are mediated by bone cells which can perceive mechanical forces, convert them to biochemical signals and induce changes in bone mass and strength. Among the first detectable signals following mechanical stimulation is the release of the energy-rich molecule ATP. Extracellular ATP was proposed as a mechanotransductive signaling molecular over 20 years ago and has been shown to signal through 15 different purinergic receptors (P2). However, the exact contribution of ATP release and P2 signaling to mechanically-induced bone adaptation remains unclear. The primary aims of this dissertation were to investigate the mechanisms of mechanically-stimulated ATP release from bone cells and to determine how the purinergic signal transmits information about the nature of the mechanical stimulus to neighbouring cells.

Many studies examining the mechanisms of mechanically-stimulated ATP release have been conducted to date. Since large-scale quantitative synthesis of basic research has not been attempted, I developed the theoretical foundation, computational resources and workflow required to conduct a meta-analysis in the basic sciences. This enabled consolidation and synthesis of quantitative data from 278 studies that investigated the amount, kinetics and mechanisms of ATP release, as well as the influence of pathologies on ATP release. I demonstrated that mechanically-stimulated ATP release is a conserved phenomenon across mammalian cells, and that mechanically-stimulated cells release 38.6 (95% confidence interval [CI]: 18.2 to 81.8) amoles ATP/cell on average with a characteristic time constant of 32 s (95% CI: 16 to 66). Importantly, vesicles and voltage sensitive calcium channels (VSCCs) were implicated in the release of ATP from mechanically-stimulated osteoblasts and osteocytes.

I next investigated the mechanisms of ATP release from osteoblasts experimentally. However, since mechanically-stimulated ATP release and ATP-mediated P2 responses are calcium-dependent processes, it was pertinent to establish a protocol for large-scale analysis of calcium responses. To do this, we developed a calcium-signal processing algorithm capable of characterizing calcium signatures, thereby automating and standardizing the analysis process.

I determined that mechanical stimulation of a single murine osteoblast led to the release of 70 ± 24 amole ATP, which stimulated calcium responses in neighboring cells. Osteoblasts were

found to contain ATP-rich vesicles that were released upon mechanical stimulation, however, pharmacological interventions that promoted vesicular exocytosis reduced ATP release, while inhibitors of vesicular release potentiated ATP release. In search of an alternative route of ATP release, I found that mechanical stresses induced reversible cell membrane injury *in vitro* and *in vivo*. Calcium/PKC-dependent vesicular exocytosis facilitated membrane repair, thereby ensuring cell viability and reducing ATP release. Thus, I propose that exocytosis of ATP-containing vesicles limits the much larger efflux of intracellular ATP through reversibly damaged membranes by facilitating membrane repair. To reconcile our findings with prior work, I suggest that non-lytic routes of ATP release predominate in basal and low mechanical agitation conditions, while injury-related ATP release becomes prevalent only when the stimulus surpasses a certain threshold.

To understand how the purinergic signal conveys information about the mechanical stimulus to neighbouring bone cells, I developed a mathematical model describing injury-related ATP and ADP release, extracellular diffusion and degradation, and purinergic responses. The model was validated using experimental data obtained by mechanically-stimulating a single osteoblast and measuring ATP release, membrane repair and calcium signaling in neighboring cells. I found that the total amount of ATP released, peak extracellular ATP concentration and the ADP-mediated signaling component contributed complementary information regarding the mechanical stimulation event. Specifically, the total amount of ATP released determined the maximal distance from the injury at which purinergic responses were stimulated, as well as the overall number of responders. Peak ATP concentrations allowed cells to discriminate between minor and severe injuries that led to the release of similar amounts of ATP due to different injury repair kinetics. ADP-mediated signaling became relevant in larger tissue-level injuries, conveying information about the distance to the injury site and its geometry. Therefore, mechanotransductive purinergic signalling fields are tuned by the severity of injury and dynamics of repair, thereby enabling neighbouring cellular populations to evoke position- and injury-appropriate responses.

Overall, the studies presented in this dissertation demonstrate that (*i*) bone cell injury is critical for purinergic mechanotransduction, (*ii*) membrane repair occurs through calcium/PKC-dependent vesicular exocytosis, and (*iii*) information about the severity of injury and cellular mechano-adaptive status is integrated at the level of the purinergic signal that communicates mechanical information to neighbouring cells. Importantly, identification of molecular mediators, including PKCμ, may represent future therapeutic targets in prevention of disuse-related bone loss.

Résumé

Les squelettes des athlètes deviennent plus forts à l'entraînement, tandis que les os s'affaiblissent chez les personnes qui ne peuvent pas bouger ou chez les astronautes en apesanteur. Ces changements sont médiés par les cellules osseuses qui peuvent percevoir les forces mécaniques, les convertir en signaux biochimiques et induire des changements dans la masse et la force osseuses. Parmi les premiers signaux détectables à la suite d'une stimulation mécanique figure la libération d'une molécule riche en énergie, l'ATP. L'ATP extracellulaire a été proposé comme molécule de signalisation mécanotransductive il y a plus de 20 ans et il a été démontré qu'il est signalé par 15 récepteurs purinergiques différents (P2). Cependant, la contribution exacte de la libération d'ATP et de la signalisation P2 à l'adaptation osseuse induite mécaniquement demeure incertaine. Les principaux objectifs de cette thèse étaient d'étudier les mécanismes de la libération d'ATP stimulée mécaniquement par les cellules osseuses et de déterminer comment le signal purinergique transmet l'information selon la nature du stimulus mécanique aux cellules voisines.

De nombreuses études portant sur les mécanismes de libération d'ATP stimulée mécaniquement ont été menées à ce jour. Comme aucune synthèse quantitative à grande échelle de la recherche fondamentale n'a été entreprise, j'ai mis au point les bases théoriques, les ressources informatiques et le déroulement du travail nécessaires pour effectuer une méta-analyse en sciences fondamentales. Cela a permis de consolider et de synthétiser les données quantitatives de 278 études portant sur la quantité, la cinétique et les mécanismes de libération de l'ATP, ainsi que l'influence des pathologies sur la libération de l'ATP. J'ai démontré que la libération d'ATP stimulée mécaniquement est un phénomène conservé dans les cellules de mammifères, et que les cellules stimulées mécaniquement libèrent 38,6 (intervalle de confiance à 95 % [IC]: 18,2 à 81,8) amoles ATP/cellule en moyenne avec une constante de temps caractéristique de 32 s (IC 95 %: 16 à 66). Il est important de noter que les vésicules et les canaux calciques sensibles au voltage (VSCC) ont été impliqués dans la libération d'ATP des ostéoblastes et ostéocytes stimulés mécaniquement.

J'ai ensuite étudié expérimentalement les mécanismes de libération de l'ATP par les ostéoblastes. Toutefois, comme la libération d'ATP stimulée mécaniquement et les réponses P2 médiées par l'ATP sont des processus dépendant du calcium, il était pertinent d'établir un protocole pour une analyse à grande échelle des réponses calciques. Pour ce faire, nous avons développé un

algorithme de traitement des signaux calciques capable de caractériser les signatures calciques, automatisant et standardisant ainsi le processus d'analyse.

J'ai déterminé que la stimulation mécanique d'un seul ostéoblaste murin a conduit à la libération de 70 ± 24 amole ATP, qui stimulait les réponses calciques dans les cellules voisines. Les ostéoblastes contiennent des vésicules riches en ATP qui sont libérées par stimulation mécanique, mais les interventions pharmacologiques qui favorisent l'exocytose vésiculaire réduisent la libération d'ATP, tandis que les inhibiteurs de la libération vésiculaire potentialisent la libération d'ATP. À la recherche d'une autre voie de libération de l'ATP, j'ai découvert que les contraintes mécaniques provoquaient des lésions réversibles de la membrane cellulaire in vitro et in vivo. L'exocytose vésiculaire dépendante du calcium et du PKC a facilité la réparation de la membrane, assurant ainsi la viabilité cellulaire et réduisant la libération d'ATP. Ainsi, je propose que l'exocytose des vésicules contenant de l'ATP limite le flux beaucoup plus important d'ATP intracellulaire à travers les membranes endommagées de façon réversible en facilitant la réparation des membranes. Pour concilier nos constatations avec les travaux antérieurs, je suggère que les voies non électrolytiques de libération d'ATP prédominent dans les conditions d'agitation basale et de faible agitation mécanique, tandis que la libération d'ATP liée aux blessures ne devient prévalente que lorsque le stimulus dépasse un certain seuil.

Pour comprendre comment le signal purinergique transmet l'information sur le stimulus mécanique aux cellules osseuses voisines, j'ai mis au point un modèle mathématique décrivant la libération d'ATP et d'ADP liée à une lésion, la diffusion et la dégradation extracellulaires et les réactions purinergiques. Le modèle a été validé à l'aide de données expérimentales obtenues en stimulant mécaniquement un seul ostéoblaste et en mesurant la libération d'ATP, la réparation des membranes et la signalisation du calcium dans les cellules voisines. J'ai constaté que la quantité totale d'ATP libérée, la concentration maximale extracellulaire d'ATP et la composante de signalisation médiée par l'ADP ont fourni des renseignements complémentaires concernant l'événement de stimulation mécanique. Plus précisément, la quantité totale d'ATP libérée a déterminé la distance maximale de la blessure à laquelle les réponses purinergiques ont été stimulées, ainsi que le nombre total de répondants. Les concentrations maximales d'ATP ont permis aux cellules de faire la distinction entre les blessures mineures et les blessures graves, ce qui a entraîné la libération de quantités similaires d'ATP en raison de la cinétique de réparation différente des blessures. La signalisation médiée par l'ADP est devenue pertinente pour les lésions

tissulaires de plus grande envergure, transmettant de l'information sur la distance jusqu'au site de la lésion et sur sa géométrie. Par conséquent, les champs de signalisation purinergiques mécanotransducteurs sont réglés en fonction de la gravité de la blessure et de la dynamique de réparation, ce qui permet aux populations cellulaires voisines d'évoquer des réponses adaptées à la position et à la blessure.

Dans l'ensemble, les études présentées dans cette thèse démontrent que (*i*) les lésions des cellules osseuses sont critiques pour la mécanotransduction purinergique, (*ii*) la réparation membranaire se produit par exocytose vésiculaire dépendante du calcium/PKC, et (*iii*) les informations sur la gravité des lésions et le statut mécano-adaptatif cellulaire sont intégrées au niveau du signal purinergique qui communique des informations mécaniques aux cellules voisines. Il est important de noter que l'identification des médiateurs moléculaires, y compris la PKCμ, pourrait représenter des cibles thérapeutiques futures dans la prévention de la perte osseuse liée à l'utilisation.

Rationale and objectives of thesis

Primary *research* objectives

Millions of people worldwide are affected by musculoskeletal disorders related to bone loss, such as osteoporosis. Mechanical cues are critical for bone health, as loss of mechanical stimulation – such as in astronauts exposed to microgravity or immobilized/bedridden patients – leads to bone loss. Over 20 years ago, extracellular ATP was proposed as a mediator that converts mechanical cues to biochemical signals. ATP acts through 15 unique purinergic (P2) receptors. However, the exact contribution of ATP release and P2 receptor signaling to skeletal mechanobiology remains unclear. The focus of this dissertation was to advance the current understanding of purinergic mechanotransduction in bone, with an emphasis on understanding how ATP release from mechanically-stimulated bone cells coordinates bone adaption in response to physiological forces.

First research objective. Determine the relationship between mechanical stimulation and early signaling events in bone cells, with an emphasis on ATP release and calcium signaling.

Second research objective. Investigate how spatiotemporal variations in the purinergic signal convey information about the nature of the mechanical stimulus.

Secondary *methodological* objectives

The field of purinergic research, like many basic sciences, is extensive and there is over 20 years of published data available. However, large-scale quantitative efforts to synthesize findings in the basic sciences are non-existent due to a lack of appropriate tools to enable such analyses. Similarly, dynamic processes, like calcium signalling, are prevalent across cell biology. However, a lack of standardized methods to quantify such data-sets make findings from various studies challenging to compare, relate and generalize. Therefore, the secondary objective of this dissertation was to develop tools that would assist in achieving our primary research objectives.

First methodological objective. Develop the theoretical foundation, computational resources and workflow required to conduct a rapid/systematic review and meta-analysis in the basic sciences.

Second methodological objective. Develop a signal-processing algorithm to facilitate and standardize the parametric characterization of calcium signals

Originality and contributions

The contents of this thesis are original, and the distinct contributions to knowledge and individual author contributions are summarized as follows:

Manuscript 1 (Chapter 3)

Mikolajewicz N., Komarova SV. (2019) Meta-analytic methodology for basic research: A practical guide. *Front Physiol*., 10:203. doi: 10.3389/fphys.2019.00203

Originality. I described the theoretical foundation, computation resources and workflow for systematic and rapid reviews followed by meta-analysis in basic research studies. I also developed a supporting software package, MetaLab in MATLAB R2016b, aimed to promote efforts to quantitatively consolidate existing evidence to support translational/pre-clinical study design. This work has been published in *Frontiers in Physiology*.

Contributions. Both authors contributed to the study conception and design, data acquisition and interpretation and drafting and critical revision of the manuscript. NM developed MetaLab. Both authors contributed to the critical revision and approval of the final manuscript.

Manuscript 2 (Chapter 4)

Mikolajewicz N., Mohammed A., Morris M., Komarova SV. (2018). Mechanically-stimulated ATP release from mammalian cells: systematic review and meta-analysis. *J Cell Sci*, 131(22). doi: 10.1242/jcs.223354.

Originality. Using the meta-analytic methodology described above, a large-scale systematic review and meta-analysis of mechanically-stimulated ATP release from mammalian cells was conducted. From 278 identified studies, I quantitatively characterized the amount, kinetics, and mechanisms of ATP release, and determined the influence of different pathologies on ATP release. This study has been published in *Journal of Cell Science*.

Contributions. Study conception and design: NM, SVK. Search strategy: MM. Data acquisition: NM, AM. Analysis and interpretation of data: NM, AM, SVK. Drafting of Manuscript: NM, SVK.

All authors contributed to the critical revision of manuscript and approved the final version to be published.

Manuscript 3 (Chapter 5)

Mackay L.*, Mikolajewicz N.*, Komarova SV., Khadra A. (2016) Systematic characterization of dynamic parameters of intracellular calcium signals. *Front. Physiol*., 7:525. doi: 10.3389/fphys.2016.00525. *indicates equal contribution.

Originality. In collaboration with Laurent MacKay (Ph.D. student, McGill University), I developed a computational algorithm in MATLAB 2016b to automate and standardize the parametric characterization of intracellular calcium signals, like those that occur during purinergic mechanotransduction (algorithm is used throughout this thesis). This study has been published in *Frontiers in Physiology*.

Contributions. Study conception and design: LM, NM, SVK, AK. Algorithm development: LM, AK. Acquisition of data: NM. Analysis and interpretation of data: LM, NM. Drafting of Manuscript: LM, NM, SVK, AK. All authors contributed to the critical revision of manuscript and approved the final version to be published.

Manuscript 4 (Chapter 6)

Mikolajewicz N., Zimmermann EA., Willie BM., Komarova SV. (2018). Mechanically stimulated ATP release from murine bone cells is regulated by a balance of injury and repair. *eLife*, 16:7. doi: 10.7554/eLife.37812.

Originality. This study investigated the mechanism of mechanically-stimulated ATP release from osteoblasts. I demonstrated that *in vitro* or *in vivo* mechanical stimuli routinely induce reversible membrane injury in osteoblastic cells resulting in ATP release by spillage, rather than by conductive or vesicular release. I further showed that mechanically-induced injuries are non-lethal and are rapidly repaired via a mechanism involving calcium/PKC-dependent vesicular exocytosis. Importantly, such injuries occur during physiological loading *in vivo*, and that the amount of ATP released from cellular injury is governed by the rate of membrane resealing. Together these findings have provided novel insights into how early mechanotransductive ATP release and signaling is linked to cellular membrane integrity and mechanosensitivity. The *in vivo* portion of

this study was performed in collaboration with Dr. Elizabeth A. Zimmermann and Dr. Bettina M. Willie at the Shriners Hospital for Children, Montreal. This study has been published in *eLife*.

Contributions. Study conception and design: NM, SVK, BW. Acquisition of data: NM, BW. Analysis and interpretation of data: NM, SVK, EZ, BW. Drafting of Manuscript: NM, SVK. All authors contributed to the critical revision and approval of the final manuscript.

Manuscript 5 (Chapter 7)

Mikolajewicz, N., Sehayek, S., Wiseman, P. W., & Komarova, S. V. (2019). Transmission of mechanical information by purinergic signaling. *Biophys J.*

Originality. In collaboration with Simon Sehayek (Ph.D. student, McGill University), I developed a mathematical model of purinergic mechanotransduction that has been experimentally validated and used to model mechanically-stimulated ATP release, diffusion, degradation and signalling. This study provided insights into how information pertaining to the severity and location of a mechanical stimulus is conveyed through the purinergic signalling network in bone cells. This work has been published in *Biophysical Journal*.

Contributions. Study conception and design: NM, SVK. Model development: SS, NM. Acquisition of data: NM, SS. Analysis and interpretation of data: NM, SS, PWW, SVK. Drafting of Manuscript: NM, SS, PWW, SVK. All authors contributed to the critical revision of manuscript and approved the final version to be published.

Chapter One

Introduction to Skeletal Mechanobiology

I begin with a review of the current state of research in the field of skeletal mechanobiology. This chapter explores the types of mechanical forces experienced by the body and introduces the tissue- and cellular-level mechanisms involved in perceiving and converting these mechanical cues into biological outcomes.

1.1 Interplay between the body and the mechanical environment

The human body is in constant interaction with the physical world. Forces generated, internally and externally, are critical to the development, maintenance and adaptation of various tissues in the body. The body itself can exert internal forces relating to the various physiological functions. These types of forces include blood flow through the vasculature, urinary bladder distension related to urine filling, peristaltic movement through the alimentary tube, ventilation-related lung distension and skeletal muscle related constriction. The body also encounters and can sense external forces, such as those related to movement- and activity-related stresses like walking or running, and gravity-related forces which affect fluid distributions and skeletal loading. Encoded within these forces is information pertaining to the physical environment, which is perceived and integrated at the cellular level, and manifesting as complex cellular- and tissue- level behaviours.

1.1.1 Diseases related to mechanobiology

The coupling between human physiology and the mechanical environment is in a delicate balance and when disrupted can lead to the development and progression of disease. A large number of disease are associated with changes in internal forces, such as altered vascular blood flow, which has been associated with increased plaque formation in atherosclerosis (Knowles & Maeda, 2000), or glaucoma which is characterized by increased intraocular pressures due to heightened flow-resistance (Overby et al., 2014). Other diseases related to abnormal mechanotransduction include (but are not limited to) bladder dysfunction, congenital deafness, pulmonary hypertension, ventilator injury, musculodystrophies, polycystic kidney disease, osteoporosis, rheumatoid arthritis, chronic back pain, metastasis and irritable bowel syndrome (Ingber, 2003). The mechanical basis of these diseases is diverse, including changes in cellular mechanics, alterations in tissue structure and disrupted mechanical-to-biochemical signal conversion (Ingber, 2003). The cell- and tissue-level mechanical environment is also influenced by external factors, such as gravity. This is emphasized when gravitational forces on the body are altered, such as in cases of immobility (i.e., paraplegic or bedridden patients) or microgravity (i.e., astronauts) (Jo & Shin, 2015). Prolonged bed-rest is marked by significant loss in bone mass, estimated by one group to decrease bone mineral density (BMD) by 3-4% over a 17-week period (Leblanc, Schneider, Evans, Engelbretson, & Krebs, 1990). Weightlessness in space causes astronauts to experience muscle atrophy and bone loss which is not preventable by exercise countermeasures, especially in load-

bearing regions such as the heel bone and lower limbs (Kohrt, Barry, & Schwartz, 2009). Thus, while the pathological manifestations of disrupted mechanical processes emphasize the importance of mechanobiology throughout the human body, this dissertation will be specifically focusing on the mechanobiology of bone.

1.2 Bone structure and composition

1.2.1 Anatomy and composition

The adult skeleton consists of 213 bones that are involved in the skeletal support, locomotion, protection of internal structures, calcium and phosphate homeostasis, acid-base balance and accommodation of hematopoiesis (Clarke, 2008). Long bones, such as the femur or tibia, are characterized by their long hollow diaphyseal shafts, cone-like metaphyseal regions below the growth plate, and rounded epiphyseal extremities above the growth plate (**Fig 1-1A**). The diaphysis is composed of compact cortical bone, while the metaphysis and epiphysis are composed of spongy-like trabecular bone. In general, our skeletal system consists of approximately 80% cortical bone and 20% trabecular bone (Clarke, 2008). Trabecular bone is a highly porous and cellular structure which is spongy in appearance, contrary to compact bone which is much denser and exhibits a lower cell-to-bone ratio. At the microscopic scale (10-500 μm diameter) cortical bones are composed of osteons, or Haversian systems, which are cylindric ensembles of concentric lamella (**Fig 1-1B, C**). Lamellae (~3-7 μm wide) are made up of mineralized collagen fibers situated around a central canal which supplies vasculature to the Haversian system. These collagen fibers are composed of collagen fibrils, which make up nearly 90% of the organic matrix in bone and serve as scaffolding upon which inorganic calcium and phosphate precipitate to form hydroxyapatite crystals [$Ca_{10}(PO_4)_6(OH)_2$] (**Fig 1-1D**). With an overall composition of 50-70% mineral, 20-40% organic matrix, 5-10% water, <3% lipids and porosity of <5% (Clarke, 2008), this hard, yet light-weight composite material is what we know as bone.

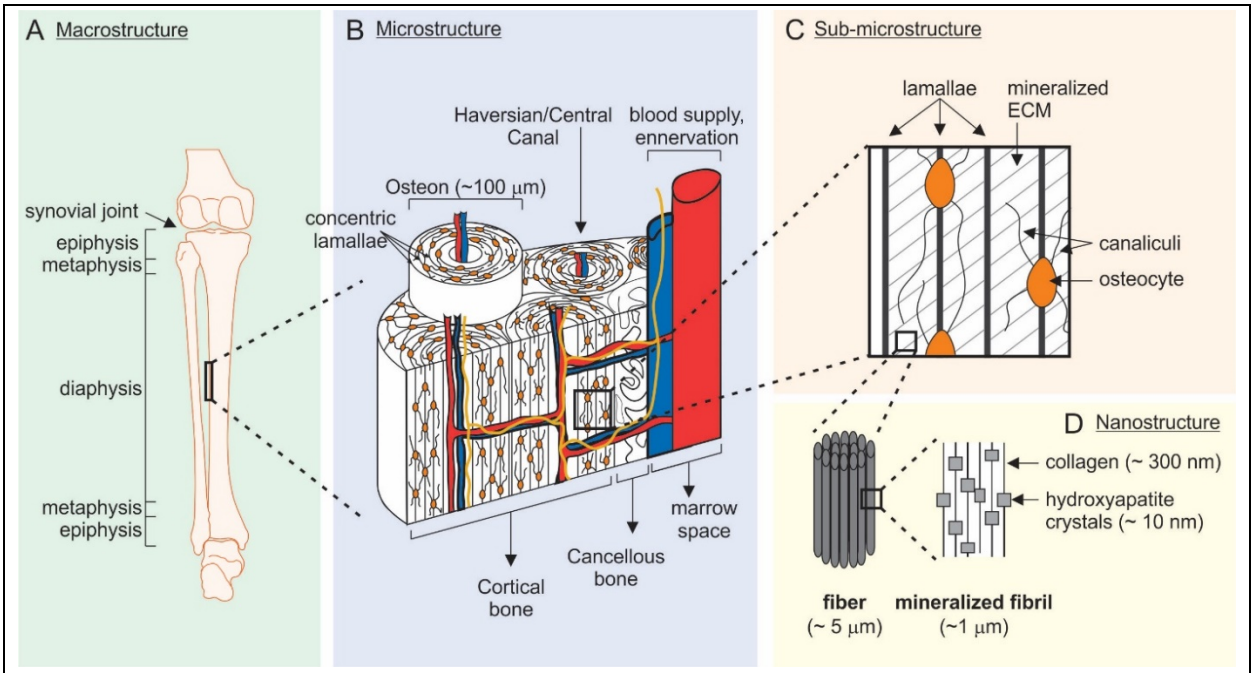

Figure 1-1. **Hierarchical bone structure**. **(A)** Long bone macrostructure consists of long hollow diaphyseal shafts, cone-like metaphyseal regions, and rounded epiphyseal extremities above metaphysis. **(B)** Microstructure consists of osteons which are cylindric ensembles of concentric lamella surrounding central Haversian canal which supplies vasculature and innervation to the osteon. **(C)** Sub-microstructure consists of osteocytes embedded in mineralized extracellular matrix (ECM) in concentric lamellar layers. **(D)** Nanostructure consists of collagen fibers composed of bundles of collagen fibrils that serve as scaffolding upon which inorganic calcium and phosphate precipitate to form hydroxyapatite crystals.

1.2.2 Cells of the bone

Bone is a highly cellular organ. It is synthesized during development and maintained throughout our adult lives by three main cell types: osteoblasts, osteoclasts and osteocytes. Together these cells orchestrate the growth, modelling and remodeling of bone, adapting the mineralized structure to systemic signals and mechanical stimuli.

Osteoblasts. Osteoblasts are cuboidal bone forming cells that comprise 4-6% of the resident bone cells (Florencio-Silva, Sasso, Sasso-Cerri, Simões, & Cerri, 2015). They are derived from mesenchymal stem cells (MSC), which are multipotent cells capable of differentiating into myoblasts, osteoblasts, chondrocytes and adipocytes. MSC commitment to the osteoprogenitor lineage requires expression of "master transcriptional regulators" Runt-related transcription factor 2 (Runx2), Distal-less homeobox 5 (Dlx5) and Osterix (Osx) (Florencio-Silva et al., 2015). Runx2 expression and transcriptional activity is promoted by several upstream signals, including Wnt/β-

catenin, BMP2/4 and Vitamin D, and is suppressed by Jagged/Notch (promotes degradation of β-catenin), Dickopf (DKK1/2, antagonizes Wnt signal) and TGFβ (inhibits Runx2 via SMAD3) (Rutkovskiy, Stensløkken, & Vaage, 2016). Runx2 upregulates several osteogenic genes including Col1A1, ALP, BSP, BGLAP, and OCN (Fakhry, Hamade, Badran, Buchet, & Magne, 2013). Osx is induced by Runx2 (Nishio et al., 2006) or BMP-2 (Lee, Kwon, Park, Wozney, & Ryoo, 2003) and Dlx5 is also induced stimulated by BMP stimulation (Han et al., 2011). Osteoblast differentiation proceeds through a proliferation phase followed by transition to a mature matrix-secreting phenotype. The organic matrix that is secreted by osteoblasts is known as osteoid (which serves as the scaffolding for subsequent mineralization) and is composed of type I collagen, non-collagenous protein (osteocalcin, osteonectin, bone sialoprotein II, osteopontin, etc.) and proteoglycans (such as decorine and biglycan) (Florencio-Silva et al., 2015). To mineralize the osteoid, calcium and phosphate must precipitate in the form of hydroxyapatite crystals. This process is not entirely understood, however key players are known. Hydroxyapatite precipitation is favored in supersaturated solutions of calcium and phosphate which are achieved within matrix vesicles released by osteoblasts. Upon rupture of the matrix vesicles, hydroxyapatite crystals spread to the surrounding matrix. As the organic matrix mineralizes, some osteoblasts undergo programmed cell death known as apoptosis. A subpopulation of non-apoptotic osteoblasts extends cytoplasmic processes towards the bone matrix and eventually becomes imbedded within the newly mineralized tissue. These osteoblasts go on to differentiate into osteocytes. The rest remain on the bone surface as bone-lining cells which neither resorb or form bone, however they have been proposed to sequester bone surface (Florencio-Silva et al., 2015) since they cover over 90% of the bone surface (A. G. Robling & C. H. Turner, 2009) thereby preventing osteoclasts from resorbing those regions. Additionally, these bone-lining cells produce osteoprotegerin (OPG) and receptor activator of nuclear factor kappa-B ligand (RANKL), factors that are critical in regulating osteoclast differentiation.

Osteoclasts. Osteoclasts are highly specialized macrophage-like cells that resorb bone (Florencio-Silva et al., 2015). They are multinucleated cells that are derived from the hematopoietic lineage. Due to the destructive nature of osteoclasts, osteoclastogenesis is tightly regulated, and terminally differentiated osteoclasts undergo apoptosis shortly (< 2 weeks) after maturation (Manolagas, 2000). Macrophage-colony stimulating factor (M-CSF) derived from osteoblasts and related osteoprogenitor cells is necessary to recruit and initiate the proliferation of monocytic precursors.

RANKL, which is secreted by osteoblasts and osteocytes, is the necessary to commit these cells to osteoclastogenesis. RANKL signals through its cognate receptor, RANK, and stimulates expression of NFATc1. NFATc1 then proceeds to stimulate osteoclast-specific gene expression, such as DC-STAMP which is critical for the fusion of mononuclear osteoclast precursor cells into multinuclear osteoclasts, and Cathepsin K which is important for osteoclast function. The RANKL/RANK signaling axes is antagonized by a secreted decoy receptor OPG, which is produced by osteoblasts and stromal cells and binds RANKL directly, sequestering it from interacting with RANK. Thus, the RANKL/RANK/OPG axis plays a central role in regulating osteoclastogenesis. Terminally differentiated osteoclasts are polarized cells with an apical and basolateral domain delineated by the sealing zone and ruffled borders which are in direct contact with the bone matrix. The sealing zone is maintained by $\alpha_v\beta_3$ integrins and ensures the basolateral domain is isolated from the surrounding extracellular space, thereby allowing osteoclasts to establish a specialized microenvironment between the bone and osteoclast basolateral surface where resorption occurs. This space is acidified by lysosomes and protons secreted by vacuolar-type H^+-ATPases which results in the dissolution of hydroxyapatite. Proteolytic enzymes, such as cathepsin K and matrix metalloproteinase (MMP)-9, then degrade the remaining organic matrix and degradation products are trafficked through the osteoclast. Pathological resorption is associated with conditions like osteoporosis, bone metastases or inflammatory arthritis which result in osteolytic lesions.

Osteocytes. Osteocytes are the terminally differentiated cell of the osteoprogenitor lineage, arising from osteoblasts that became imbedded within the mineralized matrix. Osteocytes are the most abundant and long living cell type in bone, making up 90-95% of the resident bone cells and living up to 25 years (Florencio-Silva et al., 2015). They function in maintaining and adapting bone to various stimuli and regulate the interactions and functions of osteoblasts and osteoclasts. Unlike the osteoblasts which are columnar, osteocytes have a distinct morphology that is characterized by a small soma (cell body) and long and numerous cytoplasmic processes that extend between osteocytes within the bone. Osteocytes are located within lacunae and their cytoplasmic processes form the lacuna-canalicular system. It is estimated that there are ~42 billion osteocytes in an average human skeleton with an astounding ~3.7 trillion cytosolic projections, amounting to a level of complexity that is found in the neural network of the brain (Buenzli & Sims, 2015). Given their strategic localization within the bone, osteocytes are recognized as the principle bone

mechano-sensors. They perceive the surrounding physical environment and convert mechanical stimuli to biochemical signals, which then orchestrate the downstream cellular responses of osteoclasts and osteoblasts.

1.3 Bone mechanobiology

1.3.1 Tissue-scale forces

The skeletal system is routinely exposed to physical forces. A combination of gravitational and activity-related forces acts on the skeleton. It is believed that the predominant forces impacting bone metabolism and adaptation are activity-related impact forces (Kohrt et al., 2009). On average, daily activity engenders strains of 0.05% (500 με) experienced at a frequency of 1-3 Hz (Burr et al., 1996; Fritton, McLeod, & Rubin, 2000), with larger strains (>0.1%) occurring only a few times a day, and smaller strains (<0.001%) occurring thousands of times a day (Fritton et al., 2000). Activities such as running or jumping can lead to strains as high as 0.2-0.35%, with irreversible deformation occurring at 0.7% and failure (i.e. fracture) at 1-3% (Lynch & Fischbach, 2014; Reilly & Burstein, 1975). Trabecular bones articulate with the joints and are involved in transferring loads onto the cortical bone. The architecture and mineral-collagen composition of the trabecular lattice is optimized to transfer these loads efficiently. As forces are dispersed through the skeletal structure, mechanical perturbations are perceived at the cellular level and integrated into an adaptive response. There are several types of forces that are experienced throughout bone (Lynch & Fischbach, 2014; Oftadeh, Perez-Viloria, Villa-Camacho, Vaziri, & Nazarian, 2015). Physical deformation of the bone matrix exposes adherent cells to substrate strains. Loading induces flow through the canaliculi, such that interstitial fluid flows along a pressure gradient throughout the lacuna-canalicular network (Weinbaum, Cowin, & Zeng, 1994). Related to canalicular flow, the flow of ionic fluids along charged surfaces in the lacuna-canalicular spaces can build up of electrical streaming potentials which themselves stimulate cells (Guzelsu & Walsh, 1990). Additionally, flow in the marrow space exerts forces upon cells lining the endosteal surfaces of the mineralized structure (T. R. Coughlin & Niebur, 2012). Thus, tissue-level strains, pressures and fluid shear forces are prominent in bone.

1.3.2 Tissue-level mechanoresponse

Mechano-adaptation theory. In the 19th century, Julius Wolff noticed that bone is shaped in a way that optimizes the transfer of force through the skeleton (Carter & Beaupré, 2007). Reasoning that there is a relationship between skeletal form and mechanical function, Wolff argued that

> "*alterations of the internal architecture [of bone] clearly observed, and following mathematical rules, as well as secondary alterations of the external form of the bone following the same mathematical rules, occur as a consequence of primary changes in the shape and stressing or in the stressing of the bones*"(Ruff, Holt, & Trinkaus, 2006)

This became known as Wolff's law, however, conventional interpretations are more reminiscence of arguments made by one of Wolff's contemporaries, Wilhelm Roux, who emphasized that organisms are capable of adapting to different external factors and that bone specifically responds to altered mechanical loads (Carter & Beaupré, 2007; Ruff et al., 2006). A refinement of Wolff's law was the Mechanostat Theory introduced by Harold Frost in 1983 (Frost, 1983). Frost proposed that bone adapts according to various mechanical set points (similar to a thermostat) such that loading promotes bone gain and unloading results in bone loss, thereby optimizing the mechanical properties of bone to the mechanical environment (Pivonka, 2018). To no surprise, this was an oversimplification of skeletal mechanobiology, however it continues to serve as a useful conceptual model. Based on subsequent experimental findings, Charles Turner added three rules of skeletal mechanoadaptation (Carter & Beaupré, 2007; Turner, 1998):

(i) bone adapts to dynamic rather than static loads
(ii) adaptive responses diminish as duration of loading increases
(iii) bone cells accommodate to habitual loads, thereby shifting their basal mechano-setpoints

Which Tim Skerry later extended to include (Carter & Beaupré, 2007; Skerry, 2006):

(iv) that the number loading cycles after a certain threshold no longer matters
(v) and recovery periods between bouts of loading potentiate the osteogenic effect

Each of these additional principles exemplifies a memory-like capacity in bone, such that bone "remembers" the effects of past mechanical loads and adapts accordingly. The goal of these adaptations has been inferred to maintain tissue-level strains at a minimum, while minimizing tissue mass (Pivonka, 2018).

1.3.3 Mechano-adaptive bone modelling and remodelling

Bone adapts to mechanical loads through modeling or remodeling processes (**Fig 1-2**).

Modelling. Bone modelling refers to the independent actions of bone forming osteoblasts in "formation modeling" or bone resorbing osteoclasts in "resorption modelling" (Pivonka, 2018). Modelling processes directly affect the shape and architecture of bone by widening/narrowing, changing axis or adding/removing bone at appropriate surfaces. Bone modelling is more pronounced during bone development and becomes less active in adults. In the context of mechano-adaptation, as loading increases, periosteal bone formation acts to increase the midshaft diameter of long bones, thus reducing the levels of experienced strain (Robling, Castillo, & Turner, 2006) (**Fig 1-2D**).

Remodeling. Remodeling processes refer to the spatially- and temporally- coupled actions of osteoclasts and osteoblasts in an anatomical structure that is called a basic multicellular unit (BMU) (Pivonka, 2018). Remodeling ensures that bone is constantly renewed to maintain its material properties and ensure it is accessible for mineral homeostasis. Remodeling proceeds through a three-step process, in which (i) osteoclasts resorb bone, forming a cutting cone that progressively advances through the tissue, (ii) there is a transition from resorption to formation and (iii) osteoblasts form new bone thereby closing the cone created by osteoclasts (Florencio-Silva et al., 2015). The average lifetime of a BMU is 4 months and there are ~2×10^6 BMUs in the human skeleton at any given moment (Tyrovola, 2015). Although remodeling and modelling processes are distinct in their functions, the mechanisms by which the cellular constituents are coupled (or uncoupled) are unclear. Osteocytes, the third major bone cell type, are believed to orchestrate these processes (Pivonka, 2018). Bone remodeling processes are responsive to a broad range of different mechanical environments. The relationship mechanical loads and remodeling has been described as a U-shaped curve (A. G. Robling & C. H. Turner, 2009) (**Fig 1-2E**). Insufficient loads related to disuse or microgravity are associated with elevated bone remodeling.

Similarly, excessive loads introduce microdamage at the tissue level, initiating remodeling as a repair mechanism (Mori & Burr, 1993; A. G. Robling & C. H. Turner, 2009). In between these two extremes are physiologically-relevant loads at which remodeling processes are minimal (Robling et al., 2006). The net bone gained or lost is ultimately governed by the balance of remodeling and modeling processes, such that when formation exceeds resorption, bone is gained, and when resorption exceed formation, bone is lost.

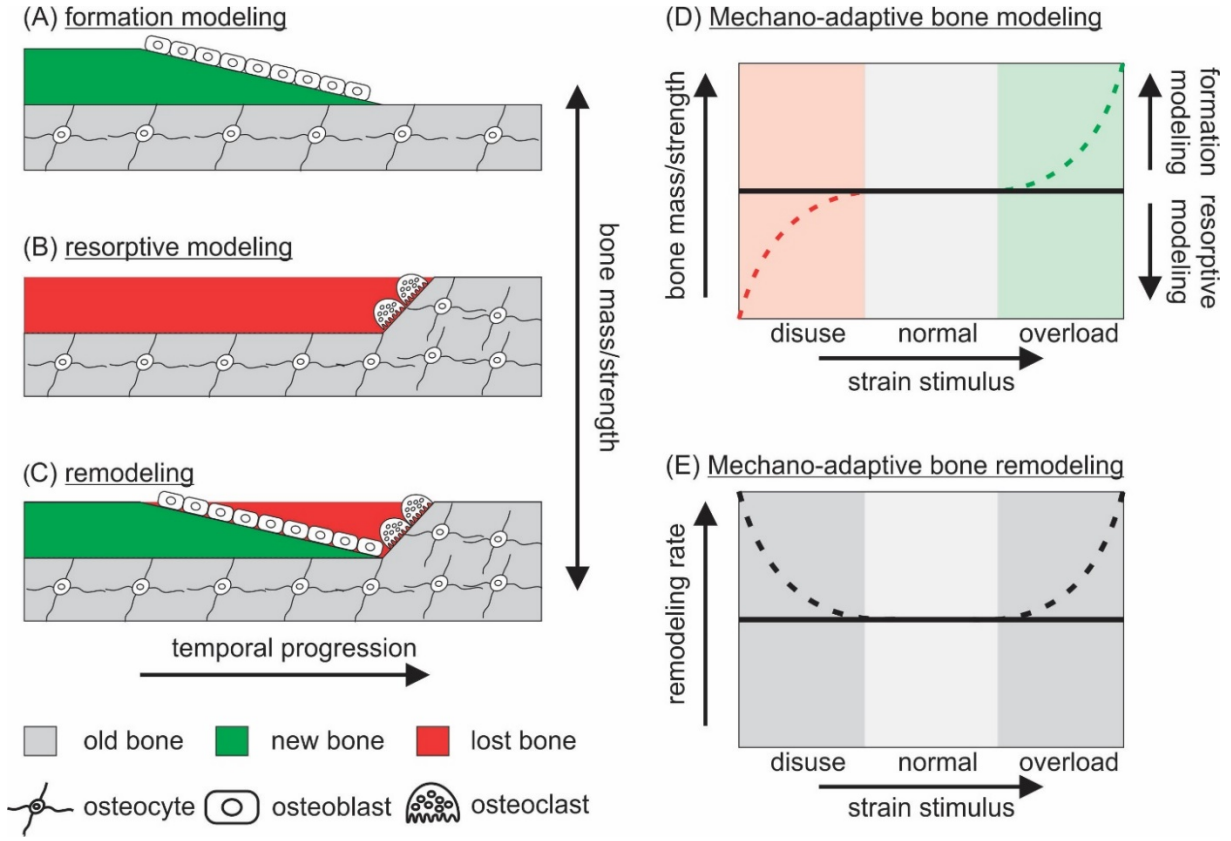

Figure 1-2. **Mechano-adaptive bone modelling and remodeling**. **(A, B)** Bone modelling adapts the mineralized structure to mechanical loads by changing the shape and architecture of bone through the independent actions of osteoblasts in formation modeling **(A)** and osteoclasts in resorptive modeling **(B)**. **(C)** Bone remodeling maintains the structure integrity of the mineralized tissue through the spatiotemporally coupled actions of osteoclasts and osteoblasts, known as the basic multicellular unit. **(D)** Strain-dependent bone modeling. *Grey zone*: physiological strains maintain bone mass, *red zone/line*: Disuse results in decrease in bone mass due to resorptive modeling, *green zone/line*: High strain results in increase in bone mass due formation modelling. **(E)** U-shaped strain-remodeling relationship. *Light grey zone*: physiological strains maintain low basal remodeling rates, *dark grey zone*: Increased remodeling rates associated with disuse and overload.

1.4 Cellular mechanobiology

1.4.1 Experimental models of physiological forces

Physiological forces vary over a quadrillion-fold, ranging from piconewtons (10^{-12}) in the cochlea to kilonewtons (10^{3}) in tendons (Addae-Mensah & Wikswo, 2008). To study the biological effects of such forces, experimentally applied forces must reliably reproduce the magnitude and types of force experienced physiologically. Force (F) is calculated as a vector that accelerates (a) a mass (m) in a specified direction.

$$F = ma$$

When force is applied to a surface (A), the resulting stress (σ) is then expressed as

$$\sigma = \frac{F}{A}$$

Applying these fundamental concepts of mechanics, *in vitro* methods have been developed to model membrane deformation, shear stress, strain, and gravity-related forces (Addae-Mensah & Wikswo, 2008).

Membrane deformations. Direct membrane deformations have been studied using atomic force microscopy (AFM), magnetic tweezers, microfluidic chambers, micropipette aspiration or deformation and optical tweezers (Addae-Mensah & Wikswo, 2008). AFM consists of a tip attached to a flexible cantilever which is used to directly probe cells and deflections in the cantilever are used to estimate the amounts of force applied. Microfluidics chamber pass cells through narrow channels thereby causing membrane deformation. Magnetic tweezers use magnetic fields to manipulate magnetic particles that have been conjugated to or taken up by the cell. Cells can also be deformed using a micropipette to apply suction to the surface of the cell. Alternatively, the micropipette can be used to directly deform the cellular membrane, similar to AFM. Optical tweezers are a variation of magnetic tweezers, but instead of magnetic fields and particles, lasers and dielectric beads are used.

Shear stresses. The effects of fluid flow-related shear stresses on cells are predominantly studied using cone and plate viscometers or parallel plate flow chambers (Addae-Mensah & Wikswo, 2008). Cone and plate viscometers typically consist of (i) a circular plane upon which cells are plated and (ii) a cone-like stirrer which rotates close to the surface to generate flow. Alternatively,

parallel plate flow chambers consist of two parallel plates and a cell monolayer attached on one surface. Flow is then generated by applying a pressure gradient along the length of the chamber. For either experimental model, laminar or turbulent flow can be applied. In a parallel plate setup, the shear (τ) generated at the chamber wall under ideal laminar flow conditions is proportionate to the flow rate (Q) and fluid viscosity (μ), and inversely proportional to the dimensions of the chamber.

$$\tau = \frac{3Q\mu}{2wh^2}$$

where *w* and *h* are chamber width and height dimensions, respectively. Shears are typically expressed in terms dynes per squared centimeter (dyne/cm^2) which is a measure of force per unit area, or stress (σ = F/A).

Strain. Strain, or stretch, is applied using deformable substrates or osmotic pressures. Cells are cultured on elastic substrates, usually made from flexible silicon sheets and sometimes modified with ECM proteins (Addae-Mensah & Wikswo, 2008). These substrates can then be stretched statically or cyclically on a uniaxial or biaxial plane. Alternatively, reducing osmolality to achieve hypotonicity causes cellular swelling and membrane stretch (Alam Shibly, Ghatak, Sayem Karal, Moniruzzaman, & Yamazaki, 2016). The amount of strain (ε) applied can be quantified as a normalized measure of deformation experienced due to stress. For small strains (<10% stretch) in the physiological range, strain is expressed as:

$$\varepsilon = \frac{L - L_0}{L_0}$$

Where L is the final length of the body and L_0 is the initial length. Strain is a unitless measure that can be related to stress. This relationship is dependent on how an object elongates when exposed to stress which is a material property known as the elastic modulus (E):

$$E = \frac{\sigma}{\varepsilon}$$

Thus, given the strain and elastic modulus, the applied stress can be estimated.

Gravitational. The effects of microgravity on cellular mechanobiology have studied to discern the effects of normal gravity on the human body. Studies have collaborated with space programs in

the past to send samples into space (Tamma et al., 2009). However, such space flight experiments are often unfeasible and devices to simulate microgravity on earth have been developed. These devices aim to establish weightlessness, defined as a lack of particle sedimentation within a vessel (Hemmersbach, von der Wiesche, & Seibt, 2006). Clinostats are one example of such a device which rotate samples perpendicular to the force of gravity, with the rationale that continuously reoriented biological systems result in a time-averaged gravitational vector of near-zero (Hemmersbach et al., 2006; Sarkar, Nagaya, Koga, & Seo, 1999). Results obtained using simulated microgravitational devices are generally consistent, albeit less pronounced than results obtained in space experiments (Hemmersbach et al., 2006; Tamma et al., 2009). Other devices have also been developed including rotating wall vessels, free-fall machines and random positioning machines (Herranz et al., 2013).

1.4.2 Mechanical forces at the cellular level

Cells are constantly probing their microenvironment, sensing and responding to environmental cues that impact their cellular behaviour. The immediate environment in which cells are situated directly influences the kinds of mechanical forces that cells are exposed to (**Fig 1-3**). Osteoblasts line the surface of the mineralized tissue while osteocytes are imbedded within. Thus, it is not surprising that osteoblasts and osteocytes inherently experience different mechanical environments. In fact, strains experienced at the surface of bone are much smaller than those experienced within bone (M. G. Mullender & Huiskes, 1995). To stimulate a mechanical response in bone cells, strains must exceed 0.5%, however, surface-residing osteoblasts are rarely exposed to physiological strains that exceed 0.2% (Burr et al., 1996; Fritton et al., 2000). The bone marrow is however highly porous and experiences fluid flow due to load-induced pressure differentials, generating shears as high as 50 dyne/cm^2 at endosteal surface of the bone (T. R. Coughlin & Niebur, 2012). Within the mineralized tissue, strain is also not the principal force acting on osteocytes, highlighted by the fact that bone cells are less sensitive to strains than to fluid flow (Oftadeh et al., 2015; J. You et al., 2000). The lacuna-canalicular network in which osteocytes reside is filled with viscous fluid. When loads are applied, pressure gradients within the bone force this fluid to flow through the canalicular canals generating shears up to 8-30 dyne/cm^2 at the osteocytic membrane (Weinbaum et al., 1994). Additionally, the long cytoplasmic processes that extend between osteocytes are directly anchored to the canalicular wall via $\alpha_V\beta_3$ integrins (Y.

Wang, McNamara, Schaffler, & Weinbaum, 2007). A growing body of evidence suggests that these tethering fibers are involved in amplifying forces applied to the osteocyte (A. G. Robling & C. H. Turner, 2009; Santos, Bakker, & Klein-Nulend, 2009). Fluid that flows past these tethers causes a drag effect, which effectively tenses the tethering fibers and produces radial strain on the cytoplasmic processes. Theoretical models have estimated that this mechanism of amplification results in a 10- to 100- fold increase in perceived force, sufficient to stimulate downstream signaling (L. You, Cowin, Schaffler, & Weinbaum, 2001).

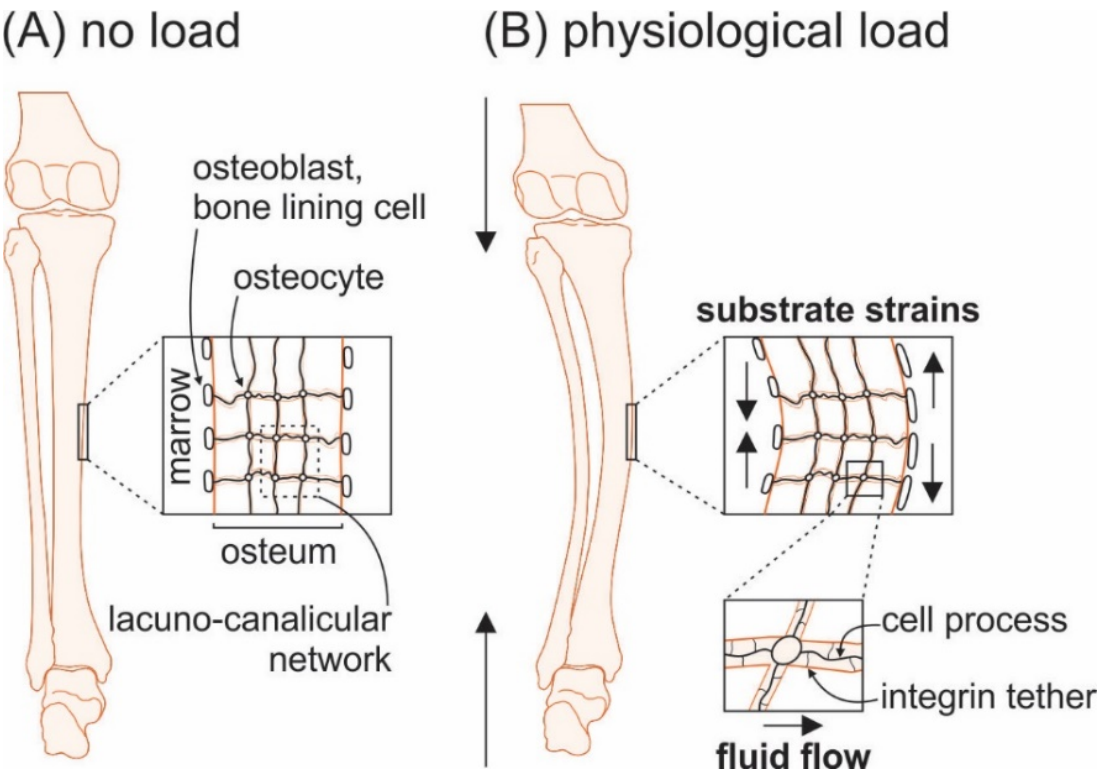

Figure 1-3. **Mechanical forces at cellular level**. **(A)** Non-loaded tibia illustrated with enlarged marrow-osteum interface shows surface-residing osteoblasts and bone-lining cells, and osteum-embedded osteocytes forming lacuna-canalicular network. **(B)** Physiological loads deform tibia and cause substrate strains that deform surface cells and generate pressure gradients within bone, forcing fluid flow through canalicular canals and creating shears on osteocytic membranes. Also, drag force on integrin- anchored tethers produces radial strain on cytoplasmic processes. *Arrows*: Direction of force.

1.4.3 Molecular basis of cellular force transmission

Mechanical stimuli are converted to biochemical signals at the cellular level through several independent and overlapping mechanisms (**Fig 1-4**).

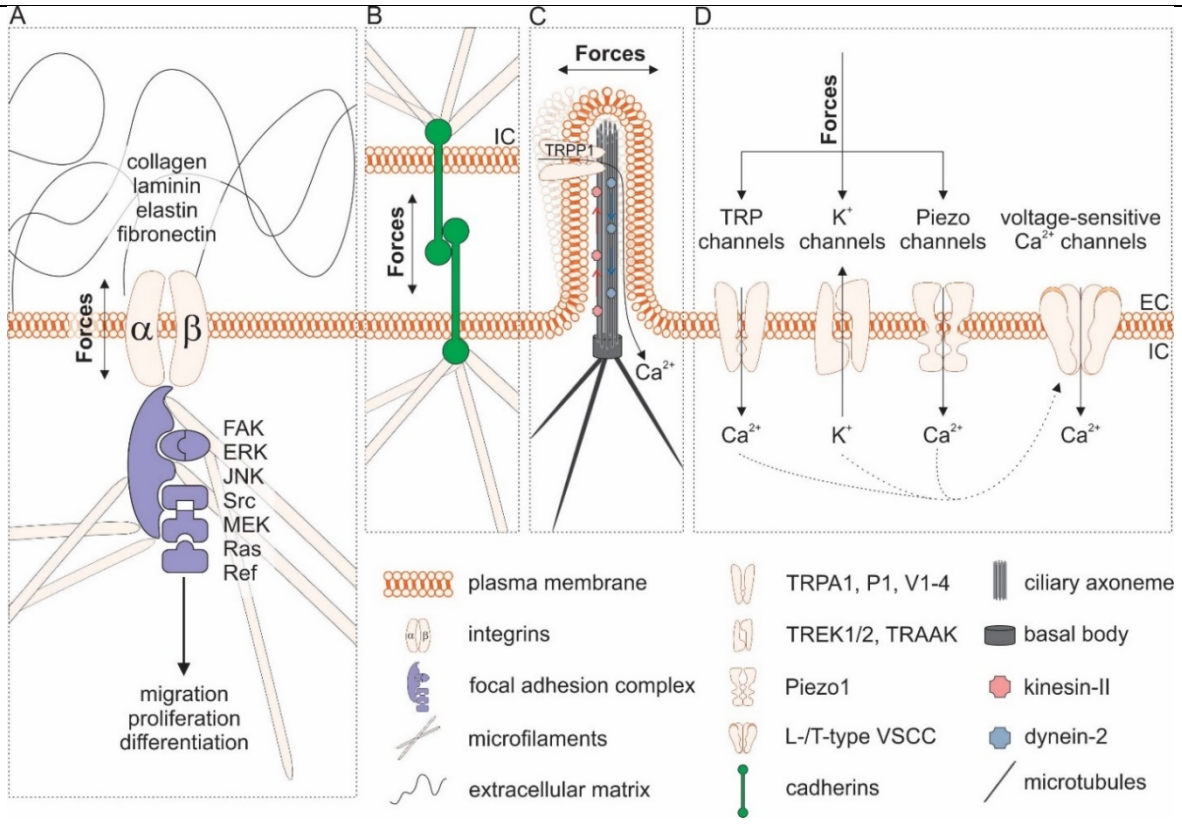

Figure 1-4. **Molecular basis of cellular forces transmission**. **(A) ECM-cell transmission**: Integrin/focal adhesion complex mediates bidirectional transmission of forces between cytoskeleton and extracellular matrix, while concurrently initiating intracellular signaling. **(B) Cell-cell transmission**: Cadherins between adjacent cells form adherent junctions and mediate bidirectional force transmission between cells. **(C, D) Force-cell transmission**: Primary cilia are deflected (C) and membrane channels are activated (D) by external forces. IC: intracellular, EC: extracellular

Cytoskeleton. At the center of cellular force transmission lies the cytoskeleton, which is the subcellular framework that provides support and structural integrity to the cell while concurrently sustaining essential cellular modalities such as shape, growth, division and differentiation (J. Eyckmans, T. Boudou, X. Yu, & C. S. Chen, 2011; Jeroen Eyckmans, Thomas Boudou, Xiang Yu, & Christopher S. Chen, 2011). The cytoskeleton consists of microtubules, intermediate filaments, and microfilaments. Polymerized tubulin forms hollow cylindric microtubules which associate with various motor proteins, such as kinesins and dyneins, and are involved in mediating

intracellular transport functions such as vesicular trafficking. Microtubules are also integral to the development of primary cilia, which function as mechanosensory organelles that perceive fluid flow (Downs, Nguyen, Herzog, Hoey, & Jacobs, 2014). Intermediate filaments, consisting of vimentin, keratin and laminin monomers, tether the nucleus to various subcellular compartments and are predominantly involved in maintaining the cellular structural integrity. Microfilaments consist of polymerized filamentous actin and they associate with myosin filaments, forming the contractile apparatus of the cell. The actomyosin network exerts traction forces, transfers forces to and from extracellular adhesions and generates forces along the length of the cell to control morphological and mechanical behaviours of the cell (Gardel; Owen et al., 2017).

Integrins and focal adhesions. The extracellular matrix (ECM) is mechanically linked to the cytoskeleton through macromolecular complexes known as focal adhesions (FA) (**Fig 1-4A**) (J. Eyckmans et al., 2011). Integrins, a family of transmembrane heterodimers consisting of α and β subunits, are mechanoreceptors that play a central role in focal adhesions (N. Wang, Butler, & Ingber, 1993). Osteoblasts express α_2, α_3, α_4, α_5, α_V, α_6, β_1, β_3, β_5 integrin subunits (Grzesik & Robey, 1994; Sinha & Tuan, 1996). The extracellular domains of integrins serve as ECM anchors, which commonly interact with RGD (Arg-Gly-Asp) peptides found in many extracellular proteins (Rodan & Rodan, 1997). When integrins bind the ECM, the intracellular integrin domains cluster into focal adhesion ensembles – for instance, shear-induced α5β3 clustering occurs in osteoblasts (Weyts, Li, van Leeuwen, Weinans, & Chien, 2002). FAs are localized at the ends of stress fibers, which are bundled actin filaments, thereby coupling the ECM to the actin cytoskeleton (Hoon, Tan, & Koh, 2016). This clustering event also recruits a variety of signalling proteins including FAK, ERK, JNK, Src, MEK, Ras and Raf, which are involved in functions like migration, proliferation and differentiation (Parsons, Horwitz, & Schwartz, 2010). Thus, integrins serve a dual function by first anchoring the cytoskeleton to the ECM and then coupling this linkage to various intracellular signalling pathways. However, this coupling is not just designed to transmit forces unidirectionally, from the ECM to the cytoskeleton. Intracellular forces generated by actomyosin contractions can be transmitted through FAs to deform the ECM, serving as a reciprocal mechanism by which cells can interact with their physical microenvironment. Many fundamental cellular processes such as mitosis and migration cannot occur without the generation of such endogenous forces (Civelekoglu-Scholey & Scholey, 2010; Renkawitz & Sixt, 2010). In the context of bone physiology, mechanical transduction through the FA-related FAK/ERK/Runx2

signalling axis has been proposed as a mechanism by which mesenchymal stems cell may commit to the osteogenic lineage (Biggs & Dalby, 2010). Moreover, as mentioned earlier, $\alpha_V\beta_3$ integrins in osteocytes tether the actin cytoskeleton to the canalicular canal, mechanically-coupling the extracellular environment to intracellular signaling machinery (Y. Wang et al., 2007).

Extracellular Matrix (ECM). The ECM is an organic mesh of cross-linked proteins which are "glued" together by hyaluronic acid and proteoglycans (J. Eyckmans et al., 2011). Its composition is tissue-dependent, incorporating varying amounts of collagen, laminin, elastin and fibronectin fibers, and its material properties directly influence the mechanobiology of residing cells. Several features highlight the ECM's role in mechanobiology. Forces acting on the ECM can directly induce alternations in quaternary protein structure (i.e., aggregate conformation of interacting protein subunits), thereby altering function (Krammer, Lu, Isralewitz, Schulten, & Vogel, 1999). Similarly, the ECM serves as a reservoir for soluble proteins and mechanical forces can result in the liberation of the ECM-bound factors, like TGFβ, which can then initiate cellular signalling (Wipff, Rifkin, Meister, & Hinz, 2007). The passive mechanical properties of the ECM, such as bulk, local stiffness and topography (Holle et al., 2018), can also influence cellular behaviour. For instance, cells exert stronger traction forces on stiffer surfaces, thereby affecting cell shape, motility, proliferation and signalling (J. Eyckmans et al., 2011). In the context of bone, osteocyte differentiation is enhanced within softer scaffolds suggesting that osteoblasts initiate their differentiation into osteocytes after becoming imbedded within soft unmineralized bone matrix (Mc Garrigle, Mullen, Haugh, Voisin, & McNamara, 2016). Thus, it is clear that the content and material properties of the ECM play an important role in cell-ECM mechanical interactions.

Intercellular Adhesion Junctions. Not only do cellular populations interact physically with the ECM, but they can also do so with one another. Cells articulate with their neighbours through adherent junction (AJ) which link the intracellular cortical actin filaments of adjacent cells through a complex of calcium-dependent cadherins (Harris & Tepass, 2010) (**Fig 1-4B**). Cells tug and pull on one another, and these mechanical stresses reinforce AJs in a myosin/Rac1-dependent manner (Z. Liu et al., 2010), representing a positive feedback loop by which cellular ensembles can remain intact. The implications for such intercellular linkages are apparent when considering multicellular sheets of cells (Nelson et al., 2005). Symmetric contractions can manifest in asymmetric distributions of mechanical forces, thereby governing the geometry of cellular sheets and resulting

in complex pattern formation and morphogenesis. Such geometrically imposed patterns of stress govern differentiation trajectories in mesenchymal stem cells (Ruiz & Chen, 2008). Mesenchymal stem cells located in low tension regions favor the adipocyte lineage while high tension regions are associated with osteogenic differentiation (Ruiz & Chen, 2008). Additionally, mechanical strains applied to mesenchymal stem cells initiate β-catenin nuclear translation in a manner dependent on the adhesion protein Cadherin, representing a mechanism of mechanically-induced osteoblastogenesis and emphasizing the role of cell-cell junctions in cellular force transduction (Arnsdorf, Tummala, & Jacobs, 2009; Norvell, Alvarez, Bidwell, & Pavalko, 2004).

Primary cilia. Primary cilia are microtubules-based structures that emanate from the cell surface of differentiated, non-dividing cells (Satir, Pedersen, & Christensen, 2010) (**Fig 1-4C**). The presence of the cilium is cell-cycle dependent, such that the cilium is assembled following mitosis. The mitotic mother centriole is repurposed into a basal body that anchors the cilium for the duration of the quiescent (G_0) or the post-mitotic gap (G_1) phase (Quarmby & Parker, 2005). Primary cilia consist of an axoneme of nine microtubule doublets spanning from the basal body into the extracellular space (Nguyen & Jacobs, 2013). Since protein synthesis cannot occur in the ciliary body, ciliary protein must be transported to and from the cilia by anterograde kinesin II and retrograde dynein 2, respectively (Sara Temiyasathit & Jacobs, 2010). Although primary cilia were proposed to be sensory organelles nearly a century ago (Zimmermann, 1898), experimental support for this hypothesis was non-existent until the 1980's when renal primary cilia were demonstrated to bend in response to fluid flow (Roth, Rieder, & Bowser, 1988) and mediate intracellular calcium signalling (Praetorius & Spring, 2001). The role of ciliary mechanotransduction in bone is unresolved. On one hand, osteoblast- and osteocyte-specific Kif3a knockout (essential protein for cilia formation and function) in mice partly diminished the osteogenic response to loading (S. Temiyasathit et al., 2012). On the other hand, primary cilia are present on only 4% of osteocytes, 4.6% of bone lining cells and 1% of cells within the marrow space (Thomas R. Coughlin, Voisin, Schaffler, Niebur, & McNamara, 2015). The low prevalence of primary cilia raises the question of whether primary cilia serve as mechano-sensors in a small subpopulation of cells, or whether the mechano-sensory role of primary cilia is secondary to some other function(Thomas R. Coughlin et al., 2015).

Membrane channels. Mechanosensitive channels are abundantly present in our sensory systems where they mediate mechano-sensation related to hearing, touch and pain (Ranade, Syeda, & Patapoutian, 2015). In non-sensory tissues, mechanosensitive channels are involved in converting a diverse range of mechanical stimuli into biochemical signals. Mechanosensitive channels are in a two-state (open/close) tension-dependent equilibrium (Sukharev, Blount, Martinac, & Kung, 1997). Transitions between the open and closed states has been described using one of two contended models: The tethered (trap-door) model or the membrane-mediated (force-from-lipid) model (Haswell, Phillips, & Rees, 2011; Ranade et al., 2015). The former postulates that forces are transmitted to the channel by some intermediary structure, such as the ECM or cytoskeleton. The latter model is simpler and suggests that forces transmitted along the lipid bilayer are sufficient to activate mechanosensitive channels. In fact, it has been established that mechanosensitive channels respond best to forces applied parallel to the membrane (e.g., tension), rather than those applied normal to the plane of the membrane (e.g., hydrostatic pressure) (Sokabe & Sachs, 1990; Sokabe, Sachs, & Jing, 1991). Features such as hydrophobic mismatch and the intrinsic membrane curvature also influence channel mechanosensitivity. Hydrophobic mismatch refers to a situation in which the thickness of the hydrophobic region of a membrane channel is different from the thickness of the membrane it spans (Duque, Li, Katsov, & Schick, 2002). While this mismatch is insufficient to activate mechanosensitive channels, it can exert a pressure bias which alters the channel open probability (Perozo, Kloda, Cortes, & Martinac, 2002). Similarly, surface tension is proportional to the extent of membrane curvature, thus the activation thresholds of mechanosensitive channels are lower when lipid bilayers are increasingly curved (Bacabac et al., 2008). There are several families of mechanosensitive channels, however, I will focus on the subsets that are relevant to skeletal mechanobiology, namely transient receptor potential (TRP) channels, mechanosensitive potassium (K^+) channels and piezo channels. I will also introduce voltage sensitive calcium channels (VSCC) which are not strictly mechanosensitive but are involved in mechanotransduction (**Fig 1-4D**).

Transient receptor potential (TRP) Channels. The TRP family of non-selective cation channels consists of 7 subclasses (Christensen & Corey, 2007). Although TRP mechanosensitivity is clearly established in invertebrates, the TRP mechanosensitivity in mammalian cells is less clear, although still evident in certain subtypes including TRPV1, TRPV2, TRPV4, TRPP1 and TRPA1 (Egbuniwe et al., 2014; Mizoguchi et al., 2008; Nauli et al., 2003; Shibukawa et al., 2015; Xiao et

al., 2011). In humans, TRPV4 mutations have been associated with skeletal dysplasia, characterized by severe dwarfism and kyphoscoliosis amongst other symptoms (S. S. Kang, Shin, Auh, & Chun, 2012; Leddy, McNulty, Guilak, & Liedtke, 2014). TRPV4$^{-/-}$ mice exhibit no morphological changes by embryonic day 16.5, but show delayed mineralization (Weinstein, Tompson, Chen, Lee, & Cohn, 2014) and are protected from disuse-related bone loss (Mizoguchi et al., 2008). Moreover, expression of mutant TRPV4 in mice recapitulates many features of TRPV4-related skeletal dysplasia seen in humans (Weinstein et al., 2014). The mechano-sensory properties of TRPP1 were originally demonstrated in kidney epithelial cells (Nauli et al., 2003). TRPP1 is predominantly localized to the primary cilium (Malicki & Avidor-Reiss, 2014; Nauli et al., 2003) where it is activated by ciliary deflection and it initiates mechanotransductive calcium signalling (Patel & Honore, 2010). Load-induced bone formation is reduced by 70% in TRPP1$^{-/-}$ mice (Xiao et al., 2011). TRPA1 is also a mechanosensitive ion channel (Kwan, Glazer, Corey, Rice, & Stucky, 2009; Vilceanu & Stucky, 2010) and in odontoblasts, TRPA1 as well as TRPV1, TRPV2 and TRPV4 are activated by mechanically stimulation (Egbuniwe et al., 2014; Shibukawa et al., 2015).

Potassium (K^+) Channels. TREK-1 (Fink et al., 1996), TREK-2 (Bang, Kim, & Kim, 2000; Lesage, Terrenoire, Romey, & Lazdunski, 2000) and TRAAK (Fink et al., 1998) are mechanosensitive potassium (K^+) channels from the 4 transmembrane two-pore domain potassium channel (K_{2p}) family. They are primarily involved in neuronal sensation, specifically tuning the activities of mechanosensitive dorsal root ganglion neurons (Ranade et al., 2015). Osteoblasts have also been reported to express TREK-1, TREK-2 and TRAAK, although investigations of their roles in skeletal mechanotransduction have been limited (Steven Hughes et al., 2006). TREK-2 is involved in the induction of mechanically-stimulated PTH-related protein (PTHrp) expression, possibly mediating an anabolic effect (X. Chen, Macica, Ng, & Broadus, 2005). Mechanistic studies focusing on TREK-1 and TRAAK have demonstrated that these channels are activated by negative or positive pressures. Importantly, their activation is intrinsically gated by membrane tension (Berrier et al., 2013; Brohawn, Su, & MacKinnon, 2014) thereby providing insight into the mechanism of mechanical force transduction at the membrane.

Piezo channels. Piezo channels are a recently discovered family of mechanosensitive cation channels (Coste et al., 2010) and have been implicated in Hereditary Stomatocytosis [Piezo1 (Albuisson et al., 2013)] and Distal Arthrogryposis [Piezo2 (Coste et al., 2013)]. These channels

are necessary to transduce mechanical forces in certain mechanosensitive cells, and sufficient to confer mechanosensitivity in naïve cells. Their function has been predominantly studied in erythrocytes, where they have been realized to link mechanical forces to cellular volume (Cahalan et al., 2015). In the context of skeletal mechanobiology, mesenchymal stem cells were shown to upregulate Piezo1 expression following exposure to hydrostatic pressure (A. Sugimoto et al., 2017). Subsequent stimulation of Piezo1 was associated with BMP2 expression and osteoblast differentiation (A. Sugimoto et al., 2017).

Voltage sensitive calcium channels (VSCC). VSCCs are a peculiar class of ion channels in the sense that they are not strictly mechanosensitive, yet their activation is consistently observed in parallel to some other unidentified mechanosensitive channel in osteoblasts (J. Zhang, Ryder, Bethel, Ramirez, & Duncan, 2006) and osteocytes (Brown, Leong, & Guo, 2016). VSCCs are multimeric complexes composed of pore forming α1 and auxiliary α2δ/β subunits. Long-lasting (L-)VSCCs and transient (T-)VSCCs are the main types of VSCCs found in bone (Catterall, 1995; Shao, Alicknavitch, & Farach-Carson, 2005), with L-VSCC predominantly expressed in osteoblasts and T-VSCCs in osteocytes (Thompson, Rubin, & Rubin, 2012). Importantly, both VSCC subtypes are involved in load-induced bone formation, which links them to a role in skeletal mechanobiology (J. Li, Duncan, Burr, & Turner, 2002; Srinivasan et al., 2015). Since VSCCs are not intrinsically mechanosensitive, they are postulated to be coupled to the mechanical stimulus through force-induced membrane depolarizations mediated by some mechanosensitive channel.

1.4.4 Cellular mechanoresponse

Following mechanical stimulation, there is a temporal cascade of signaling events that ultimately manifests in cell- and tissue-level adaptations. In bone, mechanical stimulation can influence cellular proliferation, survival and differentiation, as well as matrix deposition, mineralization and resorption. This carefully orchestrated sequence of events is both temporally and spatially organized, requiring the collective cooperation of residing bone cells to execute the mechanotransductive signaling cascade. There are various ways to classify and conceptualize the events that proceed following mechanical stimulation. I will keep to a hierarchical organization, focusing first on the signaling events that are detectable within seconds to minutes to hours, and then on the cellular effects that manifest hours and days after.

1.4.4.1 Signalling Cascades

Within seconds of experiencing a mechanical load, the cellular microenvironment is disrupted, fluid shears and substrate strains distort the extracellular matrix, integrin/FA complexes are prompted to respond, forces transmitted through FAs initiate cytoskeletal reorganizations, and mechanosensitive channels are activated as the membrane yields to applied forces. Just as quickly, the cell integrates all these cues and initiates a multifaceted mechanotransductive signalling cascade.

Calcium signalling. Intracellular calcium is a universal secondary messenger that encodes context-dependent information. Following mechanical stimulation of bone cells, transient intracellular free calcium ($[Ca^{2+}]_i$) elevations are among the earliest detectable events (N. X. Chen et al., 2000; Hung, Pollack, Reilly, & Brighton, 1995; Alexander G. Robling & Charles H. Turner, 2009). Mechanical stimuli can directly stimulate $[Ca^{2+}]_i$ influx from the extracellular space and release from intracellular endoplasmic reticulum (ER) stores through various mechanosensitive channels (e.g., L-VSCC) and integrin clustering (S Hughes, Dobson, & Haj, 2003; Pommerenke et al., 1996). $[Ca^{2+}]_i$ signals can also occur indirectly with the help of neighbouring cells through paracrine signals (e.g., ATP) or cell-to-cell coupling (e.g., GAP junctions). In osteoblasts, the mode of intercellular $[Ca^{2+}]_i$ propagation has been suggested to depend on differentiation state, such that early-stage osteoblasts propagate $[Ca^{2+}]_i$ signals to neighbouring cells via ATP, while mature osteoblasts shift to a direct mode of transmission via GAP junctions (Henriksen, Hiken, Steinberg, & Jorgensen, 2006).

$[Ca^{2+}]_i$ signals can vary in amplitude and duration, and can exhibit oscillatory dynamics which have been postulated to encode relevant information. While it remains less clear how this information is encoded, several mechanisms of have been proposed, including amplitude and frequency modulation (De Pitta, Volman, Levine, & Ben-Jacob, 2009), changes in spike time variations (Thurley et al., 2014) and signal integration (Hannanta-anan & Chow, 2016). In osteoclasts, calcium oscillations are a hallmark feature involved in NFAT upregulation during differentiation (Florencio-Silva et al., 2015; Hwang & Putney, 2011; Tiedemann et al., 2013; Tiedemann et al., 2009). NFAT has been proposed as a signal integrator, maintaining a memory of the cumulative calcium load, rather than discriminating against frequencies (Hannanta-anan & Chow, 2016). In osteoblast, calcium oscillation frequencies have been deemed important in load-

induced cellular adaptation, where they have been shown to desensitize if no recovery between bouts of loading is permitted (Donahue, Donahue, & Jacobs, 2003). In osteocytes, laminar and turbulent fluid shears have also been shown to modulate the frequency and amplitudes of downstream $[Ca^{2+}]_i$ responses (Lu, Huo, Park, & Guo, 2012).

The versatility of calcium as a secondary messenger is illustrated by its numerous down stream effectors including protein kinase A [PKA, (Ryder & Duncan, 2001)], protein kinase C [PKC, (Katz, Boland, & Santillan, 2006)], mitogen-activated protein kinase [MAPK, (Katz et al., 2006)], cFos (Chattopadhyay, Quinn, Kifor, Ye, & Brown, 2007), osteopontin upregulation (J. You et al., 2001), PGE_2 release (Genetos, Geist, Liu, Donahue, & Duncan, 2005), ATP release (Genetos, Kephart, Zhang, Yellowley, & Donahue, 2007) and NO production (McAllister & Frangos, 1999). Thus, calcium elevations are information-saturated signals that occur immediately following mechanical stimulation and are deciphered in context- and effector-dependent manners.

ATP. Following mechanical stimulation, adenosine triphosphate (ATP) release is detected within seconds, on a similar time scale as the calcium response (A. G. Robling & C. H. Turner, 2009). ATP is abundantly present in the cytosol (~1-10 mM) and maintained at low concentration in the extracellular space (~1-10 nM) by ecto-nucleotidases and is a potent extracellular signalling mediator. The mechanotransductive role of ATP is the central focus of this dissertation, so I provide a comprehensive review of ATP and its cognate purinergic (P2) receptors in **Chapter 2**.

GTPases. GTPases are a family of GTP binding and hydrolyzing enzymes which act as physiological "switches". Many receptors, including those that are mechanosensitive, are coupled to heterotrimeric G-protein complex and thus known as G-protein coupled receptors (GPCR). Each G-protein complex consists of an G_α, G_β and G_γ subunit. There are several classes of G_α ($G_{\alpha s}$, $G_{\alpha i/o}$, $G_{\alpha q/11}$, and $G_{\alpha 12/13}$), each with unique downstream effector functions. In their inactivated state, G_α is associated with the $G_{\beta\gamma}$ dimer and guanosine diphosphate (GDP). GPCR activation facilitates a switch-like replacement of GDP with guanosine triphosphate (GTP) through the GPCR-associated guanine nucleotide exchange factor (GEF). This exchange results in the dissociation of G_α from $G_{\beta\gamma}$, thereby initiating downstream signalling that include changes in intracellular calcium, cyclic adenosine monophosphate (cAMP) and cyclic guanosine monophosphate (cGMP) levels (Thompson et al., 2012). Importantly, the intrinsic GTPases domain of G_α gradually converts

bound GTP to GDP, thereby inactivating the G-protein signalling cascade, and permitting re-association of G_{α} with $G_{\beta\gamma}$ in its inactivated state.

Several GPCRs are involved in the mechano-adaptive response in bone cells, including nucleotide-sensitive P2Y receptors, prostaglandin-sensitive EP receptors (Blackwell, Raisz, & Pilbeam, 2010; Y. Sugimoto & Narumiya, 2007) and the parathyroid hormone 1 receptor [PTH1R, (Y. L. Zhang, Frangos, & Chachisvilis, 2009)]. GPCRs were initially thought to be exclusively activated by ligands, however accumulating evidence suggests that certain GPCRs and G-proteins may also be activated directly by mechanical stimuli. Fluid shear was reported to activate PTH1R in MC3T3 osteoblastic cells independent of the receptor ligand interactions (Y. L. Zhang et al., 2009). Another group demonstrated that purified G-protein complexes reconstituted in GPCR-free vesicles were activated by fluid shear (Gudi, Nolan, & Frangos, 1998).

In osteoblasts, loading induces nitric oxide-dependent cGMP synthesis which activates protein kinase G (PKG) and mediates integrin mechano-signalling (Rangaswami et al., 2010). Separately, the activated $G_{\alpha i}$ subunit colocalizes with integrins and the cytoskeleton to modulate calcium signalling. In osteocytes, fluid shear suppresses cAMP production through GTPase-related pathways (Kwon, Temiyasathit, Tummala, Quah, & Jacobs, 2010). Fluid flow also activates phospholipase C (PLC) which promotes IP_3-mediated calcium signalling leading to the activation of COX-2 expression and PGE_2 signalling (Jacobs, Temiyasathit, & Castillo, 2010). Mechanical strains also activate small GTPases like RhoA GTPase. Activated RhoA induces actin cytoskeleton reorganization into stress fibers and promotes focal adhesion formation (Hoon et al., 2016; Thompson et al., 2012). In mesenchymal stem cells, lineage commitment is RhoA-dependent such that sustained RhoA activation favors osteogenic differentiation while RhoA silencing favors the adipogenic lineage (Thompson et al., 2012).

Nitric oxide. Within minutes of mechanical stimulation, nitric oxide (NO) is released into the extracellular space from osteoblasts and osteocytes (M. Mullender et al., 2004). NO is enzymatically produced by nitric oxide synthases (NOS) in an oxidation reaction dependent on NADPH and oxygen. NOS are a family of three enzymes, namely calcium-dependent endothelial NOS (eNOS) and neuronal NOS (nNOS), and calcium-independent inducible NOS (iNOS).

Upregulation of eNOS is necessary for load-induced bone formation (Kleinnulend, Semeins, Ajubi, Nijweide, & Burger, 1995; Pitsillides et al., 1995; Sterck, Klein-Nulend, Lips, & Burger,

1998; C. H. Turner, Y. Takano, I. Owan, & G. Murrell, 1996) and fracture healing (Corbett et al., 1999; Diwan, Wang, Jang, Zhu, & Murrell, 2000). In osteoblasts, low to moderate levels of NO are anabolic, promoting proliferation, osteocalcin synthesis and mineralized matrix formation (Kapur, Baylink, & Lau, 2003; S. J. Wimalawansa, 2010). These anabolic levels NO are generated independent of the type of mechanical stimulus applied (fluid shear or cyclic stretching) to osteoblasts (M. Mullender et al., 2004). However, high concentrations of NO are inhibitory making it difficult to establish a therapeutic window in which NO can be exploited as a treatment for bone loss (S. J. Wimalawansa, 2010). Although there have been few studies examining the role of NO in osteocytes, it has been shown that osteocytes produce more NO than osteoblasts following mechanical stimulation (S. J. Wimalawansa, 2010). In osteoclasts, NO is generated in a calcium-dependent manner and results in the retraction of pseudopodia and inhibition of bone resorption. In bone marrow stromal cells, NO also reduced the RANKL/OPG ratio, resulting in reduced osteoclastogenesis (Rubin, Murphy, Fan, Goldschmidt, & Taylor, 2002). When NO synthesis was inhibited *in vivo*, load-induced bone formation was suppressed (C. H. Turner, Y. Takano, I. Owan, & G. A. Murrell, 1996). NO was proposed to be one of the mediators of sex-hormone related effects in bone. Estrogen is used to reverse bone loss in osteoporosis, however in the present of NO synthesis inhibitors, estrogen is ineffective (S. Wimalawansa, De Marco, Gangula, & Yallampalli, 1996). Although the downstream targets of NO remain unclear, current evidence supports that mechanically-induced levels of NO suppress osteoclastic bone resorption and promote osteoblast proliferation and bone formation.

Prostaglandins. Prostaglandins (PG) are lipid autocrine and paracrine mediators that are produced in response to mechanical stimulation on a similar time scale as NO. Cyclooxygenases 1 and 2 (COX-1 and COX-2) synthesize PGH_2, an intermediary substrate, that is further modified by various isomerases and synthase enzymes to synthesize various prostaglandins including PGD_2, PGE_2, PGI_2 and $PGF_{2\alpha}$ (Ricciotti & FitzGerald, 2011). Thus, the secretory profile of PGs is governed by the differential expression of isomerases and synthase enzymes involved in their synthesis. COX-1 is expressed constitutively while COX-2 is rapidly inducible to high levels by various factors such as mechanical stimulation, parathyroid hormone (PTH) and BMP-2 (Blackwell et al., 2010). COX-2 is encoded by *Ptgs2*, and exhibits characteristic features of an early response gene (Y. J. Kang, Mbonye, DeLong, Wada, & Smith, 2007).

In bone, PGE_2 is considered the predominant PG of interest. The mechanism of PGE_2 release remains unresolved, however connexin hemichannels and the P2X7 receptor have been proposed as possible release conduits (Batra et al., 2012; Goodman, Hornberger, & Robling, 2015; J. Li, Liu, Ke, Duncan, & Turner, 2005; D. Liu et al., 2008). PGE_2 was first discovered to stimulate cAMP and resorption in *ex vivo* bone explants in the 1970s (Klein & Raisz, 1970). PGE_2 is associated with four GPCRs, EP1-4, of which EP2 and EP4 are the key mediating receptors in PGE_2-related mechanostransduction (Blackwell et al., 2010; Y. Sugimoto & Narumiya, 2007). EP2 and EP4 are coupled to $G_{\alpha s}$ subunits, which results in cAMP production upon stimulation and is thought to mediate the anabolic effects of PGE_2 in bone (M. Li, Thompson, & Paralkar, 2007; Yoshida et al., 2002). However, the effects of PGE_2 has been difficult to deconvolute since they vary drastically depending on the type of stimulus, local cellular milieu and effector cells. For example, PGE_2 stimulates resorption and osteoclast differentiation through a mechanism believed to involve stimulation of RANKL production and inhibition of OPG in osteoblastic cells (Bilezikian, Raisz, & Martin, 2008). However, these pro-osteoclastic effects of prostaglandins can also be inhibited by mechanically-induced NO, thereby favoring load-induced formation instead (Ralston & Grabowski, 1996). On the other hand, osteocyte-derived PGE_2 was reported to mediate load-induced bone formation by stimulating the anabolic Wnt/β-catenin pathway (L. Li, Pettit, Gregory, & Forwood, 2006). Thus, it is clear the PGs are involved in the mechanotransductive skeletal response, however whether the effects are anabolic or catabolic depends on many confounding factors (Blackwell et al., 2010).

Growth factors. Mechanical stimulation promotes growth factor secretion and signalling in bone, which can influence bone cell growth and differentiation. Insulin-like growth factor (IGF)-related signalling is critical in skeletal mechanotransduction. Mechanical loading upregulates IGF-1 expression in osteocytes within 6 hours of stimulation (Lean, Jagger, Chambers, & Chow, 1995; Reijnders et al., 2007), while unloading inhibits integrin-mediated IGF-1 signalling (Sakata et al., 2004). *In vivo* overexpression of IGF-1 enhances the osteogenic response to mechanical-loading in mice (Gross, Srinivasan, Liu, Clemens, & Bain, 2002) while conditional knockout of IGF-1 in collagen type-1 expressing cells abolishes the load-induced osteogenic effect (Kesavan, Wergedal, Lau, & Mohan, 2011). IGF-1 has been proposed to mediate its effects through Wnt/β-catenin and prostaglandin signalling pathways (K. H. Lau et al., 2013), however further work is required to fully understand the interactions between these signalling pathways. TGF-β is another growth

factor that is induced by physiological strains, but suppressed by supra-physiological strains, and is involved in Runx2 induction and matrix production and deposition in osteoblasts (Ahdjoudj, Lasmoles, Holy, Zerath, & Marie, 2002; Cillo, Gassner, Koepsel, & Buckley, 2000; Ito & Miyazono, 2003). BMPs are a class of growth factors that are concentrated in the organic matrix in bone and are released from these ECM stores following fracture or during bone resorption. Mechanical stimulation was shown to induce BMP-mediated Runx2 expression and Smad1 phosphorylation (Bikle, 2008; Celil & Campbell, 2005). VEGFs are involved in regulating vascularization during bone development and repair and are upregulated in stretch-stimulated osteoblasts (S. J. Kim, Kim, Kwon, & Kim, 2007; K Sakai, Mohtai, & Iwamoto, 1998).

Wnt/β-catenin. The canonical Wingless-related integration site (Wnt) signalling pathway is influenced by mechanical stimuli, and in turn is a central regulator of osteogenic differentiation. Secreted Wnt binds LRP5 and a 7-transmembrane co-receptor called Frizzled. Activation of this complex results in intracellular β-catenin stabilization, permitted β-catenin to translocate and accumulate in the nucleus where it regulates gene associated with enhanced osteogenesis and reduced resorption (Goodman et al., 2015).

Fluid shear stimulation of MC3T3, UMR-106, ROS 17/2.8 osteoblast cell lines or primary rodent calvarial osteoblasts results in the nuclear translocation of β-catenin (Armstrong et al., 2007; Norvell et al., 2004). Similarly *in vivo*, mechanically loading mice that express a β-catenin reporter results in rapid (<1 h) upregulation of the reporter gene in osteocytes, followed by similar upregulation in surface-residing osteoblasts 20 h later (Kim-Weroha et al., 2008). A loss of function mutation in LRP5 is associated with Osteoporosis-Pseudoglioma (OPPG) Syndrome which is characterized by extreme osteoporosis and susceptibility to skeletal fracture and deformation (Gong et al., 2001). Similarly, $LRP5^{-/-}$ mice exhibit a severe deficit in bone mass, that is more exaggerated in load-bearing regions of the skeleton. Load-induced osteogenesis was severely impaired in these mice (Sawakami et al., 2006). These findings clearly establish the Wnt/β-catenin pathway as a key mediator of mechano-adaptive bone formation.

Sclerostin is the balancing force in the Wnt/β-catenin pathway, potently suppressing Wnt-related signalling. Sclerostin (encoded by *Sost*) is an osteocyte-specific secreted glycoprotein, and when mutated, mice exhibit an increase in bone mass (Balemans et al., 2001). Sclerostin is mechanically-regulated such that loading results in a drastic down-regulation in *Sost*, while tail suspension (i.e.,

model for disuse-related bone loss) results in upregulation of *Sost* (Kim-Weroha et al., 2008; Robling et al., 2008). Consistently, overexpression of *Sost in vivo* suppressed load-induced bone formation (Tu et al., 2012), while *Sost*$^{-/-}$ mice were protected from disuse-related bone loss and showed enhanced bone formation in response to loading (Morse et al., 2014).

Sclerostin has attracted much therapeutic interest. Romosozumab, an anti-Sclerostin monoclonal antibody developed by Amgen and UCB for the treatment of osteoporosis in postmenopausal women, has completed phase III trials (Saag et al., 2017). Compared to the current gold-standard osteoporosis treatment, alendronate, administration of Romosozumab followed by alendronate reduced risk of fraction by 27% (Saag et al., 2017). However, Romosozumab was associated with a higher rate of serious cardiovascular adverse events than alendronate, likely due to the involvement of Sclerostin in the progression of vascular calcification and arterial stiffening (Evenepoel et al., 2015; Zhu, Mackenzie, Millán, Farquharson, & MacRae, 2011). Accordingly, longer-term trials clarifying the cardiovascular effects of Romosozumab have been recommended (McClung, 2018). In another case, the Sclerostin-neutralizing antibody Setrusumab is currently being evaluated by Mereo BioPharma for the treatment of Osteogenesis Imperfecta (OI; brittle bone disease). Phase IIa trials have demonstrated that Setrusumab stimulates bone formation, reduces bone resorption and increases lumbar spine bone mineral density in adults with moderate OI (Glorieux et al., 2017). Thus, Sclerostin is emerging as a promising therapeutic target that may be affected in a variety of bone-loss related conditions.

1.4.4.2 Cellular Response

In the minutes that follow mechanical stimulation, bone cells mount a full scale molecular mechanotransductive response. However, these changes do not materialize at the tissue level until much later. Load-induced adaptations in bone occur over weeks and months, manifesting from locally-induced changes in cell survival/apoptosis, proliferation, differentiation, matrix deposition, mineralization and resorption (**Fig 1-5**). In this section, I will discuss each of these functional modalities and present findings in the context of mechano-adaptive tissue-level behaviors.

Survival/apoptosis. Cell survival and programmed death (apoptosis) are opposing extremes on the same spectrum, both which are carefully regulated by external cues.

In osteoblasts, the anti-apoptotic protein Bcl-2 is elevated upon exposure to fluid shears, thereby serving as a mechanically-stimulated survival signal. Fluid shears have been associated with several other survival cues in osteoblasts including the surface expression of EGF-R (Ogata, 2003), clustering and upregulation of β1 integrins (Carvalho, Scott, & Yen, 1995), release of survival mediators IFG-1 (Cillo et al., 2000) and IGF-II (Cheng et al., 2002) and estrogen receptor stimulation (Cheng et al., 2002). Interestingly, strain-induced osteoblast survival appears to depend on differentiation state. Immature osteoblasts exposed to stretch undergo apoptosis while mature osteoblasts do not (Weyts, Bosmans, Niesing, van Leeuwen, & Weinans, 2003). In cases of unloading, as seen in microgravitational environments, osteoblasts exhibit reduced levels of Bcl-2, relative to pro-apoptotic protein Bax, concurrent with disruption of the mitochondrial membrane potential, which is characteristic of the apoptotic pathway. Thus, unloading of osteoblasts promotes apoptosis while loading promotes survival.

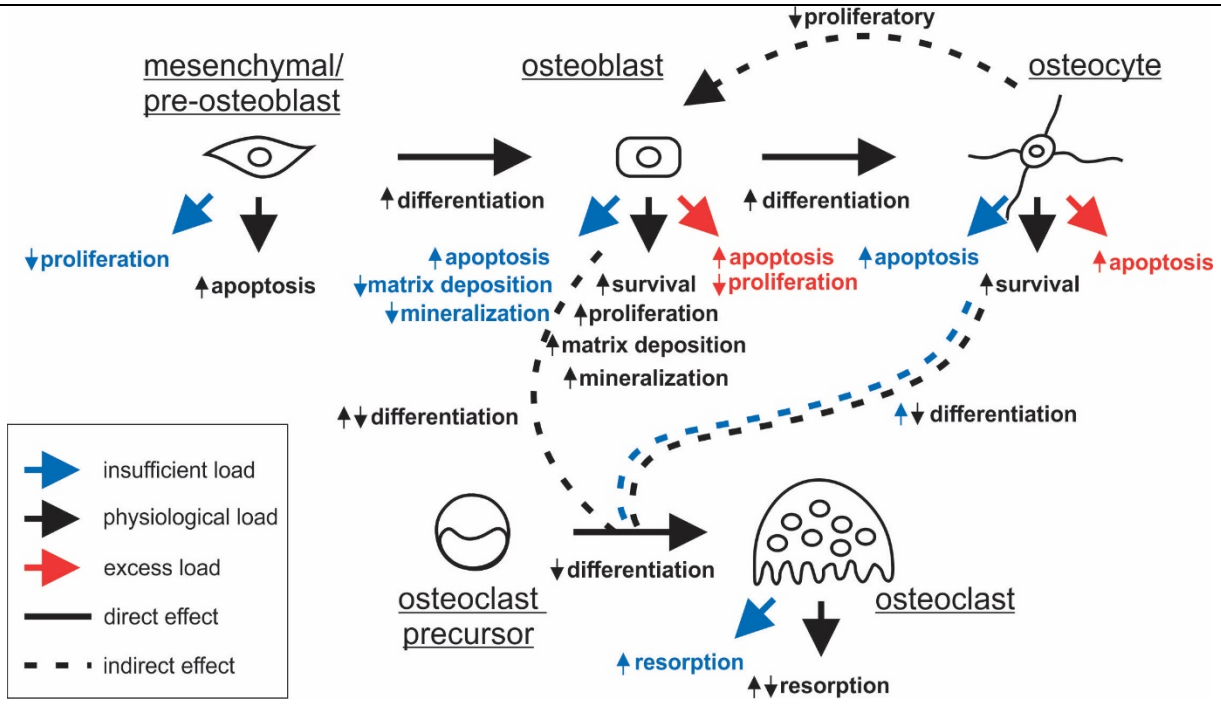

Figure 1-5. Influence of mechanical stimulation on bone cells. Effects of insufficient (*blue arrows*), physiological (*black arrows*) or excess (*red arrows*) loading on osteoblast- (*top row*) and osteoclast- (*bottom row*) lineages are summarized in flow diagram. Direct (*broken lines*) and indirect *(broken lines*, via cell-cell/paracrine interactions) are specified.

In osteocytes, physiological loads promote survival through the integrin-MAPK pathway and estrogen receptor-mediated regulation of ERK (Noble et al., 2003; Simpson et al., 2009). However, sufficiently high mechanical stresses can lead to cell death and apoptosis. Injury-related strains that exceed 10-20% result in osteoblast detachment and disruption of cellular adhesions (Lacouture, Schaffer, & Klickstein, 2002). Excessive loading also leads to osteocyte apoptosis which has been proposed as a mechanism by which osteoclasts are targeted to damaged bone regions for subsequent remodeling (Noble et al., 2003; A. G. Robling & C. H. Turner, 2009). Osteocytes that receive insufficient amount of mechanical stimulation *in situ* undergo apoptosis via a hypoxia-related mechanism (Basso & Heersche, 2006; Gross et al., 2001; Rubin et al., 2002). Thus, it appears that normal gravitational and physiological forces are necessary for the survival of osteoblasts and osteocytes, while injurious or insufficient stimuli lead to their apoptosis and subsequent invasion by osteoclast populations to initiate remodeling processes. Importantly, this relationship is consistent with the U-shaped relationship between mechanical loading and bone remodelling at the tissue level.

Proliferation. In addition to survival, cells need to be sufficiently abundant to carry out their prescribed functions. Osteocytes and osteoclasts are terminally differentiated cells and thus cannot proliferate (Ruijtenberg & van den Heuvel, 2016). Thus, a proliferation phase is essential during the differentiation of osteoblast and osteoclasts and mechanical cues can modulate the extent of this proliferation.

In osteoblasts, mechanical stresses can be either pro- or anti-proliferatory, depending on the magnitude of the stimulus. Physiological mechanical stimuli are generally associated with elevated proliferation. Flow stimulation increases osteoblast proliferation by 50-100% (Bannister et al., 2002; Kapur et al., 2003; Taylor et al., 2007). Similarly, substrate deformations stimulate osteoblast proliferation up until 0.3-1% stretch, however higher strains inhibit proliferation (Neidlinger-Wilke, Wilke, & Claes, 1994). Alternatively, hindlimb unloading in rats was reported to decrease pre-osteoblast proliferation *in vivo*, as assessed by incorporation of BrdU into newly synthesized DNA (Barou, Palle, Vico, Alexandre, & Lafage-Proust, 1998). Several molecular pathways have been implicated in the osteoblast proliferation response including NO (S. J. Wimalawansa, 2010), Wnt/β-catenin (Krishnan, Bryant, & Macdougald, 2006) and integrin/FA complex (Miyamoto et al., 1995) signalling. In particular, NO regulates proliferation in a biphasic

manner, such that low to moderate levels of NO promote proliferation while high levels are inhibitory (S. J. Wimalawansa, 2010). One group demonstrated that conditioned media take from flow-stimulated osteocytes inhibited the proliferation of osteoblasts through a mechanism that was partially dependent on NO (Vezeridis, Semeins, Chen, & Klein-Nulend, 2006). Thus, NO may explain the molecular basis of mechanically-regulated proliferation in osteoblasts, which exhibits the recurring U-shaped relationship between mechanical stimulus and outcome, such that excess or insufficient loads inhibit proliferation while physiological loads promote it.

Differentiation. The process by which cells specialize into mature functional units is known as differentiation. Bone formation and resorption processes require mature osteoblasts and osteoclasts, respectively, and the interactions between osteoblasts and osteoclasts have implications on how differentiation is triggered or enhanced in either lineage.

Mechanically stimulated mesenchymal stem cells exhibit an increase in osteogenic markers, including alkaline phosphatase and osteocalcin (Damaraju, Matyas, Rancourt, & Duncan, 2014; Guo et al., 2015; A. Kadow-Romacker, Hoffmann, Duda, Wildemann, & Schmidmaier, 2009). In contrast, mechanically-stimulated osteoclast precursors formed fewer TRAP-positive (mature osteoclast marker) multinucleated osteoclasts and resorption pits (Guo et al., 2015; A. Kadow-Romacker et al., 2009). Thus, mechanical stimulation promotes osteoblastogenesis and inhibits osteoclastogenesis, consistent with load-induced formation modeling observed at the tissue-level.

Bone cells do no however reside in isolation *in situ*. To probe the interactions between different bone cell types, coculture and conditioned-media studies have been conducted. Conditioned media from flow-stimulated MLO-Y4 osteocytes had reduced RANKL/OPG ratios which inhibited osteoclastogenesis (E. Lau et al., 2010; L. You et al., 2008). In contrast, unloading-induced osteocyte apoptosis promoted osteoclast recruitment and differentiation (Aguirre et al., 2006). Like osteocytes, osteoblasts also regulate osteoclast differentiation through soluble factors, however the effects appear to conflict with those reported for osteocytes. For instance, conditioned media taken from flow-stimulated osteoblasts inhibited osteoclast formation to a lesser extent than osteocyte-derived conditioned media (Tan et al., 2007). Other groups have reported that flow-stimulated osteoblasts can promote osteoclastogenesis. Conditioned media take from flow-stimulated SaOS-2 osteoblast-like cells promoted osteoclastogenesis in an IL-11-depedent manner (K. Sakai et al., 1999). Similarly, osteoclastic TRAP expression, pit formation and collagen degradation was

stimulated in mechanically-stimulated osteoblast and osteoclast precursor cocultures (Y.-J. Chen et al., 2015; Anke Kadow-Romacker, Duda, Bormann, Schmidmaier, & Wildemann, 2013). In comparable mechanically-strained coculture studies, increased levels of RANKL (relative to OPG) were measured (Y.-J. Chen et al., 2015; A. Kadow-Romacker et al., 2009), however this did not translate to elevated osteoclastic activity, but rather appeared to ensure normal levels of osteoclast formation were maintained by counteracting the inhibitor effects of mechanical stimulation on the osteoclast formation (A. Kadow-Romacker et al., 2009). Thus, experiments involving conditioned media from mechanically-stimulated cultures have demonstrated that osteocyte- and osteoblast-derived soluble factors can regulate osteoclast differentiation. Specifically, mechanically-stimulated osteocytes appear to suppress osteoclast formation while mechanically-stimulated osteoblasts or unloaded osteocytes can promote osteoclast formation.

Matrix deposition and mineralization. To form bone, osteoblasts deposit organic matrix which is then mineralized. Substrate strains and fluid shears enhance osteoblast ALP expression (Kapur et al., 2003), osteoid deposition [i.e., collagen, osteocalcin and osteopontin (Scott, Khan, Duronio, & Hart, 2008; J. You et al., 2000)] and matrix mineralization (Bancroft et al., 2002; Mauney et al., 2004). Similarly, compressive loading of mesenchymal stem cells or mature osteoblasts seeded on 3D scaffolds results in matrix deposition and honeycomb-like mineralization (Damaraju et al., 2014; Sittichockechaiwut, Scutt, Ryan, Bonewald, & Reilly, 2009; Vazquez et al., 2014). Consistent with prior functional modalities, microgravity results in decreased ALP, osteocalcin and collagen expression (Carmeliet, Nys, Stockmans, & Bouillon, 1998; Kunisada, Kawai, Inoue, & Namba, 1997), highlighting the necessary role of gravity in maintaining the ECM production by osteoblasts in bone (Scott et al., 2008). Thus, mechanical stimulation of mature osteoblasts promotes mineral deposition and mineralization.

Resorption. Bone remodeling or modeling processes are both stimulated by mechanical loading, leading to a complex mixture of pro- or anti-resorptive signals at the cellular level. It should be noted that the literature has predominantly focused on the mechanical responses of osteoblasts and osteocytes. This is due to the belief that osteoclasts are not mechanosensory cells, but rather regulated by mechanically stimulated signals relayed from the osteoprogenitor lineage (A. G. Robling & C. H. Turner, 2009). Consequently, the osteoclastic response has largely been inferred from factors secreted by osteoblasts and osteocytes. Further evidence informing the role of

mechanical cues in osteoclast function comes from our understanding of tissue-level responses. We know that resorptive activity is highest during periods of elevated remodeling (insufficient or excess loads) or resorptive modelling (insufficient loads or unloading). Consistent with expectations, mechanical unloading resulted in an elevated RANKL/OPG ratio which promoted osteoclast-mediated resorption (David et al., 2003; Martin et al., 2005; Tanaka et al., 2004). However data pertaining to resorption following mechanical stimulation is less consistent due to the absence of Haversian remodeling in rodents (An & Freidman, 1998), as well as heterogeneous *in vitro* loading models and responses (A. G. Robling & C. H. Turner, 2009). Nonetheless, bone cell cultures have been demonstrated to either reduce RANKL (C. H. Kim, You, Yellowley, & Jacobs; Rahnert et al., 2008; Rubin, Murphy, Nanes, & Fan, 2000) or increase RANKL (J. Liu et al., 2009), supporting that mechanical regulation of osteoclast activity converges along the RANKL/OPG signaling axis. Based on tissue level behaviors, we should expect resorption to be maintained at a minimum during normal physiological loading and elevated in response to excess loading.

1.5 Summary

Bone is in a dynamic relationship with its surrounding mechanical environment, adapting to the complex combinations of mechanical forces to maintain strength and integrity, while at the same time sustaining an optimal mass. Mechanical loading is associated with mechano-adaptive bone formation, while mechanical unloading results in bone loss which can lead to an increased risk of fracture. At the cellular level, cell-to-extracellular matrix interactions, cell-to-cell adhesions and force-to-cell transmissions constitute the structural basis by which mechanical forces are perceived and converted to biochemical signals by osteoblast, osteoclasts and osteocytes. Within seconds of mechanical stimulation, $[Ca^{2+}]_i$ elevations and ATP release are detectable, and signaling cascades involving NO, PGE, G-proteins, growth factors, and Wnt/β-catenin are initiated. The functional consequences of these signaling events are cell type- and magnitude-dependent, and regulate bone cell survival, proliferation and differentiation, and matrix deposition and mineralization in osteoblasts, and resorption in osteoclasts.

1.6 References

Addae-Mensah, K. A., & Wikswo, J. P. (2008). Measurement techniques for cellular biomechanics in vitro. *Exp Biol Med, 233*(7), 792-809. doi: 10.3181/0710-MR-278

Aguirre, J. I., Plotkin, L. I., Stewart, S. A., Weinstein, R. S., Parfitt, A. M., Manolagas, S. C., & Bellido, T. (2006). Osteocyte apoptosis is induced by weightlessness in mice and precedes osteoclast recruitment and bone loss. *J Bone Miner Res, 21*(4), 605-615. doi:10.1359/jbmr.060107

Ahdjoudj, S., Lasmoles, F., Holy, X., Zerath, E., & Marie, P. J. (2002). Transforming growth factor beta2 inhibits adipocyte differentiation induced by skeletal unloading in rat bone marrow stroma. *J Bone Miner Res, 17*(4), 668-677. doi:10.1359/jbmr.2002.17.4.668

Alam Shibly, S. U., Ghatak, C., Sayem Karal, M. A., Moniruzzaman, M., & Yamazaki, M. (2016). Experimental Estimation of Membrane Tension Induced by Osmotic Pressure. *Biophys J, 111*(10), 2190-2201. doi:10.1016/j.bpj.2016.09.043

Albuisson, J., Murthy, S. E., Bandell, M., Coste, B., Louis-Dit-Picard, H., Mathur, J., . . . Patapoutian, A. (2013). Dehydrated hereditary stomatocytosis linked to gain-of-function mutations in mechanically activated PIEZO1 ion channels. *Nat Commun, 4*, 1884. doi:10.1038/ncomms2899

An, Y. H., & Freidman, R. J. (1998). *Animal models in orthopaedic research*: CRC Press.

Armstrong, V. J., Muzylak, M., Sunters, A., Zaman, G., Saxon, L. K., Price, J. S., & Lanyon, L. E. (2007). Wnt/beta-catenin signaling is a component of osteoblastic bone cell early responses to load-bearing and requires estrogen receptor alpha. *J Biol Chem, 282*(28), 20715-20727. doi:10.1074/jbc.M703224200

Arnsdorf, E. J., Tummala, P., & Jacobs, C. R. (2009). Non-Canonical Wnt Signaling and N-Cadherin Related β-Catenin Signaling Play a Role in Mechanically Induced Osteogenic Cell Fate. *PLoS ONE, 4*(4), e5388. doi:10.1371/journal.pone.0005388

Bacabac, R. G., Mizuno, D., Schmidt, C. F., MacKintosh, F. C., Van Loon, J. J., Klein-Nulend, J., & Smit, T. H. (2008). Round versus flat: bone cell morphology, elasticity, and mechanosensing. *J Biomech, 41*(7), 1590-1598. doi:10.1016/j.jbiomech.2008.01.031

Balemans, W., Ebeling, M., Patel, N., Van Hul, E., Olson, P., Dioszegi, M., . . . Van Hul, W. (2001). Increased bone density in sclerosteosis is due to the deficiency of a novel secreted protein (SOST). *Hum Mol Genet, 10*(5), 537-543.

Bancroft, G. N., Sikavitsas, V. I., Van Den Dolder, J., Sheffield, T. L., Ambrose, C. G., Jansen, J. A., & Mikos, A. G. (2002). Fluid flow increases mineralized matrix deposition in 3D perfusion culture of marrow stromal osteoblasts in a dose-dependent manner. *Proc Natl Acad Sci U S A, 99*(20), 12600-12605.

Bang, H., Kim, Y., & Kim, D. (2000). TREK-2, a new member of the mechanosensitive tandem-pore K+ channel family. *J Biol Chem, 275*(23), 17412-17419. doi:10.1074/jbc.M000445200

Bannister, S. R., Lohmann, C. H., Liu, Y., Sylvia, V. L., Cochran, D. L., Dean, D. D., . . . Schwartz, Z. (2002). Shear force modulates osteoblast response to surface roughness. *J Biomed Mater Res, 60*(1), 167-174.

Barou, O., Palle, S., Vico, L., Alexandre, C., & Lafage-Proust, M. H. (1998). Hindlimb unloading in rat decreases preosteoblast proliferation assessed in vivo with BrdU incorporation. *Am J Physiol, 274*(1 Pt 1), E108-114.

Basso, N., & Heersche, J. N. (2006). Effects of hind limb unloading and reloading on nitric oxide synthase expression and apoptosis of osteocytes and chondrocytes. *Bone, 39*(4), 807-814. doi:10.1016/j.bone.2006.04.014

Batra, N., Burra, S., Siller-Jackson, A. J., Gu, S., Xia, X., Weber, G. F., . . . Jiang, J. X. (2012). Mechanical stress-activated integrin alpha5beta1 induces opening of connexin 43 hemichannels. *Proc Natl Acad Sci U S A, 109*(9), 3359-3364. doi:10.1073/pnas.1115967109

Berrier, C., Pozza, A., de Lacroix de Lavalette, A., Chardonnet, S., Mesneau, A., Jaxel, C., . . . Ghazi, A. (2013). The purified mechanosensitive channel TREK-1 is directly sensitive to membrane tension. *J Biol Chem, 288*(38), 27307-27314. doi:10.1074/jbc.M113.478321

Biggs, M. J. P., & Dalby, M. J. (2010). Focal adhesions in osteoneogenesis. *Proceedings of the Institution of Mechanical Engineers. Part H, Journal of engineering in medicine, 224*(12), 1441-1453.

Bikle, D. D. (2008). Integrins, insulin like growth factors, and the skeletal response to load. *Osteoporos Int, 19*(9), 1237-1246. doi:10.1007/s00198-008-0597-z

Bilezikian, J. P., Raisz, L. G., & Martin, T. J. (2008). *Principles of bone biology*: Academic Press.

Blackwell, K. A., Raisz, L. G., & Pilbeam, C. C. (2010). Prostaglandins in Bone: Bad Cop, Good Cop? *Trends in endocrinology and metabolism: TEM, 21*(5), 294-301. doi:10.1016/j.tem.2009.12.004

Brohawn, S. G., Su, Z., & MacKinnon, R. (2014). Mechanosensitivity is mediated directly by the lipid membrane in TRAAK and TREK1 K+ channels. *Proc Natl Acad Sci U S A, 111*(9), 3614-3619. doi:10.1073/pnas.1320768111

Brown, G. N., Leong, P. L., & Guo, X. E. (2016). T-type Voltage-Sensitive Calcium Channels Mediate Mechanically-Induced Intracellular Calcium Oscillations in Osteocytes by Regulating Endoplasmic Reticulum Calcium Dynamics. *Bone, 88*, 56-63. doi:10.1016/j.bone.2016.04.018

Buenzli, P. R., & Sims, N. A. (2015). Quantifying the osteocyte network in the human skeleton. *Bone, 75*, 144-150. doi:10.1016/j.bone.2015.02.016

Burr, D. B., Milgrom, C., Fyhrie, D., Forwood, M., Nyska, M., Finestone, A., . . . Simkin, A. (1996). In vivo measurement of human tibial strains during vigorous activity. *Bone, 18*(5), 405-410.

Cahalan, S. M., Lukacs, V., Ranade, S. S., Chien, S., Bandell, M., & Patapoutian, A. (2015). Piezo1 links mechanical forces to red blood cell volume. *eLife, 4*. doi:10.7554/eLife.07370

Carmeliet, G., Nys, G., Stockmans, I., & Bouillon, R. (1998). Gene expression related to the differentiation of osteoblastic cells is altered by microgravity. *Bone, 22*(5 Suppl), 139s-143s.

Carter, D. R., & Beaupré, G. S. (2007). *Skeletal function and form: mechanobiology of skeletal development, aging, and regeneration*: Cambridge University Press.

Carvalho, R. S., Scott, J. E., & Yen, E. H. (1995). The effects of mechanical stimulation on the distribution of beta 1 integrin and expression of beta 1-integrin mRNA in TE-85 human osteosarcoma cells. *Arch Oral Biol, 40*(3), 257-264.

Catterall, W. A. (1995). Structure and function of voltage-gated ion channels. *Annu Rev Biochem, 64*, 493-531. doi:10.1146/annurev.bi.64.070195.002425

Celil, A. B., & Campbell, P. G. (2005). BMP-2 and insulin-like growth factor-I mediate Osterix (Osx) expression in human mesenchymal stem cells via the MAPK and protein kinase D signaling pathways. *J Biol Chem, 280*(36), 31353-31359. doi:10.1074/jbc.M503845200

Chattopadhyay, N., Quinn, S. J., Kifor, O., Ye, C., & Brown, E. M. (2007). The calcium-sensing receptor (CaR) is involved in strontium ranelate-induced osteoblast proliferation. *Biochem Pharmacol, 74*(3), 438-447. doi:10.1016/j.bcp.2007.04.020

Chen, N. X., Ryder, K. D., Pavalko, F. M., Turner, C. H., Burr, D. B., Qiu, J., & Duncan, R. L. (2000). Ca(2+) regulates fluid shear-induced cytoskeletal reorganization and gene expression in osteoblasts. *Am J Physiol Cell Physiol, 278*(5), C989-997.

Chen, X., Macica, C. M., Ng, K. W., & Broadus, A. E. (2005). Stretch-induced PTH-related protein gene expression in osteoblasts. *J Bone Miner Res, 20*(8), 1454-1461. doi:10.1359/jbmr.050325

Chen, Y.-J., Shie, M.-Y., Hung, C., Jr., Liu, S.-L., Huang, T.-H., & Kao, C.-T. (2015). Osteoblasts subjected to tensile force induce osteoclastic differentiation of murine macrophages in a coculture system. *Journal of Dental Sciences, 10*(1), 81-87. doi:https://doi.org/10.1016/j.jds.2013.11.003

Cheng, M. Z., Rawlinson, S. C., Pitsillides, A. A., Zaman, G., Mohan, S., Baylink, D. J., & Lanyon, L. E. (2002). Human osteoblasts' proliferative responses to strain and 17beta-estradiol are mediated by the estrogen receptor and the receptor for insulin-like growth factor I. *J Bone Miner Res, 17*(4), 593-602. doi:10.1359/jbmr.2002.17.4.593

Christensen, A. P., & Corey, D. P. (2007). TRP channels in mechanosensation: direct or indirect activation? *Nat Rev Neurosci, 8*(7), 510-521. doi:10.1038/nrn2149

Cillo, J. E., Jr., Gassner, R., Koepsel, R. R., & Buckley, M. J. (2000). Growth factor and cytokine gene expression in mechanically strained human osteoblast-like cells: implications for distraction osteogenesis. *Oral Surg Oral Med Oral Pathol Oral Radiol Endod, 90*(2), 147-154. doi:10.1067/moe.2000.107531

Civelekoglu-Scholey, G., & Scholey, J. M. (2010). Mitotic force generators and chromosome segregation. *Cell Mol Life Sci, 67*(13), 2231-2250. doi:10.1007/s00018-010-0326-6

Clarke, B. (2008). Normal Bone Anatomy and Physiology. *Clin J Am Soc Nephrol, 3*(Suppl 3), S131-S139. doi:10.2215/CJN.04151206

Corbett, S., Hukkanen, M., Batten, J., McCarthy, I., Polak, J., & Hughes, S. (1999). Nitric oxide in fracture repair: Differential localisation, expression and activity of nitric oxide synthases. *J Bone Joint Surg Br, 81*(3), 531-537.

Coste, B., Houge, G., Murray, M. F., Stitziel, N., Bandell, M., Giovanni, M. A., . . . Patapoutian, A. (2013). Gain-of-function mutations in the mechanically activated ion channel PIEZO2 cause a subtype of Distal Arthrogryposis. *Proc Natl Acad Sci U S A, 110*(12), 4667-4672. doi:10.1073/pnas.1221400110

Coste, B., Mathur, J., Schmidt, M., Earley, T. J., Ranade, S., Petrus, M. J., . . . Patapoutian, A. (2010). Piezo1 and Piezo2 are essential components of distinct mechanically activated cation channels. *Science, 330*(6000), 55-60. doi:10.1126/science.1193270

Coughlin, T. R., & Niebur, G. L. (2012). Fluid shear stress in trabecular bone marrow due to low-magnitude high-frequency vibration. *J Biomech, 45*(13), 2222-2229. doi:10.1016/j.jbiomech.2012.06.020

Coughlin, T. R., Voisin, M., Schaffler, M. B., Niebur, G. L., & McNamara, L. M. (2015). Primary Cilia Exist in a Small Fraction of Cells in Trabecular Bone and Marrow. *Calcified tissue international, 96*(1), 65-72. doi:10.1007/s00223-014-9928-6

Damaraju, S., Matyas, J. R., Rancourt, D. E., & Duncan, N. A. (2014). The Effect of Mechanical Stimulation on Mineralization in Differentiating Osteoblasts in Collagen-I Scaffolds. *Tissue Engineering. Part A, 20*(23-24), 3142-3153. doi:10.1089/ten.tea.2014.0026

David, V., Laroche, N., Boudignon, B., Lafage-Proust, M.-H., Alexandre, C., Ruegsegger, P., & Vico, L. (2003). Noninvasive In Vivo Monitoring of Bone Architecture Alterations in Hindlimb-Unloaded Female Rats Using Novel Three-Dimensional Microcomputed Tomography. *Journal of Bone and Mineral Research, 18*(9), 1622-1631. doi:10.1359/jbmr.2003.18.9.1622

De Pitta, M., Volman, V., Levine, H., & Ben-Jacob, E. (2009). Multimodal encoding in a simplified model of intracellular calcium signaling. *Cognitive processing, 10*(1), 55.

Diwan, A. D., Wang, M. X., Jang, D., Zhu, W., & Murrell, G. A. (2000). Nitric oxide modulates fracture healing. *Journal of Bone and Mineral Research, 15*(2), 342-351.

Donahue, S. W., Donahue, H. J., & Jacobs, C. R. (2003). Osteoblastic cells have refractory periods for fluid-flow-induced intracellular calcium oscillations for short bouts of flow and display multiple low-magnitude oscillations during long-term flow. *J Biomech, 36*(1), 35-43.

Downs, M. E., Nguyen, A. M., Herzog, F. A., Hoey, D. A., & Jacobs, C. R. (2014). An experimental and computational analysis of primary cilia deflection under fluid flow. *Comput Methods Biomech Biomed Engin, 17*(1), 2-10. doi:10.1080/10255842.2011.653784

Duque, D., Li, X.-j., Katsov, K., & Schick, M. (2002). Molecular theory of hydrophobic mismatch between lipids and peptides. *The Journal of chemical physics, 116*(23), 10478-10484.

Egbuniwe, O., Grover, S., Duggal, A. K., Mavroudis, A., Yazdi, M., Renton, T., . . . Grant, A. D. (2014). TRPA1 and TRPV4 Activation in Human Odontoblasts Stimulates ATP Release. *Journal of Dental Research, 93*(9), 911-917. doi:10.1177/0022034514544507

Evenepoel, P., Goffin, E., Meijers, B., Kanaan, N., Bammens, B., Coche, E., . . . Jadoul, M. (2015). Sclerostin Serum Levels and Vascular Calcification Progression in Prevalent Renal Transplant Recipients. *The Journal of Clinical Endocrinology & Metabolism, 100*(12), 4669-4676. doi:10.1210/jc.2015-3056

Eyckmans, J., Boudou, T., Yu, X., & Chen, C. S. (2011). A hitchhiker's guide to mechanobiology. *Dev Cell, 21*(1), 35-47. doi:10.1016/j.devcel.2011.06.015

Eyckmans, J., Boudou, T., Yu, X., & Chen, C. S. (2011). A Hitchhiker's Guide to Mechanobiology. *Developmental cell, 21*(1), 35-47. doi:10.1016/j.devcel.2011.06.015

Fakhry, M., Hamade, E., Badran, B., Buchet, R., & Magne, D. (2013). Molecular mechanisms of mesenchymal stem cell differentiation towards osteoblasts. *World journal of stem cells, 5*(4), 136.

Fink, M., Duprat, F., Lesage, F., Reyes, R., Romey, G., Heurteaux, C., & Lazdunski, M. (1996). Cloning, functional expression and brain localization of a novel unconventional outward rectifier K+ channel. *Embo j, 15*(24), 6854-6862.

Fink, M., Lesage, F., Duprat, F., Heurteaux, C., Reyes, R., Fosset, M., & Lazdunski, M. (1998). A neuronal two P domain K+ channel stimulated by arachidonic acid and polyunsaturated fatty acids. *Embo j, 17*(12), 3297-3308. doi:10.1093/emboj/17.12.3297

Florencio-Silva, R., Sasso, G. R., Sasso-Cerri, E., Simões, M. J., & Cerri, P. S. (2015). Biology of Bone Tissue: Structure, Function, and Factors That Influence Bone Cells. *Biomed Res Int, 2015*.

Fritton, S. P., McLeod, K. J., & Rubin, C. T. (2000). Quantifying the strain history of bone: spatial uniformity and self-similarity of low-magnitude strains. *J Biomech, 33*(3), 317-325.

Frost, H. M. (1983). A determinant of bone architecture. The minimum effective strain. *Clin Orthop Relat Res*(175), 286-292.

Gardel, M. Force Transmission in the Actin Cytoskeleton. *Biophysical Journal, 102*(3), 407a. doi:10.1016/j.bpj.2011.11.2222

Genetos, D. C., Geist, D. J., Liu, D., Donahue, H. J., & Duncan, R. L. (2005). Fluid shear-induced ATP secretion mediates prostaglandin release in MC3T3-E1 osteoblasts. *J Bone Miner Res, 20*(1), 41-49. doi:10.1359/jbmr.041009

Genetos, D. C., Kephart, C. J., Zhang, Y., Yellowley, C. E., & Donahue, H. J. (2007). Oscillating fluid flow activation of gap junction hemichannels induces ATP release from MLO-Y4 osteocytes. *J Cell Physiol, 212*(1), 207-214. doi:10.1002/jcp.21021

Glorieux, F. H., Devogelaer, J. P., Durigova, M., Goemaere, S., Hemsley, S., Jakob, F., . . . Winkle, P. J. (2017). BPS804 Anti-Sclerostin Antibody in Adults With Moderate Osteogenesis Imperfecta: Results of a Randomized Phase 2a Trial. *J Bone Miner Res, 32*(7), 1496-1504. doi:10.1002/jbmr.3143

Gong, Y., Slee, R. B., Fukai, N., Rawadi, G., Roman-Roman, S., Reginato, A. M., . . . Warman, M. L. (2001). LDL receptor-related protein 5 (LRP5) affects bone accrual and eye development. *Cell, 107*(4), 513-523.

Goodman, C. A., Hornberger, T. A., & Robling, A. G. (2015). Bone and Skeletal Muscle: Key Players in Mechanotransduction and Potential Overlapping Mechanisms. *Bone, 80*, 24-36. doi:10.1016/j.bone.2015.04.014

Gross, T. S., Akeno, N., Clemens, T. L., Komarova, S., Srinivasan, S., Weimer, D. A., & Mayorov, S. (2001). Selected Contribution: Osteocytes upregulate HIF-1alpha in response to acute disuse and oxygen deprivation. *J Appl Physiol (1985), 90*(6), 2514-2519. doi:10.1152/jappl.2001.90.6.2514

Gross, T. S., Srinivasan, S., Liu, C. C., Clemens, T. L., & Bain, S. D. (2002). Noninvasive loading of the murine tibia: an in vivo model for the study of mechanotransduction. *J Bone Miner Res, 17*(3), 493-501. doi:10.1359/jbmr.2002.17.3.493

Grzesik, W. J., & Robey, P. G. (1994). Bone matrix RGD glycoproteins: immunolocalization and interaction with human primary osteoblastic bone cells in vitro. *J Bone Miner Res, 9*(4), 487-496. doi:10.1002/jbmr.5650090408

Gudi, S., Nolan, J. P., & Frangos, J. A. (1998). Modulation of GTPase activity of G proteins by fluid shear stress and phospholipid composition. *Proc Natl Acad Sci U S A, 95*(5), 2515-2519.

Guo, Y., Wang, Y., Liu, Y., Wang, H., Guo, C., Zhang, X., & Bei, C. (2015). Effect of the same mechanical loading on osteogenesis and osteoclastogenesis in vitro. *Chinese Journal of Traumatology, 18*(3), 150-156. doi:https://doi.org/10.1016/j.cjtee.2014.09.004

Guzelsu, N., & Walsh, W. R. (1990). Streaming potential of intact wet bone. *Journal of biomechanics, 23*(7), 673-685. doi:https://doi.org/10.1016/0021-9290(90)90167-2

Han, Y., Jin, Y.-H., Yum, J., Jeong, H.-M., Choi, J.-K., Yeo, C.-Y., & Lee, K.-Y. (2011). Protein kinase A phosphorylates and regulates the osteogenic activity of Dlx5. *Biochem Biophys Res Commun, 407*(3), 461-465. doi:https://doi.org/10.1016/j.bbrc.2011.03.034

Hannanta-anan, P., & Chow, B. Y. (2016). Optogenetic control of calcium oscillation waveform defines NFAT as an integrator of calcium load. *Cell Systems, 2*(4), 283-288.

Harris, T. J., & Tepass, U. (2010). Adherens junctions: from molecules to morphogenesis. *Nature reviews Molecular cell biology, 11*(7), 502.

Haswell, E. S., Phillips, R., & Rees, D. C. (2011). Mechanosensitive channels: what can they do and how do they do it? *Structure (London, England : 1993), 19*(10), 1356-1369. doi:10.1016/j.str.2011.09.005

Hemmersbach, R., von der Wiesche, M., & Seibt, D. (2006). Ground-based experimental platforms in gravitational biology and human physiology. *SITA Signal Transduction, 6*(6), 381-387.

Henriksen, Z., Hiken, J. F., Steinberg, T. H., & Jorgensen, N. R. (2006). The predominant mechanism of intercellular calcium wave propagation changes during long-term culture of human osteoblast-like cells. *Cell Calcium, 39*(5), 435-444. doi:10.1016/j.ceca.2006.01.012

Herranz, R., Anken, R., Boonstra, J., Braun, M., Christianen, P. C. M., de Geest, M., . . . Hemmersbach, R. (2013). Ground-Based Facilities for Simulation of Microgravity: Organism-Specific Recommendations for Their Use, and Recommended Terminology. *Astrobiology, 13*(1), 1-17. doi:10.1089/ast.2012.0876

Holle, A. W., Young, J. L., Van Vliet, K. J., Kamm, R. D., Discher, D., Janmey, P., . . . Saif, T. (2018). Cell-Extracellular Matrix Mechanobiology: Forceful Tools and Emerging Needs for Basic and Translational Research. *Nano Lett, 18*(1), 1-8. doi:10.1021/acs.nanolett.7b04982

Hoon, J. L., Tan, M. H., & Koh, C.-G. (2016). The Regulation of Cellular Responses to Mechanical Cues by Rho GTPases. *Cells, 5*(2), 17. doi:10.3390/cells5020017

Hughes, S., Dobson, J., & Haj, A. E. (2003). Mechanical stimulation of calcium signaling pathways in human bone cells using ferromagnetic micro-particles: implications for tissue engineering. *Eur Cell Mater, 6*, 43.

Hughes, S., Magnay, J., Foreman, M., Publicover, S. J., Dobson, J. P., & El Haj, A. J. (2006). Expression of the mechanosensitive 2PK+ channel TREK-1 in human osteoblasts. *Journal of cellular physiology, 206*(3), 738-748. doi:10.1002/jcp.20536

Hung, C. T., Pollack, S. R., Reilly, T. M., & Brighton, C. T. (1995). Real-time calcium response of cultured bone cells to fluid flow. *Clin Orthop Relat Res*(313), 256-269.

Hwang, S.-Y., & Putney, J. W. (2011). Calcium signaling in osteoclasts. *Biochimica et Biophysica Acta (BBA) - Molecular Cell Research, 1813*(5), 979-983. doi:https://doi.org/10.1016/j.bbamcr.2010.11.002

Ingber, D. (2003). Mechanobiology and diseases of mechanotransduction. *Annals of medicine, 35*(8), 564-577.

Ito, Y., & Miyazono, K. (2003). RUNX transcription factors as key targets of TGF-beta superfamily signaling. *Curr Opin Genet Dev, 13*(1), 43-47.

Jacobs, C. R., Temiyasathit, S., & Castillo, A. B. (2010). Osteocyte mechanobiology and pericellular mechanics. *Annu Rev Biomed Eng, 12*, 369-400. doi:10.1146/annurev-bioeng-070909-105302

Jo, H., & Shin, J. H. (2015). Special issue on mechanobiology and diseases. *Biomedical Engineering Letters, 5*(3), 159-161. doi:10.1007/s13534-015-0203-1

Kadow-Romacker, A., Duda, G. N., Bormann, N., Schmidmaier, G., & Wildemann, B. (2013). Slight Changes in the Mechanical Stimulation Affects Osteoblast- and Osteoclast-Like Cells in Co-Culture. *Transfusion Medicine and Hemotherapy, 40*(6), 441-447. doi:10.1159/000356284

Kadow-Romacker, A., Hoffmann, J. E., Duda, G., Wildemann, B., & Schmidmaier, G. (2009). Effect of Mechanical Stimulation on Osteoblast- and Osteoclast-Like Cells in vitro. *Cells Tissues Organs, 190*(2), 61-68.

Kang, S. S., Shin, S. H., Auh, C.-K., & Chun, J. (2012). Human skeletal dysplasia caused by a constitutive activated transient receptor potential vanilloid 4 (TRPV4) cation channel mutation. *Experimental & Molecular Medicine, 44*(12), 707-722. doi:10.3858/emm.2012.44.12.080

Kang, Y. J., Mbonye, U. R., DeLong, C. J., Wada, M., & Smith, W. L. (2007). Regulation of intracellular cyclooxygenase levels by gene transcription and protein degradation. *Prog Lipid Res, 46*(2), 108-125. doi:10.1016/j.plipres.2007.01.001

Kapur, S., Baylink, D. J., & Lau, K. H. (2003). Fluid flow shear stress stimulates human osteoblast proliferation and differentiation through multiple interacting and competing signal transduction pathways. *Bone, 32*(3), 241-251.

Katz, S., Boland, R., & Santillan, G. (2006). Modulation of ERK 1/2 and p38 MAPK signaling pathways by ATP in osteoblasts: involvement of mechanical stress-activated calcium influx, PKC and Src activation. *Int J Biochem Cell Biol, 38*(12), 2082-2091. doi:10.1016/j.biocel.2006.05.018

Kesavan, C., Wergedal, J. E., Lau, K. H., & Mohan, S. (2011). Conditional disruption of IGF-I gene in type 1alpha collagen-expressing cells shows an essential role of IGF-I in skeletal anabolic response to loading. *Am J Physiol Endocrinol Metab, 301*(6), E1191-1197. doi:10.1152/ajpendo.00440.2011

Kim-Weroha, N. A., Ferris, A., Holladay, B., Kotha, S. P., Kamel, M., & Johnson, M. (2008). *In vivo load activated propagation of b-catenin signaling in osteocytes through coordinated downregulation of inhibitors of Lrp5*.

Kim, C. H., You, L., Yellowley, C. E., & Jacobs, C. R. Oscillatory fluid flow-induced shear stress decreases osteoclastogenesis through RANKL and OPG signaling. *Bone, 39*(5), 1043-1047. doi:10.1016/j.bone.2006.05.017

Kim, S. J., Kim, S. Y., Kwon, C. H., & Kim, Y. K. (2007). Differential effect of FGF and PDGF on cell proliferation and migration in osteoblastic cells. *Growth Factors, 25*(2), 77-86. doi:10.1080/08977190701398977

Klein, D. C., & Raisz, L. G. (1970). Prostaglandins: stimulation of bone resorption in tissue culture. *Endocrinology, 86*(6), 1436-1440. doi:10.1210/endo-86-6-1436

Kleinnulend, J., Semeins, C., Ajubi, N., Nijweide, P., & Burger, E. (1995). Pulsating fluid flow increases nitric oxide (NO) synthesis by osteocytes but not periosteal fibroblasts-correlation with prostaglandin upregulation. *Biochem Biophys Res Commun, 217*(2), 640-648.

Knowles, J. W., & Maeda, N. (2000). Genetic modifiers of atherosclerosis in mice. *Arterioscler Thromb Vasc Biol, 20*(11), 2336-2345.

Kohrt, W. M., Barry, D. W., & Schwartz, R. S. (2009). Muscle Forces or Gravity: What Predominates Mechanical Loading on Bone? *Med Sci Sports Exerc, 41*(11), 2050-2055. doi:10.1249/MSS.0b013e3181a8c717

Krammer, A., Lu, H., Isralewitz, B., Schulten, K., & Vogel, V. (1999). Forced unfolding of the fibronectin type III module reveals a tensile molecular recognition switch. *Proc Natl Acad Sci U S A, 96*(4), 1351-1356.

Krishnan, V., Bryant, H. U., & Macdougald, O. A. (2006). Regulation of bone mass by Wnt signaling. *J Clin Invest, 116*(5), 1202-1209. doi:10.1172/jci28551

Kunisada, T., Kawai, A., Inoue, H., & Namba, M. (1997). Effects of simulated microgravity on human osteoblast-like cells in culture. *Acta Med Okayama, 51*(3), 135-140. doi:10.18926/amo/30798

Kwan, K. Y., Glazer, J. M., Corey, D. P., Rice, F. L., & Stucky, C. L. (2009). TRPA1 modulates mechanotransduction in cutaneous sensory neurons. *J Neurosci, 29*(15), 4808-4819. doi:10.1523/jneurosci.5380-08.2009

Kwon, R. Y., Temiyasathit, S., Tummala, P., Quah, C. C., & Jacobs, C. R. (2010). Primary cilium-dependent mechanosensing is mediated by adenylyl cyclase 6 and cyclic AMP in bone cells. *Faseb J, 24*(8), 2859-2868. doi:10.1096/fj.09-148007

Lacouture, M. E., Schaffer, J. L., & Klickstein, L. B. (2002). A comparison of type I collagen, fibronectin, and vitronectin in supporting adhesion of mechanically strained osteoblasts. *J Bone Miner Res, 17*(3), 481-492. doi:10.1359/jbmr.2002.17.3.481

Lau, E., Al-Dujaili, S., Guenther, A., Liu, D., Wang, L., & You, L. (2010). Effect of low-magnitude, high-frequency vibration on osteocytes in the regulation of osteoclasts. *Bone, 46*(6), 1508-1515. doi:10.1016/j.bone.2010.02.031

Lau, K. H., Baylink, D. J., Zhou, X. D., Rodriguez, D., Bonewald, L. F., Li, Z., . . . Sheng, M. H. (2013). Osteocyte-derived insulin-like growth factor I is essential for determining bone mechanosensitivity. *Am J Physiol Endocrinol Metab, 305*(2), E271-281. doi:10.1152/ajpendo.00092.2013

Lean, J. M., Jagger, C. J., Chambers, T. J., & Chow, J. W. (1995). Increased insulin-like growth factor I mRNA expression in rat osteocytes in response to mechanical stimulation. *Am J Physiol, 268*(2 Pt 1), E318-327. doi:10.1152/ajpendo.1995.268.2.E318

Leblanc, A. D., Schneider, V. S., Evans, H. J., Engelbretson, D. A., & Krebs, J. M. (1990). Bone mineral loss and recovery after 17 weeks of bed rest. *J Bone Miner Res, 5*(8), 843-850. doi:10.1002/jbmr.5650050807

Leddy, H. A., McNulty, A. L., Guilak, F., & Liedtke, W. (2014). Unraveling the mechanism by which TRPV4 mutations cause skeletal dysplasias. *Rare Diseases, 2*(1), e962971. doi:10.4161/2167549X.2014.962971

Lee, M.-H., Kwon, T.-G., Park, H.-S., Wozney, J. M., & Ryoo, H.-M. (2003). BMP-2-induced Osterix expression is mediated by Dlx5 but is independent of Runx2. *Biochem Biophys Res Commun, 309*(3), 689-694. doi:https://doi.org/10.1016/j.bbrc.2003.08.058

Lesage, F., Terrenoire, C., Romey, G., & Lazdunski, M. (2000). Human TREK2, a 2P domain mechano-sensitive K+ channel with multiple regulations by polyunsaturated fatty acids, lysophospholipids, and Gs, Gi, and Gq protein-coupled receptors. *J Biol Chem, 275*(37), 28398-28405. doi:10.1074/jbc.M002822200

Li, J., Duncan, R. L., Burr, D. B., & Turner, C. H. (2002). L-type calcium channels mediate mechanically induced bone formation in vivo. *J Bone Miner Res, 17*(10), 1795-1800. doi:10.1359/jbmr.2002.17.10.1795

Li, J., Liu, D., Ke, H. Z., Duncan, R. L., & Turner, C. H. (2005). The P2X7 nucleotide receptor mediates skeletal mechanotransduction. *J Biol Chem, 280*(52), 42952-42959. doi:10.1074/jbc.M506415200

Li, L., Pettit, A. R., Gregory, L. S., & Forwood, M. R. (2006). Regulation of bone biology by prostaglandin endoperoxide H synthases (PGHS): a rose by any other name. *Cytokine Growth Factor Rev, 17*(3), 203-216. doi:10.1016/j.cytogfr.2006.01.005

Li, M., Thompson, D. D., & Paralkar, V. M. (2007). Prostaglandin E(2) receptors in bone formation. *Int Orthop, 31*(6), 767-772. doi:10.1007/s00264-007-0406-x

Liu, D., Genetos, D. C., Shao, Y., Geist, D. J., Li, J., Ke, H. Z., . . . Duncan, R. L. (2008). ACTIVATION OF EXTRACELLULAR-SIGNAL REGULATED KINASE (ERK1/2) BY FLUID SHEAR IS CA(2+)- AND ATP-DEPENDENT IN MC3T3-E1 OSTEOBLASTS. *Bone, 42*(4), 644-652. doi:10.1016/j.bone.2007.09.058

Liu, J., Zhao, Z., Zou, L., Li, J., Wang, F., Li, X., . . . Wang, J. (2009). Pressure-loaded MSCs during early osteodifferentiation promote osteoclastogenesis by increase of RANKL/OPG ratio. *Ann Biomed Eng, 37*(4), 794-802. doi:10.1007/s10439-009-9638-9

Liu, Z., Tan, J. L., Cohen, D. M., Yang, M. T., Sniadecki, N. J., Ruiz, S. A., . . . Chen, C. S. (2010). Mechanical tugging force regulates the size of cell-cell junctions. *Proc Natl Acad Sci U S A, 107*(22), 9944-9949. doi:10.1073/pnas.0914547107

Lu, X. L., Huo, B., Park, M., & Guo, X. E. (2012). Calcium Response in Osteocytic Networks under Steady and Oscillatory Fluid Flow. *Bone, 51*(3), 466-473. doi:10.1016/j.bone.2012.05.021

Lynch, M., & Fischbach, C. (2014). Biomechanical forces in the skeleton and their relevance to bone metastasis: biology and engineering considerations. *Advanced drug delivery reviews, 0*, 119-134. doi:10.1016/j.addr.2014.08.009

Malicki, J., & Avidor-Reiss, T. (2014). From the cytoplasm into the cilium: bon voyage. *Organogenesis, 10*(1), 138-157. doi:10.4161/org.29055

Manolagas, S. C. (2000). Birth and death of bone cells: basic regulatory mechanisms and implications for the pathogenesis and treatment of osteoporosis. *Endocr Rev, 21*(2), 115-137. doi:10.1210/edrv.21.2.0395

Martin, A., de Vittoris, R. l., David, V., Moraes, R., Bégeot, M., Lafage-Proust, M.-H. l. n., . . . Thomas, T. (2005). Leptin Modulates both Resorption and Formation while Preventing Disuse-Induced Bone Loss in Tail-Suspended Female Rats. *Endocrinology, 146*(8), 3652-3659. doi:10.1210/en.2004-1509

Mauney, J. R., Sjostorm, S., Blumberg, J., Horan, R., O'Leary, J. P., Vunjak-Novakovic, G., . . . Kaplan, D. L. (2004). Mechanical stimulation promotes osteogenic differentiation of human bone marrow stromal cells on 3-D partially demineralized bone scaffolds in vitro. *Calcif Tissue Int, 74*(5), 458-468. doi:10.1007/s00223-003-0104-7

Mc Garrigle, M. J., Mullen, C. A., Haugh, M. G., Voisin, M. C., & McNamara, L. M. (2016). Osteocyte differentiation and the formation of an interconnected cellular network in vitro. *Eur Cell Mater, 31*, 323-340.

McAllister, T. N., & Frangos, J. A. (1999). Steady and transient fluid shear stress stimulate NO release in osteoblasts through distinct biochemical pathways. *J Bone Miner Res, 14*(6), 930-936. doi:10.1359/jbmr.1999.14.6.930

McClung, M. R. (2018). Romosozumab for the treatment of osteoporosis. *Osteoporosis and Sarcopenia, 4*(1), 11-15. doi:https://doi.org/10.1016/j.afos.2018.03.002

Miyamoto, S., Teramoto, H., Coso, O., Gutkind, J., Burbelo, P., Akiyama, S., & Yamada, K. (1995). Integrin function: molecular hierarchies of cytoskeletal and signaling molecules. *J Cell Biol, 131*(3), 791-805.

Mizoguchi, F., Mizuno, A., Hayata, T., Nakashima, K., Heller, S., Ushida, T., . . . Noda, M. (2008). Transient receptor potential vanilloid 4 deficiency suppresses unloading-induced bone loss. *J Cell Physiol, 216*(1), 47-53. doi:10.1002/jcp.21374

Mori, S., & Burr, D. B. (1993). Increased intracortical remodeling following fatigue damage. *Bone, 14*(2), 103-109.

Morse, A., McDonald, M. M., Kelly, N. H., Melville, K. M., Schindeler, A., Kramer, I., . . . Little, D. G. (2014). Mechanical load increases in bone formation via a sclerostin-independent pathway. *J Bone Miner Res, 29*(11), 2456-2467. doi:10.1002/jbmr.2278

Mullender, M., El Haj, A. J., Yang, Y., van Duin, M. A., Burger, E. H., & Klein-Nulend, J. (2004). Mechanotransduction of bone cells in vitro: mechanobiology of bone tissue. *Med Biol Eng Comput, 42*(1), 14-21.

Mullender, M. G., & Huiskes, R. (1995). Proposal for the regulatory mechanism of Wolff's law. *J Orthop Res, 13*(4), 503-512. doi:10.1002/jor.1100130405

Nauli, S. M., Alenghat, F. J., Luo, Y., Williams, E., Vassilev, P., Li, X., . . . Zhou, J. (2003). Polycystins 1 and 2 mediate mechanosensation in the primary cilium of kidney cells. *Nat Genet, 33*(2), 129-137. doi:10.1038/ng1076

Neidlinger-Wilke, C., Wilke, H. J., & Claes, L. (1994). Cyclic stretching of human osteoblasts affects proliferation and metabolism: a new experimental method and its application. *J Orthop Res, 12*(1), 70-78. doi:10.1002/jor.1100120109

Nelson, C. M., Jean, R. P., Tan, J. L., Liu, W. F., Sniadecki, N. J., Spector, A. A., & Chen, C. S. (2005). Emergent patterns of growth controlled by multicellular form and mechanics. *Proceedings of the National Academy of Sciences of the United States of America, 102*(33), 11594-11599. doi:10.1073/pnas.0502575102

Nguyen, A. M., & Jacobs, C. R. (2013). Emerging Role of Primary Cilia as Mechanosensors in Osteocytes. *Bone, 54*(2), 196-204. doi:10.1016/j.bone.2012.11.016

Nishio, Y., Dong, Y., Paris, M., O'Keefe, R. J., Schwarz, E. M., & Drissi, H. (2006). Runx2-mediated regulation of the zinc finger Osterix/Sp7 gene. *Gene, 372*, 62-70. doi:https://doi.org/10.1016/j.gene.2005.12.022

Noble, B. S., Peet, N., Stevens, H. Y., Brabbs, A., Mosley, J. R., Reilly, G. C., . . . Lanyon, L. E. (2003). Mechanical loading: biphasic osteocyte survival and targeting of osteoclasts for bone destruction in rat cortical bone. *Am J Physiol Cell Physiol, 284*(4), C934-943. doi:10.1152/ajpcell.00234.2002

Norvell, S. M., Alvarez, M., Bidwell, J. P., & Pavalko, F. M. (2004). Fluid shear stress induces beta-catenin signaling in osteoblasts. *Calcif Tissue Int, 75*(5), 396-404. doi:10.1007/s00223-004-0213-y

Oftadeh, R., Perez-Viloria, M., Villa-Camacho, J. C., Vaziri, A., & Nazarian, A. (2015). Biomechanics and mechanobiology of trabecular bone: a review. *J Biomech Eng, 137*(1). doi:10.1115/1.4029176

Ogata, T. (2003). Increase in epidermal growth factor receptor protein induced in osteoblastic cells after exposure to flow of culture media. *Am J Physiol Cell Physiol, 285*(2), C425-432. doi:10.1152/ajpcell.00505.2002

Overby, D. R., Zhou, E. H., Vargas-Pinto, R., Pedrigi, R. M., Fuchshofer, R., Braakman, S. T., . . . Johnson, M. (2014). Altered mechanobiology of Schlemm's canal endothelial cells in glaucoma. *Proc Natl Acad Sci U S A, 111*(38), 13876-13881. doi:10.1073/pnas.1410602111

Owen, L. M., Adhikari, A. S., Patel, M., Grimmer, P., Leijnse, N., Kim, M. C., . . . Dunn, A. R. (2017). A cytoskeletal clutch mediates cellular force transmission in a soft, three-dimensional extracellular matrix. *Molecular Biology of the Cell, 28*(14), 1959-1974. doi:10.1091/mbc.E17-02-0102

Parsons, J. T., Horwitz, A. R., & Schwartz, M. A. (2010). Cell adhesion: integrating cytoskeletal dynamics and cellular tension. *Nat Rev Mol Cell Biol, 11*(9), 633-643. doi:10.1038/nrm2957

Patel, A., & Honore, E. (2010). Polycystins and renovascular mechanosensory transduction. *Nat Rev Nephrol, 6*(9), 530-538. doi:10.1038/nrneph.2010.97

Perozo, E., Kloda, A., Cortes, D. M., & Martinac, B. (2002). Physical principles underlying the transduction of bilayer deformation forces during mechanosensitive channel gating. *Nat Struct Biol, 9*(9), 696-703. doi:10.1038/nsb827

Pitsillides, A. A., Rawlinson, S., Suswillo, R., Bourrin, S., Zaman, G., & Lanyon, L. (1995). Mechanical strain-induced NO production by bone cells: a possible role in adaptive bone (re) modeling? *The FASEB Journal, 9*(15), 1614-1622.

Pivonka, P. (2018). *Multiscale Mechanobiology of Bone Remodeling and Adaptation*: Springer.

Pommerenke, H., Schreiber, E., Durr, F., Nebe, B., Hahnel, C., Moller, W., & Rychly, J. (1996). Stimulation of integrin receptors using a magnetic drag force device induces an intracellular free calcium response. *Eur J Cell Biol, 70*(2), 157-164.

Praetorius, H. A., & Spring, K. R. (2001). Bending the MDCK cell primary cilium increases intracellular calcium. *J Membr Biol, 184*(1), 71-79.

Quarmby, L. M., & Parker, J. D. (2005). Cilia and the cell cycle? *J Cell Biol, 169*(5), 707-710. doi:10.1083/jcb.200503053

Rahnert, J., Fan, X., Case, N., Murphy, T. C., Grassi, F., Sen, B., & Rubin, J. (2008). The role of nitric oxide in the mechanical repression of RANKL in bone stromal cells. *Bone, 43*(1), 48-54. doi:10.1016/j.bone.2008.03.006

Ralston, S. H., & Grabowski, P. S. (1996). Mechanisms of cytokine induced bone resorption: role of nitric oxide, cyclic guanosine monophosphate, and prostaglandins. *Bone, 19*(1), 29-33.

Ranade, S. S., Syeda, R., & Patapoutian, A. (2015). Mechanically Activated Ion Channels. *Neuron, 87*(6), 1162-1179. doi:10.1016/j.neuron.2015.08.032

Rangaswami, H., Schwappacher, R., Marathe, N., Zhuang, S., Casteel, D. E., Haas, B., . . . Pilz, R. B. (2010). Cyclic GMP and protein kinase G control a Src-containing mechanosome in osteoblasts. *Sci Signal, 3*(153), ra91. doi:10.1126/scisignal.2001423

Reijnders, C. M. A., Bravenboer, N., Holzmann, P. J., Bhoelan, F., Blankenstein, M. A., & Lips, P. (2007). In Vivo Mechanical Loading Modulates Insulin-Like Growth Factor Binding Protein-2 Gene Expression in Rat Osteocytes. *Calcified tissue international, 80*(2), 137-143. doi:10.1007/s00223-006-0077-4

Reilly, D. T., & Burstein, A. H. (1975). The elastic and ultimate properties of compact bone tissue. *J Biomech, 8*(6), 393-405.

Renkawitz, J., & Sixt, M. (2010). Mechanisms of force generation and force transmission during interstitial leukocyte migration. *EMBO Rep, 11*(10), 744-750. doi:10.1038/embor.2010.147

Ricciotti, E., & FitzGerald, G. A. (2011). Prostaglandins and Inflammation. *Arterioscler Thromb Vasc Biol, 31*(5), 986-1000. doi:10.1161/ATVBAHA.110.207449

Robling, A. G., Castillo, A. B., & Turner, C. H. (2006). Biomechanical and molecular regulation of bone remodeling. *Annu Rev Biomed Eng, 8*, 455-498. doi:10.1146/annurev.bioeng.8.061505.095721

Robling, A. G., Niziolek, P. J., Baldridge, L. A., Condon, K. W., Allen, M. R., Alam, I., . . . Turner, C. H. (2008). Mechanical stimulation of bone in vivo reduces osteocyte expression of Sost/sclerostin. *J Biol Chem, 283*(9), 5866-5875. doi:10.1074/jbc.M705092200

Robling, A. G., & Turner, C. H. (2009). Mechanical signaling for bone modeling and remodeling. *Crit Rev Eukaryot Gene Expr, 19*(4), 319-338.

Robling, A. G., & Turner, C. H. (2009). Mechanical Signaling for Bone Modeling and Remodeling. *Crit Rev Eukaryot Gene Expr, 19*(4), 319-338.

Rodan, S. B., & Rodan, G. A. (1997). Integrin function in osteoclasts. *J Endocrinol, 154 Suppl*, S47-56.

Roth, K. E., Rieder, C. L., & Bowser, S. S. (1988). Flexible-substratum technique for viewing cells from the side: some in vivo properties of primary (9+0) cilia in cultured kidney epithelia. *J Cell Sci, 89 (Pt 4)*, 457-466.

Rubin, J., Murphy, T., Nanes, M. S., & Fan, X. (2000). Mechanical strain inhibits expression of osteoclast differentiation factor by murine stromal cells. *Am J Physiol Cell Physiol, 278*(6), C1126-1132. doi:10.1152/ajpcell.2000.278.6.C1126

Rubin, J., Murphy, T. C., Fan, X., Goldschmidt, M., & Taylor, W. R. (2002). Activation of extracellular signal-regulated kinase is involved in mechanical strain inhibition of RANKL expression in bone stromal cells. *J Bone Miner Res, 17*(8), 1452-1460. doi:10.1359/jbmr.2002.17.8.1452

Ruff, C., Holt, B., & Trinkaus, E. (2006). Who's afraid of the big bad Wolff?: Wolff's law and bone functional adaptation. *AJPA American Journal of Physical Anthropology, 129*(4), 484-498.

Ruijtenberg, S., & van den Heuvel, S. (2016). Coordinating cell proliferation and differentiation: Antagonism between cell cycle regulators and cell type-specific gene expression. *Cell Cycle, 15*(2), 196-212. doi:10.1080/15384101.2015.1120925

Ruiz, S. A., & Chen, C. S. (2008). Emergence of patterned stem cell differentiation within multicellular structures. *Stem Cells, 26*(11), 2921-2927. doi:10.1634/stemcells.2008-0432

Rutkovskiy, A., Stensløkken, K.-O., & Vaage, I. J. (2016). Osteoblast Differentiation at a Glance. *Medical Science Monitor Basic Research, 22*, 95-106. doi:10.12659/MSMBR.901142

Ryder, K. D., & Duncan, R. L. (2001). Parathyroid hormone enhances fluid shear-induced [Ca2+]i signaling in osteoblastic cells through activation of mechanosensitive and voltage-sensitive Ca2+ channels. *J Bone Miner Res, 16*(2), 240-248. doi:10.1359/jbmr.2001.16.2.240

Saag, K. G., Petersen, J., Brandi, M. L., Karaplis, A. C., Lorentzon, M., Thomas, T., . . . Grauer, A. (2017). Romosozumab or Alendronate for Fracture Prevention in Women with Osteoporosis. *New England Journal of Medicine, 377*(15), 1417-1427. doi:10.1056/NEJMoa1708322

Sakai, K., Mohtai, M., & Iwamoto, Y. (1998). Fluid shear stress increases transforming growth factor beta 1 expression in human osteoblast-like cells: modulation by cation channel blockades. *Calcified tissue international, 63*(6), 515-520.

Sakai, K., Mohtai, M., Shida, J., Harimaya, K., Benvenuti, S., Brandi, M. L., . . . Iwamoto, Y. (1999). Fluid shear stress increases interleukin-11 expression in human osteoblast-like cells: its role in osteoclast induction. *J Bone Miner Res, 14*(12), 2089-2098. doi:10.1359/jbmr.1999.14.12.2089

Sakata, T., Wang, Y., Halloran, B. P., Elalieh, H. Z., Cao, J., & Bikle, D. D. (2004). Skeletal unloading induces resistance to insulin-like growth factor-I (IGF-I) by inhibiting activation of the IGF-I signaling pathways. *J Bone Miner Res, 19*(3), 436-446. doi:10.1359/jbmr.0301241

Santos, A., Bakker, A. D., & Klein-Nulend, J. (2009). The role of osteocytes in bone mechanotransduction. *Osteoporosis International, 20*(6), 1027-1031. doi:10.1007/s00198-009-0858-5

Sarkar, D., Nagaya, T., Koga, K., & Seo, H. (1999). Culture in vector-averaged gravity environment in a clinostat results in detachment of osteoblastic ROS 17/2.8 cells. *Environ Med, 43*(1), 22-24.

Satir, P., Pedersen, L. B., & Christensen, S. T. (2010). The primary cilium at a glance. *Journal of Cell Science, 123*(4), 499-503. doi:10.1242/jcs.050377

Sawakami, K., Robling, A. G., Ai, M., Pitner, N. D., Liu, D., Warden, S. J., . . . Turner, C. H. (2006). The Wnt co-receptor LRP5 is essential for skeletal mechanotransduction but not for the anabolic bone response to parathyroid hormone treatment. *J Biol Chem, 281*(33), 23698-23711. doi:10.1074/jbc.M601000200

Scott, A., Khan, K. M., Duronio, V., & Hart, D. A. (2008). Mechanotransduction in human bone: in vitro cellular physiology that underpins bone changes with exercise. *Sports Med, 38*(2), 139-160.

Shao, Y., Alicknavitch, M., & Farach-Carson, M. C. (2005). Expression of voltage sensitive calcium channel (VSCC) L-type Cav1.2 (alpha1C) and T-type Cav3.2 (alpha1H) subunits during mouse bone development. *Dev Dyn, 234*(1), 54-62. doi:10.1002/dvdy.20517

Shibukawa, Y., Sato, M., Kimura, M., Sobhan, U., Shimada, M., Nishiyama, A., . . . Tazaki, M. (2015). Odontoblasts as sensory receptors: transient receptor potential channels, pannexin-1, and ionotropic ATP receptors mediate intercellular odontoblast-neuron signal transduction. *Pflugers Arch, 467*(4), 843-863. doi:10.1007/s00424-014-1551-x

Simpson, A. E., Stoddart, M. J., Davies, C. M., Jahn, K., Furlong, P. I., Gasser, J. A., . . . Richards, R. G. (2009). TGFbeta3 and loading increases osteocyte survival in human cancellous bone cultured ex vivo. *Cell Biochem Funct, 27*(1), 23-29. doi:10.1002/cbf.1529

Sinha, R. K., & Tuan, R. S. (1996). Regulation of human osteoblast integrin expression by orthopedic implant materials. *Bone, 18*(5), 451-457.

Sittichockechaiwut, A., Scutt, A. M., Ryan, A. J., Bonewald, L. F., & Reilly, G. C. (2009). Use of rapidly mineralising osteoblasts and short periods of mechanical loading to accelerate matrix maturation in 3D scaffolds. *Bone, 44*(5), 822-829.

Skerry, T. (2006). One mechanostat or many? Modifications of the site-specific response of bone to mechanical loading by nature and nurture. *Journal of Musculoskeletal and Neuronal Interactions, 6*(2), 122.

Sokabe, M., & Sachs, F. (1990). The structure and dynamics of patch-clamped membranes: a study using differential interference contrast light microscopy. *J Cell Biol, 111*(2), 599-606.

Sokabe, M., Sachs, F., & Jing, Z. Q. (1991). Quantitative video microscopy of patch clamped membranes stress, strain, capacitance, and stretch channel activation. *Biophys J, 59*(3), 722-728. doi:10.1016/s0006-3495(91)82285-8

Srinivasan, P. P., Parajuli, A., Price, C., Wang, L., Duncan, R. L., & Kirn-Safran, C. B. (2015). Inhibition of T-Type Voltage Sensitive Calcium Channel Reduces Load-Induced OA in Mice and Suppresses the Catabolic Effect of Bone Mechanical Stress on Chondrocytes. *PLoS ONE, 10*(5), e0127290. doi:10.1371/journal.pone.0127290

Sterck, J. G., Klein-Nulend, J., Lips, P., & Burger, E. H. (1998). Response of normal and osteoporotic human bone cells to mechanical stress in vitro. *American Journal of Physiology-Endocrinology and Metabolism, 274*(6), E1113-E1120.

Sugimoto, A., Miyazaki, A., Kawarabayashi, K., Shono, M., Akazawa, Y., Hasegawa, T., . . . Iwamoto, T. (2017). Piezo type mechanosensitive ion channel component 1 functions as a regulator of the cell fate determination of mesenchymal stem cells. *Sci Rep, 7*(1), 17696. doi:10.1038/s41598-017-18089-0

Sugimoto, Y., & Narumiya, S. (2007). Prostaglandin E receptors. *J Biol Chem, 282*(16), 11613-11617. doi:10.1074/jbc.R600038200

Sukharev, S. I., Blount, P., Martinac, B., & Kung, C. (1997). Mechanosensitive channels of Escherichia coli: the MscL gene, protein, and activities. *Annu Rev Physiol, 59*, 633-657. doi:10.1146/annurev.physiol.59.1.633

Tamma, R., Colaianni, G., Camerino, C., Di Benedetto, A., Greco, G., Strippoli, M., . . . Zallone, A. (2009). Microgravity during spaceflight directly affects in vitro osteoclastogenesis and bone resorption. *Faseb J, 23*(8), 2549-2554. doi:10.1096/fj.08-127951

Tan, S. D., de Vries, T. J., Kuijpers-Jagtman, A. M., Semeins, C. M., Everts, V., & Klein-Nulend, J. (2007). Osteocytes subjected to fluid flow inhibit osteoclast formation and bone resorption. *Bone, 41*(5), 745-751. doi:10.1016/j.bone.2007.07.019

Tanaka, S., Sakai, A., Tanaka, M., Otomo, H., Okimoto, N., Sakata, T., & Nakamura, T. (2004). Skeletal Unloading Alleviates the Anabolic Action of Intermittent PTH(1–34) in Mouse Tibia in Association With Inhibition of PTH-Induced Increase in c-fos mRNA in Bone Marrow Cells. *Journal of Bone and Mineral Research, 19*(11), 1813-1820. doi:10.1359/JBMR.040808

Taylor, A. F., Saunders, M. M., Shingle, D. L., Cimbala, J. M., Zhou, Z., & Donahue, H. J. (2007). Mechanically stimulated osteocytes regulate osteoblastic activity via gap junctions. *Am J Physiol Cell Physiol, 292*(1), C545-552. doi:10.1152/ajpcell.00611.2005

Temiyasathit, S., & Jacobs, C. R. (2010). The osteocyte primary cilium and its role in bone mechanotransduction. *Annals of the New York Academy of Sciences, 1192*, 422-428. doi:10.1111/j.1749-6632.2009.05243.x

Temiyasathit, S., Tang, W. J., Leucht, P., Anderson, C. T., Monica, S. D., Castillo, A. B., . . . Jacobs, C. R. (2012). Mechanosensing by the primary cilium: deletion of Kif3A reduces bone formation due to loading. *PLoS ONE, 7*(3), e33368. doi:10.1371/journal.pone.0033368

Thompson, W. R., Rubin, C. T., & Rubin, J. (2012). Mechanical Regulation of Signaling Pathways in Bone. *Gene, 503*(2), 179-193. doi:10.1016/j.gene.2012.04.076

Thurley, K., Tovey, S. C., Moenke, G., Prince, V. L., Meena, A., Thomas, A. P., . . . Falcke, M. (2014). Reliable encoding of stimulus intensities within random sequences of intracellular Ca2+ spikes. *Sci. Signal., 7*(331), ra59-ra59.

Tiedemann, K., Boraschi-Diaz, I., Rajakumar, I., Kaur, J., Roughley, P., Reinhardt, D. P., & Komarova, S. V. (2013). Fibrillin-1 directly regulates osteoclast formation and function by a dual mechanism. *Journal of Cell Science, 126*(Pt 18), 4187-4194. doi:10.1242/jcs.127571

Tiedemann, K., Hussein, O., Sadvakassova, G., Guo, Y., Siegel, P. M., & Komarova, S. V. (2009). Breast Cancer-derived Factors Stimulate Osteoclastogenesis through the Ca(2+)/Protein Kinase C and Transforming Growth Factor-β/MAPK Signaling Pathways. *J Biol Chem, 284*(48), 33662-33670. doi:10.1074/jbc.M109.010785

Tu, X., Rhee, Y., Condon, K. W., Bivi, N., Allen, M. R., Dwyer, D., . . . Bellido, T. (2012). Sost downregulation and local Wnt signaling are required for the osteogenic response to mechanical loading. *Bone, 50*(1), 209-217. doi:10.1016/j.bone.2011.10.025

Turner, C. H. (1998). Three rules for bone adaptation to mechanical stimuli. *Bone, 23*(5), 399-407.

Turner, C. H., Takano, Y., Owan, I., & Murrell, G. (1996). Nitric oxide inhibitor L-NAME suppresses mechanically induced bone formation in rats. *American Journal of Physiology-Endocrinology and Metabolism, 270*(4), E634-E639.

Turner, C. H., Takano, Y., Owan, I., & Murrell, G. A. (1996). Nitric oxide inhibitor L-NAME suppresses mechanically induced bone formation in rats. *Am J Physiol, 270*(4 Pt 1), E634-639. doi:10.1152/ajpendo.1996.270.4.E634

Tyrovola, J. B. (2015). The "Mechanostat Theory" of Frost and the OPG/RANKL/RANK System. *J Cell Biochem, 116*(12), 2724-2729. doi:10.1002/jcb.25265

Vazquez, M., Evans, B. A. J., Riccardi, D., Evans, S. L., Ralphs, J. R., Dillingham, C. M., & Mason, D. J. (2014). A New Method to Investigate How Mechanical Loading of Osteocytes Controls Osteoblasts. *Frontiers in Endocrinology, 5*, 208. doi:10.3389/fendo.2014.00208

Vezeridis, P. S., Semeins, C. M., Chen, Q., & Klein-Nulend, J. (2006). Osteocytes subjected to pulsating fluid flow regulate osteoblast proliferation and differentiation. *Biochem Biophys Res Commun, 348*(3), 1082-1088. doi:10.1016/j.bbrc.2006.07.146

Vilceanu, D., & Stucky, C. L. (2010). TRPA1 mediates mechanical currents in the plasma membrane of mouse sensory neurons. *PLoS ONE, 5*(8), e12177. doi:10.1371/journal.pone.0012177

Wang, N., Butler, J. P., & Ingber, D. E. (1993). Mechanotransduction across the cell surface and through the cytoskeleton. *Science, 260*(5111), 1124-1127.

Wang, Y., McNamara, L. M., Schaffler, M. B., & Weinbaum, S. (2007). A model for the role of integrins in flow induced mechanotransduction in osteocytes. *Proc Natl Acad Sci U S A, 104*(40), 15941-15946. doi:10.1073/pnas.0707246104

Weinbaum, S., Cowin, S. C., & Zeng, Y. (1994). A model for the excitation of osteocytes by mechanical loading-induced bone fluid shear stresses. *J Biomech, 27*(3), 339-360.

Weinstein, M. M., Tompson, S. W., Chen, Y., Lee, B., & Cohn, D. H. (2014). Mice Expressing Mutant Trpv4 Recapitulate the Human TRPV4 Disorders(). *Journal of bone and mineral research : the official journal of the American Society for Bone and Mineral Research, 29*(8), 1815-1822. doi:10.1002/jbmr.2220

Weyts, F. A., Bosmans, B., Niesing, R., van Leeuwen, J. P., & Weinans, H. (2003). Mechanical control of human osteoblast apoptosis and proliferation in relation to differentiation. *Calcif Tissue Int, 72*(4), 505-512. doi:10.1007/s00223-002-2027-0

Weyts, F. A., Li, Y. S., van Leeuwen, J., Weinans, H., & Chien, S. (2002). ERK activation and alpha v beta 3 integrin signaling through Shc recruitment in response to mechanical stimulation in human osteoblasts. *J Cell Biochem, 87*(1), 85-92. doi:10.1002/jcb.10278

Wimalawansa, S., De Marco, G., Gangula, P., & Yallampalli, C. (1996). Nitric oxide donor alleviates ovariectomy-induced bone loss. *Bone, 18*(4), 301-304.

Wimalawansa, S. J. (2010). Nitric oxide and bone. *Ann N Y Acad Sci, 1192*, 391-403. doi:10.1111/j.1749-6632.2009.05230.x

Wipff, P. J., Rifkin, D. B., Meister, J. J., & Hinz, B. (2007). Myofibroblast contraction activates latent TGF-beta1 from the extracellular matrix. *J Cell Biol, 179*(6), 1311-1323. doi:10.1083/jcb.200704042

Xiao, Z., Dallas, M., Qiu, N., Nicolella, D., Cao, L., Johnson, M., . . . Quarles, L. D. (2011). Conditional deletion of Pkd1 in osteocytes disrupts skeletal mechanosensing in mice. *Faseb J, 25*(7), 2418-2432. doi:10.1096/fj.10-180299

Yoshida, K., Oida, H., Kobayashi, T., Maruyama, T., Tanaka, M., Katayama, T., . . . Narumiya, S. (2002). Stimulation of bone formation and prevention of bone loss by prostaglandin E EP4 receptor activation. *Proc Natl Acad Sci U S A, 99*(7), 4580-4585. doi:10.1073/pnas.062053399

You, J., Reilly, G. C., Zhen, X., Yellowley, C. E., Chen, Q., Donahue, H. J., & Jacobs, C. R. (2001). Osteopontin gene regulation by oscillatory fluid flow via intracellular calcium mobilization and activation of mitogen-activated protein kinase in MC3T3-E1 osteoblasts. *J Biol Chem, 276*(16), 13365-13371. doi:10.1074/jbc.M009846200

You, J., Yellowley, C. E., Donahue, H. J., Zhang, Y., Chen, Q., & Jacobs, C. R. (2000). Substrate deformation levels associated with routine physical activity are less stimulatory to bone cells relative to loading-induced oscillatory fluid flow. *J Biomech Eng, 122*(4), 387-393.

You, L., Cowin, S. C., Schaffler, M. B., & Weinbaum, S. (2001). A model for strain amplification in the actin cytoskeleton of osteocytes due to fluid drag on pericellular matrix. *J Biomech, 34*(11), 1375-1386.

You, L., Temiyasathit, S., Lee, P., Kim, C. H., Tummala, P., Yao, W., . . . Jacobs, C. R. (2008). Osteocytes as mechanosensors in the inhibition of bone resorption due to mechanical loading. *Bone, 42*(1), 172-179. doi:10.1016/j.bone.2007.09.047

Zhang, J., Ryder, K. D., Bethel, J. A., Ramirez, R., & Duncan, R. L. (2006). PTH-induced actin depolymerization increases mechanosensitive channel activity to enhance mechanically stimulated Ca2+ signaling in osteoblasts. *J Bone Miner Res, 21*(11), 1729-1737. doi:10.1359/jbmr.060722

Zhang, Y. L., Frangos, J. A., & Chachisvilis, M. (2009). Mechanical stimulus alters conformation of type 1 parathyroid hormone receptor in bone cells. *Am J Physiol Cell Physiol, 296*(6), C1391-1399. doi:10.1152/ajpcell.00549.2008

Zhu, D., Mackenzie, N. C. W., Millán, J. L., Farquharson, C., & MacRae, V. E. (2011). The Appearance and Modulation of Osteocyte Marker Expression during Calcification of Vascular Smooth Muscle Cells. *PLoS ONE, 6*(5), e19595. doi:10.1371/journal.pone.0019595

Zimmermann, K. W. (1898). Beiträge zur Kenntniss einiger Drüsen und Epithelien. *Archiv für mikroskopische Anatomie, 52*(3), 552-706.

Chapter Two

Purinergic Signalling in Skeletal Mechanobiology

This chapter is dedicated to purinergic signalling, with an emphasis on its role in skeletal mechanobiology. I provide a brief historical account of purinergics and introduce the physiological relevance of purinergic signalling in different tissues. I then proceed to discuss the mechanisms of mechanically-stimulated ATP release, diffusion and transport of ATP, extracellular metabolism of ATP, and signalling through the purinergic (P2) receptor family. I finish by discussing the outlook of purinergic signalling in basic, translation and clinical research.

2.1 A brief history of purinergics

The history of purines dates back to 1776 when Carl Wilhelm Scheele isolated uric acid from bladder stones [**Fig 2-1** (Scheele, 1776)]. Purines are heterocyclic aromatic organic compounds consisting of a pyrimidine fused to a imidazole ring (Rosemeyer, 2004), and by the end of the 19th century, guanine, adenine, xanthine and hypoxantine had been identified. By this time, "purine" was coined by Emil Fischer who adopted the term from *purum uricum* meaning pure uric acid (Fischer, 2013). Soon after in 1929, the energy-rich adenine nucleotide ATP was discovered independently by two separate groups (Fiske & Subbarow, 1929; Lohmann, 1929).

Although the significance of the finding was not clear at the time, the first evidence that suggested a role for purines in extracellular signalling came from experiments that showed that crude tissue extracts applied to guinea pig hearts nearly induced cardiac arrest (Drury & Szent-Györgyi, 1929). However, these early studies were difficult to interpret due to impurities in purine species and unaccounted extracellular metabolism of purine compounds (Geoffrey Burnstock & Verkhratsky, 2012). The role of purines in extracellular signalling was investigated more formally in 1947, this time in the nervous system. ATP injected into the cervical segments of the feline spinal cord was found to induce tetanus-like contractions (Buchthal & Engbaek, 1947). Pamela Holton later demonstrated that ATP release could be detected from sensory neurons innervating the rabbit ear artery (Holton, 1959). Building upon these earlier findings, Geoffrey Burnstock came to realize that ATP satisfied the criteria for a neurotransmitter – This prompted him to formulate the purinergic signaling hypothesis in 1972 (G Burnstock, 1972).

At this time, the role of ATP in intracellular energetics had already been established (Lipmann, 1941) and the suggestion that ATP could have a physiological function elsewhere was considered absurd. Burnstock's idea was rejected by colleagues and he was called the "inventor of the pur*imagine* hypothesis" (Geoffrey Burnstock, 2014). Aware that his hypothesis needed further experimental support, Burnstock set out to find and describe the ATP-sensitive purinergic receptor.

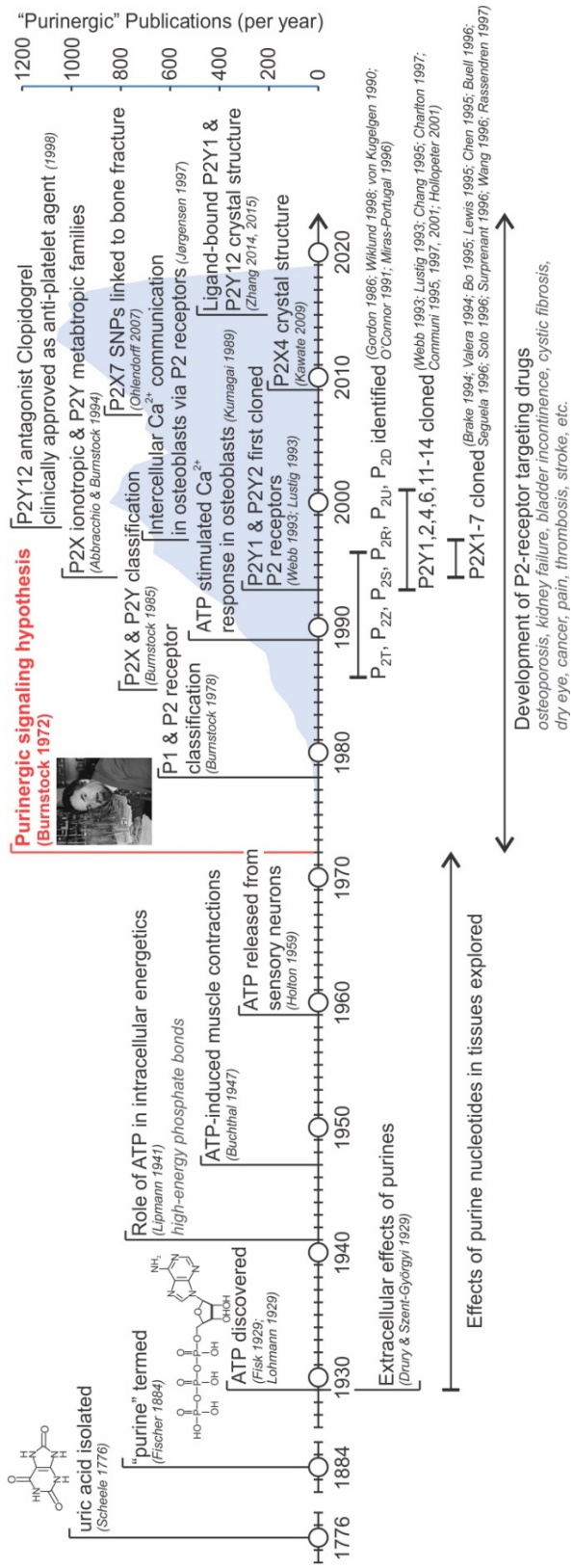

Figure 2-1. Milestones in purinergic research. Number of publications (per year) in the purinergic field shown in *blue*, publication history retrieved from PubMed on December 10th, 2018 using "purinergic" query.

By 1978, Burnstock had proposed that purinergic receptors be classified as P1 purinoceptors (responsive to adenosine) and P2 purinoreceptors (responsive to ATP and ADP) on the basis of differential pharmacological profiles and physiological responses (Geoffrey Burnstock & Verkhratsky, 2012). This attracted attention, and in subsequent years the rapid discovery of many receptor subtypes, including P_{2T} and P_{2Z} (Gordon, 1986), P_{2S} (Wiklund & Gustafsson, 1988), P_{2R} (von Kügelgen & Starke, 1990), P_{2U} (O'Connor, Dainty, & Leff, 1991) and P_{2D} (Miras-Portugal, Castro, Mateo, & Pintor, 1996), paralleled the rising acceptance of the purinergic hypothesis. However, the rate at which receptors were being identified was becoming problematic since subtype classifications were largely informal and based on pharmacological studies. A standardized nomenclature was finally proposed in 1994, suggesting that P2 receptors be grouped into two major classes: ligand-gated P2X channels and G-protein coupled P2Y receptors

(Maria P Abbracchio & Burnstock, 1994; Bertil B Fredholm et al., 1994). Around this time the first P2 receptors, P2Y1 (Webb et al., 1993) and P2Y2 (Lustig, Shiau, Brake, & Julius, 1993), were clone and findings were published 2 weeks apart.

Interest in purinergics has since surged, and to date, 15 unique P2 receptors have been discovered and cloned. It is now established that P2 receptors are expressed ubiquitously throughout the body and virtually every mammalian cell releases ATP in response to stresses [e.g., mechanical loading, injury and hypoxia (Eduardo R. Lazarowski, Sesma, Seminario-Vidal, & Kreda, 2011; Lim To, Kumar, & Marshall, 2015)] and various GPCR agonists (Eduardo R. Lazarowski et al., 2011). Today Geoffrey Burnstock is widely regarded as the founding father of purinergics and he currently carries out his work in Australia, collaborating with young clinicians to oversee the translation of his discovery to the clinic.

2.2 Mechano-physiological relevance of ATP

ATP is released in response to mechanical stimulation and it is involved in a variety of tissue-specific mechano-perceptive functions. Mechanically-stimulated ATP release intimately couples extracellular ATP to its cognate purinergic receptors (P2R), which are expressed in tissue-specific patterns throughout the body (Geoffrey Burnstock, 2014), allowing for diverse signalling cascades and outcomes. The mechano-perceptive physiology of mechanically-stimulated ATP release is broadly classified as (*i*) mechano-sensory and (*ii*) mechano-adaptive (**Fig 2-2**).

Mechano-sensory roles are characterised by the purinergic coupling of non-neuronal tissue to the nervous system. Unlike synaptic transmission, paracrine ATP signalling does not require ultrastructural synaptic specialization to facilitate the transmission of information (Roper, 2006). Thus, ATP released from mechanically stimulated tissue, such as the skin (Takahashi et al., 2013), bladder (Shiina, Hayashida, Ishikawa, & Kawatani, 2016), or gastrointestinal tract (Berglund et al., 2013), can convey long-range sensory communication about the mechanical environment. Dysregulation of ATP in mechano-sensation is associated with pain (Chizh & Illes, 2001).

Mechano-adaptive roles of mechanically-stimulated ATP release enable a dynamic relationship between tissue-level function and the mechanical environment. Two levels of temporal organization are evident for mechano-adaptive ATP release: Short- and long-term (Geoffrey Burnstock, 2016). The short-term effects of mechanically-stimulated ATP release are involved in

mechanical homeostasis, by facilitating responses to mechanical perturbations that demand immediate physiological feedback. These involve functions such as vasodilation and regulation of blood flow in vascular endothelia (Crecelius et al., 2011), ion transport and osmo-regulation in the kidney (Sinke & Deen, 2011) and muco-ciliary clearance and surfactant secretion in airway epithelia (E. R. Lazarowski & Boucher, 2009). The rapid extracellular degradation of ATP by ecto-nucleotidases permits these systems to maintain low basal extracellular ATP concentrations (H. Zimmermann, 2000), thereby ensuring sensitivity to acute exposures of ATP released following mechanical stimulation. However, acute intermittent exposures to ATP are also sufficient to initiate signalling cascades that manifest over the longer term (Geoffrey Burnstock, 2016), representing a long-term mechano-adaptive role for mechanically-stimulated ATP release. Isolating the longer-term consequences of ATP-mediated signalling has been experimentally challenging due to the inevitable release of ATP during routine handling of samples (G. Burnstock & G. E. Knight, 2017), however longer-term effects have been associated with changes in gene expression, proliferation and differentiation. At the tissue-level, these changes manifest as complex phenotypes such as skeletal bone remodeling or breast cancer metastases.

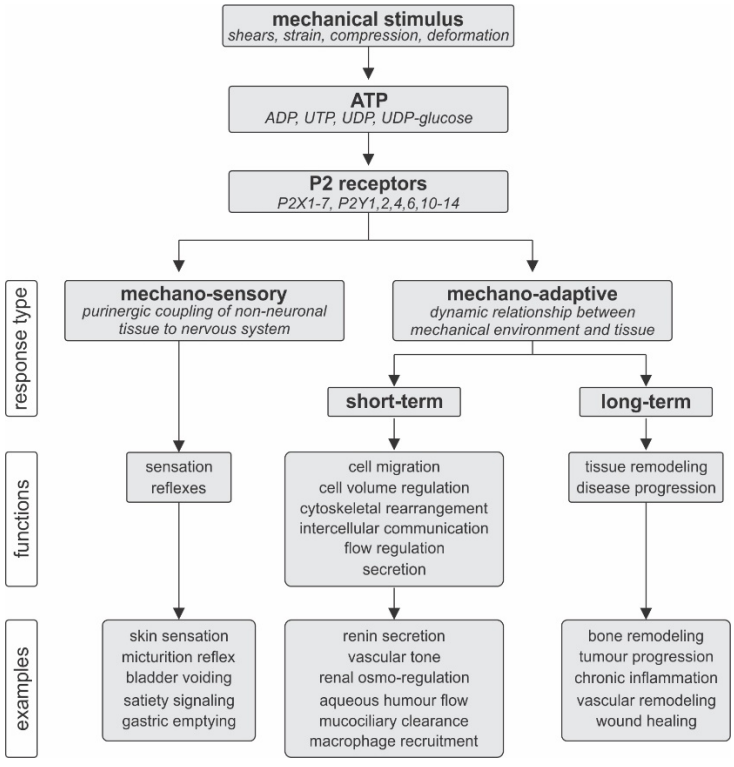

Figure 2-2. Mechanotransductive Purinergic Signaling.

2.3 Experimental methods to measure ATP release

The luciferin-luciferase bioluminescence assay is the gold standard for measuring ATP. In the presence of ATP, luciferase oxidizes luciferin and produces light proportional to the amount of ATP present.

$$\text{Luciferin} + O_2 + \mathbf{ATP} \xrightarrow{+\text{luciferase}} \text{Oxyluciferin} + CO_2 + \text{AMP} + \text{PPi} + \boldsymbol{Light}$$

Several other methods have also been used to measure ATP, including biosensors (Ildikó Toma et al., 2008), amperometry probes (B. A. Patel, 2014), high-performance liquid chromatography [HPLC; (Bhatt, Chen, Geiger, & Rosenberger, 2012; von Papen, Gambaryan, Schütz, & Geiger, 2013)], luciferin-fluorescence assay (Sørensen & Novak, 2001), and surface-conjugated luciferase (Beigi, Kobatake, Aizawa, & Dubyak, 1999; Yamamoto et al., 2011). The biosensor approach involves monitoring intracellular calcium levels in P2 receptor-expressing cells – In the presence of ATP, calcium elevations can be detected and ATP concentrations can be estimated based on a pre-established ATP dose-response curve. Amperometric ATP sensors consist of electrode-conjugated enzymes which generate currents in the presence of ATP in a manner dependent on competing reactions, such as between hexokinase and glucose oxidase (Bhavik Anil Patel, Rogers, Wieder, O'Hare, & Boutelle, 2011). HPLC techniques enable the resolution, identification and quantification of ATP present in a sample passed through a chromatography column. The luciferin-fluorescence assay is an adaptation of the luciferin-bioluminescence assay which exploits the inherent fluorescent properties of luciferin – as the luciferin substrate is depleted in the presence of ATP and luciferase, luciferin fluorescence decreases proportional to the amount of ATP added to the reaction (Sørensen & Novak, 2001).

Most ATP measurement methods depend on bulk sampling techniques, i.e., the sampling of small volumes from a larger volume of interest. This can lead to misrepresentative ATP estimates due to inadequate equilibration of ATP in the media. Cell surface-bound luciferase constructs have been developed to overcome this limitation (Beigi et al., 1999; Yamamoto et al., 2011).

Depending on the choice of assay, ATP measurements can be online (real-time monitoring) or offline (sample collected and measured elsewhere). Online measurements of ATP concentrations are only possible with luciferin-luciferase bioluminescence assays and amperometric probes.

2.4 Mechanically-stimulated ATP release

In mammalian cells, the main mechanisms of ATP release are (*i*) vesicular release (*ii*) conductive release via channels and (*iii*) injury-related release through damaged cellular plasma membranes (G. Burnstock & Verkhratskii, 2012) (**Fig 2-3**). These mechanisms vary by cell type and employ different regulatory pathways. ATP is released in response to a variety of stimuli including mechanical loads and shears (Genetos, Geist, Liu, Donahue, & Duncan, 2005), hypoxia (Orriss et al., 2009) and vitamin D_3 (Biswas & Zanello, 2009). ATP is also released constitutively under basal conditions, ensuring that nanomolar extracellular concentrations of ATP are maintained (Orriss, Key, Hajjawi, & Arnett, 2013).

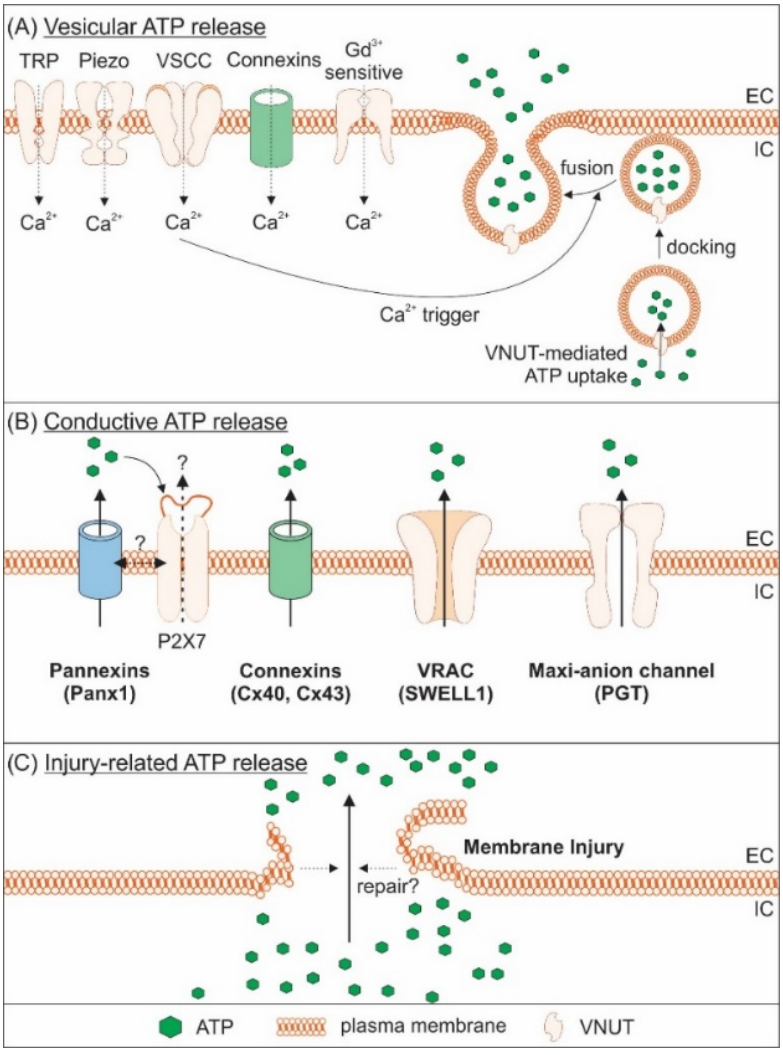

Figure 2-3. Mechanisms of mechanically-stimulated ATP release.

(A) Vesicular exocytosis is triggered by calcium influx through mechanosensitive cation channels. Vesicles uptake of ATP is mediated by VNUT.

(B) Mechano-sensitive membrane channels conduct ATP.

(C) Membrane injury permits spillage of intracellular ATP content into extracellular space. Role of passive or active membrane repair in ATP release is unknown.

EC: extracellular, Gd^{3+}: gadolinium, IC: intracellular, PGT: prostaglandin transporter, TRP: transient potential channels, VNUT: vesicular nucleotide uptake transporter, VRAC: volume-regulated anion channels, VSCC: L- or T-type voltage sensitive calcium channels.

2.4.1 Vesicular ATP release

Vesicular Pathway. ATP rich vesicles can release their contents into the extracellular space by fusing with the plasma membrane upon mechanical stimulation (**Fig 2-3A**). This phenomenon (as a response to mechanical stimulus) was first observed by Bodin and Burnstock (2001) who reported that blocking vesicular transport mechanisms suppressed ATP release from shear-stimulated vascular endothelia (Bodin & Burnstock, 2001). A vesicle-associated protein necessary for vesicular ATP release was recently discovered and characterized as the vesicular nucleotide transporter (VNUT, encoded by *SLC17A9*) involved in ATP uptake into vesicles (Sawada et al., 2008). VNUT and fluorescent analogs of ATP localize in quinacrine-positive vesicles [quinacrine is acidophilic marker that accumulates in adenine-rich compartments (Haanes et al., 2014; Kowal, Yegutkin, & Novak, 2015)]. When VNUT was knocked down in biliary cells, there was a marked reduction in quinacrine-positive vesicles and swell-induced ATP release (Sathe et al., 2011). Lysosomes likely constitute the pool of vesicles involved in mechanically-stimulated ATP release, which is suggested by colocalization of lysosomal markers with acidophilic quinacrine and VNUT (Gonzales et al., 2010).

Vesicular exocytosis is triggered by a massive influx of calcium following mechanical stimulation (Estevez-Herrera et al., 2016; J. Lee et al., 2015; Pangrsic et al., 2007). Many cation-selective channels have been implicated in ATP release, which mediate the mechanical-stimulated $[Ca^{2+}]_i$ elevations that are required for vesicular release. These channels are typically mechanosensitive like Piezo1 (Syeda, Florendo, et al., 2016), TRPV4 (Suzuki, 2008), Gd^{3+}-sensitive channels (Simon, Benos, & Hamill, 2011) and connexins (Sáez & Leybaert, 2014). Additionally, L- and T-type voltage sensitive calcium channels (VSCC) have been implicated in vesicular ATP release, although VSCCs are not mechanosensitive (D. C. Genetos et al., 2005). The heterogenous expression and involvement of these channels suggests that they may confer cell-type specific regulation of ATP release at the level of calcium entry. Experimental evidence favouring (and opposing) this hypothesis is lacking; however, such a framework would enable most cells to release ATP through a common vesicular pathway yet exhibit differential sensitivities and regulation.

2.4.2 Conductive ATP release

Several conductive mechanisms have been implicated in mechanically stimulated ATP release, including the cystic fibrosis transmembrane conductance regulator (CFTR), connexins, voltage-sensitive calcium channels [L- and T-type VSCC (D. C. Genetos, D. J. Geist, L. Dawei, H. J. Donahue, & R. L. Duncan, 2005; Thompson et al., 2011a)], maxi-anion channels, P2X7 receptor [P2RX7 (A. Li et al., 2012)], pannexins [Panx1 (Bao, Locovei, & Dahl, 2004)], Piezo1 (Bae, Gnanasambandam, Nicolai, Sachs, & Gottlieb, 2013), TRPV4 (Rahman, Sun, Mukherjee, Nilius, & Janssen, 2018) and volume-regulated anion channels [VRAC (Qiu et al., 2014)]. However, cytosolic ATP is anionic [ATP^{4-} (Sabirov & Okada, 2005)] and large (~507 Da), disqualifying many of the implicated channels as direct routes of ATP release since they are either selective towards cations (L- and T-type VSCCs, Piezo1, TRPV4), or do not form sufficiently large pores [CFTR (Grygorczyk & Hanrahan, 1997; A. Hazama et al., 2000)]. The only channels that directly conduct ATP in response to mechanical stimulation are (*i*) pannexins (Bao et al., 2004), (*ii*) connexins (Kang et al., 2008), (*iii*) maxi-anion channels (Dutta, Okada, & Sabirov, 2002; Sabirov et al., 2017; Sabirov & Okada, 2009) and (*iv*) VRACs (Gaitán-Peñas et al., 2016; Y. Okada, Sato, & Numata, 2009) (**Fig 2-3B**).

2.4.2.1 ATP conducting channels

Pannexins. Pannexins are a family of hemichannels consisting of three members (Panx1, Panx2 and Panx3). They are related to invertebrate innexins, which are analogs of the vertebrate connexin family of gap junctions (Panchin et al., 2000). Pannexins predominantly form uncoupled hemichannels and link the intracellular space to the extracellular compartment (Chiu, Ravichandran, & Bayliss, 2014). Panx1 hemichannels were proposed as a mechanosensitive conduit for ATP by Bao et al. (2004) who used electrophysiological recordings to demonstrate that Panx1 channels were mechanosensitive and permeable to ATP and soon after showed that ATP was released from osmotically-stressed RBCs via pannexins (Bao et al., 2004; Locovei, Bao, & Dahl, 2006).

Panx1 has been suggested to intimately couple with the P2X7 receptor (Pelegrin & Surprenant, 2006). The P2X7 receptor is an ATP-gated cation-selective channel belonging to the P2X receptor family and has a low-affinity for ATP. Under permissive conditions, the P2X7 receptor forms a

pore that was sufficiently large to conduct ATP, as demonstrated through various dye uptake assays (Lemaire, Falzoni, Zhang, Pellegatti, & Di Virgilio, 2011; J. Li, Liu, Ke, Duncan, & Turner, 2005b; Negoro et al., 2014). Co-immunoprecipitation experiments have shown that Panx1 and P2X7 are physically coupled in periodontal ligament cells (Kanjanamekanant, Luckprom, & Pavasant, 2014) and osteocytes (Z. Seref-Ferlengez et al., 2016). However, it remains disputed whether this pore-forming capacity is an intrinsic property of the P2X7 receptor itself, or rather characteristic of the Panx1 channel that has coupled to the P2X7 receptor (Di Virgilio, Schmalzing, & Markwardt, 2018; Wicki-Stordeur & Swayne, 2013).

Connexins. Connexins are a family of membrane channels consisting of twenty members which participate in the formation of intercellular GAP junctions between neighbouring cells. When uncoupled, connexins form hemichannels like pannexins and are permeable to ATP, as demonstrated indirectly using dye transfer experiments (Lohman & Isakson, 2014; Weber, Chang, Spaeth, Nitsche, & Nicholson, 2004) and directly using a method that combined patch clamp recordings with bioluminescent detection of ATP flux (Kang et al., 2008). Connexin-mediated mechanically-stimulated ATP release was first reported by Graff et al. (2000) who demonstrated that ATP release from cyclically compressed chondron pellets was suppressed by connexin blocker octanol (Graff, Lazarowski, Banes, & Lee, 2000). Using RNA interference or knockout animal models, Cx40, Cx43 and Cx45 have been confirmed as mechanosensitive ATP-releasing connexins in various cell types including cardiac fibroblasts (D. Lu, Soleymani, Madakshire, & Insel, 2012), ligament cells (Luckprom, Kanjanamekanant, & Pavasant, 2011), possibly osteocytes (Genetos, Kephart, Zhang, Yellowley, & Donahue, 2007b) and renal epithelial cells (Chi, Gao, Zhang, Takeda, & Yao, 2014), and glomerular endothelial cells (I. Toma et al., 2008).

VRAC. The ubiquitously expressed voltage-regulated anion channel (VRAC) is involved in maintaining cellular volume when exposed to osmotic pressures by conducting chloride and organic anions in a process called regulatory volume decrease (RVD) (Hoffmann, Sørensen, Sauter, & Lambert, 2015). The VRAC has been characterized by its sensitivity to changes in volume, outward rectifying current and anion selectivity (Y. Okada et al., 2009). However, study of VRACs has been hindered by its elusive molecular identity and lack of selective molecular tools to probe its function. Recently, two separate groups identified LRRC8A (i.e., SWELL1) as an essential component of the VRAC complex (Qiu et al., 2014; Voss et al., 2014) which constituted

the VRAC pore (Syeda, Qiu, et al., 2016). No genetic studies have yet been conducted to verify the role of LRRC8A in mechanically-stimulated ATP release in mammalian cells, however exogenous LRRC8 expressed in non-mammalian xenopus oocytes were demonstrated to facilitate ATP release in response to hypotonic stress (Gaitán-Peñas et al., 2016).

Maxi-anion channel. The maxi-anion channel is ubiquitously expressed throughout the body and was first implicated in mechanically-stimulated ATP release from osmotically stressed mammary epithelial cells (Dutta et al., 2002). Despite its enigmatic molecular identity, the maxi anion was characterized by its conductive properties and bell-shaped voltage dependence curve (Sabirov & Okada, 2009). The plasmalemmal voltage-dependent anion channel (pl-VDAC) was a longtime candidate of the maxi-anion channel (Dutta et al., 2002) and was supported by data demonstrated that mechanically-stimulated ATP release was reduced in VDAC-1$^{-/-}$ lung fibroblasts (S. F. Okada et al., 2004). However, the electrophysiological single channel properties of VDAC and maxi-anion channel were concluded to be distinct, representing two separate channels (Sabirov & Merzlyak, 2012). Connexins and pannexins were also been explored as maxi-anion channel candidates, however they were pharmacologically distinct and therefore dismissed (Islam, Uramoto, Okada, Sabirov, & Okada, 2012; Sabirov & Okada, 2009). In a breakthrough finding, the maxi-anion channel was finally identified by Sabirov et al. (2017) as the prostaglandin transport PGT (member of organic anion transporting family, encoded by *SLCO2A1*) using a combination of siRNA screening, CRISPR/Cas-9 mediated knockout and heterologous overexpression approaches (Sabirov et al., 2017). PGT was demonstrated to elicit maxi-anion-like currents and was sensitive to maxi-anion channel blocker Gd^{3+}. Most importantly, silencing *SLCO2A1* in C127 mammary cells suppressed hypotonic stress induced ATP release.

2.4.3 Injury-related ATP release

Membrane injury and ATP release. ATP spillage is a consequence of mechanical cell injury, often associated with traumatic injury and wounding (**Fig 2-3C**) (Barbee, 2006; Yin, Xu, Zhang, Kumar, & Yu, 2007). However, mechanically-active tissues such as the loaded skeleton, dilated vasculature and distended bladder are exposed to mechanical stresses that routinely damage cellular membranes (Miyake & McNeil, 2003). Despite the occurrence of injury, cells are capable

of rapidly resealing their membrane, thereby minimizing spillage of intracellular contents (Steinhardt, Bi, & Alderton, 1994).

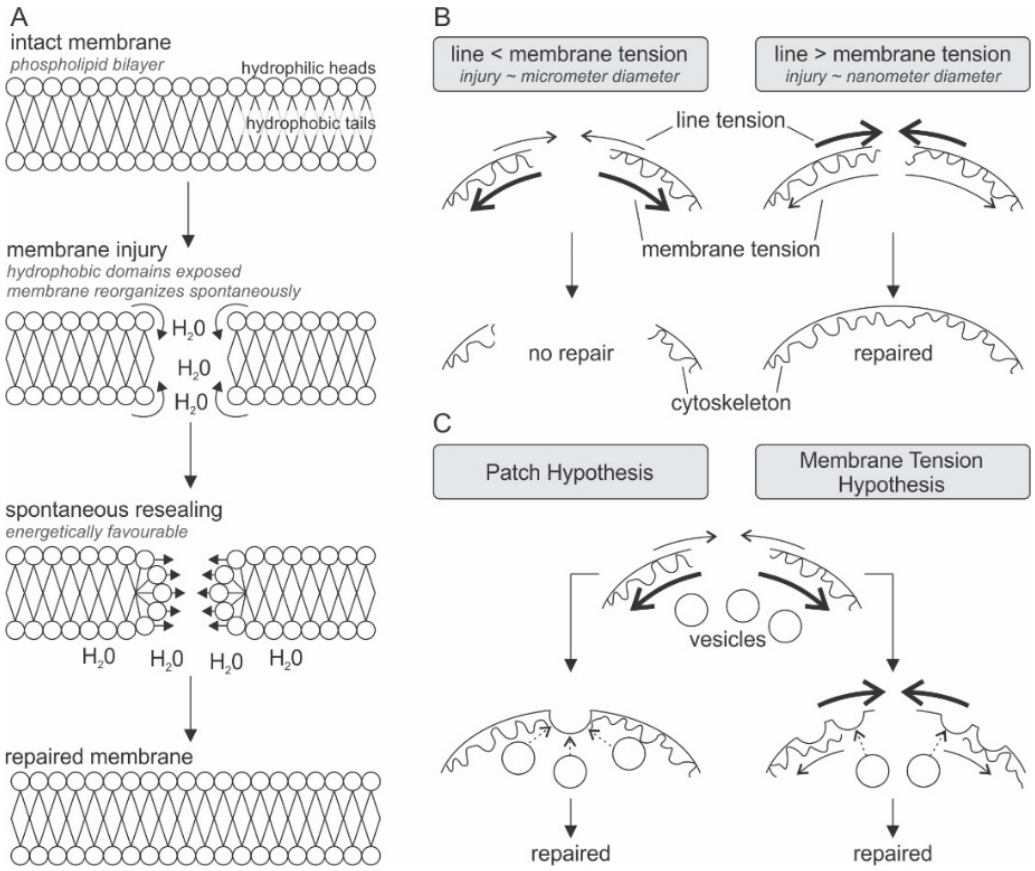

Figure 2-4. Mechanisms of membrane repair. (A) Cell injury exposes hydrophobic regions of the phospholipid bilayer, resulting in rapid conformational change to more energetically favorable state that allows membrane to spontaneously reseal. **(B)** Spontaneous membrane resealing occurs if line tensions generated from lipid disorder exceeds membrane tension generated by underlying cytoskeleton. **(C)** Vesicles mediate active membrane resealing by either patching membrane lesion directly (*left*; *patch hypothesis*) or by adding membrane to non-specific sites resulting in overall reduction in membrane tension (*right*; *membrane tension hypothesis*).

The ability for cells to repair a membrane disruption arose early in evolutionary history. Primitive prokaryotes were protected from the harsh external environment by a cell wall that was rigid and impermeable. However, the evolutionary transition of prokaryotes to eukaryotes was marked by the loss of this protective outer shell, leaving pro-eukaryotic cells vulnerable and prone to injury (Sandra T. Cooper & Paul L. McNeil, 2015). To compensate for this loss, primordial eukaryotes exploited their newly evolved endomembrane compartment as a sort of "reservoir" membrane which would aid membrane repair upon injury, thereby ensuring survival (Sandra T. Cooper &

Paul L. McNeil, 2015; S. T. Cooper & P. L. McNeil, 2015; Dacks & Field, 2007; Godell et al., 1997; Lai et al., 2009). Erythrocytes lack an endomembrane compartment, and unlike nucleated eukaryotes, they fail to reseal following laser- or shear-induced membrane disruption (McNeil, Miyake, & Vogel, 2003). Interestingly, hemolysis has been proposed as the primary route of ATP release in erythrocytes (Sikora, Orlov, Furuya, & Grygorczyk, 2014). Considering membrane repair mechanisms are primitive and conserved across eukaryotic cells (Sandra T. Cooper & Paul L. McNeil, 2015), and that membrane injury occurs routinely under physiological conditions (Miyake & McNeil, 2003), injury-related ATP release may represent a mechanism of regulated ATP release by which the rate of membrane repair governs the amount of ATP spilled from the cell prior to complete resealing.

Mechanisms of membrane repair. Upon cellular membrane injury, the hydrophobic regions of the phospholipid bilayer become exposed. This orientation is energetically unfavorable and results in the rapid lipid rearrangement so that hydrophilic (polar) phospholipid head groups become oriented towards the aqueous medium (Sandra T. Cooper & Paul L. McNeil, 2015). The line tensions generated by lipid disorder at the edge then drive the membrane to spontaneously reseal (**Fig 2-4A**). At the same time, spontaneous membrane resealing is opposed by membrane tensions generated by the underlying cytoskeleton that is tethered to the phospholipid bilayer, thereby acting to "tear" the injured membrane (**Fig 2-4B**). Small injuries (nanometer scale) can reseal spontaneously since attractive forces arising from lipid disorder exceed membrane tension forces at this scale. However, larger injuries (micrometer scale) require an active mechanism to reduce the overall membrane tension. Mass calcium influx through the disrupted membrane triggers a cascade of membrane repair pathways (T. Togo, Alderton, Bi, & Steinhardt, 1999). Among these, vesicular exocytosis is the most studied and has been proposed to promote membrane resealing in at least two ways (**Fig 2-4C**). There is the patch hypothesis in which vesicles are recruited to the site of injury and crudely "patch" the disrupted membrane (Terasaki, Miyake, & McNeil, 1997). Alternatively, there is there is the membrane tension hypothesis that suggests injury-induced exocytosis induces a decrease in membrane tension by membrane addition (Tatsuru Togo, Krasieva, & Steinhardt, 2000). In 3T3 fibroblasts, membrane tether forces decrease within 5 seconds of injury with complete membrane resealing occurring within 25 seconds, as measured by membrane impermeable dye leakage (Tatsuru Togo et al., 2000). This suggests that reduction in

membrane tension precedes cell membrane repair, and that this entire sequence of events occurs on a second-time scale. Interest in cellular and molecular mechanisms of membrane repair has surged in recent years with the realization that membrane injury underlies several pathophysiologies including ischemia-reperfusion injury in the case of heart attack and stroke, and pore formation by bacterial pathogens (Sandra T. Cooper & Paul L. McNeil, 2015). Key mediators of membrane repair include SNARES, dysferlin, calpains, annexins, mitsigumin-53, ESCRT, mucolipin-1 and the cytoskeleton, and together they represent potential therapeutic targets for a spectrum of human disorders characterized by membrane injury (Sandra T. Cooper & Paul L. McNeil, 2015).

2.4.4 Auxiliary regulators of ATP release

There are several mechanisms and pathways that have been implicated in mechanically-stimulated ATP release but are not involved in directly facilitating the transport of ATP from the intracellular space to the extracellular compartment. I have provided an overview of a few notable examples.

CFTR. CFTR is an ATP-binding cassette (ABC) transporter that functions as a chloride channel that mediates transmembrane anion currents and whose mutation results in cystic fibrosis. The involvement of CFTR in mechanically-stimulated ATP release has been contended for years, and still it remains unclear how it participates in ATP release (Grygorczyk & Hanrahan, 1997; A. Hazama et al., 2000). It was proposed as a candidate ATP release channel since it can augment ATP release through a route that is sensitive to non-specific mechanosensitive channel blocker gadolinium (Braunstein et al., 2001; A. Hazama et al., 2000); however, several groups using different methods such patch clamps and lipid bilayer and luminometry techniques have now independently concluded that the CFTR cannot directly conduct ATP (Grygorczyk & Hanrahan, 1997; A. Hazama et al., 2000; Reddy et al., 1996).

TRPV4 and Primary cilia. Primary cilia have been proposed to constitute a part of the ATP release machinery in certain cell types. Treatment of cholangiocytes with a deciliation agent, chloral hydrate, or disruption of microtubules with nocodazole significantly reduced ATP released following mechanical stimulation. Immunofluorescence labeling of cholangiocytes revealed that TRPV4 expression was localized to the primary cilia and vesicular ATP release was suppressed in TRPV4 knockdown cholangiocytes (S. A. Gradilone et al., 2007). Thus, primary cilia are

mechanosensitive organelles that mediate calcium influx via TRPV4 and subsequently release ATP through vesicular release – this collectively represents a complete ATP secretion apparatus (Sergio A. Gradilone et al., 2007). Despite the presence of primary cilia in osteoblasts (Malone et al., 2007) and osteocytes (Temiyasathit & Jacobs, 2010), TRPV4- or primary cilia-related ATP release has not been observed.

P2X7 receptor. The P2X7 receptor has also been prpoposed as an ATP release route, however mechanically-stimulated ATP release in $P2X7^{-/-}$ osteoblasts is indistinguishable from osteoblasts isolated from wild-type littermates (J. Li, Liu, Ke, Duncan, & Turner, 2005a). Oddly, there are inconsistencies between the expression and involvement of molecular mediators of ATP release. For instance, osteoblasts and osteocytes both *express* P2X7 receptor (Cheung et al., 2016; Nattapon Panupinthu et al., 2008) and hemichannels (Plotkin & Stains, 2015); however these channels are only *involved* in mechanically-stimulated ATP release in osteocytes (T. M. Kringelbach et al., 2015; Zeynep Seref-Ferlengez et al., 2016). More perplexing is the reported involvement of P2X7 in basal ATP release in osteoblasts (Andrea Brandao-Burch, Key, Patel, Arnett, & Orriss, 2012). This suggests there exists a regulatory network that is involved in coupling ATP release machinery to functional ATP release or perhaps to mechanosensitivity, however how this works is not known.

Cytoskeletal components. ATP release routes interact with the cytoskeleton. The maxi-anion channel is activated by fragmentation and depolymerization of f-actin (Sabirov & Okada, 2009). Pannexins are stabilized at the cell surface by actin, but not microtubules (Bhalla-Gehi, Penuela, Churko, Shao, & Laird, 2010). Vesicular exocytosis is increased when the actin cytoskeleton is disrupted (A. Li, Leung, Peterson-Yantorno, Stamer, & Civan, 2011) and impaired when microtubules are disrupted (Feranchak et al., 2010). The integrity of the cytoskeleton is thus essential for the assembly and function of ATP release machinery.

2.4.5 Bone-specific ATP release

Rodent and human osteoblasts have been demonstrated to release ATP in response to fluid shear stress (D. Genetos, D. Geist, L. Dawei, H. Donahue, & R. Duncan, 2005; J. Li et al., 2005a; Y. Li et al., 2013; Pines et al., 2003; Ning Wang et al., 2013a; Y. Xing et al., 2011), osmotic pressure (Pines et al., 2003; Romanello et al., 2005) and ultrasonic stimulation (Alvarenga et al., 2010;

Hayton et al., 2005; Manaka et al., 2015) through mechanisms involving vesicular exocytosis (D. Genetos et al., 2005; Romanello et al., 2005) and L-type VSCCs (D. Genetos et al., 2005; Hecht, Liedert, Ignatius, Mizaikoff, & Kranz, 2013). Rodent osteocytes also release ATP in response to fluid shear (Genetos, Kephart, Zhang, Yellowley, & Donahue, 2007a) and mechanical injury (T. M. Kringelbach et al., 2015). In osteocytes, shear induced ATP release was facilitated by vesicular exocytosis (T. M. Kringelbach et al., 2015), hemichannels [i.e., pannexins, connexins (T. M. Kringelbach et al., 2015; Zeynep Seref-Ferlengez et al., 2016)], P2X7 (Zeynep Seref-Ferlengez et al., 2016) and T-type VSCC (Thompson et al., 2011b). Shear-stressed osteoclasts release ATP (Hajjawi et al., 2013) and similarly macrophages have been shown to release ATP in response to osmotic pressure (Burow, Klapperstuck, & Markwardt, 2015). The mechanisms of ATP release have not been studied in osteoclasts, however in the study demonstrating ATP release from macrophages, VRACs were implicated as the route of ATP release (Burow et al., 2015). Taken together, at least four out of the five major ATP release mechanisms (i.e., vesicles, connexins, pannexins and VRACs) may be involved in mechanically-stimulated ATP release in bone, with differential involvement in each bone cell type.

2.5 ATP diffusion and extracellular metabolism

Following release into the extracellular space, ATP diffuses and is simultaneously metabolised by extracellular enzymes. Together these two processes influence the spatiotemporal content of ATP and its metabolites, thereby influencing downstream purinergic signalling.

2.5.1 Diffusion

Diffusion is a fundamental physical phenomenon that describes the passive movement of particles in a medium. In biology, diffusion governs many physiological processes that involve transport across space and time, like the exchange of gases in the lungs, movement of water across a semi-permeable membrane (known as osmosis) or dispersion of a signal mediator, such as ATP, between cells. The principles of diffusion were first formulated by Adolf Fick in 1855 who proposed that in a heterogeneous mixture, particle flux J across a medium is proportional to the concentration gradient (Fick, 1855). This is known as Fick's first law of diffusion:

$$J = -D\frac{\partial c}{\partial x}$$

Where D is the diffusion coefficient, c is concentration and x is space. From the First Law, Fick derived his Second Law which governs how the concentration of a diffusing species changes with respect to time and space:

$$\frac{\partial c}{\partial t} = D\frac{\partial^2 c}{\partial x^2}$$

Therefore, as particles become homogenously distributed, flux tends to zero representing an equilibrium at which there is no more change in particle density, or concentration, with respect to time (**Fig 2-5A**):

$$\frac{\partial c}{\partial t} = 0$$

Remarkably, Fick devised his laws of diffusion long before we established the existence of atoms which participate in this microscopic "random walk" process. Instead, Fick's laws of diffusion were devised to describe the conductance of heat and represented a macroscopic approach to diffusion. It was in fact Albert Einstein who established the microscopic basis for diffusion in 1905 in his doctoral thesis on Brownian Motion, representing the first direct evidence that atoms exist (Einstein, 1905).

The rate at which an atom, or molecule, diffuses is dictated by its diffusion coefficient D, which is a physical property related to the size and shape of a molecule (Erickson, 2009). Larger asymmetric molecules will diffuse slower than small symmetric molecules. For instance, ATP has a diffusion coefficient of approximately 347 $\mu m^2 s^{-1}$, while its smaller metabolite ADP has a diffusion coefficient of approximately 377 $\mu m^2 s^{-1}$ and therefore ADP would diffuse faster than ATP (Bennett, Farnell, Gibson, & Karunanithi, 1995; Diehl, Ihlefeld, & Schwegler, 2013; Hubley, Moerland, & Rosanske, 1995).

In a simplified one-dimensional case of diffusion, the spatial concentration of diffusing particles from a single instantaneous point source resembles a bell curve that spreads over time (**Fig 2-5B, C**) and is mathematically described as

$$c(x,t) = \frac{c_0}{\sqrt{4\pi Dt}} e^{-\frac{x^2}{4Dt}}$$

In this case all particles are assumed to originate from a single point source at t = 0, where x is the distance from the source, c_0 is the initial concentration and D is the diffusion coefficient. Rarely are diffusion problems so simple, often complicated by the geometric constraints of a system. The geometric and material complexity of bone contributes to complex and non-symmetric patterns of dispersal.

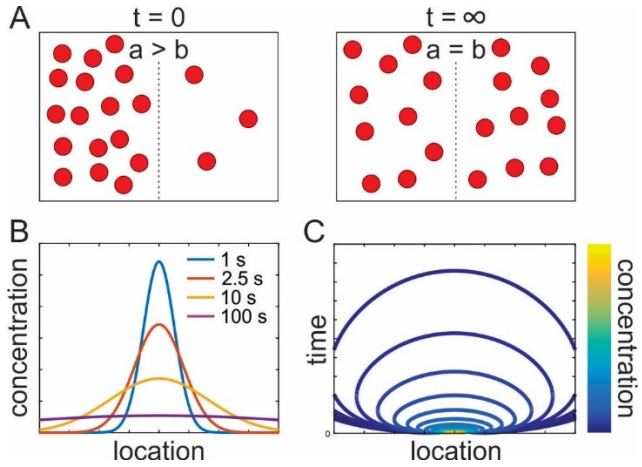

Figure 2-5. **Diffusion**. **(A)** Flux of particles (*red balls*) between compartments *a* and *b* separated by semi-permeable membrane (*dashed line*) with unequal particle distribution at t = 0, and equilibrated distributions at t = ∞. **(B, C)** Concentration profile of diffusing particles from a single instantaneous point source. **(B)** Spatial concentrations at t = 1, 2.5, 10 and 100 s. **(C)** Spatiotemporal concentrations (contour graph).

In 1952 Alan Turing published his seminal work "The Chemical Basis of Morphogenesis", which described how a simple diffusion-reaction system can result in the complex manifestation of stripes, spots and spirals in otherwise equilibrated systems (Turing, 1952). In his work, Turing demonstrated that coupling a reaction, such as degradation, to a diffusive process is sufficient to explain the mechanism of embryonic patterning during early stages of development. His work exemplified biology's capacity to harness the physical properties of diffusion to give rise to complex phenomena from a seemingly simple environment. Turing-like reaction-diffusion systems are omnipresent in biology, and comparable mechanisms of pattern formation have been described for Wnt/DKK in murine hair follicles (Sick, Reinker, Timmer, & Schlake, 2006), TGFβ/BMPs in skeletal limb patterning (Salmon, 2015) and RANKL/OPG in the formation of the trabecular bone architecture (Salmon, 2004). However, a much simpler system consisting of diffusion alone can encode similarly complex information within the spatiotemporal variations in ligand concentrations (Shankaran, Wiley, & Resat, 2007). As a diffusive wave front moves through a medium, the duration at which mediator concentrations are sustained above a certain threshold concentration can have implications for downstream signalling (Sklar et al., 1985; Zi et al., 2011). Signalling pathways that reject transient signals and preferentially respond to sustained signals have been called "persistence detectors" (Thurley, Wu, & Altschuler, 2018) or "dynamic filters"

(Toettcher, Weiner, & Lim, 2013), and have been demonstrated for intracellular Ras (Toettcher et al., 2013) and cAMP (Mangan, Zaslaver, & Alon, 2003), and intercellular IL-6 (Litvak et al., 2009) and epidermal growth factor (Kholodenko, 2006). We will see in **Chapter 7** how information about the nature of the mechanical stimulus is encoded within the spatiotemporal variations of ATP, which are shaped by extracellular reactions and diffusion to convey information about the position and magnitude of the mechanical stimulus to neighboring cells.

2.5.1.1 Solute transport in bone

Unlike soft tissue, the mineralized bone matrix restricts the transport of solutes and nutrients to and from the cells embedded within bone (Schaffler, Cheung, Majeska, & Kennedy, 2014). In addition to diffusion, solutes are also transported throughout the lacuna-canalicular system by convection, referring to the bulk movement of fluid (Piekarski & Munro, 1977). In bone, tracer studies have shown that solutes have a relative diffusivity of 55% - 80% of that observed in water (Wen Li, You, Schaffler, & Wang, 2009). Similar to water, diffusion through bone is dependent on the size and shape of the molecule (Wen Li et al., 2009), such that globular molecules diffuse more freely than linear molecules. Small solutes (<1 kDa), such as ATP, NO_2, O_2 and CO_2, diffuse relatively unrestricted through the mineralized bone matrix in the absence of mechanical loading (L. Wang, Ciani, Doty, & Fritton, 2004). Molecules larger than 70 kDa are excluded from bone, with or without mechanical loading, which has implications for the delivery of therapeutics such as antibodies which can be over 100 kDa (C. Lu, Liu, Liu, & Motchnik, 2013; Tami, Schaffler, & Knothe Tate, 2003). Cyclic intermittent loading increases solute transport through bone by approximately 30% compared to diffusion alone (Price, Zhou, Li, & Wang, 2011). Therefore, in the presence of mechanical loading, bone embedded osteocytes experience better perfusion which results in better distribution of signalling mediators thereby facilitating intercellular communication and the mechanotransductive response.

2.5.2 Extracellular metabolism of ATP and other purines

Ecto-nucleotidase play a central role in regulating purinergic transmission and salvaging extracellular purines. They metabolize extracellular ATP, effectively terminating residual P2 receptor signalling, and maintain low basal concentrations to ensure a low-noise signalling environment. Ecto-nucleotidases are evolutionarily conserved and consist of four classes: (*i*)

ectonucleoside triphosphate diphophohydrolases (NTPDase), (*ii*) ecto-5'-nucleotidase (eN), (*iii*) ecto-nucleotide pyrophosphatase/phosphodiesterases (NPP) and (*iv*) alkaline phosphatases (ALP) (Herbert Zimmermann, Zebisch, & Sträter, 2012) (**Fig 2-6**). This diversity allows ecto-nucleotidase substrates, metabolites and activities to vary substantially between sub-types. Substrates include (mono- or di-) nucleoside (mono-, di-, tri- or poly-) phosphates which can be hydrolyzed to nucleoside (mono- or di-) phosphates, nucleosides or inorganic phosphate or pyrophosphate. Among these substrates, ATP, ADP, UTP, UDP and UDP-glucose are the most relevant for purinergic signalling (Siegel, 1999). Some metabolites are recycled by the cell and rephosphorylated intracellularly (King, Ackley, Cass, Young, & Baldwin, 2006), while others participate in autocrine and paracrine signalling or are further metabolized. In general, ecto-nucleotidases are surface-bound enzymes which are anchored by glycosylphosphatidylinositol (GPI) or transmembrane helices. Subtypes which lack these anchors (eN, ALP, NPP2) or are attached to released microvesicles (eN, ALP, NTPDase1) can act over longer ranges and are also known as exo-nucleotidases. The catalytic activity of ecto-nucleotidases is dependent on substrate availability and various ions such as Ca^{2+}, Mg^{2+} and in some cases Zn^{2+}. Most ecto-nucleotidases have a micromolar affinity for ATP such that ATP metabolism at basal nanomolar levels is minimal (Yegutkin, 2008). Upon ATP release, these ecto-nucleotidases become more catalytically active and directly compete with nucleotide receptors by sequestering and hydrolyzing their substrates.

Genetic studies resulting in impaired metabolism of extracellular nucleotides have helped resolve the functions of specific ecto-nucleotidases, as well as associated pathological implications. For instance, eN is involved in generating extracellular adenosine, which signals through a family of P1 receptors [A_1, A_{2A}, A_{2B}, A_3 subtypes (B. B. Fredholm, AP, Jacobson, Klotz, & Linden, 2001)]. Mice lacking eN exhibit an osteopenic bone phenotype (Masahide Takedachi et al., 2012), impaired tubuloglomerular feedback (Castrop et al., 2004), altered thromboregulation and vascular inflammatory responses (Koszalka et al., 2004), and resistance to experimental metastasis (Stagg et al., 2011). Genetic studies of the NPP class of ecto-nucleotidase have demonstrated that NPP-deficient mice develop pathological crystal deposition in the joints, tumor metastasis and diabetes (Goding, Grobben, & Slegers, 2003). Surprisingly, double knockout of tissue nonspecific ALP (TNAP) and NPP1 resulted in a milder mineralization deficiency than observed in NPP1-

knockouts. This unexpected phenotype is explained by the reciprocal action of NPP1 and TNAP, such that NPP1 produces and TNAP hydrolyzes a common substrate PP_i (Anderson et al., 2005; Terkeltaub, 2006). Much of this reciprocity arises from differential substrate specificity and function. Thus, the differential expression of ecto-nucleotidases can drastically shape the balance of extracellular metabolites and associated (patho)physiology. Currently, the bulk of the evidence suggests that eN and NTPDases are the predominant ecto-nucleotidases involved in purinergic signalling (Herbert Zimmermann et al., 2012).

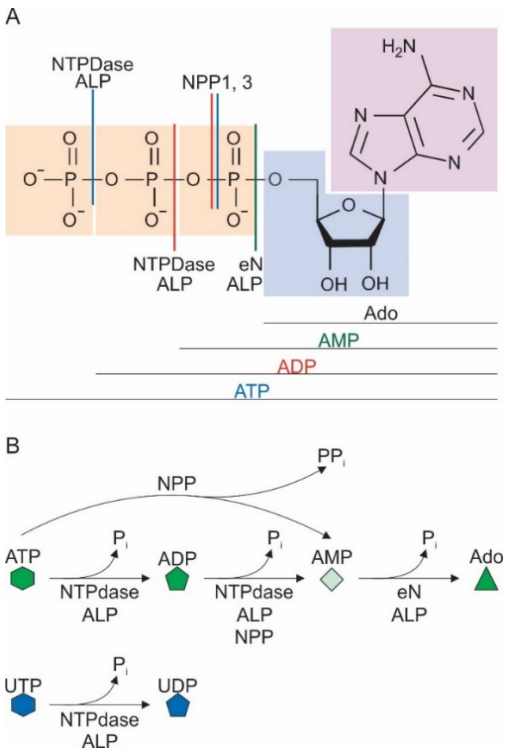

Figure 2-6. Extracellular nucleotide metabolism. **(A)** Structure of adenine nucleotides and corresponding metabolic cleavage sites. *Purple box*: nucleotide base (adenine), *blue box*: ribose sugar, *orange box*: phosphates, *blue/red/green vertical lines*: enzyme-specific cleavage sites for ATP, ADP and AMP, respectively.

(B) Extracellular metabolism of purinergic receptor-activating adenine- (*green*) and uridine- (*blue*) nucleotides. *Light green*: purinergic receptor inactive metabolite.

Ado: adenosine, ALP: alkaline phosphatases, eN: ecto-5'-nucleotidase, NPP: ecto-nucleotide pyrophosphatase/phosphodiesterases, NTPDase: ectonucleoside triphosphate diphophohydrolases, P_i: phosphate, PP_i: pyrophosphate.

2.5.2.1 ATP metabolism and metabolites in bone

In bone, the extracellular metabolism of ATP serves several functions, including termination of P2 receptor signalling and generation of various metabolites including adenosine, and inorganic phosphates P_i and pyrophosphates PP_i which regulate mineralization. Osteoblasts express NPP1-3 (Johnson et al., 2000; Orriss et al., 2007), eN [also known as CD73 (Bradaschia-Correa et al., 2017)], TNAP (Collin et al., 1992) and NTPdases 1-6 (Orriss, Key, Hajjawi, Millán, & Arnett, 2015), while osteoclasts express NPP1, 3 (Hajjawi et al., 2013) and NTPdase1, 3 (Hajjawi et al., 2013). P_i is necessary for mineralization, while PP_i is a potent inhibitor of mineralization (Fleisch & Bisaz, 1962), therefore the ratio of P_i to PP_i is central to the regulation of bone mineralization.

In bone, the predominant source of P_i is the TNAP-mediated hydrolysis of phosphate-containing substrates such as ATP and PP_i (Hamade, Azzar, Radisson, Buchet, & Roux, 2003). However, TNAP and NPP1 antagonise one another (Johnson et al., 2000) and carry out opposing functions, such that TNAP favors production of P_i (Hamade et al., 2003) and NPP1 favors production of PP_i (Orriss et al., 2007), thereby positioning these two extracellular enzymes as regulators of P_i/PP_i homeostasis in bone (Johnson et al., 2000). Their activities are sensitive to extracellular ATP levels such that when ATP is depleted, TNAP activity decreases while NPP activity increases (Orriss et al., 2013). Stimulation of P2X1, P2X3 or P2X7 in osteoblasts produced similar results (Orriss et al., 2013). $P2Y13^{-/-}$ osteoblasts also exhibit reduced TNAP activity (Ning Wang et al., 2013b). In osteoblasts, acidic conditions potentiate NPP1 activity (Orriss et al., 2015) but reduce TNAP expression (A. Brandao-Burch, Utting, Orriss, & Arnett, 2005), and similarly, NPP activity is increased in acidified osteoclasts (Hajjawi et al., 2013). In NPP1-deficient osteoclasts, flow-induced ATP release was reduced but the rate of ATP degradation was unaffected (Hajjawi et al., 2013). Surprisingly, little is known about the ATP metabolising capabilities of osteocytes, however ATP released from osteocytes is thought to contribute to the local pool of PP_i which regulates mineralization within the lacunae and canaliculae (I. Orriss & T. Arnett, 2012). Adenosine is another metabolite produced during the metabolism of extracellular ATP and is involved in P1-(A_{2B} subtype)-mediated osteoblast differentiation (Rao, Shih, Kang, Kabra, & Varghese, 2015; M. Takedachi et al., 2012; Trincavelli et al., 2014). In bone, adenosine is generated by eN and eN-deficient aging mice exhibit impaired bone formation and resorption along with reduced TNAP activity (Bradaschia-Correa et al., 2017).

2.6 Purinergic signalling

2.6.1 Overview of P2 receptor family

Purinergic receptors are among the most abundant and omnipresent receptors in biology which emerged early in our evolutionary history (M. P. Abbracchio, Burnstock, Verkhratsky, & Zimmermann, 2009). There are 7 ligand-gated P2X receptor (P2X1-7) and 8 G-protein coupled P2Y receptors (P2Y1,2,4,6,11-14) (**Fig 2-7**). There is also a class of G-protein coupled P1 receptors that are sensitive to adenosine, however they will not be the focus of my discussion. Despite there being 15 unique P2 receptors, few cells express each P2 receptor subtype, with osteoblasts among these selected few (I. Orriss & T. Arnett, 2012; Zippel et al., 2012a). Instead,

subsets of P2 receptors are expressed in a tissue-specific manner, thereby enabling P2 receptors to enact specialized functions. It remains debated whether each P2 receptor enacts a unique function, or whether various combinations of P2 receptors give rise to P2 receptor networks with unique integrated outcomes. The likely reality is that there is truth in both arguments.

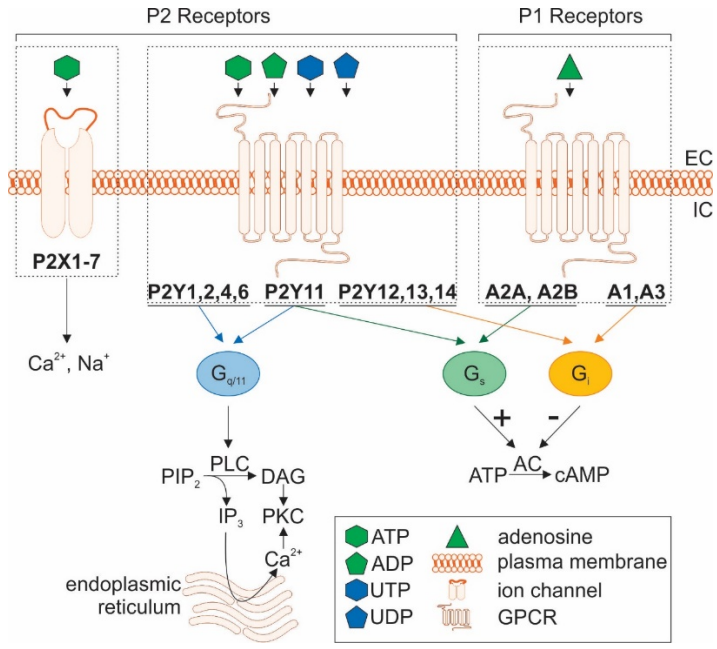

Figure 2-7. Purinergic receptor family. Purinergic receptors are classified as P2 and P1 receptors, of which P2 receptors are further subdivided into 7 P2X and 8 P2Y receptor subtypes. P2X receptors are ligand-gated cation channels. P2Yand P1 receptors are G-protein coupled receptors (GPCRs), with alpha subunit-specific ($G_{q/11}$, G_s, G_i) downstream signaling. AC: adenylyl cyclase, cAMP: cyclic adenosine monophosphate, DAG: diacylglycerol, EC: extracellular, IC: intracellular, IP_3: inositol 1,4,5-trisphosphate, PIP_2: Phosphatidylinositol 4,5-bisphosphate, PKC: Protein kinase C, PLC: Phospholipase C.

P2 receptor networks are sensitive to ATP concentrations over a million-fold range (S. Xing, Grol, Grutter, Dixon, & Komarova, 2016), however no single P2 receptor is sensitive to ATP concentrations over a thousand-fold range (S. Xing et al., 2016). This framework permits a single agonist, ATP, to stimulate different subsets of P2 receptors in a context-dependent manner. However, the study of P2 receptor network interactions is complicated by a lack of specific pharmacological tools. Consequently, studies have largely relied on the differential pharmacology of various P2 receptors, which brings me to mention that ATP is not the only P2 receptor agonist – although it is the most studied. While P2X receptors are sensitive to ATP only, P2Y receptors exhibit a range of subtype-specific sensitivities to ATP, ADP, UTP, UDP and UDP-glucose. P2 receptor-deficient mouse models have revealed that most strains of P2-deficient mice exhibit some bone abnormalities (I. Orriss et al., 2011). Genome association studies have also contributed to our understanding and have unveiled an additional layer of complexity related to the polymorphic nature of P2 receptors, such as P2Y2 (Anke Wesselius, Martijn J. L. Bours, Zanne Henriksen, et al., 2013) or P2X7 (Fuller, Stokes, Skarratt, Gu, & Wiley, 2009; Gartland et al., 2012). Despite

growing efforts to understand the role of P2 receptor signaling in bone, progress in this field has been slow due to the many complexities inherent to the P2 receptor family. Nonetheless, I consolidate and summarize our current understanding of P2 receptor physiology in bone in this section.

2.6.1.1 Ligand-gated P2X ion channels

P2X receptors are ATP-gated cation channels that form homomeric (P2X1-5, 7) and heteromeric receptors [e.g., P2X2/3 and P2X1/5 (Barrera, Ormond, Henderson, Murrell-Lagnado, & Edwardson, 2005; Torres, Egan, & Voigt, 1999)]. Each P2X subunit has two transmembrane domains linked by a 280 amino acid extracellular domain (Kaebisch, Schipper, Babczyk, & Tobiasch, 2015). To date, each P2X receptor subtype has been detected in osteoblasts (Gartland, 2012; Orriss et al., 2012; I. R. Orriss & T. R. Arnett, 2012) and osteoclasts (Gartland, 2012; Orriss, Burnstock, & Arnett, 2010; I. R. Orriss & T. R. Arnett, 2012) at the mRNA and protein level (**Table 2-1**).

P2X1. P2X1 expression is unaffected during the osteoblast differentiation (Orriss et al., 2012). In osteoblasts, P2X1 agonists inhibited mineralization without affecting collagen production or osteoblast proliferation (Orriss et al., 2012). P2X1-mediated effects were also associated with reduced ALP activity and increased NPP activity (Orriss et al., 2012), which translates to a decrease in the P_i to PP_i ratio. Consistent with these findings, P2X1 inhibitors promoted mineralization. The role of P2X1 in osteoclasts is unknown. Thus, the P2X1 receptor appears to negatively regulate mineralization.

P2X2. In osteoblasts, P2X2 expression peaks at day 8 of differentiation, but subsequently declines to undetectable levels (I. Orriss, G. Knight, S. Ranasinghe, G. Burnstock, & T. Arnett, 2006). In osteoclasts, ATP-mediated P2X2 signalling increased osteoclast resorption (Morrison, Turin, King, Burnstock, & Arnett, 1998). $P2X2^{-/-}$ mice exhibited an increase in bone mineral density, bone mineral content and weight at an early age, however this normalized with age suggesting that a compensatory mechanism exists (Orriss, Knight, Burnstock, & Arnett, 2005).

Table 2-1. P2X receptors in bone. Agonist and function of P2X receptors in osteoblasts and osteoclasts are summarized, alongside bone phenotype of knockout mice models. P2 receptors with no function/phenotype in bone are specified, otherwise non-studied fields are indicated by hyphen (-).

Type	Agonists	Osteoclasts	Osteoblasts	Knockout phenotype
X1	ATP	-	↓ mineralization, ↓ ALP, ↑ NPP ↓ P_i/P_{ii} ratio	-
X2	ATP	↑ resorption	Transiently expressed during differentiation -	↑ BMD in young mice, BMD normalizes in older mice
X3	ATP	-	Expression unaltered during differentiation	No phenotype
X4	ATP	↑ resorption	Upregulated in mature osteoblasts	-
X5	ATP	↑ maturation/ fusion	Transiently expressed during differentiation ↑ proliferation ↑ DNA synthesis, ↑ response to PDGF, IGF-1	Protected from inflammation-related bone loss
X6	ATP	-	Adipogenic lineage commitment	-
X7	ATP	↑ maturation/ fusion regulates resorption affects survival	↑ osteogenic differentiation ↑↓ mineralization ↑↓ survival	Pfizer model(Ke et al., 2003): ↓ BMD ↑ trabecular resorption ↓ periosteal formation GSK model(Chessell et al., 2005; Gartland, Buckley, Hipskind, et al., 2003): ↑ cortical thickness BMD unaffected

P2X3. In osteoblasts, P2X3 expression is unaltered during differentiation (Orriss et al., 2012; Zippel et al., 2012b). P2X3 agonists have no effect on osteoblast collagen production or proliferation, and through a differential pharmacological approach, the P2X3 receptor was concluded to not participate in mineralization (Orriss et al., 2012). Consistent with *in vitro* findings, $P2X3^{-/-}$ mice had not discernable bone phenotype (Orriss et al., 2005).

P2X4. The P2X4 receptor is upregulated in mature osteoblasts compared to proliferating pre-osteoblasts, however it is not involved in mineralization (Orriss et al., 2012). In osteoclasts, P2X4 has been proposed to stimulate bone resorption (Naemsch, Weidema, Sims, Underhill, & Dixon, 1999). Alveolar resorption was observed at the site of surgical incisions, and expression profiles of the marginal gingiva revealed significant P2X4 upregulation (Binderman et al., 2001). When ATP was hydrolyzed, or P2X4 activity was antagonised, alveolar bone loss was significantly reduced (Binderman et al., 2007). While the role of P2X4 in osteoblasts is unclear, P2X4 is possibly involved in stimulating osteoclast activity.

P2X5. P2X5 was reported to be upregulated in adipose-derived mesenchymal stem cells and downregulated in ecto-mesenchymal dental follicle cells at day 28 of osteogenic differentiation (Zippel et al., 2012b). However, in primary rat osteoblasts, P2X5 expression peaked at day 8 of differentiation and later declined to undetectable levels (I. Orriss et al., 2006). In osteoblasts, ATP-mediated P2X5 signalling increased DNA synthesis in a calcium-independent and MAPK-dependent manner (Nakamura et al., 2000). P2X5 activity also enhanced the mitogenic effects of growth factors PDGF and IGF-1 in osteoblasts (Nakamura et al., 2000). In osteoclasts, silencing P2X5 *in vitro* suppressed osteoclast maturation, suggesting that P2X5 expression is associated with osteoclast multinucleation (Kim et al., 2017). Contrary to expectations, $P2X5^{-/-}$ mice had a normal bone phenotype and the number of osteoblasts and osteoclasts on the bone surface was unaffected (Kim et al., 2017). Of interest, $P2X5^{-/-}$ mice were protected from inflammatory bone loss induced by lipopolysaccharides (Kim et al., 2017). P2X5 was concluded to mediate osteoclast maturation through inflammasome activation and IL-1β production (Kim et al., 2017). Therefore, P2X5 has a predominant role in osteoclast maturation.

P2X6. In primary rat osteoblasts, P2X6 expression transiently peaks at day 7 of differentiation (Orriss et al., 2012), and in human-derived adipose-derived mesenchymal stem cells, P2X6 expression is significantly downregulated by day 28 (Zippel et al., 2012b). Moreover, adipogenic differentiation was associated with an upregulation of P2X6 (Zippel et al., 2012b). These results suggest that P2X6 is involved in the early lineage commitment of mesenchymal stem cells (Zippel et al., 2012b). However, during *in vitro* vascular calcification of vascular smooth muscles cells (a process similar to skeletal mineralization), P2X6 expression was increased by nearly 60-fold

(Mackenzie, Zhu, Farquharson, & MacRae). Therefore, P2X6 is involved in osteogenic differentiation, however its functional role remains unclear.

P2X7. The P2X7 receptor has two features that distinguish it from other P2X receptors. First, it can form a dilated pore under permissive conditions (J. Li et al., 2005a). Second, P2X7 has a low affinity for ATP and is stimulated by high (millimolar) ATP concentrations, while other P2X receptors have a higher affinity for ATP and are stimulated by lower (micromolar) ATP concentrations (S. Xing et al., 2016). In primary rat osteoblasts, P2X7 expression was unaltered during differentiation, but was downregulated by day 15, coinciding with the maturation of osteoblasts (Orriss et al., 2012; I. Orriss et al., 2006). Similarly, P2X7 was downregulated by day 28 of osteogenic differentiation of adipose-derived mesenchymal stem cells (Zippel et al., 2012b).

In mesenchymal stem cells, shockwave or ATP application resulted in P2X7-dependent p38 MAPK activation, c-Fos and cJun mRNA transcription, increased ALP activity and osteocalcin production (Sun et al., 2013). Similarly, BzATP-mediated P2X7 signalling upregulated Runx-2 and osterix, and increased ALP activity in a Rho-kinase dependent manner (Noronha-Matos et al., 2014). These results demonstrate that P2X7 signalling in mesenchymal stem cells promotes osteogenic differentiation. P2X7 stimulation can lead to pore-mediated apoptosis (Gartland, Hipskind, Gallagher, & Bowler, 2001). P2X7 signalling also induces lysophosphatidic acid (LPA) production [via PLD and PLA_2 (N. Panupinthu et al., 2007)] which has been reported to be anti-apoptotic (Grey et al., 2002) and mitogenic (Grey et al., 2001). These inconsistent findings suggest that P2X7 can promote survival or apoptosis depending on the ATP stimulus intensity (Adinolfi, Amoroso, & Giuliani, 2012; Young et al., 2017). P2X7 also regulates prostaglandin signalling via PLA_2. PLA_2 is involved in the production of arachidonic acid which is a necessary substrate for COX to produce PGE_2. $P2X7^{-/-}$ primary osteoblasts and P2X7 inhibitor-treated MC3T3 osteoblasts failed to release PGE_2 in response to fluid shear (J. Li et al., 2005a). Consistent with these findings, COX inhibitors suppressed BzATP-enhanced mineralization in primary rat osteoblasts (Nattapon Panupinthu et al., 2008). However, when the role of P2X7 in mineralization were investigated using P2X7 agonists, mineralization was enhanced in some cases (Noronha-Matos et al., 2014; Nattapon Panupinthu et al., 2008; Sun et al., 2013), and suppressed in others (Orriss et al., 2012). Thus, P2X7 receptor signalling in osteoblasts initiates several downstream responses which regulate differentiation, proliferation, survival and apoptosis, and mineralization.

In osteoclast precursors, P2X7 knockdown reduced NFκB and PKC translocation resulting in downregulation of NFATc1, cathepsin K and TRAP (Armstrong, Pereverzev, Dixon, & Sims, 2009; Korcok, Raimundo, Ke, Sims, & Dixon, 2004). Similarly, various P2X7 antagonists were demonstrated to reduce, but not abolish, mature osteoclast formation (Agrawal et al., 2010). P2X7-deficient osteoclasts were functional although resorption was altered; Under normal culture conditions, $P2X7^{-/-}$ osteoclasts exhibited reduced resorption, but when conditions were modified (phenol-free media, heat inactivated charcoal stripped fetal bovine serum), osteoclast number and resorption was enhanced (Gartland, Buckley, Bowler, & Gallagher, 2003; Ning Wang, Agrawal, Jørgensen, & Gartland, 2018). When human osteoclasts were stimulated with P2X7 agonist BzATP or high concentrations of ATP, *in vitro* resorption was also enhanced (R. Hazama et al., 2009). At the same time, P2X7 stimulation (Miyazaki et al., 2012) and inhibition (Penolazzi et al., 2005) have both been reported to reduce survival, and with reduced survival there was less resorption. Thus, there is clear evidence that P2X7 is involved in osteoclast formation, resorption and survival, however, conflicting reports indicate that the role of P2X7 in osteoclast biology is complex, and possibly depends on the duration and magnitude of P2X7 stimulation (Agrawal & Gartland, 2015).

There have been conflicting reports of the $P2X7^{-/-}$ bone phenotype in mice. $P2X7^{-/-}$ mice generated by Pfizer exhibited reduced bone mineral content, which was associated with enhanced trabecular resorption and reduced periosteal formation (Ke et al., 2003). However, $P2X7^{-/-}$ mice generated by GlaxoSmithKline [GSK (Chessell et al., 2005)] exhibited increased cortical thickness with no effect on the bone mineral content (Gartland, Buckley, Hipskind, et al., 2003). The heterogeneous roles of P2X7 are believed to be related to the polymorphic nature of P2X7. There are over 30 non-synonymous amino-acid altering SNPs currently identified for the P2X7 receptor, which differentially alter P2X7 channel and pore function (Fuller et al., 2009). B6 mice harbour a mutation that replaces proline with leucine at position 451 (P451L) in the cytoplasmic tail of the P2X7 receptor (Adriouch et al., 2002) which has been associated with reduced responsiveness (Adriouch et al., 2002) and apoptosis (Le Stunff, Auger, Kanellopoulos, & Raymond, 2004). The Pfizer $P2X7^{-/-}$ mouse was maintained on a B6 × DBA/2 background while the GSK $P2X7^{-/-}$ mouse were maintained on a B6 background (Susanne Syberg et al., 2012). To investigate the influence of the P451 allele on the bone phenotype, mouse strains harbouring the wild allele (P451) have

been compared to strains harboring the mutated P451L allele. Strains with the P451 allele had a higher bone mineral content, stronger femurs and higher levels of bone resorption markers in their serum(Susanne Syberg et al., 2012). These findings suggest that the P2X7 polymorphisms underlie the inconsistencies between the $P2X7^{-/-}$ bone phenotypes and further suggest that P2X7-mediated signalling (P451 allele) promotes bone remodeling with a positive bone balance, similar to the effects of PTH (O'Brien et al., 2008). The cellular basis for these findings in osteoclasts and osteoblasts has yet to be resolved.

2.6.1.2 G-protein coupled P2Y receptors

P2Y receptors are GPCRs that are activated by various nucleotides including ATP, ADP, UTP, UDP and UDP-glucose and have been broadly implicated in bone cell function (**Table 2-2**).

P2Y1. The P2Y1 receptor is a $G_{q/11}$-coupled receptor (I. Orriss & T. Arnett, 2012) that is sensitive to ATP and ADP, and is expressed in osteoblasts (I. Orriss & T. Arnett, 2012; Orriss et al., 2012) and osteoclasts (Orriss et al., 2010). Osteogenic differentiation of adipose-derived mesenchymal stem cells, ecto-mesenchymal dental follicle cells and primary rat osteoblasts was consistently associated with the downregulation of P2Y1 (I. Orriss et al., 2006; Zippel et al., 2012a). Treatment of MC3T3 osteoblasts with P2Y1 antagonist MRS2179 reduced ALP activity following osteogenic induction, suggesting a role for P2Y1 in differentiation (Rodrigues-Ribeiro, Alvarenga, Calio, Paredes-Gamero, & Ferreira, 2015). In osteoblasts, P2Y1 is also involved in ultrasound-induced proliferation (Alvarenga et al., 2010) and modulation of the osteoblastic response to systematic factors (Bowler et al., 1999; Buckley et al., 2001). Specifically, P2Y1 potentiates the effects of PTH, shown by increased calcium signalling and c-fos upregulation (Bowler et al., 1999; Buckley et al., 2001). In osteoclasts, P2Y1 stimulation promotes osteoclast formation, calcium dissolution and resorption (Hoebertz, Mahendran, Burnstock, & Arnett, 2002; Hoebertz, Meghji, Burnstock, & Arnett, 2001). Unexpectedly, P2Y1-deficient mice exhibit reduced bone mineral density and trabecular number with no changes detected in cortical bone parameters (I. Orriss et al., 2011). This suggests that P2Y1 has a more substantial role in osteoblasts than in osteoclasts.

Table 2-2. P2Y receptors in bone. Agonist and function of P2Y receptors in osteoblasts and osteoclasts are summarized, alongside bone phenotype of knockout mice models. P2 receptors with no function/phenotype in bone are specified, otherwise non-studied fields are indicated by hyphen (-).

Subtype	Agonists	Osteoclasts	Osteoblasts	Knockout phenotype
Y1	ADP>ATP	↑ formation, ↑ resorption	↑ proliferation, ↑ ALP ↑ response to systemic factors	↓ BMD, ↓ trabecular number
Y2	ATP= UTP	↑ resorption	↓ mineralization, ↑ proliferation, ↑ Runx2	↑ BMD
Y4	UTP>ATP	No effect	-	-
Y6	UDP>>ATP	↑ formation, ↑ resorption, ↑ survival	Mineralization unaffected, ↑ proliferation, Regulates ALP, Associated with differentiation	↑ BMD
Y11	ATP	-	Adipogenic lineage commitment	-
Y12	ADP>>ATP	↑ adhesion, ↑ resorption	↑ proliferation, ↑ differentiation, ↑ survival, ↑ mineralization, ↑ ALP activity, collagen formation	Protected from bone loss related to arthritis, tumour growth and ovariectomy-induced osteoporosis
Y13	ADP>ATP	↑ formation	Osteogenic lineage commitment, ↑ mineralization, ↑ osterix, collagen 1 expression, ↑ ALP activity, ↓ RANKL/OPG, Regulates phosphate homeostasis	Age-dependent phenotype, ↓ bone turnover, ↓ osteoblasts/ osteoclasts on bone surface, ↑ osteogenic response to mechanical loading
Y14	UDP-glucose	Upregulated during differentiation ↑ formation	Downregulated during differentiation	-

P2Y2. The P2Y2 receptor is a $G_{q/11}$-coupled receptor (I. Orriss & T. Arnett, 2012) that is activated by ATP and UTP, and is expressed in osteoblasts (I. Orriss & T. Arnett, 2012; Orriss et al., 2012) and osteoclasts (Bowler, Littlewood-Evans, Bilbe, Gallagher, & Dixon, 1998; Orriss et al., 2010). Osteogenic differentiation of adipose-derived mesenchymal stem cells and ecto-mesenchymal dental follicle cells was consistently associated with the downregulation of P2Y2 (Zippel et al., 2012a), however differentiation and maturation of primary rat osteoblasts coincided with a sharp increase in P2Y2 expression (I. Orriss et al., 2006). In osteoblasts, P2Y2 mediates the intercellular purinergic calcium signalling (Jorgensen et al., 2000) and activates several intracellular signalling pathways, including PKC-/PLC-dependent P38 mitogen-activated protein kinase [p38 MAPK (S. Katz, Boland, & Santillán, 2006)], Egr-1 [transcription regulator responsible for activating Col1A2 (Pines et al., 2003)], Src (S. Katz, Boland, & Santillán, 2006), cJun NH_2-terminal protein kinase [JNK (I. Orriss & T. Arnett, 2012)] and Runx2 (Costessi et al., 2005). UTP and ATP mediated P2Y2 signalling inhibits mineralization in osteoblasts (Hoebertz et al., 2002) and promotes proliferation (Sebastián Katz, Ayala, Santillán, & Boland, 2011). In osteoclasts, P2Y2 is expressed at low levels (IR. Orriss et al., 2011) and was originally thought to have no effect on resorption (Hoebertz et al., 2001); however, recently $P2Y2^{-/-}$ osteoclasts were shown to exhibit a 65% reduction in resorptive activity (Orriss et al., 2017). Consistent with its inhibitory effects on mineralization and resorption *in vitro*, P2Y2-deficient mice exhibit increased trabecular and cortical bone mass (Orriss et al., 2017; I. Orriss et al., 2011).

P2Y4. The P2Y4 receptor is a $G_{q/11}$-coupled receptor (I. Orriss & T. Arnett, 2012) that is sensitive to ATP an UTP and is expressed in osteoblasts (Orriss et al., 2012) and osteoclasts (Orriss et al., 2010). In primary rat osteoblasts, P2Y4 was transiently upregulated between days 8-13 of differentiation (I. Orriss et al., 2006), and in adipose-derived mesenchymal stem cells and ecto-mesenchymal dental follicle cells P2Y4 was downregulated by day 28 of osteogenic differentiation (Zippel et al., 2012a). Silencing P2Y4 with siRNA did not affect osteogenic gene expression, suggesting P2Y4 is not involved in osteoblastogenesis (Wenkai Li et al., 2016). Lack of sensitivity of osteoclasts to UTP was used to dismiss the involvement of P2Y4 (Jorgensen et al., 2002); however, this lack of sensitivity to UTP is surprising given the involvement of UTP-sensitive P2Y2 in osteoclasts (Orriss et al., 2017). Taken together, there is little evidence to support a role for P2Y4 in bone.

P2Y6. The P2Y6 receptor is a $G_{q/11}$-coupled receptor (I. Orriss & T. Arnett, 2012) that is predominantly sensitive to UDP and is expressed in osteoblasts (Orriss et al., 2012) and osteoclasts (Orriss et al., 2010; IR. Orriss et al., 2011). In primary rat osteoblasts, P2Y6 expression was similar to P2Y4 and was transiently upregulated between days 8-13 of differentiation (I. Orriss et al., 2006). In osteoblasts, UDP-mediated P2Y6 signalling either increased or had not effect on ALP activity (Ayala-Peña, Scolaro, & Santillán, 2013; Noronha-Matos et al., 2012), and did not affect mineralization (Ayala-Peña et al., 2013). P2Y6-agonist UDP also promoted proliferation in osteoblasts (Alvarenga et al., 2010). Together these data implicate P2Y6 in osteogenic differentiation and proliferation. P2Y6 is also involved in osteoclast physiology. UDP-induced translocation and activation of NFκB, a factor regulating osteoclastogenesis, in immature and mature osteoclasts (Korcok, Raimundo, Du, Sims, & Dixon, 2005). Similarly, P2Y6 activation stimulated osteoclast formation and resorption (IR. Orriss et al., 2011). P2Y6 also promotes osteoclast survival, since P2Y6 activation protected osteoclasts from apoptosis induced by TNFα (Korcok et al., 2005). Consistent with these findings, $P2Y6^{-/-}$ mice have an increased bone mass due to reduced P2Y6-dependent osteoclast function (I. Orriss et al., 2011).

P2Y11. The P2Y11 receptor is a $G_{q/11}$ and G_s-coupled receptor (I. Orriss & T. Arnett, 2012) that is sensitive to ATP, and is expressed in human osteoclasts (Orriss et al., 2010) and osteoblasts (Orriss et al., 2012; Zippel et al., 2012a). This is the only P2 receptor capable of producing cAMP via the G_s-adenylyl cyclase pathway (Dreisig & Kornum, 2016). P2Y11 is significantly elevated during adipogenic differentiation of adipose-derived mesenchymal stem cells and ecto-mesenchymal dental follicle cells, but unaltered during osteogenic differentiation (Zippel et al., 2012a), suggesting that P2Y11 plays a role in adipocytes. Due to a lack of *P2RY11* orthologue in rodents (Dreisig & Kornum, 2016), no functional studies have been performed to investigate the role of the P2Y11 receptor in bone.

P2Y12. The P2Y12 receptor is a G_i-coupled receptor (I. Orriss & T. Arnett, 2012) that is predominantly sensitive to ADP and is expressed in osteoblasts (Orriss et al., 2012) and osteoclasts (Orriss et al., 2010). P2Y12 is significantly upregulated during osteoblast and osteoclast differentiation (S. Syberg et al., 2012). In osteoblasts, P2Y12 inhibition reduced proliferation, differentiation, mineralization, ALP activity, collagen formation and viability (Mediero et al., 2016; S. Syberg et al., 2012). In $P2Y12^{-/-}$ osteoclasts, differentiation markers were normal but

resorption was reduced (Su et al., 2012). P2Y12 activity was associated with enhanced osteoclast adhesion and resorption (Su et al., 2012). Clopidogrel, a FDA-approved P2Y12 receptor antagonist (Damman, Woudstra, Kuijt, de Winter, & James, 2012), has been used to study P2Y12 function in bone, however results have been inconsistent, possibly due to age- or dose-dependent effects. Syberg et al. treated 20-week-old ovariectomized mice with 1 mg/kg/day clopidorgel and reported reduced trabecular and cortical bone volumes in the tibia and femur (S. Syberg et al., 2012). In contrast, Su et al. treated 6 to 10-week-old mice with 30 mg/kg/day clopidorgel and found that mice were protected against pathological osteolysis related to arthritis, tumour growth, and ovariectomy-induced osteoporosis (Su et al., 2012). A Dutch cohort study examining the effects of clopidogrel over a 10-year period showed that recommended doses of clopidogrel [75 mg/day (Jiang, Samant, Lesko, & Schmidt, 2015)] were associated with a 50% increased risk of fracture compared to the control group (Jorgensen, Grove, Schwarz, & Vestergaard, 2012). However, suboptimal doses of clopidogrel (<1% daily dose) were associated with decreased fracture risk (Jorgensen et al., 2012), contrary to what would be expected based on the animal studies mentioned above. Thus, P2Y12 appears to be involved in promoting osteoblast and osteoclast function, however the relative contribution of P2Y12 in either cell type may govern the tissue-level phenotype associated with P2Y12 deficiency.

P2Y13. The P2Y13 receptor is a G_i-coupled receptor (I. Orriss & T. Arnett, 2012) that is predominantly sensitive to ADP and is expressed in osteoblasts (Orriss et al., 2012) and osteoclasts (Alvarenga et al., 2010; Orriss et al., 2010). P2Y13 signalling facilitates mesenchymal stem cell commitment to the osteogenic lineage and is associated with expression of ALP, osterix and collagen type-I (Biver et al., 2013b). $P2Y13^{-/-}$ osteoblasts exhibited down-regulated RhoA/Rock1 pathway and reduced RANKL/OPG ratio (N. Wang et al., 2012), and accumulated extracellular ATP due to reduced ALP activity (N. Wang et al., 2013). Although $P2Y13^{-/-}$ osteoblast proliferation was unaffected, *in vitro* mineralization was reduced by almost 50% (N. Wang et al., 2012). $P2Y13^{-/-}$ osteoclast differentiation was impaired, but the amount of resorption per functional osteoclast was unaffected (N. Wang et al., 2012). Accordingly, $P2Y13^{-/-}$ mice exhibit a significant decrease in bone turnover (Biver et al., 2013a; Ning Wang et al., 2012), associated with a reduction in osteoblasts and osteoclasts present on the bone surface (Biver et al., 2013a). Another group reported that the bone-phenotype was age-dependent, such that young 4-week-old $P2Y13^{-/-}$ mice

had higher bone mass than wild-types (associated with 35% more osteoblasts and 73% fewer osteoclasts), but older >10-week-old P2Y13$^{-/-}$ mice had lower bone mass [associated with 22% fewer osteoblasts (N. Wang, Robaye, Gossiel, Boeynaems, & Gartland, 2014)]. These changes correlated with serum phosphorus and FGF-23 levels, which were higher in young P2Y13$^{-/-}$ mice and unchanged in mature P2Y13$^{-/-}$ mice, consistent with the participation of P2Y13 in phosphate homeostasis (N. Wang et al., 2014; N. Wang et al., 2013). Mechanically-loaded P2Y13$^{-/-}$ mice showed a stronger osteogenic response compared to wild-type littermates, which coincided with reduced ALP activity (N. Wang et al., 2014; N. Wang et al., 2013). These results demonstrate that P2Y13 regulates differentiation and maturation of bone cells, and that it influences systemic phosphate homeostasis.

P2Y14. The P2Y14 receptor is a G_i-coupled receptor (I. Orriss & T. Arnett, 2012) that is activated by various UDP-sugars, such as UDP-glucose (Eduardo R. Lazarowski & Harden, 2015), and is expressed in osteoblasts (Orriss et al., 2012) and osteoclasts (Alvarenga et al., 2010; Orriss et al., 2010). Osteogenic differentiation of adipose-derived mesenchymal stem cells and ecto-mesenchymal dental follicle cells was consistently associated with the downregulation of P2Y14 (Zippel et al., 2012a). In osteoclasts, P2Y14 expression was significantly upregulated by RANKL in a P38 MAPK-dependent manner (S. A. Lee, Park, & Lee, 2013). Subsequent treatment with UDP-glucose promoted RANKL-induced osteoclastogenesis (Kook, Cho, Lee, & Lee, 2013; S. A. Lee et al., 2013) and when P2Y14 was knocked down, osteoclast formation was inhibited (S. A. Lee et al., 2013). Thus, P2Y14 is downregulated during osteoblastogenesis and upregulated during osteoclastogenesis, suggesting that it is predominantly involved in mediating osteoclast differentiation. The bone phenotype has not been examined in P2Y14$^{-/-}$ mice, however *in vitro* results predict an increase in bone mass due to defective osteoclast differentiation.

2.6.2 P2 receptors in osteocyte biology

Very little is known about purinergic signalling in osteocytes, owing to their inconvenient location in bone and difficulty to isolate. However, mechanically-stimulated ATP release from MLO-Y4 osteocytes has been reported, and mRNA for P2X1-3, 5, 7 and protein for P2X2, 7 have been detected (Tina M. Kringelbach et al., 2015). Moreover, based on the known expression of P2Y receptors in mature osteoblasts, it can be reasonably inferred that P2Y receptors are involved in

osteocyte biology. Recently, direct evidence of P2 receptor signalling in osteocytes was demonstrated using a pharmacological P2 receptor inhibitor to block *in situ* intracellular calcium oscillations that were recorded in osteocytes in intact mouse long bones exposed to dynamic mechanical loading (Jing et al., 2014). Beyond this, the functional role of P2 receptors in osteocytes remains elusive.

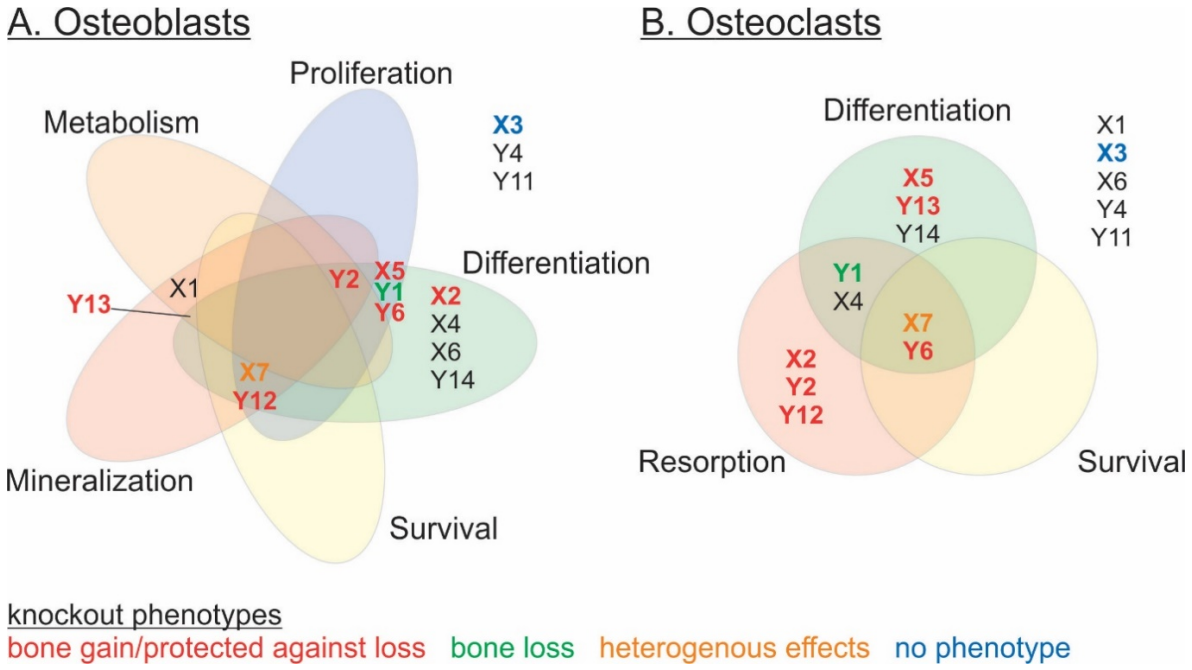

Figure 2-8. **Role of P2 receptors in bone**. **(A, B)** Venn diagrams show role of P2 receptors in osteoblasts **(A)** and osteoclasts **(B)**. P2 receptor knockout animal models exhibited bone gain (*red label*), bone loss (*green label*), heterogenous phenotype (*orange label*), no phenotype (*blue label*), or have not been studied (*black label*).

2.6.3 The role of nucleotides in bone

So, what do extracellular nucleotides accomplish in bone? Some P2 receptors appear to promote bone formation, while others appear to be favor bone loss, but the net outcome following stimulation by ATP is not evident from considering single receptor functions. *In vitro*, every P2 receptor studied in osteoclasts promotes either osteoclast formation or resorption. In osteoblasts, P2 receptor functions are more heterogenous, promoting proliferation, differentiation and survival in some cases, and inhibiting mineralization, production of osteoclastogenic factors, and survival in others (**Fig 2-8**). A complete knockout of the P2 receptor network has not been attempted, however broad P2R agonists (e.g., ATP) and antagonists (e.g., suramin, PPADS), as well as

exogenously added ecto-nucleotidases (e.g., apyrase) have been used to probe P2R network-level functions. Nucleotides induce dose-dependent calcium responses in osteoblasts (I. R. Orriss, G. E. Knight, S. Ranasinghe, G. Burnstock, & T. R. Arnett, 2006; S. Xing et al., 2016) and osteoclasts (Mackay, Mikolajewicz, Komarova, & Khadra, 2016) over a million-fold range, with the upper limit of sensitivity approaching that of intracellular nucleotide concentrations.

When applied to osteoblast cultures, low concentrations of ATP and UTP (1-10 μM) inhibited bone mineralization without affecting matrix deposition (Hoebertz et al., 2002; Orriss et al., 2007), while higher ATP concentrations (100 μM) promoted mineralization (Ayala-Peña et al., 2013) and ADP and UDP (10 μM) had no effect (I. R. Orriss et al., 2006). Thus, the effects of ATP on mineralization appear to be biphasic in osteoblasts. ATP (10-100 μM) also had an effect on osteoblast differentiation, marked by upregulation of ALP, BMP-2, -4 and 5, and BSP (Ayala-Peña et al., 2013), and Run2x DNA binding via PKC/ERK1/2-dependent mechanisms (Costessi et al., 2005; S. Katz, Boland, & Santillan, 2006). When extracellular ATP was depleted by apyrase, osteoblast numbers were reduced by ~25% within 72 hours, highlighting the role of basal extracellular ATP in promoting proliferation (Orriss et al., 2013). ATP stimulation upregulated osteoclastogenic factor RANKL [2.5-100 μM ATP (Buckley, Hipskind, Gartland, Bowler, & Gallagher, 2002)] and interleukin-6 [10-100 μM ATP (Ihara, Hirukawa, Goto, & Togari, 2005)] and stimulated PGE_2 release [0.1-1 mM ATP (D. C. Genetos et al., 2005)].

In osteoclasts, the effects of ATP are biphasic, promoting osteoclast formation and resorption at low concentrations (0.2-2 μM) and inhibiting formation at higher concentrations (20-200 μM)(Bowler et al., 1998). ADP (0.02-2 μM) is also osteolytic (Hoebertz, Arnett, & Burnstock, 2003; Hoebertz et al., 2001), and UDP (1-100 μM) promoted survival and stimulated formation and resorption (Korcok et al., 2005; IR. Orriss et al., 2011), while UTP (10 μM) reportedly has no effect (Bowler et al., 1998).

The surveyed studies demonstrate that the full spectrum of P2 receptor effects can be observed using non-specific agonists (e.g., ATP, ADP) of the P2 receptor network, with a particularly interesting biphasic ATP-mediated response at low and high concentrations in osteoblasts and osteoclasts. Based on these trends, we can infer that the P2 receptor network mediates opposing effects depending on the extent of P2 receptor stimulation, which is governed by the amount of ATP released by mechanical or other stimuli. Currently, many studies focus on single P2 receptors

at a time and use a limited range of nucleotide doses to understand P2 receptor function. These outcomes demonstrate the non-trivial nature of the P2 receptor network and emphasizes the necessity to systematically investigate the full spectrum of effects that the P2 receptor network is capable of mediating.

2.7 Challenges in studying P2 receptor physiology

The study of purinergic signalling is complicated by our lack of control over processes that regulate extracellular ATP during standard experimental protocols. Media changes, cell washes and centrifugation are part of the routine cell culture procedure, and inevitably lead to ATP release and purinergic signalling. Control cultures are subject to the same purinergic consequences; thus, it is notoriously difficult to control for these sources of variability and to isolate the effects of purinergic signalling from other phenomena being studied, especially if downstream effect pathways are convergent. Additionally, the temporal sequence of cellular events are difficult to deconvolute since it is unclear whether the observed effects are short- or long-term manifestations of purinergic signalling (Geoffrey Burnstock & Gillian E. Knight, 2017). The P2 receptor network is also highly dynamic, and P2 receptor expression can change according to passage number (Crain, Nikodemova, & Watters, 2009), differentiation state (Chamley, Campbell, & Burnstock, 1974) and duration in culture (Turner, Weisman, & Camden, 1997). Despite these overwhelming concerns, there is little to be done to circumvent these limitations given our current understanding of P2 receptor signalling.

Another challenge in studying purinergic signalling is that different model systems express different subsets of P2 receptors. I briefly mentioned that each P2 receptor has been found expressed in osteoblasts. However, these data reflect the aggregate expression profile across all osteoblast models studied (I. Orriss & T. Arnett, 2012; Orriss et al., 2010). Expression profiles in most models are inconsistent with expression profiles reported by different research groups. To handle these inconsistencies, a systematic review and meta-analysis will be needed to map the species- and differentiation-state dependent expressions of these P2 receptors. Experimentally, it may also be informative to determine the extent of heterogeneity of P2 receptor expression within cellular populations. This can be accomplished using single-cell RNA-seq to obtain single-cell gene expression profiles (Efroni, Ip, Nawy, Mello, & Birnbaum, 2015), or similarly using

microfluidics assays to obtain single cell protein expression profiles (James Magness et al., 2017). These approaches will also help address the largely unanswered question of whether these receptors are to some extent redundant, or whether certain subtypes are necessary to carry out their prescribed functions.

2.8 Targeting P2 receptors therapeutically

Bone diseases related to bone metabolism, pain and degeneration has been associated with various P2 receptors. To date there are no approved P2 receptor drugs for treatment of musculoskeletal disease, however several lines of investigation have produced promising results with anticipated clinical applications in the future.

2.8.1 P2 receptors and skeletal disease

Osteoporosis. Osteoporosis is a bone disease characterized by a disbalance of bone remodeling processes (i.e., resorption exceeds formation) that leads to lower bone mass and higher fracture risk and is associated with chronic pain, disability and a decline in quality of life (Kling, Clarke, & Sandhu, 2014). Several clinical studies have demonstrated the P2X7-associated SNPs are linked to increased fracture risk, lower bone mineral density and increased bone loss in humans (Jørgensen, Adinolfi, Orriss, & Schwarz, 2013; Ohlendorff et al., 2007), as well as periprosthetic osteolysis (Mrazek, Gallo, Stahelova, & Petrek, 2010). The P2Y2 receptor is also polymorphic, with at least 4 nonsynonymous SNPs identified (Wesselius et al., 2011). SNPs of P2Y2, along with P2X4, were associated with lower BMD and heightened risk of osteoporosis in a cohort of Dutch fracture patients (A. Wesselius et al., 2013; Anke Wesselius, Martijn J. L. Bours, Niklas R. Jørgensen, et al., 2013). Thus, P2 receptor SNPs associated with osteoporosis represent potential screening tools for early detection of individuals at risk of osteoporosis. P2 receptors associated with bone loss have also been considered as therapeutic strategies for osteoporosis. P2Y2 (I. Orriss et al., 2011) and P2Y6 (I. Orriss et al., 2011) knockout mice were associated with increases in BMD, due to elevated mineralization and reduced resorption, respectively. As mentioned earlier, a Dutch cohort study also suggested that low doses of Clopidogrel, a P2Y12 antagonist, may reduce fracture risk (Jorgensen et al., 2012), although the exact mechanisms involved need to be investigated since these findings contradict animal studies (Ning Wang & Gartland, 2014). Finally, P2Y13-deficient mice exhibit enhanced osteogenic responses to mechanical loading (N. Wang et

al., 2014; N. Wang et al., 2013). Thus, these findings suggest that P2Y2, P2Y6 or P2Y12, and P2Y13 may be therapeutically targeted in combination with exercise, thus serving as a possible way of treating osteoporosis (Ning Wang & Gartland, 2014).

Rheumatoid arthritis. Rheumatoid arthritis is a chronic inflammatory autoimmune disease characterized by joint swelling, bone erosion, joint deformation and pain (Angelotti et al., 2017). Rheumatoid arthritis -associated articular bone erosion is the major cause of disability of patients, resulting from the formation of synovial osteoclasts (Schett, 2006). P2X7-associated SNPs have been associated with the pathogenesis of rheumatoid arthritis (Al-Shukaili et al., 2011). In synoviocytes, P2X7 activity results in the release of proinflammatory cytokines [i.e., IL-1β, IL-6 and prostaglandins (Baroja-Mazo & Pelegrin, 2012; Portales-Cervantes et al., 2012)]. P2X7 antagonism was shown to reduce the pathogenesis of collagen-induced arthritis in mice (Ardissone et al., 2011). However, initial efforts to exploit P2X7 clinically to treat rheumatoid arthritis failed in phase IIb/III trials and a new generation of P2X7 antagonists with better "drug-like" properties are currently in the early stages of testing (Baroja-Mazo & Pelegrin, 2012). Bisphosphonates are a class of antiresorptive drugs used to treat osteoporosis which are also anti-inflammatory (Maksymowych, 2002) and have been shown to block proinflammatory IL-1β release from macrophages (Pennanen, Lapinjoki, Urtti, & Monkkonen, 1995). Thus, the combination of P2X7 antagonists and bisphosphonates has been proposed as a possible therapeutic strategy for rheumatoid arthritis. P2X5-deficient mouse models were protected from inflammatory bone loss (Kim et al., 2017) suggesting that P2X5 antagonism may also offer some protection against rheumatoid arthritis-associated bone erosion.

Osteoarthritis. Osteoarthritis is a degenerative joint disease characterized by the deterioration of articular cartilage leading to pain and disability (Van Manen, Nace, & Mont, 2012). Our understanding of the role of P2 receptors in osteoarthritis is limited, however given the role of P2 receptors in inflammation, P2 receptors may serve as potential therapeutic avenue of interest in the future (Ning Wang & Gartland, 2014).

2.8.2 P2 receptor drug-development and clinical trials

It has been over 20 years since the first P2 receptors were cloned, and since then, interest in the physiological roles and therapeutic potential has surged. Here I briefly describe current challenges, strategies, and progress in the development of P2 receptor therapeutics.

Translational challenges. The central challenge in P2 receptor drug development is identifying drug candidates with favorable absorption, distribution, metabolism and excretion properties (Conroy, Kindon, Kellam, & Stocks, 2016). P2 receptors are particularly nontrivial to target, owing to the widespread distribution of P2 receptor in the body, their polymorphic nature, and countless ATP recognition sites. Moreover, P2 receptor activities are modulated by dozens of natural substances derived from various plants, animals and microorganisms, which may possibly serve as lead compounds in drug discovery, but also as factors that need consideration in normal P2 receptor physiology (Bartlett, Stokes, & Sluyter, 2014; Faria, Ferreira, Bezerra, Frutuoso, & Alves, 2012). Overall, the future of purinergic therapeutics is promising, but remains unpredictable (Geoffrey Burnstock & Volonté, 2012).

Drug development strategies. Several strategies to identify P2 receptor drug candidates are being used. High-throughput methods have been used to identify lead compounds with satisfactory receptor affinity and selectivity for subsequent optimization. In the context of P2 receptors, $[Ca^{2+}]_i$ elevations are most commonly used as a readout of P2 receptor activation. Following the identification of lead compounds, optimization strategies focus on improving physicochemical properties (e.g., solubility, stability) before proceeding to preclinical and clinical testing. A more direct approach to identifying lead compounds is based on elucidating the target (P2 receptor) structure and comparing its binding sites to a database of lead compounds ranked according to predicted binding and selectivity (Ferreira, Dos Santos, Oliva, & Andricopulo, 2015). To date, our understanding of P2 receptor structure is largely based on X-ray crystallography of ligand-bound P2Y1 (Zhang et al., 2015) and P2Y12 receptors (J. Zhang et al., 2014; K. Zhang et al., 2014), and close- and open-state zebrafish P2X4 receptors (Hattori & Gouaux, 2012; Kawate, Michel, Birdsong, & Gouaux, 2009). These structural data are further complemented by over 15 years of functional mutagenesis studies (Evans, 2010). Similarities drawn between established crystal structures and structures of other P2 receptors allows drugs to be developed with region-specific targets, which can be advantageous. For instance, P2X receptors can be targeted at the ATP binding

pocket, transmembrane region or permeation pathway (North & Jarvis, 2013). Nucleotide analogs are usually the starting lead compounds when targeting the ATP-binding pocket, however these are difficult to work with due to multiple (ATP-) recognition sites. Alternatively, the transmembrane region may be allosterically regulated or antagonized, or the permeation path may by directly blocked. In P2X receptors, the permeation path offers a unique therapeutic target since two open states have been described, suggesting that subsets of receptor-related functions may be selectively targeted (Khadra et al., 2013; Rokic & Stojilkovic, 2013). Thus, using a variety of high-throughput and structure-based approaches, P2 receptor-targeting compounds are now rapidly progressing along the drug development pipeline, with several ongoing preclinical and clinical trials.

Clinical trials. There have only been four FDA-approved P2 receptor antagonists in the last 20 years, all targeting the P2Y12 receptor and classified as antithrombotic drugs (Conroy et al., 2016). However, major efforts have been made to develop P2 receptor antagonists for other pathologies. The P2X7 receptor antagonists AZD9056 and CE-224,535 were separated evaluated in phase II trials for the treatment of rheumatoid arthritis, however they were concluded to not be significantly efficacious, possibly due to P2X7 genotype-dependent antagonism (Keystone et al., 2011; Stock et al., 2012). Fortunately, AZD9056 and CE-224,535 were demonstrated to be safe and well tolerated in patients, indicating that P2X7 may be safely targeted in other pathologies, including a variety of implicated neurological diseases and injuries, inflammatory conditions and musculoskeletal disorders (Bartlett et al., 2014). The P2X3 antagonist AF-219 has also completed phase II trials and was shown to reduce coughing frequency by 75% in patients with treatment-resistant chronic cough caused by neuronal hypersensitivity (Abdulqawi et al., 2015; Geoffrey Burnstock, 2009). AF-219, named Gefapixant (-pixant being the suffix assigned to P2X drugs), is now proceeding to phase III trials (recruitment began in February 2018) which are expected to be complete by January 2021. A phase II trial of AF-219 in women with interstitial cystitis/bladder pain syndrome has also proven promising, with patients reporting improved pain scores and reduced urinary urgency (Moldwin et al., 2015). Thus, P2 receptor drugs are slowly entering the realm of clinical medicine, however no drugs have yet been approved for use in musculoskeletal disease. Several P2 receptors have been identified as possible targets for the treatment of osteoporosis and arthritis, including P2X7, P2Y6, P2Y12 and P2Y13 (Ning Wang & Gartland,

2014). Mechanistic studies are still necessary to elucidate the mechanisms of P2 receptor involvement in these pathologies, however early preclinical work can begin to probe how emerging drug-like P2X7 antagonists and available P2Y12 antagonists can be used to treat these conditions. Unfortunately, few P2Y6 antagonists are available and those that have been used to probe P2Y6 function have unfavorable drug-like properties (Conroy et al., 2016). Similarly, current P2Y13 antagonists require further optimization before clinical utility can be considered (Conroy et al., 2016). Nonetheless, the therapeutic potential of targeting P2 receptors in musculoskeletal disease is supported, and the future of purinergics in medicine is anticipated.

2.9 Summary

In the past 25 years, there has been a surge in interest in the purinergic field. The purinergic synapse, if you will, consists of "pre-synaptic" ATP release, "inter-synaptic" extracellular diffusion and degradation, and "post-synaptic" signaling via P2 receptors. To date, five main routes of mechanically-stimulated non-lytic ATP release have been identified, including vesicles, pannexins, connexins, VRACs and maxi-anion channels. In osteoblasts and osteocytes, the vesicular route has been implicated in mechanically-stimulated ATP release. Additionally, ATP can be released through injury. Once in the extracellular space, ATP diffuses and is concurrently metabolized by extracellular ecto-nucleotidases which serve to regulate P2 receptor signaling and to generate nucleotide metabolites, such as P_i and PP_i. ATP and other P2 agonists (e.g., ADP, UTP, UDP-glucose) then bind and signal through a network of P2 receptors. The P2 receptor family consists of fifteen members, eight of which are G-protein coupled P2Y receptors and seven are ionotropic P2X receptors. To date, each P2 receptor subtype has been shown to be express in osteoblasts and osteocytes, with a diverse plethora of functional outcomes shown to modulate many of the mediators involved in mechanotransduction (**Chapter 1**). Using specific P2 receptor agonists and antagonists, as well as genetic interventions, individual P2 receptor functions in osteoblasts and osteoclasts have been described. Moreover, studies that broadly stimulate of the P2 receptor network using non-specific agonists (e.g. ATP) have provided insights into how individual P2 receptors cooperate at the network level. While there remain several challenges in understanding the complexities of P2 receptor physiology in bone, P2 receptors have been identified as promising therapeutic targets in several bone diseases including osteoporosis, rheumatoid arthritis and osteoarthritis.

2.10 References

Abbracchio, M. P., & Burnstock, G. (1994). Purinoceptors: are there families of P2X and P2Y purinoceptors? *Pharmacology & therapeutics, 64*(3), 445-475.

Abbracchio, M. P., Burnstock, G., Verkhratsky, A., & Zimmermann, H. (2009). Purinergic signalling in the nervous system: an overview. *Trends Neurosci, 32*(1), 19-29. doi:10.1016/j.tins.2008.10.001

Abdulqawi, R., Dockry, R., Holt, K., Layton, G., McCarthy, B. G., Ford, A. P., & Smith, J. A. (2015). P2X3 receptor antagonist (AF-219) in refractory chronic cough: a randomised, double-blind, placebo-controlled phase 2 study. *The Lancet, 385*(9974), 1198-1205.

Adinolfi, E., Amoroso, F., & Giuliani, A. L. (2012). P2X7 Receptor Function in Bone-Related Cancer. *J Osteoporos, 2012*, 637863. doi:10.1155/2012/637863

Adriouch, S., Dox, C., Welge, V., Seman, M., Koch-Nolte, F., & Haag, F. (2002). Cutting edge: a natural P451L mutation in the cytoplasmic domain impairs the function of the mouse P2X7 receptor. *J Immunol, 169*(8), 4108-4112.

Agrawal, A., Buckley, K. A., Bowers, K., Furber, M., Gallagher, J. A., Gartland, A., . . . Gartland, A. (2010). The effects of P2X7 receptor antagonists on the formation and function of human osteoclasts in vitro. *Purinergic Signalling, 6*, 307-315.

Agrawal, A., & Gartland, A. (2015). P2X7 receptors: role in bone cell formation and function. *J Mol Endocrinol, 54*(2), R75-88. doi:10.1530/jme-14-0226

Al-Shukaili, A., Al-Kaabi, J., Hassan, B., Al-Araimi, T., Al-Tobi, M., Al-Kindi, M., . . . Al-Ansari, A. (2011). P2X7 receptor gene polymorphism analysis in rheumatoid arthritis. *Int J Immunogenet, 38*(5), 389-396. doi:10.1111/j.1744-313X.2011.01019.x

Alvarenga, E. C., Rodrigues, R., Caricati-Neto, A., Silva-Filho, F. C., Paredes-Gamero, E. J., & Ferreira, A. T. (2010). Low-intensity pulsed ultrasound-dependent osteoblast proliferation occurs by via activation of the P2Y receptor: role of the P2Y1 receptor. *Bone, 46*(2), 355-362. doi:http://dx.doi.org/10.1016/j.bone.2009.09.017

Anderson, H. C., Harmey, D., Camacho, N. P., Garimella, R., Sipe, J. B., Tague, S., . . . Millan, J. L. (2005). Sustained osteomalacia of long bones despite major improvement in other hypophosphatasia-related mineral deficits in tissue nonspecific alkaline phosphatase/nucleotide pyrophosphatase phosphodiesterase 1 double-deficient mice. *Am J Pathol, 166*(6), 1711-1720. doi:10.1016/s0002-9440(10)62481-9

Angelotti, F., Parma, A., Cafaro, G., Capecchi, R., Alunno, A., & Puxeddu, I. (2017). One year in review 2017: pathogenesis of rheumatoid arthritis. *Clin Exp Rheumatol, 35*(3), 368-378.

Ardissone, V., Radaelli, E., Zaratin, P., Ardizzone, M., Ladel, C., Gattorno, M., . . . Traggiai, E. (2011). Pharmacologic P2X purinergic receptor antagonism in the treatment of collagen-induced arthritis. *Arthritis & Rheumatism, 63*(11), 3323-3332. doi:10.1002/art.30556

Armstrong, S., Pereverzev, A., Dixon, S. J., & Sims, S. M. (2009). Activation of P2X7 receptors causes isoform-specific translocation of protein kinase C in osteoclasts. *J Cell Sci, 122*(Pt 1), 136-144. doi:10.1242/jcs.031534

Ayala-Peña, V. B., Scolaro, L. A., & Santillán, G. E. (2013). ATP and UTP stimulate bone morphogenetic protein-2,-4 and -5 gene expression and mineralization by rat primary osteoblasts involving PI3K/AKT pathway. *Experimental Cell Research, 319*(13), 2028-2036. doi:https://doi.org/10.1016/j.yexcr.2013.05.006

Bae, C., Gnanasambandam, R., Nicolai, C., Sachs, F., & Gottlieb, P. A. (2013). Xerocytosis is caused by mutations that alter the kinetics of the mechanosensitive channel PIEZO1. *Proc Natl Acad Sci U S A, 110*(12), E1162-1168. doi:10.1073/pnas.1219777110

Bao, L., Locovei, S., & Dahl, G. (2004). Pannexin membrane channels are mechanosensitive conduits for ATP. *FEBS Lett, 572*(1-3), 65-68. doi:10.1016/j.febslet.2004.07.009

Barbee, K. A. (2006). Mechanical Cell Injury. *NYAS Annals of the New York Academy of Sciences, 1066*(1), 67-84.

Baroja-Mazo, A., & Pelegrin, P. (2012). *Modulating P2X7 Receptor Signaling during Rheumatoid Arthritis: New Therapeutic Approaches for Bisphosphonates* (Vol. 2012).

Barrera, N. P., Ormond, S. J., Henderson, R. M., Murrell-Lagnado, R. D., & Edwardson, J. M. (2005). Atomic force microscopy imaging demonstrates that P2X2 receptors are trimers but that P2X6 receptor subunits do not oligomerize. *J Biol Chem, 280*(11), 10759-10765. doi:10.1074/jbc.M412265200

Bartlett, R., Stokes, L., & Sluyter, R. (2014). The P2X7 receptor channel: recent developments and the use of P2X7 antagonists in models of disease. *Pharmacological reviews, 66*(3), 638-675.

Beigi, R., Kobatake, E., Aizawa, M., & Dubyak, G. R. (1999). Detection of local ATP release from activated platelets using cell surface-attached firefly luciferase. *American Journal of Physiology, 276*(1), C267-278. doi:10.1152/ajpcell.1999.276.1.C267

Bennett, M. R., Farnell, L., Gibson, W. G., & Karunanithi, S. (1995). Quantal transmission at purinergic junctions: stochastic interaction between ATP and its receptors. *Biophys J, 68*(3), 925-935. doi:10.1016/s0006-3495(95)80268-7

Berglund, E., Berglund, D., Akcakaya, P., Ghaderi, M., Daré, E., Berggren, P.-O., . . . Bränström, R. (2013). Evidence for Ca(2+)-Regulated ATP Release in Gastrointestinal Stromal Tumors. *Experimental Cell Research, 319*(8), 1229-1238. doi:10.1016/j.yexcr.2013.03.001

Bhalla-Gehi, R., Penuela, S., Churko, J. M., Shao, Q., & Laird, D. W. (2010). Pannexin1 and Pannexin3 Delivery, Cell Surface Dynamics, and Cytoskeletal Interactions. *The Journal of biological chemistry, 285*(12), 9147-9160. doi:10.1074/jbc.M109.082008

Bhatt, D. P., Chen, X., Geiger, J. D., & Rosenberger, T. A. (2012). A sensitive HPLC-based method to quantify adenine nucleotides in primary astrocyte cell cultures. *Journal of Chromatography. B, Analytical Technologies in the Biomedical and Life Sciences, 889-890*, 110-115. doi:10.1016/j.jchromb.2012.02.005

Binderman, I., Adut, M., Zohar, R., Bahar, H., Faibish, D., & Yaffe, A. (2001). Alveolar bone resorption following coronal versus apical approach in a mucoperiosteal flap surgery procedure in the rat mandible. *Journal of periodontology, 72*(10), 1348-1353.

Binderman, I., Bahar, H., Jacob-Hirsch, J., Zeligson, S., Amariglio, N., Rechavi, G., . . . Yaffe, A. (2007). P2X4 is up-regulated in gingival fibroblasts after periodontal surgery. *Journal of Dental Research, 86*(2), 181-185.

Biswas, P., & Zanello, L. P. (2009). 1alpha,25(OH)(2) vitamin D(3) induction of ATP secretion in osteoblasts. *J Bone Miner Res, 24*(8), 1450-1460. doi:10.1359/jbmr.090306

Biver, G., Wang, N., Gartland, A., Orriss, I., Arnett, T., Boeynaems, J., & Robaye, B. (2013a). Role of the P2Y13 Receptor in the Differentiation of Bone Marrow Stromal Cells into Osteoblasts and Adipocytes. *Stem Cells, 31*(12), 2747-2758. doi:10.1002/stem.1411

Biver, G., Wang, N., Gartland, A., Orriss, I., Arnett, T., Boeynaems, J., & Robaye, B. (2013b). Role of the P2Y13 receptor in the differentiation of bone marrow stromal cells into osteoblasts and adipocytes. *Stem Cells, 31*(12), 2747-2758. doi:10.1002/stem.1411

Bodin, P., & Burnstock, G. (2001). Evidence that release of adenosine triphosphate from endothelial cells during increased shear stress is vesicular. *Journal of Cardiovascular Pharmacology, 38*(6), 900-908.

Bowler, W. B., Dixon, C. J., Halleux, C., Maier, R., Bilbe, G., Fraser, W. D., . . . Hipskind, R. A. (1999). Signaling in human osteoblasts by extracellular nucleotides. Their weak induction of the c-fos proto-oncogene via Ca2+ mobilization is strongly potentiated by a parathyroid hormone/cAMP-dependent protein kinase pathway independently of mitogen-activated protein kinase. *J Biol Chem, 274*(20), 14315-14324.

Bowler, W. B., Littlewood-Evans, A., Bilbe, G., Gallagher, J. A., & Dixon, C. J. (1998). P2Y2 receptors are expressed by human osteoclasts of giant cell tumor but do not mediate ATP-induced bone resorption. *Bone, 22*(3), 195-200.

Bradaschia-Correa, V., Josephson, A. M., Egol, A. J., Mizrahi, M. M., Leclerc, K., Huo, J., . . . Leucht, P. (2017). Ecto-5'-nucleotidase (CD73) regulates bone formation and remodeling during intramembranous bone repair in aging mice. *Tissue Cell, 49*(5), 545-551. doi:10.1016/j.tice.2017.07.001

Brandao-Burch, A., Key, M. L., Patel, J. J., Arnett, T. R., & Orriss, I. R. (2012). The P2X7 Receptor is an Important Regulator of Extracellular ATP Levels. *Frontiers in Endocrinology, 3*, 41. doi:10.3389/fendo.2012.00041

Brandao-Burch, A., Utting, J., Orriss, I., & Arnett, T. (2005). Acidosis inhibits bone formation by osteoblasts in vitro by preventing mineralization. *Calcif Tissue Int, 77*(3), 167-174. doi:10.1007/s00223-004-0285-8

Braunstein, G. M., Roman, R. M., Clancy, J. P., Kudlow, B. A., Taylor, A. L., Shylonsky, V. G., . . . Schwiebert, E. M. (2001). Cystic fibrosis transmembrane conductance regulator facilitates ATP release by stimulating a separate ATP release channel for autocrine control of cell volume regulation. *Journal of Biological Chemistry, 276*(9), 6621-6630.

Buchthal, F., & Engbaek, L. (1947). Application of adenosine triphosphate and related compounds to the spinal cord of the cat. *The Journal of Physiology, 106*(1), 3.

Buckley, K. A., Hipskind, R. A., Gartland, A., Bowler, W. B., & Gallagher, J. A. (2002). Adenosine triphosphate stimulates human osteoclast activity via upregulation of osteoblast-expressed receptor activator of nuclear factor-kappa B ligand. *Bone, 31*(5), 582-590.

Buckley, K. A., Wagstaff, S. C., McKay, G., Gaw, A., Hipskind, R. A., Bilbe, G., . . . Bowler, W. B. (2001). Parathyroid hormone potentiates nucleotide-induced [Ca2+]i release in rat osteoblasts independently of Gq activation or cyclic monophosphate accumulation. A mechanism for localizing systemic responses in bone. *J Biol Chem, 276*(12), 9565-9571. doi:10.1074/jbc.M005672200

Burnstock, G. (1972). Purinergic nerves. *Pharmacological reviews, 24*(3), 509-581.

Burnstock, G. (2009). Purinergic mechanosensory transduction and visceral pain. *Molecular pain, 5*(1), 69.

Burnstock, G. (2014). Purinergic signalling: from discovery to current developments. *Experimental Physiology, 99*(1), 16-34. doi:10.1113/expphysiol.2013.071951

Burnstock, G. (2016). Short- and long-term (trophic) purinergic signalling. *Philosophical Transactions of the Royal Society B: Biological Sciences, 371*(1700), 20150422. doi:10.1098/rstb.2015.0422

Burnstock, G., & Knight, G. E. (2017). Cell culture: complications due to mechanical release of ATP and activation of purinoceptors. *Cell and Tissue Research, 370*(1), 1-11. doi:10.1007/s00441-017-2618-8

Burnstock, G., & Knight, G. E. (2017). Cell culture: complications due to mechanical release of ATP and activation of purinoceptors. *Cell Tissue Res, 370*(1), 1-11. doi:10.1007/s00441-017-2618-8

Burnstock, G., & Verkhratskii, A. N. (2012). *Purinergic signalling and the nervous system*. Berlin; London: Springer.

Burnstock, G., & Verkhratsky, A. (2012). Early history of purinergic signalling. In *Purinergic Signalling and the Nervous System* (pp. 7-66): Springer.

Burnstock, G., & Volonté, C. (2012). *Editorial: Pharmacology and Therapeutic Activity of Purinergic Drugs for Disorders of the Nervous System* (Vol. 11).

Burow, P., Klapperstuck, M., & Markwardt, F. (2015). Activation of ATP secretion via volume-regulated anion channels by sphingosine-1-phosphate in RAW macrophages. *Pflugers Arch, 467*(6), 1215-1226. doi:10.1007/s00424-014-1561-8

Castrop, H., Huang, Y., Hashimoto, S., Mizel, D., Hansen, P., Theilig, F., . . . Schnermann, J. (2004). Impairment of tubuloglomerular feedback regulation of GFR in ecto-5'-nucleotidase/CD73-deficient mice. *J Clin Invest, 114*(5), 634-642. doi:10.1172/jci21851

Chamley, J. H., Campbell, G. R., & Burnstock, G. (1974). Dedifferentiation, redifferentiation and bundle formation of smooth muscle cells in tissue culture: the influence of cell number and nerve fibres. *J Embryol Exp Morphol, 32*(2), 297-323.

Chessell, I. P., Hatcher, J. P., Bountra, C., Michel, A. D., Hughes, J. P., Green, P., . . . Buell, G. N. (2005). Disruption of the P2X7 purinoceptor gene abolishes chronic inflammatory and neuropathic pain. *Pain, 114*(3), 386-396. doi:10.1016/j.pain.2005.01.002

Cheung, W. Y., Fritton, J. C., Morgan, S., Seref-Ferlengez, Z., Basta-Pljakic, J., Thi, M. M., . . . Schaffler, M. B. (2016). Pannexin-1 and P2X7-receptor are required for apoptotic osteocytes in fatigued bone to trigger RANKL production in neighboring bystander osteocytes. *Journal of bone and mineral research : the official journal of the American Society for Bone and Mineral Research, 31*(4), 890-899. doi:10.1002/jbmr.2740

Chi, Y., Gao, K., Zhang, H., Takeda, M., & Yao, J. (2014). Suppression of cell membrane permeability by suramin: involvement of its inhibitory actions on connexin 43 hemichannels. *British Journal of Pharmacology, 171*(14), 3448-3462. doi:http://dx.doi.org/10.1111/bph.12693

Chiu, Y.-H., Ravichandran, K. S., & Bayliss, D. A. (2014). Intrinsic properties and regulation of Pannexin 1 channel. *Channels, 8*(2), 103-109. doi:10.4161/chan.27545

Chizh, B. A., & Illes, P. (2001). P2X Receptors and Nociception. *Pharmacological reviews, 53*(4), 553.

Collin, P., Nefussi, J. R., Wetterwald, A., Nicolas, V., Boy-Lefevre, M. L., Fleisch, H., & Forest, N. (1992). Expression of collagen, osteocalcin, and bone alkaline phosphatase in a mineralizing rat osteoblastic cell culture. *Calcif Tissue Int, 50*(2), 175-183.

Conroy, S., Kindon, N., Kellam, B., & Stocks, M. J. (2016). Drug-like Antagonists of P2Y Receptors—From Lead Identification to Drug Development. *Journal of Medicinal Chemistry, 59*(22), 9981-10005. doi:10.1021/acs.jmedchem.5b01972

Cooper, S. T., & McNeil, P. L. (2015). Membrane Repair: Mechanisms and Pathophysiology. *Physiol Rev, 95*(4), 1205-1240. doi:10.1152/physrev.00037.2014

Cooper, S. T., & McNeil, P. L. (2015). Membrane Repair: Mechanisms and Pathophysiology. *Physiol Rev, 95*(4), 1205-1240. doi:10.1152/physrev.00037.2014

Costessi, A., Pines, A., D'Andrea, P., Romanello, M., Damante, G., Cesaratto, L., . . . Tell, G. (2005). Extracellular nucleotides activate Runx2 in the osteoblast-like HOBIT cell line: a possible molecular link between mechanical stress and osteoblasts' response. *Bone, 36*(3), 418-432.

Crain, J. M., Nikodemova, M., & Watters, J. J. (2009). Expression of P2 nucleotide receptors varies with age and sex in murine brain microglia. *Journal of Neuroinflammation, 6*, 24-24. doi:10.1186/1742-2094-6-24

Crecelius, A. R., Kirby, B. S., Richards, J. C., Garcia, L. J., Voyles, W. F., Larson, D. G., . . . Dinenno, F. A. (2011). Mechanisms of ATP-mediated vasodilation in humans: modest role for nitric oxide and vasodilating prostaglandins. *Am J Physiol Heart Circ Physiol, 301*(4), H1302-1310. doi:10.1152/ajpheart.00469.2011

Dacks, J. B., & Field, M. C. (2007). Evolution of the eukaryotic membrane-trafficking system: origin, tempo and mode. *J Cell Sci, 120*(Pt 17), 2977-2985. doi:10.1242/jcs.013250

Damman, P., Woudstra, P., Kuijt, W. J., de Winter, R. J., & James, S. K. (2012). P2Y12 platelet inhibition in clinical practice. *Journal of Thrombosis and Thrombolysis, 33*(2), 143-153. doi:10.1007/s11239-011-0667-5

Di Virgilio, F., Schmalzing, G., & Markwardt, F. (2018). The Elusive P2X7 Macropore. *Trends in Cell Biology, 28*(5), 392-404. doi:10.1016/j.tcb.2018.01.005

Diehl, H., Ihlefeld, H., & Schwegler, H. (2013). *Physik für Biologen*: Springer-Verlag.

Dreisig, K., & Kornum, B. R. (2016). A critical look at the function of the P2Y11 receptor. *Purinergic Signal, 12*(3), 427-437. doi:10.1007/s11302-016-9514-7

Drury, A., & Szent-Györgyi, A. v. (1929). The physiological activity of adenine compounds with especial reference to their action upon the mammalian heart. *The Journal of Physiology, 68*(3), 213-237.

Dutta, A., Okada, Y., & Sabirov, R. (2002). Regulation of an ATP-conductive large-conductance anion channel and swelling-induced ATP release by arachidonic acid. *Journal of Physiology, 542*(Pt 3), 803-816.

Efroni, I., Ip, P. L., Nawy, T., Mello, A., & Birnbaum, K. D. (2015). Quantification of cell identity from single-cell gene expression profiles. *Genome Biol, 16*, 9. doi:10.1186/s13059-015-0580-x

Einstein, A. (1905). Investigations on the Theory of the Brownian Movement. *Ann. der Physik*.

Erickson, H. P. (2009). Size and Shape of Protein Molecules at the Nanometer Level Determined by Sedimentation, Gel Filtration, and Electron Microscopy. *Biol Proced Online, 11*, 32-51. doi:10.1007/s12575-009-9008-x

Estevez-Herrera, J., Dominguez, N., Pardo, M. R., Gonzalez-Santana, A., Westhead, E. W., Borges, R., & Machado, J. D. (2016). ATP: The crucial component of secretory vesicles. *Proc Natl Acad Sci U S A, 113*(28), E4098-4106. doi:10.1073/pnas.1600690113

Evans, R. J. (2010). Structural interpretation of P2X receptor mutagenesis studies on drug action. *Br J Pharmacol, 161*(5), 961-971. doi:10.1111/j.1476-5381.2010.00728.x

Faria, R., Ferreira, L., Bezerra, R., Frutuoso, V., & Alves, L. (2012). Action of natural products on P2 receptors: A reinvented era for drug discovery. *Molecules, 17*(11), 13009-13025.

Feranchak, A. P., Lewis, M. A., Kresge, C., Sathe, M., Bugde, A., Luby-Phelps, K., . . . Fitz, J. G. (2010). Initiation of purinergic signaling by exocytosis of ATP-containing vesicles in liver epithelium. *J Biol Chem, 285*(11), 8138-8147. doi:10.1074/jbc.M109.065482

Ferreira, L. G., Dos Santos, R. N., Oliva, G., & Andricopulo, A. D. (2015). Molecular docking and structure-based drug design strategies. *Molecules, 20*(7), 13384-13421. doi:10.3390/molecules200713384

Fick, A. (1855). Ueber Diffusion. *Annalen der Physik, 170*(1), 59-86. doi:10.1002/andp.18551700105

Fischer, E. (2013). *Untersuchungen in der Puringruppe:(1882—1906)*: Springer-Verlag.

Fiske, C. H., & Subbarow, Y. (1929). Phosphorus compounds of muscle and liver. *Science, 70*(1816), 381-382.

Fleisch, H., & Bisaz, S. (1962). [Isolation from the plasma of pyrophosphate, an inhibitor of calcification]. *Helv Physiol Pharmacol Acta, 20*, C52-53.

Fredholm, B. B., Abbracchio, M. P., Burnstock, G., Daly, J. W., Harden, T. K., Jacobson, K. A., . . . Williams, M. (1994). Nomenclature and classification of purinoceptors. *Pharmacological reviews, 46*(2), 143-156.

Fredholm, B. B., AP, I. J., Jacobson, K. A., Klotz, K. N., & Linden, J. (2001). International Union of Pharmacology. XXV. Nomenclature and classification of adenosine receptors. *Pharmacol Rev, 53*(4), 527-552.

Fuller, S. J., Stokes, L., Skarratt, K. K., Gu, B. J., & Wiley, J. S. (2009). Genetics of the P2X7 receptor and human disease. *Purinergic Signalling, 5*(2), 257-262. doi:10.1007/s11302-009-9136-4

Gaitán-Peñas, H., Gradogna, A., Laparra-Cuervo, L., Solsona, C., Fernández-Dueñas, V., Barrallo-Gimeno, A., . . . Estévez, R. (2016). Investigation of LRRC8-Mediated Volume-Regulated Anion Currents in Xenopus Oocytes. *Biophysical Journal, 111*(7), 1429-1443. doi:https://doi.org/10.1016/j.bpj.2016.08.030

Gartland, A. (2012). P2X receptors in bone. *WMTS Wiley Interdisciplinary Reviews: Membrane Transport and Signaling, 1*(2), 221-227.

Gartland, A., Buckley, K. A., Bowler, W. B., & Gallagher, J. A. (2003). Blockade of the pore-forming P2X7 receptor inhibits formation of multinucleated human osteoclasts in vitro. *Calcif Tissue Int, 73*(4), 361-369. doi:10.1007/s00223-002-2098-y

Gartland, A., Buckley, K. A., Hipskind, R. A., Perry, M. J., Tobias, J. H., Buell, G., . . . Gallagher, J. A. (2003). Multinucleated osteoclast formation in vivo and in vitro by P2X7 receptor-deficient mice. *Crit Rev Eukaryot Gene Expr, 13*(2-4), 243-253.

Gartland, A., Hipskind, R. A., Gallagher, J. A., & Bowler, W. B. (2001). Expression of a P2X7 receptor by a subpopulation of human osteoblasts. *J Bone Miner Res, 16*(5), 846-856. doi:10.1359/jbmr.2001.16.5.846

Gartland, A., Skarratt, K. K., Hocking, L. J., Parsons, C., Stokes, L., Jørgensen, N. R., . . . Wiley, J. S. (2012). Polymorphisms in the P2X7 receptor gene are associated with low lumbar spine bone mineral density and accelerated bone loss in post-menopausal women. *European Journal of Human Genetics, 20*(5), 559-564. doi:10.1038/ejhg.2011.245

Genetos, D., Geist, D., Dawei, L., Donahue, H., & Duncan, R. (2005). Fluid Shear-Induced ATP Secretion Mediates Prostaglandin Release in MC3T3-E1 Osteoblasts. *J Bone Miner Res, 20*(1), 41-49. doi:10.1359/JBMR.041009

Genetos, D. C., Geist, D. J., Dawei, L., Donahue, H. J., & Duncan, R. L. (2005). Fluid Shear-Induced ATP Secretion Mediates Prostaglandin Release in MC3T3-E1 Osteoblasts. *Journal of bone and mineral research : the official journal of the American Society for Bone and Mineral Research, 20*(1), 41-49. doi:10.1359/JBMR.041009

Genetos, D. C., Geist, D. J., Liu, D., Donahue, H. J., & Duncan, R. L. (2005). Fluid shear-induced ATP secretion mediates prostaglandin release in MC3T3-E1 osteoblasts. *J Bone Miner Res, 20*(1), 41-49. doi:10.1359/jbmr.041009

Genetos, D. C., Kephart, C. J., Zhang, Y., Yellowley, C. E., & Donahue, H. J. (2007a). Oscillating fluid flow activation of gap junction hemichannels induces ATP release from MLO-Y4 osteocytes. *J Cell Physiol, 212*(1), 207-214. doi:10.1002/jcp.21021

Genetos, D. C., Kephart, C. J., Zhang, Y., Yellowley, C. E., & Donahue, H. J. (2007b). Oscillating fluid flow activation of gap junction hemichannels induces ATP release from MLO-Y4 osteocytes. *Journal of Cellular Physiology, 212*(1), 207-214.

Godell, C. M., Smyers, M. E., Eddleman, C. S., Ballinger, M. L., Fishman, H. M., & Bittner, G. D. (1997). Calpain activity promotes the sealing of severed giant axons. *Proc Natl Acad Sci U S A, 94*(9), 4751-4756.

Goding, J. W., Grobben, B., & Slegers, H. (2003). Physiological and pathophysiological functions of the ecto-nucleotide pyrophosphatase/phosphodiesterase family. *Biochim Biophys Acta, 1638*(1), 1-19.

Gonzales, E., Julien, B., Serriere-Lanneau, V., Nicou, A., Doignon, I., Lagoudakis, L., . . . Tordjmann, T. (2010). ATP release after partial hepatectomy regulates liver regeneration in the rat. *Journal of Hepatology, 52*(1), 54-62. doi:http://dx.doi.org/10.1016/j.jhep.2009.10.005

Gordon, J. L. (1986). Extracellular ATP: effects, sources and fate. *Biochemical Journal, 233*(2), 309.

Gradilone, S. A., Masyuk, A. I., Splinter, P. L., Banales, J. M., Huang, B. Q., Tietz, P. S., . . . LaRusso, N. F. (2007). Cholangiocyte cilia express TRPV4 and detect changes in luminal tonicity inducing bicarbonate secretion. *Proc Natl Acad Sci U S A, 104*(48), 19138-19143. doi:10.1073/pnas.0705964104

Gradilone, S. A., Masyuk, A. I., Splinter, P. L., Banales, J. M., Huang, B. Q., Tietz, P. S., . . . Larusso, N. F. (2007). Cholangiocyte cilia express TRPV4 and detect changes in luminal tonicity inducing bicarbonate secretion. *Proceedings of the National Academy of Sciences of the United States of America, 104*(48), 19138-19143.

Graff, R. D., Lazarowski, E. R., Banes, A. J., & Lee, G. M. (2000). ATP release by mechanically loaded porcine chondrons in pellet culture. *Arthritis & Rheumatism, 43*(7), 1571-1579.

Grey, A., Banovic, T., Naot, D., Hill, B., Callon, K., Reid, I., & Cornish, J. (2001). Lysophosphatidic acid is an osteoblast mitogen whose proliferative actions involve G(i) proteins and protein kinase C, but not P42/44 mitogen-activated protein kinases. *Endocrinology, 142*(3), 1098-1106. doi:10.1210/endo.142.3.8011

Grey, A., Chen, Q., Callon, K., Xu, X., Reid, I. R., & Cornish, J. (2002). The phospholipids sphingosine-1-phosphate and lysophosphatidic acid prevent apoptosis in osteoblastic cells via a signaling pathway involving G(i) proteins and phosphatidylinositol-3 kinase. *Endocrinology, 143*(12), 4755-4763. doi:10.1210/en.2002-220347

Grygorczyk, R., & Hanrahan, J. W. (1997). CFTR-independent ATP release from epithelial cells triggered by mechanical stimuli. *American Journal of Physiology, 272*(3 Pt 1), C1058-1066.

Haanes, K. A., Kowal, J. M., Arpino, G., Lange, S. C., Moriyama, Y., Pedersen, P. A., & Novak, I. (2014). Role of vesicular nucleotide transporter VNUT (SLC17A9) in release of ATP from AR42J cells and mouse pancreatic acinar cells. *Purinergic signalling, 10*(3), 431-440. doi:http://dx.doi.org/10.1007/s11302-014-9406-7

Hajjawi, M., Macrae, V., Huesa, C., Luis Millan, J., Arnett, T., & Orriss, I. (2013). *Do ecto-nucleotidases play a role in the regulation of osteoclast function?*

Hamade, E., Azzar, G., Radisson, J., Buchet, R., & Roux, B. (2003). Chick embryo anchored alkaline phosphatase and mineralization process in vitro. *Eur J Biochem, 270*(9), 2082-2090.

Hattori, M., & Gouaux, E. (2012). Molecular mechanism of ATP binding and ion channel activation in P2X receptors. *Nature, 485*(7397), 207-212. doi:10.1038/nature11010

Hayton, M. J., Dillon, J. P., Glynn, D., Curran, J. M., Gallagher, J. A., & Buckley, K. A. (2005). Involvement of adenosine 5'-triphosphate in ultrasound-induced fracture repair. *Ultrasound in Medicine and Biology, 31*(8), 1131-1138. doi:10.1016/j.ultrasmedbio.2005.04.017

Hazama, A., Fan, H. T., Abdullaev, I., Maeno, E., Tanaka, S., Ando-Akatsuka, Y., & Okada, Y. (2000). Swelling-activated, cystic fibrosis transmembrane conductance regulator-augmented ATP release and Cl- conductances in murine C127 cells. *Journal of Physiology, 523 Pt 1*, 1-11.

Hazama, R., Qu, X., Yokoyama, K., Tanaka, C., Kinoshita, E., He, J., . . . Tohyama, Y. (2009). ATP-induced osteoclast function: the formation of sealing-zone like structure and the secretion of lytic granules via microtubule-deacetylation under the control of Syk. *Genes to Cells, 14*, 871-884.

Hecht, E., Liedert, A., Ignatius, A., Mizaikoff, B., & Kranz, C. (2013). Local detection of mechanically induced ATP release from bone cells with ATP microbiosensors. *Biosensors and Bioelectronics, 44*, 27-33. doi:http://dx.doi.org/10.1016/j.bios.2013.01.008

Hoebertz, A., Arnett, T. R., & Burnstock, G. (2003). Regulation of bone resorption and formation by purines and pyrimidines. *Trends Pharmacol Sci, 24*(6), 290-297. doi:10.1016/s0165-6147(03)00123-8

Hoebertz, A., Mahendran, S., Burnstock, G., & Arnett, T. R. (2002). ATP and UTP at low concentrations strongly inhibit bone formation by osteoblasts: a novel role for the P2Y2 receptor in bone remodeling. *J Cell Biochem, 86*(3), 413-419. doi:10.1002/jcb.10236

Hoebertz, A., Meghji, S., Burnstock, G., & Arnett, T. R. (2001). Extracellular ADP is a powerful osteolytic agent: evidence for signaling through the P2Y(1) receptor on bone cells. *Faseb J, 15*(7), 1139-1148.

Hoffmann, E. K., Sørensen, B. H., Sauter, D. P. R., & Lambert, I. H. (2015). Role of volume-regulated and calcium-activated anion channels in cell volume homeostasis, cancer and drug resistance. *Channels, 9*(6), 380-396. doi:10.1080/19336950.2015.1089007

Holton, P. (1959). The liberation of adenosine triphosphate on antidromic stimulation of sensory nerves. *The Journal of Physiology, 145*(3), 494-504.

Hubley, M. J., Moerland, T. S., & Rosanske, R. C. (1995). Diffusion coefficients of ATP and creatine phosphate in isolated muscle: pulsed gradient 31P NMR of small biological samples. *NMR Biomed, 8*(2), 72-78.

Ihara, H., Hirukawa, K., Goto, S., & Togari, A. (2005). ATP-stimulated interleukin-6 synthesis through P2Y receptors on human osteoblasts. *Biochem Biophys Res Commun, 326*(2), 329-334. doi:10.1016/j.bbrc.2004.11.037

Islam, M., Uramoto, H., Okada, T., Sabirov, R., & Okada, Y. (2012). Maxi-anion channel and pannexin 1 hemichannel constitute separate pathways for swelling-induced ATP release in murine L929 fibrosarcoma cells. *Am J Physiol Cell Physiol, 303*(9), C924-935. doi:10.1152/ajpcell.00459.2011

James Magness, A., A Squires, J., Griffiths, B., Khan, K., Swain, A., R Willison, K., . . . R Klug, D. (2017). *Multiplexed single cell protein expression analysis in solid tumours using a miniaturised microfluidic assay* (Vol. 3).

Jiang, X.-L., Samant, S., Lesko, L. J., & Schmidt, S. (2015). Clinical Pharmacokinetics and Pharmacodynamics of Clopidogrel. *Clinical Pharmacokinetics, 54*(2), 147-166. doi:10.1007/s40262-014-0230-6

Jing, D., Baik, A. D., Lu, X. L., Zhou, B., Lai, X., Wang, L., . . . Guo, X. E. (2014). In situ intracellular calcium oscillations in osteocytes in intact mouse long bones under dynamic mechanical loading. *The FASEB Journal, 28*(4), 1582-1592. doi:10.1096/fj.13-237578

Johnson, K. A., Hessle, L., Vaingankar, S., Wennberg, C., Mauro, S., Narisawa, S., . . . Terkeltaub, R. (2000). Osteoblast tissue-nonspecific alkaline phosphatase antagonizes and regulates PC-1. *Am J Physiol Regul Integr Comp Physiol, 279*(4), R1365-1377. doi:10.1152/ajpregu.2000.279.4.R1365

Jørgensen, N., Adinolfi, E., Orriss, I., & Schwarz, P. (2013). Purinergic Signaling in Bone. *J Osteoporos, 2013*, 673684. doi:10.1155/2013/673684

Jorgensen, N. R., Grove, E. L., Schwarz, P., & Vestergaard, P. (2012). Clopidogrel and the risk of osteoporotic fractures: a nationwide cohort study. *J Intern Med, 272*(4), 385-393. doi:10.1111/j.1365-2796.2012.02535.x

Jorgensen, N. R., Henriksen, Z., Brot, C., Eriksen, E. F., Sorensen, O. H., Civitelli, R., & Steinberg, T. H. (2000). Human osteoblastic cells propagate intercellular calcium signals by two different mechanisms. *J Bone Miner Res, 15*(6), 1024-1032. doi:10.1359/jbmr.2000.15.6.1024

Jorgensen, N. R., Henriksen, Z., Sorensen, O. H., Eriksen, E. F., Civitelli, R., & Steinberg, T. H. (2002). Intercellular calcium signaling occurs between human osteoblasts and osteoclasts and requires activation of osteoclast P2X7 receptors. *J Biol Chem, 277*(9), 7574-7580. doi:10.1074/jbc.M104608200

Kaebisch, C., Schipper, D., Babczyk, P., & Tobiasch, E. (2015). The role of purinergic receptors in stem cell differentiation. *Computational and Structural Biotechnology Journal, 13*, 75-84. doi:10.1016/j.csbj.2014.11.003

Kang, J., Kang, N., Lovatt, D., Torres, A., Zhao, Z., Lin, J., & Nedergaard, M. (2008). Cx43 hemichannels are permeable to ATP. *The Journal of neuroscience : the official journal of the Society for Neuroscience, 28*(18), 4702-4711. doi:10.1523/JNEUROSCI.5048-07.2008

Kanjanamekanant, K., Luckprom, P., & Pavasant, P. (2014). P2X7 receptor-Pannexin1 interaction mediates stress-induced interleukin-1 beta expression in human periodontal ligament cells. *Journal of Periodontal Research, 49*(5), 595-602. doi:http://dx.doi.org/10.1111/jre.12139

Katz, S., Ayala, V., Santillán, G., & Boland, R. (2011). Activation of the PI3K/Akt signaling pathway through P2Y2 receptors by extracellular ATP is involved in osteoblastic cell proliferation. *Arch Biochem Biophys, 513*(2), 144-152. doi:https://doi.org/10.1016/j.abb.2011.06.013

Katz, S., Boland, R., & Santillan, G. (2006). Modulation of ERK 1/2 and p38 MAPK signaling pathways by ATP in osteoblasts: involvement of mechanical stress-activated calcium influx, PKC and Src activation. *Int J Biochem Cell Biol, 38*(12), 2082-2091. doi:10.1016/j.biocel.2006.05.018

Katz, S., Boland, R., & Santillán, G. (2006). Modulation of ERK 1/2 and p38 MAPK signaling pathways by ATP in osteoblasts: involvement of mechanical stress-activated calcium influx, PKC and Src activation. *The international journal of biochemistry & cell biology, 38*(12), 2082-2091. doi:10.1016/j.biocel.2006.05.018

Kawate, T., Michel, J. C., Birdsong, W. T., & Gouaux, E. (2009). Crystal structure of the ATP-gated P2X(4) ion channel in the closed state. *Nature, 460*(7255), 592-598. doi:10.1038/nature08198

Ke, H. Z., Qi, H., Weidema, A. F., Zhang, Q., Panupinthu, N., Crawford, D. T., . . . Thompson, D. D. (2003). Deletion of the P2X7 nucleotide receptor reveals its regulatory roles in bone formation and resorption. *Mol Endocrinol, 17*(7), 1356-1367. doi:10.1210/me.2003-0021

Keystone, E. C., Wang, M. M., Layton, M., Hollis, S., McInnes, I. B., & Team, D. S. (2011). Clinical evaluation of the efficacy of the P2X7 purinergic receptor antagonist AZD9056 on the signs and symptoms of rheumatoid arthritis in patients with active disease despite treatment with methotrexate or sulphasalazine. *Ann Rheum Dis*, annrheumdis143578.

Khadra, A., Tomić, M., Yan, Z., Zemkova, H., Sherman, A., & Stojilkovic, Stanko S. (2013). Dual Gating Mechanism and Function of P2X7 Receptor Channels. *Biophysical Journal, 104*(12), 2612-2621. doi:10.1016/j.bpj.2013.05.006

Kholodenko, B. N. (2006). CELL SIGNALLING DYNAMICS IN TIME AND SPACE. *Nat Rev Mol Cell Biol, 7*(3), 165-176. doi:10.1038/nrm1838

Kim, H., Walsh, M. C., Takegahara, N., Middleton, S. A., Shin, H. I., Kim, J., & Choi, Y. (2017). The purinergic receptor P2X5 regulates inflammasome activity and hyper-multinucleation of murine osteoclasts. *Sci Rep, 7*(1), 196. doi:10.1038/s41598-017-00139-2

King, A. E., Ackley, M. A., Cass, C. E., Young, J. D., & Baldwin, S. A. (2006). Nucleoside transporters: from scavengers to novel therapeutic targets. *Trends Pharmacol Sci, 27*(8), 416-425. doi:10.1016/j.tips.2006.06.004

Kling, J. M., Clarke, B. L., & Sandhu, N. P. (2014). Osteoporosis Prevention, Screening, and Treatment: A Review. *Journal of Women's Health, 23*(7), 563-572. doi:10.1089/jwh.2013.4611

Kook, S., Cho, J., Lee, S. B., & Lee, B.-C. (2013). The nucleotide sugar UDP-glucose mobilizes long-term repopulating primitive hematopoietic cells. *J Clin Invest, 123*(8), 3420-3435. doi:10.1172/JCI64060

Korcok, J., Raimundo, L. N., Du, X., Sims, S. M., & Dixon, S. J. (2005). P2Y6 nucleotide receptors activate NF-kappaB and increase survival of osteoclasts. *J Biol Chem, 280*(17), 16909-16915. doi:10.1074/jbc.M410764200

Korcok, J., Raimundo, L. N., Ke, H. Z., Sims, S. M., & Dixon, S. J. (2004). Extracellular nucleotides act through P2X7 receptors to activate NF-kappaB in osteoclasts. *J Bone Miner Res, 19*(4), 642-651. doi:10.1359/jbmr.040108

Koszalka, P., Ozuyaman, B., Huo, Y., Zernecke, A., Flogel, U., Braun, N., . . . Schrader, J. (2004). Targeted disruption of cd73/ecto-5'-nucleotidase alters thromboregulation and augments vascular inflammatory response. *Circ Res, 95*(8), 814-821. doi:10.1161/01.RES.0000144796.82787.6f

Kowal, J. M., Yegutkin, G. G., & Novak, I. (2015). ATP release, generation and hydrolysis in exocrine pancreatic duct cells. *Purinergic signalling, 11*(4), 533-550. doi:http://dx.doi.org/10.1007/s11302-015-9472-5

Kringelbach, T. M., Aslan, D., Novak, I., Ellegaard, M., Syberg, S., Andersen, C. K., . . . Jorgensen, N. R. (2015). Fine-tuned ATP signals are acute mediators in osteocyte mechanotransduction. *Cell Signal, 27*(12), 2401-2409. doi:10.1016/j.cellsig.2015.08.016

Kringelbach, T. M., Aslan, D., Novak, I., Ellegaard, M., Syberg, S., Andersen, C. K. B., . . . Jørgensen, N. R. (2015). Fine-tuned ATP signals are acute mediators in osteocyte mechanotransduction. *Cell Signal, 27*(12), 2401-2409. doi:https://doi.org/10.1016/j.cellsig.2015.08.016

Lai, Y., Thomas, G. D., Yue, Y., Yang, H. T., Li, D., Long, C., . . . Duan, D. (2009). Dystrophins carrying spectrin-like repeats 16 and 17 anchor nNOS to the sarcolemma and enhance exercise performance in a mouse model of muscular dystrophy. *J Clin Invest, 119*(3), 624-635. doi:10.1172/jci36612

Lazarowski, E. R., & Boucher, R. C. (2009). Purinergic receptors in airway epithelia. *Curr Opin Pharmacol, 9*(3), 262-267. doi:10.1016/j.coph.2009.02.004

Lazarowski, E. R., & Harden, T. K. (2015). UDP-Sugars as Extracellular Signaling Molecules: Cellular and Physiologic Consequences of P2Y(14) Receptor Activation. *Mol Pharmacol, 88*(1), 151-160. doi:10.1124/mol.115.098756

Lazarowski, E. R., Sesma, J. I., Seminario-Vidal, L., & Kreda, S. M. (2011). Chapter 8 - Molecular Mechanisms of Purine and Pyrimidine Nucleotide Release. In K. A. Jacobson & J. Linden (Eds.), *Advances in Pharmacology* (Vol. 61, pp. 221-261): Academic Press.

Le Stunff, H., Auger, R., Kanellopoulos, J., & Raymond, M. N. (2004). The Pro-451 to Leu polymorphism within the C-terminal tail of P2X7 receptor impairs cell death but not phospholipase D activation in murine thymocytes. *J Biol Chem, 279*(17), 16918-16926. doi:10.1074/jbc.M313064200

Lee, J., Chun, Y.-E., Han, K.-S., Lee, J., Woo, D. H., & Lee, C. J. (2015). Ca(2+) Entry is Required for Mechanical Stimulation-induced ATP Release from Astrocyte. *Experimental Neurobiology, 24*(1), 17-23. doi:10.5607/en.2015.24.1.17

Lee, S. A., Park, J. H., & Lee, S. Y. (2013). Selective Induction of P2Y14 Receptor by RANKL Promotes Osteoclast Formation. *Molecules and Cells, 36*(3), 273-277. doi:10.1007/s10059-013-0226-3

Lemaire, I., Falzoni, S., Zhang, B., Pellegatti, P., & Di Virgilio, F. (2011). The P2X7 receptor and Pannexin-1 are both required for the promotion of multinucleated macrophages by the inflammatory cytokine GM-CSF. *Journal of Immunology, 187*(7), 3878-3887. doi:http://dx.doi.org/10.4049/jimmunol.1002780

Li, A., Leung, C. T., Peterson-Yantorno, K., Stamer, W. D., & Civan, M. M. (2011). Cytoskeletal dependence of adenosine triphosphate release by human trabecular meshwork cells. *Investigative Ophthalmology & Visual Science, 52*(11), 7996-8005. doi:http://dx.doi.org/10.1167/iovs.11-8170

Li, A., Leung, C. T., Peterson-Yantorno, K., Stamer, W. D., Mitchell, C. H., & Civan, M. M. (2012). Mechanisms of ATP release by human trabecular meshwork cells, the enabling step in purinergic regulation of aqueous humor outflow. *J Cell Physiol, 227*(1), 172-182. doi:10.1002/jcp.22715

Li, J., Liu, D., Ke, H. Z., Duncan, R. L., & Turner, C. H. (2005a). The P2X7 nucleotide receptor mediates skeletal mechanotransduction. *J Biol Chem, 280*(52), 42952-42959. doi:10.1074/jbc.M506415200

Li, J., Liu, D., Ke, H. Z., Duncan, R. L., & Turner, C. H. (2005b). The P2X7 nucleotide receptor mediates skeletal mechanotransduction. *Journal of Biological Chemistry, 280*(52), 42952-42959.

Li, W., Wei, S., Liu, C., Song, M., Wu, H. U. A., & Yang, Y. (2016). Regulation of the osteogenic and adipogenic differentiation of bone marrow-derived stromal cells by extracellular uridine triphosphate: The role of P2Y2 receptor and ERK1/2 signaling. *International Journal of Molecular Medicine, 37*(1), 63-73. doi:10.3892/ijmm.2015.2400

Li, W., You, L., Schaffler, M. B., & Wang, L. (2009). The dependency of solute diffusion on molecular weight and shape in intact bone. *Bone, 45*(5), 1017-1023. doi:10.1016/j.bone.2009.07.076

Li, Y., Luo, Y., Huang, K., Xing, J., Xie, Z., Lin, M., . . . Wang, Y. (2013). The responses of osteoblasts to fluid shear stress depend on substrate chemistries. *Arch Biochem Biophys, 539*(1), 38-50. doi:10.1016/j.abb.2013.09.005

Lim To, W. K., Kumar, P., & Marshall, J. M. (2015). Hypoxia is an effective stimulus for vesicular release of ATP from human umbilical vein endothelial cells. *Placenta, 36*(7), 759-766. doi:10.1016/j.placenta.2015.04.005

Lipmann, F. (1941). Metabolic generation and utilization of phosphate bond energy. *Adv. Enzymol. Relat. Areas Mol. Biol, 1*, 99-162.

Litvak, V., Ramsey, S. A., Rust, A. G., Zak, D. E., Kennedy, K. A., Lampano, A. E., . . . Aderem, A. (2009). Function of C/EBPδ in a regulatory circuit that discriminates between transient and persistent TLR4-induced signals. *Nature immunology, 10*(4), 437.

Locovei, S., Bao, L., & Dahl, G. (2006). Pannexin 1 in erythrocytes: function without a gap. *Proceedings of the National Academy of Sciences of the United States of America, 103*(20), 7655-7659.

Lohman, A. W., & Isakson, B. E. (2014). Differentiating connexin hemichannels and pannexin channels in cellular ATP release. *FEBS Lett, 588*(8), 1379-1388. doi:http://doi.org/10.1016/j.febslet.2014.02.004

Lohmann, K. (1929). Über die pyrophosphatfraktion im muskel. *Naturwissenschaften, 17*(31), 624-625.

Lu, C., Liu, D., Liu, H., & Motchnik, P. (2013). Characterization of monoclonal antibody size variants containing extra light chains. *mAbs, 5*(1), 102-113. doi:10.4161/mabs.22965

Lu, D., Soleymani, S., Madakshire, R., & Insel, P. A. (2012). ATP released from cardiac fibroblasts via connexin hemichannels activates profibrotic P2Y2 receptors. *FASEB Journal, 26*(6), 2580-2591. doi:http://dx.doi.org/10.1096/fj.12-204677

Luckprom, P., Kanjanamekanant, K., & Pavasant, P. (2011). Role of connexin43 hemichannels in mechanical stress-induced ATP release in human periodontal ligament cells. *Journal of Periodontal Research, 46*(5), 607-615. doi:http://dx.doi.org/10.1111/j.1600-0765.2011.01379.x

Lustig, K. D., Shiau, A. K., Brake, A. J., & Julius, D. (1993). Expression cloning of an ATP receptor from mouse neuroblastoma cells. *Proceedings of the National Academy of Sciences, 90*(11), 5113-5117.

Mackay, L., Mikolajewicz, N., Komarova, S. V., & Khadra, A. (2016). Systematic Characterization of Dynamic Parameters of Intracellular Calcium Signals. *Frontiers in Physiology, 7*(525). doi:10.3389/fphys.2016.00525

Mackenzie, N., Zhu, D., Farquharson, C., & MacRae, V. E. Upregulation of P2X6 during the differentiation and calcification of vascular smooth muscle cells. *Bone, 47*, S231. doi:10.1016/j.bone.2010.04.553

Maksymowych, W. (2002). *Bisphosphonates-Anti-Inflammatory Properties* (Vol. 1).

Malone, A. M. D., Anderson, C. T., Tummala, P., Kwon, R. Y., Johnston, T. R., Stearns, T., & Jacobs, C. R. (2007). Primary cilia mediate mechanosensing in bone cells by a calcium-independent mechanism. *Proceedings of the National Academy of Sciences of the United States of America, 104*(33), 13325-13330. doi:10.1073/pnas.0700636104

Manaka, S., Tanabe, N., Kariya, T., Naito, M., Takayama, T., Nagao, M., . . . Miyazaki, M. (2015). Low-intensity pulsed ultrasound-induced ATP increases bone formation via the P2X7 receptor in osteoblast-like MC3T3-E1 cells. *FEBS Lett, 589*(3), 310-318. doi:10.1016/j.febslet.2014.12.013

Mangan, S., Zaslaver, A., & Alon, U. (2003). The Coherent Feedforward Loop Serves as a Sign-sensitive Delay Element in Transcription Networks. *Journal of Molecular Biology, 334*(2), 197-204. doi:https://doi.org/10.1016/j.jmb.2003.09.049

McNeil, P. L., Miyake, K., & Vogel, S. S. (2003). The endomembrane requirement for cell surface repair. *Proceedings of the National Academy of Sciences, 100*(8), 4592.

Mediero, A., Wilder, T., Reddy, V. S. R., Cheng, Q., Tovar, N., Coelho, P. G., . . . Cronstein, B. N. (2016). Ticagrelor regulates osteoblast and osteoclast function and promotes bone formation in vivo via an adenosine-dependent mechanism. *The FASEB Journal, 30*(11), 3887-3900. doi:10.1096/fj.201600616R

Miras-Portugal, M. T., Castro, E., Mateo, J., & Pintor, J. (1996). The diadenosine polyphosphate receptors: P2D purinoceptors. *P2 Purinoceptors: Localization, Function and Transduction Mechanisms*, 35-47.

Miyake, K., & McNeil, P. L. (2003). Mechanical injury and repair of cells. *Crit Care Med, 31*(8 Suppl), S496-501. doi:10.1097/01.ccm.0000081432.72812.16

Miyazaki, T., Iwasawa, M., Nakashima, T., Mori, S., Shigemoto, K., Nakamura, H., . . . Tanaka, S. (2012). Intracellular and extracellular ATP coordinately regulate the inverse correlation between osteoclast survival and bone resorption. *Journal of Biological Chemistry, 287*, 37808-37823.

Moldwin, R., Kitt, M., Mangel, J., Beyer, R., Hanno, P., Butera, P., & Ford, A. (2015). *A phase 2 study in women with interstitial cystitis/bladder pain syndrome (IC/BPS) of the novel P2X3 antagonist AF-219.* Paper presented at the NEUROUROLOGY AND URODYNAMICS.

Morrison, M., Turin, L., King, B., Burnstock, G., & Arnett, T. (1998). ATP is a potent stimulator of the activation and formation of rodent osteoclasts. *J Physiol, 511 (Pt 2)*, 495-500.

Mrazek, F., Gallo, J., Stahelova, A., & Petrek, M. (2010). Functional variants of the P2RX7 gene, aseptic osteolysis, and revision of the total hip arthroplasty: a preliminary study. *Hum Immunol, 71*(2), 201-205. doi:10.1016/j.humimm.2009.10.013

Naemsch, L. N., Weidema, A. F., Sims, S. M., Underhill, T. M., & Dixon, S. J. (1999). P2X(4) purinoceptors mediate an ATP-activated, non-selective cation current in rabbit osteoclasts. *J Cell Sci, 112 (Pt 23)*, 4425-4435.

Nakamura, E., Uezono, Y., Narusawa, K., Shibuya, I., Oishi, Y., Tanaka, M., . . . Izumi, F. (2000). ATP activates DNA synthesis by acting on P2X receptors in human osteoblast-like MG-63 cells. *Am J Physiol Cell Physiol, 279*(2), C510-519.

Negoro, H., Urban-Maldonado, M., Liou, L. S., Spray, D. C., Thi, M. M., & Suadicani, S. O. (2014). Pannexin 1 channels play essential roles in urothelial mechanotransduction and intercellular signaling. *PLoS ONE [Electronic Resource], 9*(8), e106269. doi:http://dx.doi.org/10.1371/journal.pone.0106269

Noronha-Matos, J. B., Coimbra, J., Sa-e-Sousa, A., Rocha, R., Marinhas, J., Freitas, R., . . . Correia-de-Sa, P. (2014). P2X7-induced zeiosis promotes osteogenic differentiation and mineralization of postmenopausal bone marrow-derived mesenchymal stem cells. *Faseb J, 28*(12), 5208-5222. doi:10.1096/fj.14-257923

Noronha-Matos, J. B., Costa, M. A., Magalhaes-Cardoso, M. T., Ferreirinha, F., Pelletier, J., Freitas, R., . . . Correia-de-Sa, P. (2012). Role of ecto-NTPDases on UDP-sensitive P2Y(6) receptor activation during osteogenic differentiation of primary bone marrow stromal cells from postmenopausal women. *J Cell Physiol, 227*(6), 2694-2709. doi:10.1002/jcp.23014

North, R. A., & Jarvis, M. F. (2013). P2X Receptors as Drug Targets. *Mol Pharmacol, 83*(4), 759-769. doi:10.1124/mol.112.083758

O'Brien, C. A., Plotkin, L. I., Galli, C., Goellner, J. J., Gortazar, A. R., Allen, M. R., . . . Bellido, T. (2008). Control of Bone Mass and Remodeling by PTH Receptor Signaling in Osteocytes. *PLoS ONE, 3*(8), e2942. doi:10.1371/journal.pone.0002942

O'Connor, S. E., Dainty, I. A., & Leff, P. (1991). Further subclassification of ATP receptors based on agonist studies. *Trends in pharmacological sciences, 12*, 137-141.

Ohlendorff, S. D., Tofteng, C. L., Jensen, J. E., Petersen, S., Civitelli, R., Fenger, M., . . . Jorgensen, N. R. (2007). Single nucleotide polymorphisms in the P2X7 gene are associated to fracture risk and to effect of estrogen treatment. *Pharmacogenet Genomics, 17*(7), 555-567. doi:10.1097/FPC.0b013e3280951625

Okada, S. F., O'Neal, W. K., Huang, P., Nicholas, R. A., Ostrowski, L. E., Craigen, W. J., . . . Boucher, R. C. (2004). Voltage-dependent anion channel-1 (VDAC-1) contributes to ATP release and cell volume regulation in murine cells. *Journal of General Physiology, 124*(5), 513-526.

Okada, Y., Sato, K., & Numata, T. (2009). Pathophysiology and puzzles of the volume-sensitive outwardly rectifying anion channel. *The Journal of Physiology, 587*(Pt 10), 2141-2149. doi:10.1113/jphysiol.2008.165076

Orriss, I., & Arnett, T. (2012). P2Y receptors in bone. *Wiley Interdisciplinary Reviews: Membrane Transport and Signaling, 1*(6), 805-814. doi:10.1002/wmts.67

Orriss, I., Burnstock, G., & Arnett, T. (2010). Purinergic signalling and bone remodelling. *Curr Opin Pharmacol, 10*(3), 322-330. doi:10.1016/j.coph.2010.01.003

Orriss, I., Guneri, D., Hajjawi, M., Shaw, K., Patel, J., & Arnett, T. (2017). Activation of the P2Y2 receptor regulates bone cell function by enhancing ATP release. *J Endocrinol, 233*(3), 341-356. doi:10.1530/joe-17-0042

Orriss, I., Key, M., Brandao-Burch, A., Patel, J., Burnstock, G., & Arnett, T. (2012). The regulation of osteoblast function and bone mineralisation by extracellular nucleotides: The role of p2x receptors. *Bone, 51*(3), 389-400. doi:10.1016/j.bone.2012.06.013

Orriss, I., Key, M., Hajjawi, M., & Arnett, T. (2013). Extracellular ATP Released by Osteoblasts Is A Key Local Inhibitor of Bone Mineralisation. *PLoS ONE, 8*(7), e69057. doi:10.1371/journal.pone.0069057

Orriss, I., Key, M. L., Hajjawi, M., Millán, J., & Arnett, T. (2015). Acidosis Is a key regulator of osteoblast ecto-nucleotidase pyrophosphatase/phosphodiesterase 1 (NPP1) expression and activity. *Journal of cellular physiology, 230*(12), 3049-3056. doi:10.1002/jcp.25041

Orriss, I., Knight, G., Burnstock, G., & Arnett, T. (2005). *P2X (2) but not P2X (3) receptor knockout mice demonstrate increased bone mass and weight*.

Orriss, I., Knight, G., Ranasinghe, S., Burnstock, G., & Arnett, T. (2006). Osteoblast responses to nucleotides increase during differentiation. *Bone, 39*(2), 300-309. doi:10.1016/j.bone.2006.02.063

Orriss, I., Knight, G., Utting, J., Taylor, S., Burnstock, G., & Arnett, T. (2009). Hypoxia stimulates vesicular ATP release from rat osteoblasts. *J Cell Physiol, 220*(1), 155-162. doi:10.1002/jcp.21745

Orriss, I., Syberg, S., Wang, N., Robaye, B., Gartland, A., Jorgensen, N., . . . Boeynaems, J. (2011). Bone phenotypes of P2 receptor knockout mice. *Front Biosci (Schol Ed), 3*, 1038-1046.

Orriss, I., Utting, J., Brandao-Burch, A., Colston, K., Grubb, B., Burnstock, G., & Arnett, T. (2007). Extracellular nucleotides block bone mineralization in vitro: evidence for dual inhibitory mechanisms involving both P2Y2 receptors and pyrophosphate. *Endocrinology, 148*(9), 4208-4216. doi:10.1210/en.2007-0066

Orriss, I., Wang, N., Burnstock, G., Arnett, T., Gartland, A., Robaye, B., & Boeynaems, J. (2011). The P2Y6 Receptor Stimulates Bone Resorption by Osteoclasts. *Endocrinology, 152*(10), 3706-3716. doi:10.1210/en.2011-1073

Orriss, I. R., & Arnett, T. R. (2012). P2Y receptors in bone. *Wiley Interdisciplinary Reviews: Membrane Transport and Signaling, 1*(6), 805-814.

Orriss, I. R., Knight, G. E., Ranasinghe, S., Burnstock, G., & Arnett, T. R. (2006). Osteoblast responses to nucleotides increase during differentiation. *Bone, 39*(2), 300-309. doi:https://doi.org/10.1016/j.bone.2006.02.063

Panchin, Y., Kelmanson, I., Matz, M., Lukyanov, K., Usman, N., & Lukyanov, S. (2000). A ubiquitous family of putative gap junction molecules. *Curr Biol, 10*(13), R473-474.

Pangrsic, T., Potokar, M., Stenovec, M., Kreft, M., Fabbretti, E., Nistri, A., . . . Zorec, R. (2007). Exocytotic release of ATP from cultured astrocytes. *J Biol Chem, 282*(39), 28749-28758. doi:10.1074/jbc.M700290200

Panupinthu, N., Rogers, J. T., Zhao, L., Solano-Flores, L. P., Possmayer, F., Sims, S. M., & Dixon, S. J. (2008). P2X7 receptors on osteoblasts couple to production of lysophosphatidic acid: a signaling axis promoting osteogenesis. *J Cell Biol, 181*(5), 859-871. doi:10.1083/jcb.200708037

Panupinthu, N., Zhao, L., Possmayer, F., Ke, H. Z., Sims, S. M., & Dixon, S. J. (2007). P2X7 nucleotide receptors mediate blebbing in osteoblasts through a pathway involving lysophosphatidic acid. *J Biol Chem, 282*(5), 3403-3412. doi:10.1074/jbc.M605620200

Patel, B. A. (2014). Mucosal adenosine triphosphate mediates serotonin release from ileal but not colonic guinea pig enterochromaffin cells. *Neurogastroenterol Motil, 26*(2), 237-246. doi:10.1111/nmo.12254

Patel, B. A., Rogers, M., Wieder, T., O'Hare, D., & Boutelle, M. G. (2011). ATP microelectrode biosensor for stable long-term in vitro monitoring from gastrointestinal tissue. *Biosensors and Bioelectronics, 26*(6), 2890-2896. doi:https://doi.org/10.1016/j.bios.2010.11.033

Pelegrin, P., & Surprenant, A. (2006). Pannexin-1 mediates large pore formation and interleukin-1beta release by the ATP-gated P2X7 receptor. *Embo j, 25*(21), 5071-5082. doi:10.1038/sj.emboj.7601378

Pennanen, N., Lapinjoki, S., Urtti, A., & Monkkonen, J. (1995). Effect of liposomal and free bisphosphonates on the IL-1 beta, IL-6 and TNF alpha secretion from RAW 264 cells in vitro. *Pharm Res, 12*(6), 916-922.

Penolazzi, L., Bianchini, E., Lambertini, E., Baraldi, P. G., Romagnoli, R., Piva, R., & Gambari, R. (2005). N-Arylpiperazine modified analogues of the P2X7 receptor KN-62 antagonist are potent inducers of apoptosis of human primary osteoclasts. *J Biomed Sci, 12*(6), 1013-1020. doi:10.1007/s11373-005-9029-7

Piekarski, K., & Munro, M. (1977). Transport mechanism operating between blood supply and osteocytes in long bones. *Nature, 269*(5623), 80-82.

Pines, A., Romanello, M., Cesaratto, L., Damante, G., Moro, L., D'Andrea, P., & Tell, G. (2003). Extracellular ATP stimulates the early growth response protein 1 (Egr-1) via a protein kinase C-dependent pathway in the human osteoblastic HOBIT cell line. *Biochem J, 373*(Pt 3), 815-824. doi:10.1042/bj20030208

Plotkin, L. I., & Stains, J. P. (2015). Connexins and pannexins in the skeleton: gap junctions, hemichannels and more. *Cellular and molecular life sciences : CMLS, 72*(15), 2853-2867. doi:10.1007/s00018-015-1963-6

Portales-Cervantes, L., Nino-Moreno, P., Salgado-Bustamante, M., Garcia-Hernandez, M. H., Baranda-Candido, L., Reynaga-Hernandez, E., . . . Portales-Perez, D. P. (2012). The His155Tyr (489C>T) single nucleotide polymorphism of P2RX7 gene confers an enhanced function of P2X7 receptor in immune cells from patients with rheumatoid arthritis. *Cell Immunol, 276*(1-2), 168-175. doi:10.1016/j.cellimm.2012.05.005

Price, C., Zhou, X., Li, W., & Wang, L. (2011). Real-Time Measurement of Solute Transport Within the Lacunar-Canalicular System of Mechanically Loaded Bone: Direct Evidence for Load-Induced Fluid Flow. *Journal of Bone and Mineral Research, 26*(2), 277-285. doi:10.1002/jbmr.211

Qiu, Z., Dubin, A. E., Mathur, J., Tu, B., Reddy, K., Miraglia, L. J., . . . Patapoutian, A. (2014). SWELL1, a plasma membrane protein, is an essential component of volume-regulated anion channel. *Cell, 157*(2), 447-458. doi:10.1016/j.cell.2014.03.024

Rahman, M., Sun, R., Mukherjee, S., Nilius, B., & Janssen, L. J. (2018). TRPV4-stimulation Releases ATP via Pannexin Channels in Human Pulmonary Fibroblasts. *Am J Respir Cell Mol Biol*. doi:10.1165/rcmb.2017-0413OC

Rao, V., Shih, Y.-R. V., Kang, H., Kabra, H., & Varghese, S. (2015). Adenosine Signaling Mediates Osteogenic Differentiation of Human Embryonic Stem Cells on Mineralized Matrices. *Frontiers in Bioengineering and Biotechnology, 3*, 185. doi:10.3389/fbioe.2015.00185

Reddy, M. M., Quinton, P. M., Haws, C., Wine, J. J., Grygorczyk, R., Tabcharani, J. A., . . . Kopito, R. R. (1996). Failure of the cystic fibrosis transmembrane conductance regulator to conduct ATP. *Science, 271*(5257), 1876-1879.

Rodrigues-Ribeiro, R., Alvarenga, É. C., Calio, M. L., Paredes-Gamero, E. J., & Ferreira, A. T. (2015). Dual Role of P2 Receptors during Osteoblast Differentiation. *Cell Biochemistry and Biophysics, 71*(2), 1225-1233. doi:10.1007/s12013-014-0332-7

Rokic, M. B., & Stojilkovic, S. S. (2013). Two open states of P2X receptor channels. *Frontiers in Cellular Neuroscience, 7*, 215. doi:10.3389/fncel.2013.00215

Romanello, M., Codognotto, A., Bicego, M., Pines, A., Tell, G., & D'Andrea, P. (2005). Autocrine/paracrine stimulation of purinergic receptors in osteoblasts: Contribution of vesicular ATP release. *Biochem Biophys Res Commun, 331*(4), 1429-1438. doi:http://dx.doi.org/10.1016/j.bbrc.2005.03.246

Roper, S. D. (2006). Cell communication in taste buds. *Cellular and molecular life sciences : CMLS, 63*(13), 1494-1500. doi:10.1007/s00018-006-6112-9

Rosemeyer, H. (2004). The Chemodiversity of Purine as a Constituent of Natural Products. *Chemistry & Biodiversity, 1*(3), 361-401. doi:10.1002/cbdv.200490033

Sabirov, R., & Merzlyak, P. (2012). Plasmalemmal VDAC controversies and maxi-anion channel puzzle. *Biochimica et Biophysica Acta (BBA) - Biomembranes, 1818*(6), 1570-1580. doi:https://doi.org/10.1016/j.bbamem.2011.09.024

Sabirov, R., Merzlyak, P., Okada, T., Islam, M., Uramoto, H., Mori, T., . . . Okada, Y. (2017). The organic anion transporter SLCO2A1 constitutes the core component of the Maxi-Cl channel. *The EMBO Journal, 36*(22), 3309-3324. doi:10.15252/embj.201796685

Sabirov, R., & Okada, Y. (2005). ATP release via anion channels. *Purinergic Signalling, 1*(4), 311-328. doi:10.1007/s11302-005-1557-0

Sabirov, R., & Okada, Y. (2009). The maxi-anion channel: a classical channel playing novel roles through an unidentified molecular entity. *The Journal of Physiological Sciences, 59*(1), 3-21. doi:10.1007/s12576-008-0008-4

Sáez, J. C., & Leybaert, L. (2014). Hunting for connexin hemichannels. *FEBS Lett, 588*(8), 1205-1211. doi:https://doi.org/10.1016/j.febslet.2014.03.004

Salmon, P. (2004). Loss of Chaotic Trabecular Structure in OPG-Deficient Juvenile Paget's Disease Patients Indicates a Chaogenic Role for OPG in Nonlinear Pattern Formation of Trabecular Bone. *Journal of Bone and Mineral Research, 19*(5), 695-702.

Salmon, P. (2015). Non-Linear Pattern Formation in Bone Growth and Architecture. *Frontiers in Endocrinology, 5*(239). doi:10.3389/fendo.2014.00239

Sathe, M. N., Woo, K., Kresge, C., Bugde, A., Luby-Phelps, K., Lewis, M. A., & Feranchak, A. P. (2011). Regulation of purinergic signaling in biliary epithelial cells by exocytosis of SLC17A9-dependent ATP-enriched vesicles. *Journal of Biological Chemistry, 286*(28), 25363-25376. doi:http://dx.doi.org/10.1074/jbc.M111.232868

Sawada, K., Echigo, N., Juge, N., Miyaji, T., Otsuka, M., Omote, H., . . . Moriyama, Y. (2008). Identification of a vesicular nucleotide transporter. *Proceedings of the National Academy of Sciences of the United States of America, 105*(15), 5683-5686. doi:10.1073/pnas.0800141105

Schaffler, M. B., Cheung, W.-Y., Majeska, R., & Kennedy, O. (2014). Osteocytes: Master Orchestrators of Bone. *Calcified tissue international, 94*(1), 5-24. doi:10.1007/s00223-013-9790-y

Scheele, K. W. (1776). Examen chemicum calculi urinarii. *Opuscula, 2*(73), 1776.

Schett, G. (2006). Rheumatoid arthritis: inflammation and bone loss. *Wiener Medizinische Wochenschrift, 156*(1), 34-41. doi:10.1007/s10354-005-0244-7

Seref-Ferlengez, Z., Maung, S., Schaffler, M. B., Spray, D. C., Suadicani, S. O., & Thi, M. M. (2016). P2X7R-Panx1 Complex Impairs Bone Mechanosignaling under High Glucose Levels Associated with Type-1 Diabetes. *PLoS ONE, 11*(5), e0155107. doi:10.1371/journal.pone.0155107

Seref-Ferlengez, Z., Maung, S., Schaffler, M. B., Spray, D. C., Suadicani, S. O., & Thi, M. M. (2016). P2X7R-Panx1 Complex Impairs Bone Mechanosignaling under High Glucose Levels Associated with Type-1 Diabetes. *PLoS ONE [Electronic Resource], 11*(5), e0155107. doi:http://dx.doi.org/10.1371/journal.pone.0155107

Shankaran, H., Wiley, H. S., & Resat, H. (2007). Receptor downregulation and desensitization enhance the information processing ability of signalling receptors. *BMC Systems Biology, 1*(1), 1-15. doi:10.1186/1752-0509-1-48

Shiina, K., Hayashida, K. I., Ishikawa, K., & Kawatani, M. (2016). ATP release from bladder urothelium and serosa in a rat model of partial bladder outlet obstruction. *Biomed Res, 37*(5), 299-304. doi:10.2220/biomedres.37.299

Sick, S., Reinker, S., Timmer, J., & Schlake, T. (2006). WNT and DKK determine hair follicle spacing through a reaction-diffusion mechanism. *Science, 314*(5804), 1447-1450.

Siegel, G. J. (1999). *Basic neurochemistry: molecular, cellular and medical aspects*.

Sikora, J., Orlov, S. N., Furuya, K., & Grygorczyk, R. (2014). Hemolysis is a primary ATP-release mechanism in human erythrocytes. *Blood, 124*(13), 2150-2157. doi:10.1182/blood-2014-05-572024

Simon, S. A., Benos, D. J., & Hamill, O. P. (2011). *Mechanosensitive Ion Channels* (Vol. 59): Academic Press.

Sinke, A. P., & Deen, P. M. (2011). The physiological implication of novel proteins in systemic osmoregulation. *Faseb J, 25*(10), 3279-3289. doi:10.1096/fj.11-188433

Sklar, L. A., Hyslop, P. A., Oades, Z. G., Omann, G. M., Jesaitis, A. J., Painter, R. G., & Cochrane, C. G. (1985). Signal transduction and ligand-receptor dynamics in the human neutrophil. Transient responses and occupancy-response relations at the formyl peptide receptor. *J Biol Chem, 260*(21), 11461-11467.

Sørensen, C. E., & Novak, I. (2001). Visualization of ATP release in pancreatic acini in response to cholinergic stimulus Use of fluorescent probes and confocal microscopy. *Journal of Biological Chemistry, 276*(35), 32925-32932.

Stagg, J., Divisekera, U., Duret, H., Sparwasser, T., Teng, M. W., Darcy, P. K., & Smyth, M. J. (2011). CD73-deficient mice have increased antitumor immunity and are resistant to experimental metastasis. *Cancer Res, 71*(8), 2892-2900. doi:10.1158/0008-5472.can-10-4246

Steinhardt, R. A., Bi, G., & Alderton, J. M. (1994). Cell membrane resealing by a vesicular mechanism similar to neurotransmitter release. *Science, 263*(5145), 390-393.

Stock, T. C., Bloom, B. J., Wei, N., Ishaq, S., Park, W., Wang, X., . . . Mebus, C. A. (2012). Efficacy and safety of CE-224,535, an antagonist of P2X7 receptor, in treatment of patients with rheumatoid arthritis inadequately controlled by methotrexate. *J Rheumatol, 39*(4), 720-727.

Su, X., Floyd, D. H., Hughes, A., Xiang, J., Schneider, J. G., Uluckan, O., . . . Weilbaecher, K. N. (2012). The ADP receptor P2RY12 regulates osteoclast function and pathologic bone remodeling. *J Clin Invest, 122*(10), 3579-3592. doi:10.1172/jci38576

Sun, D., Junger, W. G., Yuan, C., Zhang, W., Bao, Y., Qin, D., . . . Yu, T. (2013). Shockwaves induce osteogenic differentiation of human mesenchymal stem cells through ATP release and activation of P2X7 receptors. *Stem Cells, 31*(6), 1170-1180. doi:10.1002/stem.1356

Suzuki, M. (2008). Mechanosensitive Channel TRPV4. In A. Kamkin & I. Kiseleva (Eds.), *Mechanosensitive Ion Channels* (pp. 203-231). Dordrecht: Springer Netherlands.

Syberg, S., Brandao-Burch, A., Patel, J. J., Hajjawi, M., Arnett, T. R., Schwarz, P., . . . Orriss, I. R. (2012). Clopidogrel (Plavix), a P2Y12 receptor antagonist, inhibits bone cell function in vitro and decreases trabecular bone in vivo. *J Bone Miner Res, 27*(11), 2373-2386. doi:10.1002/jbmr.1690

Syberg, S., Schwarz, P., Petersen, S., Steinberg, T. H., Jensen, J.-E. B., Teilmann, J., & Jørgensen, N. R. (2012). Association between P2X7 Receptor Polymorphisms and Bone Status in Mice. *J Osteoporos, 2012*, 637986. doi:10.1155/2012/637986

Syeda, R., Florendo, M. N., Cox, C. D., Kefauver, J., Santos, J. S., Martinac, B., & Patapoutian, A. (2016). Piezo1 channels are inherently mechanosensitive. *Cell reports, 17*(7), 1739-1746. doi:10.1016/j.celrep.2016.10.033

Syeda, R., Qiu, Z., Dubin, Adrienne E., Murthy, Swetha E., Florendo, Maria N., Mason, Daniel E., . . . Patapoutian, A. (2016). LRRC8 Proteins Form Volume-Regulated Anion Channels that Sense Ionic Strength. *Cell, 164*(3), 499-511. doi:10.1016/j.cell.2015.12.031

Takahashi, T., Kimura, Y., Niwa, K., Ohmiya, Y., Fujimura, T., Yamasaki, K., & Aiba, S. (2013). In Vivo Imaging Demonstrates ATP Release from Murine Keratinocytes and Its Involvement in Cutaneous Inflammation after Tape Stripping. *Journal of Investigative Dermatology, 133*(10), 2407-2415. doi:https://doi.org/10.1038/jid.2013.163

Takedachi, M., Oohara, H., Smith, B. J., Iyama, M., Kobashi, M., Maeda, K., . . . Murakami, S. (2012). CD73-generated adenosine promotes osteoblast differentiation. *J Cell Physiol, 227*(6), 2622-2631. doi:10.1002/jcp.23001

Takedachi, M., Oohara, H., Smith, B. J., Iyama, M., Kobashi, M., Maeda, K., . . . Murakami, S. (2012). CD73-generated adenosine promotes osteoblast differentiation. *Journal of cellular physiology, 227*(6), 2622-2631. doi:10.1002/jcp.23001

Tami, A. E., Schaffler, M. B., & Knothe Tate, M. L. (2003). Probing the tissue to subcellular level structure underlying bone's molecular sieving function. *Biorheology, 40*(6), 577-590.

Temiyasathit, S., & Jacobs, C. R. (2010). Osteocyte primary cilium and its role in bone mechanotransduction. *Ann N Y Acad Sci, 1192*, 422-428. doi:10.1111/j.1749-6632.2009.05243.x

Terasaki, M., Miyake, K., & McNeil, P. L. (1997). Large plasma membrane disruptions are rapidly resealed by Ca2+-dependent vesicle-vesicle fusion events. *J Cell Biol, 139*(1), 63-74.

Terkeltaub, R. (2006). Physiologic and pathologic functions of the NPP nucleotide pyrophosphatase/phosphodiesterase family focusing on NPP1 in calcification. *Purinergic Signal, 2*(2), 371-377. doi:10.1007/s11302-005-5304-3

Thompson, W. R., Majid, A. S., Czymmek, K. J., Ruff, A. L., Garcia, J., Duncan, R. L., & Farach-Carson, M. C. (2011a). Association of the alpha(2)delta(1) subunit with Ca(v)3.2 enhances membrane expression and regulates mechanically induced ATP release in MLO-Y4 osteocytes. *J Bone Miner Res, 26*(9), 2125-2139. doi:10.1002/jbmr.437

Thompson, W. R., Majid, A. S., Czymmek, K. J., Ruff, A. L., Garcia, J., Duncan, R. L., & Farach-Carson, M. C. (2011b). Association of the alpha(2)delta(1) subunit with Ca(v)3.2 enhances membrane expression and regulates mechanically induced ATP release in MLO-Y4 osteocytes. *Journal of Bone & Mineral Research, 26*(9), 2125-2139. doi:http://dx.doi.org/10.1002/jbmr.437

Thurley, K., Wu, L. F., & Altschuler, S. J. (2018). Modeling Cell-to-Cell Communication Networks Using Response-Time Distributions. *Cell Systems, 6*(3), 355-367. e355.

Toettcher, Jared E., Weiner, Orion D., & Lim, Wendell A. (2013). Using Optogenetics to Interrogate the Dynamic Control of Signal Transmission by the Ras/Erk Module. *Cell, 155*(6), 1422-1434. doi:10.1016/j.cell.2013.11.004

Togo, T., Alderton, J. M., Bi, G. Q., & Steinhardt, R. A. (1999). The mechanism of facilitated cell membrane resealing. *J Cell Sci, 112 (Pt 5)*, 719-731.

Togo, T., Krasieva, T. B., & Steinhardt, R. A. (2000). A Decrease in Membrane Tension Precedes Successful Cell-Membrane Repair. *Molecular Biology of the Cell, 11*(12), 4339-4346.

Toma, I., Bansal, E., Meer, E. J., Kang, J. J., Vargas, S. L., & Peti-Peterdi, J. (2008). Connexin 40 and ATP-dependent intercellular calcium wave in renal glomerular endothelial cells. *American Journal of Physiology-Regulatory, Integrative and Comparative Physiology, 294*(6), R1769-R1776.

Toma, I., Bansal, E., Meer, E. J., Kang, J. J., Vargas, S. L., & Peti-Peterdi, J. (2008). Connexin 40 and ATP-dependent intercellular calcium wave in renal glomerular endothelial cells. *American Journal of Physiology - Regulatory Integrative & Comparative Physiology, 294*(6), R1769-1776. doi:http://dx.doi.org/10.1152/ajpregu.00489.2007

Torres, G. E., Egan, T. M., & Voigt, M. M. (1999). Hetero-oligomeric assembly of P2X receptor subunits. Specificities exist with regard to possible partners. *J Biol Chem, 274*(10), 6653-6659.

Trincavelli, M. L., Daniele, S., Giacomelli, C., Taliani, S., Da Settimo, F., Cosimelli, B., . . . Martini, C. (2014). Osteoblast differentiation and survival: A role for A2B adenosine receptor allosteric modulators. *Biochim Biophys Acta, 1843*(12), 2957-2966. doi:10.1016/j.bbamcr.2014.09.013

Turing, A. M. (1952). The chemical basis of morphogenesis. *Philosophical Transactions of the Royal Society of London. Series B, Biological Sciences, 237*(641), 37-72.

Turner, J. T., Weisman, G. A., & Camden, J. M. (1997). Upregulation of P2Y2 nucleotide receptors in rat salivary gland cells during short-term culture. *Am J Physiol, 273*(3 Pt 1), C1100-1107. doi:10.1152/ajpcell.1997.273.3.C1100

Van Manen, M. D., Nace, J., & Mont, M. A. (2012). Management of primary knee osteoarthritis and indications for total knee arthroplasty for general practitioners. *J Am Osteopath Assoc, 112*(11), 709-715.

von Kügelgen, I., & Starke, K. (1990). Evidence for two separate vasoconstriction-mediating nucleotide receptors, both distinct from the P 2x-receptor, in rabbit basilar artery: a receptor for pyrimidine nucleotides and a receptor for purine nucleotides. *Naunyn-Schmiedeberg's Archives of Pharmacology, 341*(6), 538-546.

von Papen, M., Gambaryan, S., Schütz, C., & Geiger, J. (2013). Determination of ATP and ADP Secretion from Human and Mouse Platelets by an HPLC Assay. *Transfusion Medicine and Hemotherapy, 40*(2), 109-116. doi:10.1159/000350294

Voss, F. K., Ullrich, F., Munch, J., Lazarow, K., Lutter, D., Mah, N., . . . Jentsch, T. J. (2014). Identification of LRRC8 heteromers as an essential component of the volume-regulated anion channel VRAC. *Science, 344*(6184), 634-638. doi:10.1126/science.1252826

Wang, L., Ciani, C., Doty, S. B., & Fritton, S. P. (2004). Delineating bone's interstitial fluid pathway in vivo. *Bone, 34*(3), 499-509. doi:10.1016/j.bone.2003.11.022

Wang, N., Agrawal, A., Jørgensen, N. R., & Gartland, A. (2018). P2X7 receptor regulates osteoclast function and bone loss in a mouse model of osteoporosis. *Scientific Reports, 8*(1), 3507. doi:10.1038/s41598-018-21574-9

Wang, N., & Gartland, A. (2014). Targeting P2 receptors—current progress in treating musculoskeletal diseases. *Curr Opin Pharmacol, 16*, 122-126. doi:https://doi.org/10.1016/j.coph.2014.05.004

Wang, N., Robaye, B., Agrawal, A., Skerry, T. M., Boeynaems, J.-M., & Gartland, A. (2012). Reduced Bone Turnover in Mice Lacking the P2Y(13) Receptor of ADP. *Molecular Endocrinology, 26*(1), 142-152. doi:10.1210/me.2011-1083

Wang, N., Robaye, B., Agrawal, A., Skerry, T. M., Boeynaems, J. M., & Gartland, A. (2012). Reduced bone turnover in mice lacking the P2Y13 receptor of ADP. *Mol Endocrinol, 26*(1), 142-152. doi:10.1210/me.2011-1083

Wang, N., Robaye, B., Gossiel, F., Boeynaems, J. M., & Gartland, A. (2014). The P2Y13 receptor regulates phosphate metabolism and FGF-23 secretion with effects on skeletal development. *Faseb J, 28*(5), 2249-2259. doi:10.1096/fj.13-243626

Wang, N., Rumney, R. M., Yang, L., Robaye, B., Boeynaems, J. M., Skerry, T. M., & Gartland, A. (2013). The P2Y13 receptor regulates extracellular ATP metabolism and the osteogenic response to mechanical loading. *J Bone Miner Res, 28*(6), 1446-1456. doi:10.1002/jbmr.1877

Wang, N., Rumney, R. M. H., Yang, L., Robaye, B., Boeynaems, J.-M., Skerry, T. M., & Gartland, A. (2013a). The P2Y13 receptor regulates extracellular ATP metabolism and the osteogenic response to mechanical loading. *J Bone Miner Res, 28*(6), 1446-1456. doi:10.1002/jbmr.1877

Wang, N., Rumney, R. M. H., Yang, L., Robaye, B., Boeynaems, J.-M., Skerry, T. M., & Gartland, A. (2013b). The P2Y13 receptor regulates extracellular ATP metabolism and the osteogenic response to mechanical loading. *Journal of Bone and Mineral Research, 28*(6), 1446-1456. doi:10.1002/jbmr.1877

Webb, T. E., Simon, J., Krishek, B. J., Bateson, A. N., Smart, T. G., King, B. F., . . . Barnard, E. A. (1993). Cloning and functional expression of a brain G-protein-coupled ATP receptor. *FEBS Lett, 324*(2), 219-225.

Weber, P. A., Chang, H.-C., Spaeth, K. E., Nitsche, J. M., & Nicholson, B. J. (2004). The Permeability of Gap Junction Channels to Probes of Different Size Is Dependent on Connexin Composition and Permeant-Pore Affinities. *Biophysical Journal, 87*(2), 958-973. doi:10.1529/biophysj.103.036350

Wesselius, A., Bours, M. J., Agrawal, A., Gartland, A., Dagnelie, P. C., Schwarz, P., & Jorgensen, N. R. (2011). [Frontiers in Bioscience 16, 2572-2585, June 1, 2011] Role of purinergic receptor polymorphisms in human bone. *Frontiers in Bioscience, 16*, 2572-2585.

Wesselius, A., Bours, M. J., Henriksen, Z., Syberg, S., Petersen, S., Schwarz, P., . . . Dagnelie, P. C. (2013). Association of P2Y(2) receptor SNPs with bone mineral density and osteoporosis risk in a cohort of Dutch fracture patients. *Purinergic Signal, 9*(1), 41-49. doi:10.1007/s11302-012-9326-3

Wesselius, A., Bours, M. J. L., Henriksen, Z., Syberg, S., Petersen, S., Schwarz, P., . . . Dagnelie, P. C. (2013). Association of P2Y(2) receptor SNPs with bone mineral density and osteoporosis risk in a cohort of Dutch fracture patients. *Purinergic Signalling, 9*(1), 41-49. doi:10.1007/s11302-012-9326-3

Wesselius, A., Bours, M. J. L., Jørgensen, N. R., Wiley, J., Gu, B., van Helden, S., . . . Dagnelie, P. C. (2013). Non-synonymous polymorphisms in the P2RX(4) are related to bone mineral density and osteoporosis risk in a cohort of Dutch fracture patients. *Purinergic Signalling, 9*(1), 123-130. doi:10.1007/s11302-012-9337-0

Wicki-Stordeur, L. E., & Swayne, L. A. (2013). The emerging Pannexin 1 signalome: a new nexus revealed? *Frontiers in Cellular Neuroscience, 7*, 287. doi:10.3389/fncel.2013.00287

Wiklund, P., & Gustafsson, L. (1988). Agonist and antagonist characterization of the P2-purinoceptors in the guinea pig ileum. *Acta Physiologica, 132*(1), 15-21.

Xing, S., Grol, M. W., Grutter, P. H., Dixon, S. J., & Komarova, S. V. (2016). Modeling Interactions among Individual P2 Receptors to Explain Complex Response Patterns over a Wide Range of ATP Concentrations. *Frontiers in Physiology, 7*(294). doi:10.3389/fphys.2016.00294

Xing, Y., Gu, Y., Xu, L. C., Siedlecki, C. A., Donahue, H. J., & You, J. (2011). Effects of membrane cholesterol depletion and GPI-anchored protein reduction on osteoblastic mechanotransduction. *J Cell Physiol, 226*(9), 2350-2359. doi:10.1002/jcp.22579

Yamamoto, K., Furuya, K., Nakamura, M., Kobatake, E., Sokabe, M., & Ando, J. (2011). Visualization of flow-induced ATP release and triggering of Ca2+ waves at caveolae in vascular endothelial cells. *Journal of Cell Science, 124*(Pt 20), 3477-3483. doi:10.1242/jcs.087221

Yegutkin, G. G. (2008). Nucleotide- and nucleoside-converting ectoenzymes: Important modulators of purinergic signalling cascade. *Biochim Biophys Acta, 1783*(5), 673-694. doi:10.1016/j.bbamcr.2008.01.024

Yin, J., Xu, K., Zhang, J., Kumar, A., & Yu, F.-S. X. (2007). Wound-induced ATP release and EGF receptor activation in epithelial cells. *Journal of Cell Science, 120*(Pt 5), 815-825. doi:10.1242/jcs.03389

Young, C. N. J., Chira, N., Rog, J., Al-Khalidi, R., Benard, M., Galas, L., . . . Gorecki, D. C. (2017). Sustained activation of P2X7 induces MMP-2-evoked cleavage and functional purinoceptor inhibition. *J Mol Cell Biol*. doi:10.1093/jmcb/mjx030

Zhang, D., Gao, Z. G., Zhang, K., Kiselev, E., Crane, S., Wang, J., . . . Wu, B. (2015). Two disparate ligand-binding sites in the human P2Y1 receptor. *Nature, 520*(7547), 317-321. doi:10.1038/nature14287

Zhang, J., Zhang, K., Gao, Z. G., Paoletta, S., Zhang, D., Han, G. W., . . . Zhao, Q. (2014). Agonist-bound structure of the human P2Y12 receptor. *Nature, 509*(7498), 119-122. doi:10.1038/nature13288

Zhang, K., Zhang, J., Gao, Z. G., Zhang, D., Zhu, L., Han, G. W., . . . Zhao, Q. (2014). Structure of the human P2Y12 receptor in complex with an antithrombotic drug. *Nature, 509*(7498), 115-118. doi:10.1038/nature13083

Zi, Z., Feng, Z., Chapnick, D. A., Dahl, M., Deng, D., Klipp, E., . . . Liu, X. (2011). Quantitative analysis of transient and sustained transforming growth factor-β signaling dynamics. *Molecular Systems Biology, 7*, 492-492. doi:10.1038/msb.2011.22

Zimmermann, H. (2000). Extracellular metabolism of ATP and other nucleotides. *Naunyn-Schmiedebergs Archives of Pharmacology, 362*(4-5), 299-309.

Zimmermann, H., Zebisch, M., & Sträter, N. (2012). Cellular function and molecular structure of ecto-nucleotidases. *Purinergic Signalling, 8*(3), 437-502. doi:10.1007/s11302-012-9309-4

Zippel, N., Limbach, C. A., Ratajski, N., Urban, C., Luparello, C., Pansky, A., . . . Tobiasch, E. (2012a). Purinergic receptors influence the differentiation of human mesenchymal stem cells. *Stem cells and development, 21*(6), 884-900.

Zippel, N., Limbach, C. A., Ratajski, N., Urban, C., Luparello, C., Pansky, A., . . . Tobiasch, E. (2012b). Purinergic receptors influence the differentiation of human mesenchymal stem cells. *Stem Cells Dev, 21*(6), 884-900. doi:10.1089/scd.2010.0576

Chapter Three

Meta-Analytic Methodology for Basic Research

The field of purinergic research, like many basic sciences, is extensive with decades of published data available. However, large-scale quantitative efforts to synthesize findings in the basic sciences are non-existent due to a lack of appropriate analytic tools. The aim of this study (***methodological objective 1*** of dissertation) was to develop the theoretical foundation, computational resources and workflow required to conduct a meta-analysis in the basic sciences. The methods developed here are later used in **Chapter 4** to consolidate and synthesis over 20 years of research on mechanically-stimulated ATP release.

3.1 Abstract

Basic life science literature is rich with information, however methodically quantitative attempts to organize this information are rare. Unlike clinical research, where consolidation efforts are facilitated by systematic review and meta-analysis, the basic sciences seldom use such rigorous quantitative methods. The goal of this study is to present a brief theoretical foundation,

computational resources and workflow outline along with a working example for performing systematic or rapid reviews of basic research followed by meta-analysis. Conventional meta-analytic techniques are extended to accommodate methods and practices found in basic research. Emphasis is placed on handling heterogeneity that is inherently prevalent in studies that use diverse experimental designs and models. We introduce *MetaLab*, a meta-analytic toolbox developed in MATLAB R2016b which implements the methods described in this methodology and is provided for researchers and statisticians at Git repository (https://github.com/NMikolajewicz/MetaLab). Through the course of the manuscript, a rapid review of intracellular ATP concentrations in osteoblasts is used as an example to demonstrate workflow, intermediate and final outcomes of basic research meta-analyses. In addition, the features pertaining to larger datasets are illustrated with a systematic review of mechanically-stimulated ATP release kinetics in mammalian cells. We discuss the criteria required to ensure outcome validity, as well as exploratory methods to identify influential experimental and biological factors. Thus, meta-analyses provide informed estimates for biological outcomes and the range of their variability, which are critical for the hypothesis generation and evidence-driven design of translational studies, as well as development of computational models.

3.2 Introduction

Evidence-based medical practice aims to consolidate best research evidence with clinical and patient expertise. Systematic reviews and meta-analyses are essential tools for synthesizing evidence needed to inform clinical decision making and policy. Systematic reviews summarize available literature using specific search parameters followed by critical appraisal and logical synthesis of multiple primary studies (Gopalakrishnan & Ganeshkumar, 2013). Meta-analysis refers to the statistical analysis of the data from independent primary studies focused on the same question, which aims to generate a quantitative estimate of the studied phenomenon, for example, the effectiveness of the intervention (Gopalakrishnan & Ganeshkumar, 2013). In clinical research, systematic reviews and meta-analyses are a critical part of evidence-based medicine. However, in basic science, attempts to evaluate prior literature in such rigorous and quantitative manner are rare, and narrative reviews are prevalent. The goal of this manuscript is to provide a brief theoretical foundation, computational resources and workflow outline for performing a systematic or rapid review followed by a meta-analysis of basic research studies.

Meta-analyses can be a challenging undertaking, requiring tedious screening and statistical understanding. There are several guides available that outline how to undertake a meta-analysis in clinical research (Higgins, Green et al., 2011). Software packages supporting clinical meta-analyses include the Excel plugins MetaXL (Barendregt, J., & Doi, S. 2009) and Mix 2.0 (Bax, 2016), Revman (Cochrane Collaboration, 2011), Comprehensive Meta-Analysis Software [CMA (Borenstein, Hedges et al., 2005)], JASP (JASP Team, 2018) and MetaFOR library for R (Viechtbauer, 2010). While these packages can be adapted to basic science projects, difficulties may arise due to specific features of basic science studies, such as large and complex datasets and heterogeneity in experimental methodology. To address these limitations, we developed a software package aimed to facilitate meta-analyses of basic research, *MetaLab* in MATLAB R2016b, with an intuitive graphical interface that permits users with limited statistical and coding background to proceed with a meta-analytic project. We organized *MetaLab* into six modules (**Fig 3-1**), each focused on different stages of the meta-analytic process, including graphical-data extraction, model parameter estimation, quantification and exploration of heterogeneity, data-synthesis and meta-regression.

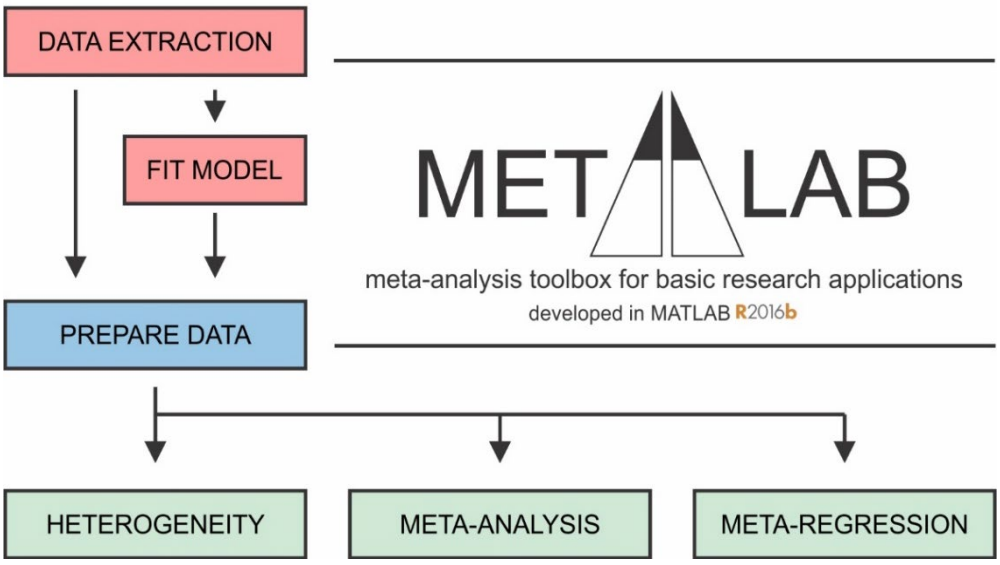

Figure 3-1. General framework of MetaLab. The *Data Extraction* module assists with graphical data extraction from study figures. *Fit Model* module applies Monte-Carlo error propagation approach to fit complex datasets to model of interest. Prior to further analysis, reviewers have opportunity to manually curate and consolidate data from all sources. *Prepare Data* module imports datasets from a spreadsheet into MATLAB in a standardized format. *Heterogeneity*, *Meta-analysis* and *Meta-regression* modules facilitate meta-analytic synthesis of data.

In the present manuscript, we describe each step of the meta-analytic process with emphasis on specific considerations made when conducting a review of basic research. The complete workflow of parameter estimation using *MetaLab* is demonstrated for evaluation of intracellular ATP content in osteoblasts (OB $[ATP]_{ic}$ dataset) based on a rapid literature review. In addition, the features pertaining to larger datasets are explored with the ATP release kinetics from mechanically-stimulated mammalian cells (ATP release dataset) obtained as a result of a systematic review in our prior work (Mikolajewicz, Mohammed et al, 2018).

MetaLab can be freely accessed at Git repository (https://github.com/NMikolajewicz/MetaLab), and a detailed documentation of how to use MetaLab together with a working example is available in **Appendix A1**.

3.3 Validity of evidence in the basic sciences

To evaluate the translational potential of basic research, the validity of evidence must first be assessed, usually by examining the approach taken to collect and evaluate the data. Studies in the basic sciences are broadly grouped as hypothesis-generating and hypothesis-driven. The former tend to be small-sampled proof-of-principle studies and are typically exploratory and less valid than the latter. An argument can even be made that studies that report novel findings fall into this group as well, since their findings remain subject to external validation prior to being accepted by the broader scientific community. Alternatively, hypothesis-driven studies build upon what is known or strongly suggested by earlier work. These studies can also validate prior experimental findings with incremental contributions. Although such studies are often overlooked and even dismissed due to a lack of substantial novelty, their role in external validation of prior work is critical for establishing the translational potential of findings.

Another dimension to the validity of evidence in the basic sciences is the selection of experimental model. The human condition is near-impossible to recapitulate in a laboratory setting, therefore experimental models (e.g., cell lines, primary cells, animal models) are used to mimic the phenomenon of interest, albeit imperfectly. For these reasons, the best quality evidence comes from evaluating the performance of several independent experimental models. This is accomplished through systematic approaches that consolidate evidence from multiple studies, thereby filtering the signal from the noise and allowing for side-by-side comparison. While systematic reviews can be conducted to accomplish a qualitative comparison, meta-analytic

approaches employ statistical methods which enable hypothesis generation and testing. When a meta-analysis in the basic sciences is hypothesis-driven, it can be used to evaluate the translational potential of a given outcome and provide recommendations for subsequent translational- and clinical-studies. Alternatively, if meta-analytic hypothesis testing is inconclusive, or exploratory analyses are conducted to examine sources of inconsistency between studies, novel hypotheses can be generated, and subsequently tested experimentally. **Figure 3-2** summarizes this proposed framework.

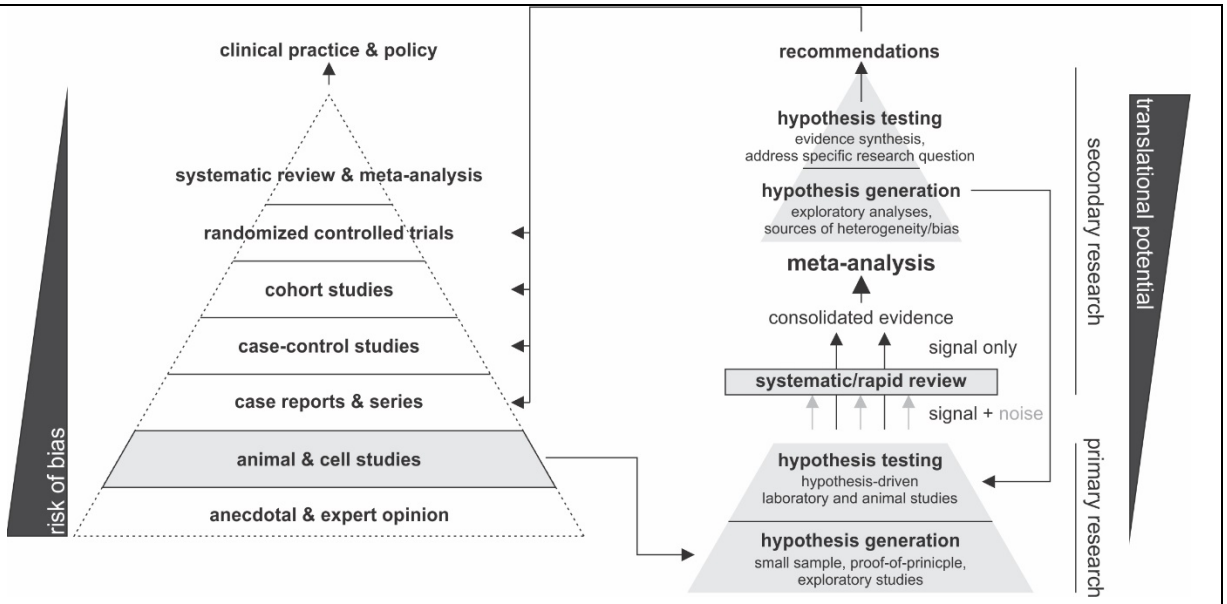

Figure 3-2. Schematic of proposed hierarchy of translational potential in basic research.

3.4 Steps in Quantitative Literature Review

Identification of relevant literature precedes meta-analytic evidence synthesis, typically proceeding through the following steps:

1) **Formulate research question**
    - Define primary and secondary objectives
    - Determine breadth of question
2) **Identify relevant literature**
    - Construct search strategy: rapid or systematic search
    - Screen studies and determine eligibility
3) **Extract and consolidate study-level data**

- Extract data from relevant studies
- Collect relevant study-level characteristics and experimental covariates
- Evaluate quality of studies
- Estimate model parameters for complex relationships (optional)

4) **Data appraisal and preparation**
    - Compute appropriate outcome measure
    - Evaluate extent of between-study inconsistency (heterogeneity)
    - Perform relevant data transformations
    - Select meta-analytic model
5) **Synthesize study-level data into summary measure**
    - Pool data and calculate summary measure and confidence interval
6) **Exploratory analyses**
    - Explore potential sources of heterogeneity (ex. biological or experimental)
    - Subgroup and meta-regression analyses
7) **Knowledge synthesis**
    - Interpret findings
    - Provide recommendations for future work

3.5 Meta-analysis methodology

3.5.1 Search and selection strategies

The first stage of any review involves formulating a primary objective in the form of a research question or hypothesis. Reviewers must explicitly define the objective of the review before starting the project, which serves to reduce the risk of data dredging, where reviewers later assign meaning to significant findings. Secondary objectives may also be defined; however, precaution must be taken as the search strategies formulated for the primary objective may not entirely encompass the body of work required to address the secondary objective. Depending on the purpose of a review, reviewers may choose to undertake a rapid or systematic review. While the meta-analytic methodology is similar for systematic and rapid reviews, the scope of literature assessed tends to be significantly narrower for rapid reviews permitting the project to proceed faster.

3.5.1.1 Systematic review and meta-analysis

Systematic reviews involve comprehensive search strategies that enable reviewers to identify all relevant studies on a defined topic (DeLuca, Mullins et al., 2008). Meta-analytic methods then permit reviewers to quantitatively appraise and synthesize outcomes across studies to obtain information on statistical significance and relevance. Systematic reviews of basic research data have the potential of producing information-rich databases which allow extensive secondary analysis. To comprehensively examine the pool of available information, search criteria must be sensitive enough not to miss relevant studies. Key terms and concepts that are expressed as synonymous keywords and index terms, such as Medical Subject Headings (MeSH) must be combined using Boolean operators AND, OR and NOT (Ecker & Skelly, 2010). Truncations, wildcards, and proximity operators can also help refine a search strategy by including spelling variations and different wordings of the same concept (Ecker & Skelly, 2010). Search strategies can be validated using a selection of expected relevant studies. If the search strategy fails to retrieve even one of the selected studies, the search strategy requires further optimization. This process is iterated, updating the search strategy in each iterative step until the search strategy performs at a satisfactory level (Finfgeld-Connett & Johnson, 2013). A comprehensive search is expected to return a large number of studies, many of which are not relevant to the topic, commonly resulting in a specificity of less than 10% (McGowan & Sampson, 2005). Therefore, the initial stage of sifting through the library to select relevant studies is time-consuming (may take six months to two years) and prone to human error. At this stage, it is recommended to include at least two independent reviewers to minimize selection bias and related errors. Nevertheless, systematic reviews have a potential to provide the highest quality quantitative evidence synthesis to directly inform the experimental and computational basic, preclinical and translational studies.

3.5.1.2 Rapid reviews and meta-analysis

The goal of the rapid review, as the name implies, is to decrease the time needed to synthesize information. Rapid reviews are a suitable alternative to systematic approaches if reviewers prefer to get a general idea of the state of the field without an extensive time investment. Search strategies are constructed by increasing search specificity, thus reducing the number of irrelevant studies identified by the search at the expense of search comprehensiveness (Haby, Chapman et al., 2016). The strength of a rapid review is in its flexibility to adapt to the needs of the reviewer, resulting in

a lack of standardized methodology (Mattivi & Buchberger, 2016). Common shortcuts made in rapid reviews are: (*i*) narrowing search criteria, (*ii*) imposing date restrictions, (*iii*) conducting the review with a single reviewer, (*iv*) omitting expert consultation (i.e. librarian for search strategy development), (*v*) narrowing language criteria (ex. English only), (*vi*) foregoing the iterative process of searching and search term selection, (*vii*) omitting quality checklist criteria and (*viii*) limiting number of databases searched (Ganann, Ciliska et al., 2010). These shortcuts will limit the initial pool of studies returned from the search, thus expediting the selection process, but also potentially resulting in the exclusion of relevant studies and introduction of selection bias. While there is a consensus that rapid reviews do not sacrifice quality, or synthesize misrepresentative results (Haby et al., 2016), it is recommended that critical outcomes be later verified by systematic review (Ganann et al., 2010). Nevertheless, rapid reviews are a viable alternative when parameters for computational modeling need to be estimated. While systematic and rapid reviews rely on different strategies to select the relevant studies, the statistical methods used to synthesize data from the systematic and rapid review are identical.

3.5.1.3 Screening and selection

When the literature search is complete (the date articles were retrieved from the databases needs to be recorded), articles are extracted and stored in a reference manager for screening. Before study screening, the inclusion and exclusion criteria must be defined to ensure consistency in study identification and retrieval, especially when multiple reviewers are involved. The critical steps in screening and selection are 1) removing duplicates, 2) screening for relevant studies by title and abstract, and 3) inspecting full texts to ensure they fulfill the eligibility criteria. There are several reference managers available including Mendeley and Rayyan, specifically developed to assist with screening systematic reviews. However, 98% of authors report using Endnote, Reference Manager or RefWorks to prepare their reviews (Lorenzetti & Ghali, 2013). Reference managers often have deduplication functions; however, these can be tedious and error-prone (Kwon, Lemieux et al., 2015). A protocol for faster and more reliable de-duplication in Endnote has been recently proposed (Bramer, Giustini et al., 2016). The selection of articles should be sufficiently broad not to be dominated by a single lab or author. In basic research articles, it is common to find data sets that are reused by the same group in multiple studies. Therefore additional precautions should be taken when deciding to include multiple studies published by a single group. At the end

of the search, screening and selection process, the reviewer obtains a complete list of eligible full-text manuscripts. The entire screening and selection process should be reported in a PRISMA diagram, which maps the flow of information throughout the review according to prescribed guidelines published elsewhere (Moher, Liberati et al., 2009). **Figure 3-3** provides a summary of the workflow of search and selection strategies using the OB $[ATP]_{ic}$ rapid review and meta-analysis as an example.

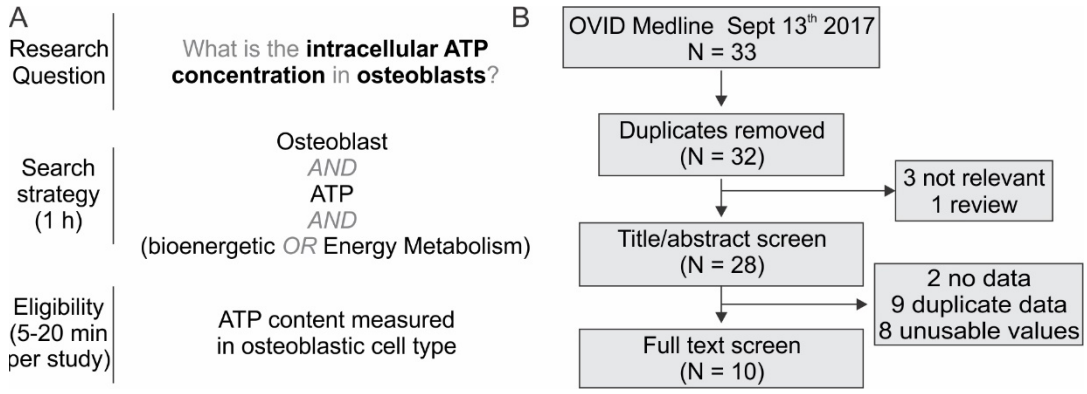

Figure 3-3. Example of the rapid review literature search. (A) Development of the search parameters to find literature on the intracellular ATP content in osteoblasts. **(B)** PRISMA diagram for the information flow.

3.5.2 Data extraction, initial appraisal, and preparation

3.5.2.1 Identification of parameters to be extracted

It is advised to predefine analytic strategies before data extraction and analysis. However, the availability of reported effect measures and study designs will often influence this decision. When reviewers aim to estimate the absolute mean difference (absolute effect), normalized mean difference, response ratio or standardized mean difference (ex. Hedges' g), they need to extract study-level means (θ_i), standard deviations $\left(sd(\theta_i)\right)$, and sample sizes ($n_i$), for control (denoted θ_i^c, $sd(\theta_i^c)$, and n_i^c) and intervention (denoted θ_i^r, $sd(\theta_i^r)$, and n_i^r) groups, for studies i. To estimate absolute mean effect, only the mean (θ_i^r), standard deviation $(sd(\theta_i^r),)$ and sample size (n_i^r) are required. In basic research, it is common for a single study to present variations of the same observation (ex. measurements of the same entity using different techniques). In such cases, each point may be treated as an individual observation, or common outcomes within a study can be pooled by taking the mean weighted by the sample size. Another consideration is inconsistency

between effect size units reported on the absolute scale, for example, protein concentrations can be reported as g/cell, mol/cell, g/g wet tissue or g/g dry tissue. In such cases, conversion to a common representation is required for comparison across studies, for which appropriate experimental parameters and calibrations need to be extracted from the studies. While some parameters can be approximated by reviewers, such as cell-related parameters found in BioNumbers database (Milo, Jorgensen et al., 2010) and equipment-related parameters presumed from manufacturer manuals, reviewers should exercise caution when making such approximations as they can introduce systematic errors that manifest throughout the analysis. When data conversion is judged to be difficult but negative/basal controls are available, scale-free measures (i.e., normalized, standardized, or ratio effects) can still be used in the meta-analysis without the need to convert effects to common units on the absolute scale. In many cases, reviewers may only be able to decide on a suitable effect size measure after data extraction is complete.

It is regrettably common to encounter unclear or incomplete reporting, especially for the sample sizes and uncertainties. Reviewers may choose to reject studies with such problems due to quality concerns or to employ conservative assumptions to estimate missing data. For example, if it is unclear if a study reports the standard deviation or standard error of the mean, it can be assumed to be a standard error, which provides a more conservative estimate. If a study does not report uncertainties but is deemed important because it focuses on a rare phenomenon, imputation methods have been proposed to estimate uncertainty terms (Chowdhry, Dworkin et al., 2016). If a study reports a range of sample sizes, reviewers should extract the lowest value. Strategies to handle missing data should be pre-defined and thoroughly documented.

In addition to identifying relevant primary parameters, *a priori* defined study-level characteristics that have a potential to influence the outcome, such as species, cell type, specific methodology, should be identified and collected in parallel to data extraction. This information is valuable in subsequent exploratory analyses and can provide insight into influential factors through between-study comparison.

3.5.2.2 Quality assessment

Formal quality assessment allows the reviewer to appraise the quality of identified studies and to make informed and methodical decision regarding exclusion of poorly conducted studies. In

general, based on initial evaluation of full texts, each study is scored to reflect the study's overall quality and scientific rigor. Several quality-related characteristics have been described (Sena, van der Worp et al., 2007), such as: (*i*) published in peer-reviewed journal, (*ii*) complete statistical reporting, (*iii*) randomization of treatment or control, (*iv*) blinded analysis, (*v*) sample size calculation prior to the experiment, (*vi*) investigation of a dose-response relationship, and (*vii*) statement of compliance with regulatory requirements. We also suggest that the reviewers of basic research studies assess (*viii*) objective alignment between the study in question and the meta-analytic project. This involves noting if the outcome of interest was the primary study objective or was reported as a supporting or secondary outcome, which may not receive the same experimental rigor and is subject to expectation bias (Sheldrake, 1997). Additional quality criteria specific to experimental design may be included at the discretion of the reviewer. Once study scores have been assembled, study-level aggregate quality scores are determined by summing the number of satisfied criteria, and then evaluating how outcome estimates and heterogeneity vary with study quality. Significant variation arising from poorer quality studies may justify study omission in subsequent analysis.

3.5.2.3 Extraction of tabular & graphical data

The next step is to compile the meta-analytic data set, which reviewers will use in subsequent analysis. For each study, the complete dataset which includes parameters required to estimate the target outcome, study characteristics, as well as data necessary for unit conversion needs to be extracted. Data reporting in basic research are commonly tabular or graphical. Reviewers can accurately extract tabular data from the text or tables. However, graphical data often must be extracted from the graph directly using time consuming and error prone methods. The Data Extraction Module in *MetaLab* was developed to facilitate systematic and unbiased data extraction; Reviewers provide study figures as inputs, then specify the reference points that are used to calibrate the axes and extract the data (**Fig 3-4A, B**).

To validate the performance of the *MetaLab* Data Extraction Module, we generated figures using 319 synthetic data points plotted with varying markers sizes (**Fig 3-4C**). Extracted and actual values were correlated ($R^2 = 0.99$) with the relationship slope estimated as 1.00 (95% CI: 0.99 to 1.01) (**Fig 3-4D**). Bias was absent, with a mean percent error of 0.00 % (95% CI: -0.02 to 0.02 %) (**Fig 3-4E**). The narrow range of errors between -2.00 and 1.37 %, and consistency between the

median and mean error indicated no skewness. Data marker size did not contribute to the extraction error, as 0.00% of the variation in absolute error was explained by marker size, and the slope of the relationship between marker size and extraction error was 0.000 (95% CI: -0.001, 0.002) (**Fig 3-4F**). There data demonstrate that graphical data can be reliably extracted using *MetaLab*.

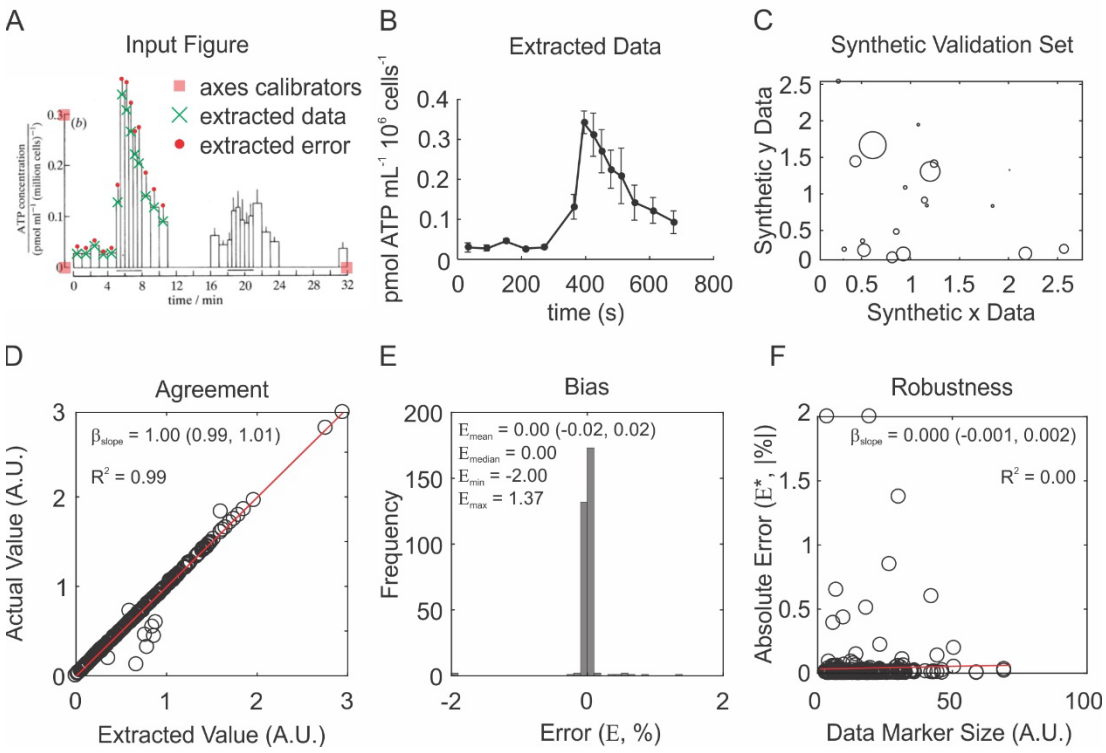

Figure 3-4. MetaLab data extraction procedure is accurate, unbiased and robust to quality of data presentation. **(A, B)** Example of graphical data extraction using MetaLab. **(A)** Original figure with axes, data points and corresponding errors marked by reviewer (Bodin, Milner et al., 1992). **(B)** Extracted data with error terms. **(C-F)** Validation of MetaLab data-extraction module. **(C)** Synthetic datasets were constructed using randomly generated data coordinates and marker sizes. **(D)** Extracted values were consistent with true values evaluated by linear regression with the slope β_{slope}, *red line*: line of equality. **(E)** Data extraction was unbiased, evaluated with distribution of percent errors between true and extracted values. E_{mean}, E_{median}, E_{min}, and E_{max} are mean, median, minimum and maximum % error respectively. **(F)** The absolute errors of extracted data were independent of data marker size, evaluated by linear regression with the slope β_{slope}, *red line*: line regression.

3.5.2.4 Extracting data form complex relationships

Basic science often focuses on natural processes and phenomena characterized by complex relationships between a series of inputs (e.g., exposures) and outputs (e.g., response). The results are commonly explained by an accepted model of the relationship, such as Michaelis-Menten

model of enzyme kinetics which involves two parameters – V_{max} for the maximum rate and K_m for the substrate concentration half of V_{max}. For meta-analysis, model parameters characterizing complex relationships are of interest as they allow direct comparison of different multi-observational datasets. However, study-level outcomes for complex relationships often (*i*) lack consistency in reporting, and (*ii*) lack estimates of uncertainties for model parameters. Therefore, reviewers wishing to perform a meta-analysis of complex relationships may need to fit study-level data to a unified model $y = f(x, \beta)$ to estimate parameter set β characterizing the relationship (**Table 3-1**) and assess the uncertainty in β.

Table 3-1. Commonly used models to explain complex relationships in the basic sciences

Model	Equation	Parameter Meaning	Applications
Linear model	$y = \beta_1 x + \beta_2$	β_1: slope, magnitude of relationship β_2: intercept, response at x = 0	reaction rates
Quadratic model (vertex form)	$y = \beta_1 (x - \beta_2)^2 + \beta_3$	β_1: curvature factor β_2: x at global max/min β_3: global maxima/minimal	trajectory modeling
Exponential model	$y = \beta_1 e^{\beta_2 x}$	β_1: intercept, response at x = 0 β_2: decay/growth constant	population decay/growth
Michaelis-Menten Saturation Curve, hyperbolic curve	$y = \frac{\beta_1 x}{\beta_2 + x}$	β_1: max response β_2: x at half max response	enzyme kinetics, reaction rates, infection rates, drug clearance
Sigmoidal E_{max} Model, Hill Function	$y = \frac{\beta_1 x^{\beta_3}}{(\beta_2)^{\beta_3} + x^{\beta_3}}$	β_1: max response β_2: x at half max response β_3: slope-related term	dose-response relationships, pharmacodynamics

The study-level data can be fitted to a model using conventional fitting methods, in which the model parameter error terms depend on the goodness of fit and number of available observations. Alternatively, a Monte Carlo simulation approach (Cox, Harris et al., 2003) allows for the propagation of study-level variances (uncertainty in the model inputs) to the uncertainty in the model parameter estimates (**Fig 3-5**). Suppose that for a reported set of predictor variables $x = \{\bar{x}_1\ \bar{x}_2 \dots \bar{x}_k\}$ there is an array of observations $\theta = \{\bar{\theta}_1\ \bar{\theta}_2 \dots \bar{\theta}_k\}$ along with the corresponding standard deviations $sd(\theta) = \{sd(\bar{\theta}_1), sd(\bar{\theta}_2) \dots sd(\bar{\theta}_k)\}$ and sample sizes $n = \{n_1, n_2 \dots n_k\}$ (**Fig 3-5A**). The Monte Carlo error propagation method assumes that observations are normally

distributed, enabling pseudo random observations to be sampled from a distribution approximated by $\mathcal{N}(\bar{\theta}_k, sd(\bar{\theta}_k)^2)$. The pseudo random observations are then averaged to obtain a Monte-Carlo estimate $\bar{\theta}_k^*$ for each observation such that

$$\bar{\theta}_k^* = \frac{1}{n_k}\sum_{j=1}^{n_k}(\theta_{kj}^*) \quad (1)$$

where θ_{kj}^* represents a pseudo-random variable sampled n_k times from $\mathcal{N}(\bar{\theta}_k, sd(\bar{\theta}_k)^2)$. The model of interest is fitted to set $\{\bar{\theta}_1^*, \ldots, \bar{\theta}_k^*\}$ using the least-squares method to obtain an estimate of model parameters β (**Fig 3-5B**). After many iterations of resampling and fitting, a distribution of parameter estimates $\mathcal{N}(\bar{\beta}, sd(\bar{\beta})^2)$ is obtained, from which the parameter means $\bar{\beta}$ and variances $sd(\bar{\beta})^2$ can be estimated (**Fig 3-5C, D**). As the number of iterations M tend to infinity, the parameter estimate converges to the expected value $E(\beta)$.

$$\lim_{M\to\infty}\frac{1}{M}(\beta_1 + \beta_2 + \cdots + \beta_M) = E(\beta) \quad (2)$$

It is critical for reviewers to ensure the data is consistent with the model such that the estimated parameters sufficiently capture the information conveyed in the underlying study-level data. In general, reliable model fittings are characterized by normal parameter distributions (**Fig 3-5D**) and have a high goodness of fit as quantified by R^2. The advantage of using the Monte-Carlo approach is that it works as a black box procedure that does not require complex error propagation formulas, thus allowing handling of correlated and independent parameters without additional consideration.

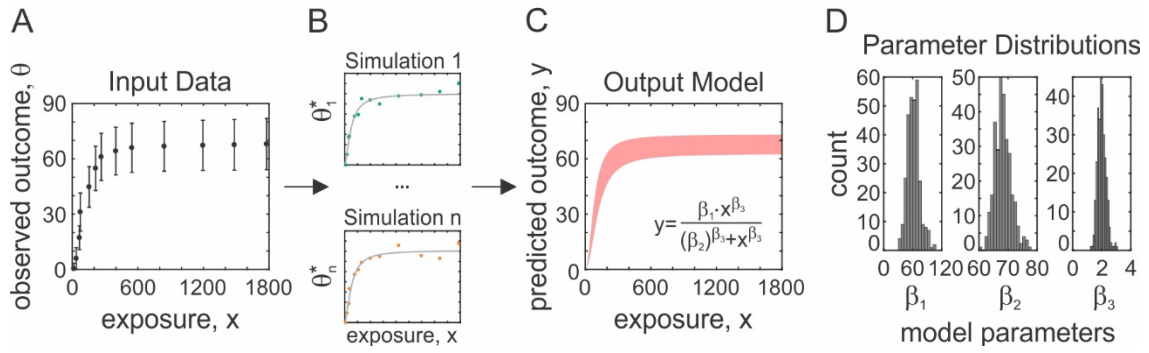

Figure 3-5. Model parameter estimation with Monte-Carlo error propagation. **(A)** Study-level data taken from ATP release meta-analysis. **(B)** Assuming sigmoidal model, parameters were estimated using MetaLab by randomly sampling data from distributions defined by study level data and model parameters were estimated for each set of sampled data. **(C)** Final model using parameters estimated from 400 simulations. **(D)** Distributions of parameters estimated for given dataset are unimodal and symmetrical.

3.5.2.5 Study-level effect sizes

Depending on the purpose of the review product, study-level outcomes θ_i can be expressed as one of several effect size measures. The absolute effect size, computed as a mean outcome or absolute difference from baseline, is the simplest, is independent of variance, and retains information about the context of the data (Baguley, 2009). However, the use of absolute effect size requires authors to report on a common scale or provide conversion parameters. In cases where a common scale is difficult to establish, a scale-free measure, such as standardized, normalized or relative measures can be used. Standardized mean differences, such Hedges' g or Cohen d, report the outcome as the size of the effect (difference between the means of experimental and control groups) relative to the overall variance (pooled and weighted standard deviation of combined experimental and control groups). The standardized mean difference, in addition to odds or risk ratios, is widely used in meta-analysis of clinical studies (Vesterinen, Sena et al., 2014), since it allows to summarize metrics that do not have unified meaning (e.g., a pain score), and takes into account the variability in the samples. However, the standardized measure is rarely used in basic science since study outcomes are commonly a defined measure, sample sizes are small, and variances are highly influenced by experimental and biological factors. Other measures that are more suited for basic science are the normalized mean difference, which expresses the difference between the outcome and baseline as a proportion of the baseline (alternatively called the percentage difference), and response ratio, which reports the outcome as a proportion of the baseline. All discussed measures have been included in *MetaLab* (**Table 3-2**).

Table 3-2. Types of Effect Sizes. Provided are formulas to calculate the mean and standard error for the specified effect sizes.

Measure	Mean	Standard Error
Absolute	$\theta_i = \begin{cases} \theta_i^r - \theta_i^c, \ if\ \theta_i^c\ reported \\ \theta_i^r, else \end{cases}$	$se(\theta_i) = \begin{cases} \sqrt{\frac{n_i^c + n_i^r}{n_i^c n_i^r}} sd(\theta_i)^2, \ if\ \theta_i^c\ reported \\ \frac{sd(\theta_i^r)}{\sqrt{n_i^r}}, else \end{cases}$ Where $sd(\theta_i) = \sqrt{\frac{(n_i^c-1)sd(\theta_i^c)+(n_i^r-1)sd(\theta_i^r)}{n_i^c+n_i^r-2}}$
Standardized (Hedges' g)	$\theta_i = \frac{\theta_i^r - \theta_i^c}{sd(\theta_i)} \cdot \left(1 - \frac{3}{4(n_i^c + n_i^r) - 9}\right)$	$se(\theta_i) = \sqrt{\frac{n_i^c + n_i^r}{n_i^c n_i^r} + \frac{\theta_i^2}{2\left((n_i^c + n_i^r) - 3.94\right)}}$

	Where $sd(\theta_i) = \sqrt{\frac{(n_i^c-1)sd(\theta_i^c)+(n_i^r-1)sd(\theta_i^r)}{n_i^c+n_i^r-2}}$	
Normalized	$\theta_i = \frac{\theta_i^r - \theta_i^c}{\theta_i^c}$	$se(\theta_i) = \sqrt{\frac{\left(\frac{sd(\theta_i^c)}{\theta_i^c}\right)^2}{n_i^c} + \frac{\left(\frac{sd(\theta_i^r)}{\theta_i^r}\right)^2}{n_i^r}}$
Ratio	$\theta_i = \frac{\theta_i^r}{\theta_i^c}$	$se(\theta_i) = \sqrt{\frac{(\theta_i^r)^2}{(\theta_i^c)^2}\left(\frac{sd(\theta_i^r)^2}{n_i^r(\theta_i^r)^2} + \frac{sd(\theta_i^c)^2}{n_i^c(\theta_i^c)^2}\right)}$

3.5.3 Data synthesis

The goal of any meta-analysis is to provide an outcome estimate that is representative of all study-level findings. One important feature of the meta-analysis is its ability to incorporate information about the quality and reliability of the primary studies by weighing larger, better reported studies more heavily. The two quantities of interest are the overall estimate and the measure of the variability in this estimate. Study-level outcomes θ_i are synthesized as a weighted mean $\hat{\theta}$ according to the study-level weights w_i:

$$\hat{\theta} = \frac{\sum_i(\theta_i \cdot w_i)}{\sum_i(w_i)} \quad (3)$$

The choice of a weighting scheme dictates how study-level variances are pooled to estimate the variance of the weighted mean. The weighting scheme thus significantly influences the outcome of meta-analysis, and if poorly chosen, potentially risks over-weighing less precise studies and generating a less valid, non-generalizable outcome. Thus, the notion of defining an *a priori* analysis protocol has to be balanced with the need to assure that the dataset is compatible with the chosen analytic strategy, which may be uncertain prior to data extraction. We provide strategies to compute and compare different study-level and global outcomes and their variances.

3.5.3.1 Weighting schemes

To generate valid estimates of cumulative knowledge, studies are weighed according to their reliability. This conceptual framework, however, deteriorates if reported measures of precision are themselves flawed. The most commonly used measure of precision is the inverse variance which is a composite measure of total variance and sample size, such that studies with larger sample sizes and lower experimental errors are more reliable and more heavily weighed. Inverse variance

weighting schemes are valid when (*i*) sampling error is random, (*ii*) the reported effects are homoscedastic, i.e., have equal variance and (*iii*) the sample size reflects the number of independent experimental observations. When assumptions (*i*) or (*ii*) are violated, sample size weighing can be used as an alternative. Despite sample size and sample variance being such critical parameters in the estimation of the global outcome, they are often prone to deficient reporting practices.

Potential problems with sample variance and sample size. The standard error $se(\theta_i)$ is required to compute inverse variance weights, however, primary literature as well as meta-analysis reviewers often confuse standard errors with standard deviations $sd(\theta_i)$ (Altman & Bland, 2005). Additionally, many assays used in basic research often have uneven error distributions, such that the variance component arising from experimental error depends on the magnitude of the effect (Bittker & Ross, 2016). Such uneven error distributions will lead to biased weighing that does not reflect true precision in measurement. Fortunately, the standard error and standard deviation have characteristic properties that can be assessed by the reviewer to determine whether inverse variance weights are appropriate for a given dataset. The study-level standard error $se(\theta_i)$ is a measure of precision and is estimated as the product of the sample standard deviation $sd(\theta_i)$ and margin of error $\frac{1}{\sqrt{n_i}}$ for study i. Therefore, the standard error is expected to be approximately inversely proportionate to the root of the study-level sample size n_i

$$se(\theta_i) \sim \frac{1}{\sqrt{n_i}} \tag{4}$$

Unlike the standard error, the standard deviation – a measure of the variance of a random variable $sd(\theta)^2$ – is assumed to be independent of the sample size because it is a descriptive statistic rather than a precision statistic. Since the total observed study-level sample variance is the sum of natural variability (assumed to be constant for a phenomenon) and random error, no relationship is expected between reported standard deviations and sample sizes. These assumptions can be tested by correlation analysis and can be used to inform the reviewer about the reliability of the study-level uncertainty measures. For example, a relationship between sample size and sample variance was observed for the OB $[ATP]_{ic}$ dataset (**Fig 3-6A)**, but not for the ATP release data (**Fig 3-6B**). Therefore, in the case of the OB $[ATP]_{ic}$ data set, lower variances are not associated with higher precision and inverse variance weighting is not appropriate. Sample sizes are also frequently

misrepresented in the basic sciences, as experimental replicates and repeated experiments are often reported interchangeably (incorrectly) as sample sizes (Vaux, Fidler et al., 2012). Repeated (independent) experiments refer to number of randomly sampled observations, while replicates refer to the repeated measurement of a sample from one experiment to improve measurement precision. Statistical inference theory assumes random sampling, which is satisfied by independent experiments but not by replicate measurements. Misrepresentative reporting of replicates as the sample size may artificially inflate the reliability of results. While this is difficult to identify, poor reporting may be reflected in the overall quality score of a study.

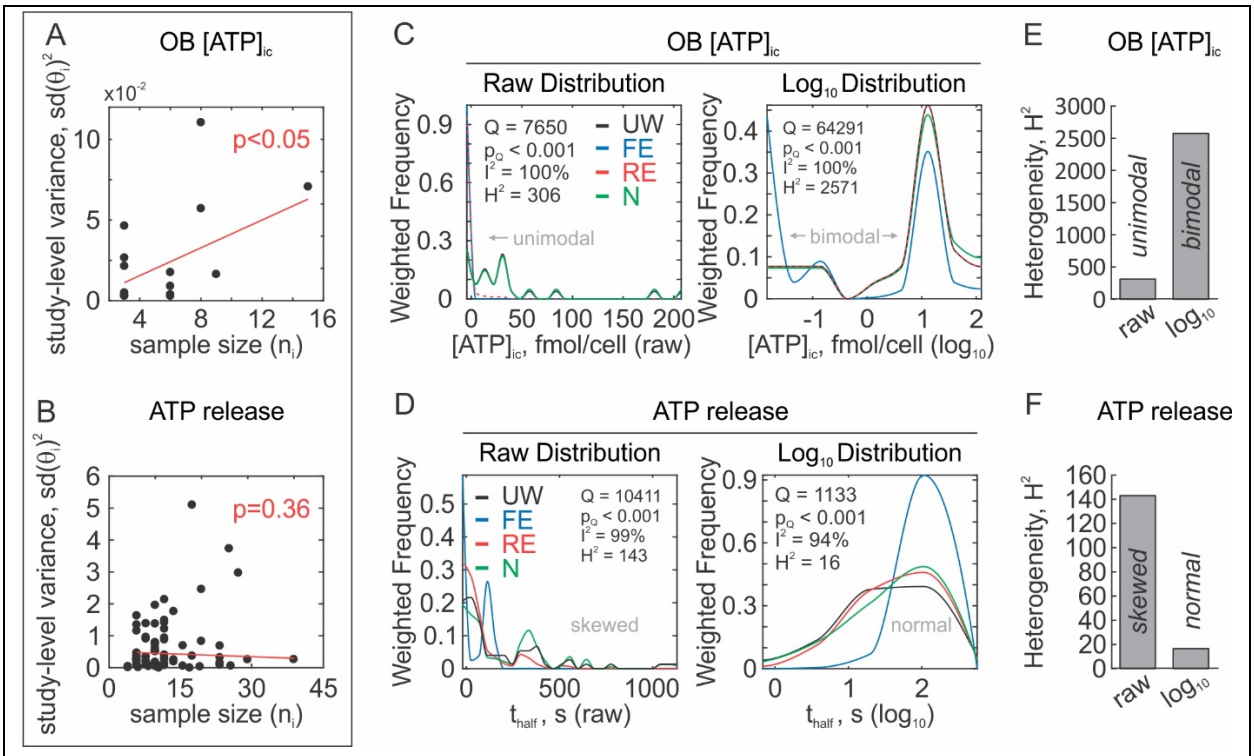

Figure 3-6. Assessment of study-level outcomes. (A, B) Reliability of study-level error measures. Relationship between study-level squared standard deviation $sd(\theta_i)^2$ and sample sizes n_i are assumed to be independent when reliably reported. Association between $sd(\theta_i)^2$ and n_i was present in OB $[ATP]_{ic}$ data set **(A)** and absent in ATP release data set **(B)**, *red line*: linear regression. **(C, D)** Distributions of study-level outcomes. Assessment of unweighted (UW – *black*) and weighted (fixed effect; FE – *blue*, random effects; RE – *red*, sample-size weighting; N – *green*) study-level distributions of data from OB $[ATP]_{ic}$ (**C**) and ATP release (**D**) data sets, before (*left*) and after $\log_{10}$ transformation (*right*). Heterogeneity was quantified by Q, I^2 and H^2 heterogeneity statistics. **(E, F)** After $\log_{10}$ transformation, H^2 heterogeneity statistics increased for OB $[ATP]_{ic}$ data set (**E**) and decreased for ATP release (**F**) data set.

Inverse variance weighting. The inverse variance is the most common measure of precision, representing a composite measure of total variance and sample size. Widely used weighting schemes based on the inverse variance are fixed effect or random effects meta-analytic models. The fixed effect model assumes that all the studies sample one true effect γ. The observed outcome θ_i for study i is then a function of a within-study error ε_i, $\theta_i = \gamma + \varepsilon_i$, where ε_i is normally distributed $\varepsilon_i \sim \mathcal{N}(0, se(\theta_i)^2)$. The standard error $se(\theta_i)$ is calculated from the sample standard deviation $sd(\theta_i)$ and sample size n_i as:

$$se(\theta_i) = \frac{sd(\theta_i)}{\sqrt{n_i}} \tag{5}$$

Alternatively, the random effects model supposes that each study samples a different true outcome μ_i, such that the combined effect μ is the mean of a population of true effects. The observed effect θ_i for study i is then influenced by the intrastudy error ε_i and interstudy error ξ_i $\theta_i = \mu_i + \varepsilon_i + \xi_i$, where ξ_i is also assumed to be normally distributed $\xi_i \sim \mathcal{N}(0, \tau^2)$, with τ^2 representing the extent of heterogeneity, or between-study (interstudy) variance.

Study-level estimates for a fixed effect or random effects model are weighted using the inverse variance:

$$w_i = \begin{cases} \dfrac{1}{se(\theta_i)^2}, \text{fixed effect} \\ \dfrac{1}{se(\theta_i)^2 + \tau^2}, \text{random effects} \end{cases} \tag{6}$$

These weights are used to calculate the global outcome $\hat{\theta}$ (Eq. 3) and the corresponding standard error $se(\hat{\theta})$:

$$se(\hat{\theta}) = \frac{1}{\sqrt{\sum_i w_i}} \tag{7}$$

In practice, random effects models are favored over the fixed effect model, due to the prevalence of heterogeneity in experimental methods and biological outcomes. However, when there is no between-study variability ($\tau^2 = 0$), the random effects model reduces to a fixed effect model. In contrast, when τ^2 is exceedingly large and interstudy variance dominates the weighting term [$\tau^2 \gg se(\theta_i)^2$], random effects estimates will tend to an unweighted mean.

Interstudy variance τ^2 estimators. Under the assumptions of a random effects model, the total variance is the sum of the intrastudy variance (experimental sampling error) and interstudy variance τ^2 (variability of true effects). Since the distribution of true effects is unknown, we must estimate the value of τ^2 based on study-level outcomes (Borenstein, 2009). The DerSimonian and Laird (DL) method is the most commonly used in meta-analyses (DerSimonian & Laird, 1986). Other estimators such as the Hunter & Schmidt (Hunter & Schmidt, 2004), Hedges (Hedges & Olkin, 1985), Hartung-Makambi (Hartung & Makambi, 2002), Sidik-Jonkman (Sidik & Jonkman, 2005) and Paule-Mandel (Paule & Mandel, 1982) estimators have been proposed as either alternatives or improvements over the DL estimator (Sanchez-Meca & Marin-Martinez, 2008) and have been implemented in *MetaLab* (**Table 3-3)**. Negative values of τ^2 are truncated at zero. An overview of the various τ^2 estimators along with recommendations on their use can be found elsewhere (Veroniki, Jackson et al., 2016).

Sample size weighting. Sample-size weighting is preferred in cases where variance estimates are unavailable or unreliable. Under this weighting scheme, study-level sample sizes are used in place of inverse variances as weights. The sampling error is then unaccounted for; however, since sampling error is random, larger sample sizes will effectively average out the error and produce more dependable results. This is contingent on reliable reporting of sample sizes which is difficult to assess and can be erroneous as detailed above. For a sample size weighted estimate, study-level sample sizes n_i replace weights that are used to calculate the global effect size $\hat{\theta}$, such that

$$w_i = n_i \tag{8}$$

The pooled standard error $se(\hat{\theta})$ for the global effect is then:

$$se(\hat{\theta}) = \sqrt{\frac{\sum_i (se(\theta_i)^2 \cdot (n_i - 1))}{\sum_i (n_i - 1)}} \tag{9}$$

While sample size weighting is less affected by sampling variance, the performance of this estimator depends on the availability of studies (Marin-Martinez & Sanchez-Meca, 2010). When variances are reliably reported, sample-size weights should roughly correlate to inverse variance weights under the fixed effect model.

Table 3-3. Interstudy variance estimators (Sanchez-Meca & Marin-Martinez, 2008)

Estimator	τ^2 estimate
DerSimonian-Laird (DL)* †	$\tau^2_{DL} = \frac{Q-(N-1)}{c}$
Hunter-Schmidt (HS)*	$\tau^2_{HS} = \frac{Q-N}{\sum_i se(\theta_i)^{-2}}$
Hedges (H)	$\tau^2_H = \frac{\sum_i \left(\theta_i - \left(\frac{\sum_i \theta_i}{N}\right)\right)^2}{N-1} - \frac{\sum_i se(\theta_i)^2}{N}$
Hartung-Makambi (HM)* †	$\tau^2_{HM} = \frac{Q^2}{(2(N-1)+Q)\cdot c}$
Sidik-Jonkman (SJ)	$\tau^2_{SJ} = \frac{\sum_i v_i^{-1}\left(\theta_i - \left(\frac{\sum_i v_i^{-1}\theta_i}{\sum_i v_i^{-1}}\right)\right)^2}{N-1}$, Where $v_i = \left(\frac{se(\theta_i)^2}{\left(\frac{\sum_i(\theta_i-\bar{\theta})^2}{N}\right)} + 1\right)$ and $\bar{\theta} = \frac{1}{N}\sum_i \theta_i$
Paule-Mandel (PM)#	$\tau^2_{PM} = \frac{\sum_i w_i\left(\theta_i - \hat{\theta}_{PM}\right)^2 - \left(\sum_i w_i^2 se(\theta_i)^2 - \left(\frac{\sum_i w_i^2 se(\theta_i)^2}{\sum_i w_i}\right)\right)}{\sum_i w_i - \left(\frac{\sum_i w_i^2}{\sum_i w_i}\right)}$ Where $\hat{\theta}_{PM} = \frac{\sum_i(\theta_i \cdot w_i)}{\sum_i(w_i)}$

* $Q = \sum_i \left(se(\theta_i)^{-2}\left(\theta_i - \frac{\sum_i se(\theta_i)^{-2}\theta_i}{\sum_i se(\theta_i)^{-2}}\right)^2\right)$

† $c = \sum_i se(\theta_i)^{-2} - \frac{\sum_i\left(se(\theta_i)^{-2}\right)^2}{\sum_i se(\theta_i)^{-2}}$

iterative estimator

Meta-analytic data distributions

One important consideration the reviewer should attend to is the normality of the study-level effects distributions assumed by most meta-analytic methods. Non-parametric methods that do not assume normality are available but are more computationally intensive and inaccessible to non-statisticians (Karabatsos, Talbott et al., 2015). The performance of parametric meta-analytic methods has been shown to be robust to non-normally distributed effects (Kontopantelis & Reeves, 2012). However, this robustness is achieved by deriving artificially high estimates of heterogeneity for non-normally distributed data, resulting in conservatively wide confidence intervals and severely underpowered results (Jackson & Turner, 2017). Therefore, it is prudent to characterize

the underlying distribution of study-level effects and perform transformations to normalize distributions to preserve the inferential integrity of the meta-analysis.

Assessing data distributions. Graphical approaches, such as the histogram, are commonly used to assess the distribution of data; however, in a meta-analysis, they can misrepresent the true distribution of effect sizes that may be different due to unequal weights assigned to each study. To address this, we can use a weighted histogram to evaluate effect size distributions (**Fig 3-6**). A weighted histogram can be constructed by first binning studies according to their effect sizes. Each bin is then assigned weighted frequencies, calculated as the sum of study-level weights within the given bin. The sum of weights in each bin are then normalized by the sum of all weights across all bins

$$P_j = \frac{\sum_i w_{ij}}{\sum_j^{nBins} \sum_i w_{ij}} \tag{10}$$

where P_j is the weighted frequency for bin j, w_{ij} is the weight for the effect size in bin j from study i, and $nBins$ is the total number of bins. If the distribution is found deviate from normality, the most common explanations are that (i) the distribution is skewed due to inconsistencies between studies, (ii) subpopulations exist within the dataset giving rise to multimodal distributions or (iii) the studied phenomenon is not normally distributed. The source of inconsistencies and multimodality can be explored during the analysis of heterogeneity (i.e., to determine whether study-level characteristics can explain observed discrepancies). Skewness may however be inherent to the data when values are small, variances are large, and values cannot be negative (Limpert, Stahel et al., 2001) and has been credited to be characteristic of natural processes (Grönholm & Annila, 2007). For sufficiently large sample sizes the central limit theorem holds that the means of a skewed data are approximately normally distributed. However, due to common limitation in the number of studies available for meta-analyses, meta-analytic global estimates of skewed distributions are often sensitive to extreme values. In these cases, data transformation can be used to achieve a normal distribution on the logarithmic scale (i.e., lognormal distribution).

Lognormal distributions. Since meta-analytic methods typically assume normality, the log transformation is a useful tool used to normalize skewed distributions (**Fig 3-6C-F**). In the ATP release dataset, we found that log transformation normalized the data distribution. However, in the

case of the OB $[ATP]_{ic}$ dataset, log transformation revealed a bimodal distribution that was otherwise not obvious on the raw scale.

Data normalization by log transformation allows meta-analytic techniques to maintain their inferential properties. The outcomes synthesized on the logarithmic scale can then be transformed to the original raw scale to obtain asymmetrical confidence intervals which further accommodate the skew in the data. Study-level effect sizes θ_i can be related to the logarithmic mean Θ_i through the forward log transformation, meta-analyzed on the logarithmic scale, and back-transformed to the original scale using one of the back-transformation methods (**Table 3-4**). We have implemented three different back-transformation methods into MetaLab, including geometric approximation (anti-log), naïve approximation (rearrangement of forward-transformation method) and tailor series approximation (Higgins, White et al., 2008). The geometric back-transformation will yield an estimate of $\hat{\theta}$ that is approximately equal to the median of the study-level effects. The naïve or tailor series approximation differ in how the standard errors are approximated, which is used to obtain a point estimate on the original raw scale. The naïve and tailor series approximations were shown to maintain adequate inferential properties in the meta-analytic context (Higgins et al., 2008).

Table 3-4. Logarithmic Transformation Methods. Forward-transformation of study-level estimates θ_i to corresponding log-transformed estimates Θ_i, and back-transformation of meta-analysis outcome $\widehat{\Theta}$ to the corresponding outcome $\hat{\theta}$ on the raw scale (Higgins et al., 2008). $v_{1-\alpha/2}$: confidence interval critical value, α: significance level.

Forward-Transformation (raw to log_{10})		
	Mean	**Standard error**
	$\Theta_i = log_{10}(\theta_i) - \left(\frac{se(\Theta_i)^2}{2}\right)$	$se(\Theta_i)^2 = \sqrt{log_{10}\left(\frac{se(\theta_i)^2}{\theta_i^{\,2}} + 1\right)}$
Back-Transformation (log_{10} to raw)		
Method	**Mean**	**Standard error**
Geometric	$\hat{\theta} = 10^{\widehat{\Theta}}$	$\pm CI_{1-\alpha/2}(\hat{\theta}) = 10^{\widehat{\Theta} \pm v_{1-\alpha/2} \cdot se(\widehat{\Theta})}$ $se(\hat{\theta}) = \frac{\left(+CI_{1-\alpha/2}(\hat{\theta})\right) - \left(-CI_{1-\alpha/2}(\hat{\theta})\right)}{2v_{1-\alpha/2}}$ Where $v_{1-\alpha/2}$ corresponds to critical value
Naïve approx.	$\hat{\theta} = 10^{\left(\widehat{\Theta} + \frac{se(\widehat{\Theta})^2}{2}\right)}$	$se(\hat{\theta}) = \frac{1}{\sqrt{n_i}}\left(10^{sd(\widehat{\Theta})^2} - 1\right)10^{2\widehat{\Theta} + sd(\widehat{\Theta})^2}$

Tailor Series approx.	$\hat{\theta} = 10^{\left(\hat{\Theta}+\frac{se(\hat{\Theta})^2}{2}\right)}$	$se(\hat{\theta}) = \sqrt{\frac{1}{n_i}10^{(2\hat{\Theta}+sd(\hat{\Theta})^2)}sd(\hat{\Theta})^2\left(1+\left(\frac{sd(\hat{\Theta})^2}{2}\right)\right)}$

3.5.3.2 Confidence intervals

Once the meta-analysis global estimate and standard error has been computed, reviewers may proceed to construct the confidence intervals (CI). The CI represents the range of values within which the true mean outcome is contained with the probability of 1-α. In meta-analyses, the CI conveys information about the significance, magnitude and direction of an effect, and is used for inference and generalization of an outcome. Values that do not fall in the range of the CI may be interpreted as significantly different. In general, the CI is computed as the product of the standard error $se(\hat{\theta})$ and the critical value $v_{1-\alpha/2}$:

$$\pm CI = \pm v_{1-\alpha/2} \cdot se(\hat{\theta}) \quad (11)$$

CI estimators. The critical value $v_{1-\alpha/2}$ is derived from a theoretical distribution and represents the significance threshold for level α. A theoretical distribution describes the probability of any given possible outcome occurrence for a phenomenon. Extreme outcomes that lie furthest from the mean are known as the tails. The most commonly used theoretical distributions are the z-distribution and t-distribution, which are both symmetrical and bell-shaped, but differ in how far reaching or 'heavy' the tails are. Heavier tails will result in larger critical values which translate to wider confidence intervals, and vice versa. Critical values drawn from a z-distribution, known as z-scores (*z*), are used when data are normal, and a sufficiently large number of studies are available (>30). The tails of a z-distribution are independent of the sample size and reflect those expected for a normal distribution. Critical values drawn from a t-distribution, known as t-scores (t), also assume data are normally-distributed, however, are used when there are fewer available studies (<30) because the t-distribution tails are heavier. This produces more conservative (wider) CIs, which help ensure that the data are not misleading or misrepresentative when there is limited evidence available. The heaviness of the t-distribution tails is dictated by the degree of freedom *df*, which is related to the number of available studies *N* (*df* = *N* – *1*) such that fewer studies will result in heavier t-distribution tails and therefore larger critical values. Importantly, the t-distribution is asymptotically normal and will thus converge to a z-distribution for a sufficiently

large number of studies, resulting in similar critical values. For example, for a significance level α = 0.05 (5% false positive rate), the z-distribution will always yield a critical value $v = 1.96$, regardless of how many studies are available. The t-distribution will however yield $v = 2.78$ for 5 studies, $v = 2.26$ for 10 studies, $v = 2.05$ for 30 studies and $v = 1.98$ for 100 studies, gradually converging to 1.96 as the number of studies increases. We have implemented the z-distribution and t-distribution CI estimators into MetaLab.

3.5.3.3 Evaluating meta-analysis performance

In general, 95% of study-level outcomes are expected to fall within the range of the 95% global CI. To determine whether the global 95% CI is consistent with the underlying study-level outcomes, the coverage of the CI can be computed as the proportion of study-level 95% CIs that overlap with the global 95% CI:

$$\begin{aligned} \left|\hat{\theta} - \theta_i\right| &\leq v_{1-\frac{\alpha}{2}} \cdot se\left(\hat{\theta}\right) + v_{1-\frac{\alpha}{2}} \cdot se(\theta_i), && \text{covered} \\ \left|\hat{\theta} - \theta_i\right| &> v_{1-\alpha/2} \cdot se(\hat{\theta}) + v_{1-\frac{\alpha}{2}} \cdot se(\theta_i), && \text{not covered} \end{aligned} \tag{12}$$

The coverage is a performance measure used to determine whether inference made on the study-level is consistent with inference made on the meta-analytic level. Coverage that is less than expected for a specified significance level (i.e., <95% coverage for α = 0.05) may be indicative of inaccurate estimators, excessive heterogeneity or inadequate choice of meta-analytic model, while coverage exceeding 95% may indicate an inefficient estimator that results in insufficient statistical power.

Overall, the performance of a meta-analysis is heavily influenced by the choice of weighting scheme and data transformation (**Fig 3-7**). This is especially evident in the smaller datasets, such as our OB $[ATP]_i$ example, where both the global estimates and the confidence intervals are dramatically different under different weighting schemes (**Fig 3-7A**). Working with larger datasets, such as ATP release kinetics, allows to somewhat reduce the influence of the assumed model (**Fig 3-7B**). However, normalizing data distribution (by log transformation) produces much more consistent outcomes under different weighting schemes for both datasets, regardless of the number of available studies (**Fig 3-7A, B**, *log_{10} synthesis*).

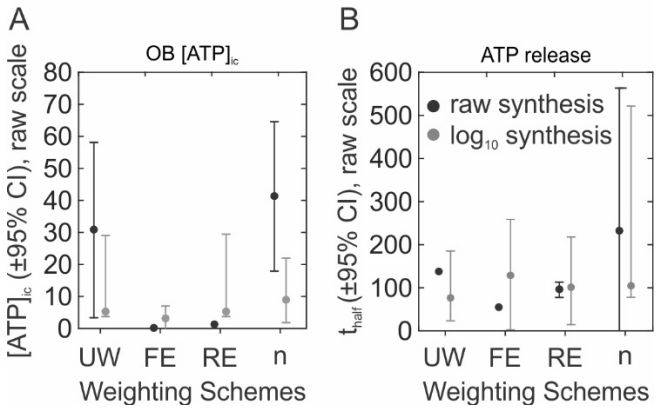

Figure 3-7. Comparison of global effect estimates using different weighting schemes. **(A, B)** Global effect estimates for OB $[ATP]_{ic}$ **(A)** and ATP release **(B)** following synthesis on original data (raw, *black*) or on log_{10}-transformed data followed by back-transformation to original scale (log_{10}, *gray*). Global effects ± 95% CI were obtained with unweighted data (UW), or using fixed effect (FE), random effects (RE) and sample-size (n) weighting schemes.

3.5.4 Analysis of heterogeneity

Heterogeneity refers to inconsistency between studies. A large part of conducting a meta-analysis involves quantifying and accounting for sources of heterogeneity that may compromise the validity of meta-analysis. Basic research meta-analytic datasets are expected to be heterogeneous because (*i*) basic research literature searches tend to retrieve more studies than clinical literature searches and (*ii*) experimental methodologies used in basic research are more diverse and less standardized compared to clinical research. The presence of heterogeneity may limit the generalizability of an outcome due to the lack of study-level consensus. Nonetheless, exploration of heterogeneity sources can be insightful for the field in general, as it can identify biological or methodological factors that influence the outcome.

3.5.4.1 Quantifying heterogeneity

Higgins & Thompson emphasized that a heterogeneity metric should be (*i*) dependent on magnitude of heterogeneity, (*ii*) independent of measurement scale, (*iii*) independent of sample size and (*iv*) easily interpretable (Higgins & Thompson, 2002). Regrettably, the most commonly used test of heterogeneity is the Cochrane's Q test (Borenstein, 2009), which has been repeatedly shown to have undesirable statistical properties (Higgins, Thompson et al., 2003). Nonetheless, we will introduce it here, not because of its widespread use, but because it is an intermediary statistic used to obtain more useful measures of heterogeneity, H^2 and I^2. The measure of total variation Q_{total} statistic is calculated as the sum of the weighted squared differences between the study-level means θ_i and the fixed effect estimate $\hat{\theta}_{FE}$:

$$Q_{total} = \sum_{i=1}^{N} \left(w_i \cdot \left(\theta_i - \hat{\theta}_{FE} \right)^2 \right)$$
$$\text{where } \hat{\theta}_{FE} = \frac{\sum_i se(\theta_i)^{-2}\theta_i}{\sum_i se(\theta_i)^{-2}} \text{ and } w_i = se(\theta_i)^{-2} \quad (13)$$

The Q_{total} statistic is compared to a chi-square (χ^2) distribution (*df = N-1*) to obtain a p-value, which, if significant, supports the presence of heterogeneity. However, the Q-test has been shown to be inadequately powered when the number of studies is too low (N < 10) and excessively powered when study number is too high (N > 50) (Gavaghan, Moore et al., 2000; Higgins et al., 2003). Additionally, the Q_{total} statistic is not a measure of the magnitude of heterogeneity due to its inherent dependence on the number of studies. To address this limitation, H^2 heterogeneity statistics was developed as the relative excess in Q_{total} over degrees of freedom df:

$$H^2 = \frac{Q_{total}}{df} \quad (14)$$

H^2 is independent of the number of studies in the meta-analysis and is indicative of the magnitude of heterogeneity (Higgins & Thompson, 2002). For values less than 1, H^2 is truncated at 1, therefore values of H^2 can range from one to infinity, where $H^2 = 1$ indicates homogeneity. The corresponding confidence intervals for H^2 are

$$H^2 \pm 95\%\ \text{CI} = \left(e^{\ln(H) \pm 1.96 \cdot \sqrt{\frac{1}{2(df-1)}\left(1 - \frac{1}{3(df)^2}\right)}} \right)^2 \quad (15)$$

Intervals that do not overlap with 1 indicate significant heterogeneity. A more easily interpretable measure of heterogeneity is the I^2 statistic, which is a transformation of H^2:

$$I^2 = \frac{H^2 - 1}{H^2} \cdot 100\% \quad (16)$$

The corresponding 95% CI for I^2 is derived from the 95% CI for H^2

$$I^2 \pm 95\%\ CI = \frac{(\text{H}^2 \pm 95\%\ \text{CI}) - 1}{(\text{H}^2 \pm 95\%\ \text{CI})} \cdot 100\% \quad (17)$$

Values of I^2 range between 0 to 100% and describe the percentage of total variation that is attributed to heterogeneity. Like H^2, I^2 provides a measure of the magnitude of heterogeneity. Values of I^2 at 25%, 50% and 75% are generally graded as low, moderate and high heterogeneity,

respectively (Higgins & Thompson, 2002; Pathak, Nand Dwivedi et al., 2017). However, several limitations have been noted for the I^2 statistic. I^2 has a nonlinear dependence on τ^2, thus I^2 will appear to saturate as it approaches 100% (Huedo-Medina, Sanchez-Meca et al., 2006). In cases of excessive heterogeneity, if heterogeneity is partially explained through subgroup analysis or meta-regression, residual unexplained heterogeneity may still be sufficient to maintain I^2 near saturation. Therefore, I^2 will fail to convey the decline in overall heterogeneity, while H^2 statistic that has no upper limit will allow to track changes in heterogeneity more meaningfully. In addition, a small number of studies (<10) will bias I^2 estimates, contributing to uncertainties inevitable associated with small meta-analyses (von Hippel, 2015). Of the three heterogeneity statistics Q_{total}, H^2 and I^2 described, we recommend that H^2 is used as it best satisfies the criteria for a heterogeneity statistic defined by Higgins & Thompson (Higgins & Thompson, 2002).

3.5.4.2 Identifying bias

Bias refers to distortions in the data that may result in misleading meta-analytic outcomes. In the presence of bias, meta-analysis outcomes are often contradicted by higher quality large sample-sized studies (Egger, Smith et al., 1997), thereby compromising the validity of the meta-analytic study. Sources of observed bias include publication bias, methodological inconsistencies and quality, data irregularities due to poor quality design, inadequate analysis or fraud, and availability or selection bias (Ahmed, Sutton et al., 2012; Egger et al., 1997). At the level of study identification and inclusion for meta-analysis, systematic searches are preferred over rapid review search strategies, as narrow search strategies may omit relevant studies. Withholding negative results is also a common source of publication bias, which is further exacerbated by the small-study effect (the phenomenon by which smaller studies produce results with larger effect sizes than larger studies) (Schwarzer, Carpenter et al., 2015). By extension, smaller studies that produce negative results are more likely to not be published compared to larger studies that produce negative results. Identifying all sources of bias is unfeasible, however, tools are available to estimate the extent of bias present.

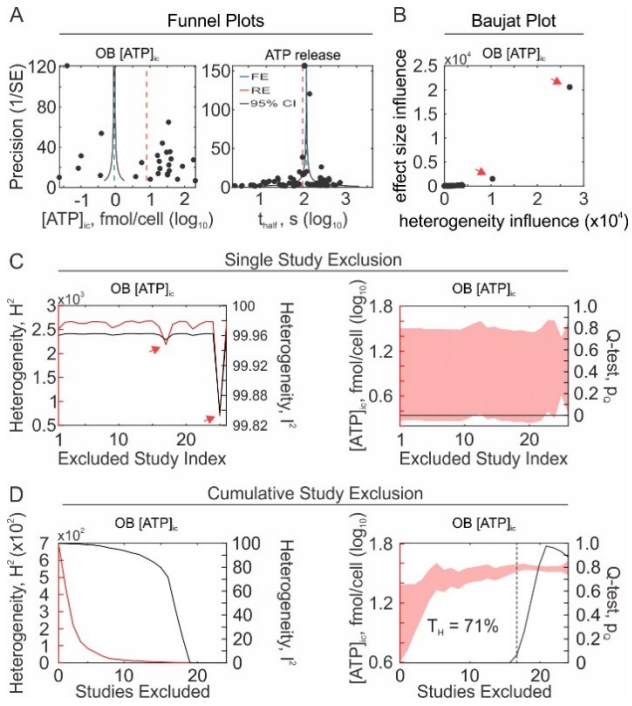

Figure 3-8. Analysis of bias and heterogeneity, and identification of influential studies. **(A)** Bias and heterogeneity in OB $[ATP]_{ic}$ (*left*) and ATP release (*right*) data sets were assessed with funnel plots. Log_{10}-transformed study-level effect sizes (black markers) were plotted in relation to their precision assessed as inverse of standard error (1/SE). *Blue dashed line*: fixed effect estimate, *red dashed line*: random effects estimate, *grey lines*: Expected 95% confidence interval (95% CI) in the absence of bias/heterogeneity. **(B)** OB $[ATP]_{ic}$ were evaluated using Baujat plot and inconsistent and influential studies were identified in top right corner of plot (*black arrows*). **(C, D)** Effect of the single study exclusion (**C**) and cumulative sequential exclusion of the most inconsistent studies (**D**). *Left*: heterogeneity statistics, H^2 (*red line*) and I^2 (*black line*). *Right*: ± 95% CI (*red band*) and Q-test p-value (*black line*). *Black arrows*: influential studies (same as those identified using Baujat Plot). *Dashed Black line*: homogeneity threshold $T_{H,}$ where Q-test p = 0.05.

Funnel plots. Funnel plots have been widely used to assess the risk of bias and examine meta-analysis validity (Borenstein, 2009; Light & Pillemer, 1984). The logic underlying the funnel plot is that in the absence of bias, studies are symmetrically distributed around the fixed effect size estimate, due to sampling error being random. Moreover, precise study-level estimates are expected to be more consistent with the global effect size than less precise studies, where precision is inversely related to the study-level standard error. Thus, for an unbiased set of studies, study-level effects θ_i plotted in relation to the inverse standard error $1/se(\theta_i)$ will produce a funnel shaped plot. Theoretical 95% CIs for the range of plotted standard errors are included as reference to visualize the expected distribution of studies in the absence of bias (Sterne & Harbord, 2004). When bias is present, study-level effects will be asymmetrically distributed around the global fixed-effect estimate. In the past, funnel plot asymmetries have been attributed solely to publication bias, however they should be interpreted more broadly as a general presence of bias or heterogeneity (Sterne, Sutton et al., 2011). It should be noted that rapid reviews (**Fig 3-8A**, *left*)

are far more subject to bias than systematic reviews (**Fig 3-8A**, *right*), due to the increased likelihood of relevant study omission.

3.5.4.3 Heterogeneity sensitivity analyses

Inconsistencies between studies can arise for a number of reasons, including methodological or biological heterogeneity (Patsopoulos, Evangelou et al., 2008). Since accounting for heterogeneity is an essential part of any meta-analysis, it is of interest to identify influential studies that may contribute to the observed heterogeneity.

Baujat Plot. The Baujat Plot was proposed as a diagnostic tool to identify the studies that contribute most to heterogeneity and influence the global outcome (Baujat, 2002). The graph illustrates the contribution Q_i^{inf} of each study to heterogeneity on the x-axis

$$Q_i^{inf} = \frac{\theta_i - \hat{\theta}_{FE}}{se(\theta_i)^2} \tag{18}$$

and contribution θ_i^{inf} to global effect on the y-axis

$$\theta_i^{inf} = \frac{\hat{\theta}_{-i} - \hat{\theta}_{FE}}{se\left(\hat{\theta}_{-i}\right)^2} \tag{19}$$

Studies that strongly influence the global outcome and contribute to heterogeneity are visualized in the upper right corner of the plot (**Fig 3-8B**). This approach has been used to identify outlying studies in the past (Anzures-Cabrera & Higgins, 2010).

Single-Study Exclusion Sensitivity. Single-study exclusion analysis assesses the sensitivity of the global outcome and heterogeneity to exclusion of single studies. The global outcomes and heterogeneity statistics are computed for a dataset with a single omitted study; single study exclusion is iterated for all studies; and influential outlying studies are identified by observing substantial declines in observed heterogeneity, as determined by Q_{total}, H^2, or I^2, and by significant differences in the global outcome (**Fig 3-8C**). Influential studies should not be blindly discarded, but rather carefully examined to determine the reason for inconsistency. If a cause for heterogeneity can be identified, such as experimental design flaw, it is appropriate to omit the

study from the analysis. All reasons for omission must be justified and made transparent by reviewers.

Cumulative-Study Exclusion Sensitivity. Cumulative study exclusion sequentially removes studies to maximize the decrease in total variance Q_{total}, such that a more homogenous set of studies with updated heterogeneity statistics is achieved with each iteration of exclusion (**Fig 3-8D**).

$$\hat{\theta}_{-j} \pm 95\%\, CI_{-j} \quad \text{where } j = \arg\max_{i}(Q - Q_{-i}) \tag{20}$$

This method was proposed by Patsopoulos et al. to achieve desired levels of homogeneity (Patsopoulos et al., 2008), however, Higgins argued that its application should remain limited to (*i*) quantifying the extent to which heterogeneity permeates the set of studies and (*ii*) identifying sources of heterogeneity (Higgins, 2008). We propose the homogeneity threshold T_H as a measure of heterogeneity that can be derived from cumulative-study exclusion sensitivity analysis. The homogeneity threshold describes the percentage of studies that need to be removed (by the maximal Q-reduction criteria) before a homogenous set of studies is achieved. For example, in the OB $[ATP]_{ic}$ dataset, the homogeneity threshold was 71%, since removal of 71% of the most inconsistent studies resulted in a homogeneous dataset (**Fig 3-8D**, *right*). After homogeneity is attained by cumulative exclusion, the global effect generally stabilizes with respect to subsequent study removal. This metric provides information about the extent of inconsistency present in the set of studies that is scale invariant (independent of the number of studies), and is easily interpretable.

3.5.4.4 Exploratory analyses

The purpose of an exploratory analysis is to understand the data in ways that may not be represented by a pooled global estimate. This involves identifying sources of observed heterogeneity related to biological and experimental factors. Subgroup and meta-regression analyses are techniques used to explore known data groupings define by study-level characteristics (i.e., covariates). Additionally, we introduce the cluster-covariate dependence analysis, which is an unsupervised exploratory technique used to identify covariates that coincide well will natural

groupings within the data, and the intrastudy regression analysis, which is used to validate meta-regression outcomes.

Cluster-covariate dependence analysis. Natural groupings within the data can be informative and serve as a basis to guide further analysis. Using an unsupervised k-means clustering approach (Lloyd, 1982), we can identify natural groupings within the study-level data and assign cluster memberships to these data (**Fig 3-9A**). Reviewers then have two choices: either proceed directly to subgroup analysis (**Fig 3-9B**) or look for covariates that co-cluster with cluster memberships (**Fig 3-9C**) In the latter case, dependencies between cluster memberships and known data covariates can be tested using Pearson's Chi-Squared test for independence. Covariates that coincide with clusters can be verified by subgroup analysis (**Fig 3-9D**). The dependence test is limited by the availability of studies and requires that at least 80% of covariate-cluster pairs are represented by at least 5 studies (McHugh, 2013). Clustering results should be considered exploratory and warrant further investigation due to several limitations. If the subpopulations were identified through clustering, however they do not depend on extracted covariates, reviewers risk assigning misrepresentative meaning to these clusters. Moreover, conventional clustering methods always converge to a result, therefore the data will still be partitioned even in the absence of natural data groupings. Future adaptations of this method might involve using different clustering algorithms (hierarchical clustering) or independence tests (G-test for independence) as well as introducing weighting terms to bias clustering to reflect study-level precisions.

Subgroup analysis. Subgroup analyses attempt to explain heterogeneity and explore differences in effects by partitioning studies into characteristic groups defined by study-level categorical covariates (**Fig 3-9B,D, Table 3-5**). Subgroup effects are estimated along with corresponding heterogeneity statistics. To evaluate the extent to which subgroup covariates contribute to observed inconsistencies, the explained heterogeneity $Q_{between}$ and unexplained heterogeneity Q_{within} can be calculated.

$$Q_{within} = \sum_{j=1}^{S} \left(\sum_{i=1}^{N_j} \left(se(\theta_i)^{-2} \cdot \left(\theta_i - \hat{\theta}_{(FE)j} \right)^2 \right) \right) \tag{21}$$

where S is the total number of subgroups per given covariate and each subgroup j contains N_j studies.

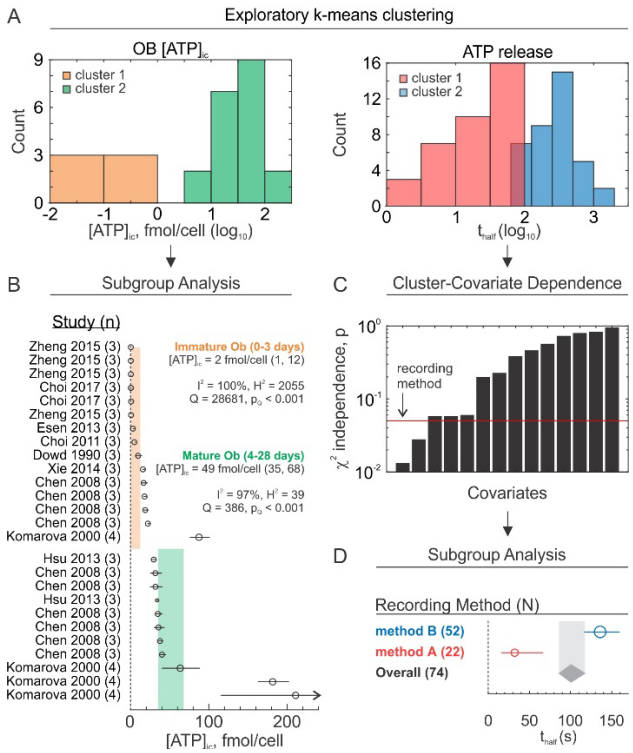

Figure 3-9. Exploratory subgroup analysis. **(A)** Exploratory k-means clustering was used to partition OB $[ATP]_{ic}$ (*left*) and ATP release (*right*) data into potential clusters/ subpopulations of interest. **(B)** Subgroup analysis of OB $[ATP]_{ic}$ data by differentiation status (immature – 0 to 3 day osteoblasts vs. mature – 4 to 28 day osteoblasts). Subgroup outcomes (fmol ATP/cell) estimated using sample-size weighting-scheme. *black markers*: Study-level outcomes ± 95% CI, marker sizes are proportional to sample size, *n*. *Orange and green bands*: 95% CI for immature and mature osteoblast subgroups, respectively. **(C)** Dependence between ATP release cluster membership and known covariates/ characteristics was assessed using Pearson's $\chi 2$ independence test. *Black bars*: $\chi 2$ test p-values for each covariate-cluster dependence test. *Red line*: α=0.05 significance threshold. *Black arrow*: covariate (ex. recording method) that is most dependent on cluster membership. **(D)** Subgroup analysis of ATP release by recording method. Subgroup outcomes (t_{half}) estimated using random effects weighting, τ^2 computed using DerSimonian-Laird estimator. *Round markers*: subgroup estimates ± 95% CI, marker sizes are proportional to number of studies per subgroup, *N*. *Grey band/diamond*: global effect ± 95% CI.

The explained heterogeneity $Q_{between}$ is then the difference between total and subgroup heterogeneity:

$$Q_{between} = Q_{total} - Q_{within} \tag{22}$$

If the p-value for the χ^2 distributed statistic $Q_{between}$ is significant, the subgrouping can be assumed to explain a significant amount of heterogeneity (Borenstein, 2009). Similarly, Q_{within} statistic can be used to test whether there is any residual heterogeneity present within the subgroups.

The $R^2_{explained}$ is a related statistic that can be used to describe the percent of total heterogeneity that was explained by the covariate and is estimated as

$$R^2_{explained} = \left(1 - \frac{\tau^2_{within}}{\tau^2_{total}}\right) \cdot 100\% \quad (23)$$

Where pooled heterogeneity within subgroups τ^2_{within} represents the remaining unexplained variation (Borenstein, 2009):

$$\tau^2_{within} = \frac{\sum_{j=1}^{s} Q_{(within)j} - \sum_{j=1}^{s} df_j}{\sum_{j=1}^{s} c_j}$$
$$\text{where } c_j = \sum_{i=1}^{N_j} se(\theta_i)^{-2} - \frac{\sum_i \left(se(\theta_i)^{-2}\right)^2}{\sum_i se(\theta_i)^{-2}} \quad (24)$$

Subgroup analysis of the ATP release dataset revealed that recording method had a major influence on ATP release outcome, such that method A produced significantly lower outcomes than method B (**Fig 3-9D**, **Table 3-5;** significance determined by non-overlapping 95% CIs). Additionally, recording method accounted for a significant amount of heterogeneity ($Q_{between}$, p<0.001), however it represented only 4% ($R^2_{explained}$) of the total observed heterogeneity. Needless to say, the remaining 96% of heterogeneity is significant (Q_{within}, p<0.001). To explore the remaining heterogeneity, additional subgroup analysis can be conducted by further stratifying method A and method B subgroups by other covariates. However, in many meta-analyses multi-level data stratification may be unfeasible if covariates are unavailable or if the number of studies within subgroups are low.

Table 3-5. **Exploratory subgroup analysis.** Effect and heterogeneity estimates of ATP release by recording method.

Subgroup summary statistics

Group (N)	$\hat{\theta}$ **± 95% CI (sec)**	**I² (%)**	**H²**	**Q**
Total (74)	101 (86, 117)	94	16	1133
Method A (22)	32 (16, 66)	94	17	358
Method B (52)	136 (117, 159)	92	13	669

Accounting for heterogeneity with subgroup analysis

	Q	***df***	**p-value**	**Interpretation**
Total	1133	73	<0.001	
Method A	358	21	<0.001	data are heterogeneous
Method B	669	51	<0.001	
between	106	1	<0.001	subgrouping explained significant heterogeneity
within	1027	72	<0.001	significant heterogeneity remains

Multiple comparisons. When multiple subgroups are present for a given covariate, and the reviewer wishes to investigate the statistical differences between the subgroups, the problem of

multiple comparisons should be addressed. Error rates are multiplicative and increase substantially as the number of subgroup comparisons increases. The Bonferroni correction has been advocated to control for false positive findings in meta-analyses (Hedges & Olkin, 1985) which involves adjusting the significance threshold:

$$\alpha^* = \frac{\alpha}{m} \tag{25}$$

α^* is the adjusted significance threshold to attain intended error rates α for m subgroup comparisons. Confidence intervals can then be computed using α^* in place of α:

$$\pm CI = \pm v_{1-\alpha^*/2} \cdot se(\hat{\theta}) \tag{26}$$

Meta-regression. Meta-regression attempts to explain heterogeneity by examining the relationship between study-level outcomes and continuous covariates while incorporating the influence of categorical covariates (**Fig 3-10A**). The main differences between conventional linear regression and meta-regression are (i) the incorporation of weights and (ii) covariates are at the level of the study rather than the individual sample. The magnitude of the relationship β_n between the covariates x_n and outcome y_i are of interest when conducting a meta-regression analysis. It should be noted that the intercept β_0 of a meta-regression with negligible effect of covariates is equivalent to the estimate approximated by a weighted mean. The generalized meta-regression model is specified as

$$y_i = \beta_0 + \beta_1 x_1 + \cdots + \beta_n x_n + \eta_i + \varepsilon_i \tag{27}$$

where intrastudy variability ε_i is

$$\varepsilon \sim \mathcal{N}(0, \sigma^2) \tag{28}$$

and the study-specific deviation from the distribution η_i depends on the chosen meta-analysis model:

$$\eta_i \sim \begin{cases} 0, fixed\ effect \\ \mathcal{N}(0, \tau^2), random\ effets \end{cases} \tag{29}$$

The residual Q statistic that explains the dispersion of the studies from the regression line is calculated as follows

$$Q_{residual} = \sum_{i=1}^{N} (w_i \cdot (\theta_i - y_i)^2) \tag{30}$$

Where y_i is the predicted value at x_i according to the meta-regression model. $Q_{residual}$ is analogous to $Q_{between}$ computed during subgroup analysis and is used to test the degree of remaining unaccounted heterogeneity. $Q_{residual}$ is also used to approximate the unexplained interstudy variance $\tau^2_{residual}$

$$\tau^2_{residual} = \frac{Q_{residual} - df}{c_{total}}$$
$$\text{where } c_{total} = \sum_i se(\theta_i)^{-2} - \frac{\sum_i (se(\theta_i)^{-2})^2}{\sum_i se(\theta_i)^{-2}} \quad (31)$$

Which can be used to calculate $R^2_{explained}$ estimated as

$$R^2_{explained} = \left(1 - \frac{\tau^2_{residual}}{\tau^2_{total}}\right) \cdot 100\% \quad (32)$$

Q_{model} quantifies the amount of heterogeneity explained by the regression model and is analogous to Q_{within} computed during subgroup analysis.

$$Q_{model} = Q_{total} - Q_{residual} \quad (33)$$

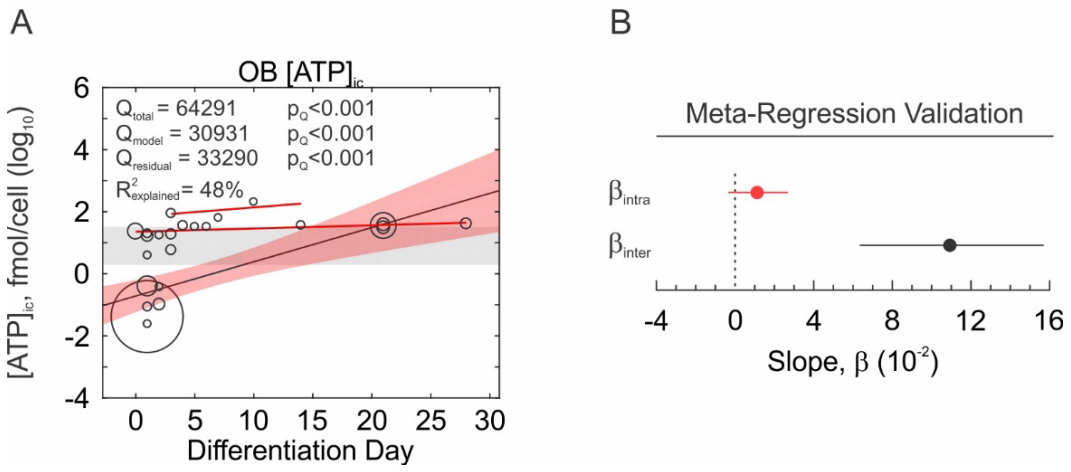

Figure 3-10. Meta-regression analysis and validation. (A) Relationship between osteoblast differentiation day (covariate) and intracellular ATP content (outcome) investigated by meta-regression analysis. Outcomes are on $\log_{10}$ scale, meta-regression markers sizes are proportional to weights. *Red bands*: 95% CI. *Grey bands*: 95% CI of intercept only model. *Solid red lines*: intrastudy regression. **(B)** Meta-regression coefficient β_{inter} (*black*) compared to intrastudy regression coefficient β_{intra} (*red*). Shown are regression coefficients ± 95% CI.

Intrastudy regression analysis. The challenge of interpreting results from a meta-regression is that relationships that exist within studies may not necessarily exist across studies, and vice versa. Such inconsistencies are known as aggregation bias and in the context of meta-analyses can arise from excess heterogeneity or from confounding factors at the level of the study. This problem has been

acknowledged in clinical meta-analyses (Thompson & Higgins 2002), however cannot be corrected without access to individual patient data. Fortunately, basic research studies often report outcomes at varying predictor levels (ex. dose-response curves), permitting for intrastudy (within-study) relationships to be evaluated by the reviewer. If study-level regression coefficients can be computed for several studies (**Fig 3-10A,** *red lines*), they can be pooled to estimate an overall effect β_{intra}. The meta-regression interstudy coefficient β_{inter} and the overall intrastudy-regression coefficient β_{intra} can then be compared in terms of magnitude and sign. Similarity in the magnitude and sign validates the existence of the relationship and characterizes its strength, while similarity in sign but not the magnitude, still supports the presence of the relationship, but calls for additional experiments to further characterize it. For the Ob $[ATP]_i$ dataset, the magnitude of the relationship between osteoblast differentiation day and intracellular ATP concentration was inconsistent between intrastudy and interstudy estimates, however the estimates were of consistent sign (**Fig 3-10B**).

When performed with knowledge and care, exploratory analysis of meta-analytic data has an enormous potential for hypothesis generation, cataloging current practices and trends, and identifying gaps in the literature. Thus, we emphasize the inherent limitations of exploratory analyses:

Data dredging. A major pitfall in meta-analyses is data dredging (also known as p-hacking), which refers to searching for significant outcomes only to assign meaning later. While exploring the dataset for potential patterns can identify outcomes of interest, reviewers must be wary of random patterns that can arise in any dataset. Therefore, if a relationship is observed it should be used to generate hypotheses, which can then be tested on new datasets. Steps to avoid data dredging involve defining an *a priori* analysis plan for study-level covariates, limiting exploratory analysis of rapid review meta-analyses and correcting for multiple comparisons.

Statistical power. The statistical power reflects the probability of rejecting the null hypothesis when the alternative is true. Meta-analyses are believed to have higher statistical power than the underlying primary studies, however this is not always true (Hedges & Pigott, 2001; Jackson & Turner, 2017). Random effects meta-analyses handle data heterogeneity by accounting for between-study variance, however this weakens the inference properties of the model. To maintain statistical powers that exceed those of the contributing studies in a random effects meta-

analysis, at least five studies are required (Jackson & Turner, 2017). This consequently limits subgroup analyses that partition studies into smaller groups to isolate covariate-dependent effects. Thus, reviewers should ensure that group are not under-represented to maintain statistical power. Another determinant of statistical power is the expected effect size, which if small, will be much more difficult to support with existing evidence than if it is large. Thus, if reviewers find that there is insufficient evidence to conclude that a small effect exists, this should not be interpreted as evidence of no effect.

Causal inference. Meta-analyses are not a tool for establishing causal inference. However, there are several criteria for causality that can be investigated through exploratory analyses that include consistency, strength of association, dose-dependence and plausibility (Weed, 2000, 2010). For example, consistency and the strength of association and dose-dependence can help establish that the outcome is dependent on exposure. However, reviewers are still posed with the challenge of accounting for confounding factors and bias. Therefore, while meta-analyses can explore various criteria for causality, causal claims are inappropriate, and outcomes should remain associative.

3.6 Concluding remarks

Meta-analyses of basic research can offer critical insights into the current state of knowledge. In this manuscript, we have adapted meta-analytic methods to basic science applications and provided a theoretical foundation, using OB $[ATP]_i$ and ATP release datasets, to illustrate the workflow. Since the generalizability of any meta-analysis relies on the transparent, unbiased and accurate methodology, the implications of deficient reporting practices and the limitations of the meta-analytic methods were discussed. Emphasis was placed on the analysis and exploration of heterogeneity. Additionally, several alternative and supporting methods have been proposed, including a method for validating meta-regression outcomes – intrastudy regression analysis, and a novel measure of heterogeneity – the homogeneity threshold. All analyses were conducted using *MetaLab*, a meta-analysis toolbox that we have developed in MATLAB R2016b. *MetaLab* has been provided for free to promote meta-analyses in basic research (https://github.com/NMikolajewicz/MetaLab).

In its current state, the translational pipeline from benchtop to bedside is an inefficient process, in one case estimated to produce ~1 clinically favorable clinical outcome for ~1000 basic research

studies (O'Collins, Macleod et al., 2006). The methods we have described here serve as a general framework for comprehensive data consolidation, knowledge gap-identification, evidence-driven hypothesis generation and informed parameter estimation in computation modeling, which we hope will contribute to meta-analytic outcomes that better inform translation studies, thereby minimizing current failures in translational research.

3.7 References

Ahmed, I., Sutton, A. J., & Riley, R. D. (2012). Assessment of publication bias, selection bias, and unavailable data in meta-analyses using individual participant data: a database survey. *Br Med J, 344*: d7762

Altman, D. G., & Bland, J. M. (2005). Standard deviations and standard errors. *Br Med J, 331*(7521), 903-903.

Anzures-Cabrera, J., & Higgins, J. P. T. (2010). Graphical displays for meta-analysis: An overview with suggestions for practice. *Res Synth Methods, 1*(1), 66-80.

Baguley, T. (2009). Standardized or simple effect size: What should be reported? *Br J Soc Psychol, 100*(3), 603-617.

Barendregt, J., & Doi, S. (2009). MetaXL User Guide: Version 1.0. *Wilston, Australia: EpiGear International Pty Ltd*.

Baujat, B. (2002). A graphical method for exploring heterogeneity in meta-analyses: application to a meta-analysis of 65 trials. *Stat Med, 21*(18).

Bax, L. (2016). MIX 2.0 – Professional software for meta-analysis in Excel. Version 2.0.1.5. BiostatXL. https://www.meta-analysis-made-easy.com.

Bittker, J. A., & Ross, N. T. (2016). *High throughput screening methods: evolution and refinement* Cambridge: Royal Society of Chemistry.

Bodin, P., Milner, P., Winter, R., & Burnstock, G. (1992). Chronic hypoxia changes the ratio of endothelin to ATP release from rat aortic endothelial cells exposed to high flow. *Proc Biol Sci, 247*(1319), 131-135.

Borenstein, M. (2009). *Introduction to meta-analysis*. Chichester, U.K.: John Wiley & Sons.

Borenstein, M., Hedges, L., Higgins, J. P. T., & Rothstein, H. R. (2005). *Comprehensive meta-analysis (Version 2.2.027) [Computer software]* 11.

Bramer, W. M., Giustini, D., de Jonge, G. B., Holland, L., & Bekhuis, T. (2016). De-duplication of database search results for systematic reviews in EndNote. *J Med Libr Assoc, 104*(3), 240-243.

Chowdhry, A. K., Dworkin, R. H., & McDermott, M. P. (2016). Meta-analysis with missing study-level sample variance data. *Stat Med, 35*(17), 3021-3032.

Cochrane Collaboration. (2011). Review manager (RevMan) [computer program].

Cox, M., Harris, P., & Siebert, B. R.-L. (2003). Evaluation of Measurement Uncertainty Based on the Propagation of Distributions Using Monte Carlo Simulation. *Measurement Techniques, 46*(9), 824-833.

DeLuca, J. B., Mullins, M. M., Lyles, C. M., Crepaz, N., Kay, L., & Thadiparthi, S. (2008). Developing a comprehensive search strategy for evidence based systematic reviews. *Evid Based Libr Inf Pract*, 3(1), 3-32.

DerSimonian, R., & Laird, N. (1986). Meta-analysis in clinical trials. *Control Clin Trials, 7*(3), 177-188.

Ecker, E. D., & Skelly, A. C. (2010). Conducting a winning literature search. *Evid Based Spine Care J,* 1(1), 9-14.

Egger, M., Smith, G. D., Schneider, M., & Minder, C. (1997). Bias in meta-analysis detected by a simple, graphical test. *Br Med J, 315*(7109), 629-634.

Finfgeld-Connett, D., & Johnson, E. D. (2013). Literature search strategies for conducting knowledge-building and theory-generating qualitative systematic reviews. *J Adv Nurs, 69*(1), 194-204.

Ganann, R., Ciliska, D., & Thomas, H. (2010). Expediting systematic reviews: methods and implications of rapid reviews. *Implementation Sci, 5*(1), 56-56.

Gavaghan, D. J., Moore, R. A., & McQuay, H. J. (2000). An evaluation of homogeneity tests in meta-analyses in pain using simulations of individual patient data. *Pain, 85*(3), 415-424.

Gopalakrishnan, S., & Ganeshkumar, P. (2013). Systematic Reviews and Meta-analysis: Understanding the Best Evidence in Primary Healthcare. *J Family Med Prim Care, 2*(1), 9-14.

Grönholm, T., & Annila, A. (2007). Natural distribution. *Math Biosci,* 210(2), 659-667.

Haby, M. M., Chapman, E., Clark, R., Barreto, J., Reveiz, L., & Lavis, J. N. (2016). What are the best methodologies for rapid reviews of the research evidence for evidence-informed decision making in health policy and practice: a rapid review. *Health Res Policy Syst, 14*(1), 83.

Hartung, J., & Makambi, K. H. (2002). Positive estimation of the between-study variance in meta-analysis: theory and methods. *S Afr Stat J*, 36(1), 55-76.

Hedges, L. V., & Olkin, I. (1985). *Statistical Methods for Meta-Analysis*. New York: Academic Press.

Hedges, L. V., & Pigott, T. D. (2001). The power of statistical tests in meta-analysis. *Psychol Methods, 6*(3), 203-217.

Higgins, J. P. (2008). Commentary: Heterogeneity in meta-analysis should be expected and appropriately quantified. *Int J Epidemiol, 37*(5), 1158-1160.

Higgins, J. P., & Thompson, S. G. (2002). Quantifying heterogeneity in a meta-analysis. *Stat Med, 21*(11), 1539-1558.

Higgins, J. P., Thompson, S. G., Deeks, J. J., & Altman, D. G. (2003). Measuring inconsistency in meta-analyses. *Br Med J (Clin Res Ed), 327*(7414), 557-560.

Higgins, J. P., & Green, S. (Eds.). (2011). *Cochrane handbook for systematic reviews of interventions* (Vol. 4). John Wiley & Sons.

Higgins, J. P., White, I. R., & Anzures-Cabrera, J. (2008). Meta-analysis of skewed data: Combining results reported on log-transformed or raw scales. *Stat Med, 27*(29), 6072-6092.

Huedo-Medina, T. B., Sanchez-Meca, J., Marin-Martinez, F., & Botella, J. (2006). Assessing heterogeneity in meta-analysis: Q statistic or I2 index? *Psychol Methods, 11*(2), 193-206.

Hunter, J. E., & Schmidt, F. L. (2004). *Methods of meta-analysis: Correcting error and bias in research findings*. Thousand Oaks, Calif: Sage

Jackson, D., & Turner, R. (2017). Power analysis for random-effects meta-analysis. *Res Synth Methods, 8*(3), 290-302.

JASP Team (2018). JASP (Verision 0.9) [Computer Software].

Karabatsos, G., Talbott, E., & Walker, S. G. (2015). A Bayesian nonparametric meta-analysis model. *Res Synth Methods, 6*(1), 28-44.

Kontopantelis, E., & Reeves, D. (2012). Performance of statistical methods for meta-analysis when true study effects are non-normally distributed: A simulation study. *Stat Methods Med Res, 21*(4), 409-426.

Kwon, Y., Lemieux, M., McTavish, J., & Wathen, N. (2015). Identifying and removing duplicate records from systematic review searches. *J Med Libr Assoc, 103*(4), 184-188.

Light, R. J., & Pillemer, D. B. (1984). Summing up: the science of reviewing research. Cambridge, MA: Harvard University Press.

Limpert, E., Stahel, W. A., & Abbt, M. (2001). Log-normal Distributions across the Sciences: Keys and Clues: On the charms of statistics, and how mechanical models resembling gambling machines offer a link to a handy way to characterize log-normal distributions, which can provide deeper insight into variability and probability—normal or log-normal: That is the question. *AIBS Bulletin*, 51(5), 341-352.

Lorenzetti, D. L., & Ghali, W. A. (2013). Reference management software for systematic reviews and meta-analyses: an exploration of usage and usability. *BMC Med Res Methodol, 13*, 141-141.

Marin-Martinez, F., & Sanchez-Meca, J. (2010). Weighting by Inverse Variance or by Sample Size in Random-Effects Meta-Analysis. *Educ Psychol Meas, 70*(1), 56-73.

Mattivi, J. T., & Buchberger, B. (2016). Using the amstar checklist for rapid reviews: is it feasible? *Int J Technol Assess Health Care, 32*(4), 276-283.

McGowan, J., & Sampson, M. (2005). Systematic reviews need systematic searchers. *J Med Libr Assoc, 93*(1), 74-80.

McHugh, M. L. (2013). The Chi-square test of independence. *Biochem Med, 23*(2), 143-149.

Milo, R., Jorgensen, P., Moran, U., Weber, G., & Springer, M. (2010). BioNumbers—the database of key numbers in molecular and cell biology. *Nucleic Acids Res, 38*(Database issue), D750-D753.

Mikolajewicz, N., Mohammed, A., Morris, M., Komarova, S. V. (2018). Mechanically-stimulated ATP release from mammalian cells: systematic review and meta-analysis. *J Cell Sci*, *131*(22). doi: 10.1242/jcs.223354.

Moher, D., Liberati, A., Tetzlaff, J., & Altman, D. G. (2009). Preferred reporting items for systematic reviews and meta-analyses: the PRISMA statement. *PLoS Med, 6*(7), e1000097.

O'Collins, V. E., Macleod, M. R., Donnan, G. A., Horky, L. L., van der Worp, B. H., & Howells, D. W. (2006). 1,026 experimental treatments in acute stroke. *Ann Neurol, 59*(3), 467-477.

Lloyd, S. (1982). Least squares quantization in PCM. *IEEE Trans Inf Theory*, 28(2), 129-137.

Pathak, M., Dwivedi, S. N., Deo, S. V. S., Sreenivas, V., & Thakur, B. (2017) Which is the Preferred Measure of Heterogeneity in Meta-Analysis and Why? A Revisit. *Biostat Biometrics Open Acc*. *1*(1).

Patsopoulos, N. A., Evangelou, E., & Ioannidis, J. P. A. (2008). Sensitivity of between-study heterogeneity in meta-analysis: proposed metrics and empirical evaluation. *Int J Epidemiol, 37*(5), 1148-1157.

Paule, R. C., & Mandel, J. (1982). Consensus values and weighting factors. *J Res Natl Bur Stand, 87*(5), 377-385.

Sanchez-Meca, J., & Marin-Martinez, F. (2008). Confidence intervals for the overall effect size in random-effects meta-analysis. *Psychol Methods, 13*(1), 31-48.

Schwarzer, G., Carpenter, J. R., & Rücker, G. (2015). Small-Study Effects in Meta-Analysis. In G. Schwarzer, J. R. Carpenter, & G. Rücker (Eds.), *Meta-Analysis with R* (pp. 107-141). Cham: Springer International Publishing.

Sena, E., van der Worp, H. B., Howells, D., & Macleod, M. (2007). How can we improve the pre-clinical development of drugs for stroke? *Trends Neurosci, 30*(9), 433-439.

Sheldrake, R. (1997). Experimental Effects in Scientific Research: How Widely are They Neglected? *Bull Sci Technol Soc*, 17(4), 171-174.

Sidik, K., & Jonkman, J. N. (2005). Simple heterogeneity variance estimation for meta-analysis. *J R Stat Soc Ser C Appl Stat*, 54(2), 367-384.

Sterne, J.A., Sutton, A.J., Ioannidis, J.P., Terrin, N., Jones, D.R., Lau, J., Carpenter, J., Rücker, G., Harbord, R.M., Schmid, C.H. and Tetzlaff, J. (2011). Recommendations for examining and interpreting funnel plot asymmetry in meta-analyses of randomised controlled trials. *Br Med J*, 343, d4002.

Sterne, J. A. C., & Harbord, R. (2004). Funnel plots in meta-analysis. *Stata J, 4*(2), 127-141.

Vaux, D. L., Fidler, F., & Cumming, G. (2012). Replicates and repeats—what is the difference and is it significant?: A brief discussion of statistics and experimental design. *EMBO Rep, 13*(4), 291-296.

Veroniki, A.A., Jackson, D., Viechtbauer, W., Bender, R., Bowden, J., Knapp, G., Kuss, O., Higgins, J., Langan, D. and Salanti, G. (2016). Methods to estimate the between-study variance and its uncertainty in meta-analysis. *Res Synth Methods*, 7(1), 55-79.

Vesterinen, H.M., Sena, E.S., Egan, K.J., Hirst, T.C., Churolov, L., Currie, G.L., Antonic, A., Howells, D.W. and Macleod, M.R. (2014). Meta-analysis of data from animal studies: a practical guide. *J Neurosci Methods*, 221, 92-102.

Viechtbauer, W. (2010). Conducting meta-analyses in R with the metafor package. *J Stat Softw*, 36(3), 1-48.

von Hippel, P. T. (2015). The heterogeneity statistic I(2) can be biased in small meta-analyses. *BMC Med Res Methodol, 15*, 35.

Weed, D. L. (2000). Interpreting epidemiological evidence: how meta-analysis and causal inference methods are related. *Int J Epidemiol, 29*(3), 387-390.

Weed, D. L. (2010). Meta-Analysis and Causal Inference: A Case Study of Benzene and Non-Hodgkin Lymphoma. *Ann Epidemiol, 20*(5), 347-355.

Chapter Four

Mechanically-Stimulated ATP Release from Mammalian Cells: Systematic Review and Meta-Analysis

Using the methods described in **Chapter 3**, we performed a large-scale quantitative synthesis of 278 studies that investigated mechanically-stimulated ATP release in mammalian cells. This study provided insights into the amounts, kinetics, and mechanisms of ATP release, as well as the influence of various pathologies on ATP release. Importantly, this advanced our understanding of mechanically-stimulated ATP release from osteoblasts and osteocytes, aligning with ***research objective 1*** of this dissertation. Supplemental materials for this chapter are in **Appendix A2**.

4.1 Abstract

Body tissues are exposed to a complex mechanical environment which is perceived by cells and converted to biochemical signals, such as ATP release. We performed a meta-analysis of 278 systematically identified studies that investigated mechanically-stimulated ATP release (MSAR) to quantify the amounts, kinetics and mechanisms of ATP release under normal and pathological conditions. Mechanically-stimulated mammalian cells were shown to release 38.6 (95% CI: 18.2 to 81.8) amoles ATP/cell on average with a characteristic time constant of 32 s (95% CI: 16 to 66). Analysis of ATP release mechanisms revealed the existence of conserved and tissue-specific release routes. We assessed ATP release in pathophysiological states and found that ATP release was elevated in inflammation and injury and attenuated in hereditary (cystic fibrosis, xerocytosis) and metabolic (type II diabetes, primary pulmonary hypertension) conditions. Our study links cell-

specific ATP release mechanisms to pathophysiological changes in ATP release and allows ATP release-targeting interventions to be mapped to site-specific effects. This work demonstrates that quantitative synthesis of basic research can generate non-trivial hypotheses and inform evidence-driven translational studies.

4.2 Introduction

The discovery that mechanical stimuli elicit ATP release from mammalian cells was made over 25 years ago (Milner et al., 1990) and represented a paradigm shift in how we understand the interaction between the body and the mechanical environment. The body is constantly exposed to a complex combination of shear forces, strains, osmotic stresses and pressures. These forces are perceived at the cellular level and converted to biochemical signals, one of which involves the release of ATP, a high-energy content purine molecule that represents the primary source of cellular energy (Bergman, 1999). It is now clear that extracellular ATP is as an autocrine and paracrine signaling molecule that exerts its effects through purinergic receptors (Burnstock, 2014).

In this study, we systematically reviewed the literature pertaining to mechanically-stimulated ATP release from mammalian cells and conducted a meta-analysis on relevant studies. The primary objective was to provide quantitative estimates of amount and kinetics of ATP release in response to mechanical stimulation. The secondary objective was to extend our analysis to address problems that are otherwise difficult to investigate at the single study level, including comparing the effects of different mechanical stimuli, as well as consolidating the available intervention and pathology-related data. In addition to our research objectives, we sought to demonstrate the feasibility and value of conducting meta-analyses at the basic research level to complement existing lines of evidence used to inform translational research.

4.3 Results

4.3.1 Overview of relevant studies

We systematically identified 278 studies that directly measured ATP release from mechanically-stimulated mammalian cells (**Fig 4-1A**). In these studies, 9 unique models of mechanical stimulation, including osmotic pressure, fluid shear stress (FSS), strain and compression, were used to stimulate ATP release from mammalian cells (**Fig 4-1B**). Cells derived from 12 different organ systems were studied, most commonly originating from the urinary and musculoskeletal

systems (**Fig 4-1C**). Most studies measured ATP using the luciferin-luciferase bioluminescence assay (91.6%), while others used high performance liquid chromatography (4%), hexokinase-based enzymatic assays (1.8%), surface-bound luciferase probes (1.1%), microelectrodes (1.1%) and cell-based biosensors (0.004%).

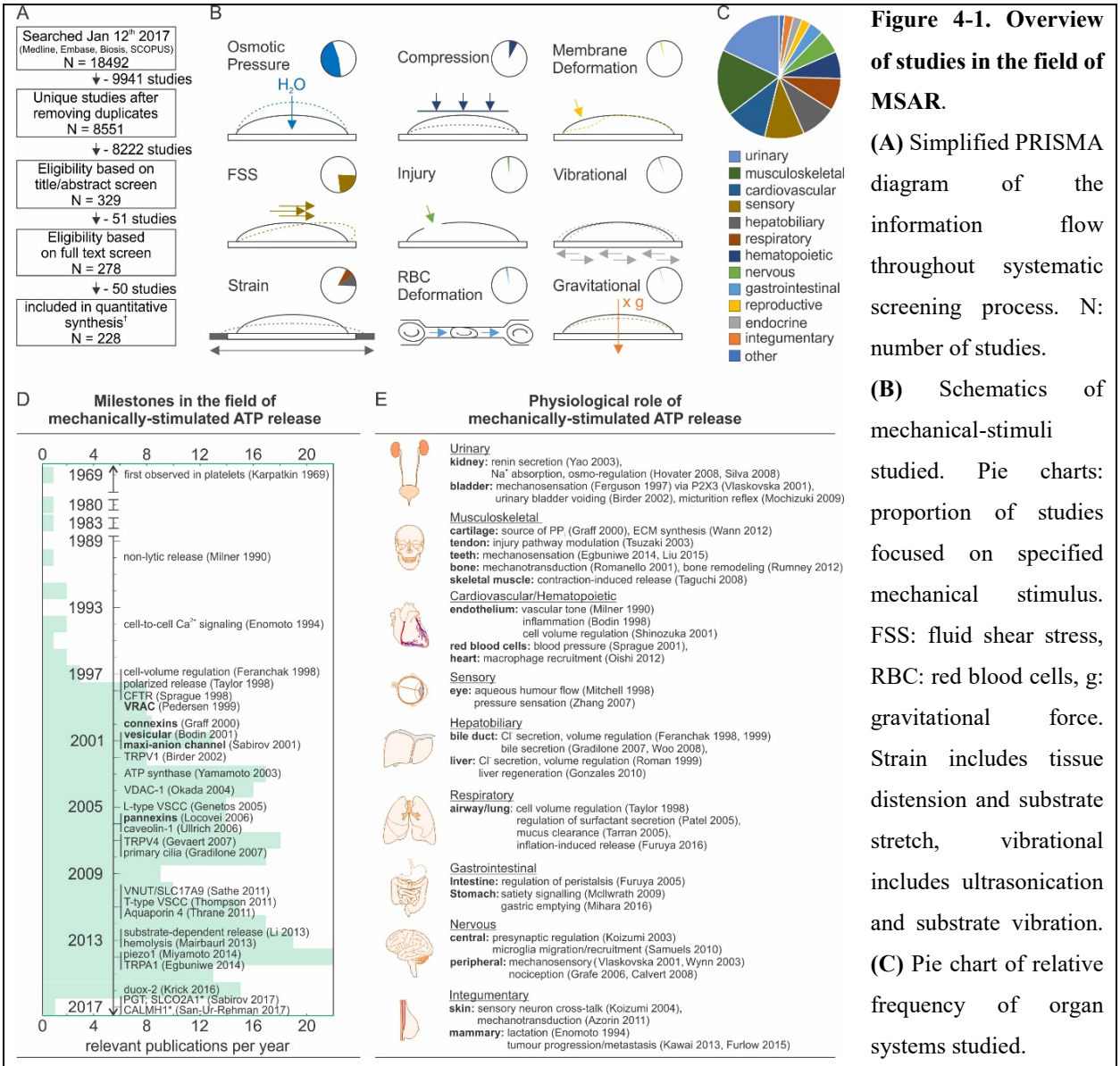

Figure 4-1. Overview of studies in the field of MSAR.

(A) Simplified PRISMA diagram of the information flow throughout systematic screening process. N: number of studies.

(B) Schematics of mechanical-stimuli studied. Pie charts: proportion of studies focused on specified mechanical stimulus. FSS: fluid shear stress, RBC: red blood cells, g: gravitational force. Strain includes tissue distension and substrate stretch, vibrational includes ultrasonication and substrate vibration.

(C) Pie chart of relative frequency of organ systems studied.

(D) Milestones in the field of mechanically-stimulated ATP release. *Time-line*: key publications or notable discoveries, *bolded*: main routes of ATP release identified, *bar-graph (green)*: Number of relevant publications per year. *key contributions published after systematic search: Prostaglandin transporter (PGT) constitutes core component of maxi-anion channel (Ravshan Z Sabirov et al., 2017), calcium homeostasis modulator 1 (CALHM1) (Sana-Ur-Rehman, Markus, Moore, Mansfield, & Liu, 2017). **(E)** Overview of physiological role of mechanically-stimulated ATP release in different tissues.

We tracked the discovery of non-lytic ATP release to Milner et. al. who described the phenomenon in fluid-shear stimulated endothelial cells in 1990 (Milner et al., 1990) (**Fig 4-1D**). The physiological relevance of mechanically-stimulated ATP release (MSAR) was soon after realized and widespread interest surged around the 2000s. It is now clear that MSAR is physiologically involved in virtually every organ system and plays a role in facilitating responses to mechanical perturbations that demand immediate physiological feedback (**Fig 4-1E**). To date, the general physiological relevance has been established, and current work in the field is focused on understanding the mechanistic and potential therapeutic relevance of MSAR.

4.3.2 Mechanically-stimulated ATP release is a conserved phenomenon in mammalian cells

We quantified ATP release as the amount of ATP liberated into the extracellular space after mechanical stimulation (**Fig 4-2A**). Using a random effects model, we estimated that mechanically-stimulated mammalian cells released 38.6 (95% CI: 18.2 to 81.8) amoles ATP/cell over basal extracellular amount of 8.1 (95% CI: 3.9 to 16.6) amoles ATP/cell. The total intracellular ATP content was estimated to be 5.0 (95% CI: 2.6 to 9.5) fmoles ATP/cell in nucleated cells and 0.14 (95% CI: 0.12, 0.18) fmoles ATP/cell in red blood cells (RBC) (**Fig 4-2B**, **Table 4-S1**). ATP release estimates were considerably inconsistent between studies, ranging over 10-orders of magnitude (**Fig 4-S1, Table 4-S1**). We found that 80% of the heterogeneity was explained by a correlation between basal ATP (A_{base}) and ATP release (A_{mech}) estimates that arose only between studies but was absent within studies (**Fig 4-2C**). Furthermore, we found that heterogeneity in basal ATP was not explained by differences in methodologies (**Fig 4-2D**), suggesting that the primary source of heterogeneity was inconsistent ATP calibrations between studies. Estimates of relative ATP release were more consistent between studies and were unaffected by the overall quality of the study, although some publication bias was evident (**Fig 4-S1**). We found that every cell type investigated responded to mechanical stimulation by releasing ATP, resulting in a 4.3-fold (95% CI: 3.8 to 4.8) increase in extracellular ATP above baseline (**Fig 2E**). Remarkably, the amount of ATP released was generally robust to variations in experimental methodology and biological characteristics (**Fig 4-S2, Table 4-S2**). In particular, different cell types, cells from different species, embryonic origin and most organ systems released similar amounts of ATP upon mechanical stimulation. Among the factors that did influence ATP release, we found that neutralization of ATP degradation or application of cyclic mechanical stimuli were

associated with relatively lower ATP release (**Fig 4-S2A**), and polarized epithelia released significantly higher amounts of ATP from the apical surface compared to the basolateral membrane (**Fig 4-S2B**). We conclude that MSAR is a conserved phenomenon in mammalian cells, and provide robust quantitative estimates for the absolute and relative amounts of ATP released upon mechanical stimulation.

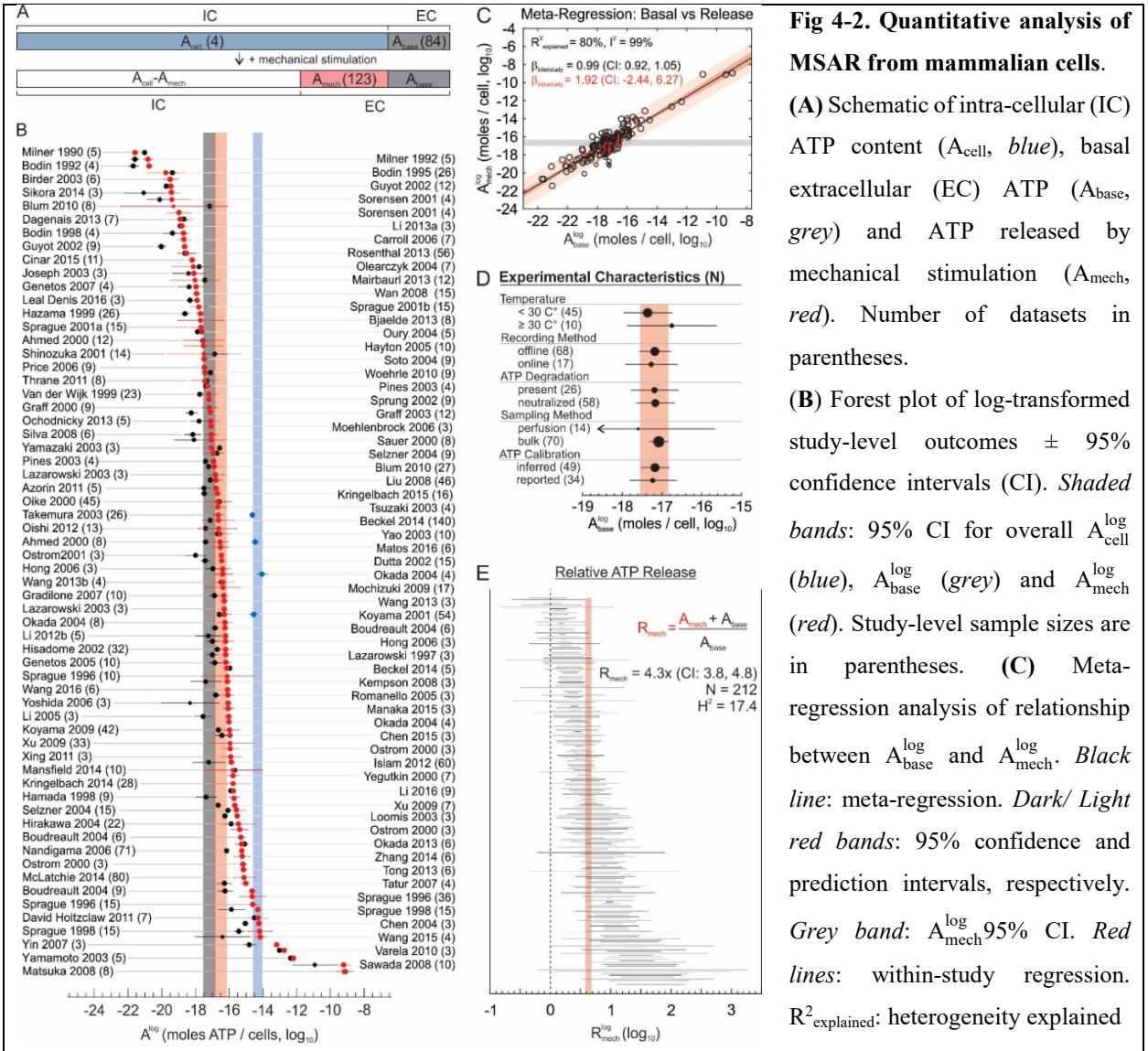

Fig 4-2. Quantitative analysis of MSAR from mammalian cells.
(A) Schematic of intra-cellular (IC) ATP content (A_{cell}, *blue*), basal extracellular (EC) ATP (A_{base}, *grey*) and ATP released by mechanical stimulation (A_{mech}, *red*). Number of datasets in parentheses.
(**B**) Forest plot of log-transformed study-level outcomes ± 95% confidence intervals (CI). *Shaded bands*: 95% CI for overall A^{log}_{cell} (*blue*), A^{log}_{base} (*grey*) and A^{log}_{mech} (*red*). Study-level sample sizes are in parentheses. **(C)** Meta-regression analysis of relationship between A^{log}_{base} and A^{log}_{mech}. *Black line*: meta-regression. *Dark/ Light red bands*: 95% confidence and prediction intervals, respectively. *Grey band*: A^{log}_{mech}95% CI. *Red lines*: within-study regression. $R^2_{explained}$: heterogeneity explained by regression, I^2: variance due to heterogeneity, $\beta_{interstudy}$: slope ± 95% of between-study relationship, $\beta_{intrastudy}$: average slope ± 95% of within-study relationship **(D)** Effects of experimental factors on A^{log}_{base}. *Black markers/lines*: subgroup estimates ± 95% CI. *Red band*: Overall A^{log}_{base} 95% CI. **(E)** Forest plot of study-level 95% CI for relative ATP release R^{log}_{mech}. *Shaded band*: Overall 95% CI for R^{log}_{mech}, *dashed black line*: No ATP released reference. H^2: heterogeneity statistic, N: number of included datasets. Detailed statistics in **Table 4-S1, 4-S2**.

4.3.3 The amount of ATP release is proportional to the magnitude of mechanical stimulation

We next investigated the relationship between the type of mechanical stimulation and ATP release. We found that similar amounts of ATP were released in response to all studied mechanical stimuli (**Fig 4-3A, Table 4-S3**). Only locally-applied membrane deformations resulted in lower ATP release compared to other forms of stimulation. We used a combination of meta-regression and within-study regression to investigate the relationship between the magnitude of mechanical stimulation and the amount of ATP released (**Fig 4-3B-G, Table 4-S3**). Within studies, ATP release was consistently proportional to the magnitude of mechanical stimulation, while between studies this relationship was less pronounced. Nevertheless, the directions of association were consistently positive for all types of mechanical stimulation (**Fig 4-3H**). Thus, despite evident aggregation bias, we conclude that the amount of ATP released is governed by the magnitude of mechanical stimulation.

4.3.4 ATP release kinetics are stimulus-dependent

To quantify the kinetics of ATP release, we fitted study-level time-series data to a sigmoidal model using a Monte-Carlo fitting procedure and estimated the time to half max ATP release t_{half} (**Fig 4-4A**). Meta-analysis demonstrated that the characteristic half-max ATP release time was 101 s (95% CI: 83 to 117 s) (**Fig 4-4B**). ATP release kinetic estimates were moderately heterogeneous with no discernable publication bias and they were not influenced by study quality (**Fig 4-S3**). However, we found that real-time online recordings of ATP release yielded significantly faster release kinetics of 32 s (95% CI: 16 to 66 s) compared to offline measurement methods which yielded slower kinetics of 136 s (95% CI: 117 to 159 s) (**Fig 4-4C-D, Table 4-S4**). We stratified the data by recording method prior to further analysis. ATP release kinetics were robust to differences in all other experimental factors but not to biological factors (**Fig 4-S4, Table 4-S4**). ATP release was relatively slower in certain species (guinea pigs, porcine, rabbits) and cells from different embryonic origins (ectoderm) and organ systems (sensory). Importantly, the kinetics of ATP release depended on the type of mechanical stimulus applied. FSS evoked significantly faster ATP release compared to osmotic pressures (**Fig 4-4E-F, Table 4-S4**). Thus, systematic large-scale data synthesis allowed us to identify a previously unknown relationship between ATP release kinetics and the type of mechanical stimulation, suggesting that it needs to be further explored experimentally.

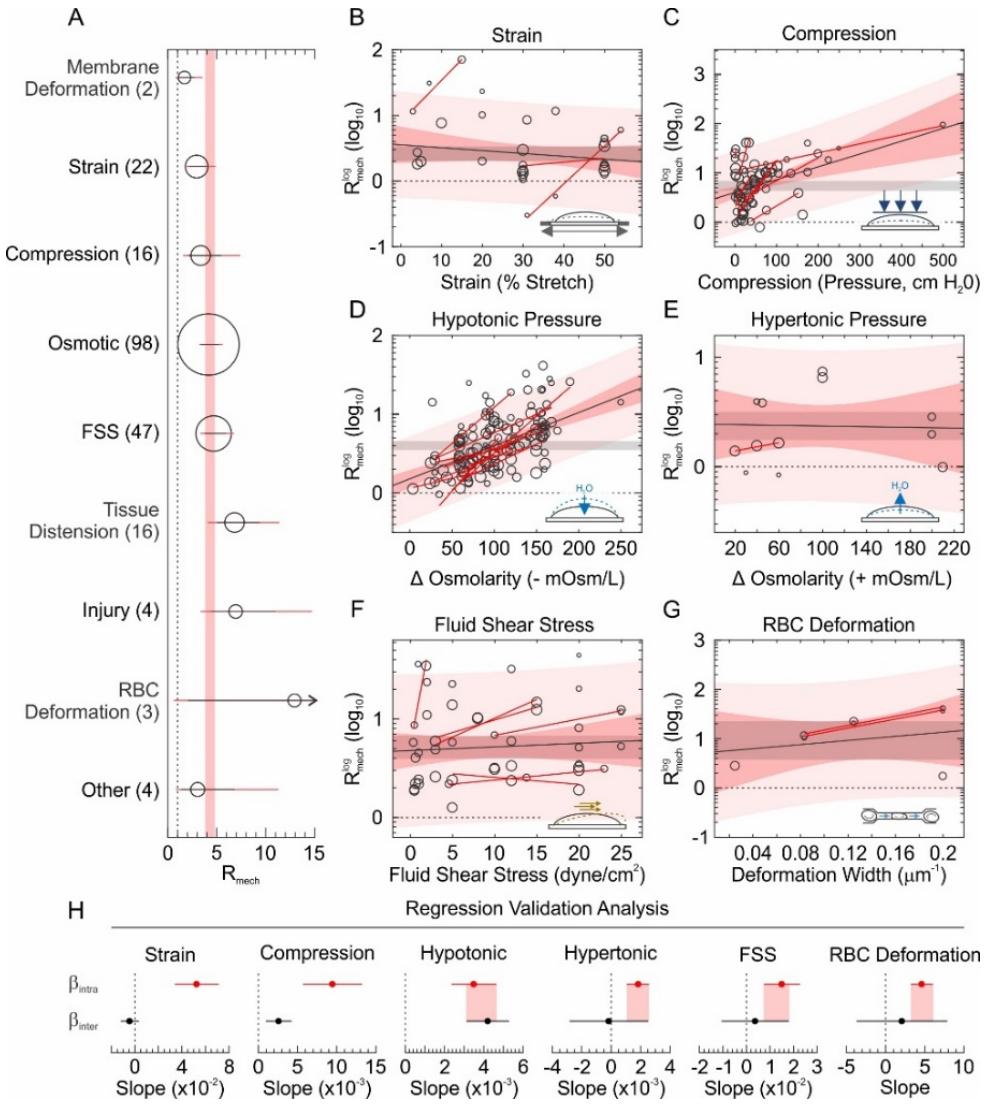

Figure 4-3. Relationship between mechanical stimuli and ATP release. (A) Relative amount of ATP (R_{mech}) released in response to different mechanical stimuli. Number of datasets in parentheses. *Black circles*: Subgroup estimates, *Horizontal black lines*: ± 95% CI, *Horizontal red lines*: ± Bonferroni-adjusted 95% CI, *Red band*: 95% CI for overall R_{mech}, *dashed black line*: No ATP released reference. (**B-G**) Meta-regression analysis of relationship between magnitude of mechanical stimulation and R^{log}_{mech} following stimulation by strain **(B)**, compression **(C)**, hypotonic pressure **(D)**, hypertonic pressure **(E)**, FSS **(F)** or deformation of RBCs **(G)**. *Black line*: meta-regression. *Dark/Light red bands*: 95% confidence and prediction intervals. *Grey band*: 95% CI of R^{log}_{mech} for indicated stimulus. *Red lines*: intrastudy regression. *Insets*: schematic of mechanical stimuli. **(H)** Comparison of intrastudy (β_{intra}, *red*) and interstudy (β_{inter}, *black*) regression slopes ± 95% CI. *Red bands*: 95% CI overlap, *dashed lines*: no relationship reference. Detailed statistics are in **Table 4-S3**.

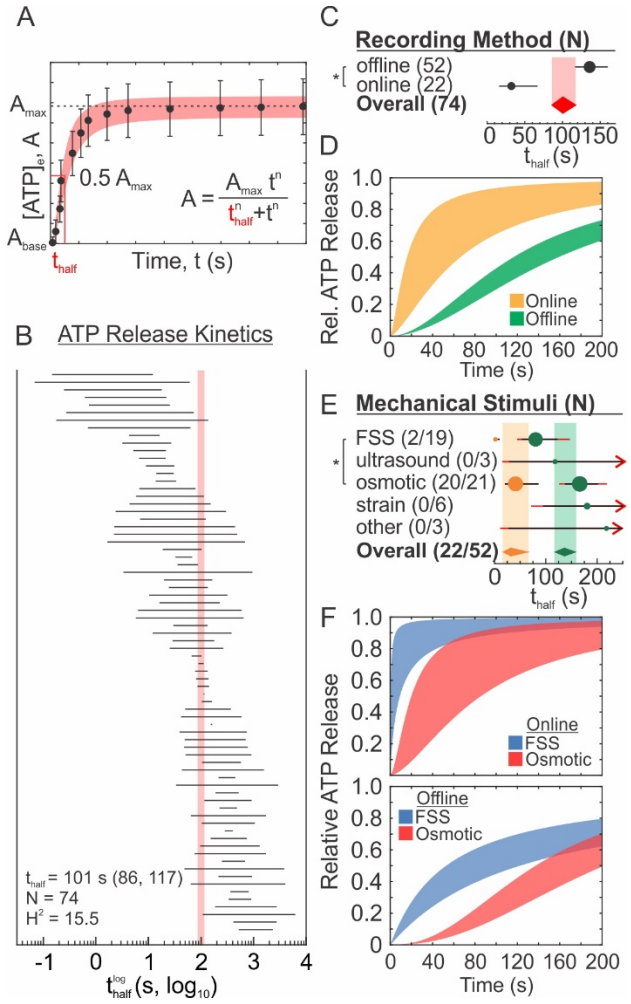

Figure 4-4. Kinetics of ATP release.

(A) Study-level ATP release kinetics (*black markers*) were fit to sigmoidal function using Monte-Carlo method and characteristic time to half-max release (t_{half}, *red*) with standard error was estimated. *Dashed black line*: A_{max}; max ATP released, *red band*: sigmoidal function 95% CI. **(B)** Forest plot of log-transformed study-level 95% CIs for t_{half} (t_{half}^{log}). *Shaded band*: 95% CI for overall t_{half}^{log}. N: Number of datasets, H^2: heterogeneity statistic. **(C, D)** Subgroup estimates of t_{half} ± 95% CI **(C)** and 95% CI temporal profiles of ATP release **(D)** recorded using online or offline methods. *Red band*: 95% CI for overall t_{half}. **(E, F)** t_{half} stratified by recording method for different mechanical stimuli. **(E)** Subgroup t_{half} estimates. *Green*: offline recording, *yellow*: online recording. *Horizontal black lines*: ± 95% CI, *horizontal red lines*: ± Bonferroni-adjusted 95% CI, *bands/diamonds*: overall t_{half} ± 95% CI. **(F)** Comparison of FSS- (*blue*) and osmotic pressure- (*red*) stimulated ATP release 95% CI temporal profiles when recorded online (*top*) or offline (*bottom*). Detailed statistics in **Table 4-S4**.

4.3.5 Mechanisms of mechanically-stimulated ATP release

We next synthesized the data pertaining to the mechanisms of MSAR. Pharmacological and genetic interventions were grouped by common molecular targets (**Table 4-S5**) and their relative inhibitory effects were quantified for each cell type (**Fig 4-5, Table 4-S6**). The five main direct routes of mechanically stimulated ATP release that have been identified in mammalian cells are vesicles (Bodin & Burnstock, 2001; Sathe et al., 2011), pannexins (Locovei, Bao, & Dahl, 2006), connexins (Graff, Lazarowski, Banes, & Lee, 2000), volume-regulated anion channels (VRAC) (Pedersen, Pedersen, Nilius, Lambert, & Hoffmann, 1999; Qiu et al., 2014; Voss et al., 2014) and maxi-anion channels (MAC) (Ravshan Z. Sabirov, Dutta, & Okada, 2001; Ravshan Z Sabirov et al., 2017). Vesicles were involved in 70% (14/20) of studied cell types from all organ systems except for the integumentary (i.e., keratinocytes, mammary epithelial cells) (**Fig 4-5A**). Pannexins

were the second most common route of ATP release, involved in 58% (15/26) of all studied cell types. Pannexin-mediated ATP release occurred in hematopoietic cells, astrocytes and most epithelial cells (including digestive, airway and ocular). Connexins, VRACs and MACs were implicated in ATP release in 35% (7/20), 36% (4/11) and 23% (3/13) of all cells studied, respectively. Connexin-mediated ATP release was highly prevalent in ocular cell types and in the kidney, but was absent in airway epithelia and smooth muscle. VRACs exhibited no discernable tissue-specific pattern of involvement, while MACs were almost exclusively implicated in ATP release from integumentary cells. This data-driven summary of MSAR mechanisms allowed us to establish tissue-level generalizations and suggest the existence of common (vesicular) and tissue-specific (pannexin, connexins, MAC) routes of ATP release.

We conducted a co-occurrence analysis to screen for possibly codependent pathways of ATP release (**Fig 4-5B**). The main routes of ATP release (i.e., vesicular, pannexin, connexin, VRAC and MAC) co-occurred pairwise in 27-67% of studied cells, except for vesicle- and MAC-mediated ATP release routes which were mutually exclusive (co-occurred in 0 of the 4 cell types studied; 0/4). We investigated whether the main routes of ATP release contributed to the total amount of ATP released in an additive manner by accounting for the relative contributions of each route (**Table 4-1**). In certain cell types, the total amount of ATP released was accounted for by the additive contribution of the main routes of ATP release. However, in cardiomyocytes, ligament cells, pancreatic and renal epithelia, and urothelial cells, the additive contributions exceeded the amount of ATP released. Although there is a possibility that pharmacological non-specificity contributed to this effect, genetic methods were in agreement. For instance, siRNA-mediated knockdown of Cx43 and Panx1 in ligament cells inhibited ATP release by 73.1% (95% CI: 68.7, 77.4) (Luckprom, Kanjanamekanant, & Pavasant, 2011) and 73.6% (95% CI: 69.2, 78.0) (Kanjanamekanant, Luckprom, & Pavasant, 2014), respectively. These findings suggest the existence of a cell type-specific synergistic interaction between ATP release routes previously thought to be functionally independent.

We investigated the association between the main ATP release routes and other implicated regulatory and auxiliary pathways. Vesicular ATP release consistently coincided with the involvement of intracellular calcium ($[Ca^{2+}]_i$, 8/8 cell types studied), Rho kinases (3/3) and microtubules (4/4). Rho kinases (3/3) and microtubules (3/3) were also involved in pannexin-

mediated ATP release. No pathway consistently co-occurred with connexin-mediated ATP release. VRAC-mediated ATP release coincided with the involvement of P2X7 receptors (5/5), but never with ATP synthase (0/3), and MAC-mediated ATP release co-occurred with ATP synthase-related ATP release (3/3), but never with $[Ca^{2+}]_i$-dependent ATP release (0/3). Thus, we have identified conserved cell-independent signaling patterns that warrant further experimental investigation.

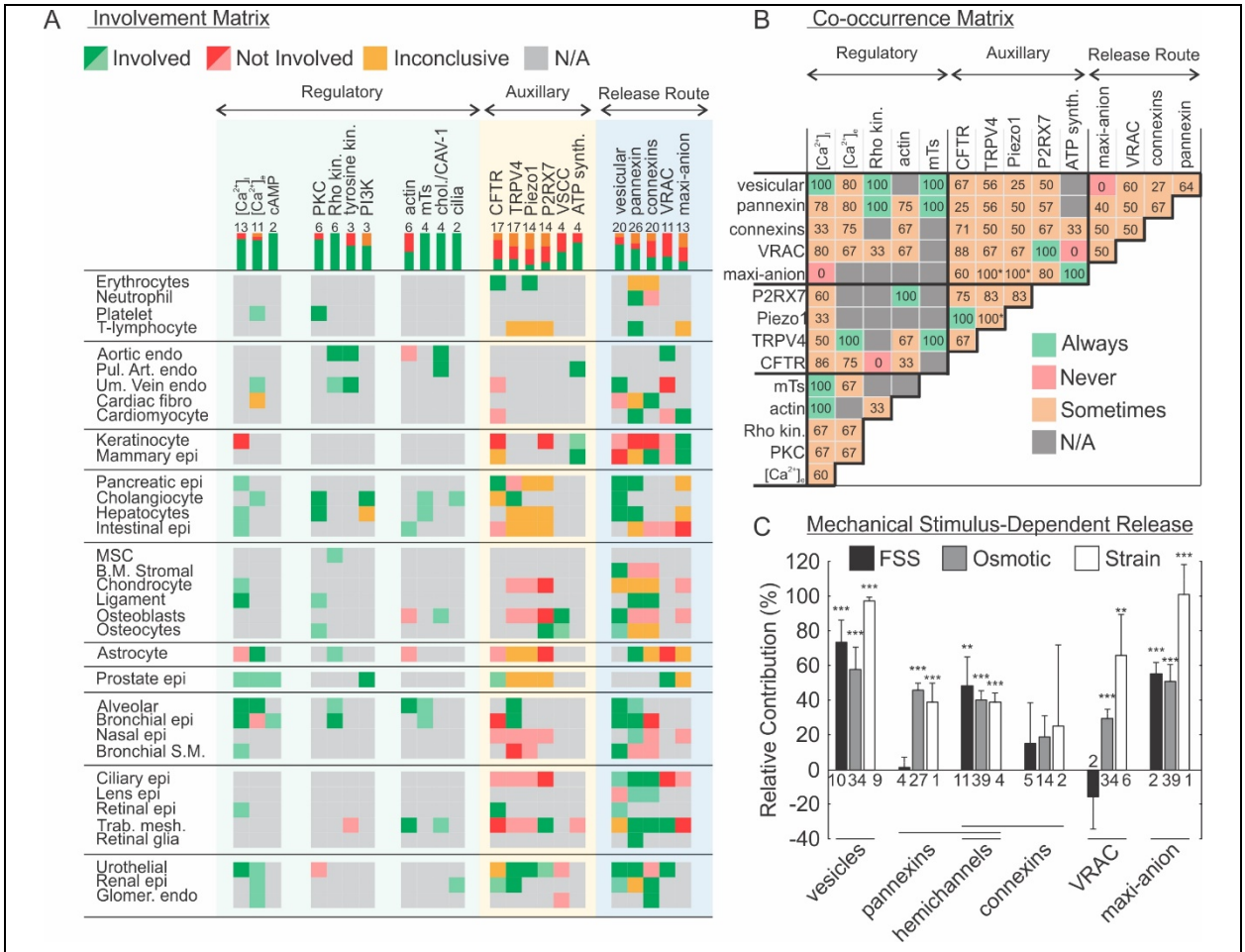

Figure 4-5. Mechanisms of mechanically-stimulated ATP release. (A) Involvement of the most commonly studied MSAR mechanisms (*columns*) for each cell type (*rows*). *Stacked bars*: Relative frequencies of involvement for each mechanism. Number of unique cell types studied per mechanism is indicated. *Dark green/red*: findings replicated by separate study/method, *light green/red*: not-replicated. **(B)** Percentage of cells types in which implicated mechanisms co-occurred. Results shown for mechanism pairs studied in >2 cell types. *pairwise co-occurrences confounded by common pharmacological interventions. **(C)** Relative contributions of main ATP release routes to ATP release in cells stimulated by FSS, osmotic pressure or strain, approximated by inhibitory effect (%) ± standard errors of interventions. **p<0.01 and ***p<0.001 indicate significant contribution assessed by t-test, compared to reference value 0 (i.e., no contribution to ATP release). Number of datasets are indicated. Intervention data used to construct matrices are in **Table 4-S5, 4-S6**.

Table 4-1. **Total contribution of the main routes of ATP release**.

Cell type	Studied mechanisms	Joint Contributions (% ± 95% CI)	Proposed Interaction
Astrocytes	Px, Cx, VRAC, MAC	118 (67.8, 168.2)	Additive
Cardiomyocytes	Px, VRAC, MAC	176.6 (140.4, 212.8)	Synergy
Chondrocytes	Vesicle, Px, Cx, MAC	99.2 (32.9, 165.5)	Additive
Ciliary Epithelia	Vesicle, Px, Cx, VRAC, MAC	122.1 (39.8, 204.4)	Additive
Keratinocytes	Vesicle, Px, Cx, VRAC, MAC	92.7 (-18.7, 204.1)	Additive
Ligament cells	Px, Cx	146.6 (139.9, 153.3)	Synergy
Mammary epithelia	Vesicle, Px, Cx, VRAC, MAC	53.9 (-64.3, 172.1)	Additive
Pancreatic epithelia	Vesicle, Px	164.3 (144.8, 183.8)	Synergy
Renal epithelia	Vesicle, Px, Cx	220.2 (132.4, 308)	Synergy
Trabecular meshwork	Vesicle, Px, Cx, VRAC, MAC	110.9 (35.3, 186.5)	Additive
Urothelial Cells	Vesicle, Px, Cx, VRAC	248.1 (137.6, 358.6)	Synergy

The relative contributions (determined from genetic and pharmacological interventions, **Table 4-S6**) of each ATP release route were added together. Contributions that added to 100% (contained by 95% CI) were interpreted as additive, and those exceeding 100% were interpreted as synergistic. Shown are cell types in which at least 4 of the 5 main routes of ATP release were studied, except for cell types that exhibited synergy-like interactions, in which case not restriction was placed on minimum number of routes studied.

We next explored whether the mechanisms of ATP release depend on the type of mechanical stimulation (**Fig 4-5C**). We examined the contribution of the main routes of ATP release in response to mechanical stimuli with sufficiently large datasets (FSS, osmotic pressure and strain). All 5 routes of ATP release were implicated in osmotic pressure- and strain-induced ATP release with the similar patterns of contribution. In contrast, VRAC and possibly pannexins were not involved in FSS-induced ATP release. Thus, consistent with our findings that FSS- and osmotic pressure-induced ATP release exhibit distinct release kinetics, these data suggest that distinct mechanisms may contribute to stretch- and shear-related responses.

4.3.6 Mechanically-stimulated ATP release in pathologies

Aberrant ATP release has been implicated in multiple pathophysiological conditions (**Fig 4-6A**). Inflammation and injury related conditions were associated with elevated levels of MSAR, compared to unaffected controls (**Fig 4-6B, Table 4-S7**). On the other hand, attenuated ATP release was observed in hereditary conditions such as cystic fibrosis and xerocytosis, and in type II diabetes and primary pulmonary hypertension (**Fig 4-6C, Table 4-S7**). In some pathologies, the magnitude or direction of changes in MSAR were cell- or stimulus-specific. In cystic fibrosis, RBCs and pancreatic epithelia released less ATP upon stimulation, while airway epithelia and astrocytes were unaffected. Acute hypoxia potentiated ATP release from endothelial cells, while chronically hypoxic cells released less ATP (**Fig 4-6D**, **Table 4-S7**). In polycystic kidney disease (PKD), renal epithelia released less ATP upon FSS stimulation in both autosomal dominant and

recessive cases, while osmotic swelling-induced ATP release was unaffected in autosomal recessive and potentiated in autosomal dominant PKD (**Fig 4-6D**, **Table 4-S7**), again suggesting distinct cell processing of shear- and stretch-related stimuli. Thus, we demonstrate the presence of specific patterns of MSAR alteration with respect to the type of pathology, affected cells, and applied stimulus, and suggest that inhibitory and stimulatory interventions targeting MSAR can be of therapeutic interest, but need to be applied with caution. Our study maps the potential anatomical sites and situations in which targeting MSAR may have (patho-) physiological consequences.

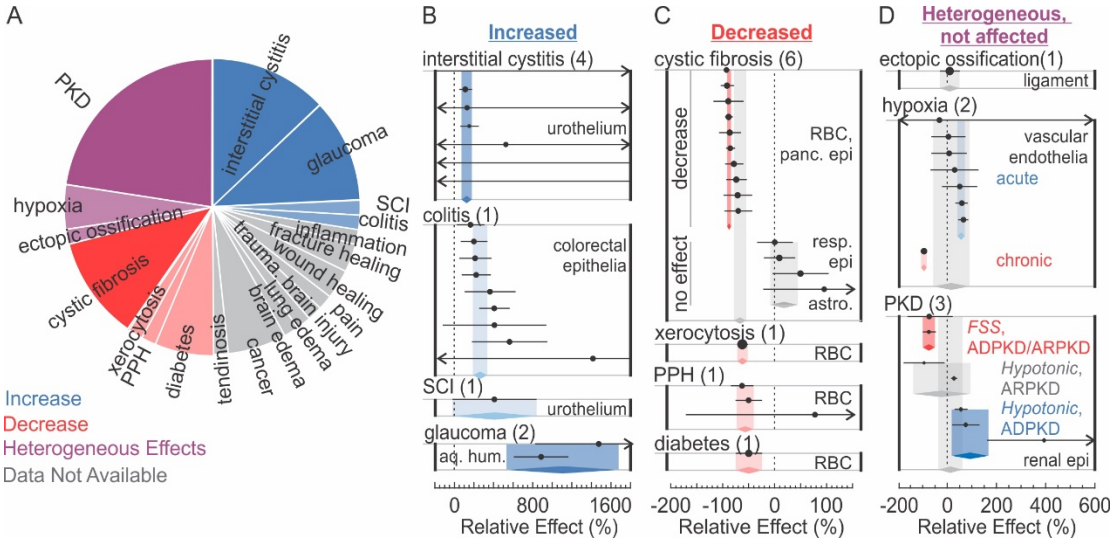

Figure 4-6. Pathological ATP release. (A) Pie chart of relative frequency of clinically-relevant conditions studied or implicated in aberrant MSAR (61 studies total). *Blue*: increased ATP release, *red*: decreased ATP release, *grey*: implicated but not measured, *purple*: heterogenous effects. *Light shade*: reported by single study, *Dark shade*: replicated findings. **(B-D)** Forest plots of relative effect (%) of pathologies (specified in top left) on MSAR from cells (specified on the right) compared to unaffected controls. *Black markers/lines*: study-level relative effects ± 95% CI, *bands*: 95% CI of overall pathology-specific effect. Marker sizes are proportional to study-level sample sizes, number of independent studies for each pathology are in parentheses. *Black dashed lines*: no effect reference. **(B)** Pathologies associated with increased MSAR. **(C)** Pathologies associated with decreased MSAR. **(D)** Pathologies that had heterogeneous or no effect on MSAR.

4.4 Discussion

4.4.1 Overview

We have conducted a systematic large-scale data synthesis to quantitatively characterize the amounts, kinetics and mechanisms of mechanically-stimulated ATP release under normal and pathological conditions. From 228 systematically selected studies, we extracted 123 estimates of absolute and 212 estimates of relative amount of ATP released, 74 kinetic time-series, 592 pharmacological and 89 genetic intervention outcomes, and 51 pathophysiological comparisons. Using a meta-analytic approach, we have established that mechanically-stimulated mammalian cells release 38.6 (95% CI: 18.2 to 81.8) amoles ATP/cell, with a characteristic time constant of 32 s (95% CI: 16 to 66) measured using real-time recording methods. We have found that MSAR is a universally conserved phenomenon in mammalian cells, and that cells from different species, embryonic origin and most organ systems release similar amount of ATP when mechanically stimulated. Our data-driven summary of MSAR mechanisms allowed us to infer tissue-level generalizations that suggest the existence of common and tissue-specific routes of ATP release, and to identify conserved cell type-independent signaling patterns. We have found that inflammation and injury were associated with increased MSAR, while hereditary and metabolic conditions resulted in attenuated ATP release. Importantly, several lines of evidence including (i) differences in release kinetics, (ii) implicated mechanisms and (iii) pathophysiological effects in polycystic kidney disease, suggest that cells can discriminate between stretch- and shear-related forces. Thus, consolidating and quantifying over 25 years of basic research data generated in 64 unique cell types derived from 12 organ systems and stimulated by 9 distinct force applications allowed us to generate novel testable hypotheses, and provide evidence-driven recommendations for translational studies.

4.4.2 Study limitations

The studies included in this meta-analysis were highly heterogeneous, however this was expected due to the higher methodological variability in exploratory basic science studies (Bradbury & Pluckthun, 2015; Fontoura-Andrade, Amorim, & Sousa, 2017; Soehnlein & Silvestre-Roig, 2017). Importantly, accounting for interstudy differences in ATP calibration and recording methods allowed us to dramatically reduce heterogeneity. We found minimal evidence of publication bias.

We also demonstrated that the quality of the studies did not significantly affect study-level outcomes, despite quality scores varying substantially across studies. It is known that subgroup analyses come at the expense of lower statistical power, however the large number of available datasets permitted statistically powered analysis for numerous secondary outcomes (Jackson & Turner, 2017). Analysis of MSAR mechanisms was limited by overlapping and off-target effects of many inhibitors, as well as lack of within-study inhibitor validation and overreliance on assumed pharmacological targets. We minimized false positive outcomes by applying random effects meta-analytic models and considering Bonferroni adjustments for multiple comparison analyses (Glass, 1986). There remains a distinct possibility of false negative outcomes due to limited sample sizes in some subgroups, aggregation bias and heterogeneity (Higgins & Thompson, 2002).

4.4.3 Quantitative characterization

We estimated that mechanically-stimulated mammalian cells release 38.6 (95% CI: 18.2 to 81.8) amoles ATP/cell, resulting in a 4.3-fold (95% CI: 3.8 to 4.8) increase in ATP above basal levels of 8.1 (95% CI: 3.9 to 16.6) amoles ATP/cell. Intracellular ATP content was estimated to be 3 orders of magnitude higher than basal ATP levels in nucleated cells, 5.0 (95% CI: 2.6 to 9.5) fmoles ATP/cell, and 2 orders of magnitude higher in RBCs, 0.14 (95% CI: 0.12, 0.18) fmoles ATP/RBC. Study-level estimates of the absolute amount of ATP released ranged over 10 orders of magnitude, with 5 studies reporting more ATP release than can be contained within a cell, suggesting that more caution must be taken when performing ATP calibrations and measurements, and that basal, released and total ATP content should be reported to obtain relative measures. The characteristic time to half-max ATP release was strongly influenced by the recording method, yielding almost 4 times faster estimates by real-time recordings compared to estimates acquired by bulk sampling and offline measurement. This difference can be potentially explained by the diffusion time required to equilibrate the concentration within the volume of the culture medium. In this regard, the volume into which ATP is released is an important (but not routinely controlled for) determinant of the effective ATP concentration available for autocrine and paracrine signaling, including ATP-regulated ATP release (Bodin & Burnstock, 1996; Dillon et al., 2013). We found that less ATP is released in response to cyclic stimulation, however no studies reported the kinetics of ATP release in response to repeated or cyclical stimulations, even though physiological stimuli are often cyclical (Burr et al., 1996; Eyckmans, Boudou, Yu, & Chen, 2011; Fritton, McLeod, &

Rubin, 2000). Of interest, studies in which cell injury was assessed and detected or intentionally induced, reported a tendency for higher ATP release. However, the amount of injury-related ATP release never reached amounts expected following cell destruction and was not statistically different from osmotic pressure- or FSS-induced ATP release. Thus, quantitative synthesis of basic science studies employing diverse approaches with complex endpoints is feasible and has allowed us to identify methodological variations of consequence.

4.4.4 Dependence on mechanical stimulus

We compared ATP release induced by 9 different types of mechanical stimulation, including stretch-related stimuli, such as substrate strain, osmotic pressure and tissue distention, and FSS and local membrane deformation. Although all types of mechanical stimulation resulted in release of comparable amounts of ATP, we found significant differences in the kinetics of ATP release, which were much faster in response to fluid shear compared to stretch-related stimuli. In addition, we found that VRAC and possibly pannexins were involved in mediating swell- and strain-, but not shear-induced responses. Finally, MSAR from PKD-afflicted renal epithelia was differentially sensitive to FSS and hypotonic swelling. These results strongly suggest that mammalian cells can discriminate between different types of mechanical stimuli. Theoretical models have previously demonstrated that shear stresses induce more cell membrane deformation than stretch-related stimuli (Lynch & Fischbach, 2014; McGarry, Klein-Nulend, Mullender, & Prendergast, 2005). Direct comparison of mechanisms involved in hypotonic pressure- and strain-induced ATP release has demonstrated that these stretch-related stimuli recruit common ATP release pathways (A. Li, Leung, Peterson-Yantorno, Stamer, & Civan, 2011), however no study has directly compared shear- and stretch-related ATP release. Thus, we recommend a direct comparison between shear- and stretch-induced cell deformation, and ATP release to be investigated in future work.

4.4.5 Intervention studies

We quantified the effects of pharmacological and genetic intervention for 681 combinations of cell type, mechanical stimulation and interventions. From the five main routes of ATP release (vesicular (Bodin & Burnstock, 2001; Sathe et al., 2011), pannexin (Locovei et al., 2006), connexin (Graff et al., 2000), VRAC (Pedersen et al., 1999; Qiu et al., 2014; Voss et al., 2014) and MAC (Ravshan Z. Sabirov et al., 2001; Ravshan Z Sabirov et al., 2017)), at least 2, and often 3 were

consistently implicated in the same cell type, with the exception of keratinocytes, in which all 5 pathways were studied, but only MAC was found to mediate ATP release. The involvement of multiple independent release mechanisms may confer a redundancy that ensures cellular ATP release is robust. Alternatively, it is possible that different routes work collaboratively within the same pathway. Of interest, we demonstrated a lack of additivity in the relative contributions of main release routes in certain cell types. We found that different ATP release routes shared common intracellular signaling pathways. In particular, Rho kinases and microtubules always co-occurred with vesicular and pannexin pathways, and $[Ca^{2+}]_i$ co-occurred with all 5 routes of ATP release in 33-100% of cases. Thus, it can be hypothesized that different routes of release are functionally independent but are regulated by common intracellular signaling. At this time, this hypothesis is difficult to test experimentally, partly because pharmacological agents used to study mechanisms of MSAR suffer from extensively overlapping antagonistic profiles (Azorin et al., 2011; A. Li, Leung, Peterson-Yantorno, Mitchell, & Civan, 2010; Liu, Toychiev, Takahashi, Sabirov, & Okada, 2008; Sauer, Hescheler, & Wartenberg, 2000; Wang et al., 2005). Targeted genetic studies (e.g. siRNA, CRISPR, animal models) are needed to further our understanding of MSAR. To date, genetic interventions have been used to study the involvement of vesicle-related VNUT (SLC17A9) (Sathe et al., 2011; Sawada et al., 2008), pannexin 1 (Panx1) (Bao, Locovei, & Dahl, 2004; Beckel et al., 2014; Kanjanamekanant et al., 2014; Lu, Soleymani, Madakshire, & Insel, 2012; Seminario-Vidal et al., 2011; Woehrle et al., 2010), pannexin 2 (Panx2) (Oishi et al., 2012), connexin 40 (Cx40) (Toma et al., 2008), connexin 43 (Cx43) (Chi, Gao, Zhang, Takeda, & Yao, 2014; Genetos, Kephart, Zhang, Yellowley, & Donahue, 2007; Lu et al., 2012; Luckprom et al., 2011) and connexin 45 (Cx45)(Lu et al., 2012). Recently, SWELL1 (LRRC8A) was identified as a the pore component of the VRAC complex (Qiu et al., 2014; Syeda et al.; Voss et al., 2014), and the prostaglandin transporter PGT (encoded by SLCO2A1) was recognized as the MAC (Ravshan Z Sabirov et al., 2017). Of interest, Sana-Ur-Rehman et al (Sana-Ur-Rehman et al., 2017) and Workman et al (Workman et al., 2017) have recently reported the calcium homoeostatic modulator 1 (CALHM1) as a novel mediator of MSAR in nasal epithelia and the urothelium, however, it remains unclear whether CALHM1 is a direct or indirect conduit of ATP release and its investigation is complicated by its sensitivity to non-specific inhibitors ruthenium red and gadolinium (Taruno, 2018). A comprehensive review of recent evidence supporting the role of CALHM1 in ATP release can be found elsewhere (Taruno, 2018). Nonetheless, now that the

molecular identity of each main route of ATP release has been identified, genetic studies to resolve ATP release mechanisms are feasible. Thus, systematic analysis of prior data allowed us to pinpoint specific mechanistic features that warrant further experimental investigation, such as differential involvement of VRAC in FSS- and osmotic pressure-induced ATP release, and to suggest that certain ATP release mechanisms are cell type- and stimulation type-dependent.

4.4.6 Therapeutic potential

Our systematic assessment of MSAR involvement in different pathologies included data from 10 cell types/tissues from 11 pathological conditions. We have found that inflammation and injury coincided with higher ATP release from epithelial cells, which may contribute to pain commonly present in these conditions (Butrick, Howard, & Sand, 2010; Docherty, Jones, & Wallace, 2011; Taweel & Seyam, 2015; Weinreb, Aung, & Medeiros, 2014). In contrast, in hereditary and metabolic conditions, lower ATP release from RBCs was consistently reported. Thus, both MSAR inhibitory and stimulatory interventions can be of therapeutic interest. The downstream actions of MSAR are mediated by 15 members of the purinergic (P2) receptor family (Burnstock, 2014), which have been identified as valuable therapeutic targets for treatment of pain, inflammation, SCI and bladder dysfunction (North & Jarvis, 2013). There are several advantages of targeting MSAR over the P2 receptor network. First, the impact of disproportionally targeting single P2 receptors has poorly understood implications for signaling by the entire P2 receptor network. Instead, manipulating MSAR allows proportional reduction or increase in the stimulation of all P2 receptors. Second, many of the drugs used to inhibit MSAR, including mefloquine (Lee, ter Kuile, Price, Luxemburger, & Nosten, 2017), carbenoxolone (Doll, Hill, & Hutton, 1965), probenecid (S. Li et al., 2016), flufenamic acid (Flemming & Jones, 2015), glybenclamide (Sola et al., 2015), and clodronate (Ghinoi & Brandi, 2002) (recently demonstrated to potently inhibit VNUT (Kato et al., 2017)) are already used in clinic. Although these drugs are relatively non-specific, strategies to therapeutically repurpose them for diseases with aberrant MSAR may be considered. As for any potential therapy, unintended drug effects need to be taken into account. In this regard, our systematic approach allowed to identify cell- and stimulus-specific effects of various pathologies. Thus, comprehensive assessment of cell type-specific mechanisms of ATP release, considered together with known pathophysiological changes can be used to map site-specific effects of therapeutic MSAR interventions, and predict any unintended (patho)physiological consequences.

4.5 Methods

4.5.1 Software

Reference manager: Endnote X7 (Thomson Reuters). *Data extraction and analysis*: MetaLab meta-analysis toolbox in MATLAB (MathWorks) (Mikolajewicz & Komarova, 2018). *Data storage*: Excel 2016 (Microsoft). *Figure preparation*: CorelDRAW X8 (Corel).

4.5.2 Search strategy and inclusion criteria

A medical librarian (MM) prepared the systematic search strategy. The search strategy was constructed around key terms "ATP" and "mechanical stimulation". Search terms were validated by ensuring the search retrieved a selection of articles, representative of relevant works. Medline, Embase, Biosis and SCOPUS databases were searched on January 12th, 2017 using search terms listed in **Table 4-S8** and articles were exported to Endnote. Reviews, books, letters, editorials and conference proceedings were excluded, language was restricted to English and there was no restriction on date of publication. Studies in which mammalian cells were mechanically stimulated and ATP release was assayed were included. No restrictions were imposed on experimental setup. Abstracts were screened independently by two reviewers (NM and AM). Full-text screens were conducted to confirm eligibility. Differences between two reviewers were resolved through discussion and consensus. The complete list of systematically identified studies is in **Table 4-S9**.

4.5.3 Data extraction

Study characteristics and data were extracted by a single non-blinded reviewer (NM) and independently verified by another reviewer (AM) to minimize user-related error. For all studies, study design and biological characteristics were recorded (**Table 4-S10**). For experiments using a perfusion-based sampling method, perfusion intervals and volumes were extracted to estimate cumulative ATP release. For experiments reporting outcomes in units other than moles ATP per cell, relevant conversion parameters were extracted. For intervention/pathology studies, we collected information on pharmacological agents, genetic targets or pathological states. MetaLab data extraction module was used facilitate graphical data extraction (Mikolajewicz & Komarova, 2018). For each data set, we extracted baseline ATP levels and mechanically-stimulated ATP along with measures of variance. In some studies, multiple datasets were extracted if reported. For

temporal recordings of ATP release, entire time-series were extracted and used to estimate the time to half-max ATP release for analysis of ATP release kinetics. From these times series, the maximal amount of ATP release was also used for analysis of amount of ATP released. For intervention or pathology studies, basal ATP and amount of ATP released in the absence and presence of the intervention/pathology was extracted for subsequent calculation of the intervention inhibitory effect (%)or relative effect (%) of pathology. Sample sizes and type of variance measures (standard error, standard deviation) used were recorded. When variance measure was unclear, error was extracted as standard error, lending to more conservative estimates. When sample size was unclear but there was indication of multiple trials, we set the sample size to three. When a range of sample sizes was reported, the smallest value was extracted.

4.5.4 Standardization of measures

ATP was commonly reported as an amount or concentration of ATP released per cell(s). Accordingly, conversion factors were estimated for each study to express ATP amount in terms of moles per cell. In cases where certain conversion parameters were not reported, assumptions were made according to the table reported in **Table 4-S11**. Cell-related parameters were estimated using the BioNumbers database (Milo, Jorgensen, Moran, Weber, & Springer, 2010) which were compared to our in-lab experience and deemed appropriate. Volume assumptions for culture dishes were made per manufacturer recommended volumes. For each type of mechanical stimulation, if enough information was provided, magnitude of stimulus was converted to a common unit. Experiments that applied osmotic pressure commonly reported changes in osmolarity as a percentage of basal osmolarity (isotonic). Since basal osmolarity varied across studies, we expressed the magnitude of osmotic stress in terms of change in mOsm/KgH_2O (δ mOsm/L).

4.5.5 Quality assessment

Quality of studies was assessed according to an 8-item quality check-list: Publication in peer reviewed journal, control of temperature, control of sample degradation, cell viability checked, mechanical stimulus regime reported, ATP calibration, negative control and statement of potential conflicts of interest reported. Outcomes were stratified by aggregate quality score to determine influence of study quality on reported results.

4.5.6 Study-level outcomes

In this section we provide general outcome calculations; a detailed statistical methodology (including variance estimation, heterogeneity analysis) is described in our previous work (Mikolajewicz & Komarova, 2018). Five outcomes were synthesized in this study: **(i)** absolute ATP released (A_{mech}), **(ii)** relative ATP released above baseline (R_{mech}), **(iii)** time to half max ATP releasea (t_{half}), **(iv)** Effect of pharmacological/genetic intervention on ATP release *(% inhibition*), and **(v)** Effect of pathology on ATP release (*relative effect, %*).

Study-level absolute ATP release. The amount of ATP released was calculated as the difference in extracellular ATP before and after mechanical stimulation:

$$A_{mech} = A_{EC} - A_{base} \tag{1}$$

Where A_{mech} was mechanically-induced ATP release, A_{EC} was total extracellular ATP following mechanically-stimulation and A_{base} was basal extracellular ATP.

Study-level relative ATP release. The relative amount of ATP released above baseline R_{mech} was computed as:

$$R_{mech} = \frac{A_{mech} + A_{base}}{A_{base}} \cdot 100\% \tag{2}$$

Estimation of cumulative ATP release. Extracted ATP release time series were reported as cumulative ATP release or rates of ATP release. Release rates data were converted to cumulative ATP release over the reported period following mechanical stimulation:

$$A(t) = \int_0^b a(t)\, dt \approx \sum_1^b (a(t)) \tag{3}$$

where a was the cellular release rate (units ATP per unit time per cell), $A(t)$ was the cumulative extracellular ATP, b was the reported time period and t was time.

Study-level ATP release kinetics. Study-level ATP release time series recordings with at least 4-time points were fit to a sigmoidal function (Eqn. 4) using a Monte-Carlo error propagation method and the characteristic time to half-max release t_{half} with standard error was estimated. Recordings

that extended beyond the time of maximal ATP release were truncated to restrict the fitting of the sigmoid curve to the relevant period over which ATP is being released.

$$A(t) = \frac{A_{max} \cdot t^n}{t_{half}^n + t^n} \tag{4}$$

where A_{max} was maximal ATP release, $A(t)$ was cumulative ATP release with respect to time, n was coefficient related to the slope of activation, t was time and $\boldsymbol{t_{half}}$ was time to half-max release. The Monte Carlo fitting method allowed us to propagate study-level variances (uncertainty in the model inputs) to the uncertainty in the model parameter estimates (Cox, Harris, & Siebert, 2003). This approach assumes that study-level estimates are normally distributed, enabling pseudo random observations to be sampled from a distribution defined by the study-level means and standard deviations. The pseudo random observations were then averaged to obtain a Monte-Carlo estimate for each time point and the sigmoidal model was fit to the Monte Carlo estimates using the least-squared method. This procedure of pseudo-random sampling and model fitting was iterated 1000 times, and the distribution of 1000 t_{half} estimates was used to compute a mean and variance that was then used as the study-level estimate of t_{half}. Model goodness of fit was assessed quantitatively by R^2 and visually verified.

Study-level percent inhibition. For intervention studies, the effect of genetic and pharmacological interventions was computed as percent inhibition, compared to unaffected control ATP release:

$$inhibition\ (\%) = \frac{A_{mech}^{control} - A_{mech}^{treated}}{A_{mech}^{control}} \cdot 100\% \tag{5}$$

$A_{mech}^{control}$ and $A_{mech}^{treated}$ were computed same as A_{mech} (i.e., basal ATP release is accounted for). Negative values of percent inhibition outcomes indicate increased ATP release, and positive values indicate decreased ATP release.

Study-level relative effects. For pathophysiological conditions, the relative effect size was calculated as follows:

$$effect\ (\%) = \frac{A_{mech}^{affected} - A_{mech}^{control}}{A_{mech}^{control}} \cdot 100\% \tag{6}$$

Where $A_{mech}^{affected}$ was ATP released from the pathologically affected cell/tissue type and $A_{mech}^{control}$ was ATP released from healthy control samples.

4.5.7 Quantitative synthesis

For each study i, study-level outcomes θ_i and standard errors $se(\theta_i)$ were estimated and synthesized as described in our previous work (Mikolajewicz & Komarova, 2018). θ_i is a general study-level outcome used to represent A_{mech}, R_{mech}, t_{half}, inhibition (%) or effect (%).

Data transformation and normalization. Prior to synthesis, skewed distributions of study-level outcomes θ_i were identified by histograms and were normalized by transformation to the logarithmic scale:

$$\Theta_i = log_{10}(\theta_i) - \left(\frac{se(\Theta_i)^2}{2}\right) \tag{7}$$

Where Θ_i is a log-transformed study-level outcome which we reported in the study as either A_{mech}^{log}, R_{mech}^{log}or t_{half}^{log}. The corresponding standard error $se(\Theta_i)$ was approximated as:

$$se(\Theta_i) = \sqrt{log_{10}\left(\frac{se(\theta_i)^2}{{\theta_i}^2} + 1\right)} \tag{8}$$

Log transformation was applied as shown to A_{mech}, R_{mech} and t_{half} datasets. Outcomes were synthesized on the logarithmic scale, transformed back to the original raw scale and reported.

Analysis of heterogeneity. To quantify the extent of inconsistency, or heterogeneity, present between datasets, we calculated Q, I^2 and H^2 heterogeneity statistics. Q is a measure of total variation and was calculated as the sum of the weighted squared differences between the study-level means θ_i and the fixed effect estimate $\hat{\theta}_{FE}$:

$$Q = \sum_{i=1}^{N} \left(se(\theta_i)^{-2} \cdot \left(\theta_i - \hat{\theta}_{FE}\right)^2\right) \tag{9}$$

$$\text{where } \hat{\theta}_{FE} = \frac{\sum_i se(\theta_i)^{-2}\theta_i}{\sum_i se(\theta_i)^{-2}},$$

Q is a χ^2 distributed statistic with N-1 degrees of freedom and the corresponding p-value P_Q was used to evaluate the null hypothesis that all datasets reported the same effect. For example, $P_Q>0.05$ indicates that outcomes are consistent and describe the same effect, while $P_Q<0.05$ indicates that outcomes are inconsistent or heterogeneous. H^2 is another heterogeneity metric that is independent of the number of datasets available, and describes the relative excess of Q over the degrees of freedom df:

$$H^2 = \frac{Q}{df} \tag{10}$$

I^2 is a transformation of H^2 that describes the percentage of variance that is due to heterogeneity:

$$I^2 = \frac{H^2 - 1}{H^2} \cdot 100\% \tag{11}$$

H^2 is preferred over I^2 for highly heterogenous data because it has an unbound upper limit, however I^2 is more easily interpretable. Values of $Q = 0$, $I^2 = 0$ or $H^2 = 1$ indicate that data are homogenous.

Heterogeneity and publication bias were assessed using funnel plots and cumulative-study exclusion plots (Mikolajewicz & Komarova, 2018). The homogeneity threshold T_H was calculated from cumulative exclusion analysis and specifies the percentage of studies that need to be removed (according to maximal Q-reduction criteria) before a homogenous set of studies is attained, as determined by the p-value P_Q corresponding to the Q heterogeneity statistic (Mikolajewicz & Komarova, 2018).

Meta-analysis. Study-level outcomes were synthesized under the assumptions of a random effects model to obtain an overall outcome $\hat{\theta}$:

$$\hat{\theta} = \frac{\sum_i(\theta_i \cdot w_i)}{\sum_i(w_i)} \tag{12}$$

Where the random effects study-level weights w_i were estimated as

$$w_i = \frac{1}{se(\theta_i)^2 + \tau^2} \tag{13}$$

And the interstudy variance was approximated using the DerSimonian-Laird estimator:

$$\tau^2 = \frac{Q - (N-1)}{c}$$
$$\text{Where } c = \sum_i se(\theta_i)^{-2} - \frac{\sum_i \left(se(\theta_i)^{-2}\right)^2}{\sum_i se(\theta_i)^{-2}} \tag{14}$$

Q is the heterogeneity statistic (introduced above), c is a scaling factor and N is the number of datasets being synthesized. The standard error corresponding to the overall outcome was estimated as:

$$se(\hat{\theta}) = \frac{1}{\sqrt{\sum_i w_i}} \tag{15}$$

And the corresponding confidence intervals were constructed using critical values $z_{1-\alpha/2}$ obtained from a z-distribution:

$$\pm CI = \pm z_{1-\alpha/2} \cdot se(\hat{\theta}) \tag{16}$$

Where $\alpha = 0.05$ corresponds to a 95% significance level.

Subgroup analyses were conducted to identify sources of heterogeneity and explore the influence of different experimental and biological factors on the outcome of interest. Study-level data were stratified into characteristic groups defined by study-level covariates and study-level outcomes within each subgroup were synthesized as above. When multiple subgroups comparisons were made, the Bonferroni correction was used to adjust the significance threshold to control for false positive findings:

$$\alpha^* = \frac{\alpha}{m} \tag{17}$$

Where α^* is the adjusted significance threshold to attain intended error rates α for m subgroup comparisons.

Meta-Regression. To assess the bivariate relationship between study-level predictors and outcomes, a random-effects meta-regression model was constructed in the following form:

$$\theta_i = \beta_0 + \beta_{inter} x_i + \eta_i + \varepsilon_i \tag{18}$$

Where β_0 is the intercept, β_{inter} is the slope coefficient describing the relationship between predictor x_i and outcome θ_i, ε_i is the intrastudy variability approximated by $\mathcal{N}(0, se(\theta_i)^2)$, and η_i is the interstudy variability approximated by $\mathcal{N}(0, \tau^2)$. In addition to the meta-regression analysis conducted to assess the *between-study* relationship of study-level predictors and outcomes, we also conducted a intrastudy regression analysis to assess the *within study* relationship between study-level predictors and outcomes (Mikolajewicz & Komarova, 2018). Within-study regression coefficients were computed and pooled using the meta-analytic methods described above to estimate an overall effect β_{intra}. The magnitude and sign of β_{inter} and β_{intra} were then compared to evaluated whether the observed relationships between- and within- studies were in agreement. For additional details, refer to our previous work (Mikolajewicz & Komarova, 2018).

Analysis of ATP release mechanisms. To evaluate the cell-type specific mechanisms of ATP release, pharmacological and genetic intervention outcomes were grouped by common molecular targets and their inhibitory effects were estimated and synthesized as above. Due to the non-specific effects of certain inhibitors, differential pharmacological effects were considered to differentiate between ATP release pathways that shared common pharmacological profiles. Depending on the panel of available inhibitor data for each cell type, more targeted interventions allowed us to narrow down the pathways affected by nonspecific inhibitors. For example, carbenoxolone inhibits connexin and pannexin activity, while flufenamic acid is a more targeted connexin inhibitor. For cells in which carbenoxolone inhibited ATP release, but flufenamic acid did not, we inferred the involvement of pannexins. In some cases, nonspecific interventions were used to support or dismiss the involvement of several pathways at a time. For instance, cells in which Gd^{3+} had no effect on ATP release allowed us to putatively dismiss ATP release pathways related to maxi anion channels, P2X7, Piezo1 and TRP channels. To reflect the varying degrees of evidence (i.e., availability of data, specificity of interventions, separate replication of findings), we distinguished between cell-type specific mechanisms that were reported once, those that were verified by different methods/groups, and those for which data was available but inconclusive (often due to nonspecific nature of interventions). These outcomes were summarized in a cell-by-mechanism involvement matrix indicating whether the pathway was involved in ATP release and the degree of evidence supporting the conclusion. Based on the mechanisms summarized in the involvement matrix, a co-occurrence analysis was then conducted to screen for possibly codependent pathways of ATP release. Results were summarized in a co-occurrence matrix for

cases in which at least three cell-types could be evaluated and were expressed as the percentage of cell types in which the pairs of mechanisms were co-occurrent.

To determine whether the separate routes of ATP release were additive, the effects of ATP release inhibitors were used to approximate of relative contribution *RC* of that pathway to ATP release:

$$RC \sim inhibitory\ effect\ (\%) \tag{19}$$

The joint contribution *JC* was then computed as:

$$JC = RC_{vesicles} + RC_{px} + RC_{cx} + RC_{VRAC} + RC_{MAC} \tag{20}$$

And the standard error was

$$se(JC) = \sqrt{se(RC_{vesicles})^2 + se\left(RC_{px}\right)^2 + se(RC_{cx})^2 + se(RC_{VRAC})^2 + se(RC_{MAC})^2} \tag{21}$$

95% CI for joint contributions were constructed using Eqn. 16. Joint contributions that were insignificantly different from 100% (contained by 95% CI) were interpreted as additive, and those exceeding 100% were interpreted as synergistic. Cell types in which at least 4 of the 5 main routes of ATP release were studied were included in this analysis, except for cell types that exhibited synergy-like interactions, in which case not restriction was placed on minimum number of routes studied since including the relative contributions of additional release routes would have only added to the joint contribution.

4.6 References

Azorin, N., Raoux, M., Rodat-Despoix, L., Merrot, T., Delmas, P., & Crest, M. (2011). ATP signalling is crucial for the response of human keratinocytes to mechanical stimulation by hypo-osmotic shock. *Experimental Dermatology, 20*(5), 401-407. doi:http://dx.doi.org/10.1111/j.1600-0625.2010.01219.x

Bao, L., Locovei, S., & Dahl, G. (2004). Pannexin membrane channels are mechanosensitive conduits for ATP. *FEBS Lett, 572*(1-3), 65-68. doi:10.1016/j.febslet.2004.07.009

Beckel, J. M., Argall, A. J., Lim, J. C., Xia, J., Lu, W., Coffey, E. E., . . . Mitchell, C. H. (2014). Mechanosensitive release of adenosine 5'-triphosphate through pannexin channels and mechanosensitive upregulation of pannexin channels in optic nerve head astrocytes: a mechanism for purinergic involvement in chronic strain. *GLIA, 62*(9), 1486-1501. doi:http://dx.doi.org/10.1002/glia.22695

Bergman, J. (1999). ATP: the perfect energy currency for the cell. *Creation Research Society Quarterly, 36*(1), 2-9.

Bodin, P., & Burnstock, G. (1996). ATP-stimulated release of ATP by human endothelial cells. *J Cardiovasc Pharmacol, 27*(6), 872-875.

Bodin, P., & Burnstock, G. (2001). Evidence that release of adenosine triphosphate from endothelial cells during increased shear stress is vesicular. *Journal of Cardiovascular Pharmacology, 38*(6), 900-908.

Bradbury, A., & Pluckthun, A. (2015). Standardize antibodies used in research: to save millions of dollars and dramatically improve reproducibility, protein-binding reagents must be defined by their sequences and

produced as recombinant proteins, say Andrew Bradbury, Andreas Pluckthun and 110 co-signatories. *Nature, 518*(7537), 27-30.

Burnstock, G. (2014). Purinergic signalling: from discovery to current developments. *Experimental Physiology, 99*(1), 16-34. doi:10.1113/expphysiol.2013.071951

Burr, D. B., Milgrom, C., Fyhrie, D., Forwood, M., Nyska, M., Finestone, A., . . . Simkin, A. (1996). In vivo measurement of human tibial strains during vigorous activity. *Bone, 18*(5), 405-410.

Butrick, C. W., Howard, F. M., & Sand, P. K. (2010). Diagnosis and treatment of interstitial cystitis/painful bladder syndrome: a review. *J Womens Health (Larchmt), 19*(6), 1185-1193. doi:10.1089/jwh.2009.1702

Chi, Y., Gao, K., Zhang, H., Takeda, M., & Yao, J. (2014). Suppression of cell membrane permeability by suramin: involvement of its inhibitory actions on connexin 43 hemichannels. *Br J Pharmacol, 171*(14), 3448-3462. doi:http://dx.doi.org/10.1111/bph.12693

Cox, M., Harris, P., & Siebert, B. R.-L. (2003). Evaluation of Measurement Uncertainty Based on the Propagation of Distributions Using Monte Carlo Simulation. *Measurement Techniques, 46*(9), 824-833. doi:10.1023/B:METE.0000008439.82231.ad

Dillon, J. P., Vindigni, G., Collins, J., Wilson, P. J., Ranganath, L. R., Milner, P. I., & Gallagher, J. A. (2013). ATP-Stimulated ATP release and metabolic acid production:-regulating life and death decisions in articular chondrocytes. *Osteoarthritis and Cartilage, 21*, S111. doi:10.1016/j.joca.2013.02.233

Docherty, M. J., Jones, R. C. W., & Wallace, M. S. (2011). Managing Pain in Inflammatory Bowel Disease. *Gastroenterology & Hepatology, 7*(9), 592-601.

Doll, R., Hill, I., & Hutton, C. (1965). Treatment of gastric ulcer with carbenoxolone sodium and oestrogens. *Gut, 6*(1), 19.

Eyckmans, J., Boudou, T., Yu, X., & Chen, C. S. (2011). A hitchhiker's guide to mechanobiology. *Dev Cell, 21*(1), 35-47. doi:10.1016/j.devcel.2011.06.015

Flemming, K. D., & Jones, L. K. (2015). *Mayo Clinic Neurology Board Review: Clinical Neurology for Initial Certification and MOC*: Oxford University Press.

Fontoura-Andrade, J. L., Amorim, R. F. B. d., & Sousa, J. B. d. (2017). Improving reproducibility and external validity. The role of standardization and data reporting of laboratory rat husbandry and housing. *Acta cirurgica brasileira, 32*(3), 251-262.

Fritton, S. P., McLeod, K. J., & Rubin, C. T. (2000). Quantifying the strain history of bone: spatial uniformity and self-similarity of low-magnitude strains. *J Biomech, 33*(3), 317-325.

Genetos, D. C., Kephart, C. J., Zhang, Y., Yellowley, C. E., & Donahue, H. J. (2007). Oscillating fluid flow activation of gap junction hemichannels induces ATP release from MLO-Y4 osteocytes. *Journal of Cellular Physiology, 212*(1), 207-214.

Ghinoi, V., & Brandi, M. L. (2002). Clodronate: mechanisms of action on bone remodelling and clinical use in osteometabolic disorders. *Expert Opin Pharmacother, 3*(11), 1643-1656. doi:10.1517/14656566.3.11.1643

Glass, G. V. (1986). Statistical Methods for Meta-Analysis. Larry V. Hedges , Ingram Olkin. *American Journal of Sociology, 92*(1), 255-256. doi:10.1086/228501

Graff, R. D., Lazarowski, E. R., Banes, A. J., & Lee, G. M. (2000). ATP release by mechanically loaded porcine chondrons in pellet culture. *Arthritis & Rheumatism, 43*(7), 1571-1579.

Higgins, J. P., & Thompson, S. G. (2002). Quantifying heterogeneity in a meta-analysis. *Stat Med, 21*(11), 1539-1558. doi:10.1002/sim.1186

Jackson, D., & Turner, R. (2017). Power analysis for random-effects meta-analysis. *Res Synth Methods, 8*(3), 290-302. doi:10.1002/jrsm.1240

Kanjanamekanant, K., Luckprom, P., & Pavasant, P. (2014). P2X7 receptor-Pannexin1 interaction mediates stress-induced interleukin-1 beta expression in human periodontal ligament cells. *Journal of Periodontal Research, 49*(5), 595-602. doi:http://dx.doi.org/10.1111/jre.12139

Kato, Y., Hiasa, M., Ichikawa, R., Hasuzawa, N., Kadowaki, A., Iwatsuki, K., . . . Miyaji, T. (2017). Identification of a vesicular ATP release inhibitor for the treatment of neuropathic and inflammatory pain. *Proceedings of the National Academy of Sciences, 114*(31), E6297-E6305. doi:10.1073/pnas.1704847114

Lee, S. J., ter Kuile, F. O., Price, R. N., Luxemburger, C., & Nosten, F. (2017). Adverse effects of mefloquine for the treatment of uncomplicated malaria in Thailand: A pooled analysis of 19, 850 individual patients. *PLoS ONE [Electronic Resource], 12*(2), e0168780. doi:10.1371/journal.pone.0168780

Li, A., Leung, C. T., Peterson-Yantorno, K., Mitchell, C. H., & Civan, M. M. (2010). Pathways for ATP release by bovine ciliary epithelial cells, the initial step in purinergic regulation of aqueous humor inflow. *American Journal of Physiology - Cell Physiology, 299*(6), C1308-1317. doi:http://dx.doi.org/10.1152/ajpcell.00333.2010

Li, A., Leung, C. T., Peterson-Yantorno, K., Stamer, W. D., & Civan, M. M. (2011). Cytoskeletal dependence of adenosine triphosphate release by human trabecular meshwork cells. *Investigative Ophthalmology & Visual Science, 52*(11), 7996-8005. doi:http://dx.doi.org/10.1167/iovs.11-8170

Li, S., Yang, H., Guo, Y., Wei, F., Yang, X., Li, D., . . . Wang, Y. (2016). Comparative efficacy and safety of urate-lowering therapy for the treatment of hyperuricemia: a systematic review and network meta-analysis. *Scientific Reports, 6*, 33082. doi:10.1038/srep33082

https://www.nature.com/articles/srep33082#supplementary-information

Liu, H. T., Toychiev, A. H., Takahashi, N., Sabirov, R. Z., & Okada, Y. (2008). Maxi-anion channel as a candidate pathway for osmosensitive ATP release from mouse astrocytes in primary culture. *Cell Research, 18*(5), 558-565. doi:http://dx.doi.org/10.1038/cr.2008.49

Locovei, S., Bao, L., & Dahl, G. (2006). Pannexin 1 in erythrocytes: function without a gap. *Proceedings of the National Academy of Sciences of the United States of America, 103*(20), 7655-7659.

Lu, D., Soleymani, S., Madakshire, R., & Insel, P. A. (2012). ATP released from cardiac fibroblasts via connexin hemichannels activates profibrotic P2Y2 receptors. *FASEB Journal, 26*(6), 2580-2591. doi:http://dx.doi.org/10.1096/fj.12-204677

Luckprom, P., Kanjanamekanant, K., & Pavasant, P. (2011). Role of connexin43 hemichannels in mechanical stress-induced ATP release in human periodontal ligament cells. *Journal of Periodontal Research, 46*(5), 607-615. doi:http://dx.doi.org/10.1111/j.1600-0765.2011.01379.x

Lynch, M., & Fischbach, C. (2014). Biomechanical forces in the skeleton and their relevance to bone metastasis: biology and engineering considerations. *Advanced drug delivery reviews, 0*, 119-134. doi:10.1016/j.addr.2014.08.009

McGarry, J. G., Klein-Nulend, J., Mullender, M. G., & Prendergast, P. J. (2005). A comparison of strain and fluid shear stress in stimulating bone cell responses--a computational and experimental study. *FASEB Journal, 19*(3), 482-484. doi:10.1096/fj.04-2210fje

Mikolajewicz, N., & Komarova, S. (2018). Meta-analytic methodology for basic research. *Submitted*.

Milner, P., Kirkpatrick, K. A., Ralevic, V., Toothill, V., Pearson, J., & Burnstock, G. (1990). Endothelial cells cultured from human umbilical vein release ATP, substance P and acetylcholine in response to increased flow. *Proceedings of the Royal Society of London - Series B: Biological Sciences, 241*(1302), 245-248.

Milo, R., Jorgensen, P., Moran, U., Weber, G., & Springer, M. (2010). BioNumbers—the database of key numbers in molecular and cell biology. *Nucleic Acids Research, 38*(Database issue), D750-D753. doi:10.1093/nar/gkp889

North, R. A., & Jarvis, M. F. (2013). P2X Receptors as Drug Targets. *Mol Pharmacol, 83*(4), 759-769. doi:10.1124/mol.112.083758

Oishi, S., Sasano, T., Tateishi, Y., Tamura, N., Isobe, M., & Furukawa, T. (2012). Stretch of atrial myocytes stimulates recruitment of macrophages via ATP released through gap-junction channels. *Journal of Pharmacological Sciences, 120*(4), 296-304.

Pedersen, S., Pedersen, S. F., Nilius, B., Lambert, I. H., & Hoffmann, E. K. (1999). Mechanical stress induces release of ATP from Ehrlich ascites tumor cells. *Biochimica et Biophysica Acta, 1416*(1-2), 271-284.

Qiu, Z., Dubin, A. E., Mathur, J., Tu, B., Reddy, K., Miraglia, L. J., . . . Patapoutian, A. (2014). SWELL1, a plasma membrane protein, is an essential component of volume-regulated anion channel. *Cell, 157*(2), 447-458. doi:10.1016/j.cell.2014.03.024

Sabirov, R. Z., Dutta, A. K., & Okada, Y. (2001). Volume-Dependent Atp-Conductive Large-Conductance Anion Channel as a Pathway for Swelling-Induced Atp Release. *The Journal of General Physiology, 118*(3), 251-266.

Sabirov, R. Z., Merzlyak, P. G., Okada, T., Islam, M. R., Uramoto, H., Mori, T., . . . Okada, Y. (2017). The organic anion transporter SLCO2A1 constitutes the core component of the Maxi-Cl channel. *The EMBO Journal, 36*(22), 3309-3324. doi:10.15252/embj.201796685

Sana-Ur-Rehman, H., Markus, I., Moore, K. H., Mansfield, K. J., & Liu, L. (2017). Expression and localization of pannexin-1 and CALHM1 in porcine bladder and their involvement in modulating ATP release. *Am J Physiol Regul Integr Comp Physiol, 312*(5), R763-r772. doi:10.1152/ajpregu.00039.2016

Sathe, M. N., Woo, K., Kresge, C., Bugde, A., Luby-Phelps, K., Lewis, M. A., & Feranchak, A. P. (2011). Regulation of purinergic signaling in biliary epithelial cells by exocytosis of SLC17A9-dependent ATP-enriched vesicles. *Journal of Biological Chemistry, 286*(28), 25363-25376. doi:http://dx.doi.org/10.1074/jbc.M111.232868

Sauer, H., Hescheler, J., & Wartenberg, M. (2000). Mechanical strain-induced Ca(2+) waves are propagated via ATP release and purinergic receptor activation. *American Journal of Physiology - Cell Physiology, 279*(2), C295-307.

Sawada, K., Echigo, N., Juge, N., Miyaji, T., Otsuka, M., Omote, H., . . . Moriyama, Y. (2008). Identification of a vesicular nucleotide transporter. *Proceedings of the National Academy of Sciences of the United States of America, 105*(15), 5683-5686. doi:10.1073/pnas.0800141105

Seminario-Vidal, L., Okada, S. F., Sesma, J. I., Kreda, S. M., van Heusden, C. A., Zhu, Y., . . . Lazarowski, E. R. (2011). Rho signaling regulates pannexin 1-mediated ATP release from airway epithelia. *Journal of Biological Chemistry, 286*(30), 26277-26286. doi:http://dx.doi.org/10.1074/jbc.M111.260562

Soehnlein, O., & Silvestre-Roig, C. (2017). Basic research: Standardizing animal atherosclerosis studies to improve reproducibility. *Nature Reviews Cardiology, 14*(10), 574.

Sola, D., Rossi, L., Schianca, G. P. C., Maffioli, P., Bigliocca, M., Mella, R., . . . Derosa, G. (2015). Sulfonylureas and their use in clinical practice. *Archives of Medical Science : AMS, 11*(4), 840-848. doi:10.5114/aoms.2015.53304

Syeda, R., Qiu, Z., Dubin, Adrienne E., Murthy, Swetha E., Florendo, Maria N., Mason, Daniel E., . . . Patapoutian, A. LRRC8 Proteins Form Volume-Regulated Anion Channels that Sense Ionic Strength. *Cell, 164*(3), 499-511. doi:10.1016/j.cell.2015.12.031

Taruno, A. (2018). ATP Release Channels. *International Journal of Molecular Sciences, 19*(3), 808. doi:10.3390/ijms19030808

Taweel, W. A., & Seyam, R. (2015). Neurogenic bladder in spinal cord injury patients. *Research and Reports in Urology, 7*, 85-99. doi:10.2147/RRU.S29644

Toma, I., Bansal, E., Meer, E. J., Kang, J. J., Vargas, S. L., & Peti-Peterdi, J. (2008). Connexin 40 and ATP-dependent intercellular calcium wave in renal glomerular endothelial cells. *American Journal of Physiology - Regulatory Integrative & Comparative Physiology, 294*(6), R1769-1776. doi:http://dx.doi.org/10.1152/ajpregu.00489.2007

Voss, F. K., Ullrich, F., Munch, J., Lazarow, K., Lutter, D., Mah, N., . . . Jentsch, T. J. (2014). Identification of LRRC8 heteromers as an essential component of the volume-regulated anion channel VRAC. *Science, 344*(6184), 634-638. doi:10.1126/science.1252826

Wang, E. C., Lee, J. M., Ruiz, W. G., Balestreire, E. M., von Bodungen, M., Barrick, S., . . . Apodaca, G. (2005). ATP and purinergic receptor-dependent membrane traffic in bladder umbrella cells. *Journal of Clinical Investigation, 115*(9), 2412-2422.

Weinreb, R. N., Aung, T., & Medeiros, F. A. (2014). The Pathophysiology and Treatment of Glaucoma: A Review. *JAMA, 311*(18), 1901-1911. doi:10.1001/jama.2014.3192

Woehrle, T., Yip, L., Manohar, M., Sumi, Y., Yao, Y., Chen, Y., & Junger, W. G. (2010). Hypertonic stress regulates T cell function via pannexin-1 hemichannels and P2X receptors. *Journal of Leukocyte Biology, 88*(6), 1181-1189. doi:http://dx.doi.org/10.1189/jlb.0410211

Workman, A. D., Carey, R. M., Chen, B., Saunders, C. J., Marambaud, P., Mitchell, C. H., . . . Cohen, N. A. (2017). CALHM1-Mediated ATP Release and Ciliary Beat Frequency Modulation in Nasal Epithelial Cells. *Scientific Reports, 7*(1), 6687. doi:10.1038/s41598-017-07221-9

Chapter Five

Systematic Characterization of Dynamic Parameters of Intracellular Calcium Signals

There is an intimate relationship between purinergic mechanotransduction and intracellular calcium signalling, as seen in mechanically-stimulated ATP release (**Chapter 4**) and purinergic signalling (**Chapter 2**). Consequently, calcium signals obtained from live-cell recordings are often used as a proxy outcome measure to study purinergic mechanotransduction. While these signals are saturated with relevant information, experimental datasets are typically extensive with a high degree of variability, which precludes large-scale comprehensive analysis. In line with ***methodological objective 2***, we developed a computational toolset to standardize and automate parametric characterization of calcium signals and validated the performance of the algorithm using ATP-mediated calcium signals from osteoclast precursor cells. The algorithm developed here was used extensively to analyze calcium recordings in **Chapters 6** and **7,** and can be accessed freely at https://github.com/NMikolajewicz/Calcium-Signal-Analyzer. Supplemental methods and the user-guide referenced in this chapter can be found in **Appendix A3** and **A4**, respectively.

5.1 Abstract

Dynamic processes, such as intracellular calcium signaling, are hallmark of cellular biology. As real-time imaging modalities become widespread, a need for analytical tools to reliably

characterize time-series data without prior knowledge of the nature of the recordings becomes more pressing. The goal of this study is to develop a signal-processing algorithm for MATLAB that autonomously computes the parameters characterizing prominent single transient responses (TR) and/or multi-peaks responses (MPR). The algorithm corrects for signal contamination and decomposes experimental recordings into contributions from drift, TRs and MPRs. It subsequently provides numerical estimates for the following parameters: time of onset after stimulus application, activation time (time for signal to increase from 10% to 90% of peak), and amplitude of response. It also provides characterization of the (i) TRs by quantifying their area under the curve, response duration (time between ½ amplitude on ascent and descent of the transient), and decay constant of the exponential decay region of the deactivation phase of the response, and (ii) MPRs by quantifying the number of peaks, mean peak magnitude, mean periodicity, standard deviation of periodicity, oscillatory persistence (time between first and last discernable peak) and duty cycle (fraction of period during which system is active) for all the peaks in the signal, as well as coherent oscillations (i.e. deterministic spikes). We demonstrate that the signal detection performance of this algorithm is in agreement with user-mediated detection and that parameter estimates obtained manually and algorithmically are correlated. We then apply this algorithm to study how metabolic acidosis affects purinergic (P2) receptor-mediated calcium signalling in osteoclast precursor cells. Our results reveal that acidosis significantly attenuates the amplitude and AUC calcium responses at high ATP concentrations. Collectively, our data validated this algorithm as a general framework for comprehensively analyzing dynamic time-series.

5.2 Introduction

Cellular biology is vastly populated with dynamic processes, which can be altered dramatically or subtly by pathological causes. Calcium signals, characterized by fast and transient increases in cytosolic free calcium concentration ($[Ca^{2+}]_i$), which vary in amplitude and duration and can exhibit oscillatory dynamics with frequency-dependent downstream effects (Clapham, 2007), represent a prominent example of such dynamic processes (**Fig 5-1**). To fully understand the data of such dynamic complexity, a robust methodology to analyse and characterize these responses is necessary. Numerous studies have investigated $[Ca^{2+}]_i$ dynamics, but the analysis have in many cases been limited to qualitative assessments (Cao, Lin, Westphale, Beyer, & Steinberg, 1997; Frame & de Feijter, 1997; Isakson, Evans, & Boitano, 2001; Jorgensen, Geist, Civitelli, &

Steinberg, 1997; Jorgensen et al., 2003; Romanello & D'Andrea, 2001). Studies that have pursued quantitative analysis of calcium time-series reported a number of different, often non-overlapping characteristics of the response (**Table 5-1**). In cases where experiments were conducted on a smaller-scale, manual analysis was achievable. However, to achieve larger-scale analyses for experiments with hundreds of individual recordings, open-source signal-processing algorithms are required and becoming increasingly relied on to overcome these bottlenecks in productivity. None of 11 published algorithms we examined provided a comprehensive analysis of the entire response observed within a recording (**Table 5-2**). As a direct consequence of the lack of a standardized methodology to quantify such data-sets, findings from various studies are challenging to compare, relate and generalize. Hence, the motivation of this study was to achieve faster analysis while standardizing the methodology involved, thereby minimizing user-bias and ensuring consistency in the analysis of complex physiological signals. While such a tool may or may not change the conclusions of individual studies, it would improve comparability between different studies, and potentially enable meta-analysis of different experiments. We have therefore developed an algorithm that addresses these concerns and focused on the dynamic signals generated by purinergic (P2) receptors to demonstrate its utility.

Purinergic receptors that evoke intracellular responses upon extracellular stimulation with nucleotides, such as ATP and ADP, are known to induce complex $[Ca^{2+}]_i$ signals. P2 receptors are subdivided into two families, P2X and P2Y receptors, which are omnipresent in virtually all mammalian tissue (Burnstock & Verkhratsky, 2009). The mammalian P2X receptor family, consisting of seven subtypes ($P2X_{1-7}$), are ionotropic ligand-gated cation channels that can permit the influx of extracellular calcium upon stimulation (Kaczmarek-Hajek, Lorinczi, Hausmann, & Nicke, 2012). The mammalian P2Y receptor family, consisting of eight subtypes ($P2Y_{1-2,4,6,11-14}$), are metabotropic G-protein coupled receptors that can indirectly modulate the release of calcium from intracellular calcium stores through inositol triphosphate (von Kugelgen & Hoffmann, 2016). P2 receptors have been demonstrated to play an important role on bone physiology (Lenertz, Baughman, Waldschmidt, Thaler, & van Wijnen, 2015). Since individual bone cells commonly express multiple active P2 receptors (Gallagher & Buckley, 2002), responses to purinergic stimulation result in complex, concentration-dependent $[Ca^{2+}]_i$ transients (Xing, Grol, Grutter, Dixon, & Komarova, 2016). While it remains difficult to experimentally isolate the contribution of individual receptors, a number of studies have demonstrated that various P2 receptor subtypes

have distinct calcium response kinetics and signatures. For instance, various P2X receptors desensitize at distinct rates under sustained agonist stimulation (Koshimizu, Koshimizu, & Stojilkovic, 1999). $P2X_7$-mediated responses in particular are biphasic (Yan et al., 2010) and characterized by sustained $[Ca^{2+}]_i$ elevation (Nobile, Monaldi, Alloisio, Cugnoli, & Ferroni, 2003). It is becoming increasingly clear, however, that P2 receptors cannot be studied and manipulated as individual components, but rather must be regarded as building blocks of a far more "dynamic architecture" that permits diverse functionality and flexibility (Volonte, Amadio, D'Ambrosi, Colpi, & Burnstock, 2006).

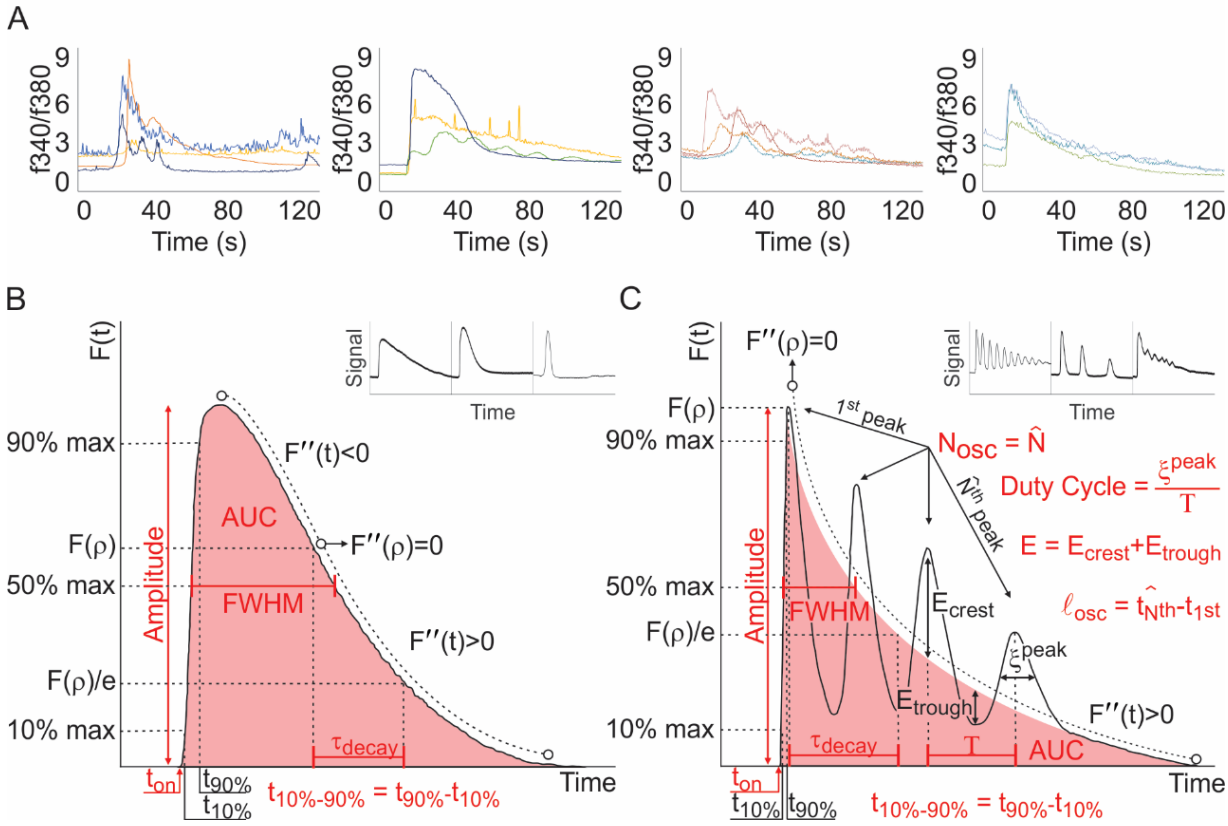

Figure 5-1. Characterization of dynamic calcium signals. **(A)** Examples of heterogeneity of $[Ca^{2+}]_i$ responses observed in various live-cell recordings; note many signature forms that TRs and MPRs can exhibit. **(B)** Analysis of parameters for single-peak TRs. **(C)** Analysis of parameters for MPRs. Time of onset: t_{onset}; area under curve: AUC; full-width half-max: FWHM; activation time: $t_{10\%-90\%}$; decay constant: τ_{decay}; periodicity: T; number of peaks: N_{osc}; oscillatory peak magnitude: E; width of oscillatory peaks: ξ^{peak}; point of inflection in deactivation phase of TR: $F''(\rho)$. Arrows/text in red illustrate how parameters of interest are obtained.

Table 5-1. Commonly reported parameters in studies investigating calcium dynamics

Amplitude	t_{onset}	$t_{10\%-90\%}$	FWHM	FDHM*	AUC	τ_{decay}	Period	Reference
x	x							Abu Khamidakh, Juuti-Uusitalo, Larsson, Skottman, and Hyttinen (2013)
x			x				x	(Appleby, Shabir, Southgate, & Walker, 2015)
x								(Churchill, Atkinson, & Louis, 1996)
x	x			x			x	(Dickinson & Parker, 2013)
x			x					(Francis et al., 2016)
x	x							(Hansen, Boitano, Dirksen, & Sanderson, 1993)
x	x	x			x		x	(James et al., 2011)
x								(Rast et al., 2015)
x								(Shabir & Southgate, 2008)
x		x	x			x		(Smith, Wiltgen, & Parker, 2009)
x			x					(Sun, Berry, Leong, & Veldhuis, 1997)
x								(Zhao, Walczysko, & Zhao, 2008)

*FDHM: Full Duration Half Maximum.

The goal of this study is to develop a universal signal-processing algorithm for MATLAB (MathWorks, Natick, MA) that would facilitate and standardize the parameter characterization of time series calcium imaging recordings containing prominent single transient responses (TR) and/or multi-peaked responses (MPR). All signals, no matter their complexity, can be reduced to a set of defined characteristics that describe the magnitude and kinetics of a given response. Based on our expertise and literature review (**Table 1 & 2**), we have selected the following parameters: time of onset after stimulus application (t_{onset}), activation time (time for signal to increases from 10% to 90% of peak; $t_{10\%-90\%}$), and amplitude of response. Additionally, TRs are specifically described by their area under the curve (AUC), response duration (time between ½ amplitude on ascent and descent of the transient; FWHM), and decay constant of the exponential decay region of the deactivation phase of the response (τ_{decay}, **Fig 5-1B**) while MPRs are described by their

number of peaks (N_{osc}), mean peak magnitude (E), mean periodicity (T), standard deviation of periodicity (σ_T), oscillatory persistence (time between first and last discernable peak; ℓ_{osc}) and duty cycle (fraction of period during which system is active; ξ^{peak}/T, where ξ^{peak} is the width of the oscillatory peaks, **Fig 5-1C**). Since MPRs can be either stochastic or deterministic (Dupont & Combettes, 2009; Dupont, Combettes, Bird, & Putney, 2011; Skupin et al., 2008), the algorithm reports two sets of MPR parameters. The first describes MPR parameters for all the peaks present, while the second set reports the MPR parameters describing the subset of coherent oscillations, to omit the influence of stochastic processes and to focus on the deterministic properties of the signal.

Table 5-2. Published signal-processing algorithms

Amplitude	t_{onset}	$t_{10\%-90\%}$	FWHM	FDHM	AUC	τ_{decay}	$t_{90\%-10\%}$	Period	Classifier*	Reference
x		x	x	x						(Bray, Geisse, & Parker, 2007)
x		x					x			(Ellefsen, Settle, Parker, & Smith, 2014)
	x						x			(Fritzsche et al., 2015)
									x	(Juhola et al., 2015)
x		x	x				x			(Lock, Ellefsen, Settle, Parker, & Smith, 2015)
x		x					x	x		(Patel, Man, Firestein, & Meaney, 2015)
x		x	x	x		x				(Picht, Zima, Blatter, & Bers, 2007)
								x		(Ruffinatti et al., 2011)
x		x					x			(Stoehr et al., 2014)
x			x			x		x		(Steele & Steele, 2014)
x										(Wong, Lu, Tan, & Fivaz, 2010)

*Classifier: grouping of time-series by characteristic signature of response.

Live cell recordings will inevitably contain signal contaminations arising from experimental conditions and instrumentation, including (a) photochemical effects induced by the measurement process and (b) unrelated biological processes. While these imperfections are inherent to the experimental process, dynamic processes of interest can still be extracted from these recordings.

This process in itself can be complicated and highly subjective depending on the extent to which the raw data are corrupted by noise and drift. Therefore, to reliably evaluate the magnitude and kinetics of these signals, we have developed a systematic way of first identifying unwanted signal contaminations, and then removing their effects when determining the parameters of interest. Following algorithm validation, we have also investigated the effect of acidosis on ATP-mediated $[Ca^{2+}]_i$ responses in bone-marrow derived osteoclast precursors to demonstrate the efficacy of this algorithm in characterizing real-time cellular dynamics.

5.3 Results

Although the notation used throughout the text implies that the recorded signals are fluorescence, the methodology remains the same for any other type of signals. For fluorescent recordings, the measured fluorescence F may consist of multiple parts: the drift, TR including the activation and deactivation phases, and the superimposed MPR. It can be expressed as the sum of the actual signal, F_{true}, and the normally distributed noise with a standard deviation σ.

$$F(t) = F_{true}(t) + \mathcal{N}(0, \sigma). \quad (1)$$

To characterize parameters that reliably reflect $F_{true}(t)$, $F(t)$ is first preprocessed to remove the effects of noise and to estimate the contributions of drift to $F_{true}(t)$. Next, the activation phase of TR is fit while simultaneously refining the estimated contribution of the drift. This approach allows us to determine if the recording is consistent with the expected model of a TR superimposed on a drifting baseline (i.e. whether activation phase is followed by a deactivation phase). If a TR is detected, we proceed by fitting the full set of TR model parameters simultaneously with the drift parameters. In the case where there remain multiple significant deviations in the data from the TR model, we investigate and characterize the presence of oscillatory MPRs. The fitting of the TR is refined to remove the effects of the multiple peaks on the initial fit, in order to provide the best estimate of the baseline around which the MPRs oscillate. The deviations resulting from this secondary fitting of the TR are then analyzed to determine those resulting from coherent oscillatory processes. At each step throughout the fitting procedure, an updated estimate of the optimal set of parameters (e.g., the drift parameters) is obtained. These parameters are then used in a feed-forward manner, where the optimal set of parameters of the preceding fit is used as an initial guess for the subsequent step. This ensures that the algorithm produces high-fidelity fittings. Finally, the

algorithm performance and utility is demonstrated with a new data set describing the effect of acidosis on ATP-induced calcium signaling in osteoclast precursors.

5.3.1 Noise characterization

The first step in the processing of data is to evaluate four values that will be used for the remainder of the text: the derivative ($\hat{u}$) of the noisy signal, the standard deviation of noise ($\sigma\_$), indices at which this noise is not prevalent (j), and the noise-to-signal ratio (ϕ). $\hat{u}$ will be used to separate the TR from the underlying drift. Data points excluded by j (i.e. noise) will be omitted. The methodology detailed throughout the following section is an iterative procedure. In the instances where those quantities are used, we are referring to the value determined by the final iteration of the procedure.

5.3.1.1 Euler-Lagrange formalism

The presence of noise in a recording renders naïve methods of derivative estimation inadequate (Chartrand, 2011). This is particularly exacerbated by the intermittent presence of large amplitude noise (spikes) related to the use of high gain settings on instrumentation. To reliably delimit (i.e., define the boundaries of) the drift in a recording of a noisy transient signal, we have adapted the total-variational (TV) technique commonly used to estimate the first derivative of a signal contaminated with various types of noise (Chartrand, 2011; Chartrand & Staneva, 2008; Chartrand & Wohlberg, 2010). This technique performs better than the low-pass filter in distinguishing the drift from the transient response, as it does not indiscriminately remove high frequency components that affect the overall trend of the signal.

Our TV-based methodology seeks a function, $\hat{u}(t)$, which represents the derivative of $F_{true}(t)$, that solves the optimization problem.

$$\min_u \alpha \int_0^L \left|\frac{du}{dx}\right| dx + \frac{1}{2}\int_0^L \left|\left(Au(x) - F(x)\right)\right|^2 dx . \quad (2)$$

The first term in Eq. (2) is a regularization term which penalizes sudden changes in the derivative (to make the fitting smooth), the second term is an L^2 data fidelity term, where A is the anti-differentiation operator ($Au \approx F_{true}$), and α is a parameter dictating the balance between the two

terms. In order to solve this minimization problem, we have to find the stationary solution to the following equation

$$u_t(x) = \alpha \frac{d}{dx} \frac{u'(x)}{|u'(x)|} - A^T\left(Au(x) - F\right) \tag{3}$$

derived from the Euler-Lagrange equation associated with Eq. (2), where $A^T v(x) = \int_x^L v dx$ is the L^2 -adjoint of A. Within the context of ratiometric fluorescent dyes (such as Fura2 AM used for $[Ca^{2+}]_i$ recordings in this study) the recorded signal is the ratio of two Poisson random variables. The variance and the mean of such a signal follow a complex, and seemingly non-linear, function of the photon count rates at each wavelength. Since these rates are assumed to be unknown *a posteriori* in a recording, we cannot accurately determine how the noise is distributed. However, we will assume that instrumentation and experimental settings contribute to a noise distribution that is approximately Gaussian. Moreover, in the specific case of ratiometric dyes, we have found that true noise distribution is a complex function of time, but can be represented reliably using a time-dependent Gaussian noise model. Therefore, to reduce data-fidelity and conversely increase regularity in the regions of highest amplitude noise while accurately reproducing data in regions of lowest noise, we find instead a stationary solution to the following equation

$$u_t(x) = \alpha \frac{d}{dx} \frac{u'(x)}{|u'(x) + \varepsilon|} - \frac{A^T\left(Au(x) - F\right)}{\psi(x,u) + \eta}, \tag{4}$$

where $\psi(\mathrm{x},\mathrm{u})$ is an iteratively determined weighting function (as described below), and ε and η , are parameters introduced to avoid dividing by zero.

At the n^{th} iteration of the algorithm, we solve for u^{n+1} by setting the left-hand-side of Eq. (4) to zero, and linearizing the problem through substituting every u appearing in the denominators by the value of u^n obtained from the previous iterate. For a more detailed descritption of the means used to solve this type of problem, see (Chartrand & Staneva, 2008; Chartrand & Wohlberg, 2010; Vogel, 2002). It is known that an appropriate choice of the denominator offsets, ε and η, is necessary to produce acceptable minimizations (Chartrand, 2007), yet this choice is rarely considered beyond their status as parameters that must be tweaked to obtain acceptable results (Chambolle, Caselles, Novaga, Cremers, & Pock, 2009; Li, Shen, Fan, & Shen, 2007; Oh, Woo,

Yun, & Kang, 2013). In what follows, we detail a methodology on how to determine the parameters α, ε, η, and the function $\psi(t)$, based on the data $F(t)$ and the derivative estimate $u(t)$.

5.3.1.2 Dynamic determination of total-variational parameters

Given a set of fluorescence recordings $\{F_i\}$ of length N, at the n^{th} iterate of the regularization algorithm, we identify the set of indices $j = \{i = 1,2,\cdots,N \,|\, \psi^n(t_i) \neq \infty\}$ whose data are not likely dominated by noise and thus should contribute to the fidelity term of Eq. (4). Letting $\Delta_i = F_i - F_{i-1}$, we can define the weighting sequence $g_i = 1 - |\Delta_i| / \max_i |\Delta_i|$ in order to provide an upper bound on the noise of the signal, given by

$$\sigma_+^n = \frac{\sum_j |\Delta_j| g_j}{\sum_j g_j}.$$

The weights g_i will tend to zero as Δ_i approach their maximum, and converge to a positive number(<1) as $|\Delta_i|$ approach their minimum. We can thus conclude that the weighted average of $|\Delta_j|$ will identify the smallest differences as being the most informative of the magnitude of noise. Large discrete differenecs, whether they result from transient increases in the noise level or from the fact that the signal is non-stationary, contribute only modestly to the estimate σ_+^n. On the other hand, we can also estimate a lower bound on the noise using

$$\sigma_-^n = mean\left(\left|\zeta_j^n\right|\right), \tag{5}$$

where $\zeta_i^n = F_i - (Au^n)_i$, i.e., by taking the difference between the data and the cumulative integral of u. Because we use the discrete differences Δ_i as our initial solution: $u_i^0 = \Delta_i$, the integral of u^n ($n > 0$) will likely diverge away from the data with each succesive iteration of the algortithm due to the action of the regularization term in Eq. (4). This tends to result in σ_-^n being smaller than σ_+^n, although this is not always strictly true. The use of the two different estimators for the noise allows for a more robust performance of the methodology, as both estimators are prone to

becoming inaccurate in different scenarios. With an estimate of the noise, we can also estimate the noise-to-signal ratio by

$$\phi^n = \frac{\sigma_+^n}{\max\left(Au^n\right)}.$$

The value of ϕ is a critical parameter in our algorithm as it discreminates between small and large values of various quantities. For example, it is employed to calculate an appropriate value of ε, defined in Eq. (4), based on the scale of variations of small values of u', as follows

$$\varepsilon^n = std\left(\left\{ \left|u_r'\right| : \left|u_r'\right| \le \left(\phi^n\right)^2 \max_i\left(\left|u_i'\right| \right), r \in i \right\} \right).$$

The calculation of η requires defining another weighting sequence $h_i = \left|u_i'\right| \Big/ \max_i \left|u_i'\right|$, which tends to zero when u is the most regular, as well as an estimate for the upper bound on the total error, χ, between the integral of u and the data in the least regular regions of the solution, given by

$$\chi^n = \frac{\sum_i h_i \left|\zeta_i^n\right|}{\sigma_-^n}.$$

When χ is small, η must be made large enough to improve the smoothness of the fitting (at the expense of data-fidelity). This can be acheived by making η a decreasing function of χ. However, if a recording does not contain any rapid jumps or noise spikes (but is nonetheless noisy), such a relation between χ and η will not be sufficient to infer a proper choice of η given χ. Thus, we must include another term independent of χ which will produce modest data-fidelity for signals dominated by drift. We therefore define η to be

$$\eta^n = \frac{\exp}{\sigma_+^n}\left[-\left(\frac{\chi^n + 1}{2\sigma_-^n} \max\left(\left\{ \left|F_i - F_{i-1}\right| - std\left(\left\{ \left|F_r - F_{r-1}\right| : r = 2,\ldots,N \right\} \right) : i = 2,\ldots,N \right\} \right) \right)^{\frac{\sqrt{\chi^n}}{2}} \right]$$

$$+ mean\left(\underset{d \subset \left\{\delta^n\right\}}{arg\,max} \left\{ \left|d\right|_{\ell^1} : \mathrm{mean}(d) \ge 3\mathrm{std}(d) \right\} \right).$$

which includes the smallest non-zero scale of the weighted differences $\delta_i^n = \left(1 - h_i^n\right)\Delta_i^n$.

TV methods tend to smooth the fit when there are large amplitude jumps in the data, or where u is large. If a single large jump dominates the derivative, this can lead to excessive local smoothing, which can be resolved by having enhanced data-fidelity at that point. On the other hand, in the presence of large jumps in the data, small noise-driven fluctuations may be under-regularized. In this case, data-fidelity at these points must be reduced. The function ψ allows for local enhancement or reduction of data-fidelity. Unlike ε, η does not depend on ϕ, but data-fidelity must through the weighting function ψ (by making ψ proportional to ϕ). Therefore, we define ψ to be

$$\psi_i^n = \left(\phi^{\sqrt{\chi^n+2}}\right)^{J_1} + \phi^{J_2}, \tag{6}$$

where

$$J_1 = \left[\frac{1}{\left(\sigma_+^n\right)^{1+\sqrt{\phi^n}}}\sqrt{\frac{\left|u_{i+1}^{n-1}\right|}{\min\left(\left\{\left|u_r^{n-1}\right| : u_r^{n-1} \neq 0\right\}\right)}}\right], \quad J_2 = \left[\sqrt{\frac{\left(\frac{1}{\tau_{\max}}+\frac{1}{3}\right)\sigma_+^n}{\left(\chi^n+1\right)\left(\omega_i+\delta_i\right)}} + \frac{mean\left(\left|u^{n-1}\right|\right)}{\left|\max\left(\left|\upsilon^n\right|\right)-\left|\upsilon_i^n\right|+\phi^n\right|}\right],$$

$\tau_{\max}^n = \left(mean\left(\left|\zeta_j^n\right|\right) + std\left(\left|\zeta_j^n\right|\right)\right)/\sigma_+^n$ is a iterative error scale parameter, $\upsilon_i^n = u_{i+1}^{n-1} + \left(1-h_{i+1}\right)^2 u_{i-1}^{n-1}$ is an estimator of u_i based on the adjacent values of u, and ω_i is a three-point moving average of δ_i. The exponent J_1 emphasizes data-fidelity (regularity) when the derivative of the following point is large (small), whereas the exponent J_2 emphasizes data-fidelity when Δ_i are small or when the derivative is near its maximum. When Δ_i is large and u_{i-1}, u_i are regular, on the other hand, J_2 is small allowing regularity to propagate forward into regions of signal possessing large ampltidue noise (i.e., where the data is not informative). The balance between the two effects of J_2 along with the χ-dependent terms of Eq. (6) produce an acceptable compromise between the regularity of the fit and data-fidelity for recordings across a wide range of signal-to-noise ratio and extremely varied dynamics. Finally, once the maximum relative change between two iterations of the procedure becomes less than $\sqrt{\phi}$, we consider the solution to have achieved quasi-stationarity and terminate the procedure.

5.3.1.3 Removal of noise spikes

When a recording exhibits intermittent periods of high amplitude noise (noise spikes), the data contaminated by these noise spikes is minimally informative. Detecting them allows for determining the indices j (**Fig 5-2A**). Within our regularization algorithm, this is done by (a) setting ψ to infinity at those time points in such a way that Eq. (4) only penalizes irregularity at these time points, and (b) determining the fit at these points based on the surrounding (reliable) data. After each iteration, n, of the regularization algorithm, a smoother fit, Au^n, of the data is obtained. We also obtain a criterion that determines whether or not each point represents a noise spike based on a comparison between the residual differences, ζ^n, and a chosen threshold value. This threshold is specified using the parameter τ_{rm}^n, given by

$$\tau_{rm}^n = (1-\xi) + \xi\tau_{\max}^n,$$

where $\xi = \exp\left(-\left(\left(\sigma_+^n - \sigma_-^n\right)/\max\left\{\sigma_+^n, \sigma_-^n\right\}\right) - \left(\chi^n\right)^2/N\right)$ is a convergence parameter for the noise rejection method. Positive ζ_i^n are rejected if they are greater than $\tau_{rm}^n\sigma_+^n$, while negative ζ_i^n are rejected if they are less than $\left(\tau_{rm}^n\right)^2\sigma_+^n$. The use of two thresholds is due to the asymmetry of the Poisson statistics underlying data collection using photodetectors. Rejection is achieved by setting $\psi_i = \infty$, which serves as the basis for defining the set of indices j (i.e., $j = \{i = 1,2,\cdots,N \,|\, \psi^n(t_i) \neq \infty\}$ as stated before).

5.3.2 Baseline drift

When fitting data to specific functional forms, it is important to take into account temporal drifting of the baseline in a signal. The specific nature of the processes underlying this drift are not of particular interest here. Rather, we consider them as nuisance trends and aim to remove their effects from the data.

5.3.2.1 Drift model

Some drifts are quite slow compared to the timeframe of the experimental recording, and thus can be fairly well represented by linear functions, whereas others are fast and better represented by an

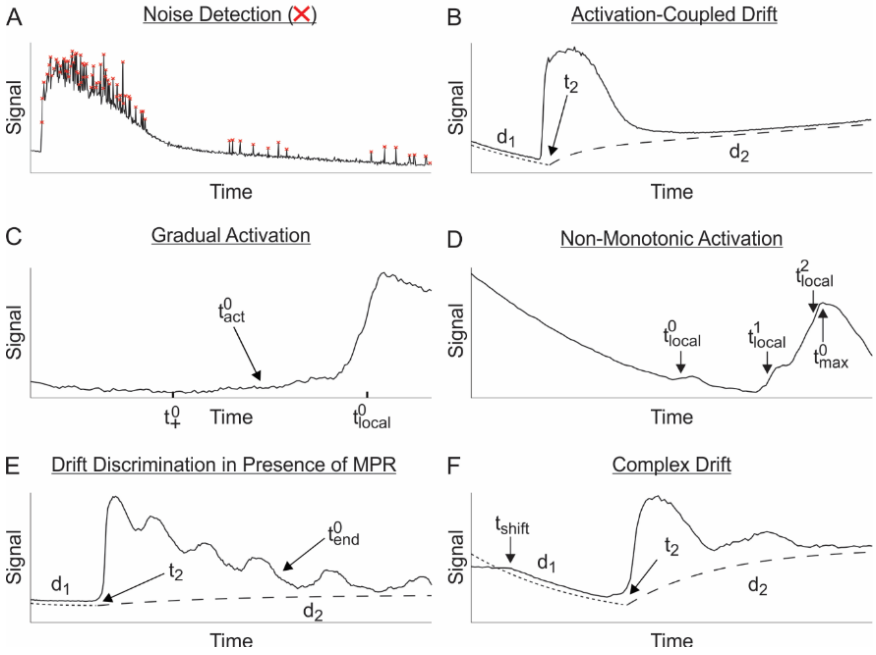

Figure 5-2. Multitude of features that must be considered during parameter characterization. **(A)** Experimental recordings are often contaminated with noise; red crosses represent noise detected and corrected. **(B)** Activation-coupled drift; Trajectory of baseline drift, d_1, can shift to secondary drift, d_2 at time t_2. **(C)** Determination of activation in the presence of gradual activation. Region of activation is restricted to $\left[t_{i^0_+}, t_{i^0_{local}}\right]$, within which the most likely point of activation, $t_{i^0_{act}}$, is statistically resolved. **(D)** Non-monotonic activation. Spurts of negligible activity, represented by the local maxima at $t_{i^0_{local}}$ and $t_{i^1_{local}}$, are disregarded as points of activation, in favor of $t_{i^2_{local}}$ which is characterized by the max peak, $t_{i^0_{max}}$. **(E)** Drift discrimination in cases where MPRs are superimposed on TRs. Underlying TR serves as a non-stationary baseline around which the MPR will oscillate for $\left[t_2, t_{i^0_{end}}\right]$ until its contribution becomes negligible and the baseline drift, d_2, dominates the MPR baseline. **(F)** Complex drift; Change in the baseline drift, t_{shift}, prior to onset of TR is ignored in favor of d_1 after the reweighting procedure.

exponential decay function. Since, in a given recording, a number of processes will result in the observed drift, we postulate that, the drift throughout the signal can be well fit to a combination of linear and exponential functions

$$d_\iota\left(t; a_\iota, \tau_\iota, m_\iota\right) = a_\iota\left[1 - \exp\left(-t/\tau_\iota\right)\right] + m_\iota t \tag{7}$$

where, a_ι, τ_ι, and m_ι are the exponential amplitude, exponential time constant and the slope of the linear component of the ι^{th} drift within the signal, respectively (examples of fitted drifts shown in **Fig 5-2B, E, F**) . With an appropriate choice of data, these are determined using the least squares

fitting. We have found numerous cases where either the linear or exponential components were not justifed. However, this knowledge is unavailable to us prior to conducting manual or automated analysis of the data, and we cannot assume *a priori* a less general form than Eq. (7). Thus we have to rely on the fitting to optimize the contribution of the two compoenets in a data-dependent manner.

It is possible for the signal to exhibit (multiple) drifts with different trends separated perhaps by a TR. In order to capture this effect in a signal, we use a global drift model that combines the intial and secondary drifts (**Fig 5-2B**) in a semi-piecewise manner in which the initial drift, d_1, continues to contribute to the overall observed drift and succesfully captures the global behaviour. This can be written as

$$D(t) = \begin{cases} d_1(t) + z & if\ t < t_2 \\ d_1(t) + d_2(t - t_2) + z & if\ t \geq t_2 \end{cases}, \quad (8)$$

where t_2 is the time at which the secondary drift, d_2, begins and z is the offset at $t = 0$. Rather than assuming that the drift is similar for all recordings and attempting to construct a standard curve, we assume that a few points in each recording are highly informative of the drift in the baseline.

5.3.2.2 Drift delimitation

To fit the drift model to the corresponding portion of the recorded signal, it is necessary to delimit the boundaries of TR by identifying the start of activation and end of deactivation. Firstly, we will aim to estimate the point in time at which the TR of a recording begins. Experimental TRs rarely activate abruptly and simultaneously for a field of imaged cells. Many factors play a role in the heterogeneity of responses observed such as variable diffusion fronts of applied agonist or heterogenous receptor expression among cells. These effects can manifest as very gradual rises or additional small amplitudes prior to a certain activation threshold being surpassed and a rapid activation phase being observed (**Fig 5-2C, D**). Therefore, analyzing the activation times of all components of the biological unit manually can be subjective. While a simple threshold value in the signal can be effective in detecting activation, the choice of the threshold requires some knowledge of the amplitude of the noise σ and is complicated by the presence of drift in the signal. Instead, we determine the end points of the time intervals dominated by the drift through statistical

analysis of an estimate of the first derivative of the signal $\hat{u}(t)$. In other words, to distinguish the drift from TR, the derivative of the latter must change in a way that is more statisically significant than that of the former.

Using the estimated time derivative, we aim to determine (*i*) the earliest possible time of activation $t_{i^0_{act}}$ (defined as the last time point exhibitng a significant increase in the first derivative before it reaches its maximum value), (*ii*) the time at which the activation reaches its maximum value $t_{i_{max}}$, and (*iii*) the time at which the deactivation ends and the signal is once again dominated by the drift $t_{i^0_{end}}$.

i. Assuming that the estimated first derivative during activation reaches a local maximum, we can find the most significant local maxima of $\hat{u}$ at the location

$$i_{local} = \left\{ i : \hat{u}_i > std(\hat{u}), \hat{u}_i \geq \hat{u}_{i-1} \text{ and } \hat{u}_i \geq \hat{u}_{i+1} \right\},$$

where we denote the first significant local maximum by $i^0_{local} = \min\{ i_{local} \}$. By focusing on the portion of the signal containing the first drift and the activation phase of the TR, we restrict our attention to the time interval in which the first derivative $\hat{u}(t)$ is non-negative to disentangle the effects of activation and drift in the data. In other words, we restrict our analysis to $\left[t_{i^0_+}, t_{i^0_{local}} \right]$, where the derivative is non-negative and

$$i^0_+ = \min_{i \in 0,\ldots,i^0_{local}} \left\{ i : \hat{u}_r \geq 0 \quad \forall r = i,\ldots,i^0_{local} \right\}.$$

Without prior knowledge about the sign of the derivative of the baseline drift, we cannot conclude that i^0_+ corresponds to the beginning of activation. To resolve this issue, we employ a statistical test to determine the likely time at which the activation occurs, located at the index

$$i^0_{act} = \max_{i \in i^0_+,\ldots,i^0_{local}} \left\{ i : \hat{u}_i < std\left(\left\{ \hat{u}_{i^0_+},\ldots,\hat{u}_{i^0_{local}} \right\} \right) \right\}.$$

This methodology, based on the properties of the derivative around its first significant local maximum, generally picks out the first visually unambiguous activation (**Fig 5-2C**). As a result, it may be necessary to trim recordings where there are (large amplitude) artifacts prior to the activation of interest.

ii. TRs may be produced by the action of multiple active units (e.g., different receptor species) within the biological system under consideration, each having distinct properties and activation times. This leads to multiple delayed activations taking place over a broad range of time (**Fig 5-2D**). Due to the superposition of the drift in the baseline with these responses, it is entirely possible for recordings to be contaminated by strongly decreasing drift and for the expected maximum TR to not coincide with the actual maximum of the data. Thus we have developed a method to search for the visually most likely point at which the TR reaches its maximum in the presence of a drift. For each one of the N_{local} significant local maxima of the first derivative along the activation phase, we find the location of the previous local minimum of the TV estimate of the data using

$$i_{local}^{min} = \left\{ \max_{n<r} \left\{ n : \hat{u} \le 0 \right\} : r \in i_{local} \right\}$$

as well as the location of the next local maximum at

$$i_{local}^{max} = \left\{ \min_{n>r} \left\{ n : \hat{u} \le 0 \right\} : r \in i_{local} \right\}.$$

From the positions of the local extrema of the data, we can estimate the value of the baseline drift from each local minimum to the next local maximum using the linear extrapolation

$$v_{\_} = \left\{ \left(A\hat{u}\right)_q + \left(t_r - t_q\right) \frac{\hat{u}_{r-1} + \hat{u}_r}{2} \quad : q = \left(i_{local}^{min}\right)_s, r = \left(i_{local}^{max}\right)_s, s \in \left\{1, \ldots, N_{local}\right\} \right\} \tag{9}$$

where A is the operator of antidifferentiation with $Au \approx F_{true}$ (see Eq. (1)). Based on this, we then estimate the average rate of activation for each significant local maximum of the derivative according to

$$\mu = \left\{ \frac{\left(A\hat{u}\right)_r - \left(v_{\_}\right)_s}{t_r - t_q} \quad : q = \left(i_{local}^{min}\right)_s, r = \left(i_{local}^{max}\right)_s, s \in \left\{1, \ldots, N_{local}\right\} \right\}$$

and select the first local maximum at the location

$$i_{max}^{0} = \min\left\{r : \mu_r \geq mean(\mu) - 3 \cdot std(\mu) \text{ and } \nu_r > mean(\nu) - std(\nu)\right\},$$

which has an average rate and magnitude within a statistically acceptable range (that excludes small outliers). $t_{i_{max}^{0}}$ is the time point at which the derivative reaches a local maximum. It may differ from the one that corresponds to the local maximum immediately following the first activation time point $t_{i_{act}^{0}}$ (**Fig 5-2D**). This is because i_{act}^{0} depends solely on the derivative around its first local maximum, while i_{max}^{0} takes into account an approximation to the average rate of change around all local maxima; the local maximum after i_{act}^{0} should only differ from i_{max}^{0} when there is a succession of activations and the first does not have the largest rate of activation.

Starting from this local maximum of the derivative, we seek the location of the first point in time $t_{i_{max}^{end}}$ where the change in the signal drops below the estimated noise level σ_{-}

$$i_{max}^{end} = \min_{i \in i_{max}^{0},\ldots,N} \left\{ i : \hat{u}_i \cdot (t_i - t_{i-1}) < \sigma_{-} \right\}, \tag{10}$$

and thus isolate the time interval in which the most significant activation occurs. Having isolated the most significant activation, we finally arrive at the location of the first estimate of the time where the response reaches its maximum

$$i_{max} = \min\left\{ \arg\max_{i \in i_{max}^{0},\ldots,i_{max}^{end}} \left(A\hat{u}\right)_i \right\}.$$

iii. Having identified the time at which activation is likely to begin $t_{i_{act}^{0}}$, we can now assume that the signal prior to this point is the drift. If the recording is of a sufficiently long duration, the response will return to baseline and the end of the recording should once again be dominated by the (secondary) drift (**Fig 5-2B**). To account for this drift, we need to estimate the time duration of deactivation. This is done in a manner nearly identical to how we determined the first time of activation $t_{i_{act}^{0}}$. However, due to the possibility of having MPR after the initiation of TR (**Fig 5-2E**), we cannot restrict ourselves to time intervals in which the first derivative is non-positive.

To solve this issue, we define a set of time points after the presumed maximum of TR, located at $i_{decay} = \{i_{max}, \ldots, N\}$, and construct a measure

$$n_{end} = \max_{n \in \{3,2,1,0\}} \left\{ n : \exists \left| \hat{u}_i \right| - mean\left(\left| \hat{u}_{i_{decay}} \right| \right) > n \cdot std\left(\left| \hat{u}_{i_{decay}} \right| \right), i \in i_{decay} \right\}$$

to quantify how far the derivative deviates from its mean during the decay. This measure allows us to robustly detect the location of the time point where TR is negligible

$$i^0_{end} = \min_{i \in i_{decay}} \left\{ i : \left| \hat{u}_i \right| - mean\left(\left| \hat{u}_{i_{decay}} \right| \right) > n_{end} \cdot std\left(\left| \hat{u}_{i_{decay}} \right| \right) \right\}.$$

The time point $t_{i^0_{end}}$ is then used to determine the start of the new drift.

5.3.2.3 Drift fitting

To isolate the TR from the drift, it is necessary to generate an accurate fit for the drift. This is achieved by employing a succession of least square fits that progressively incorporates more data and models that account for additional components of the signal (including activation and deactivation phases of TR). The first step in this successive least-square-fitting method is to obtain preliminary estimates of the parameters $\theta_{drift} = [a_1, \tau_1, m_1, a_2, \tau_2, m_2]$ of the drift model. The MATLAB implementation of the non-linear least squares method (Marquardt, 1963; Moré, 1978) is used. More specifically, we initially minimize the error function between the drift model and the data

$$S^0_{drift}(\theta_{drift}) = \sum_k \left(D(t_k; \theta_{drift}) - F_k \right)^2, \quad (11)$$

where the set of indices k is defined by $k = \left\{ \left\{ 1, \ldots, i^0_{act} \right\} \cup \left\{ i^0_{end}, \ldots, N \right\} \right\} \cap j$. We denote the first estimate of parameters obtained from the minimizaiton of Eq. (11) by θ^0_{drift}. There is no guarantee, however, that the drift model described by Eq. (8) can accurately represent the actual drift in the baseline. The emergence of drifting trends which are not related to the onset of TR (**Fig 5-2F**) may require the inclusion of more than two functions of the type described in (7), yet the decision to include more drift terms, or alternatively to truncate the signal, would require manual intervention. To circumvent this limitation, we perform a second fit where the individual terms in Eq. (11) are weighed according to a weight function w, and the first derivative of the data is taken into account.

Although the set of parameters θ^0_{drift} will be able to produce the "general" trends in the data before and after TR, the presence of multiple drifting trends necessitates the use of the derivative estimate, $\hat{u}$, to identify the segment(s) of the signal that actually follow the trend described in (8) and remove the effects of others. The inclusion of $\hat{u}$, however, in the sum of squared errors can lead to erroneous fittings when the drift is not well represented by (8). The weight function w alleviates this problem by preventing the linear and exponential trends in (7) from growing unjustifiably large.

To determine w, we require that it approaches zero when the match between $\hat{u}$ and $\dot{D}\left(t;\theta^0_{drift}\right)$ is minimal. To achieve this, we choose w to depend on $y = \left|\hat{u} - \dot{D}\left(t;\theta^0_{drift}\right)\right|$ as follows

$$w_k = \exp\left(\frac{-y_k^2}{mean\left(y_k^2\right)}\right).$$

We then apply the non-linear least squares fitting procedure to minimize the error function

$$S_{drift}\left(\theta_{drift}\right) = \sum_k w_k\left[\left(D\left(t_k;\theta_{drift}\right) - F_k\right)^2 + \left(\hat{u}_k - \dot{D}\left(t_k;\theta_{drift}\right)\right)^2\right],$$

and use θ^0_{drift} as an initial condition for the fitting procedure.

5.3.3 Activation fitting

For the activation phase of the response, we use the model

$$g_{act}\left(t;A_{act},\beta,n_{act},m_{act}\right) = A_{act}\frac{t^{n_{act}}}{t^{n_{act}} + \beta^{n_{act}}} + m_{act}\int_0^t \frac{x^{n_{act}}}{x^{n_{act}} + \beta^{n_{act}}}dx.$$

where A_{act} is the maximum of the Hill function, n_{act} is the Hill coefficient, β is the time at which the the Hill function reaches its half maximum, and m_{act} is the slope of the quasi-linear function that accounts for the trend which dominates at the end of activation. The Hill function allows for a rapid rise and switch in convexity due to many biological units being activated at once, whereas the linear trend allows for a delayed and slower rise induced by more units being progressively recruited into the generation of the signal. The values of A_{act} and m_{act} determine the magnitude

of these two trends, whereas n_{act} and β affect primarily the timescales of switching between the two. The time at which the activation phase begins is denoted as t_{on}, and its estimate is confined to the time interval $\left[t_{i_{act}^0}, t_{i_{\max}}\right]$. In order to obtain a preliminary estimate of the values of these parameters and those of the drift function, $\theta_{act} = [t_{on}, A_{act}, \beta, n_{act}, m_{act}, \theta_{drift}]$, we minimize the sum of square errors between the activation data and the model along with their derivatives, given by the function

$$S_{act}(\theta_{act}) = \sum_j \left[\phi^2 \left(F_j - G_{act}(t_j;\theta_{act})\right)^2 + \phi\left(\hat{u}_j - \dot{G}_{act}(t_j;\theta_{act})\right)^2 \right] + S_{drift}(\theta_{drift}), \tag{12}$$

where ϕ is the noise-to-signal ratio, and

$$G_{act}(t;\theta_{act}) = \begin{cases} D(t;\theta_{act}) + g_{act}(t - t_{on};\theta_{act}) & if\ t_{onset} \le t < t_{max} \\ D(t;\theta_{act}) & otherwise \end{cases}$$

is our activation data model that takes into account the effect of the drift D (defined in Eq. (8)) on the perceived activation. To abrogate the influence of noise spikes on measured parameters, the sum of squares in (12) is evaluated at the set of indices j which are not dominated by noise. Moreover, we use $\hat{\theta}_{drift}^{act}$ to denote the set of drift parameters obtained from the minimization of (12).

5.3.3.1 Signal detection

In order for the algorithm to resolve whether there is a discernable TR present in $F_{true}(t)$, three conditions must be satisfied: (i) i_{local} must be a non-empty set, (ii) the initial drift estimate

$$D\left(t;\ \arg\min_{\theta \in \left\{\hat{\theta}_{drift}, \hat{\theta}_{drift}^{act}\right\}} S_{drift}(\theta)\right)$$

must be below the TV data estimate by a detection threshold of $4\sigma_{-}$ for at least six data points, and (iii) the difference between the TV data estimate and the initial drift estimate must not be a

strictly increasing function of time after t^0_{max}. These three criteria allow for the detection of the TR and further analysis of its characteristics.

To evaluate the signal detection performance of the algorithm, 450 individual traces of ATP-induced calcium responses were used as a validation set. Manual results were then compared to automated detection of TRs to assess extent of agreement between the two methods. Classical signal detection nomenclature (i.e. true positive or negative and false positive or negative) was intentionally avoided due to lack of certainty in determining the true presence of TRs in more ambiguous cases. We found that the automated and manual methods agreed in detecting a TR in 88.1% of cases, and they disagreed in 11.9% of cases (**Fig 5-3A**). Further dissection of these results showed that 64.7% of disagreement arose from the algorithm reporting an absence of TR while visual evaluation suggested otherwise (**Fig 5-3A**), indicating that the algorithm has a tendency to be more conservative than user-mediated assessments.

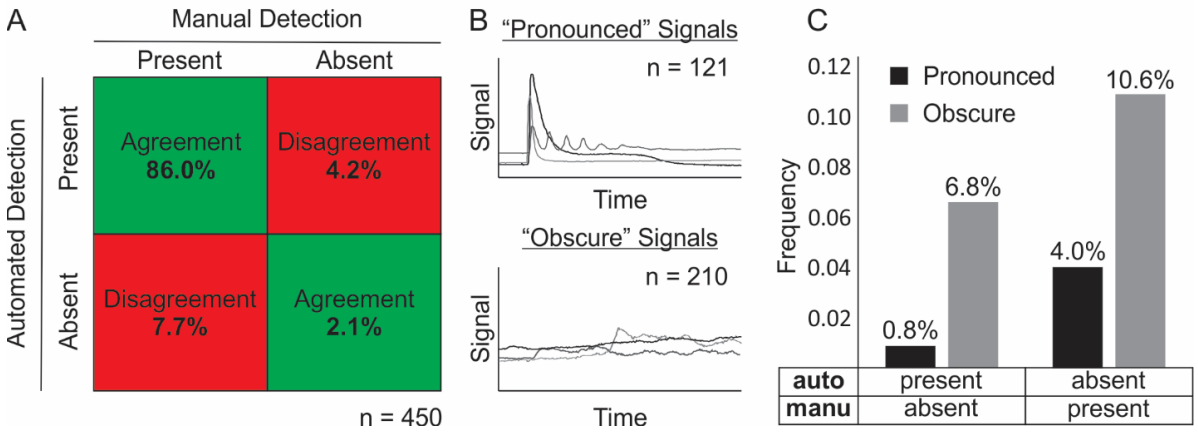

Figure 5-3. Signal detection and performance. (A) Signal detection analysis demonstrates relative selectivity and sensitivity of the algorithm as compared to user-mediated manual detection. "Agreement" refers to instances where the detection of a response was consistent between algorithm and manual methods. "Disagreement" refers to the contrary. "Present" indicates cases where a response was detected using the indicated method, while "absent" refers to cases where a response was not detected. **(B)** Representative time-series for pronounced (*top*) and obscure (*bottom*) signals. **(C)** Analysis of disagreement cases for pronounced and obscure signal selections. Automated detection, auto; manual detection, manu; sample size, n.

To determine whether there were particular types of recordings that contributed to these disagreements, time-series traces were qualitatively divided into two groups: Clean signals with clearly defined responses were classified as "pronounced" (**Fig 5-3B**, *top*), and signals containing ambiguous signals with low signal to noise ratio or strong drift were classified as "obscure" (**Fig**

5-3B, *bottom*). The total frequency of disagreement was 3.6 times greater for obscure signals compared to those classified as pronounced (17.4% vs. 4.8%; **Fig 5-3C**). Regardless of the group, the algorithm signal detection remained more conservative compared to the manual method.

5.3.4 Transient response (TR) model

Transient cellular responses are generally complex with multiple time scales and amplitudes. They may, in fact, exhibit prolonged MPRs superimposed on a more acute response (see **Fig 5-2E**). For these reasons, a complete characterization of all possible TRs is unlikely to be attainable. In order to remain as general as possible, we propose modeling TR as a continuously differentiable piece-wise defined function that first increases during the activation phase and subsequently decreases during the deactivation phase. Due to the large number of parameters required for such a description and the automated nature of our fitting procedure, we decompose the fitting of the whole TR into a sequential fitting of the activation phase alone followed by a fit of both phases simultaeously. This yields significantly more reliable results with faster convergence rates over a wide gamut of input data, because it allows for information obtained during preliminary simple fits to be used in a progressively more complex manner. In order to capture the complex fluorescence response generated by the spatially separated units in a live cell, we use a combination of Hill functions and quasi-linear functions generated by the integral of the corresponding Hill functions.

5.3.4.1 Response fitting

Following the least squares fitting of the activation data, we now seek to fit the entire recording (with the drift and TR) using a continuously differentiable function. A decreasing Hill Function is used to describe deactivation phase of the signal in a manner similar to Eq. (11), as follows

$$g_{de}(t; A_{de}, \gamma, n_{de}) = A_{de}\frac{\gamma^{n_{de}}}{t^{n_{de}} + \gamma^{n_{de}}} + m_{de}\int_0^t \frac{\gamma^{n_{de}}}{x^{n_{de}} + \gamma^{n_{de}}}dx\,,$$

where A_{de} is the amplitude of the Hill function, n_{de} is the Hill coefficient, γ is the time at which the Hill function reaches its half maximum, and m_{de} is the slope of the quasi-linear function that accounts for the trend dominating at the beginning of deactivation. The time when the response

switches to the deactivation function is denoted by t_{de}. The parameter m_{de} is chosen such that the response function returns to zero by the end of the recording and is given by

$$m_{de} = \frac{g_{act}\left(\ell_{act}; A_{act}, \beta, n_{act}, m_{act}\right) - A_{de}\dfrac{\gamma^{n_{de}}}{\left(t_N - t_{de}\right)^{n_{de}} + \gamma^{n_{de}}}}{\displaystyle\int_0^{t_N - t_{de}} \frac{\gamma^{n_{de}}}{x^{n_{de}} + \gamma^{n_{de}}} dx},$$

where $\ell_{act} = t_{de} - t_{on}$ is the time duration of the activation phase of the response. If differentiability is not enforced at the point t_{de}, where the two functions g_{act} and g_{de} meet, then the fitting may contain sharp edges indicative of unconverged solution. To solve this issue, the continuity of the first derivative of these two functions, particularly at t_{de}, is achieved through a third-order Hermite spline (Traub, 1964) on the time interval $\left[t_{de} - \varsigma_{act}, t_{de} + \varsigma_{de}\right]$, where ς_{act} and ς_{de} are two parameters that must satisfy $\varsigma_{act} < \ell_{act}$ and $\varsigma_{de} < 2\gamma$ (see **Appendix A3**). The overall response model is thus given by

$$g_{resp}\left(t;\theta_{resp}\right) = \begin{cases} g_{act}\left(t - t_{on};\theta_{resp}\right) & if\ t_{on} \le t < t_{de} - \varsigma_{act} \\ p_{Hermite}\left(t - \left(t_{de} - \rho_{act}\right);\theta_{resp}\right) & if\ t_{de} - \varsigma_{act} \le t < t_{de} + \varsigma_{de}, \\ g_{de}\left(t - t_{de};\theta_{resp}\right) & if\ t_{de} + \varsigma_{de} \le t \end{cases}$$

where $\theta_{resp} = [\theta_{act}, t_{de}, \varsigma_{act}, \varsigma_{de}, A_{de}, \gamma, n_{de}\theta_{drift}]$. Given the response model, we define the global data model as

$$G_{resp}\left(t;\theta_{resp},\theta_{drift}\right) = \begin{cases} D\left(t;\theta_{resp}\right) + g_{resp}\left(t_i;\theta_{resp}\right) & if\ t_{onset} \le t \\ D\left(t;\theta_{resp}\right) & otherwise \end{cases}, \tag{13}$$

and minimize the error function

$$\begin{aligned} S_{resp}\left(\theta_{resp}\right) = \phi \sum_j \Big[& \phi\left(F_j - G_{resp}\left(t_j;\theta_{resp}\right)\right)^2 + \left(\hat{u}_j - \dot{G}_{resp}\left(t_j;\theta_{resp}\right)\right)^2 \\ & + \kappa\phi\left(D_2\left(t_k - t_2; a_2, \tau_2, m_2\right)\right)^2 \Big] + \frac{\lambda}{\phi^2} S_{drift}\left(\theta_{drift}\right), \end{aligned} \tag{14}$$

to obtain the fitting, where κ is a parameter quantifying the apparent coherence between the drift and reponse models (D and g_{resp}), given by

$$\kappa = \left| \frac{\left(A\hat{u}\right)_N - g_{act}\left(t_{max} - t_{on}; A_{act}, \beta, n_{act}, m_{act}\right)}{\left(A\hat{u}\right)_N - \min\limits_{i \in i^0_{act}, \ldots, i_{max}} \left(A\hat{u}\right)_i} \right|,$$

λ is a parameter defined by

$$\lambda = \frac{\max\limits_{i > i^0_{end}} \left|\hat{u}_i\right|}{\max\limits_{i \in i^0_{act}, \ldots, i_{max}} \hat{u}_i},$$

and the values for the parameters A_{act}, n_{act}, β, m_{act}, and t_{onset} are taken from the activation fitting. The first two terms in the sum of squares in Eq. (14) are analgous to those in Eq. (12), whereas the third term minimizes the area under the curve for the second drift function D_2. By including the coefficient κ in this third term, however, allows D_2 to become more significant when there is a large mismatch in the value of the baseline between $t_{i^0_{act}}$ and t_N (that cannot be explained by d_1).

5.3.4.2 Activation parameter validation: t_{onset}, $t_{10\%-90\%}$, and amplitude

The three parameters, t_{onset}, $t_{10\%-90\%}$ and amplitude, are considered together because they describe what happens at the activation phase of the TR, with no regard for the deactivation phase or MPR. The time at which a TR is discernable from baseline is defined as t_{onset} and is estimated directly as the parameter t_{on} of the response function g_{resp}.There was a strong linear agreement between the manual and automated-estimates, with a linear slope of 1.06 and a correlation coefficient (r^2) of 0.94 (**Fig 5-4A**, *left*). On average, automated estimates of t_{onset} were 4.6% greater than manual estimates, with limits of agreement ranging between -10% and 19% difference (**Fig 5-4A**, *right*). The $t_{10\%-90\%}$ is also estimated numerically from the response function g_{resp}. Using the response function allows to overcome issues arising from the subsampling of rapid dynamics by numerically evaluating on a time grid ten times finer than the input times. Manual estimation of this parameter is contingent upon accurate estimation of the baseline and peak occurrences, both of which present

potential sources of error, particularly for noisy signals with drift. The relationship between manual and automated estimates had a linear slope of 0.77 and a correlation coefficient of 0.77 (**Fig 5-4B**, *left*). The higher degree of scatter away from the line of exact linear correlation is reflected by the wider Bland-Altman interval of agreement, ranging from -89% to 54% difference between manual and automated estimates. Overall, there was a -17% difference between all paired estimates of $t_{10\%-90\%}$, revealing that $t_{10\%-90\%}$ was manually overestimated compared to the automated estimates (**Fig 5-4B**, *right*). Amplitude estimates obtained by the manual and automated methods had a strong linear relationship with a slope of 1.02 and a correlation coefficient of 0.84 (**Fig 5-4C**, *left*). The limits of agreement, ranging from -26% to 25%, were narrow with a mean percent difference of -0.3% between all paired estimates of amplitude (**Fig 5-4C**, *right*).

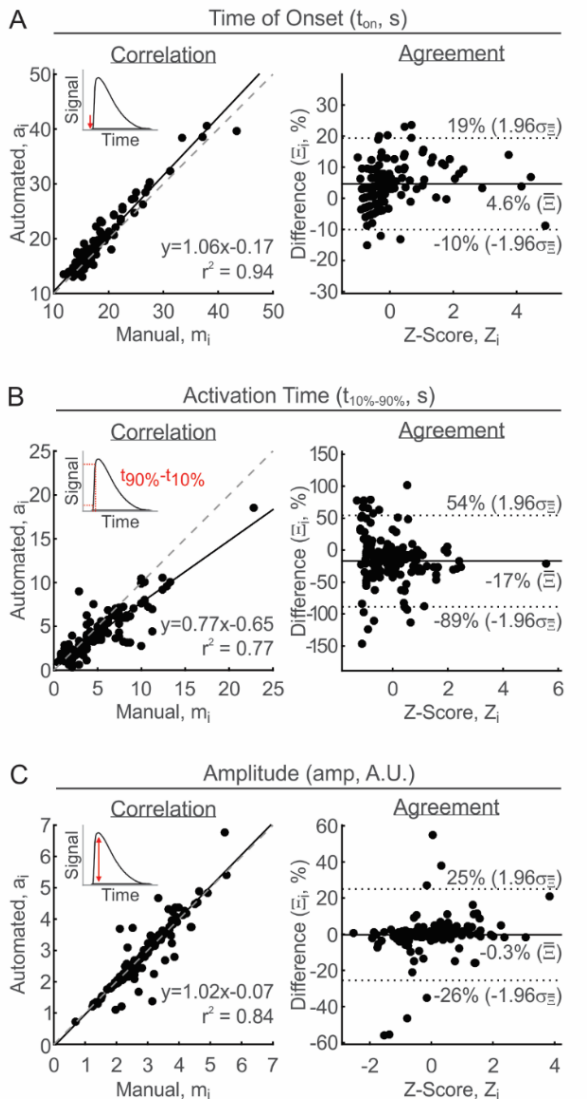

Figure 5-4. Validation of activation parameter measurements. Parameters were estimated manually and then compared with automated-estimated values using correlation analysis (*left*, *solid line*: linear regression line; *broken line*: line of equality) and Bland-Altman analysis (*right*, *solid line*: mean percent difference, $\overline{\Xi}$; *broken line*: limits of agreement, $\overline{\Xi} \pm 1.96\,\sigma_{\overline{\Xi}}$). **(A)** Time of onset, t_{onset}. **(B)** Activation time, $t_{10\%-90\%}$. **(C)** Amplitude.

5.3.4.3 TR parameter validation: AUC, FWHM, and τ_{decay}

Due to the inherent differences between TRs and MPRs and the approach taken with this algorithm, the AUC, FWHM and τ_{decay} are limited to describing TRs. Nevertheless, these parameters will be also reported in the presence of MPRs where they should be interpreted with the following considerations. (*i*) if a MPR is superimposed on a TR, the reported parameters describe the underlying TR, not the superimposed MPR. (*ii*) if TR presence is not detectable and MPR demonstrates a purely oscillatory response, the reported parameters characterize the first peak only. With these considerations in mind, manual evaluation of TR parameters was performed with a variety of signals, including MPRs. AUC estimates are manually determined using a geometric estimation of the area of a triangle whose vertices are at the start, peak and end of the TR. Algorithmically, AUC was evaluated from the area under g_{resp}, using the trapezoidal rule (Rice, 1973) implemented in MATLAB using "trapz()". Comparing the manual and automated estimates demonstrated a linear relationship with a slope of 0.85 and a correlation coefficient of 0.79 (**Fig 5-5A**, *left*). On average, automated estimates were 4.6% larger than manual estimates with an interval of agreement ranging between -38% and 47% difference (**Fig 5-5A**, *right*). Considering the geometric-approach used for manual-estimation of AUC values, it is reasonable to assume that the error arose from manual limitations.

Due to the difficulty in determining the precise time at which the signal returns to its former baseline, it would be challenging to manually describe the duration and decay characteristics of the response. Incomplete recordings and background drift are largely responsible for generating such behaviour. The full-width half-max (FWHM) is defined as the time elapsed between the two half-max coordinates of a peak. Our analysis of FWHM revealed that the linear relationship between manual and automated-estimates was strong, with a correlation coefficient of 0.87 and slope of 0.95 (**Fig 5-5B**, *left*). The Bland Altman analysis demonstrated that the agreement interval ranged from -20% to 22% difference with a mean percent difference of 0.85% between all paired estimates (**Fig 5-5B**, *right*).

Finally, to manually estimate the decay constant, the time of the inflection point (ρ) is visually estimated and the general trend of the data following ρ is represented by a mono-exponential decay. The decay constant is then determined by the time it takes for the signal to reduce to

approximately 37% of its initial value (1/e). Algorithmically, the time ρ is determined by solving for the inflection point in the deactivation function, given by

$$\rho = t_{de} + \gamma\left(\frac{n_{de}-1}{n_{de}+1}\right)^{1/n_{de}}.$$

The data following ρ is then fit to a mono-exponential decay function using least squares, to determine the time constant of decay. The slope of the linear agreement between manual and automated-estimates was 0.81 and the correlation coefficient was 0.75 (**Fig 5-5C**, left). The Bland Altman analysis revealed a strong systematic bias of -14% difference, with an agreement range of -63% to 34% difference, signifying that manual efforts to estimate the decay constant consistently overshot the values reported by the algorithm (**Fig 5-5C**, *right*).

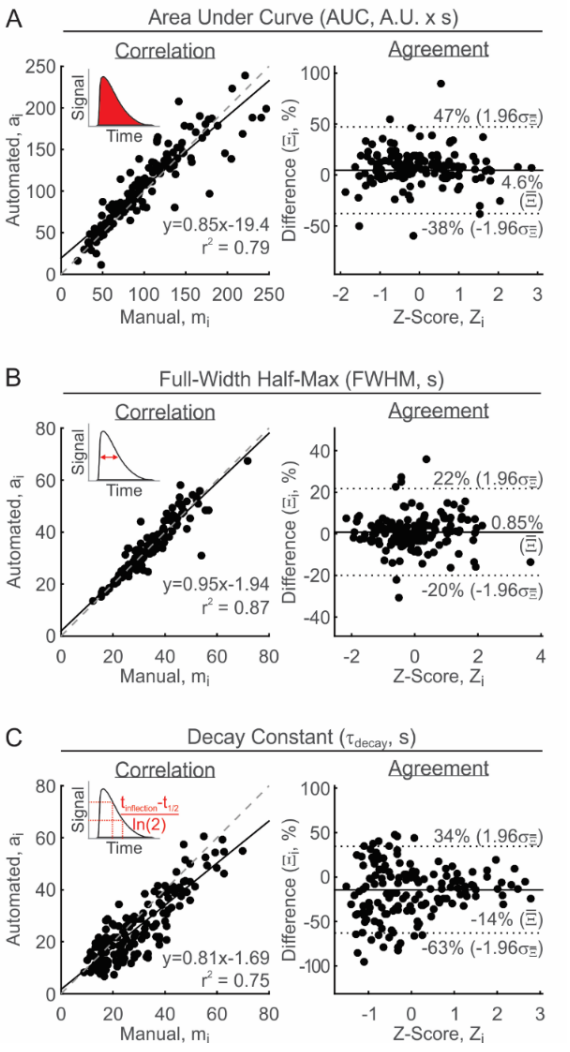

Figure 5-5. Validation of TR parameter measurements. Parameters were estimated manually and then compared with automated-estimated values using correlation analysis (*left, solid line*: linear regression line; *broken line*: line of equality) and Bland-Altman analysis (*right, solid line*: mean percent difference, $\overline{\Xi}$; *broken line*: limits of agreement, $\overline{\Xi} \pm 1.96\,\sigma_{\Xi}$ **(A)** Area under curve, AUC. **(B)** Full-width half-max, FWHM. **(C)** Decay constant, τ_{decay}.

5.3.5 Multi-peaked responses

To isolate the characteristic parameters of MPRs that are frequently superimposed on TRs, the TR model g_{resp} must be refined to serve as a non-stationary baseline around which the MPR will oscillate. This refinement is necessary because it is often the case that the TR model g_{resp} will produce sub-optimal fittings where the data deviates significantly from the TR fitting. Therefore, to accurately characterize the TR and quantify the properties of truly oscillatory MPRs, it is first necessary to adapt the least squares fitting procedure to remove the effects of data points not well represented by G_{resp}. This is done by first identifying large deviations representing MPRs from the G_{resp}-fitting (obtained by minimizing Eq. (14)), and then reweighing the sum of squares in Eq. (14) to remove the influence of those deviations from the fits. We subsequently perform a secondary fitting of G_{resp} to determine more accurately the baseline, delineating the TR, where the MPR-associated deviations originate from. Finally, we analyze the MPRs by determining whether they represent oscillations and, if so, quantify their properties.

To identify these MPR-associated deviations from the newly defined baseline, we first employ the MATLAB "findpeaks()" function. This finds the peaks and troughs of the significant deviations in the TV data estimate, $A\hat{u}(t)$, from the TR estimate, $G_{resp}\left(t;\hat{\theta}_{resp}\right)$, truncated at its half-maximums, where $\hat{\theta}_{resp}$ is the optimal parameter set obtained from minimizing Eq. (14). This truncation permits for the possibility that the onset of TR coincides with the first peak of the MPR-associated deviations. The implementation of peak-finding algorithm, on the other hand, allows for the specification of minimum heights and timing between peaks, set to be $6\sigma_{-}$ and 5 seconds, respectively. The algorithm yields the heights (E^{peak}, E^{trough}), the FWHM (ξ^{peak}, ξ^{trough}), and the times ($\widetilde{t}^{\,peak}, \widetilde{t}^{\,trough}$) of significant peaks and troughs of the deviations, respectively (**Fig 5-1C**). In total, there are $\widetilde{N} = N_{peak} + N_{trough}$ of these deviations, including N_{peak} peaks and N_{trough} troughs. If $\widetilde{N} \le 2$, then the only deviation in the signal is the TR and the algorithm can terminate. Without prior knowledge of the nature of the MPR-associated deviations, it is very difficult to determine whether they result from trends which are above, below, or symmetric to the TR. To resolve this issue, we assume that the estimated baseline underlies the signal in the absence of deviations. To

incorporate this assumption algorithmically, we define two bias parameters based on the relative heights of the first peak and trough, as follows

$$o_{peak} = \exp\left[-\left(\frac{E_1^{peak}}{E_1^{trough}}\right)^4\right] \quad \text{and} \quad o_{trough} = \exp\left[-\left(\frac{E_1^{trough}}{E_1^{peak}}\right)^4\right].$$

These quantities are then used to calculate weighting functions for the data based on the properties of peaks

$$\pi_i^{peak} = \sum_{r=1}^{N_{peak}} o_{peak} \exp\left(-\phi\left(\frac{o_{peak}\left(t_i - \tilde{t}_r^{\,peak}\right)}{\xi_r^{peak}}\right)^2\right) + \left(1 - o_{peak}\right)\left(1 - \exp\left(-\phi\left(\frac{o_{peak}\left(t_i - \tilde{t}_r^{\,peak}\right)}{\xi_r^{peak}}\right)^2\right)\right)$$

and troughs

$$\pi_i^{trough} = \sum_{r=1}^{N_{trough}} o_{trough} \exp\left(-\phi\left(\frac{o_{trough}\left(t_i - \tilde{t}_r^{\,trough}\right)}{\xi_r^{trough}}\right)^2\right) + \left(1 - o_{trough}\right)\left(1 - \exp\left(-\phi\left(\frac{o_{trough}\left(t_i - \tilde{t}_r^{\,trough}\right)}{\xi_r^{trough}}\right)^2\right)\right).$$

The weighting functions $\pi_i^{peak}, \pi_i^{trough}$ quantify the relative reliability of the data around each deviation based on how close it is to the fitting function G_{resp} and on its duration. We can also assess the reliability of each time point of the recording (including the TR, the drift, and any MPR-associated deviations present) by how well its derivative matches $\dot{G}_{resp}\left(t;\hat{\theta}_{resp}\right)$. This is done using another weighting function, defined by

$$\Gamma_i = \exp\left(-\left(\frac{\hat{u}_i - \dot{G}_{resp}\left(t;\hat{\theta}_{resp}\right)}{2\,std\left(\hat{u}_i - \dot{G}_{resp}\left(t;\hat{\theta}_{resp}\right)\right)}\right)^2\right).$$

We combine these weighting functions using the criterion that for a data point to be reliable, it must have either a large value of π^{peak} or π^{trough}, and a large value of Γ. It is implemented in the weighting function Ω, as follows

$$\Omega_i = \Gamma_i\left(\pi_i^{peak} + \pi_i^{trough} - \min_i\left(\pi_i^{peak}\right) - \min_i\left(\pi_i^{trough}\right)\right)$$

With Ω_i, we can fit the TR reliably in the presence of significant deviations from the model of Eq. (13). This is done by minimizing the error function

$$S_{resp}^{\Omega}\left(\theta_{resp}\right)=\phi\sum_{j}\Big[\ \phi\,\Omega_j^2\left(F_j-G_{resp}\left(t_j;\theta_{resp}\right)\right)^2+\Omega_j^2\left(\hat{u}_j-\dot{G}_{resp}\left(t_j;\theta_{resp}\right)\right)^2 + \kappa\phi\left(D_2\left(t_k-t_2;a_2,\tau_2,m_2\right)\right)^2\Big]+\frac{\lambda}{\phi^2}S_{drift}\left(\theta_{drift}\right) \tag{15}$$

5.3.5.1 Identifying coherent oscillations

Not all MPRs correspond to periodic oscillations (Thurley et al., 2014). To address this, the algorithm reports two sets of MPR parameters, the first to describe all the peaks detected within a MPR, and the second to describe the subset of coherent peaks present within the same MPR. This section focuses on how the subset of coherent oscillatory peaks is identified. We use a clustering algorithm which is an unsupervised learning technique that enables for the identification of natural groupings or patterns with a defined data set. By minimizing (15), we obtain the most reliable estimate of the TR (specified by the model G_{resp} and its optimal parameter set $\hat{\theta}_{resp}^{\Omega}$), which we take to be the baseline of the MPR-associated deviations. Given the estimate $G_{resp}\left(t;\theta_{resp}^{\Omega}\right)$, we repeat the peak finding steps. To determine whether or not the detected deviations represent oscillations, we use a Gaussian mixture model clustering technique. It groups together (in clusters) peaks and troughs with comparable periods, T (determined by the difference between two consecutive peak or trough times; i.e., $\tilde{t}^{\,peak}$ or $\tilde{t}^{\,trough}$) and FWHM, ξ. Two adjacent deviations are deemed to be coherent oscillations if they are grouped in the same cluster. In situations where the period or FWHM are modulated throughout time, Gaussian clustering technique may not be able to cluster all coherent oscillations adequately. We therefore process clusters by defining period- and FWHM-trends for all coherent oscillations. If this trend can accurately predict the period and FWHM of the first deviation of an adjacent cluster, then both clusters are deemed to form a set of coherent oscillations. This is repeated for all pairs of adjacent clusters, progressively updating the set of coherent oscillations with those previously deemed incoherent at prior steps.

This procedure use the Expectation Maximization (EM) clustering algorithm (McLachlan & Peel, 2005) to cluster the period and FWHM of a potential oscillatory MPRs, and to determine the optimal number of clusters using gap statistic (Tibshirani, Walther, & Hastie, 2001). It allows for

a reliable separation of oscillatory data from recording artifacts or non-oscillatory MPRs with visually different properties. It also yields a set of $\hat{N}_{peak}$ peaks ($\hat{N}_{trough}$ troughs) occurring at times $\hat{t}^{peak}$ ($\hat{t}^{trough}$), which together represent coherent oscillations. Having determined the properties of the individual features making up the oscillations, they can be used to quantify the properties of the oscillations.

5.3.5.2 Characterizing oscillatory parameters

In order for the algorithm to report the oscillatory properties of a signal, the MPR-associated deviations must satisfy $\widetilde{N} > 2$, for the set of MPR parameters describing all detected peaks. If these deviations form a coherent set of oscillations, a second set of MPR parameters characterizing this coherent oscillatory behavior is also reported. In both instances, the following parameters will be reported: the number of oscillations (N_{osc}), the average magnitude of the oscillations (defined as $E^{peak} + E^{trough}$), the average period of oscillation (T), the standard deviation of the periodicity (σ_T), the total time for which the oscillations persist (defined as $\ell_{osc} = \hat{t}^{peak}_{\hat{N}_{peak}} - \hat{t}^{peak}_{1}$), and the mean duty cycle parameter (given by ξ^{peak}/T) (Smedler & Uhlen, 2014).

5.3.5.3 MPR parameter validation: N_{osc}, E, T, ℓ_{osc} and ξ^{peak}/T

Manual estimates of N_{osc} is determined by counting the number of discernable peaks within the signal. The slope of correlation was 0.85 with an r^2-score of 0.78 (**Fig 5-6A**, *left*). The mean difference between manual and automated estimates was 15% with an interval of agreement ranging from -39% to 69% (**Fig 5-6A**, *right*). The peak magnitude of the oscillations, E, is manually estimated by the mean change between peak maxima and their subsequent trough minima, after correcting for a non-stationary baseline that is often a consequence of a concurrent TR. For most signals the non-stationary baseline can be manually estimated to be linear. However, there are a few cases where an estimate of an exponential baseline is required. The correlation between manual and automated estimates was relatively strong, with an r^2-value of 0.92 and a slope of 1.08 (**Fig 5-6B**, *left*). The agreement analysis on the other hand revealed relatively no bias, with a mean difference of -2% and limit of agreement ranging from -48% to 44% difference (**Fig 5-6B**, *right*). The periodicity is manually estimated by the average time between adjacent peaks. The linear relationship was slightly weaker with a r^2-value of 0.55 and slope of 0.65 (**Fig 5-6C**,

left). The mean difference between manual and automated estimates was negligible, at only 0.3%, indicating an absence systematic bias, and the limits of agreement spanned from -54% to 54% difference (**Fig 5-6C**, *right*). The standard deviation of periodicity was obtained from the same set of periods used to estimate the mean period. The linear slope was 0.77 and the r^2-value was 0.77 (**Fig 5-6D**, *left*). Similar to periodicity, the mean difference for the standard deviation of periodicity was a negligible -0.4%, with limits of agreement ranging from -61 to 62% difference (**Fig 5-6D**, *right*). Oscillatory persistence is chosen to describe how long oscillations are sustained within a given recording and is estimated as the elapsed time between the first and last discernable peaks in the MPR. The correlation between manual and automated estimates was supported by a r^2-value of 0.79 and slope of 0.85 (**Fig 5-6E**, *left*). The mean difference between paired estimates was only -5.3% with a limit of agreement between -47% and 37% difference (**Fig 5-6E**, *right*). Finally, the duty cycle is manually estimated by the ratio between ξ^{peak} and T. ξ^{peak} is manually determined by the mean FWHM of individual oscillatory peaks and the same T value obtained above is used to calculate ξ^{peak} /T. The linear relationship between manual and automated estimated of ξ^{peak} /T was decidedly weak with a slope of 0.51 and r^2 of 0.26 (**Fig 5-6F**, *left*). The Bland Altman analysis, however, suggests that there was a systematic bias that could explain the poorer correlation results. The mean difference between manual and automated estimated was -19% with a limit of agreement between -69% and 31% (**Fig 5-6F**, *right*).

The MPR parameter validation described above focuses on the set of parameter estimates describing all the peaks in the MPR, rather than the subset of coherent oscillations. This is because manual detection of each peak in the MPR is less subjective than detecting only the coherent peaks in the MPR. Since the algorithm sub-selects the coherent oscillatory peaks from the initial set of identified deviations, the performance reported for the characterization of all peaks extends to the subset of coherent oscillations. Furthermore, as expected, the standard deviation of the periodicity is consistently lower for coherent oscillations when compare to the σ_T reported for all peaks in the same MPR (i.e. more regular periodicities result in lower standard deviations).

To ensure confidence in the reported MPR parameters, users of this algorithm are urged to visually verify the quality of the signal fittings to determine whether the algorithm is characterizing their peaks of interest, as these may not always coincide with the most prevalent oscillatory component of the signal (Thurley et al., 2014). Furthermore, N_{osc} reported for all peaks and coherent peaks

can be compared to be aware of how many peaks were omitted during the clustering step. Collectively, the information reported for MPRs is sufficient for the informed analysis of a diverse selection of MPRs, including those that exhibit coherent oscillations and those that do not.

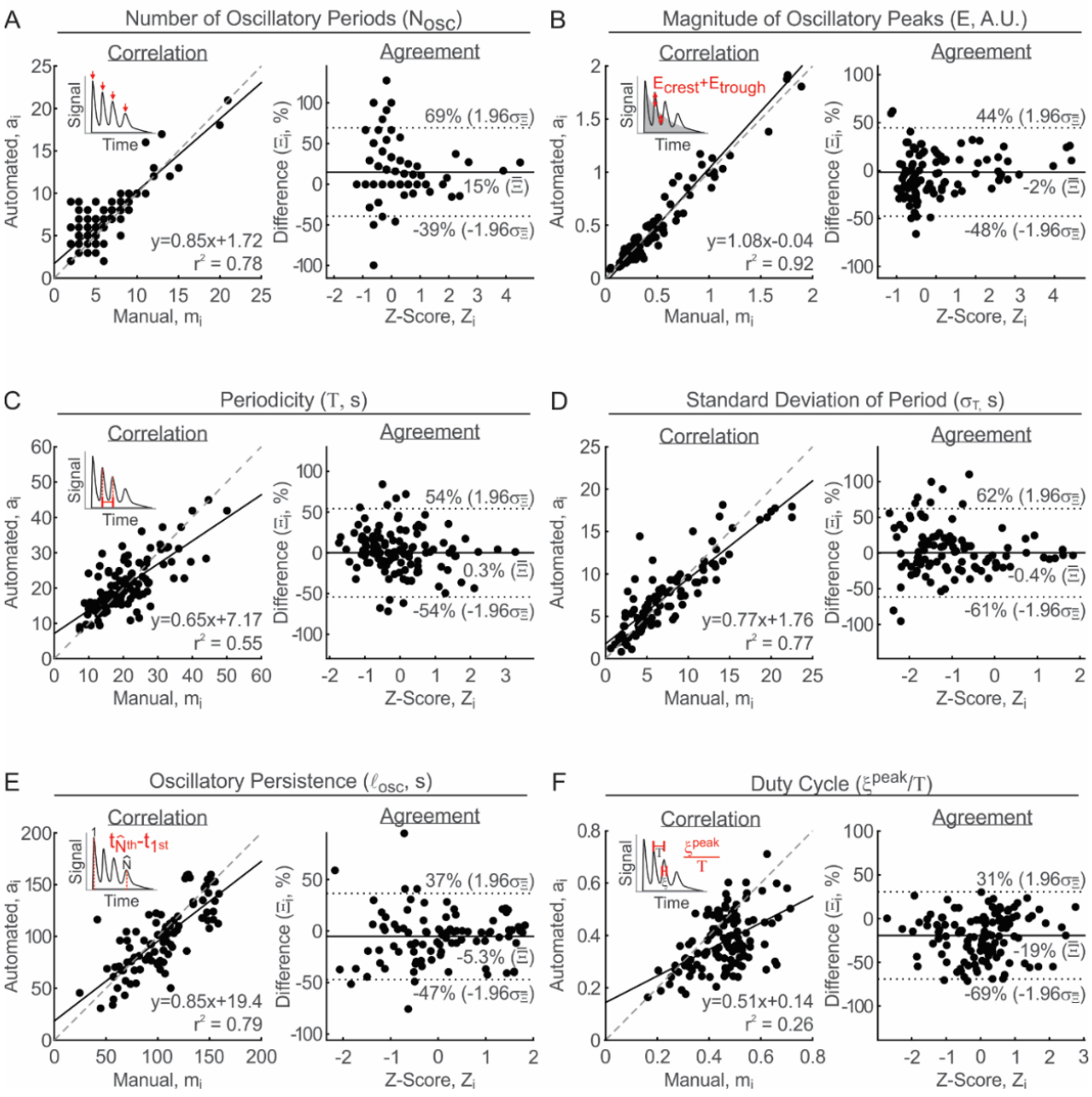

Figure 5-6. Validation of MPR parameter measurements. Parameters were estimated manually and then compared with automated-estimated values using correlation analysis (*left*, *solid line*: linear regression line; *broken line*: line of equality) and Bland-Altman analysis (*right*, *solid line*: mean percent difference, $\overline{\Xi}$; *broken line*: limits of agreement, $\overline{\Xi} \pm 1.96\,\sigma_{\Xi}$). **(A)** Number of oscillatory periods N_{osc}. **(B)** Magnitude of oscillatory peaks, E. **(C)** Periodicity, T. **(D)** Standard Deviation of Period, σ_T. **(E)** Oscillatory persistence, ℓ_{osc}. **(F)** Duty cycle, ξ^{peak}/T.

5.3.6 Application to pathophysiology

In the context of bone physiology, the deleterious consequences of disrupting extracellular nucleotide-mediated cross talk have been highlighted by the emergence of P2 receptor knockout mouse models (Lenertz et al., 2015). P2 receptors are particularly sensitive to changes in the extracellular milieu. Consequently, P2 receptor pathophysiology is often coupled to events that influence the extracellular composition, thereby compromising processes regulated by the P2 receptor network. In particular, changes in extracellular pH alter P2 receptor function (Gerevich et al., 2007; King, Wildman, Ziganshina, Pintor, & Burnstock, 1997; Langfelder, Okonji, Deca, Wei, & Glitsch, 2015; Wildman, 2009). Such conditions arise from pathological acidosis that is commonly caused by systemic acid-base disturbances, such as metabolic or respiratory acidosis (Berend, de Vries, & Gans, 2014; Krieger, Frick, & Bushinsky, 2004; Miller, 2012). More localized acidifications can also be associated with tumors (Kato et al., 2013; Martin & Jain, 1994). Since the skeleton is a common metastatic site for cancer, and participates in systemic buffering of protons, the effect of acidosis on the skeletal system is of particular interest. On the cellular level, acidosis promotes the activation of osteoclasts, resulting in elevated bone resorption which manifests itself in osteoporotic phenotype (Ahn, Kim, Lee, Kim, & Jeong, 2012; Bushinsky & Frick, 2000; Gasser, Hulter, Imboden, & Krapf, 2014; Krieger, Bushinsky, & Frick, 2003). However, it remains unclear whether the P2 receptor network plays a direct role in this cascade of events. The most immediate influence of acidosis on the P2-receptor network can be studied at the level of the $[Ca^{2+}]_i$ response evoked immediately upon application of a purinergic agonist.

We investigated the effect of acidosis on ATP-mediated $[Ca^{2+}]_i$ responses in bone-marrow derived osteoclast precursors to demonstrate the applicability of the developed algorithm. The application of ATP (100 nM to 10 mM) to the fura2-loaded osteoclast precursors evoked a $[Ca^{2+}]_i$ TR in a dose-dependent manner in control and acidosis conditions (**Fig 5-7A, B**). The response amplitudes under acidic conditions were virtually indistinguishable from the control for ATP concentrations up to 10 µM. However, above this threshold concentration, the amplitude of the control responses continued to increase with rising concentrations of ATP, while $[Ca^{2+}]_i$ responses under acidic conditions plateaued at 10 µM (**Fig 5-7C**). With respect to the AUC of the $[Ca^{2+}]_i$ responses, the observed differences between the two conditions were more gradual with a diverging trend beginning as low as 1 µM ATP and becoming more prominent at high ATP (**Fig 5-7D**). Finally,

acidosis was found to have no significant effect on the periodicity of the oscillatory responses (**Fig 5-7E**).

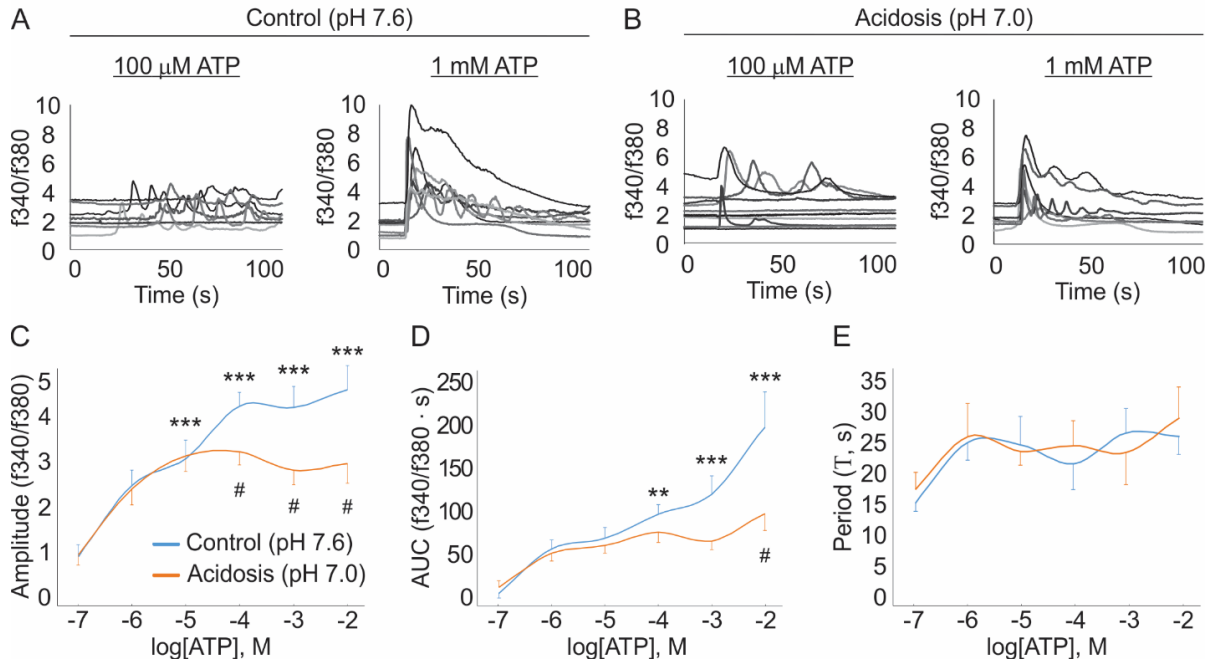

Figure 5-7. Algorithm application in characterization of pathological states. ATP (100 nM – 10 mM) was applied to Fura-2 loaded osteoclast precursors, under control (pH 7.6) and acidosis (pH 7.0) conditions, and $[Ca^{2+}]_i$ responses were recorded. Algorithm was used to obtain estimates for amplitude, AUC and periodicity. **(A)** Representative $[Ca^{2+}]_i$ response traces for 100 μM and 1 mM ATP under control conditions. **(B)** Representative $[Ca^{2+}]_i$ response traces for 100 μM and 1 mM ATP under acidosis conditions. Data are mean± S.E.M. The effect of ATP under control conditions was examined for statistical significance using one-way ANOVA (*). The effect of acidosis on ATP-mediated responses was determined using two-way ANOVA (#). The Bonferroni test was used for post hoc multi-comparison analysis. **(C)** Amplitude dose-response curves. Effect of ATP under control conditions, $p<0.001$, one-way ANOVA. Effect of acidosis on ATP-mediated responses, $p<0.05$, two-way ANOVA. **(D)** AUC dose-response curves. Effect of ATP under control conditions, $p<0.001$, one-way ANOVA. Effect of acidosis on ATP-mediated responses, $p<0.05$, two-way ANOVA. **(E)** Period dose-response curves. Results were not significant

These findings support that acidosis, while having no effect on ATP-mediated $[Ca^{2+}]_i$ responses at lower ATP concentration, significantly attenuates the magnitude of $[Ca^{2+}]_i$ transients responding to higher ATP concentrations (>10 μM ATP). Within the limited scope of this study that is focused on the development of a data analysis algorithm, we can only hypothesize on the mechanism by which these differences arise. One possibility is that the rise in extracellular $[H^+]$ has a significant influence on the electro-chemical gradient across the cellular membrane, which

may consequently alter the extent of calcium flux across certain ionotropic P2X receptors. Since the oscillations are commonly driven by inositol triphosphate-mediated release of calcium from internal calcium stores (i.e. isolated from extracellular [H^+]), it may explain why the oscillatory behavior is not affected by acidosis. Alternatively, there may exist a subset of P2 receptors that are sensitive to fluctuations in extracellular [H^+], while P2-receptors involved in oscillatory behaviour and/or responses to lower ATP concentrations (≤ 10 μM) are resilient to such changes. Regardless of the underlying mechanism, these results highlight that the P2 receptor network can be differentially modulated by extracellular pH.

5.4 Discussion

This paper presents an autonomous signal-processing algorithm capable of robustly removing signal-contaminating noise and delineating the various components seen in a calcium response, including non-stationary drift, TRs and MPRs (possibly caused by flickers, puffs and sparks) sampled with at least twice the Nyquist frequency. By fitting piece-wise defined model functions to data, the algorithm also extracts estimates for the parameters that are relevant to the characterization of cellular transient dynamics. Any time-series recordings can be used as an input for the algorithm, provided that they resemble a single or multi-peak transient response. As demonstrated in the validation process, manual estimation of certain parameters has an inherent degree of subjectivity and measurement error associated with it. In particular, the manual evaluations of AUC values, decay constant and the time of onset, as well as most of the MPR-parameter values, were found to rely on subjective estimates and thus lacked true accuracy and consistency. Because of such limitation in the validation method, manual-estimates are to be recognized as representative estimates, rather than accurate values for these parameters. Consequently, validation method applied here should be considered as a comparison against imperfect estimates.

Nevertheless, our analysis of the automated method has verified that the algorithm performs within acceptable margins of agreement when compared to manual analysis. Regarding the response detection capabilities, the algorithm behaves conservatively compared to manual assessments, especially when presented with low-magnitude TRs or ambiguous response signals. Most importantly, our algorithm has been validated against experimental $[Ca^{2+}]_i$ recording data, rather than simulated data, ensuring that the method is capable of handling variations in drift and noise

that realistically reflect signal contaminations of experimental data acquisition. We have demonstrated that this automated methodology is effective in analyzing empirical data, providing quantitative insights about them and identifying differences between them.

A particularly unique feature of this algorithm is its capacity to characterize the magnitude and temporal characteristics of MPRs exhibiting stochastic and deterministic behaviour. It is well established that a diverse amount of biochemical processes can be amplitude- and/or frequency-modulated (Adachi, Kindzelskii, Ohno, Yadomae, & Petty, 1999; Micali, Aquino, Richards, & Endres, 2015). To analyse such oscillatory data, the fast Fourier transform (FFT) is commonly used, which allows for the conversion of a signal from its time domain, into the frequency domain. Unfortunately, the variance in the frequency domain is proportional to the number of repetitive components in the time-domain. Therefore, if the oscillatory signals present few repetitive components then reliable resolution of the true periodicity of the signal is unachievable. To circumvent the limitations inherent to FFT, we apply the MATLAB "findpeaks()" function to identify peaks of interest. To isolate underlying coherent oscillations that are often present, we applied a clustering method. This is based on the principle of clustering deviations from baseline according to their temporal offset and respective FWHM. The advantage of this approach is that it allows for the reliable detection of periodic peaks, even in the presence of stochastic discharges, as is often the case in experimental recordings. Secondly, comparison of the set of MPR parameters for all peaks and subset of coherent peaks allows users to quantify the extent of stochastic activity within MPRs. Alternatively, the relationship between mean and standard deviation of periodicity in a MPR has been previously used to reveal the contribution of stochastic processes to the periodicity (Thurley et al., 2014). We anticipate this methodology will contribute to the comprehensive analysis of diverse MPRs.

Calcium signalling is by no means unique to the P2-receptor network, but rather represents the most ubiquitous and versatile messenger found in biological systems. All kinds of extracellular signals exploit calcium as a secondary messenger, including P2 agonists (i.e. ATP, ADP, UTP and UDP), endothelin-1, oxotremorine-M, norephinephrine, thrombin, PDGF, bombensin, (Balla et al., 1991; Burnstock, 2004; Palmer, 1994). The universal involvement of calcium ranges from basic physiological processes such as muscle contraction, neuronal discharge and pancreatic secretion, to early development events including mammalian egg fertilization and embryonic

pattern formation (Berridge, Lipp, & Bootman, 2000). Calcium signalling is also known to be impaired in various pathological states, as suggested for metabolic acidosis in this study, chronic renal failure (Massry et al., 1995), Alzheimer's (Brawek et al., 2014), Diabetes (Chen, Kold-Petersen, Laher, Simonsen, & Aalkjaer, 2015) and zinc deficiency (O'Dell & Browning, 2013). However, despite all that we know about calcium's role in biological processes, there remains ongoing debate on how calcium signals robustly encode information while still exhibiting a large degree of heterogeneity within and between various cellular populations. Many theories have been proposed to establish how information can be encoded. Some of these involve encoding information on the basis of calcium binding cooperativity (Larsen, Olsen, & Kummer, 2004), amplitude and frequency modulation (De Pitta, Volman, Levine, & Ben-Jacob, 2009), changes in spike time variation (Thurley et al., 2014) and signal integration (Hannanta-anan & Chow, 2016). In order to reconcile these theories and establish a universal syntax for calcium-encoded information, tools such as this algorithm will aid in the large-scale analysis of experimental data sets required for the validation of mathematical models.

The consideration of signalling nuances that are specifically found in physiological signals, but may or may not be present in non-biological signals, was a critical step in the development of this algorithm. As demonstrated in this study, physiological signals were decomposed into their elementary components and mathematically generalized to enable for the computational reconstruction of a diverse range of signature forms. In doing so, we were able to provide a foundation for further modeling of the nonlinear multi-parametric physiological signals. This study demonstrates that the accurate description of complex physiological signals is non-trivial, but rather an extensive mathematical undertaking. Therefore, we believe that, beyond serving the purpose of a signal-processing tool, this algorithm will also contribute to future efforts to modeling physiological signals.

5.5 Concluding Remarks

In summary, we have detailed an open-source MATLAB algorithm intended to facilitate the analysis of time-series recordings (User guide provided in **Appendix A4**). With minimal user-input required, this tool dramatically decreases analysis time and ensures consistency in parameter characterization of complex physiological signals. This algorithm is capable of handling noise and drift and robustly characterizes the magnitude and kinetics of dynamic processes, outputting the

amplitude, time of onset (t_{onset}), activation time ($t_{10\%-90\%}$), full-width half-max (FWHM), area under the curve (AUC), and decay constant (τ_{decay}). In the presence of MPR, six additional parameters are characterized which include number of oscillations (N_{osc}), magnitude of oscillatory peaks (E), periodicity (T), standard deviation of periodicity (σ_T), oscillatory persistence (ℓosc) and the duty cycle (ξ^{peak}/T). This algorithm is not limited to any specific data-type, but $[Ca^{2+}]_i$ recordings represent an obvious application. In addition to calcium imaging, other imaging modalities such as adapted fluorescence resonance energy transfer (FRET) biosensors, real-time bioluminescence and voltage and current measurements can generate time-series data for which characterization of signal magnitude and kinetics can provide valuable information. As data acquisition becomes more efficient and data sets become increasingly complex, automated analysis will serve as an essential tool for conducting basic research and clinical screening.

5.6 Materials and Methods

5.6.1 Cell culture

All procedures were approved by McGill University's Animal Care Committee and complied with the ethical guidelines of the Canadian Council on Animal Care. Bone marrow precursor cells were isolated from the femur and tibia of 6 week old FVB mice (Charles River), plated at a density of 7.5 x 10^3 on 48-well glass-bottom plates (No. 1.5 Coverslip, 6 mm glass diameter, uncoated, MatTek Corp.) and cultured for three days in αMEM (12,000-022, GIBCO) supplemented with 10% FBS (080152, Wisent), 1% sodium pyruvate (600-110-UL, Wisent), 1% penicillin streptomycin (450-201-EL, Wisent), 50 ng/mL MCSF (300-25, Peprotech) and 50 ng/mL RANKL according to the protocol previously described (Boraschi-Diaz & Komarova, 2016).

5.6.2 Intracellular calcium measurements

After 3 days of culture, osteoclast precursors were loaded with fura2-AM, a ratiometric fluorescent calcium dye (F1221, Invitrogen), incubated at room temperature for 30 min and washed twice with physiological solution (130 mM NaCl; 5 mM KCl; 1 mM $MgCl_2$; 1 mM $CaCl_2$; 10 mM glucose; 20 mM HEPES, pH 7.6). The final volume of 270 µL of physiological solution at pH 7.6 or pH 7.0 was added and cells were acclimatized for 10 min to reduce the effects of mechanical agitation that resulted from fura2-AM loading and washing. 10X ATP (Sigma) solutions were prepared in

physiological solution at corresponding pH and 30 µL was added after 10 s of baseline $[Ca^{2+}]_i$ recording to obtain a 1X dilution (i.e. final concentrations ranging from 1 µM - 10 mM ATP). $[Ca^{2+}]_i$ was imaged for an additional 110 s at a sampling rate of 2 images per second using a fluorescent inverted microscope (T2000, Nikon). The excitation wavelength was alternated between 340 and 380 nm using an ultra-high-speed wavelength switching illumination system (Lambda DG-4, Quorum Technologies). Regions of interest (ROI) were manually defined and the ratio of the fluorescent emission at 510 nm, following 340 and 380 nm excitation (f340/f380), was calculated and exported using the imaging software (Volocity, Improvision). All data were imported into an excel spreadsheet for subsequent analysis.

5.6.3 Validation and statistical analysis

Algorithm performance was evaluated using the algorithm generated figures for 450 individual signal fitting that enabled retrospective visual examination of both response-detection and quality of parameter fitting. Manual and automated estimates were compared using a correlation plot and Bland Altman analysis (Bland & Altman, 1986) to assess the degree of correlation and agreement, respectively. For correlation analysis, the line of exact linear correlation (i.e. $y = x$) is plotted as a reference to assess deviation of the linear regression curve from the desired 1:1 relationship between the manual and automated estimates. For the Bland Altman analysis, we compared the automated (a) and manual (m) parameter estimates of the ith recording to obtain a Z-score, given by

$$\mathrm{Z_i} = \frac{x_i - \bar{x}}{\sigma_x}$$

where $x_i = (m_i + a_i)/2$ is the average value of the estimated parameter, $\bar{x}$ is the mean value of x averaged over all recordings, and σ_x is the standard deviation of x over all recordings. Furthermore, the percent difference, Ξ_i, of the ith recording is defined by

$$\Xi_i = \frac{\text{error}}{\text{average value}} \times 100\% = \frac{a_i - m_i}{x_i} \times 100\%.$$

Ξ_i versus Z_i were plotted to illustrate systematic biases. Negative values of Ξ_i were interpreted as manual estimates being greater than automated estimates, and vice versa. A quantitative estimate of the interval of agreement, within which 95% of differences lie, is defined by

$$95\%\ \text{interval of agreement} = \overline{\Xi} \pm 1.96\sigma_{\overline{\Xi}}$$

where $\overline{\Xi}$ is mean percent difference over all recordings and $\sigma_{\overline{\Xi}}$ is the standard deviation of $\overline{\Xi}$.

Experimental data were expressed as means ± S.E.M. Effect of ATP treatment under control conditions was evaluated using one-way ANOVA followed with Bonferroni *post hoc* test. The effect of acidosis was evaluated using two-way ANOVA with Bonferroni *post hoc* test. Results were accepted as significant at $p<0.05$. Statistical analysis was performed in MATLAB.

5.7 References

Abu Khamidakh, A. E., Juuti-Uusitalo, K., Larsson, K., Skottman, H., & Hyttinen, J. (2013). Intercellular Ca(2+) wave propagation in human retinal pigment epithelium cells induced by mechanical stimulation. *Exp Eye Res, 108*, 129-139. doi:10.1016/j.exer.2013.01.009

Adachi, Y., Kindzelskii, A. L., Ohno, N., Yadomae, T., & Petty, H. R. (1999). Amplitude and Frequency Modulation of Metabolic Signals in Leukocytes: Synergistic Role of IFN-γ in IL-6- and IL-2-Mediated Cell Activation. *The Journal of Immunology, 163*(8), 4367-4374.

Ahn, H., Kim, J. M., Lee, K., Kim, H., & Jeong, D. (2012). Extracellular acidosis accelerates bone resorption by enhancing osteoclast survival, adhesion, and migration. *Biochem Biophys Res Commun, 418*(1), 144-148. doi:10.1016/j.bbrc.2011.12.149

Appleby, P. A., Shabir, S., Southgate, J., & Walker, D. (2015). Sources of variability in cytosolic calcium transients triggered by stimulation of homogeneous uro-epithelial cell monolayers. *J R Soc Interface, 12*(105). doi:10.1098/rsif.2014.1403

Balla, T., Sim, S. S., Iida, T., Choi, K. Y., Catt, K. J., & Rhee, S. G. (1991). Agonist-induced calcium signaling is impaired in fibroblasts overproducing inositol 1,3,4,5-tetrakisphosphate. *J Biol Chem, 266*(36), 24719-24726.

Berend, K., de Vries, A. P., & Gans, R. O. (2014). Physiological approach to assessment of acid-base disturbances. *N Engl J Med, 371*(15), 1434-1445. doi:10.1056/NEJMra1003327

Berridge, M. J., Lipp, P., & Bootman, M. D. (2000). The versatility and universality of calcium signalling. *Nat Rev Mol Cell Biol, 1*(1), 11-21. doi:10.1038/35036035

Bland, J. M., & Altman, D. G. (1986). Statistical methods for assessing agreement between two methods of clinical measurement. *Lancet, 1*(8476), 307-310. doi:10.1016/S0140-6736(86)90837-8

Boraschi-Diaz, I., & Komarova, S. V. (2016). The protocol for the isolation and cryopreservation of osteoclast precursors from mouse bone marrow and spleen. *Cytotechnology, 68*(1), 105-114. doi:10.1007/s10616-014-9759-3

Brawek, B., Schwendele, B., Riester, K., Kohsaka, S., Lerdkrai, C., Liang, Y., & Garaschuk, O. (2014). Impairment of in vivo calcium signaling in amyloid plaque-associated microglia. *Acta Neuropathol, 127*(4), 495-505. doi:10.1007/s00401-013-1242-2

Bray, M. A., Geisse, N. A., & Parker, K. K. (2007). Multidimensional detection and analysis of Ca2+ sparks in cardiac myocytes. *Biophys J, 92*(12), 4433-4443. doi:10.1529/biophysj.106.089359

Burnstock, G. (2004). Introduction: P2 receptors. *Curr Top Med Chem, 4*(8), 793-803.

Burnstock, G., & Verkhratsky, A. (2009). Evolutionary origins of the purinergic signalling system. *Acta Physiol (Oxf), 195*(4), 415-447. doi:10.1111/j.1748-1716.2009.01957.x

Bushinsky, D. A., & Frick, K. K. (2000). The effects of acid on bone. *Curr Opin Nephrol Hypertens, 9*(4), 369-379. doi:10.1097/00041552-200007000-00008

Cao, D., Lin, G., Westphale, E. M., Beyer, E. C., & Steinberg, T. H. (1997). Mechanisms for the coordination of intercellular calcium signaling in insulin-secreting cells. *J Cell Sci, 110 (Pt 4)*, 497-504.

Chambolle, A., Caselles, V., Novaga, M., Cremers, D., & Pock, T. (2009). An introduction to Total Variation for Image Analysis.

Chartrand, R. (2007, Sept. 16 2007-Oct. 19 2007). *Nonconvex Regularization for Shape Preservation.* Paper presented at the 2007 IEEE International Conference on Image Processing.

Chartrand, R. (2011). Numerical Differentiation of Noisy, Nonsmooth Data. *ISRN Applied Mathematics, 2011*, 1-11. doi:10.5402/2011/164564

Chartrand, R., & Staneva, V. (2008). A quasi-newton method for total variation regulatrization of images corrupted by non-gaussian noise. *IET Image Processing, 2*(3), 1-6.

Chartrand, R., & Wohlberg, B. (2010). Total-variation regularization with bound constraints. In *Proceedings of IEEE International Conference on Acoustics, Speech, and Signal Processing (ICASSP)* (pp. 766-769). Dallas, TX, USA.

Chen, H., Kold-Petersen, H., Laher, I., Simonsen, U., & Aalkjaer, C. (2015). Impaired endothelial calcium signaling is responsible for the defective dilation of mesenteric resistance arteries from db/db mice to acetylcholine. *Eur J Pharmacol, 767*, 17-23. doi:10.1016/j.ejphar.2015.09.043

Churchill, G. C., Atkinson, M. M., & Louis, C. F. (1996). Mechanical stimulation initiates cell-to-cell calcium signaling in ovine lens epithelial cells. *J Cell Sci, 109 (2)*, 355-365.

Clapham, D. E. (2007). Calcium Signaling. *Cell, 131*(6), 1047-1058. doi:10.1016/j.cell.2007.11.028

De Pitta, M., Volman, V., Levine, H., & Ben-Jacob, E. (2009). Multimodal encoding in a simplified model of intracellular calcium signaling. *Cogn Process, 10 Suppl 1*, S55-70. doi:10.1007/s10339-008-0242-y

Dickinson, G. D., & Parker, I. (2013). Temperature dependence of IP3-mediated local and global Ca2+ signals. *Biophys J, 104*(2), 386-395. doi:10.1016/j.bpj.2012.12.024

Dupont, G., & Combettes, L. (2009). What can we learn from the irregularity of Ca2+ oscillations? *Chaos, 19*(3), 037112. doi:doi:http://dx.doi.org/10.1063/1.3160569

Dupont, G., Combettes, L., Bird, G. S., & Putney, J. W. (2011). Calcium Oscillations. *Cold Spring Harb Perspect Biol, 3*(3), 10.1101/cshperspect.a004226 a004226. doi:10.1101/cshperspect.a004226

Ellefsen, K. L., Settle, B., Parker, I., & Smith, I. F. (2014). An algorithm for automated detection, localization and measurement of local calcium signals from camera-based imaging. *Cell Calcium, 56*(3), 147-156. doi:10.1016/j.ceca.2014.06.003

Frame, M. K., & de Feijter, A. W. (1997). Propagation of mechanically induced intercellular calcium waves via gap junctions and ATP receptors in rat liver epithelial cells. *Exp Cell Res, 230*(2), 197-207. doi:10.1006/excr.1996.3409

Francis, M., Waldrup, J. R., Qian, X., Solodushko, V., Meriwether, J., & Taylor, M. S. (2016). Functional Tuning of Intrinsic Endothelial Ca2+ Dynamics in Swine Coronary Arteries. *Circ Res, 118*(7), 1078-1090. doi:10.1161/CIRCRESAHA.115.308141

Fritzsche, M., Fernandes, R. A., Colin-York, H., Santos, A. M., Lee, S. F., Lagerholm, B. C., . . . Eggeling, C. (2015). CalQuo: automated, simultaneous single-cell and population-level quantification of global intracellular Ca2+ responses. *Sci Rep, 5*, 16487. doi:10.1038/srep16487

Gallagher, J. A., & Buckley, K. A. (2002). Expression and function of P2 receptors in bone. *J Musculoskelet Neuronal Interact, 2*(5), 432-439.

Gasser, J. A., Hulter, H. N., Imboden, P., & Krapf, R. (2014). Effect of chronic metabolic acidosis on bone density and bone architecture in vivo in rats. *Am J Physiol Renal Physiol, 306*(5), F517-524. doi:10.1152/ajprenal.00494.2013

Gerevich, Z., Zadori, Z. S., Koles, L., Kopp, L., Milius, D., Wirkner, K., . . . Illes, P. (2007). Dual effect of acid pH on purinergic P2X3 receptors depends on the histidine 206 residue. *J Biol Chem, 282*(47), 33949-33957. doi:10.1074/jbc.M705840200

Hannanta-anan, P., & Chow, Brian Y. (2016). Optogenetic Control of Calcium Oscillation Waveform Defines NFAT as an Integrator of Calcium Load. *Cell Systems, 2*(4), 283-288. doi:10.1016/j.cels.2016.03.010

Hansen, M., Boitano, S., Dirksen, E. R., & Sanderson, M. J. (1993). Intercellular calcium signaling induced by extracellular adenosine 5'-triphosphate and mechanical stimulation in airway epithelial cells. *J Cell Sci, 106 (Pt 4)*, 995-1004.

Isakson, B. E., Evans, W. H., & Boitano, S. (2001). Intercellular Ca2+ signaling in alveolar epithelial cells through gap junctions and by extracellular ATP. *Am J Physiol Lung Cell Mol Physiol, 280*(2), L221-228.

James, L. R., Andrews, S., Walker, S., de Sousa, P. R., Ray, A., Russell, N. A., & Bellamy, T. C. (2011). High-throughput analysis of calcium signalling kinetics in astrocytes stimulated with different neurotransmitters. *PLoS ONE, 6*(10), e26889. doi:10.1371/journal.pone.0026889

Jorgensen, N. R., Geist, S. T., Civitelli, R., & Steinberg, T. H. (1997). ATP- and gap junction-dependent intercellular calcium signaling in osteoblastic cells. *J Cell Biol, 139*(2), 497-506. doi:10.1083/jcb.139.2.497

Jorgensen, N. R., Teilmann, S. C., Henriksen, Z., Civitelli, R., Sorensen, O. H., & Steinberg, T. H. (2003). Activation of L-type calcium channels is required for gap junction-mediated intercellular calcium signaling in osteoblastic cells. *J Biol Chem, 278*(6), 4082-4086. doi:10.1074/jbc.M205880200

Juhola, M., Penttinen, K., Joutsijoki, H., Varpa, K., Saarikoski, J., Rasku, J., . . . Aalto-Setala, K. (2015). Signal analysis and classification methods for the calcium transient data of stem cell-derived cardiomyocytes. *Comput Biol Med, 61*, 1-7. doi:10.1016/j.compbiomed.2015.03.016

Kaczmarek-Hajek, K., Lorinczi, E., Hausmann, R., & Nicke, A. (2012). Molecular and functional properties of P2X receptors--recent progress and persisting challenges. *Purinergic Signal, 8*(3), 375-417. doi:10.1007/s11302-012-9314-7

Kato, Y., Ozawa, S., Miyamoto, C., Maehata, Y., Suzuki, A., Maeda, T., & Baba, Y. (2013). Acidic extracellular microenvironment and cancer. *Cancer Cell Int, 13*(1), 89. doi:10.1186/1475-2867-13-89

King, B. F., Wildman, S. S., Ziganshina, L. E., Pintor, J., & Burnstock, G. (1997). Effects of extracellular pH on agonism and antagonism at a recombinant P2X2 receptor. *Br J Pharmacol, 121*(7), 1445-1453. doi:10.1038/sj.bjp.0701286

Koshimizu, T., Koshimizu, M., & Stojilkovic, S. S. (1999). Contributions of the C-terminal domain to the control of P2X receptor desensitization. *J Biol Chem, 274*(53), 37651-37657.

Krieger, N. S., Bushinsky, D. A., & Frick, K. K. (2003). Cellular mechanisms of bone resorption induced by metabolic acidosis. *Semin Dial, 16*(6), 463-466. doi:10.1046/j.1525-139x.2003.16100.x

Krieger, N. S., Frick, K. K., & Bushinsky, D. A. (2004). Mechanism of acid-induced bone resorption. *Curr Opin Nephrol Hypertens, 13*(4), 423-436. doi:10.1097/01.mnh.0000133975.32559.6b

Langfelder, A., Okonji, E., Deca, D., Wei, W. C., & Glitsch, M. D. (2015). Extracellular acidosis impairs P2Y receptor-mediated Ca(2+) signalling and migration of microglia. *Cell Calcium, 57*(4), 247-256. doi:10.1016/j.ceca.2015.01.004

Larsen, A. Z., Olsen, L. F., & Kummer, U. (2004). On the encoding and decoding of calcium signals in hepatocytes. *Biophys Chem, 107*(1), 83-99. doi:10.1016/j.bpc.2003.08.010

Lenertz, L. Y., Baughman, C. J., Waldschmidt, N. V., Thaler, R., & van Wijnen, A. J. (2015). Control of bone development by P2X and P2Y receptors expressed in mesenchymal and hematopoietic cells. *Gene, 570*(1), 1-7. doi:10.1016/j.gene.2015.06.031

Li, F., Shen, C., Fan, J., & Shen, C. (2007). Image restoration combining a total variational filter and a fourth-order filter. *Journal of Visual Communication and Image Representation, 18*(4), 322-330. doi:10.1016/j.jvcir.2007.04.005

Lock, J. T., Ellefsen, K. L., Settle, B., Parker, I., & Smith, I. F. (2015). Imaging local Ca2+ signals in cultured mammalian cells. *J Vis Exp*(97). doi:10.3791/52516

Marquardt, D. W. (1963). An Algorithm for Least-Squares Estimation of Nonlinear Parameters. *Journal of the Society for Industrial and Applied Mathematics, 11*, 431-441. doi:10.1137/0111030

Martin, G. R., & Jain, R. K. (1994). Noninvasive Measurement of Interstitial pH Profiles in Normal and Neoplastic Tissue Using Fluorescence Ratio Imaging Microscopy. *Cancer Research, 54*(21), 5670-5674.

Massry, S. G., Klin, M., Ni, Z., Tian, J., Kedes, L., & Smogorzewski, M. (1995). Impaired agonist-induced calcium signaling in hepatocytes from chronic renal failure rats. *Kidney International, 48*(4), 1324-1331. doi:http://dx.doi.org/10.1038/ki.1995.417

McLachlan, G., & Peel, D. (2005). ML Fitting of Mixture Models. In *Finite Mixture Models* (pp. 40-80): John Wiley & Sons, Inc.

Micali, G., Aquino, G., Richards, D. M., & Endres, R. G. (2015). Accurate Encoding and Decoding by Single Cells: Amplitude Versus Frequency Modulation. *PLoS Computational Biology, 11*(6), e1004222. doi:10.1371/journal.pcbi.1004222

Miller, P. D. (2012). Unrecognized and unappreciated secondary causes of osteoporosis. *Endocrinol Metab Clin North Am, 41*(3), 613-628. doi:10.1016/j.ecl.2012.05.005

The Levenberg-Marquardt algorithm: Implementation and theory 105-116 (Springer Berlin Heidelberg 1978).

Nobile, M., Monaldi, I., Alloisio, S., Cugnoli, C., & Ferroni, S. (2003). ATP-induced, sustained calcium signalling in cultured rat cortical astrocytes: evidence for a non-capacitative, P2X7-like-mediated calcium entry. *FEBS Lett, 538*(1-3), 71-76. doi:10.1016/s0014-5793(03)00129-7

O'Dell, B. L., & Browning, J. D. (2013). Impaired Calcium Entry into Cells Is Associated with Pathological Signs of Zinc Deficiency. *Advances in Nutrition: An International Review Journal, 4*(3), 287-293. doi:10.3945/an.112.003624

Oh, S., Woo, H., Yun, S., & Kang, M. (2013). Non-convex hybrid total variation for image denoising. *Journal of Visual Communication and Image Representation, 24*(3), 332-344. doi:10.1016/j.jvcir.2013.01.010

Palmer, R. K. R. (1994). Agonist-specific calcium signaling and phosphoinositide hydrolysis in human SK-N-MCIXC neuroepithelioma cells. *Journal of Neurochemistry, 63*(6), 2099-2107.

Patel, T. P., Man, K., Firestein, B. L., & Meaney, D. F. (2015). Automated quantification of neuronal networks and single-cell calcium dynamics using calcium imaging. *J Neurosci Methods, 243*, 26-38. doi:10.1016/j.jneumeth.2015.01.020

Picht, E., Zima, A. V., Blatter, L. A., & Bers, D. M. (2007). SparkMaster: automated calcium spark analysis with ImageJ. *Am J Physiol Cell Physiol, 293*(3), C1073-1081. doi:10.1152/ajpcell.00586.2006

Rast, G., Weber, J., Disch, C., Schuck, E., Ittrich, C., & Guth, B. D. (2015). An integrated platform for simultaneous multi-well field potential recording and Fura-2-based calcium transient ratiometry in human induced pluripotent stem cell (hiPSC)-derived cardiomyocytes. *J Pharmacol Toxicol Methods, 75*, 91-100. doi:10.1016/j.vascn.2015.04.005

Rice, S. O. (1973). Efficient Evaluation of Integrals of Analytic Functions by the Trapezoidal Rule. *Bell System Technical Journal, 52*(5), 707-722. doi:10.1002/j.1538-7305.1973.tb01986.x

Romanello, M., & D'Andrea, P. (2001). Dual mechanism of intercellular communication in HOBIT osteoblastic cells: a role for gap-junctional hemichannels. *J Bone Miner Res, 16*(8), 1465-1476. doi:10.1359/jbmr.2001.16.8.1465

Ruffinatti, F. A., Lovisolo, D., Distasi, C., Ariano, P., Erriquez, J., & Ferraro, M. (2011). Calcium signals: analysis in time and frequency domains. *J Neurosci Methods, 199*(2), 310-320. doi:10.1016/j.jneumeth.2011.05.009

Shabir, S., & Southgate, J. (2008). Calcium signalling in wound-responsive normal human urothelial cell monolayers. *Cell Calcium, 44*(5), 453-464. doi:10.1016/j.ceca.2008.02.008

Skupin, A., Kettenmann, H., Winkler, U., Wartenberg, M., Sauer, H., Tovey, S. C., . . . Falcke, M. (2008). How Does Intracellular Ca(2+) Oscillate: By Chance or by the Clock? *Biophysical Journal, 94*(6), 2404-2411. doi:10.1529/biophysj.107.119495

Smedler, E., & Uhlen, P. (2014). Frequency decoding of calcium oscillations. *Biochim Biophys Acta, 1840*(3), 964-969. doi:10.1016/j.bbagen.2013.11.015

Smith, I. F., Wiltgen, S. M., & Parker, I. (2009). Localization of puff sites adjacent to the plasma membrane: functional and spatial characterization of Ca2+ signaling in SH-SY5Y cells utilizing membrane-permeant caged IP3. *Cell Calcium, 45*(1), 65-76. doi:10.1016/j.ceca.2008.06.001

Steele, E. M., & Steele, D. S. (2014). Automated detection and analysis of Ca(2+) sparks in x-y image stacks using a thresholding algorithm implemented within the open-source image analysis platform ImageJ. *Biophys J, 106*(3), 566-576. doi:10.1016/j.bpj.2013.12.040

Stoehr, A., Neuber, C., Baldauf, C., Vollert, I., Friedrich, F. W., Flenner, F., . . . Hansen, A. (2014). Automated analysis of contractile force and Ca2+ transients in engineered heart tissue. *Am J Physiol Heart Circ Physiol, 306*(9), H1353-1363. doi:10.1152/ajpheart.00705.2013

Sun, F., Berry, D. J., Leong, D. A., & Veldhuis, J. D. (1997). Recruitment of individually (all-or-none) responding cells, rather than amplitude enhancement, is the single-cell mechanism subserving the dose-responsive activation of intracellular calcium second messenger signaling by the human luteinizing-hormone receptor. *Endocrine, 7*(2), 219-226. doi:10.1007/bf02778144

Thurley, K., Tovey, S. C., Moenke, G., Prince, V. L., Meena, A., Thomas, A. P., . . . Falcke, M. (2014). Reliable encoding of stimulus intensities within random sequences of intracellular Ca2+ spikes. *Sci Signal, 7*(331), ra59. doi:10.1126/scisignal.2005237

Tibshirani, R., Walther, G., & Hastie, T. (2001). Estimating the number of clusters in a data set via the gap statistic. *Journal of the Royal Statistical Society: Series B (Statistical Methodology), 63*(2), 411-423. doi:10.1111/1467-9868.00293

Traub, J. F. (1964). On Lagrange-Hermite Interpolation. *Journal of the Society for Industrial and Applied Mathematics, 12*(4), 886-891. doi:10.1137/0112076

Vogel, C. (2002). *Computational Methods for Inverse Problem*. Philadelphia: Society for Industrial and Applied Mathematics.

Volonte, C., Amadio, S., D'Ambrosi, N., Colpi, M., & Burnstock, G. (2006). P2 receptor web: complexity and fine-tuning. *Pharmacol Ther, 112*(1), 264-280. doi:10.1016/j.pharmthera.2005.04.012

von Kugelgen, I., & Hoffmann, K. (2016). Pharmacology and structure of P2Y receptors. *Neuropharmacology, 104*, 50-61. doi:10.1016/j.neuropharm.2015.10.030

Wildman, S. S. P. (2009). Changes in tubular fluid pH and nucleotide concentration alter P2 receptor-mediated regulation of renal ENaC. *The FASEB Journal, 23*(1 Supplement), 602.605.

Wong, L. C., Lu, B., Tan, K. W., & Fivaz, M. (2010). Fully-automated image processing software to analyze calcium traces in populations of single cells. *Cell Calcium, 48*(5), 270-274. doi:10.1016/j.ceca.2010.09.008

Xing, S., Grol, M. W., Grutter, P. H., Dixon, S. J., & Komarova, S. V. (2016). Modeling Interactions among Individual P2 Receptors to Explain Complex Response Patterns over a Wide Range of ATP Concentrations. *Front Physiol, 7*, 294. doi:10.3389/fphys.2016.00294

Yan, Z., Khadra, A., Li, S., Tomic, M., Sherman, A., & Stojilkovic, S. S. (2010). Experimental characterization and mathematical modeling of P2X7 receptor channel gating. *J Neurosci, 30*(42), 14213-14224. doi:10.1523/jneurosci.2390-10.2010

Zhao, Z., Walczysko, P., & Zhao, M. (2008). Intracellular Ca2+ stores are essential for injury induced Ca2+ signaling and re-endothelialization. *J Cell Physiol, 214*(3), 595-603. doi:10.1002/jcp.21248

Chapter Six

Mechanically-Stimulated ATP Release from Murine Bone Cells is Regulated by a Balance of Injury and Repair

To address ***research objective 1***, this experimental study investigated how mechanical stimulation is associated with early signalling events in bone cells, specifically ATP release and calcium signalling. I used *in vitro* and *in vivo* approaches to understand how mechanical forces lead to ATP release within seconds of stimulation, as well as what controls the amount of ATP released from a stimulated cell. I identified a novel mechano-adaptive mechanism of ATP release from bone cells, in which the amount of ATP released is initially proportional to mechanically induced non-lethal membrane injury and is later limited by adaptive membrane repair through PKC-dependent vesicular exocytosis. The prevalence of membrane injury in osteocytes at physiological and supraphysiological mechanical strain levels was further investigated following *in vivo* cyclic compressive tibial loading. Supplemental materials for this chapter are provided in **Appendix A5**.

6.1 Abstract

Bone cells sense and actively adapt to physical perturbations to prevent critical damage. ATP release is among the earliest cellular responses to mechanical stimulation. Mechanical stimulation of a single murine osteoblast led to the release of 70 ± 24 amole ATP, which stimulated calcium responses in neighboring cells. Osteoblasts contained ATP-rich vesicles that were released upon mechanical stimulation. Surprisingly, interventions that promoted vesicular release reduced ATP

release, while inhibitors of vesicular release potentiated ATP release. Searching for an alternative ATP release route, we found that mechanical stresses induced reversible cell membrane injury *in vitro* and *in vivo*. Ca^{2+}/PLC/PKC-dependent vesicular exocytosis facilitated membrane repair, thereby minimizing cell injury and reducing ATP release. Priming cellular repair machinery prior to mechanical stimulation reduced subsequent membrane injury and ATP release, linking cellular mechanosensitivity to prior mechanical exposure. Thus, our findings position ATP release as an integrated readout of membrane injury and repair.

6.2 Introduction

The mechanical environment is an important determinant of bone health, as emphasized by a consistent bone loss in astronauts exposed to microgravity or in paralyzed or bedridden patients (Patel Nagaraja & Jo, 2014). Gravitational and muscle forces act on the skeleton during physical activity resulting in a complex combination of shear forces, strains and pressures. Bone-embedded osteocytes and bone-forming osteoblasts are widely regarded as the mechanosensitive cells in the skeletal system (Weinbaum, Cowin, & Zeng, 1994).

Following mechanical stimulation of rodent and human osteoblasts, transient intracellular free calcium ($[Ca^{2+}]_i$) elevations and ATP release are among the earliest detectable events, which result in autocrine and paracrine purinergic (P2) receptor signaling (Genetos, Geist, Dawei, Donahue, & Duncan, 2005; Robling & Turner, 2009; Romanello, Pani, Bicego, & D'Andrea, 2001). Vesicular release of lysosomes or secretory vesicles, or conductive release via channels such as Maxi anion channels, Volume-regulated anion channels, Connexins or Pannexins are the main mechanisms of regulated ATP release in mammalian cells (Burnstock & Verkhratskii, 2012). Pathological ATP spillage also occurs from traumatically damaged cells (Burnstock & Verkhratskii, 2012). Of interest, non-lethal membrane injury has been demonstrated *in vivo* in several tissues (McNeil & Steinhardt, 2003), including bone (Yu et al., 2017), under physiological conditions. The mechanism of facilitated cell membrane repair has been described and involves Ca^{2+}/PKC-dependent vesicular exocytosis (Togo, Alderton, Bi, & Steinhardt, 1999). However, the contribution of non-lethal cell injury to ATP release and related mechanotransductive purinergic signaling remains unclear.

The goal of this study was to examine the mechanism of ATP release from mechanically-stimulated cells of the osteoblastic lineage. Since we have previously demonstrated that transient

membrane disruption is required to induce global $[Ca^{2+}]_i$ elevations in osteoblasts (Lopez-Ayon et al., 2014), we were particularly interested in understanding the contribution of membrane injury to mechanically-induced ATP release. Mechanical forces were applied by local membrane deformation or turbulent fluid shear stress *in vitro* to BMP-2 transfected C2C12 osteoblastic cells (C2-OB), primary bone marrow (BM-OB) and compact bone (CB-OB)-derived osteoblasts and changes in $[Ca^{2+}]_i$, vesicular exocytosis, membrane permeability and ATP release were assessed. The prevalence of membrane injury in osteocytes at physiological and supraphysiological mechanical strain levels was investigated following *in vivo* cyclic compressive tibial loading of 10-week old female C57Bl/6J mice.

6.3 Results

6.3.1 Mechanically-stimulated osteoblasts release ATP that induces calcium responses in non-stimulated neighboring cells

Osteoblasts from three different sources, C2-OB, CB-OB, and BM-OB, were loaded with $[Ca^{2+}]_i$ dye Fura2 and mechanically stimulated with a glass micropipette, which induced qualitatively similar transient global $[Ca^{2+}]_i$ elevations, consistent with prior work (Genetos et al., 2005; Robling & Turner, 2009; Romanello et al., 2001) (**Fig. 6-1A-C**). L-type voltage-sensitive calcium channel (VSCC) inhibitor Nifedipine and P2 antagonist PPADS significantly reduced the amplitude of mechanically-stimulated $[Ca^{2+}]_i$ transients (**Fig. 6-1D**). L-type VSCC activation occurred gradually (**Fig. 6-1E**) while the P2 receptor-driven component of the response peaked within seconds of stimulation (**Fig. 6-1F**). Together, L-type VSCC and P2 receptor-driven component accounted for ~50% of the mechanical stimulated $[Ca^{2+}]_i$ transient. Consistent with previous reports (Genetos et al., 2005; Robling & Turner, 2009; Romanello et al., 2001), shortly after a single osteoblast was mechanically stimulated, neighboring cells exhibited delayed secondary $[Ca^{2+}]_i$ responses (**Fig. 6-1G**). Pharmacological interventions revealed that P2 receptors mediated the secondary response in all three osteoblast models, while a tendency for GAP junction involvement was observed in BM-OB responses (**Fig. 6-1H**). Puff application of 10 μM ATP mimicked the appearance of secondary responders in C2-OB (**Fig. 6-1I**).

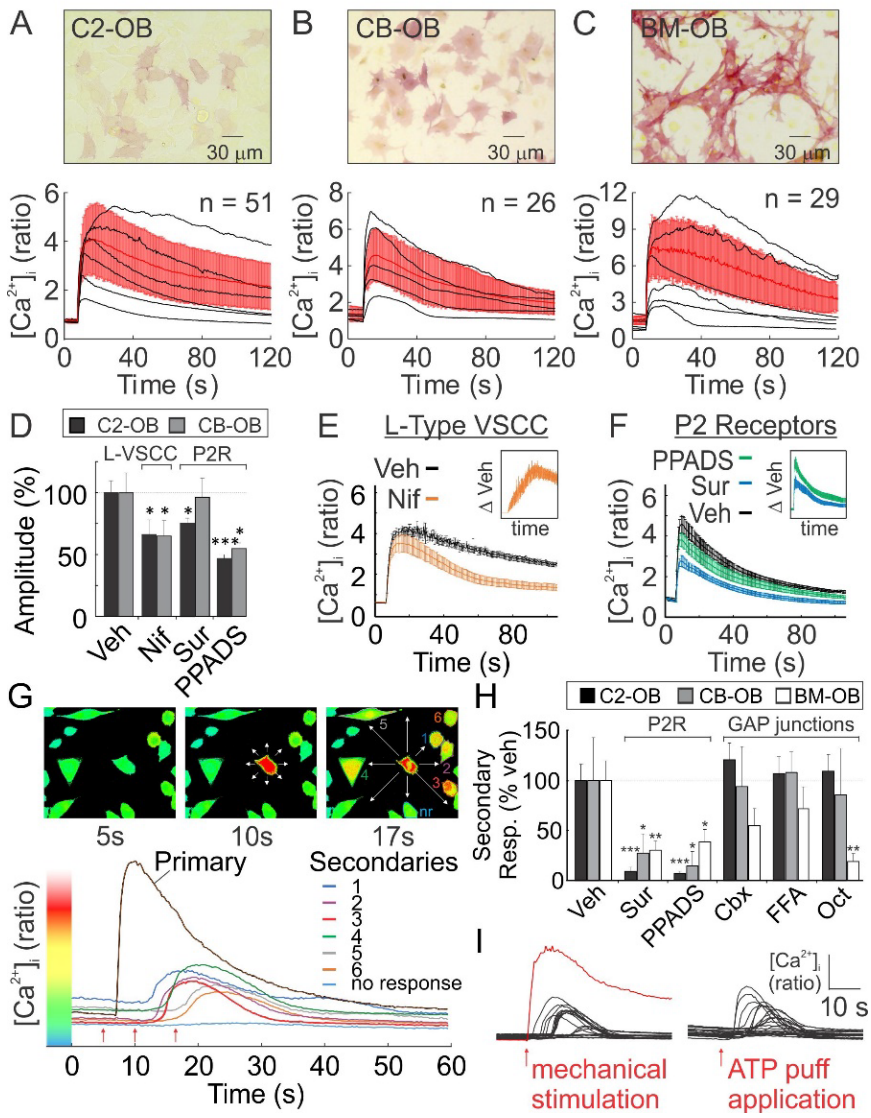

Figure 6-1. Osteoblasts are mechanosensitive (A-C) Single Fura2-loaded C2-OB (**A**), CB-OB (**B**) or BM-OB (**C**) (*Top*: ALP staning) were stimulated with micropipette and $[Ca^{2+}]_i$ was recorded. Bottom: representative traces (*black*), means ± SEM (*red*) **(D)** Amplitudes of mechanically-evoked $[Ca^{2+}]_i$ transients in osteoblasts pretreated with vehicle, Nif, Sur or PPADS (see materials & methods for abbreviations, targets and doses). Means ± SEM, n = 6-15 stimulated cells, normalized to vehicle. **(E, F)** Contribution of L-type VSCC (**E**, n = 10) and P2 receptors (**F**, n = 12) to mechanically-evoked $[Ca^{2+}]_i$ transients in C2-OB as comparison and difference (*Insets*) of mean ± SEM of vehicle and treatment $[Ca^{2+}]_i$ transients. **(G)** $[Ca^{2+}]_i$ in the stimulated (primary) and neighboring (secondary) C2-OB. *Top*, pseudocolor of 340/380 ratio, *white arrows*: directions of signal propagation; *Bottom*, $[Ca^{2+}]_i$ transients, *red arrows*: *Top* panel time points. **(H)** Secondary responsiveness in cultures pretreated with vehicle, Sur, PPADS, Cbx, FFA or Oct. Means ± SEM, n = 7-21 stimulated primary responses, normalized to vehicle. **(H)** $[Ca^{2+}]_i$ transients induced by mechanical stimulation of single C2-OB (*left*, *red curve*) or puff application of 10 µM ATP (*right*). For figure 1, *significance between treatment and control by ANOVA.

We used a luciferin fluorescence-based imaging technique (Sørensen & Novak, 2001) to directly measure ATP release ($[ATP]_e$) (**Fig 6-2**, **Fig 6-S1**). Simultaneous recording of $[ATP]_e$ and $[Ca^{2+}]_i$ demonstrated that ATP release occurred within seconds after mechanical stimulation (time to peak release: 1.64 ± 0.36 s) and preceded the onset of $[Ca^{2+}]_i$ responses in neighboring cells (**Fig 6-2**). We measured pericellular $[ATP]_e$ concentrations in the range of 0.05 – 80.5 µM corresponding to

a release of 70 ± 24 amole ATP from a single mechanically stimulated osteoblast (**Fig 6-2B**). Pericellular $[ATP]_e$ significantly correlated with the percentage of secondary responders (**Fig 6-2C**).

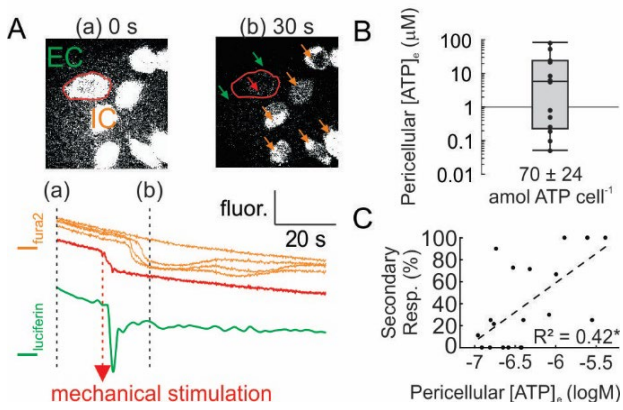

Figure 6-2. ATP release following mechanical stimulation of a single osteoblast. **(A)** Fura2-loaded C2-OB bathed in luciferin/luciferase containing PS was micropipette-stimulated. *Top*, 380 ex/510 em images before (a) and after (b) stimulation of the cell (*red outline*); *Bottom*, intracellular (IC) Fura2 fluorescence [I_{fura2}] of primary (*red*) and secondary (*orange*) responders and extracellular (EC) luciferin fluorescence [$I_{luciferin}$] (*green*). **(B)** Box plot of $[ATP]_e$ in pericellular region of stimulated C2-OB, *black markers*: observations, n = 13 stimulated cells. **(C)** Correlation between $[ATP]_e$ and percentage of secondary responders observed in C2-OB (n = 20 stimulated primary responses), *dashed line*: linear regression.

6.3.2 Vesicular ATP released upon mechanical stimulation is not the primary source of extracellular ATP

Vesicular ATP release was proposed to be a major source of extracellular ATP (Genetos et al., 2005). Using confocal microscopy, we found that an acidophilic marker quinacrine and a fluorescent ATP analog MANT-ATP co-localized in intracellular granular compartments (**Fig 6-3A**). Quinacrine-positive vesicular pool was entirely released after treatment with Ca^{2+} ionophore ionomycin, and only partially by mechanical stimulation, while negligible vesicular release was observed in unstimulated cells (**Fig 6-3B**). Interestingly, vesicular release peaked within 20 s of mechanical stimulation (**Fig. 3C, D**), while ATP release within ~2 s (**Fig 6-2A**). Basal vesicular density was 70 ± 4 × 10^{-3} vesicles/μm^2 (**Fig 6-3E**) and mechanical stimulation resulted in the cumulative release of 5 ± 1 × 10^{-3} vesicles/μm^2 over 100 s post-stimulation (7.2 ± 1.2% of the basal vesicular pool) (**Fig 6-3F**). In $[Ca^{2+}]_e$-free conditions vesicular density was unaffected, while mechanically-evoked vesicular release was markedly suppressed (**Fig 6-3E, F**). Treatment with N-ethylmaleimide (NEM) caused a 33 ± 2% increase in the vesicular density (**Fig 6-3E**), consistent with a NEM-induced increase in the readily releasable vesicular pool (Lonart & Sudhof, 2000), and a 55 ± 8% increase in mechanically-evoked vesicular exocytosis (**Fig 6-3F**). Surprisingly, the

percentage of secondary responders and activation rates for Ca^{2+} responses (response amplitude divided by time for signal to increase from 10 to 90% of peak) were unaffected in $[Ca^{2+}]_e$-free conditions, while NEM induced significant decline in the percentage of secondary responders and activation rates (**Fig 6-3G, H**). We measured bulk ATP release following mechanical stimulation by media displacement, a model for turbulent fluid shear stress (tFSS) (Rumney, Sunters, Reilly, & Gartland, 2012) (**Fig 6-3I**). Proportionally to the extent of tFSS, 21 ± 11 to 422 ± 97 amol ATP/cell were released, approaching 31.5% of total intracellular ATP at high tFSS (**Fig 6-3J**). tFSS (10x media displacements) induced release of 324 ± 50 amol ATP/cell, while ionomycin only led to release of 94 ± 5 amol ATP/cell. Moreover, tFSS-induced ATP release was significantly potentiated under $[Ca^{2+}]_e$-free conditions (961 ± 88 amol ATP/cells) and inhibited in NEM-treated cells (41 ± 24 amol ATP/cells) (**Fig 6-3K**). We also investigated conductive channels, however pharmacological inhibition of Maxi-anion channels, P2X7, Connexins, Pannexins, T-type VSCC, TRPV4 or Piezo1 channels did not affect tFSS-stimulated ATP release (**Fig 6-S2**). Although inhibition of L-Type VSCC had a small inhibitory effect (**Fig 6-S2**), our data suggest that conductive channels cannot account for ATP release observed from mechanically-stimulated osteoblasts. Importantly, our data show that increases in vesicular release were consistently associated with a reduction in mechanically-stimulated ATP release, while inhibition of vesicular exocytosis increased ATP release from mechanically-stimulated osteoblasts.

6.3.3 Mechanical stimuli regularly and reversibly compromise the integrity of the osteoblast membrane

We hypothesized that mechanically-stimulated ATP release is related to membrane injury. Adopting a Fura2-based dye-leakage assay (Togo et al., 1999), we examined changes in 340 ex/510 em Fura2 fluorescence following mechanical stimulation of osteoblasts (**Fig 6-4A**). In ~40% of micropipette-stimulated osteoblasts, intracellular Fura2 fluorescence returns to pre-stimulation basal (minor or no injury; mIn). However, in 30-40% of osteoblasts post-stimulation fluorescence was partially reduced (intermediate injury; iIn) and in 15-20% of osteoblasts completely lost (severe injury; sIn) (**Fig 6-4B**). The extent of injury sustained by a micropipette-stimulated cell correlated with the magnitude and duration of $[Ca^{2+}]_i$ elevations (**Fig 6-4C-E**), as well as the percentage of secondary responders (**Fig 6-4F**), suggesting that ATP release is related to the extent of membrane disruption. In a dye uptake assay, we added membrane impermeable

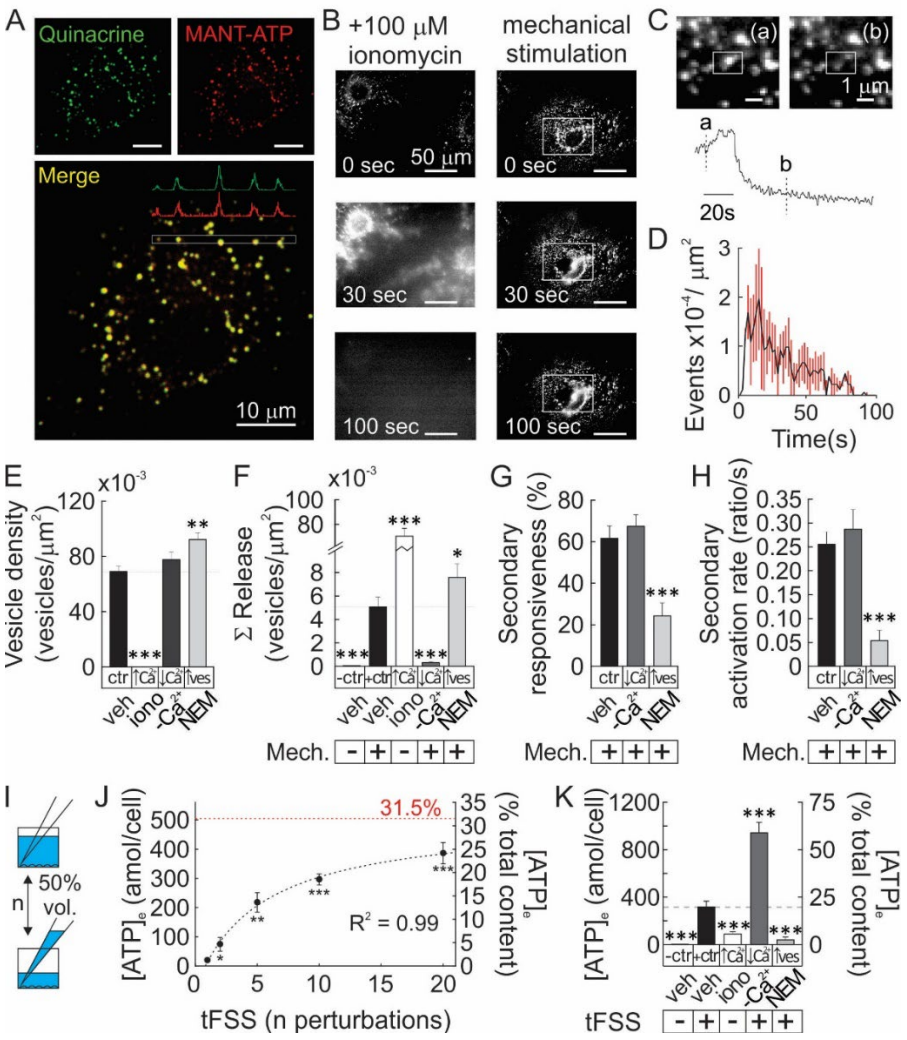

Figure 6-3. Vesicular ATP released upon mechanical stimulation is not the primary source of extracellular ATP. (A) Confocal images of CB-OB loaded with quinacrine and MANT-ATP. **(B)** Changes in quinacrine-loaded CB-OB treated with ionomycin (*left*) or stimulated with micropipette (*right*, region of interest in white). **(C)** Vesicular release event in CB-OB (*top*) coincides with a sudden drop in granular quinacrine fluorescence (*bottom*). **(D)** Kinetics of vesicular release from CB-OB stimulated by micropipette at 0 s, n = 37 stimulated cells. **(E-H)** Quinacrine- **(E, F)** or Fura2- **(G, H)** loaded CB-OB were pre-treated (10 min) with vehicle, ionomycin (iono) or NEM or placed in $[Ca^{2+}]$-depleted physiological solution, and micropipette-stimulated when indicated (+). Vesicular density (**E**) and cumulative release (**F**), secondary responsiveness (**G**) and $[Ca^{2+}]$ response activation rates (**H**) were determined, n = 7-37 primary cells. **(I)** tFSS was applied by replacing 50% media volume *n* times. **(J, K)** ATP released per cell (*left axis*) or as percent of cellular ATP content (*right axis*) was measured following CB-OB stimulation by tFSS **(J,** *black dashed line*: rational function fit; *red dashed line:* corresponding asymptote**)** or after indicated pre-treatments followed by tFSS (10x media displacements, +) (**K**), n = 6-8 independent cultures. For figure 3, means ± SEM, *significance compared to vehicle (**E-H**), basal ATP release **(J)** or to tFSS-stimulated vehicle (**K**) by ANOVA.

dyes, trypan blue (TB) or rhodamine-conjugate dextran (R-dextran), to osteoblasts before or after mechanical stimulation (**Fig 6-4G**). When the dyes were applied prior to tFSS, the proportion of dye-permeable osteoblasts positively correlated with the degree of tFSS. The extent of dye uptake was higher for TB (~900 Da) compared to R-dextran (~10 kDa) (**Fig 6-4H, I**). However, when membrane permeability was examined 300 s after stimulation, a significantly lower percentage of cells were permeable to the dyes (**Fig 6-4H, I**). Hemichannel involvement was excluded, since hemichannel blockers did not affect mechanically-stimulated $[Ca^{2+}]_i$ elevations, membrane permeability or ATP release (**Fig 6-S3**). Consistent with transient membrane disruption, lactate dehydrogenase (LDH, ~140 kDa) leaked into the extracellular media proportionally to tFSS magnitude (**Fig 6-4J**), even though cell viability was minimally affected 1 h after tFSS stimulation (**Fig 6-4K**). Examining TB uptake following micropipette stimulation, we have found that all C2-OB were TB-permeable immediately upon stimulation, decreasing to 75 ± 22% within 10 s, to 40-50% by 180 s and to 18 ± 12% by 300 s (**Fig 6-4L**). Comparing these data to dye leakage experiments suggested that minor injuries resealed within 10 s, intermediate – within 20 -180 s and severe injuries did not reseal by 300 s. (**Fig 6-4L**). Based on predicted molecular radii of the dyes (Erickson, 2009), we estimated the membrane lesion radius to be on the nanometer scale, sufficiently large to permit the efflux of smaller ATP molecules (~507 Da) (**Fig 6-4M**).

6.3.4 Osteocyte membranes are reversibly disrupted during mouse *in vivo* tibia loading

To determine whether mechanically-induced repairable membrane disruptions occur *in vivo*, 10-week-old female C57Bl/6J mice were injected with lysine-fixable Texas Red-conjugated dextran (LFTR-Dex, ~10 kDa) either 30 min prior to or 20 min after cyclic compressive tibial loading to strain magnitudes at the upper level of physiological activities (600 με) or at supraphysiological osteogenic levels (1200 με) (Willie et al., 2013) (**Fig 6-5A-D**). In the contralateral non-loaded control tibiae (which experienced habitual loads only), sclerostin-positive osteocytes were observed at a density of 3212 ± 287 cells/mm^2 (**Fig 6-S4**), ~4-7% of which demonstrated LFTR-Dex uptake, while only 2% of calvarial osteocytes were LFTR-Dex positive (**Fig 6-5E**). Cyclic compressive tibial loading in the presence of LFTR-Dex resulted in significantly increased osteocyte dye uptake compared to unloaded bone, demonstrating that *in vivo* mechanical loading results in cellular membrane disruption (**Fig 6-5F, G** *red*). Importantly, when LFTR-Dex was

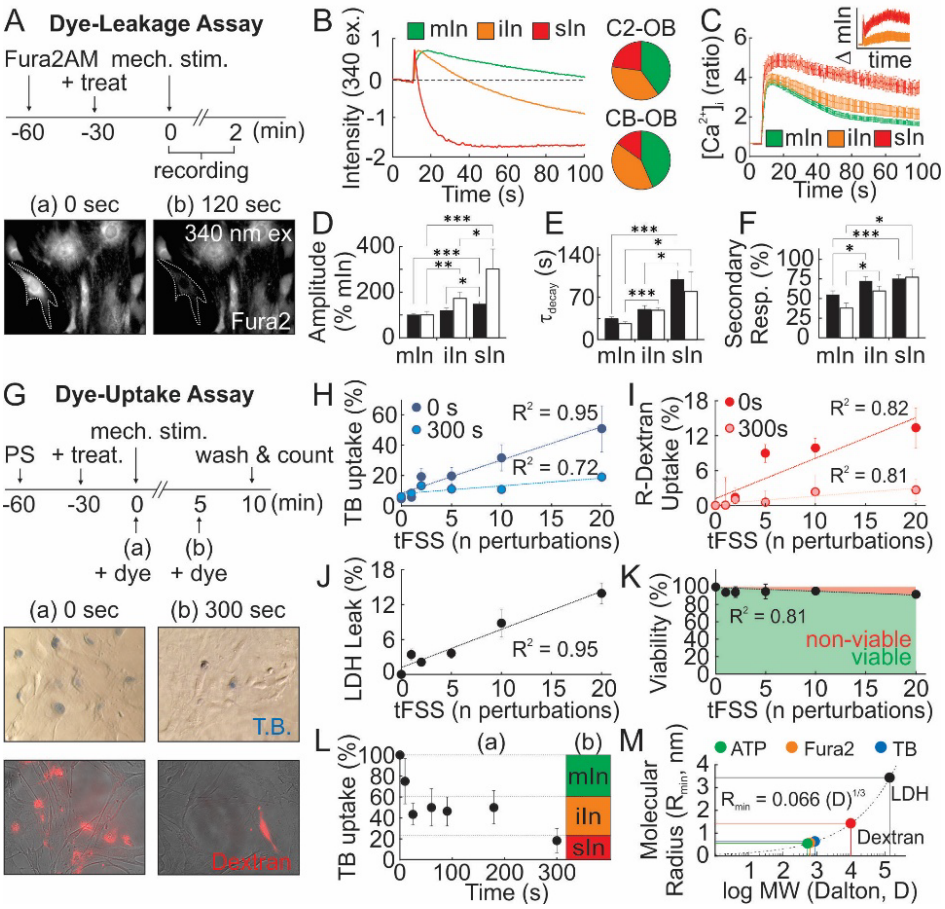

Figure 6-4. Mechanical stimuli regularly and reversibly compromise the integrity of osteoblast cell membrane. (A-F) Membrane permeability in micropipette-stimulated Fura2-loaded osteoblasts. **(A)** *Top:* Schematic of dye-leakage assay. *Bottom*: 340 ex/510 em before (a) and after (b) CB-OB stimulation (*white outline)*. **(B)** Representative Fura2 traces in C2-OB with minor (mIn), intermediate (iIn) or severe (sIn) cell injury and relative occurrence frequency (*Right*, n = 35-40 stimulated cells). **(C)** C2-OB $[Ca^{2+}]_i$ responses and differences (*Inset*) for mIn (*green*), iIn (*orange*) and sIn (*red*), n = 8–14 stimulated cells. **(D-F)** Primary $[Ca^{2+}]_i$ response amplitudes (**D**) and decay constants (**E**), and secondary responsiveness (**F**) in CB-OB (*black*; n = 40 stimulated cells) or C2-OB (*white*; n = 35 stimulated cells), grouped by cell injury status. **(G-K)** Membrane permeability in tFSS-stimulated osteoblasts. (**G**) *Top:* schematic of dye-uptake assay. *Bottom*: CB-OB stained with TB (*top*) or R-dextran (*bottom*) prior to (0 s, *left*) or after (300 s, *right*) tFSS application (10x). Uptake of TB (**H**) or R-dextran (**I**) added prior to (0 s) or after (300 s) tFSS stimulation of CB-OB (n = 4 independent cultures). **(J)** Leakage of LDH from CB-OB 5 min after tFSS (n = 8 independent cultures, normalized to total LDH). **(K)** Viability of C2-OB 1 h after tFSS assessed by alamarBlue (n = 8-16 independent cultures). **(L)** Uptake of TB added at indicated times after micropipette-stimulation of C2-OB (*a*, n = 4-23 stimulated cells) compared to relative frequencies of mIn, iIn and sIn assessed by Fura2-leakage assay (*b*). **(M)** Calculated minimum membrane lesion radius R_{min} required for permeability to LDH, R-dextran, TB, Fura2 and ATP. For figure 4, means ± SEM, *dashed lines* – linear regression, *significance by ANOVA.

administered 20-50 min after 600 με loading, the levels of cellular dye uptakes were similar to those in unloaded tibia, suggesting that damage evident immediately after loading was repaired within this time period (**Fig 6-5F** *light blue*). Of interest, when LFTR-Dex was administered 20-50 min after 1200 με loading, the proportion of osteocyte exhibiting dye uptake was significantly lower compared to non-loaded controls, suggesting that adaptive improvements in membrane integrity occurred in response to the supraphysiological strain (**Fig 6-5F, G** *dark blue*).

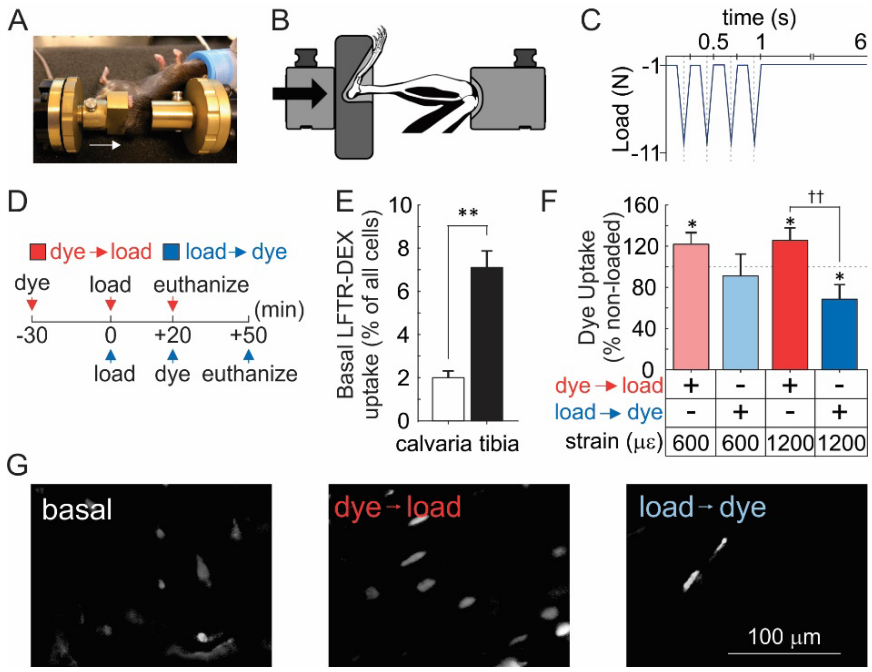

Figure 6-5. Osteocyte membranes are reversibly disrupted during *in vivo* cyclic compressive loading of the tibia.

(A, B) Left tibia of anesthetized mouse was positioned in loading device as shown on the picture **(A)** and schematic **(B)**. *Arrows* indicate direction of load. **(C)** The triangle waveform included 0.15 s symmetric active loading/unloading, with a 0.1 s rest phase (-1 N) between load cycles and a 5 s rest inserted between every four cycles. A maximum force of -5.5 N or -11 N was applied, which engenders 600 με or 1200 με, respectively at the periosteal surface of the tibia mid-diaphysis in these mice. **(D)** Experimental design schematic: animals were injected with LFTR-Dex 30 min before (*red*) or 20 min after (*blue*) *in vivo* cyclic tibial loading (5 min). **(E)** Proportion of cells exhibiting LFTR-Dex uptake in calvariae (n = 5 animals) and control tibiae (n = 20 from 10 animals), normalized to average total cell number, means ± SEM, **p<0.01. **(F)** Dye uptake in tibia injected before (*red*) or after (*blue*) loading at 600 με or 1200 με, means ± SEM, n = 5/strain/dye protocol, normalized to non-loaded contralateral tibia, *significance compared to non-loaded tibia, ††significance between dye protocols, by ANOVA. **(G)** Contrast enhanced images of dye uptake in control (*left*), and 1200 με loaded tibia injected with dye before (*middle*) or after (*right*) loading.

6.3.5 PKC regulated vesicular exocytosis and membrane resealing

Vesicular exocytosis has been demonstrated to facilitate membrane repair and improve membrane integrity in a PKC dependent manner (Togo et al., 1999). We examined the role of Ca^{2+}/PLC/PKC

pathway during mechanically-induced membrane injury and resealing. Pharmacological activation of PKC (**Fig 6-6A, Fig 6-S5A)** and NEM-induced potentiation of vesicular release (**Fig 6-S6A**) both attenuated tFSS-induced membrane disruption. Depletion of $[Ca^{2+}]_e$, or pharmacological inhibition of PLC (**Fig 6-S6A, B)** or PKC (**Fig 6-6A, B, Fig 6-S5A, B)** increased membrane disruption in osteoblasts following tFSS or micropipette stimulation. Together these findings suggest that membrane repair was regulated by extracellular calcium influx, PLC/PKC signalling and vesicular exocytosis. We next investigated the link between Ca^{2+}/PLC/PKC pathway and mechanically-stimulated $[Ca^{2+}]_i$ elevations, vesicular exocytosis and ATP release. Depletion of $[Ca^{2+}]_e$ or PLC inhibition consistently reduced the amplitude of mechanically-stimulated $[Ca^{2+}]_i$ elevations (**Fig 6-S6C**) and vesicular release (**Fig 6-S6D**), and potentiated ATP release **(Fig 6-S6E**). PKC activation had minor effect on calcium responses (**Fig 6-S6C**), augmented vesicular release (**Fig 6-6C**) and reduced ATP release (**Fig 6-6D, Fig 6-S5C**). In contrast, PKC inhibition potentiated calcium responses (**Fig 6-S6C**), suppressed vesicular release (**Fig 6-6C**) and increased ATP release (**Fig 6-6D, Fig 6-S5C**). PMA-induced PKC activation rescued vesicle pool depletion following PLC inhibition, thereby positioning PKC signalling downstream of PLC (**Fig 6-S7)**. Together these data suggest that mechanically-stimulated membrane injury and repair, vesicular release and ATP release are regulated by Ca^{2+}/PLC/PKC-dependent signalling.

We next examined which PKC isoform is involved in the mechanoresponse. Immunoblot analysis demonstrated that mechanical stimulation (using tFSS) of CB-OB activated conventional PKCα/β and PKD/PKCμ, but not atypical PKCζ/λ or novel PKCδ/θ isoforms (**Fig. 6E, Fig S8**). PMA stimulated phosphorylation of conventional and PKD/PKCμ isoforms, but not atypical or novel PKC isoforms, while only basal PKD/PKCμ phosphorylation had a tendency ($p=0.09$) to be inhibited by Bis. Total PKC levels were unaffected by pharmacological interventions or mechanical stimulation (**Fig 6-S8G**). These findings suggest that the PKD/PKCμ isoform regulates membrane resealing in osteoblasts.

To establish the relationship between vesicular release, membrane disruption and ATP release, we pooled data for the mechanically-induced responses from all treatments studied in CB-OB (**Fig 6-6F-H**). Mechanically-induced vesicular release negatively correlated with the extent of membrane disruption (**Fig 6-6F**) and the amount of ATP released (**Fig 6-6G**), while membrane disruption positively correlated with amount of ATP released in response to mechanical stimulation (**Fig 6-**

6H). These data support a model in which mechanical disruption of the cell membrane leads to ATP spillage, while the extent of membrane resealing, regulated by Ca^{2+}/PLC/PKC-dependent vesicular exocytosis, limits the amount of total ATP released (**Fig 6-7**).

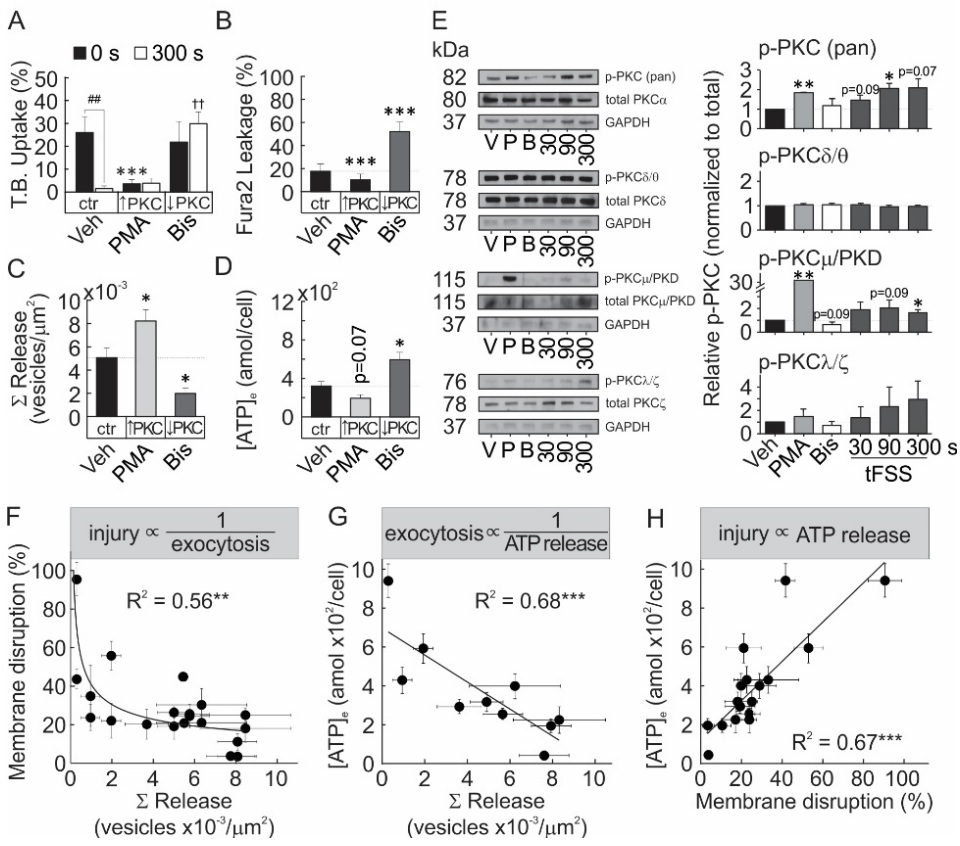

Figure 6-6. Membrane resealing depends on PKC-regulated vesicular exocytosis. (A-D) CB-OB were pretreated with vehicle, PMA or Bis, and membrane injury (**A, B**), vesicular exocytosis (**C**) and ATP release (**D**) were assessed. **(A)** TB uptake at 0 and 300 s after tFSS (10x), n = 5-8 independent cultures. **(B)** Fura2 leakage, determined as percentage of sIn cells after micropipette-stimulation, n=9-16 stimulated cells. **(C)** Cumulative vesicular release over 100 s after micropipette-stimulation, n=6-10 stimulated cells. **(D)** ATP release over 60 s following 10x tFSS stimulation, n=8 independent cultures. **(E)** Immunoblotting for PKC isoform phosphorylation in CB-OB treated with vehicle, PMA or Bis (30 min); or 30 s, 90 s or 300 s after tFSS (10x). Shown are immunoblots (*left,* complete gels in Fig S8) and densitometry (*right*) of phosphorylated and total conventional (pPKC pan), atypical (pPKC ζ/λ), novel (pPKC δ/θ), and PKD/PKCμ isoforms. Phosphorylated PKC isoforms were normalized by total PKC levels and reported relative to vehicle, n=3 independent cultures. **(F-H)** Relationships between vesicular release (pooled data from vesicular release experiments), membrane disruption (pooled from membrane integrity experiments) and ATP release (pooled from 10x tFSS experiments) following mechanical stimulation of CB-OB, *solid line* - regression. For figure 6, data are means ± SEM, *significance compared to vehicle (0 s vehicle for A), †significance compared to 300 s vehicle (A) and #significance of indicated comparisons (A), by ANOVA or by regression.

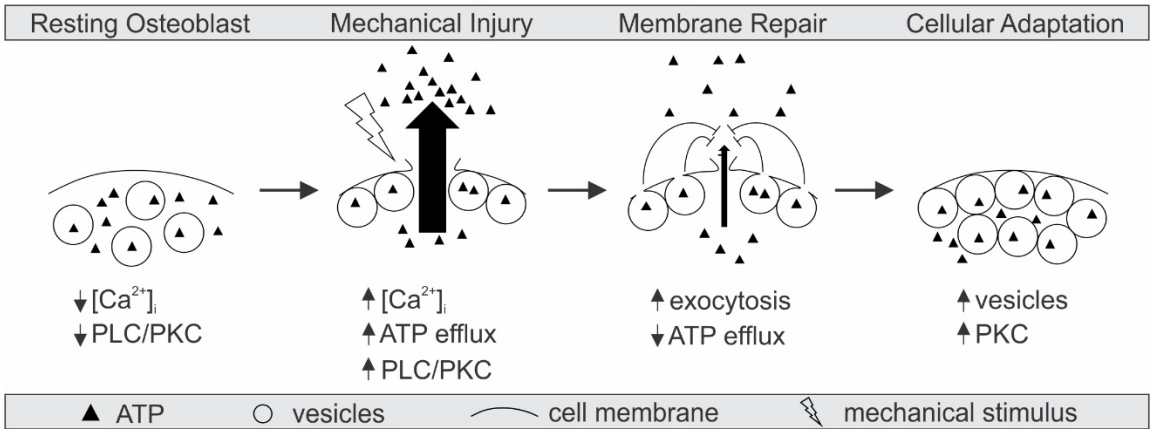

Figure 6-7. Proposed model for mechanically-stimulated ATP release in osteoblasts. *Resting Osteoblasts*: Under basal conditions, the cell membrane is intact and intracellular free calcium levels and PLC/PKC signalling are minimal. *Mechanical injury*: Mechanical stimulation results in disruption of the cellular membrane, which leads to the influx of calcium, activation of PLC/PKC signalling, and the efflux of ATP. *Membrane repair*: The disrupted membrane is rapidly repaired through a process involving Ca^{2+}/PLC/PKC-dependent vesicular exocytosis, thereby limiting ATP release. *Cellular adaptation*: Elevated PKC levels result in priming of the vesicular pathway, likely regulating cellular resilience and responsiveness to subsequence cycles of mechanical stimulation.

6.4 Discussion

6.4.1 Overview

This study establishes a novel mechanism of mechanotransduction in bone cells, which positions ATP release as the integrated outcome of membrane injury (reflective of the destructive potential of mechanical forces) and membrane repair (countering and adapting to the damage). We report that mechanical stimuli *in vitro* and *in vivo* induced reversible cell membrane disruption. This disruption resulted in ATP release predominantly through the compromised membrane, rather than through vesicular or conductive mechanisms. Ca^{2+}/PLC/PKC-dependent vesicular release was necessary for successful membrane repair and prevention of further ATP release. Importantly, prior activation of PKD/PKCμ or vesicular priming improved membrane integrity and repair, thereby minimizing membrane injury and ATP release upon subsequent mechanical stimulation and serving as a mechanism of cellular mechano-adaptive memory.

6.4.2 Membrane injury

We have demonstrated that non-lethal cell membrane injury is routine in mechanically stimulated cells. *In vitro*, single cell membrane deformation or fluid shear stress transiently compromised cell

membrane integrity in 2-30% of cells, which was repaired within 10-100 s. Consistent with findings observed using *in vitro* models of mechanical stimulation, *in vivo* cyclic compressive tibial loading engendering physiological and supraphysiological strains resulted in transient osteocyte membrane disruption in 5-10% of cells. Interestingly, supraphysiological mechanical strains improved membrane integrity post-stimulation compared to baseline levels. Previously, non-lethal reversible cell wounding was shown to occur in mechanically active tissues, with membrane-impermeable marker uptake reported in 3-20% of cells in skeletal muscle, 3-6% in skin, 25% in cardiac muscle, 2-30% in lung and aorta (McNeil & Steinhardt, 2003). Consistent with our findings, membrane disruption was reported in 20-60% of long bone osteocytes after *in vivo* treadmill loading (Yu et al., 2017). The higher prevalence of disruption reported by Yu et al. in long bones was likely a consequence of cumulative dye uptake over 18 h, while our study examined membrane disruption over a 20-50 min period. Our data demonstrated that reparable membrane injuries are common and significantly contribute to ATP release from mechanically stimulated osteoblasts and osteocytes.

6.4.3 ATP release

We observed that osteoblasts release 70 ± 24 amol ATP /cell in response to direct membrane deformation and 21 ± 11 to 422 ± 97 amol ATP/cell in response to tFSS, which is consistent with previously reported estimates ranging from 24 ± 1 to 324 ± 59 amol ATP/cell (Genetos et al., 2005; Genetos, Kephart, Zhang, Yellowley, & Donahue, 2007; Kringelbach et al., 2015; Kringelbach, Aslan, Novak, Schwarz, & Jorgensen, 2014; Manaka et al., 2015; Pines et al., 2003; Romanello et al., 2005; Wang et al., 2013). Osteoblasts have been reported to release ATP through mechanisms related to vesicular exocytosis (Genetos et al., 2005; Romanello et al., 2005), and L-type VSCC (Genetos et al., 2005). In osteocytes, hemichannels (Kringelbach et al., 2015; Seref-Ferlengez et al., 2016), P2X7 (Seref-Ferlengez et al., 2016) and T-type VSCC (Thompson et al., 2011) have also been implicated. We visualized ATP-containing quinacrine-positive vesicles and directly demonstrated their release upon mechanical stimulation. Surprisingly, the total vesicular ATP content was ~ 94 ± 5 amol ATP/cell, which, considering that only 7.2 ± 1.2% of vesicles were released upon mechanical stimulation, is much less (i.e., <10 amol ATP/cell) than mechanically-induced ATP release. Moreover, treatments that potentiated vesicular release resulted in a surprising decrease in ATP release, while treatments interfering with vesicular release enhanced

ATP release. In search for an alternative route of ATP release, we found that mechanically stimulated ATP release was proportional to the extent of membrane injury.

6.4.4 Membrane resealing

Vesicular exocytosis is believed to promote membrane repair via membrane insertion, thereby reducing membrane tension and allowing exposed hydrophobic residues to reseal (McNeil & Steinhardt, 2003). We have shown that vesicular release was critical for the repair of mechanically-induced membrane injury and that the Ca^{2+}/PLC/PKC pathway regulates vesicular exocytosis in osteoblasts. We interrogated the role of vesicular release in the mechanoresponse using NEM, a modulator of vesicular docking machinery (Lonart & Sudhof, 2000). While NEM is commonly used as an inhibitor of vesicular release (Genetos et al., 2005; Kowal, Haanes, Christensen, & Novak, 2015), it has also been shown to increase vesicular release probability through accumulation of readily-releasable vesicles (Kirmse & Kirischuk, 2006; Lonart & Sudhof, 2000). Using real-time imaging, we demonstrated that NEM increased the basal vesicular density and potentiated mechanically-stimulated vesicular exocytosis in osteoblasts. In the presence of NEM, mechanically-induced membrane injury and ATP release were significantly reduced. Vesicular exocytosis has been implicated as a mechanism of ATP release from osteoblasts and osteocytes based on the assumed inhibition of vesicular exocytosis by NEM or vesicular trafficking by brefeldin A, bafilomycin or monensin (Genetos et al., 2005; Kringelbach et al., 2015; Romanello et al., 2005). However, our data demonstrated that the role of vesicles cannot be inferred without a direct validation of the effect of NEM on vesicular release. In our study, $[Ca^{2+}]_e$ depletion abolished mechanically-stimulated vesicular release, interfered with membrane repair and increased ATP release. Calcium is one of the first mechanically-induced signals that initiates downstream responses (Robling & Turner, 2009), including exocytosis-mediated membrane repair (Cooper & McNeil, 2015). It was previously shown that during *in vivo* loading of mouse bone, the number of osteocytes exhibiting $[Ca^{2+}]_i$ elevations increased proportionally to the magnitude of applied strain (Lewis et al., 2017). We found that PLC and PKCμ, known downstream targets of Ca^{2+} signaling (Mochly-Rosen, Das, & Grimes, 2012), regulated basal vesicle abundance and membrane resealing. Our study suggests that the osteoporotic phenotype reported in PKCμ-deficient bones may be associated with defective mechanoresponsiveness (Li et al., 2017). Consistent with mechanisms of facilitated membrane resealing (Cooper & McNeil, 2015; Togo et

al., 1999), we propose that mechanical stimulation results in membrane disruption, which leads to ATP efflux and Ca^{2+} influx, triggering vesicular exocytosis and membrane repair that then limits ATP release (**Fig 6-7**).

6.4.5 Mechano-adaptive memory

Our findings suggest that osteoblast mechano-adaptive status may be influenced by PKCμ/vesicular signaling. Activation of PKC prior to mechanical stimulation or priming the vesicular pool for release with NEM resulted in drastic decreases in membrane injury and ATP release in response to subsequent mechanical stimulation. Prior work has demonstrated that mechanical loading induces the production and release of LAMP-1-positive vesicles from osteocytes [LAMP-1 colocalizes with the quinacrine tracer-dye used in this study (Cao et al., 2014)], which was critical for mechano-adaptive bone formation (Morrell et al., 2018). This mechano-adaptive effect may underlie cellular accommodation in the bone response to mechanical loading previously reported (Schriefer, Warden, Saxon, Robling, & Turner, 2005), and explain the reduced responsiveness of osteocytes exposed to higher frequency *in vivo* mechanical loading, compared to lower frequency loading of the same magnitude (Lewis et al., 2017). Our findings suggest that during repeated mechanical stimulation, the priming of PKCμ/vesicular pathway by earlier stimuli will determine osteoblast resilience and responsiveness to subsequent cycles of mechanical stimulation, representing a mechanism for cellular accommodation.

6.4.6 Concluding remarks

In this study we established the regulatory mechanisms involved in controlling the amount of ATP released following reversible cellular injury. We have demonstrated that membrane injury and repair are common under physiological stresses *in vitro* and *in vivo* and determined the critical role for PKC-regulated vesicular exocytosis in bone cell membrane repair. We suggest that rather than delivering ATP to extracellular space, exocytosis of ATP-containing vesicles limits the much larger efflux of intracellular ATP through damaged membranes. We propose a model of biological adaptation to mechanical forces, which directly links mechanosensation through reversible membrane injury and ATP release to the development of adaptive resilience against the destructive potential of mechanical forces. PKC-mediated vesicular release provides a target for potential therapeutic interventions to modulate mechano-responsiveness and mechano-resilience in humans habitually experiencing altered mechanical environment, such as astronauts or paralysis patients.

6.5 Materials & Methods

All procedures were approved by McGill's University's Animal Care Committee and complied with the ethical guidelines of the Canadian Council on Animal Care.

6.5.1 Solutions and reagents

Solutions. Phosphate-buffered saline (PBS; 140 mM NaCl, 3 mM KCl, 10 mM Na_2HPO_4, 2 mM KH_2PO_4, pH 7.4), sterilized by autoclave. Physiological solution (PS; 130 mM NaCl; 5 mM KCl; 1 mM $MgCl_2$; 1 mM $CaCl_2$; 10 mM glucose; 20 mM HEPES, pH 7.6), sterilized by 0.22 μM filtration. In [Ca^{2+}]-free PS, $CaCl_2$ was excluded and 10 mM EGTA was added to chelate any residual calcium, sterilized by 0.22 μm filtration. Bioluminescence reaction buffer (0.1 M DTT, 25 mM tricine, 5 mM $MgSO_4$, 0.1 mM EDTA, 0.1 mM NaN_3, pH 7.8), sterilized by 0.22 μm filtration. RIPA lysis buffer (50 mM Tris, pH 7.4, 150 mM NaCl, 1% Nonidet P-40, 1 mM EDTA, 1 mg/mL aprotinin, 2 mg/mL leupeptin, 0.1 mM phenylmethylsulfonyl fluoride, 20 mM NaF, 0.5 mM Na_3VO_4). TBST buffer (10 mM Tris-HCL, pH 7.5, 150 mM NaCl, 1% Tween 20).

Key Resources Table.

Reagent type	Designation	Source	Identifiers	Additional information
Cell line (M. musculus)	BMP2-transfected C2C12 myoblast cells (C2C12-BMP2; C2-OB)	Dr. M. Murshed, McGill University		osteoblast cell line
strain, strain background (M.musculus, female)	10 week-old C57Bl/6J	Jackson Laboratory	Stock #: 000664; RRID: IMSR_JAX:000644	primary osteoblast source, in vivo studies
software, algorithm	Calcium Analyser	DOI: 10.3389/fphys.2016.00525		MATLAB algorithm for calcium analysis
chemical compound, drug	MANT-ATP	AnaSpec	Cat. AS-64610	fluorescent ATP analog, 5 μM (overnight, 37°C)
chemical compound, drug	GsMTx-4; GsM	Alomone Labs	Cat. STG-100	Piezo1 inhibitor, 1 μM (10 min, room temperature)
chemical compound, drug	U73122; U73	Calbiochem	Cat. 662035	PLC inhibitor, 10 μM (10 min, room temperature)

Key Resources Table.

Reagent type	Designation	Source	Identifiers	Additional information
antibody	GAPDH (D16H11, Rabbit antibody)	Cell Signaling Technology	Cat. 5174; RRID:AB_10622025	WB, 1:1000 dilution, 5% BSA/TBST (1 h, room temperature)
antibody	β-tubulin (9F3, Rabbit antibody)	Cell Signaling Technology	Cat. 2128; RRID:AB_823664	WB, 1:1000 dilution, 5% BSA/TBST (1 h, room temperature)
antibody	p-PKC (pan; βII Ser660, Rabbit antibody)	Cell Signaling Technology	Cat. 9371; RRID:AB_330848	WB, 1:1000 dilution, 5% BSA/TBST (over night, 4°C)
antibody	PKCα (Rabbit antibody)	Cell Signaling Technology	Cat. 2056; RRID:AB_2284227	WB, 1:1000 dilution, 5% BSA/TBST (over night, 4°C)
antibody	p-PKCδ/θ (Ser643/676, Rabbit antibody)	Cell Signaling Technology	Cat. 9376; RRID:AB_330848	WB, 1:1000 dilution, 5% BSA/TBST (over night, 4°C)
antibody	PKCδ (D10E2, Rabbit anitbody)	Cell Signaling Technology	Cat. 9616; RRID:AB_10949973	WB, 1:1000 dilution, 5% BSA/TBST (over night, 4°C)
antibody	p-PKD/PKCμ (Ser744/748, Rabbit antibody)	Cell Signaling Technology	Cat. 2054; RRID:AB_330848	WB, 1:1000 dilution, 5% BSA/TBST (over night, 4°C)
antibody	PKD/PKCμ (D4J1N, Rabbit antibody)	Cell Signaling Technology	Cat. 90039	WB, 1:1000 dilution, 5% BSA/TBST (over night, 4°C)
antibody	p-PKCζ/λ (Thr410/403, Rabbit antibody)	Cell Signaling Technology	Cat. 9378; RRID:AB_330848	WB, 1:1000 dilution, 5% BSA/TBST (over night, 4°C)
antibody	PKCζ (C24E6, Rabbit antibody)	Cell Signaling Technology	Cat. 9368; RRID:AB_10693777	WB, 1:1000 dilution, 5% BSA/TBST (over night, 4°C)
antibody	anti-rabbit IgG, HRP-linked secondary antibody)	Cell Signaling Technology	Cat. 7074; RRID:AB_2099233	WB, 1:1000 dilution, 5% BSA/TBST (1 h, room temperature)

Key Resources Table.

Reagent type	Designation	Source	Identifiers	Additional information
chemical compound, drug	Minimum Essential Medium (MEM) α; αMEM	Gibco	Cat. 12,000-022	cell culture reagent
chemical compound, drug	Trypan Blue Solution, 0.4%; TB	Gibco	Cat. 15250061	in vitro injury assay dye
commercial assay or kit	Alamar Blue Cell Viability Reagent	Invitrogen	Cat. DAL1025	cell viability assay
chemical compound, drug	DAPI	Invitrogen	Cat. D1306; RRID:AB_2629482	IF, nucleur stain, 1:5000 dilution, H_20 (5 min, room temperature)
chemical compound, drug	Fura2 AM	Invitrogen	Cat. F1221	ratiometric calcium-binding dye (30 min, room temperature)
chemical compound, drug	D-Luciferin potassium salt	Invitrogen	Cat. L2916	luciferase substrate, ATP bioluminescence assay
chemical compound, drug	Lucifer Yellow CH, Lithium Salt; LY	Invitrogen	Cat. L453	GAP junction permeable dye, 10 μM (2 min, 37°C)
chemical compound, drug	Rhodamine B-conjugated 10 000 MW Dextran; R-dextran	Invitrogen	Cat. D1824	in vitro injury assay dye
chemical compound, drug	lysine-fixable Texas Red-conjugated 10 000 MW Dextra; LFTR-Dex	Invitrogen	Cat. D1863	in vivo injury assay dye
antibody	Sclerostin (Goat antibody)	R&D Systems	Cat. AF1589; RRID:AB_2195345	IF, 1:1000 dilution, 5% BSA/TBST (over night, 4°C)
chemical compound, drug	Collagenase P from *Clostridium histolyticum*	Roche	Cat. 11213857001	enzymatic digest of bone fragments
commercial assay or kit	Cytotoxicity Detection Kit^{PLUS}; LDH	Roche	Cat. 04 744 926 011	LDH leakage assay
antibody	Donkey anti-goat IgG-FITC	Santa Cruz	Cat. Sc-2024; RRID:AB_631727	IF, 1:1000 dilution, 5% BSA/TBST (1 h, room temperature)

Key Resources Table.

Reagent type	Designation	Source	Identifiers	Additional information
chemical compound, drug	Adenosine 5'-triphosphate magnesium salt; ATP	Sigma-Aldrich	Cat. A9187	
chemical compound, drug	Bisindolylmaleimide II; Bis	Sigma-Aldrich	Cat. B3056	PKC inhibitor, 1 μM (10 min, room temperature)
chemical compound, drug	Carbenoxolone disodium salt; Cbx	Sigma-Aldrich	Cat. C4790	Hemichannel blocker, 10 μM (10 min, room temperature)
chemical compound, drug	Fast Red Violet LB Salt	Sigma-Aldrich	Cat. F3381	alkaline phosphatase assay reagent
chemical compound, drug	Gadolinium (III) chloride; Gd^{3+}	Sigma-Aldrich	Cat. 439770	Mechanically-sensitive channel blocker, 10 μM (10 min, room temperature)
chemical compound, drug	GSK2193874; GSK	Sigma-Aldrich	Cat. SML0942	TRPV4 inhibitor, 100 nM (10 min, room temperature)
chemical compound, drug	HC-067047; HC	Sigma-Aldrich	Cat. SML0143	TRPV4 inhibitor, 100 nM (10 min, room temperature)
chemical compound, drug	L-ascorbic acid 2-phosphate sesquimagnesium salt hydrate	Sigma-Aldrich	Cat. A8960	osteoblast differentiation reagent, 50 μg/mL
chemical compound, drug	Luciferase from *Photinus pyralis*	Sigma-Aldrich	Cat. L9420	ATP bioluminescence assay reagent
chemical compound, drug	ML218; ML	Sigma-Aldrich	Cat. SML0385	t-type VSCC inhibitor, 10 μM (10 min, room temperature)
chemical compound, drug	Naphthol AS-MX phosphate disodium salt	Sigma-Aldrich	Cat. N5000	alkaline phosphatase assay reagent
chemical compound, drug	N-ethylmaleimide; NEM	Sigma-Aldrich	Cat. E3876	Vesicular activator, 1 mM (10 min, room temperature)
chemical compound, drug	Nifedipine; Nif	Sigma-Aldrich	Cat. N7634	l-type VSCC inhibitor, 10 μM (10 min, room temperature)
chemical compound, drug	1-octanol; Oct	Sigma-Aldrich	Cat. 297877	Connexin blocker, 1 mM (10 min, room temperature)

Key Resources Table.

Reagent type	Designation	Source	Identifiers	Additional information
chemical compound, drug	phorbol 12-myristate 13-acetate; PMA	Sigma-Aldrich	Cat. P8139	PKC activator, 100 nM (10 min, room temperature)
chemical compound, drug	Quinacrine dihydrochloride	Sigma-Aldrich	Cat. Q3251	Vesicle dye, 10 μM (15 min, room temperature)
chemical compound, drug	Flufenamic Acid; FFA	Tocris Bioscience	Cat. 4522	Hemichannel blocker, 10 μM (10 min, room temperature)
chemical compound, drug	Ionomycin calcium salt; Iono	Tocris Bioscience	Cat. 1704	calcium ionophore, 100 μM
chemical compound, drug	PPADS tetrasodium salt; PPADS	Tocris Bioscience	Cat. 0625	P2R inhibitor, 100 μM (10 min, room temperature)
chemical compound, drug	Suramin hexasodium salt; Sur	Tocris Bioscience	Cat. 1472	P2R inhibitor, 100 μM (10 min, room temperature)
chemical compound, drug	A 740003; A7	Tocris Bioscience	Cat. 3701	P2X7 inhibitor, 1 μM (10 min, room temperature)
chemical compound, drug	Dulbecco's Modified Eagle Medium; DMEM	Wisent Bio Products	Cat. 319-020 CL	cell culture reagent
chemical compound, drug	Fetal bovine Serum; FBS	Wisent Bio Products	Cat. 080152	cell culture reagent
chemical compound, drug	Penicillin Streptomycin	Wisent Bio Products	Cat. 450-201-EL	antibiotic, 1%
chemical compound, drug	Sodium Pyruvate	Wisent Bio Products	Cat. 600-110-UL	cell culture reagent
chemical compound, drug	Collagenase Type II	Worthington Biochemical Corporation	Cat. LS004176	enzymatic digest of bone fragments

6.5.2 Pharmacological interventions

The pharmacological interventions (final concentration, name (***abbreviation***): molecular target) used in this study were: 10 μM Gadolinium (Gd^{3+}): maxi-anion channel, 10 μM Carbenoxolone (***Cbx***): connexins/pannexins, 10 μM Flufenamic Acid (***FFA***): connexins, 1 mM 1-Octanol (***Oct***): connexins, 100 nM GSK 2193874 (***GSK***): TRPV4, 100 nM HC 067047 (***HC***): TRPV4, 10 μM Nifedipine (***Nif***): L-type VSCC, 10 μM ML218 (***ML***): T-type VSCC, 100 μM Suramin (***Sur***): P2 receptors (P2R), 100 μM ***PPADS***: P2 receptors, 1 μM A740003 (***A7***): P2X7 receptor, 10 μM

U73122 (***U73***): PLC, 100 nM Phorbol 12-myristate 13-acetate (***PMA***): PKC, 1 μM Bisindolylmaleimide II (***Bis***): PKC, 1 mM N-Ethylmaleimide (***NEM***): NSF, 1 μM GsMTx-4 (***GsM***): Piezo1. Unless stated otherwise, cells were treated with drugs for 10 mins prior to experiments. We validated the effects of hemichannel blockers (**Fig 6-S3**) and evaluated the effects of the inhibitors on ATP- or citrate-induced $[Ca^{2+}]_i$ responses in Fura2-loaded C2-OB cells and on luciferin/luciferase bioluminescence (**Fig 6-S9**).

6.5.3 Cell culture

Three osteoblast models were used in this study. All key experiments required to support our proposed model were performed using primary CB-OB cells, however, additional data from another primary source (bone marrow-derived; BM-OB) and cell-line (C2-OB) were reported to emphasize the validity of our findings and demonstrate how different osteoblast models perform in this study.

Bone marrow-derived osteoblasts (BM-OB): To obtain bone marrow-derived osteoblasts, 4-6 week C57Bl/6J mice (Charles River) were sacrificed and femur and tibia were collected. Bone pieces were sterilized in 70% EtOH and washed (3x, PBS). Bones were cut in half and placed into longitudinally-cut 1 mL pipette tips, with the exposed marrow end of the bone facing down. Pipette tips were centrifuged in Eppendorf tubes at 12 000 rpm (3x, 30 s) to isolate bone marrow cells. Bone marrow cells were plated at a density of 5×10^4 cells per cm^2 in osteoblastic differentiation medium (αMEM supplemented with 10% FBS, 1% sodium pyruvate, 1% penicillin streptomycin and 50 μg/mL ascorbic acid) and media was refreshed every 2-3 days. Osteoblast phenotype was observed within 7-11 days.

Compact bone-derived osteoblasts (CB-OB): Bone-marrow depleted bones, obtained after bone marrow cell isolation, were used as source of CB-OB. Epiphyseal ends of the bone were cut off and the remaining diaphysis were cut into small fragments (<1 mm^2 pieces. Bone fragments underwent a three-step enzymatic digest: (i) 10 mL αMEM (serum-free) + 125 μL 0.25% trypsin + 5 μL collagenase P (37℃, 15 min while rotating). (ii) Dispose supernatant and add 10 mL αMEM (serum-free) + 125 μL 0.25% trypsin + 10 μL 100 mg/mL collagenase P (37℃, 30 min while rotating). (iii) Dispose supernatant and add 10 mL αMEM (serum-free) + 125 μL 0.25% trypsin + 100 μL 100mg/mL collagenase II (37℃, 1 hr while rotating, shake vigorously every 10 min).

Supernatant from final digest was disposed, bone fragments were rinsed with PBS and plated in 6-well plates in αMEM (10% FBS, 1% sodium pyruvate, 1% penicillin streptomycin and 50 µg/mL ampicillin) for 3-5 days to allow cell outgrowth from fragments. Cells were detached with trypsin, filtered through 40 µm membrane and plated at a density of 1×10^4 per cm^2 in osteoblastic differentiation medium (αMEM supplemented with 10% FBS, 1% sodium pyruvate, 1% penicillin streptomycin and 50 µg/mL ascorbic acid) 2-3 days prior to experiments. Primary osteoblast cultures were sub-cultured for up to 8 passages (1:10 passages).

BMP-2 transfected C2C12 cells (C2-OB): The C2C12 cell line (ATCC CRL-1772) stably transfected with BMP-2 (courtesy of Dr. M. Murshed, McGill University) was maintained in DMEM (supplemented with 1% penicillin streptomycin, 1% sodium pyruvate and 10% FBS) at 5% CO_2, 37℃ humidified atmosphere. Cells between passages 6 – 10 were used in all experiments. 2-3 days prior to experiments, cells were plated at a density of 3×10^4 cells per cm^2.

6.5.4 Osteoblast phenotype

Cells were fixed with formalin (pH 7.4, 8 min) rinsed with PBS (3x). Alkaline phosphatase (ALP) staining solution was prepared by combining 4.5 mg fast red violet salt dissolved in 3.75 mL H_2O and 3.75 mL 0.2 M Tris-HCl, pH 8.3 with 0.75 mg Naphthol AS-MX phosphate disodium salt dissolved in 30 µL N,N-dimethylformamide. Sufficient staining solution was added to each well to ensure entire surface was covered (approx. 500 µL in 35 mm dish) and incubated at room temperature for 15 min, or until red precipitate formed. Cells were washed with H_2O and observed under bright field microscopy. Alkaline phosphate-positive cells were stained pinkish-red, while yellow hue was observed in alkaline phosphatase-negative cells.

6.5.5 Mechanical stimulation

Local membrane deformation of a single cell: Single osteoblastic cells were stimulated by local membrane deformation with a glass micropipette using a FemtoJet microinjector NI2 (Eppendorf Inc.). The micropipette was positioned approximately 10 µm from the cell membrane at a 45° angle from the horizontal plane and mechanically stimulated at a speed of 250 µm/s with a contact duration of 60 ms. Glass micropipettes were custom-made from glass capillary tubes (1.5 mm

outer diameter, King Precision Glass Inc.) using a Sutter Pipette Puller (Flaming/Brown, model P-87).

***Bulk stimulation using tFSS**:* 50% of the culture medium volume was manually withdrawn and replaced at an approximate speed of 2 resuspensions per second for an indicated number of x times (for example, 10x tFSS corresponded to 50% volume displacement performed 10 times).

6.5.6 Intracellular calcium recording and analysis

Cells plated on glass-bottom plates (MatTek Corporation) were loaded with a ratiometric fluorescent calcium dye Fura2-AM (r.t., 30 min), washed with PS and allowed to acclimatize for 10 min to reduce the effects of mechanical agitation. $[Ca^{2+}]_i$ was recorded at a sampling rate of 2 images per second (2 Hz) using a Nikon T2000 fluorescent inverted microscope with 40x objective (Tiedemann et al., 2009). Recordings consisted of ~10 s baseline $[Ca^{2+}]_i$ and additional 110-170 s following application of mechanical stimulation or treatment. The excitation wavelength was alternated between 340 and 380 nm using an ultra-high-speed wavelength switching illumination system (Lambda DG-4, Quorum Technologies). Regions of interest (ROI) were manually defined and the ratio of the fluorescent emission at 510 nm, following 340 and 380 nm excitation (f340/f380), was calculated and exported using the imaging software (Volocity, Improvision). All data were imported into an excel spreadsheet for characterization using a MATLAB algorithm previously described (Mackay, Mikolajewicz, Komarova, & Khadra, 2016). The following parameters were obtained for statistical analysis: amplitude (amp; magnitude of response), activation time ($t_{10\%-90\%}$; time between 10% and 90% of maximum response), and decay constant (τ_{decay}) of exponential decay region of deactivation phase of transient response. Micropipette stimulation experiments, secondary responsiveness was calculated as the percentage of neighboring cells exhibiting $[Ca^{2+}]_i$ elevations.

6.5.7 Vesicle labeling, imaging, and analysis

Localization: To visualize the intracellular distribution and colocalization of quinacrine and MANT-ATP, cells were loaded with MANT-ATP (5 μM, overnight, 37°C) followed by quinacrine (10 μM, 15 min, room temperature). Cells were washed with PS and imaged using a Zeiss LSM 780 laser scanning confocal microscope. An argon and diode laser were used as light sources (ex. 405 nm and 458 nm) and the detection wavelength ranges were set to 410-470 nm and 490-570

nm to ensure separation of overlapping emission spectra, for MANT-ATP and quinacrine, respectively. Images were acquired using a Zeiss Plan-Apochromat 63x/1.40 Oil immersion objective lens. Subsequent analysis was carried out using ImageJ (National Institutes of Health, USA). Vesicular density was determined using ImageJ by counting number of intracellular quinacrine-positive puncta and normalizing count to cell surface area.

Kinetics: To study vesicular release kinetics, time-lapse recordings of quinacrine-loaded cells were acquired with a Nikon T2000 fluorescent inverted microscope after a 10 min period of post-stain acclimatization to minimize the effects of mechanical agitation. Quinacrine-rich vesicles were imaged using a 40x objective at a sampling frequency of 2 Hz for 2 min. To minimize the phototoxic effects of quinacrine, the excitation intensity was set to 33% of peak intensity and the shutter was shut in between 100 ms exposures. Image sequences were exported using the imaging software (Velocity, Improvision) for subsequent analysis in ImageJ. To quantify the kinetics of vesicular release, sudden losses of fluorescence were monitored. Vesicles that gradually came in and out of focus did not qualify as release events. SparkSpotter (Babraham Bioinformatics, UK), an ImageJ plugin, was used to identify release events in temporally reversed and contrast-enhanced image stacks, so that the loss of fluorescence would instead be detected as a sudden increase by the spark identifying algorithm. Acquired data was visually evaluated and represented as either release events per second or cumulative vesicular release for indicated time frame, normalized to unit area.

6.5.8 ATP measurements

Fluorescence recordings of $[ATP]_e$: 10 nM D-luciferin- and 2 µg/mL fire-fly luciferase-containing physiological solution (PS) was added to C2-OB and extracellular luciferin fluorescence was recorded (380/510 ex/em). Using an ATP standard calibration curve (**Fig 6-S1)**, pericellular (<15 µm from stimulated cell) ATP concentrations [ATP] were obtained. The amount of ATP released by individual cells was estimated by fitting the diffusion profile obtained from the fluorescence measurements with the diffusion equation for release from an instantaneous plane source (Crank, 1975).

$$[ATP](x,t) = \frac{M}{2(\pi Dt)^{\frac{1}{2}}} \exp\left(\frac{-x^2}{4Dt}\right)$$

Where $[ATP](x,t)$ is ATP concentration at distance x from the source, the time t from the moment of release. M is the amount of ATP released at x = 0, t = 0. D is ATP diffusion coefficient, assumed at 3.3×10^{-6} cm^2/s at 22°C (Newman, 2001).

Bioluminescent recordings of [ATP]$_e$: Bioluminescence assay was used to measure ATP content in supernatant samples. Luciferin-luciferase reaction solution contained 0.45 μM D-luciferin and 40 μg/mL firefly-luciferase in bioluminsecence reaction buffer. 10 μL supernatants were sampled after tFSS stimulation, added into a glass cuvette containing 100 μL of luciferin-luciferase reaction solution, and measured using FB 12 single tube luminometer. Total cellular ATP content was measured in RIPA-lysed samples. [ATP] was estimated using calibration curves (**Fig 6-S9**).

6.5.9 Membrane integrity assays

Dye leakage: Fura2-loaded osteoblastic cells were mechanically stimulated with a glass micropipette and 510 nm emission intensity was monitored after 340 nm excitation (Togo et al., 1999). Unless stated otherwise, Fura2 leakage refers to the percentage of cells that were severely injured (sIn; complete loss of intracellular Fura2 fluorescence) following micropipette stimulation.
Dye uptake: 0.08% TB or 10 μM R-dextran were added before or 5 min after mechanical stimulation, washed with PS, and the proportion of dye-positive cells were assessed by bright field microscopy.
Cytosolic leakage: Extracellular lactate dehydrogenase (LDH) was measured using Cytotoxicity Detection Kit^{PLUS}. Total cellular LDH content was measured in RIPA-lysed samples.
Cell viability: 1 h after tFSS, AlamarBlue assay was performed according to manufacturer's protocol. Cell viability was reported as percentage of non-stimulated cells.

6.5.10 *In vivo* bone loading

10-week-old female C57Bl/6J mice were injected intraperitoneally with LFTR-Dex either 30 min before or 20 min after loading. In vivo cyclic compressive loading at 600 με or 1200 με was applied for 5 min (Willie et al., 2013). Mice were randomized into two groups, anesthetized, and *in vivo* cyclic compressive loading was applied to the left tibia [216 cycles at 4Hz the mean mouse locomotor stride frequency (Clarke & Still, 1999)], delivering a maximum force of -5.5 N and -11 N, which engenders 600 με or 1200 με, respectively at the periosteal surface of the tibia mid-diaphysis in these mice determined by prior in vivo strain gauging studies (Birkhold et al., 2014).

Previous reports have shown strain levels of 200-600 με are engendered on the medial tibia during walking in the mouse (De Souza et al., 2005; Sugiyama et al., 2012). Strain levels of 1200 με are considered supraphysiological resulting in a robust bone formation response after 5 days of mouse tibial loading (Brodt & Silva, 2010; Willie et al., 2013) and altered gene expression after only a single bout of loading (Kelly, Schimenti, Ross, & van der Meulen, 2016; Zaman et al., 2010). Mice ambulated freely after controlled loading, and were euthanized 50 min post dye-injection, weighed (**Fig 6-S4A**) and tibiae and calvariae were dissected and fixed in formalin. Tibia lengths were measured (**Fig 6-S4B**) and mid-shaft tibiae were cut into fragments, which were immunofluoresecently labeled for sclerostin, counterstained with DAPI, and visualized with Nikon T2000 fluorescence inverted microscope. Right non-loaded tibiae were used as an internal control. Female mice were used instead of males to minimize in-cage aggression and related variations in mechanical-loading. Experimenter was blinded during image analysis.

6.5.11 Immunoblotting

Cell lysates were extracted in RIPA lysis buffer and centrifuged (12 000 rpm, 10 min, 4°C). Supernatants were collected and protein concentration were determined using Quant-iT protein assay kit (Invitrogen). 70 μg cell lysates were separated on a 10% SDS-PAGE and transferred to a nitrocellulose membrane (0.45 μm, 162-0115, Bio-Rat) using a 10 mM sodium borate buffer. The membranes were blocked in 5% BSA in TBST buffer (1 h., room temperature) followed by overnight incubation at 4°C with primary antibodies (1:1000 dilution, 5% BSA in TBST) for phosphorylated PKC isoforms: p-PKC (pan; βII Ser660), p-PKCδ/θ (Ser643/676), p-PKD/PKCμ (Ser744/748) and p-PKCζ/λ (Thr410/403), or for total PKC isoforms: PKCα, PKCδ, PKD/PKCμ and PKCζ. Blots were washed and incubated with horseradish peroxidase (HRP)-conjugated secondary antibodies for 1 h at room temperature (1:1000 dilution, 5% BSA in TBST) and visualized with a chemiluminescence system.

6.5.12 GAP junction functional assay

Cells were scraped in the presence of GAP-junction permeable dye Lucifer yellow (LY, 10 μM), incubated for 2 min (37°C), rinsed and fixed with formalin (pH 7.4, 8 min). Dye transfer was visualized using wide-field epifluorescence microscopy and cell-cell coupling was visually determined by bright field microscopy. Cells that were not initially scraped but were physically

coupled and LY-positive after two minutes of staining were reported as a percentage of total cells that were physically coupled to scraped neighbors.

6.5.13 Statistical analysis

Data are representative results or means ± standard errors (S.E.M). Curve fittings and $[Ca^{2+}]_i$ transient characterization was done in MATLAB (MathWorks). Sample sizes for *in vitro* experiments indicate the total number of biological replicates (specified in figure legends as number of stimulated cells or number of independent cultures, which were isolated from different mice for primary OB, or represent different plating dates for C2-OB) pooled across a minimum of 3 independent experiments. For *in vivo* experiments, sample sizes indicate number of animals. Statistical significance was assessed by ANOVA followed by Bonferroni post-hoc test, significance levels are reported as single symbol: *p<0.05; double symbol **p<0.01 or triple symbol ***p<0.001.

6.6 References

Birkhold, A. I., Razi, H., Duda, G. N., Weinkamer, R., Checa, S., & Willie, B. M. (2014). Mineralizing surface is the main target of mechanical stimulation independent of age: 3D dynamic in vivo morphometry. *Bone, 66*(Supplement C), 15-25. doi:https://doi.org/10.1016/j.bone.2014.05.013

Brodt, M. D., & Silva, M. J. (2010). Aged mice have enhanced endocortical response and normal periosteal response compared with young-adult mice following 1 week of axial tibial compression. *Journal of Bone and Mineral Research, 25*(9), 2006-2015. doi:10.1002/jbmr.96

Burnstock, G., & Verkhratskii, A. N. (2012). *Purinergic signalling and the nervous system*. Berlin; London: Springer.

Cao, Q., Zhao, K., Zhong, X. Z., Zou, Y., Yu, H., Huang, P., . . . Dong, X. P. (2014). SLC17A9 protein functions as a lysosomal ATP transporter and regulates cell viability. *J Biol Chem, 289*(33), 23189-23199. doi:10.1074/jbc.M114.567107

Clarke, K. A., & Still, J. (1999). Gait analysis in the mouse. *Physiol Behav, 66*(5), 723-729.

Cooper, S. T., & McNeil, P. L. (2015). Membrane Repair: Mechanisms and Pathophysiology. *Physiol Rev., 95*(4), 1205-1240. doi:10.1152/physrev.00037.2014

Crank, J. (1975). *The mathematics of diffusion / by J. Crank*. Oxford [England]: Clarendon Press.

De Souza, R. L., Matsuura, M., Eckstein, F., Rawlinson, S. C., Lanyon, L. E., & Pitsillides, A. A. (2005). Non-invasive axial loading of mouse tibiae increases cortical bone formation and modifies trabecular organization: a new model to study cortical and cancellous compartments in a single loaded element. *Bone, 37*(6), 810-818. doi:10.1016/j.bone.2005.07.022

Erickson, H. P. (2009). Size and Shape of Protein Molecules at the Nanometer Level Determined by Sedimentation, Gel Filtration, and Electron Microscopy. *Biol Proced Online, 11*, 32-51. doi:10.1007/s12575-009-9008-x

Genetos, D., Geist, D., Dawei, L., Donahue, H., & Duncan, R. (2005). Fluid Shear-Induced ATP Secretion Mediates Prostaglandin Release in MC3T3-E1 Osteoblasts. *J Bone Miner Res, 20*(1), 41-49. doi:10.1359/JBMR.041009

Genetos, D., Kephart, C., Zhang, Y., Yellowley, C., & Donahue, H. (2007). Oscillating fluid flow activation of gap junction hemichannels induces ATP release from MLO-Y4 osteocytes. *J Cell Physiol, 212*(1), 207-214. doi:10.1002/jcp.21021

Kelly, N. H., Schimenti, J. C., Ross, F. P., & van der Meulen, M. C. (2016). Transcriptional profiling of cortical versus cancellous bone from mechanically-loaded murine tibiae reveals differential gene expression. *Bone, 86*, 22-29. doi:10.1016/j.bone.2016.02.007

Kirmse, K., & Kirischuk, S. (2006). N-ethylmaleimide increases release probability at GABAergic synapses in layer I of the mouse visual cortex. *European Journal of Neuroscience, 24*(10), 2741-2748. doi:10.1111/j.1460-9568.2006.05179.x

Kowal, J. M., Haanes, K. A., Christensen, N. M., & Novak, I. (2015). Bile acid effects are mediated by ATP release and purinergic signalling in exocrine pancreatic cells. *CCS, 13*, 28. doi:10.1186/s12964-015-0107-9

Kringelbach, T. M., Aslan, D., Novak, I., Ellegaard, M., Syberg, S., Andersen, C. K., . . . Jorgensen, N. R. (2015). Fine-tuned ATP signals are acute mediators in osteocyte mechanotransduction. *Cell Signal, 27*(12), 2401-2409. doi:10.1016/j.cellsig.2015.08.016

Kringelbach, T. M., Aslan, D., Novak, I., Schwarz, P., & Jorgensen, N. R. (2014). UTP-induced ATP release is a fine-tuned signalling pathway in osteocytes. *Purinergic Signal, 10*(2), 337-347. doi:10.1007/s11302-013-9404-1

Lewis, K. J., Frikha-Benayed, D., Louie, J., Stephen, S., Spray, D. C., Thi, M. M., . . . Schaffler, M. B. (2017). Osteocyte calcium signals encode strain magnitude and loading frequency in vivo. *PNAS, 114*(44), 11775-11780.

Li, S., Xu, W., Xing, Z., Qian, J., Chen, L., Gu, R., . . . Deng, F. (2017). A Conditional Knockout Mouse Model Reveals a Critical Role of PKD1 in Osteoblast Differentiation and Bone Development. *Scientific Reports, 7*, 40505. doi:10.1038/srep40505

https://www.nature.com/articles/srep40505#supplementary-information

Lonart, G., & Sudhof, T. C. (2000). Assembly of SNARE core complexes prior to neurotransmitter release sets the readily releasable pool of synaptic vesicles. *J Biol Chem, 275*(36), 27703-27707.

Lopez-Ayon, G. M., Liu, H. Y., Xing, S., Maria, O. M., LeDue, J. M., Bourque, H., . . . Komarova, S. V. (2014). Local membrane deformation and micro-injury lead to qualitatively different responses in osteoblasts. *F1000Res, 3*, 162. doi:10.12688/f1000research.4448.1

Mackay, L., Mikolajewicz, N., Komarova, S. V., & Khadra, A. (2016). Systematic Characterization of Dynamic Parameters of Intracellular Calcium Signals. *Front Physiol., 7*(525). doi:10.3389/fphys.2016.00525

Manaka, S., Tanabe, N., Kariya, T., Naito, M., Takayama, T., Nagao, M., . . . Miyazaki, M. (2015). Low-intensity pulsed ultrasound-induced ATP increases bone formation via the P2X7 receptor in osteoblast-like MC3T3-E1 cells. *FEBS Lett, 589*(3), 310-318. doi:10.1016/j.febslet.2014.12.013

McNeil, P. L., & Steinhardt, R. A. (2003). Plasma membrane disruption: repair, prevention, adaptation. *Annu Rev Cell Dev Biol, 19*, 697-731. doi:10.1146/annurev.cellbio.19.111301.140101

Mochly-Rosen, D., Das, K., & Grimes, K. V. (2012). Protein kinase C, an elusive therapeutic target? *Nature reviews. Drug discovery, 11*(12), 937-957. doi:10.1038/nrd3871

Morrell, A. E., Brown, G. N., Robinson, S. T., Sattler, R. L., Baik, A. D., Zhen, G., . . . Guo, X. E. (2018). Mechanically induced Ca2+ oscillations in osteocytes release extracellular vesicles and enhance bone formation. *Bone Research, 6*(1), 6. doi:10.1038/s41413-018-0007-x

Newman, E. A. (2001). Propagation of Intercellular Calcium Waves in Retinal Astrocytes and Müller Cells. *The Journal of neuroscience : the official journal of the Society for Neuroscience, 21*(7), 2215-2223.

Patel Nagaraja, M., & Jo, H. (2014). The Role of Mechanical Stimulation in Recovery of Bone Loss—High versus Low Magnitude and Frequency of Force. *Life, 4*(2), 117-130. doi:10.3390/life4020117

Pines, A., Romanello, M., Cesaratto, L., Damante, G., Moro, L., D'Andrea, P., & Tell, G. (2003). Extracellular ATP stimulates the early growth response protein 1 (Egr-1) via a protein kinase C-dependent pathway in the human osteoblastic HOBIT cell line. *Biochem J, 373*(Pt 3), 815-824. doi:10.1042/bj20030208

Robling, A. G., & Turner, C. H. (2009). Mechanical Signaling for Bone Modeling and Remodeling. *Crit Rev Eukaryot Gene Expr, 19*(4), 319-338.

Romanello, M., Codognotto, A., Bicego, M., Pines, A., Tell, G., & D'Andrea, P. (2005). Autocrine/paracrine stimulation of purinergic receptors in osteoblasts: Contribution of vesicular ATP release. *Biochem Biophys Res Commun, 331*(4), 1429-1438. doi:http://dx.doi.org/10.1016/j.bbrc.2005.03.246

Romanello, M., Pani, B., Bicego, M., & D'Andrea, P. (2001). Mechanically induced ATP release from human osteoblastic cells. *Biochem Biophys Res Commun, 289*(5), 1275-1281. doi:10.1006/bbrc.2001.6124

Rumney, R. M. H., Sunters, A., Reilly, G. C., & Gartland, A. (2012). Application of multiple forms of mechanical loading to human osteoblasts reveals increased ATP release in response to fluid flow in 3D cultures and differential regulation of immediate early genes. *Journal of biomechanics, 45*(3), 549-554.

Schriefer, J. L., Warden, S. J., Saxon, L. K., Robling, A. G., & Turner, C. H. (2005). Cellular accommodation and the response of bone to mechanical loading. *J Biomech, 38*(9), 1838-1845. doi:10.1016/j.jbiomech.2004.08.017

Seref-Ferlengez, Z., Maung, S., Schaffler, M. B., Spray, D. C., Suadicani, S. O., & Thi, M. M. (2016). P2X7R-Panx1 Complex Impairs Bone Mechanosignaling under High Glucose Levels Associated with Type-1 Diabetes. *PLoS ONE, 11*(5), e0155107. doi:10.1371/journal.pone.0155107

Sørensen, C. E., & Novak, I. (2001). Visualization of ATP Release in Pancreatic Acini in Response to Cholinergic Stimulus. *J Biol Chem, 276*(35), 32925-32932. doi:10.1074/jbc.M103313200

Sugiyama, T., Meakin, L. B., Browne, W. J., Galea, G. L., Price, J. S., & Lanyon, L. E. (2012). Bones' adaptive response to mechanical loading is essentially linear between the low strains associated with disuse and the

high strains associated with the lamellar/woven bone transition. *J Bone Miner Res, 27*(8), 1784-1793. doi:10.1002/jbmr.1599

Thompson, W. R., Majid, A. S., Czymmek, K. J., Ruff, A. L., Garcia, J., Duncan, R. L., & Farach-Carson, M. C. (2011). Association of the alpha(2)delta(1) subunit with Ca(v)3.2 enhances membrane expression and regulates mechanically induced ATP release in MLO-Y4 osteocytes. *J Bone Miner Res, 26*(9), 2125-2139. doi:10.1002/jbmr.437

Tiedemann, K., Hussein, O., Sadvakassova, G., Guo, Y., Siegel, P. M., & Komarova, S. V. (2009). Breast Cancer-derived Factors Stimulate Osteoclastogenesis through the Ca(2+)/Protein Kinase C and Transforming Growth Factor-β/MAPK Signaling Pathways. *J Biol Chem, 284*(48), 33662-33670. doi:10.1074/jbc.M109.010785

Togo, T., Alderton, J. M., Bi, G. Q., & Steinhardt, R. A. (1999). The mechanism of facilitated cell membrane resealing. *J Cell Sci, 112 (Pt 5)*, 719-731.

Wang, N., Rumney, R. M., Yang, L., Robaye, B., Boeynaems, J. M., Skerry, T. M., & Gartland, A. (2013). The P2Y13 receptor regulates extracellular ATP metabolism and the osteogenic response to mechanical loading. *J Bone Miner Res, 28*(6), 1446-1456. doi:10.1002/jbmr.1877

Weinbaum, S., Cowin, S. C., & Zeng, Y. (1994). A model for the excitation of osteocytes by mechanical loading-induced bone fluid shear stresses. *J Biomech, 27*(3), 339-360.

Willie, B. M., Birkhold, A. I., Razi, H., Thiele, T., Aido, M., Kruck, B., . . . Duda, G. N. (2013). Diminished response to in vivo mechanical loading in trabecular and not cortical bone in adulthood of female C57Bl/6 mice coincides with a reduction in deformation to load. *Bone, 55*(2), 335-346. doi:10.1016/j.bone.2013.04.023

Yu, K., Sellman, D. P., Bahraini, A., Hagan, M. L., Elsherbini, A., Vanpelt, K. T., . . . McGee-Lawrence, M. E. (2017). Mechanical loading disrupts osteocyte plasma membranes which initiates mechanosensation events in bone. *J Orthop Res*. doi:10.1002/jor.23665

Zaman, G., Saxon, L. K., Sunters, A., Hilton, H., Underhill, P., Williams, D., . . . Lanyon, L. E. (2010). Loading-related regulation of gene expression in bone in the contexts of estrogen deficiency, lack of estrogen receptor alpha and disuse. *Bone, 46*(3), 628-642. doi:10.1016/j.bone.2009.10.021

Chapter Seven

Transmission of Mechanical Information by Purinergic Signalling

In addition to identifying a novel regulatory mechanism of mechanically-stimulated ATP release in bone cells, we demonstrated that the magnitude of the mechanical stimulus (**Chapter 4, 6**) as well as the mechano-adaptive status of the stimulated cell (**Chapter 6**) influence the purinergic response in neighbouring non-stimulated cells. In the current study, we build upon those findings and address ***research objective 2*** by investigating how spatiotemporal variations in the purinergic signal convey information about severity of the mechanical stimulus, as well as the mechano-adaptive status of the mechanically-stimulated cell. using a combination of experimental and mathematical approaches. We developed a mathematical model describing mechanically-induced ATP release, its diffusion and degradation to ADP as well as signaling induced by these molecules. This model was validated using experimental data obtained in **Chapter 6**. This approach allowed us to scale a single-cell injury to a tissue-level injury with varying geometries and examine how neighboring cell populations detect the magnitude of injury and discern their position relative to the injury site. Supplemental figures and tables for this chapter are provided in **Appendix A6**.

7.1 Abstract

The skeleton constantly interacts and adapts to the physical world. We have previously reported that physiologically-relevant mechanical forces lead to small repairable membrane injuries in bone-forming osteoblasts, resulting in release of ATP and stimulation of purinergic (P2) calcium responses in neighbouring cells. The goal of this study was to develop a theoretical model

describing injury-related ATP and ADP release, their extracellular diffusion and degradation, and purinergic responses in neighboring cells. After validation using experimental data for intracellular free calcium elevations, ATP and vesicular release following mechanical stimulation of a single osteoblast, and model was scaled to a tissue-level injury to investigate how purinergic signaling communicates information about injuries with varying geometries. We found that total ATP released, peak extracellular ATP concentration and the ADP-mediated signaling component contributed complementary information regarding the mechanical stimulation event. The total amount of ATP released governed spatial factors, such as the maximal distance from the injury at which purinergic responses were stimulated. The peak ATP concentration reflected the severity of an individual cell injury allowing to discriminate between minor and severe injuries that released similar amounts of ATP due to differences in injury repair, and determined temporal aspects of the response, such as signal propagation velocity. ADP-mediated signaling became relevant only in larger tissue-level injuries, conveying information about the distance to the injury site and its geometry. Thus, we identified specific features of extracellular ATP and ADP spatiotemporal signals that depend on tissue mechano-resilience and encode the severity, scope and proximity of the mechanical stimulus.

7.2 Introduction

The human skeleton is constantly interacting and adapting to the physical world, as seen by the loss of bone in astronauts experiencing microgravity (Jo & Shin, 2015) or gain of bone in athletes engaged in intense activities (Kohrt, Barry, & Schwartz, 2009). The magnitude, frequency and duration of mechanical loading are known determinants of the mechano-adaptive response of bone at the tissue-level (Carter & Beaupré, 2007; Skerry, 2006; Turner, 1998) and at the cellular-level, as observed with intracellular free calcium ($[Ca^{2+}]_i$) elevations in osteocytes during *in vivo* mechanical loading (Lewis et al., 2017).

We have recently reported that physiologically-relevant mechanical loading routinely injured bone cells *in vitro* and *in vivo*, resulting in release of ATP through plasma membrane disruptions, and stimulation of calcium responses in the neighbouring cells (Mikolajewicz, Zimmermann, Willie, & Komarova, 2018). These membrane disruptions in bone cells are counteracted by rapid vesicle-mediated membrane repair (Mikolajewicz, Zimmermann, et al., 2018; K. Yu et al., 2018), which limits ATP spillage. Thus, contrary to previous generalizations that ATP is released as a bolus

proportional to mechanical stimulus (Mikolajewicz, Mohammed, Morris, & Komarova, 2018), our data suggest that mechanically-stimulated ATP release contains dynamic information about both the extent of the injury and the rate of repair.

ATP stimulates autocrine and paracrine $[Ca^{2+}]_i$ signaling through purinergic (P2) receptor network, which consists of seven ionotropic P2X receptors and eight G-protein coupled P2Y receptors (Genetos, Geist, Dawei, Donahue, & Duncan, 2005; Robling & Turner, 2009; Romanello, Pani, Bicego, & D'Andrea, 2001). Several P2 receptors have been implicated in the mechano-adaptive response in bone (Alvarenga et al., 2010; Biver et al., 2013; Li, Liu, Ke, Duncan, & Turner, 2005), however it is uncertain why so many receptors are required and how they integrate mechanical information. While individual P2 receptors are sensitive to ATP concentrations over 2-3 orders of magnitude, the entire P2 receptor network covers over a million-fold range of ATP concentrations (Grol, Pereverzev, Sims, & Dixon, 2013; Xing, Grol, Grutter, Dixon, & Komarova, 2016). In addition, many P2Y receptors are differentially sensitive to ADP and ATP. Thus, it is possible that unique subsets of P2 receptors are activated in neighboring bone cells depending on the position and severity of the mechanical stimulus.

We hypothesized that the dynamics of mechanically-stimulated ATP release reflect the balance between cell membrane injury and repair; and that ATP and ADP released from the injury site generate unique spatiotemporal signatures that convey information to non-stimulated neighboring cells, such as injury severity and distance to stimulus, as well as the state of tissue mechano-resilience. We developed a mathematical model to account for injury-related ATP and ADP release, their extracellular diffusion and degradation, as well as paracrine purinergic responsiveness of neighboring cells. The experimentally validated model was scaled to a tissue-level mechanical stimulus to investigate how a cellular population responds to mechanical stimuli with position- and severity-appropriate responses.

7.3 Results

7.3.1 Mechanical stimulation of a single osteoblast leads to release of purinergic signals that convey position- and magnitude-related information to neighboring osteoblasts

Compact bone-derived primary osteoblasts (CB-OB) or BMP-2-transfected C2C12 osteoblast-like cells (C2-OB) were loaded with calcium-indicator Fura2 and a single osteoblast (primary cell) was mechanically stimulated with a glass micropipette, which we have shown to result in a repairable plasma membrane disruption, severity of which correlates with the magnitude of $[Ca^{2+}]_i$ elevation in the stimulated cell (Mikolajewicz, Zimmermann, et al., 2018). Now we focus on $[Ca^{2+}]_i$ elevations in non-stimulated neighbouring cells (secondary responses), which were inhibited by the purinergic antagonist suramin (**Fig 7-1A**). The magnitudes of the secondary responses were proportional to the amplitude of $[Ca^{2+}]_i$ elevation in the primary cell (**Fig 7-1B**). The responding fraction of cells (observed response probability, P_O) decreased with increasing distance from the primary cell (**Fig 7-1C**), while the delay between the primary and secondary responses (observed response time, T_O) increased (**Fig 7-1D**). Using a logistic regression model, we demonstrated that the parameters of the primary Ca^{2+} response and distance to the primary cell predicted the onset of secondary responses with 76-79% accuracy ($p<0.001$, **Fig 7-1E**). These data suggest that purinergic signals convey information regarding the magnitude and proximity of the mechanical stimulus.

7.3.2 ATP release depends on the size and resealing kinetics of membrane repair following mechanical injury

We have shown that micropipette stimulation generates non-lethal membrane injury, detectable by decrease in Fura2 fluorescence (dye leakage), through which intracellular ATP is released (Mikolajewicz, Zimmermann, et al., 2018). Membrane injury is quickly repaired through PKC-dependent vesicular exocytosis, thus limiting ATP release (Mikolajewicz, Zimmermann, et al., 2018). The size of initial membrane injury, d_0, was estimated to be on the nanometer scale based on cell intake of membrane-impermeable dyes of variable size (Mikolajewicz, Zimmermann, et al., 2018). To quantify the rate of membrane resealing, we determined the repair kinetics using two independent methods: plateau of dye leakage and cessation of vesicular release (Defour, Sreetama, & Jaiswal, 2014). Depletion of Fura2 fluorescence (340 ex/510 em) after C2-OB cell

micropipette stimulation was monitored until a plateau was achieved, indicating membrane repair (**Fig 7-2A**, *top*). Alternatively, quinacrine-loaded C2-OB cells were micropipette-stimulated and vesicular release was monitored as a proxy of the membrane repair process (**Fig** 7-**2A**, *bottom*). The repair time $\tau_{1/2}$ – calculated as the exponential half-life – was 11 s (95% CI: 6 to 16) for Fura2-leakage assay (**Fig 7-2B**, *blue*) and 18 s (95% CI: 7 to 28) for vesicular release imaging (**Fig 7-2B**, *red*). Despite using two surrogate measures of membrane repair, both methods provided similar estimates of $\tau_{1/2}$ suggesting that the contribution of other processes is limited. Thus, nanometer-scale mechanically-induced membrane injury reseals with an exponential half-time of 11-18 s.

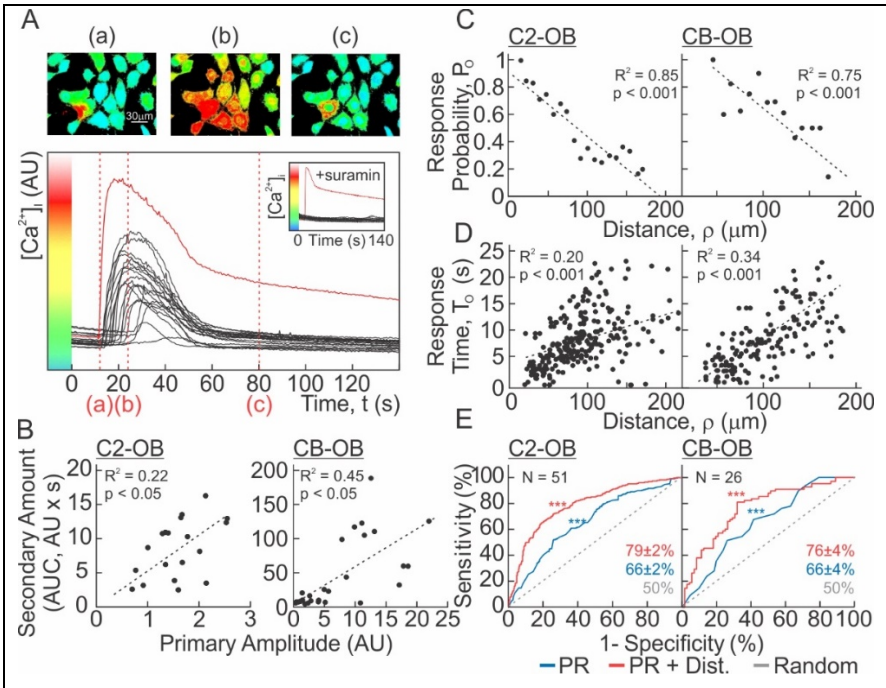

Figure 7-1. Mechanically-induced purinergic signaling conveys the magnitude and distance to stimulus. (A) Single Fura2-loaded C2-OB was mechanically stimulated by micropipette and $[Ca^{2+}]_i$ was recorded. *Top*: pseudocolored 340/380 Fura2 ratio images. *Bottom*: $[Ca^{2+}]_i$ recording of mechanically-stimulated (primary) cell (*red*) and neighboring (secondary) responders (*black*). *Red dashed lines*: Time points in top panel. *Inset*: Experiment performed in presence of P2 receptor antagonist suramin (100 μM). **(B)** Correlation between the primary response amplitude and area under curve (AUC) of secondary $[Ca^{2+}]_i$ elevations for C2-OB (*left*) and CB-OB (*right*). **(C-D)** Correlation between distance from primary cell and observed response probability P_O of neighboring cells **(C)** and observed response time T_O after mechanical stimulation **(D)** for C2-OB (*left*) and CB-OB (*right*). *Black dashed line*: linear regressions. **(E)** Receiver operating characteristic (ROC) curves demonstrate performance of logistic regression model in predicting incidence of secondary responses based on primary response (PR) parameters (*blue*), PR parameters and distance (dist., *red*) or chance alone (*grey*) for C2-OB (*left*) and CB-OB (*right*). Accuracies of logistic models ± SEM are shown, N indicates number of trials.

Mediator release model. To describes the release of mediators, such as ATP, from a mechanically-injured cell, we assumed that a circular injury (Lopez-Ayon et al., 2014; Nakamura et al., 2018) with the diameter $d(t)$, and an initial diameter d_0, is repaired with an exponential half-time $\tau_{1/2}$:

$$d(t) = d_0 2^{-t/\tau_{1/2}} \quad (1)$$

Mediator release from the injured cell was modelled as described previously by Zarnitsyn and colleagues (2008) (Zarnitsyn, Rostad, & Prausnitz, 2008) as diffusion through the membrane opening, with the rate of intracellular mediator depletion $c_{in}^{i\prime}(t)$ ($i = ATP\ or\ ADP$; $'$ indicates the time derivative) proportional to the diffusion-dependent transport coefficient β_i, which in turn depends on the injury diameter $d(t)$, cell volume V_{cell} and intracellular D_{cyto}^{i} and extracellular D_i diffusivity of ATP and ADP [$D_{cyto}^{i} \cong 0.25 D_i$ (Zarnitsyn et al., 2008), $i = ATP, ADP$]:

$$\beta_i = \left(\frac{1}{4D_{cyto}^{i} \cdot d(t)} + \frac{1}{4D_i \cdot d(t)}\right)^{-1} (V_{cell})^{-1} = \frac{4D_i}{5V_{cell}} d(t) \quad (2)$$

The rate of intracellular mediator depletion $c_{in}^{i\prime}(t)$ is then expressed as:

$$\begin{cases} c_{in}^{i\prime}(t) = -\beta_i c_{in}^{i}(t) & , \quad t > 0 \\ c_{in}^{i}(0) = c_{in,0}^{i} & , \quad t = 0 \end{cases} \quad (3)$$

Finally, the rate of mediator release at the site of the injured cell $c_{source}^{i'}(t)$ is:

$$c_{source}^{i'}(t) = -c_{in}^{i\prime}(t) \quad (4)$$

At varying d_0 and $\tau_{1/2}$, the rate of ATP release is the highest immediately after membrane disruption and declines exponentially with time (**Fig 7-2C, D**). The total amount of ATP released ($[\mathrm{ATP}]_{\mathrm{total}}$) is proportional to the initial injury size d_0 and inversely proportional to the repair half-time $\tau_{1/2}$ (**Fig 7-2E, F**). The peak of extracellular ATP ($[\mathrm{ATP}]_{\mathrm{peak}}$) is determined by the initial injury size (**Fig 7-2G**), while ATP persistence at the source ($[\mathrm{ATP}]_{\mathrm{FWHM}}$; time during which extracellular [ATP] was above half-maximal [ATP]) is governed by the rate of membrane resealing (**Fig 7-2H**). Thus, the severity and dynamics of membrane repair contribute differentially to the peak, total amount and persistence of extracellular ATP.

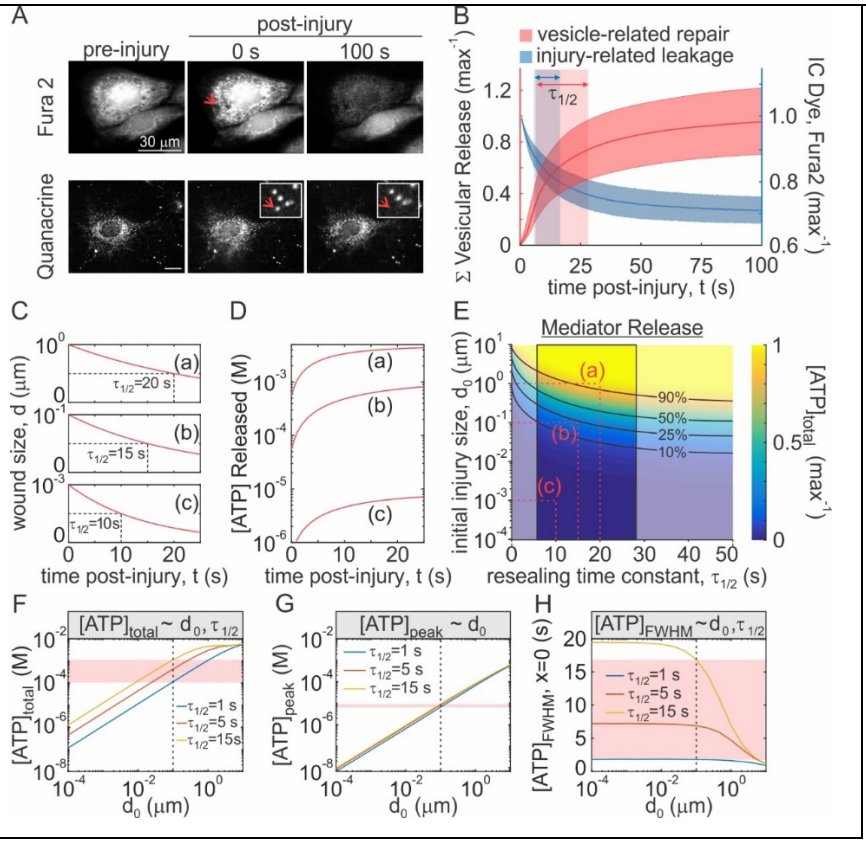

Figure 7-2. The size and resealing kinetics of the membrane injury determine the kinetics of ATP release. (A, B) Single Fura2- (**A**, *top*) or quinacrine- (**A**, *bottom*) loaded C2-OB was mechanically stimulated by micropipette and time-course of intracellular (IC) Fura2 decrease (**B**, *blue,* N=51) and cumulative vesicular release (**B**, red, N=15) was recorded. Data are means ± 95% confidence intervals (CI). *Shaded boxes*: 95% CI of time to half max ($\tau_{1/2}$) for Fura2-leakage (*blue*) or vesicular release (*red*). **(C, D)** Simulated temporal changes in injury size $d(t)$ **(C)** and ATP release **(D)** for indicated initial injury size d_0 and the characteristic membrane repair times $\tau_{1/2}$. **(E)** Solution space for injury-related ATP release with respect to changes in initial injury size d_0 and the characteristic membrane repair time $\tau_{1/2}$. *Black lines*: isoclines for parameter pairs that yield equal percentage of total ATP release. *Red dashed lines*: Parameter pairs (a, b, c) used in **C, D**. *Outlined region*: Experimentally measured $\tau_{1/2}$. **(F-H)** Relationship between initial injury size d_0 and total ATP released $[ATP]_{total}$ **(F)**, peak extracellular ATP concentration $[ATP]_{peak}$ **(G)** and full-width half max (FWHM) duration of extracellular ATP concentration $[ATP]_{FWHM}$ at the source **(H)** for $\tau_{1/2} = 1, 5, 15$ s. *Red bands* show sensitivity of ATP release parameters to changes in $\tau_{1/2}$ for $d_0 = 100$ nm (*dashed black line*).

7.3.3 Contribution of ADP to the mechanically-stimulated purinergic signal

Mediator spillage through membrane injury is nonspecific, therefore, purines present in the cytosol will be released from the cell in proportional amounts. We tested ATP, ADP, AMP and adenosine for their ability to induce calcium responses. Only ATP and ADP evoked $[Ca^{2+}]_i$ elevations in C2-OB cells (**Fig 7-3A**). Extracellular ATP and ADP is degraded by ecto-nucleotidases present on cells resident to bone, including osteoblasts, osteoclasts and bone marrow cells. Osteoblast (C2-OB) and osteoclast (Raw 264.7) precursors-like cells metabolized extracellular ATP with similar

rate constants of 0.049 min^{-1} (95% CI: 0.043 to 0.055) and 0.048 min^{-1} (95% CI: 0.044 to 0.042), respectively, while erythroid K562 cells hydrolyzed ATP significantly faster with a rate constant of 0.096 min^{-1} (95% CI: 0.085 to 0.11) (**Fig 7-3B, C, Table 7-S1**). The degradation rate was independent of cell density (**Fig 7-S1**). In C2-OB cells, ATP degradation was partially inhibited by ecto-nucleotidase inhibitor ARL 67156 (**Fig 7-3D**, *blue*), and potently inhibited by alkaline phosphatase inhibitor orthovanadate (**Fig 7-3D**, *red*). These data suggest that the mechanical signal is composed of ATP and ADP and is regulated by extracellular enzymatic degradation.

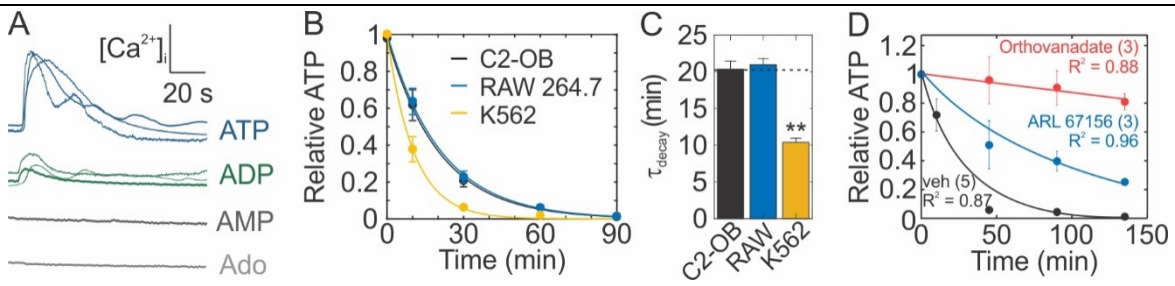

Figure 7-3. Contribution of ADP to the mechanically-stimulated purinergic signal (A) Representative $[Ca^{2+}]_i$ elevations in Fura2-loaded C2-OB stimulated by 1 μM ATP, 1 μM ADP, 10 μM AMP or 10 μM adenosine (Ado). **(B, C)** 1 μM ATP was added to cultures of C2-OB osteoblasts, RAW 264.7 osteoclast-precursors and K562 erythrocyte-like cells, ATP degradation was measured (**B**) and decay time constants were estimated τ_{decay} (**C**). **(D)** Degradation of 1 μM ATP by C2-OB in the presence of ecto-nucleotidase inhibitor ARL 67156 (10 μM) or alkaline-phosphatase inhibitor orthovanadate (10 μM). For **B-D**, data are means ± SEM, *solid curves*: fitted exponential functions (**Table 7-S1**).

7.3.4 Paracrine response probabilities and times are governed by ATP and ADP diffusion and purinergic reaction times

We next extended our mediator release model to describe the extracellular diffusion of ATP and ADP released by mechanical injury and subsequent cellular responsiveness to ATP and ADP, using experimental data to validate model predictions.

Diffusion model. We coupled ATP and ADP release and extracellular diffusion using the geometrical constraints imposed by our *in vitro* experiments. The mechanically-stimulated primary cell was modelled as a finite sphere (defined by radius R_{cell}), from which ATP and ADP molecules were released uniformly within the cell volume at a rate $c_{source}^{i'}(t)$ $(i = ATP, ADP)$. Of note, the geometry of the primary cell minimally affected ATP and ADP diffusion profiles, due to their rapid diffusion over the cell length scale $\left(\frac{R_{cell}^2}{6D_i} < 0.04s;\ i = ATP, ADP\right)$. Diffusion of

extracellular ATP and ADP ($c_{ex}^{i}(\rho,t);\ i=ATP,ADP$) with coefficients D_i was computed using the 3D radial diffusion equation with spherical boundaries of radius R_{bound}, such that the radial variable satisfied $0<\rho<R_{bound}$. This spherical boundary has no physical significance and was chosen to be much larger than the other dimensions in our problem i.e. $\sqrt{6D_i t}\ll R_{bound}$, where t is any time in the time range considered in this work. To account for extracellular degradation of ATP and ADP, we assumed the first-order degradation rate constant of ATP to ADP as k_{ATP}, and the first-order degradation rate constant of ADP out of the system as k_{ADP}. In order to impose no-flux boundary (Neumann) conditions to emulate the culture dish bottom, we doubled the concentration in the upper hemisphere (i.e. polar angle limited to $0<\theta<\pi/2$), while ignoring the solution in the lower hemisphere (i.e. $\pi/2<\theta<\pi$) after computation of the concentration in full 3D space. The equations which were solved (in full 3D space) for extracellular ATP (Eq. 5) and ADP (Eq. 6) were:

$$\begin{cases} \dfrac{\partial}{\partial t}c_{ex}^{ATP}(\rho,t)=D_{ATP}\left(\dfrac{\partial^2}{\partial\rho^2}+\dfrac{2}{\rho}\dfrac{\partial}{\partial\rho}\right)c_{ex}^{ATP}(\rho,t) \\ \qquad\qquad +I(\rho<R_{cell})c_{source}^{ATP'}(t)-k_{ATP}c_{ex}^{ATP}(\rho,t), \qquad \rho<R_{bound},t\geq 0 \\ \dfrac{\partial}{\partial t}c_{ex}^{ATP}(\rho,t)=0 \qquad\qquad , \qquad \rho=R_{bound},t\geq 0 \end{cases} \tag{5}$$

$$\begin{cases} \dfrac{\partial}{\partial t}c_{ex}^{ADP}(\rho,t)=D_{ADP}\left(\dfrac{\partial^2}{\partial\rho^2}+\dfrac{2}{\rho}\dfrac{\partial}{\partial\rho}\right)c_{ex}^{ADP}(\rho,t) \\ \qquad +I(\rho<R_{cell})c_{source}^{ADP'}(t) \\ \quad +k_{ATP}c_{ex}^{ATP}(\rho,t)-k_{ADP}c_{ex}^{ADP}(\rho,t), \qquad \rho<R_{bound},t\geq 0 \\ \dfrac{\partial}{\partial t}c_{ex}^{ADP}(\rho,t)=0 \qquad\qquad \rho=R_{bound},t\geq 0 \end{cases} \tag{6}$$

where $I(\cdot)$ denotes the indicator function (1 when true, otherwise 0). Eq. 5 and 6 were solved using the NDSolve routine provided by Mathematica 11.2 (**Fig 7-4A**).

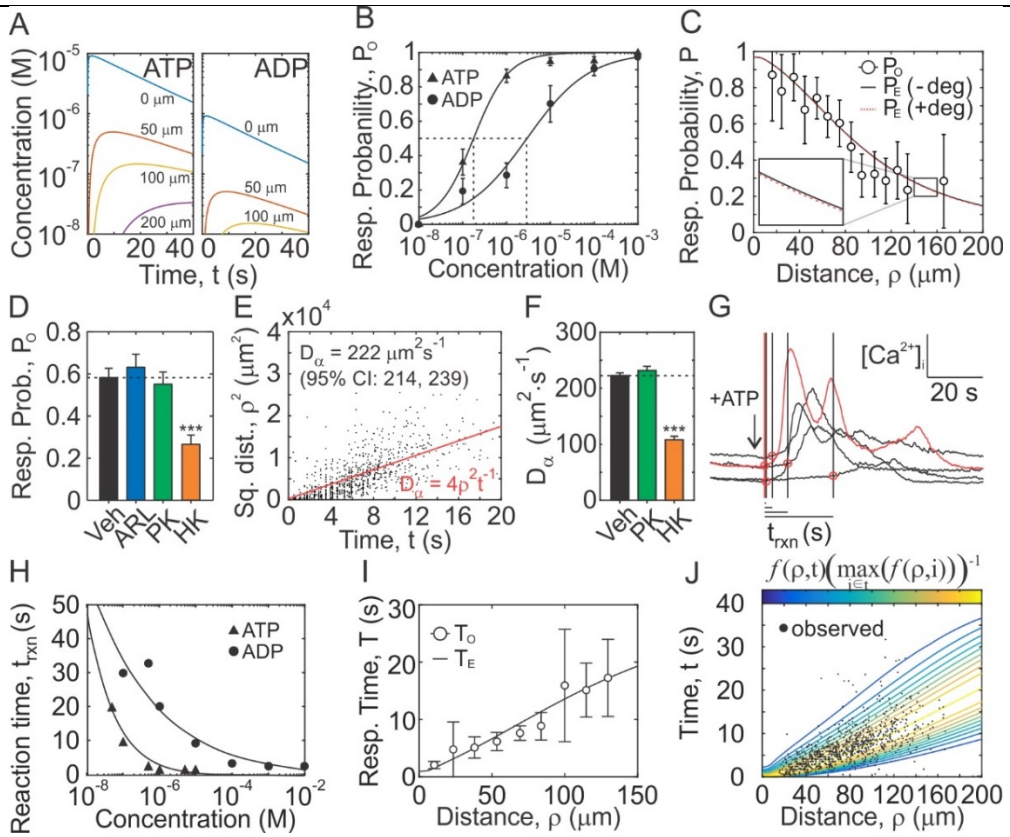

Figure 7-4. Modeling diffusion and purinergic reaction times to predict the spatial and temporal distribution of secondary responses. (A) ATP and ADP release and diffusion were numerically simulated following mechanical injury of a single cell ($d_0 = 100$ nm, $\tau_{1/2} = 15$ s, $k_{ATP} = 0$, Eq. 5, 6). **(B)** Dose-dependence of ATP and ADP response probabilities. Means ± SEM, N=6-8. *Fitted curves*: Hill functions (**Table 7-S1**). **(C)** Expected response probabilities P_E following mechanical stimulation of a single cell in the presence (+deg; $k_{ATP} = 0.05$ min^{-1}) or absence (-deg; $k_{ATP} = 0$ min^{-1}) of extracellular ATP degradation compared to observed response probabilities P_O (means ± SEM, N=51). **(D)** Observed response probabilities P_O after micropipette stimulation of C2-OB cell in the presence of vehicle, 10 μM ARL 67156 (ARL), 20 U/mL pyruvate kinase + PEP (PK) or 20 U/mL hexokinase (HK). Means ± SEM, ***p<0.001 by ANOVA. **(E)** Relationship between observed secondary response times T_O and squared distance from source. *Red line*: Apparent diffusion coefficient D_α estimated by linear regression. **(F)** D_α in presence of vehicle, PK or HK. Means ± SEM, N=10-15, ***p<0.001 assessed by ANOVA. **(G)** $[Ca^{2+}]_i$ traces demonstrating reaction times for ATP-stimulated responses (1 μM). The first discernable response in indicated in *red, black lines/red circles*: reaction times t_{rxn}. **(H)** ATP and ADP dose-dependences for t_{rxn}. *Black lines*: fitted exponential functions (**Table 7-S1**). **(I)** Comparison of expected T_E and observed T_O (means ± SEM, N=51) secondary response times. **(J)** Spatiotemporal map of secondary responses represented as probability density function f (Eq. 13) overlaid with observed raw data.

Response probabilities. To examine whether the diffusion model can predict the secondary responses after stimulation of a single primary cell, we first characterized how observed response probability P_O depends on ATP and ADP concentrations. ATP induced responses at lower concentrations compared to ADP (EC_{50}^{ATP} = 180 nM, EC_{50}^{ADP} = 2.9 μM; **Fig 7-4B, Table 7-S1**). When ATP and ADP were applied together, P_O was dictated by the nucleotide species with the highest P_O when applied alone (**Fig 7-S2A**). Next, ATP and ADP spatiotemporal concentration profiles obtained by Eq. 5 and 6 (**Fig 7-4A**) were mapped to the respective P_O (**Fig 7-4B, Fig 7-S2A**), generating a spatiotemporal map of instantaneous response probabilities denoted $p_{inst}(\rho, t)$ (**Fig 7-S2B**). The expected response probability P_E describing the proportion of cells expected to respond at distance ρ and time t was determined as the time-cumulative maxima of p_{inst} (**Fig 7-S2B**):

$$P_E(\rho, t) = \max_{j \epsilon t}\left(p_{inst}(\rho, j)\right) \quad (7)$$

$P_E(\rho, \infty)$ was computed for a range of injury-related parameters ($d_0 = 10^{-4}$ to 10^1 μm, $\tau_{1/2} = 1$ to 20 s) and compared to P_O after single cell micropipette stimulation. P_E for $\tau_{1/2} > 4$ s, $d_0 = 0.05 - 1$ μm injuries were consistent with P_O (**Fig 7-S3A**), with the best fit parameter set being $d_0 = 100$ nm and $\tau_{1/2} = 15$ s (**Fig 7-4C**).

The model also predicted that extracellular nucleotide degradation (with $k_{ATP} = 0.05$ min^{-1}, $k_{ADP} = 0.25k_{ATP}$; Eq. 5, 6) has a negligible influence on the purinergic signal released by a single cell (**Fig 7-4C**). Experimentally, we confirmed that inhibition of ATP degradation or enzymatic conversion of ADP-to-ATP using pyruvate kinase and PEP did not affect P_O following single cell micropipette stimulation, while hexokinase-mediated ATP-to-ADP conversion significantly reduced response radius and fraction (**Fig 7-S4, Fig 7-4D**).

Response times. We next examined whether ATP and ADP diffusion can predict the timing of secondary responses following single cell micropipette stimulation. The apparent diffusion coefficient D_α (**Fig 7-4E)** estimated from the slope of the linear relationship between secondary response times and squared distances from the source as 222 μm^{2}s^{-1} (95% CI: 214 to 239) was significantly lower than diffusion coefficients reported for ATP (347 μm^{2}s^{-1}) or ADP (377 μm^{2}s^{-1}) (Bennett, Farnell, Gibson, & Karunanithi, 1995; Diehl, Ihlefeld, & Schwegler, 2013; Hubley, Moerland, & Rosanske, 1995). Enzymatic conversion of ADP to ATP using pyruvate kinase and

PEP did not affect secondary response times, while hexokinase-mediated ATP to ADP conversion further reduced D_α (**Fig 7-4F**, **Fig 7-S5**), contrary to what would be expected based on the lower molecular weight of ADP compared to ATP. We hypothesized that the reaction times (t_{rxn}) of ATP- and ADP-mediated responses exhibit purine species-dependent differences. Applying ATP, ADP or their combination to Fura2-loaded C2-OBs, we estimated the average time delay between purine application (approximated by the time of discernable response in the first cell) and subsequent responses (**Fig 7-4G**). Responses induced by ADP were slower compared to ATP and reaction times were substantially slower at low nucleotide concentrations (**Fig 7-4H, Table 7-S1**). When ATP and ADP were applied together, the nucleotide that evoked the fastest response governed the observed reaction time (**Fig 7-S6A**). Thus, diffusion alone is insufficient to account for the observed response times and requires additional consideration of P2 reaction times.

Response time model. We next formulated a response time model to predict the expected response times T_E in neighbouring cells (Thurley, Wu, & Altschuler, 2018). Spatiotemporal ATP and ADP concentrations following single-cell injury were numerically simulated (**Fig 7-4A**, Eq. 5, 6) and mapped to their corresponding observed reaction times (**Fig 7-S6A, Table 7-S1**) to obtain a spatiotemporal map of instantaneous reaction times $t_{rxn}(\rho, t)$, from which was the instantaneous rate of response $\lambda(\rho, t)$ was obtained (**Fig 7-S6B**):

$$\lambda(\rho, t) = \frac{1}{t_{rxn}(\rho, t)} \tag{8}$$

which then allowed us to derive the time-dependent proportion of responding cells $S_1(\rho, t)$:

$$S_1(\rho, t) = \exp\left\{-\int_0^t \lambda(\rho, u)du\right\} \tag{9}$$

To account for situations where nucleotide concentrations are insufficient to induce response in all the cells, we partitioned the neighboring cells into three subpopulations: (*i*) cells that respond to the stimulus without delay $R(\rho, t)$, (*ii*) cells that have not yet responded, but will respond eventually $S_1(\rho, t)$, and (*iii*) cells that will not respond to the stimulus $S_0(\rho, t)$:

$$R(\rho, t) + S_1(\rho, t) + S_0(\rho, t) = 1 \tag{10}$$

These cellular subpopulations could further be expressed in terms of the expected response probability such that $R(\rho,t)+S_1(\rho,t)=P_E(\rho,t)$ and $S_0(\rho,t)=1-P_E(\rho,t)$ (**Fig 7-S6C**). This partitioning of the neighboring cell population allows us to limit our focus to the subpopulation of responders $[R(\rho,t)+S_1(\rho,t)]$, and define the conditional survival function $S^*(\rho,t)$, which describes the time-dependent proportion of responding cells:

$$S^*(\rho,t)=\frac{S_1(\rho,t)}{1-S_0(\rho,\infty)}=\frac{\exp\left\{-\int_0^t\lambda(\rho,u)du\right\}}{P_E(\rho,\infty)} \tag{11}$$

$S^*(\rho,t)$ was then integrated to obtain the expected response times $T_E(\rho)$ at distance ρ:

$$T_E(\rho)=\int_0^\infty S^*(\rho,u)du \tag{12}$$

The values of $T_E(\rho)$ derived for single-cell injuries where $\tau_{1/2}>4$ s and $d_0=100-500$ nm were consistent with T_O (**Fig 7-S3B)**, with $d_0=100$ nm and $\tau_{1/2}=15$ s remaining the best fit parameter set (**Fig 7-4I**). Importantly, the observed spatial (P_O) and temporal (T_O) responses were best predicted by the same set of injury parameters [$d_0=100$ nm and $\tau_{1/2}=15$ (**Fig 7-S3C**)]. The spatiotemporal distribution of observed secondary responses strongly correlated with predicted by the model using probability density function $f(\rho,t)$ corresponding to the conditional survival function $S^*(\rho,t)$ (Bloxom, 1984) (**Fig 7-4J**):

$$f(\rho,t)=\left(-\frac{d}{dt}\ln|S^*(\rho,t)|\right)S^*(\rho,t) \tag{13}$$

Thus, we have coupled ATP and ADP release, degradation and diffusion to the secondary response, and validated the expected response probabilities and times using experimental data. In addition, we have demonstrated that taking into account ATP and ADP reaction times is required to accurately describe the spatial and temporal aspects of secondary purinergic responses.

7.3.5 Injury severity and repair dynamics differentially affect the spatial and temporal recruitment of secondary purinergic responses.

Using the validated model, we examined how the purinergic signal guides the spatial and temporal recruitment of secondary responses. The signal radius R_{signal}, the distance at which the expected response probability declines below 5% (**Fig 7-5A**), was governed by the total amount of ATP

released, regardless of whether ATP was spilled from a severe injury or from a slowly repaired minor injury (**Fig 7-5B**). The signal velocity V_{signal}, the average speed at which the paracrine signal propagated (**Fig 7-5C**), was predominantly controlled by the peak concentration of ATP achieved following injury (**Fig 7-5D**). Thus, the total amount of ATP released, which depends on the overall damage to the stimulated cell, governs the degree of involvement of the neighbouring population, while peak ATP concentration that only depends on the size of initial injury determines how fast the neighboring cells will respond.

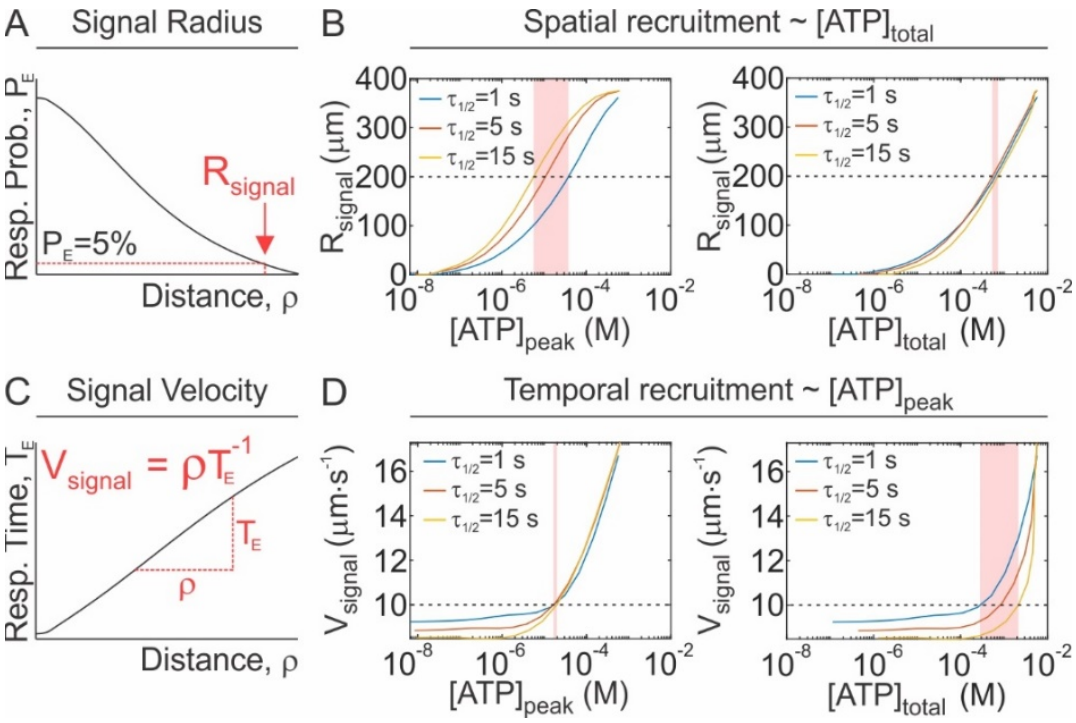

Figure 7-5. Relationship between ATP release and spatial and temporal recruitment of $[Ca^{2+}]_i$ responses. (A) Schematic of signalling radius (R_{signal}). **(B)** Relationship between ATP release parameters $[ATP]_{peak}$ and $[ATP]_{total}$ and spatial recruitment parameter R_{signal} for $\tau_{1/2} = 1, 5, 15$ s. **(C)** Schematic of signal velocity (V_{signal}) **(D)** Relationship between ATP release parameters $[ATP]_{peak}$ or $[ATP]_{total}$ and temporal recruitment parameter V_{signal} for $\tau_{1/2} = 1, 5, 15$ s. For **B** and **D**, *Shaded bands*: show sensitivity of ATP release parameters to changes in $\tau_{1/2}$ for given level of spatial ($R_{signal} = 200$ μm, **B**) or temporal ($V_{signal} = 10$ μm s^{-1}, **D**) recruitment.

Table 7-1. Model Parameters

Symbol	Description	Value(s)	Reference
$c^{i}_{in,0}$	Initial intracellular concentration, $i = ATP, ADP$	5.0 mM ATP; 0.5 mM ADP	(Traut, 1994)
$\tau_{1/2}$	Reseal half-time constant	0.1 to 20 s	Estimated in study
d_0	Initial injury (diameter)	$10^{-4}$to 10^{1}µm	Estimated in study
R_{cell}	Osteoblast cell radius	8.3 µm	Estimated for C2-OB cells
V_{cell}	Osteoblast cell volume	2400 μm^3	Estimated for C2-OB cells
D_{ATP}	ATP diffusion coefficient	347 $\mu m^2 s^{-1}$	(Bennett et al., 1995; Diehl et al., 2013; Hubley et al., 1995)
D_{ADP}	ADP diffusion coefficient	377 $\mu m^2 s^{-1}$	
k_{ATP}	ATP degradation constant	0.05 min^{-1}	Estimated in study
k_{ADP}	ADP degradation constant	$0.25k_{ATP}$	Approximated from (Kukulski et al., 2005)
P_O	Observed response probability	Table 7-S1	Estimated in study
t_{rxn}	Reaction time	Table 7-S1	Estimated in study
T_O	Observe response time	Table 7-S1	Estimated in study

Symbol	Description	Value
ρ	Distance from mechanically-stimulated cell	
t	Time post-injury	
$d(t)$	Diameter of cellular injury post-injury	Eq. (1)
$\beta_i(t)$	Transport coefficient, $i = ATP, ADP$	Eq. (2)
$c^{i}_{in}(t)$	Intracellular concentration, $i = ATP, ADP$	Eq. (3)
$c^{i,\prime}_{source}$	Rate of release at source, $i = ATP, ADP$	Eq. (4)
$c^{i}_{ex}(\rho, t)$	Extracellular concentration, $i = ATP, ADP$	Eq. (5, 6)
$p_{inst}(\rho, t)$	Instantaneous response probability	Eq. (7)
$P_E(\rho, t)$	Expected response probability	Eq. (7)
$\lambda(\rho, t)$	Instantaneous rate of response	Eq. (8)
$S_1(\rho, t)$	Proportion of cells that will eventually respond	Eq. (9, 10)
$S_0(\rho, t)$	Proportion of cells that will not respond	Eq. (10)
$R(\rho, t)$	Proportion of cells that have responded	Eq. (10)
$S^*(\rho, t)$	Conditional survival function	Eq. (11)
$T_E(\rho)$	Expected response time	Eq. (12)
$f(\rho, t)$	Probability density function of S^*; Spatio-temporal distribution of paracrine responses	Eq. (13)

Symbol	Description
$[ATP]_{total}$	Total ATP released following cell injury
$[ATP]_{peak}$	Peak extracellular ATP concentration following cell injury
$[ATP]_{FWHM}$	Duration that extracellular [ATP] was sustained above half-maximal [ATP]
R_{signal}	Distance at which the expected response probability *P* declines below 5%
V_{signal}	Average speed at which the paracrine signal propagates

7.3.6 Propagation of purinergic signal resulting from a tissue-level injury

Physiologically, mechanical stimuli affect multiple cells occupying a tissue area of a certain size and geometry. This results in the release of purinergic mediators from numerous sources in the tissue, unlike the single cell experimental setup that we have considered thus far. We extended the model to consider three injury geometries: (*i*) point source, consisting of one or 40 injured cells (**Fig 7-6A**, *left*); (*ii*) linear source, consisting of 40 or 1600 injured cells evenly distributed along a 2000 μm linear plane (**Fig 7-6A**, *middle*); and (*iii*) half-field source consisting of 800 or 8000 cells evenly arranged as a series of point sources over a 2000×4000 μm^2 surface area (**Fig 7-6A**, *right*). For each of these geometries, we assumed simultaneous and identical cell-level injury ($d_0 = 100$ nm, $\tau_{1/2} = 15$ s) and assessed expected response probability along the signalling axis perpendicular to the injury front in the presence of extracellular nucleotide degradation ($k_{ATP} = 0.05$ min^{-1}, $k_{ADP} = 0.25k_{ATP}$) and in its absence ($k_{ATP} = 0$, $k_{ADP} = 0$) (**Fig 7-6B**). Since certain P2 receptors (e.g., P2Y1, P2Y12 and P2Y13) are predominantly sensitive to ADP (von Kugelgen & Hoffmann, 2016), we also isolated the ADP-mediated response component (**Fig 7-6C**). The expected response probability was the highest at the site of injury and declined at increasing distances from the injury. For all geometries, the more cells were initially injured, the more neighboring cells exhibited P2 responses. The effect of extracellular nucleotide degradation became apparent for larger tissue-level injuries, especially when higher ATP levels (due to more injury) were sustained for longer (due to injury geometry). In these cases, ATP degradation attenuated total paracrine responsiveness while increasing the ADP-mediated signalling component (**Fig 7-6B, C**; *red vs. black curves*). Importantly, the effects of extracellular nucleotide degradation were not observed at the site of injury, but rather at increasing distances from the source. Thus, scaling a single-cell injury to a tissue-level injury with varying geometries revealed that ATP- and ADP-mediated components of the purinergic response reflect the extent of injury and differentially change with increasing distance from the injury site.

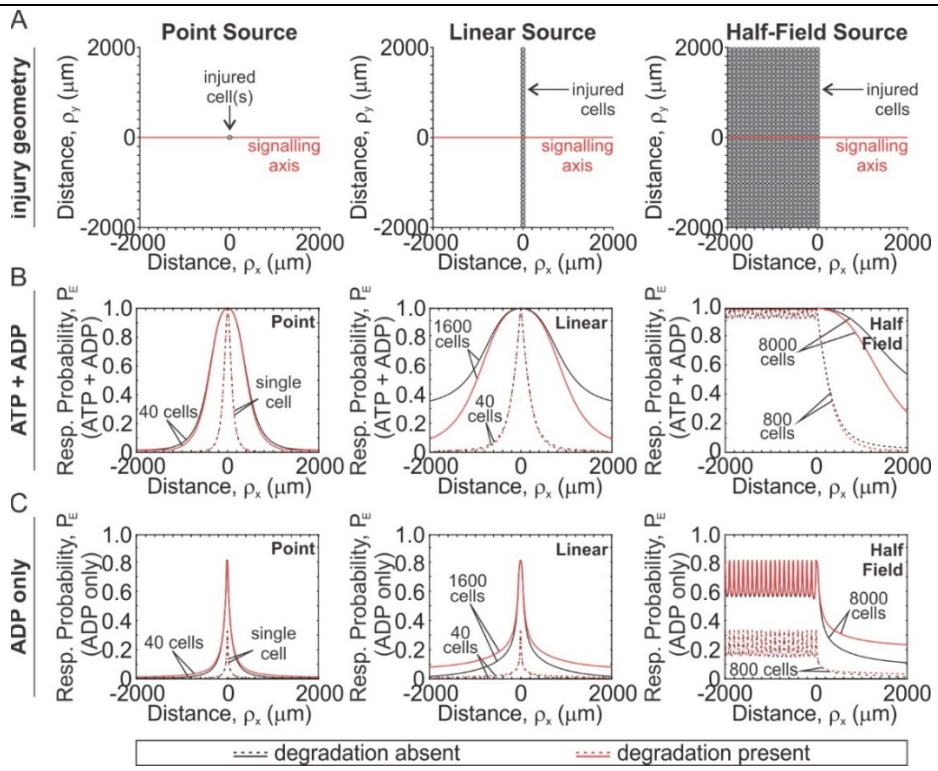

Figure 7-6. Paracrine purinergic signaling following tissue-level injury. ATP and ADP release and diffusion from point- (*left*), linear- (*middle*) and half-field- (*right*) source injuries (**A**) were numerically simulated (Eq. 5, 6) and contributions of ATP and ADP **(B)** or ADP alone **(C)** to expected response probabilities P_E were determined for varying number of injured cells in the presence (*red*) or absence (*black*) of extracellular ATP and ADP degradation. *Simulation parameters*: $k_{ATP} = 0$ (degradation absent) or 0.05 min^{-1} (degradation present), $k_{ADP} = 0.25k_{ATP}$, $d_0 = 100$ nm, $\tau_{1/2} = 15$ s.

7.4 Discussion

7.4.1 Overview

The goals of this study were (*i*) to determine how mechanically-induced cell membrane injury and repair govern ATP and ADP release dynamics, (*ii*) to characterize ATP and ADP spatiotemporal diffusion profiles and (*iii*) to understand the basic principles dictating the spatial and temporal recruitment of responses in neighboring (non-stimulated) cells to the presented levels of ATP and ADP. For each elementary step (ATP and ADP release, diffusion and degradation, and P2 responses in neighboring cells), we developed and experimentally validated mathematical descriptions. Using the combined model of ATP-driven mechanotransduction, we scaled a single-cell injury to a tissue-level injury with varying geometries and described how neighboring cells may detect the magnitude of injury and discern their proximity to the injury site. We were able to

identify specific features of the ATP and ADP spatiotemporal signal that encode the severity of mechanical stimulus, distance to the stimulus, as well as the state of tissue mechano-resilience.

7.4.2 ATP release due to mechanical injury

Several groups have shown that mechanically-induced membrane disruptions occur under physiological conditions in muscle fibers (McNeil & Khakee, 1992), gastrointestinal tract (McNeil & Ito, 1989), heart (Clarke, Caldwell, Chiao, Miyake, & McNeil, 1995), aorta (Q. C. Yu & McNeil, 1992) and bone (Mikolajewicz, Zimmermann, et al., 2018; K. Yu et al., 2018). Despite these injuries, cell death is minimal because cells can rapidly repair their membranes (Cooper & McNeil, 2015). Membrane disruption results in nonspecific spillage of intracellular content, which includes growth factors (Clarke et al., 1995; Clarke, Khakee, & McNeil, 1993) as well as ATP (Mikolajewicz, Zimmermann, et al., 2018; Sikora, Orlov, Furuya, & Grygorczyk, 2014; Yin, Xu, Zhang, Kumar, & Yu, 2007). The extent of this spillage is determined by the size of membrane disruption (parameter d_0) and the rate of membrane repair (parameter $\tau_{1/2}$). Importantly, both membrane integrity and repair rates are sensitive to pharmacological interventions along the Ca^{2+}/PLC/PKC axis (Mikolajewicz, Zimmermann, et al., 2018; T. Togo, Alderton, Bi, & Steinhardt, 1999) and are improved after exposure to mechanical stimulation (Mikolajewicz, Zimmermann, et al., 2018; Tatsuru Togo, 2012, 2017). We demonstrated that injuries with an initial size of $d_0 \sim 100$ nm that resealed exponentially with a half-time of $\tau_{1/2} \sim 15$ s predicted ATP concentrations at the surface of the mechanically-stimulated cell (~10 □M) that were consistent with experimental measurements (0.05-80.5 □M) (Mikolajewicz, Zimmermann, et al., 2018). Modelling ATP release using theoretical description developed for the transport of fluorescent dyes though membrane pores (Zarnitsyn et al., 2008), we showed that the total amount of ATP released depended on both the severity of mechanical injury d_0 and rate of membrane repair $\tau_{1/2}$, while the peak extracellular ATP was determined by the injury severity alone.The P2 receptor network consists of 15 receptor subtypes with ATP affinities covering over a million-fold range of ATP concentrations (Grol et al., 2013; Xing et al., 2016). Therefore, peak ATP release will determine the degree of activation of low-affinity P2 receptors [e.g. P2X7; EC_{50} = 1.9 mM (Xing et al., 2016)], while the total amount of ATP released will determine the area over which high-affinity P2 receptors are activated [e.g. P2Y2; EC_{50} = 200 nM (Xing et al., 2016)]. Thus, information about the extent of the injury and the rate of repair encoded in the dynamics of ATP

release can be deciphered at the level of P2 receptors network. Importantly, these mechanistic insights are applicable to any form of stimulus-related mediator release which can be described in terms of its magnitude and temporal dynamics, including conductive and vesicular ATP release.

7.4.3 Signal propagation through ATP diffusion and degradation and P2 responses in neighboring cells

Following release into the extracellular space, ATP diffuses and is concurrently metabolized by ecto-nucleotidases (Zimmermann, Zebisch, & Sträter, 2012), producing ADP, AMP and adenosine, which may also stimulate cellular responses (Alvarenga et al., 2010; Ethier & Madison, 2006; Pilitsis & Kimelberg, 1998; Rittiner et al., 2012). Moreover, since mediator spillage through a membrane injury is nonspecific, all purines present in the cytosol will be released in proportional amounts. Of the tested purine metabolites, ADP was capable of stimulating calcium responses in C2-OB, consistent with prior work (Bowler et al., 1999; Orriss, Knight, Ranasinghe, Burnstock, & Arnett, 2006). ATP degradation half-time in the extracellular space was 20 min (95% CI: 17 to 25) for C2-OB cells, compared to ~10 min by primary rat osteoblasts (Orriss et al., 2009), and ~5 min by primary murine osteoblasts (Wang et al., 2013). Osteoblastic ATP degradation was too slow to affect purinergic transmission initiated by a single cell, contrary to endothelial cells (Gomes, Srinivas, Van Driessche, Vereecke, & Himpens, 2005; Gomes, Srinivas, Vereecke, & Himpens, 2005), or keratinocytes (Ho, Yang, Lin, & Lin, 2013), in which paracrine responses following single cell stimulation were potentiated when ecto-nucleotidases were inhibited. Nevertheless, since most ecto-nucleotidases have a micromolar affinity for ATP (Zimmermann et al., 2012), low hydrolysis rates were consistent with the amounts of ATP released by a single osteoblast. Spatiotemporal ATP and ADP concentration profiles following mechanical stimulation were computed by coupling injury-related ATP release to radial diffusion. We validated the model using $[Ca^{2+}]_i$ recordings of secondary responders following micropipette stimulation of a single osteoblast, since direct ATP measurements were performed with limited sensitivity and spatial resolution (7). Surprisingly, we have found that the apparent diffusion coefficients derived from the $[Ca^{2+}]_i$ recordings were lower than previously reported (Bennett et al., 1995; Diehl et al., 2013; Hubley et al., 1995). To account for this discrepancy, we used a response-time modeling framework to predict the probability and timing of secondary $[Ca^{2+}]_i$ elevations (Thurley et al., 2018), which allowed us to explain the high degree of variability observed in $[Ca^{2+}]_i$ response times, and to predict experimentally observed propagation velocities of ~10 μm/s, consistent with

previously reported (Leybaert & Sanderson, 2012). Accounting for response times resolved the discrepancy between observed and expected ATP diffusion coefficients that was identified by us and others (Handly & Wollman, 2017). Finite wave propagation was sufficient to explain observed $[Ca^{2+}]_i$ elevations in osteoblasts, without need for regenerative propagation terms (e.g., ATP-mediated ATP release) that were proposed in airway epithelia (Warren, Tawhai, & Crampin, 2010) or astrocytes (MacDonald, Yu, Buibas, & Silva, 2008). Thus, ATP and ADP diffusion and degradation as well P2 receptor response times collectively explained the spatial and temporal recruitment of purinergic signaling events in osteoblasts.

7.4.4 Mechanical information encoding

We identified three features of purinergic signal that communicate complimentary mechanically-relevant information to neighboring cells: (i) the total amount of ATP released, (ii) the peak extracellular [ATP] and (iii) ADP-mediated signaling component. The total amount of ATP released, regulated by the injury severity (d_0) and repair dynamics ($\tau_{1/2}$), determined the P2 receptor signaling radius, thus governing the spatial recruitment of the neighboring population. The peak extracellular ATP concentration reflected the severity the cell injury (d_0 only) and strongly influenced the temporal recruitment of the neighboring population. Peak [ATP] allowed cells to discriminate between severe (large d_0) and minor (small d_0) injuries that led to the release of similar total amounts of ATP due to differences in injury repair dynamics (e.g. fast repair for large injury, slow repair for small injury). This framework enables situations in which severe injuries –associated with higher peak ATP concentrations – can recruit low-affinity P2 receptors. The third signaling feature was ADP-mediated signaling which manifested only when tissue-level injuries were considered. In the case of a single cell injury, the amounts of ADP released and produced from ATP degradation were too low to induce paracrine responses. However, when the injury included multiple cells, ATP degradation resulted in overall dampening of paracrine responses, especially at further distances from the injury site, together with the proportional increase in ADP-mediated signaling. The observed injury-related increase in ADP-mediated signaling is supported by prior work in which ADP-sensitive P2Y1 (Alvarenga et al., 2010) and P2Y13 (Wang et al., 2013) receptors were implicated in osteoblasts mechanotransduction. Thus, our findings support a model in which mechanical information – encoded within ATP and ADP diffusion waves – is differentially decoded by low affinity P2 receptors, high affinity P2 receptors

and ADP-sensitive P2 receptors (**Fig 7-7**). It is important to note that in this study we focused on the population-level responses (i.e., spatial and temporal recruitment) and did not consider specific features of $[Ca^{2+}]_i$ responses in individual cells, such as amplitude, duration and oscillatory behaviour. Based on our insights at the population-level, future efforts investigating how mechanical information is decoded at the cellular level are warranted.

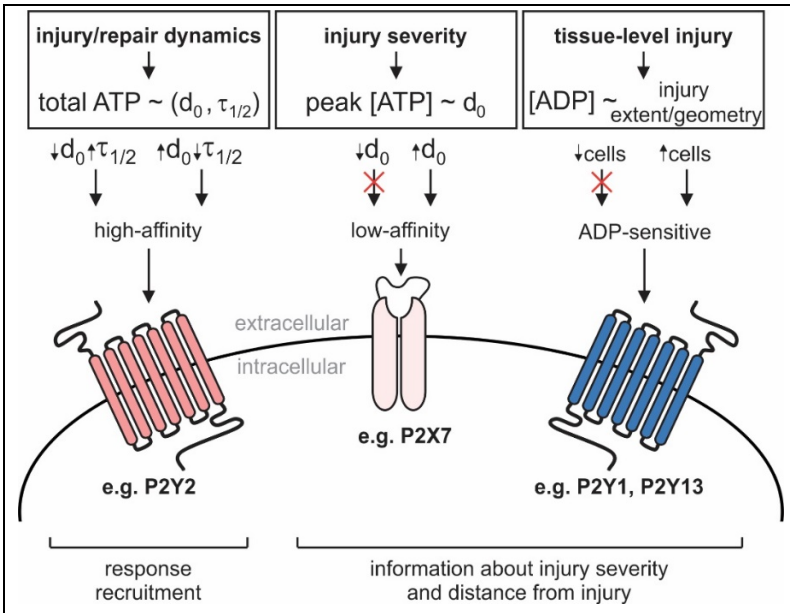

Figure 7-7. Proposed model of mechanical information decoding by the P2 receptor network. *Left*: Single cell membrane injury (d_0) and repair ($\tau_{1/2}$) dynamics regulate the total amount of ATP released and the extent of recruitment of neighboring cells (i.e., spatial recruitment) through high-affinity P2 receptors. *Middle*: Severity of injury (d_0) is conveyed to neighboring cells through peak extracellular ATP concentrations which influence the timing of responses (i.e., temporal recruitment) and low-affinity P2 receptor signaling. *Right*: Extent and geometry of tissue-level injury determines amount of ADP released and produced by ATP degradation, and thus stimulation of ADP-sensitive P2 receptors.

7.4.5 Concluding remarks

We developed and validated a theoretical model to investigate how extracellular ATP and ADP released by mechanical stimulation encode information about the position and severity of the mechanical stimulus, and how this information can be subsequently decoded at the level of the paracrine responses. We demonstrate that purinergic signalling fields are tuned by the severity of injury and dynamics of repair, thereby enabling neighbouring cells to evoke responses appropriate to the injury severity and the neighbouring cell proximity to the event.

7.5 Materials & Methods

7.5.1 Solutions and reagents

Solutions. Phosphate-buffered saline (PBS; 140 mM NaCl, 3 mM KCl, 10 mM Na_2HPO_4, 2 mM

KH_2PO_4, pH 7.4), autoclaved. Physiological solution (PS; 130 mM NaCl; 5 mM KCl; 1 mM $MgCl_2$; 1 mM $CaCl_2$; 10 mM glucose; 20 mM HEPES, pH 7.6), filtered through 0.2 μm. Bioluminescence reaction buffer (0.1 M DTT, 25 mM tricine, 5 mM $MgSO_4$, 0.1 mM EDTA, 0.1 mM NaN_3, pH 7.8), filtered through 0.2 μm.

Reagents. Minimum essential medium (MEM) α (Gibco 12,000-022); Fura2-AM (Invitrogen F1221); D-Luciferin (Invitrogen L2916); Collagenase P from *Clostridium histolyticum* (Roche 11213857001); Adenosine 5'-triphosphate (Sigma-Aldrich A9187); Adenosine 5'-diphosphate (Sigma-Aldrich A2754); Adensoine 5'-monophosphate (Sigma-Aldrich 01930); Adenosine (Sigma-Aldrich A4036), hexokinase from *Saccharomyces cerevisiae* (Sigma-Aldrich H6380); L-ascorbic acid (Sigma-Aldrich A8960); Luciferase from *Photinus pyralis* (Sigma-Aldrich L9420); Phosphoenolpyruvic acid (Sigma-Aldrich 860077); Pyruvate kinase from rabbit muscle (Sigma-Aldrich P9136); Quinacrine (Sigma-Aldrich Q3251); Venor GeM Mycoplasma PCR-based detection kit (Sigma-Aldrich MP0025); ARL 67156 (Tocris Bioscience 1283); Suramin (Tocris Bioscience 1472); Dulbecco's modified eagle medium (Wisent Bio Products 319-020 CL); Fetal bovine serum (Wisent Bio Products 080152); Penicillin streptomycin (Wisent Bio Products 450-201-EL); pyruvate (Wisent Bio Products 600-110-UL); collagenase Type II (Worthington Biochemical Corporation LS004176).

7.5.2 Cell culture

All procedures were approved by McGill's University's Animal Care Committee and complied with the ethical guidelines of the Canadian Council on Animal Care.

For compact bone-derived osteoblasts (CB-OB), 4-6 week old C57BL/6 mice (Charles River) femurs and tibia bone fragments were enzymatically digested and cultured for 3-5 days in αMEM (with 10% FBS, 1% pyruvate, 1% penicillin streptomycin) as described previously (Mikolajewicz, Zimmermann, et al., 2018). Cells were trypsinized, filtered, plated at 10^4 cells/cm^2 in osteoblast differentiation medium (+ 50 μg/mL ascorbic acid) and cultured for 2-3 days prior to experiments. The C2C12 cell line (ATCC CRL-1772), stably transfected with BMP-2 (C2-OB, courtesy of Dr. M. Murshed, McGill University) was plated at 10^4 cells/cm^2 in DMEM (with 10% FBS, 1% pyruvate, 1% penicillin streptomycin) and cultured for 2-3 days prior to experiments. Absence of

mycoplasma contamination was verified in cryo-preserved stocks of C2-OB cells using PCR-based detection kit.

7.5.3 Intracellular calcium recording and analysis

Cells plated in glass-bottom 35 mm dishes or 48-well plates (MatTek Corporation) were loaded with Fura2-AM for 30 min, bathed in physiological solution, acclimatized for 10 min on the stage of an inverted fluorescence microscope (Nikon T2000) and imaged as described previously (Tiedemann et al., 2009). The data were analyzed using a previously developed MATLAB algorithm (Mackay, Mikolajewicz, Komarova, & Khadra, 2016).

7.5.4 Generating homogenous solutions of ATP and ADP

ADP present in ATP solutions was converted to ATP by 20 U/mL pyruvate kinase in the presence of excess phosphoenolpyruvate (PEP). ATP present in ADP solutions was converted to ADP by 20 U/mL hexokinase. On the day of experiment, enzymatic reactions were carried out in PS at 37°C for 30 min, then heat inactivated at 95°C for 2 min.

7.5.5 ATP and ADP dose-dependencies

Fura2-loaded C2-OB cells in a 48-well plate were bathed in 270 µL PS and 30 µL of ATP or ADP solution at 10x of the desired final concentration were added (e.g., 30 µL of 10 µM ATP solution was added to cells to achieve 1 µM ATP stimulation). Application of PS alone evoked no discernable response. A solution containing desired concentrations of both ATP and ADP, was obtained from homogenous solutions of ATP and ADP. Response probabilities P were measured as the proportion of cells in the field of view that evoked a discernable $[Ca^{2+}]_i$ response. Reaction times t_{rxn} were measured as the average time between the first discernable $[Ca^{2+}]_i$ response and subsequent cell responses.

7.5.6 Single cell mechanical stimulation

A micropipette was positioned approximately 10 µm from the cell membrane at a 45° angle from the horizontal plane and moved at a speed of 250 µm/s with a contact duration of 60 ms using a FemtoJet microinjector NI2 (Eppendorf Inc.).

7.5.7 Vesicular release kinetics

Cells were incubated with 10 μM quinacrine solution for 15 min at room temperature, washed with physiological solution, and time-lapse recordings were acquired with a Nikon T2000 inverted fluorescence microscope at a sampling rate of 2 Hz. Vesicular release was identified as sudden loss of localized fluorescence using an ImageJ plugin SparkSpotter (Babraham Bioinformatics, UK) applied to temporally reversed and contrast-enhanced image stacks (7).

7.5.8 ATP measurement

ATP content was measured in 100 μL of supernatant by bioluminescence luciferin-luciferase assay using FB 12 single tube luminometer (Titertek-Berthold).

7.5.9 Analysis

Data are representative images and traces, or means ± SEM, with *N* indicating the number of independent trials. Statistical significance was assessed by ANOVA followed by a Bonferroni post-test, and accepted as significant at $p<0.05$. Numerical simulation of diffusion profiles was conducted in Mathematica 11.2 (Wolfram Research, Illinois, USA). Curve fitting and model-related analyses was conducted in MATLAB R2018a (MathWorks, Massachusetts, USA). Logistic regression and ROC curves were generated in SPSS 24 (IBM, New York, USA).

The model parameter space that predicted expected outcomes θ_E (where $\theta = T, P$) most consistent with experimental observations θ_O was identified by computing the bias between θ_E and θ_O as the root difference between mean squared error (MSE) ($MSE(\theta_E, \theta_O) = \frac{1}{m}\sum_{i=1}^{m}(\theta_E - \theta_O)^2$, m is the number of distances from primary cell at which observed secondary responses θ_O were compared to predicted outcomes θ_E) and sampling variance (Var),

$$Bias(\theta_E, \theta_O) = \sqrt{MSE(\theta_E, \theta_O) - Var(\theta_O)}$$

When two sets of outcome measurements were available (response time T, response probability P), the parameter space with minimal $Bias_{T,P}$ was identified by combining $Bias_T$ and $Bias_P$ as:

$$Bias_{T,P} = \sqrt{Bias_T^2 + Bias_P^2}$$

7.6 References

Alvarenga, E. C., Rodrigues, R., Caricati-Neto, A., Silva-Filho, F. C., Paredes-Gamero, E. J., & Ferreira, A. T. (2010). Low-intensity pulsed ultrasound-dependent osteoblast proliferation occurs by via activation of the P2Y receptor: role of the P2Y1 receptor. *Bone, 46*(2), 355-362. doi:http://dx.doi.org/10.1016/j.bone.2009.09.017

Bennett, M. R., Farnell, L., Gibson, W. G., & Karunanithi, S. (1995). Quantal transmission at purinergic junctions: stochastic interaction between ATP and its receptors. *Biophys J, 68*(3), 925-935. doi:10.1016/s0006-3495(95)80268-7

Biver, G., Wang, N., Gartland, A., Orriss, I., Arnett, T. R., Boeynaems, J.-M., & Robaye, B. (2013). Role of the P2Y13 Receptor in the Differentiation of Bone Marrow Stromal Cells into Osteoblasts and Adipocytes. *Stem Cells, 31*(12), 2747-2758. doi:10.1002/stem.1411

Bloxom, B. (1984). Estimating response time hazard functions: An exposition and extension. *Journal of Mathematical Psychology, 28*(4), 401-420. doi:https://doi.org/10.1016/0022-2496(84)90008-7

Bowler, W. B., Dixon, C. J., Halleux, C., Maier, R., Bilbe, G., Fraser, W. D., . . . Hipskind, R. A. (1999). Signaling in human osteoblasts by extracellular nucleotides. Their weak induction of the c-fos proto-oncogene via Ca2+ mobilization is strongly potentiated by a parathyroid hormone/cAMP-dependent protein kinase pathway independently of mitogen-activated protein kinase. *J Biol Chem, 274*(20), 14315-14324.

Carter, D. R., & Beaupré, G. S. (2007). *Skeletal function and form: mechanobiology of skeletal development, aging, and regeneration*: Cambridge University Press.

Clarke, M. S., Caldwell, R. W., Chiao, H., Miyake, K., & McNeil, P. L. (1995). Contraction-induced cell wounding and release of fibroblast growth factor in heart. *Circ Res, 76*(6), 927-934.

Clarke, M. S., Khakee, R., & McNeil, P. L. (1993). Loss of cytoplasmic basic fibroblast growth factor from physiologically wounded myofibers of normal and dystrophic muscle. *J Cell Sci, 106 (Pt 1)*, 121-133.

Cooper, S. T., & McNeil, P. L. (2015). Membrane Repair: Mechanisms and Pathophysiology. *Physiol Rev, 95*(4), 1205-1240. doi:10.1152/physrev.00037.2014

Defour, A., Sreetama, S. C., & Jaiswal, J. K. (2014). Imaging cell membrane injury and subcellular processes involved in repair. *J Vis Exp*(85), 10.3791/51106. doi:10.3791/51106

Diehl, H., Ihlefeld, H., & Schwegler, H. (2013). *Physik für Biologen*: Springer-Verlag.

Ethier, M. F., & Madison, J. M. (2006). Adenosine A1 receptors mediate mobilization of calcium in human bronchial smooth muscle cells. *Am J Respir Cell Mol Biol, 35*(4), 496-502. doi:10.1165/rcmb.2005-0290OC

Genetos, D., Geist, D., Dawei, L., Donahue, H., & Duncan, R. (2005). Fluid Shear-Induced ATP Secretion Mediates Prostaglandin Release in MC3T3-E1 Osteoblasts. *J Bone Miner Res, 20*(1), 41-49. doi:10.1359/JBMR.041009

Gomes, P., Srinivas, S. P., Van Driessche, W., Vereecke, J., & Himpens, B. (2005). ATP Release through Connexin Hemichannels in Corneal Endothelial Cells. *Investigative Ophthalmology & Visual Science, 46*(4), 1208-1218. doi:10.1167/iovs.04-1181

Gomes, P., Srinivas, S. P., Vereecke, J., & Himpens, B. (2005). ATP-Dependent Paracrine Intercellular Communication in Cultured Bovine Corneal Endothelial Cells. *Investigative Ophthalmology & Visual Science, 46*(1), 104-113. doi:10.1167/iovs.04-0846

Grol, M. W., Pereverzev, A., Sims, S. M., & Dixon, S. J. (2013). P2 receptor networks regulate signaling duration over a wide dynamic range of ATP concentrations. *J Cell Sci, 126*(Pt 16), 3615-3626. doi:10.1242/jcs.122705

Handly, L. N., & Wollman, R. (2017). Wound-induced Ca(2+) wave propagates through a simple release and diffusion mechanism. *Molecular Biology of the Cell, 28*(11), 1457-1466. doi:10.1091/mbc.E16-10-0695

Ho, C.-L., Yang, C.-Y., Lin, W.-J., & Lin, C.-H. (2013). Ecto-Nucleoside Triphosphate Diphosphohydrolase 2 Modulates Local ATP-Induced Calcium Signaling in Human HaCaT Keratinocytes. *PLoS ONE, 8*(3), e57666. doi:10.1371/journal.pone.0057666

Hubley, M. J., Moerland, T. S., & Rosanske, R. C. (1995). Diffusion coefficients of ATP and creatine phosphate in isolated muscle: pulsed gradient 31P NMR of small biological samples. *NMR Biomed, 8*(2), 72-78.

Jo, H., & Shin, J. H. (2015). Special issue on mechanobiology and diseases. *Biomedical Engineering Letters, 5*(3), 159-161. doi:10.1007/s13534-015-0203-1

Kohrt, W. M., Barry, D. W., & Schwartz, R. S. (2009). Muscle Forces or Gravity: What Predominates Mechanical Loading on Bone? *Med Sci Sports Exerc, 41*(11), 2050-2055. doi:10.1249/MSS.0b013e3181a8c717

Kukulski, F., Lévesque, S. A., Lavoie, É. G., Lecka, J., Bigonnesse, F., Knowles, A. F., . . . Sévigny, J. (2005). Comparative hydrolysis of P2 receptor agonists by NTPDases 1, 2, 3 and 8. *Purinergic Signalling, 1*(2), 193. doi:10.1007/s11302-005-6217-x

Lewis, K. J., Frikha-Benayed, D., Louie, J., Stephen, S., Spray, D. C., Thi, M. M., . . . Schaffler, M. B. (2017). Osteocyte calcium signals encode strain magnitude and loading frequency in vivo. *PNAS, 114*(44), 11775-11780.

Leybaert, L., & Sanderson, M. J. (2012). Intercellular Ca2+ Waves: Mechanisms and Function. *Physiological Reviews, 92*(3), 1359-1392. doi:10.1152/physrev.00029.2011

Li, J., Liu, D., Ke, H. Z., Duncan, R. L., & Turner, C. H. (2005). The P2X7 nucleotide receptor mediates skeletal mechanotransduction. *J Biol Chem, 280*(52), 42952-42959. doi:10.1074/jbc.M506415200

Lopez-Ayon, G. M., Liu, H. Y., Xing, S., Maria, O. M., LeDue, J. M., Bourque, H., . . . Komarova, S. V. (2014). Local membrane deformation and micro-injury lead to qualitatively different responses in osteoblasts. *F1000Res, 3*, 162. doi:10.12688/f1000research.4448.1

MacDonald, C., Yu, D., Buibas, M., & Silva, G. (2008). Diffusion modeling of ATP signaling suggests a partially regenerative mechanism underlies astrocyte intercellular calcium waves. *Frontiers in Neuroengineering, 1*(1). doi:10.3389/neuro.16.001.2008

Mackay, L., Mikolajewicz, N., Komarova, S. V., & Khadra, A. (2016). Systematic Characterization of Dynamic Parameters of Intracellular Calcium Signals. *Frontiers in Physiology, 7*(525). doi:10.3389/fphys.2016.00525

McNeil, P. L., & Ito, S. (1989). Gastrointestinal cell plasma membrane wounding and resealing in vivo. *Gastroenterology, 96*(5 Pt 1), 1238-1248.

McNeil, P. L., & Khakee, R. (1992). Disruptions of muscle fiber plasma membranes. Role in exercise-induced damage. *Am J Pathol, 140*(5), 1097-1109.

Mikolajewicz, N., Mohammed, A., Morris, M., & Komarova, S. V. (2018). Meta-analysis of mechanically-stimulated ATP release from mammalian cells. *J Cell Sci*. doi:10.1242/jcs.223354

Mikolajewicz, N., Zimmermann, E., Willie, B. M., & Komarova, S. V. (2018). Mechanically-stimulated ATP release from murine bone cells is regulated by a balance of injury and repair. *eLife*.

Nakamura, M., Dominguez, A. N. M., Decker, J. R., Hull, A. J., Verboon, J. M., & Parkhurst, S. M. (2018). Into the breach: how cells cope with wounds. *Open Biol, 8*(10). doi:10.1098/rsob.180135

Orriss, I., Knight, G., Ranasinghe, S., Burnstock, G., & Arnett, T. (2006). Osteoblast responses to nucleotides increase during differentiation. *Bone, 39*(2), 300-309. doi:10.1016/j.bone.2006.02.063

Orriss, I., Knight, G., Utting, J., Taylor, S., Burnstock, G., & Arnett, T. (2009). Hypoxia stimulates vesicular ATP release from rat osteoblasts. *J Cell Physiol, 220*(1), 155-162. doi:10.1002/jcp.21745

Pilitsis, J. G., & Kimelberg, H. K. (1998). Adenosine receptor mediated stimulation of intracellular calcium in acutely isolated astrocytes. *Brain Res, 798*(1-2), 294-303.

Rittiner, J. E., Korboukh, I., Hull-Ryde, E. A., Jin, J., Janzen, W. P., Frye, S. V., & Zylka, M. J. (2012). AMP is an adenosine A1 receptor agonist. *J Biol Chem, 287*(8), 5301-5309. doi:10.1074/jbc.M111.291666

Robling, A. G., & Turner, C. H. (2009). Mechanical Signaling for Bone Modeling and Remodeling. *Crit Rev Eukaryot Gene Expr, 19*(4), 319-338.

Romanello, M., Pani, B., Bicego, M., & D'Andrea, P. (2001). Mechanically induced ATP release from human osteoblastic cells. *Biochem Biophys Res Commun, 289*(5), 1275-1281. doi:10.1006/bbrc.2001.6124

Sikora, J., Orlov, S. N., Furuya, K., & Grygorczyk, R. (2014). Hemolysis is a primary ATP-release mechanism in human erythrocytes. *Blood, 124*(13), 2150-2157. doi:10.1182/blood-2014-05-572024

Skerry, T. (2006). One mechanostat or many? Modifications of the site-specific response of bone to mechanical loading by nature and nurture. *Journal of Musculoskeletal and Neuronal Interactions, 6*(2), 122.

Thurley, K., Wu, L. F., & Altschuler, S. J. (2018). Modeling Cell-to-Cell Communication Networks Using Response-Time Distributions. *Cell systems, 6*(3), 355-367.e355. doi:10.1016/j.cels.2018.01.016

Tiedemann, K., Hussein, O., Sadvakassova, G., Guo, Y., Siegel, P. M., & Komarova, S. V. (2009). Breast Cancer-derived Factors Stimulate Osteoclastogenesis through the Ca(2+)/Protein Kinase C and Transforming Growth Factor-β/MAPK Signaling Pathways. *J Biol Chem, 284*(48), 33662-33670. doi:10.1074/jbc.M109.010785

Togo, T. (2012). Cell Membrane Disruption Stimulates NO/PKG Signaling and Potentiates Cell Membrane Repair in Neighboring Cells. *PLoS ONE, 7*(8), e42885. doi:10.1371/journal.pone.0042885

Togo, T. (2017). Cell membrane disruption stimulates cAMP and Ca2+ signaling to potentiate cell membrane resealing in neighboring cells. *Biology Open*, bio. 028977.

Togo, T., Alderton, J. M., Bi, G. Q., & Steinhardt, R. A. (1999). The mechanism of facilitated cell membrane resealing. *J Cell Sci, 112 (Pt 5)*, 719-731.

Traut, T. W. (1994). Physiological concentrations of purines and pyrimidines. *Mol Cell Biochem Molecular and Cellular Biochemistry : An International Journal for Chemical Biology in Health and Disease, 140*(1), 1-22.

Turner, C. H. (1998). Three rules for bone adaptation to mechanical stimuli. *Bone, 23*(5), 399-407.

von Kugelgen, I., & Hoffmann, K. (2016). Pharmacology and structure of P2Y receptors. *Neuropharmacology, 104*, 50-61. doi:10.1016/j.neuropharm.2015.10.030

Wang, N., Rumney, R. M. H., Yang, L., Robaye, B., Boeynaems, J.-M., Skerry, T. M., & Gartland, A. (2013). The P2Y13 receptor regulates extracellular ATP metabolism and the osteogenic response to mechanical loading. *J Bone Miner Res, 28*(6), 1446-1456. doi:10.1002/jbmr.1877

Warren, N. J., Tawhai, M. H., & Crampin, E. J. (2010). Mathematical modelling of calcium wave propagation in mammalian airway epithelium: evidence for regenerative ATP release. *Exp Physiol, 95*(1), 232-249. doi:10.1113/expphysiol.2009.049585

Xing, S., Grol, M. W., Grutter, P. H., Dixon, S. J., & Komarova, S. V. (2016). Modeling Interactions among Individual P2 Receptors to Explain Complex Response Patterns over a Wide Range of ATP Concentrations. *Frontiers in Physiology, 7*(294). doi:10.3389/fphys.2016.00294

Yin, J., Xu, K., Zhang, J., Kumar, A., & Yu, F.-S. X. (2007). Wound-induced ATP release and EGF receptor activation in epithelial cells. *Journal of Cell Science, 120*(Pt 5), 815-825. doi:10.1242/jcs.03389

Yu, K., Sellman, D. P., Bahraini, A., Hagan, M. L., Elsherbini, A., Vanpelt, K. T., . . . McGee-Lawrence, M. E. (2018). Mechanical loading disrupts osteocyte plasma membranes which initiates mechanosensation events in bone. *J Orthop Res, 36*(2), 653-662. doi:10.1002/jor.23665

Yu, Q. C., & McNeil, P. L. (1992). Transient disruptions of aortic endothelial cell plasma membranes. *Am J Pathol, 141*(6), 1349-1360.

Zarnitsyn, V., Rostad, C. A., & Prausnitz, M. R. (2008). Modeling Transmembrane Transport through Cell Membrane Wounds Created by Acoustic Cavitation. *Biophysical journal, 95*(9), 4124-4138. doi:10.1529/biophysj.108.131664

Zimmermann, H., Zebisch, M., & Sträter, N. (2012). Cellular function and molecular structure of ecto-nucleotidases. *Purinergic Signalling, 8*(3), 437-502. doi:10.1007/s11302-012-9309-4

Chapter Eight

Discussion and Outlook

In this final chapter, I recap the objectives of this dissertation and position my findings in the context of purinergic mechanotransduction in bone. Along side these discussions, I propose future directions and draw attention to select pilot experiments which warrant further investigation.

8.1 Thesis objectives

8.1.1 Primary *research* objectives

The ***first research objective*** of this dissertation to determine the relationship between mechanical stimulation and early responses in bone cells, specifically focusing on ATP release and calcium signaling was addressed by systematic review and meta-analysis in **Chapter 4** and using a combination of experimental and mathematical methods in **Chapters 6** and **7**.

The ***second research objective*** to examine how spatiotemporal variations in the purinergic signal conveys information about the nature of the mechanical stimulus was investigated in **Chapter 7** using a mathematical model validated with experimental data.

8.1.2 Secondary *methodological* objectives

The ***first methodological objective*** of this dissertation was to develop the theoretical foundation, computational resources and workflow required to conduct a rapid/systematic review and meta-analysis in the basic sciences. The resulting methodology is described in **Chapter 3**.

The ***second methodological objective*** to develop a signal-processing algorithm to facilitate parametric characterization of calcium signals was accomplished in **Chapter 5**.

8.2 Mechanically-stimulated ATP release

8.2.1 Overview

Through systematic review and meta-analysis, we demonstrated that ATP release is among the earliest detectable cellular responses following mechanical stimulation, which is conserved across mammalian cells. In osteoblasts, ATP release was found to occur predominantly through mechanisms related to vesicular exocytosis (Genetos, Geist, Dawei, Donahue, & Duncan, 2005; Romanello et al., 2005) and L-type VSCCs (Genetos et al., 2005), while in osteocytes, vesicles (Kringelbach et al., 2015), hemichannels (Kringelbach et al., 2015; Seref-Ferlengez et al., 2016), P2X7 (Seref-Ferlengez et al., 2016) and T-type VSCC (Thompson et al., 2011) have been implicated.

Consistent with prior findings, we confirmed that osteoblasts contain ATP-rich vesicles and that vesicular exocytosis and L-type VSCCs are involved in mechanically-stimulated ATP release.

However, we also found that mechanical stimuli routinely and reversibly induce membrane disruptions in osteoblasts *in vitro*, and in osteocytes *in vivo*. When vesicular release was interrogated pharmacologically, we found that promoting vesicular exocytosis resulted in reduced ATP release and vice versa, suggesting that vesicular exocytosis is involved in preventing mechanically-stimulated ATP release through micro-injuries. Mathematical modeling further revealed that experimentally observed membrane disruptions were ~100nm in diameter and resealed with a half-time of ~15 seconds. Therefore, I propose that in addition to delivering ATP to the extracellular space, exocytosis of ATP-containing vesicles limits the much larger efflux of intracellular ATP through the non-lethal membrane disruption.

8.2.2 Discussion

Physiological and pathological cell injury. ATP release occurring through a disrupted/injured membrane is not a novel finding. In fact, ATP release is an expected during trauma and cell injury. However, ATP release through a disrupted cell membrane is not considered a physiological route of ATP release and is rather viewed as pathological consequence of trauma or necrotic and apoptotic processes (Ayna et al., 2012; Barbee, 2006; Dahl, 2015; Yin, Xu, Zhang, Kumar, & Yu, 2007). We have challenged this assertion by demonstrating that mechanically-induced membrane injuries occur routinely and are rapidly repaired within moments of stimulation without affecting cell viability. Consistent with these findings, non-lethal reversible cell membrane disruption has been demonstrated using membrane-impermeable tracers in a variety of mechanically-active tissues, including skeletal muscle, skin, cardiac muscle, lung and aorta (McNeil & Steinhardt, 2003), as well as bone (Yu et al., 2017). Thus, rather than amalgamating all ATP release related to membrane injury as pathological, it is necessary to demarcate physiological (**Fig 8-1A, B**) and pathological cases (**Fig 8-1C**), since the former appears to be involved in regular mechanotransductive processes.

Intact and disrupted membrane-related ATP release mechanisms. Our systematic review and meta-analysis on mechanically-stimulated ATP release made it clear that there is widespread consensus that physiological ATP release occurs in the presence of an intact cell membrane. Based on our survey of the literature, this disproportionate over-representation of non-disruptive mechanisms in the literature is likely biased, because most studies that studied ATP release would intentionally discard trials if membrane disruption or injury was evident (Koizumi, Fujishita,

Tsuda, Shigemoto-Mogami, & Inoue, 2003; Leal Denis et al., 2016). However, I must emphasize that evidence of cell membrane injury is not the same as evidence of cell death. Moreover, studies frequently claimed that no membrane disruption occurred by citing prior work (Hovater et al., 2008), without direct verification (Kroemer et al., 2008).

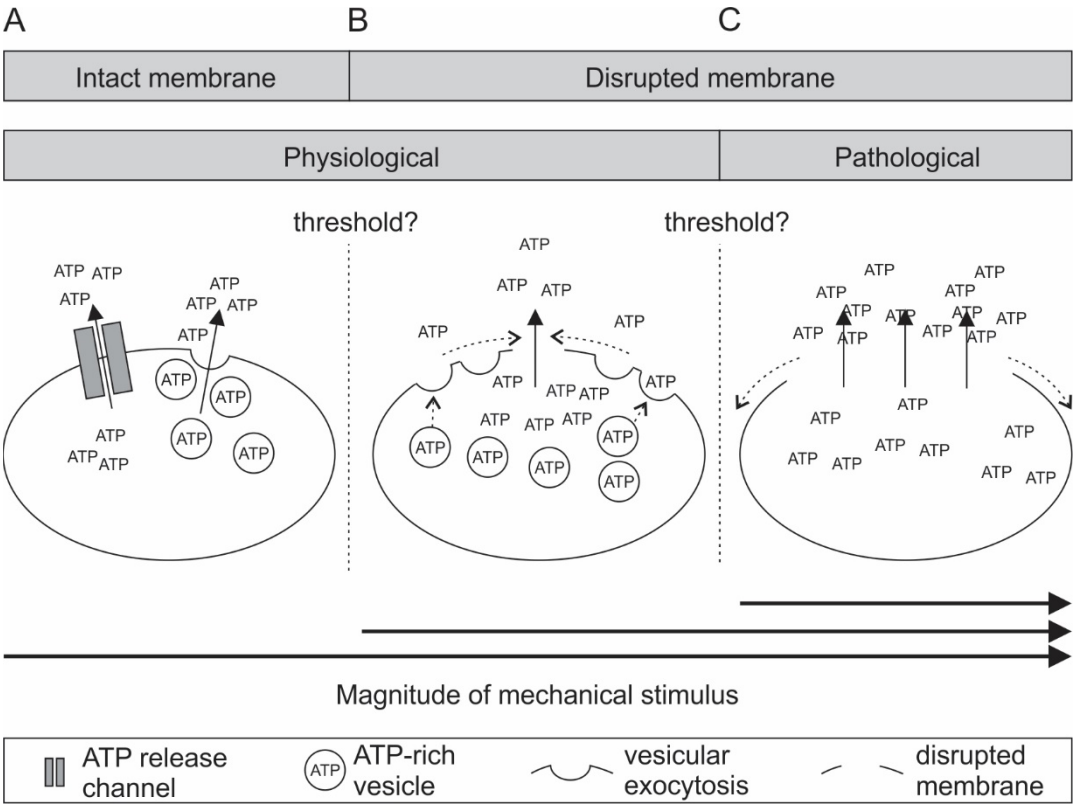

Figure 8-1. Proposed model for mechanically-stimulated ATP release. (A) For low magnitude mechanical stimuli, ATP release is predominantly mediated through intact membrane-related mechanisms, i.e., vesicular and conductive mechanisms. **(B)** Injury-related ATP release occurs when mechanical stimuli exceed the injury threshold, resulting in membrane disruption. ATP spillage is then actively limited by the rate of exocytosis-mediated membrane repair. **(C)** Mechanical stimuli that disrupt the cell membrane beyond repair are pathological. The mechanical thresholds that delineate ATP release through intact- and disrupted-membrane related mechanisms, as well as physiological and pathological ATP release have yet to be characterized.

Based our findings, I suggest that ATP release in the presence of an intact cell membrane occurs predominantly in basal and low mechanical agitation conditions (**Fig 8-1A**), and only when the mechanical stimulus surpasses a certain threshold, ATP released through a disrupted membrane becomes the major source of extracellular ATP (**Fig 8-1B**). Although I did not characterize this injury threshold, Li and colleagues (2016) showed that 20 dynes/cm^2 – but not 12 dynes/cm^2 – shears induced LDH release from calvarian osteoblasts (Y. Li, Wang, Xing, Wang, & Luo, 2016).

Considering that the lacuna-canalicular network can generate shears up to 8-30 dyne/cm^2 at the osteocyte membrane (Weinbaum, Cowin, & Zeng, 1994), and shears up to 50 dyne/cm^2 have been described at the endosteal surface of bone (Coughlin & Niebur, 2012), the membrane disruption threshold lies well within the physiological range of expected forces.

Mechano-adaptation. During our investigation of membrane disruption-related ATP release, we discovered a link between cellular mechanosensitivity and the mechanism involved in membrane repair. Following membrane disruption, vesicular release was critical for the membrane repair and was regulated by the Ca^{2+}/PLC/PKC signalling axis. Importantly, pharmacological activation of PKC prior to mechanical stimulation or priming the vesicular pool for release with NEM resulted in a substantial decrease in membrane disruption and ATP release in response to subsequent mechanical stimulation (**Chapter 6**). Consistent with these findings, meta-analysis of mechanically-stimulated ATP release demonstrated that cyclic stimuli were associated with significantly less ATP release than static (non-oscillatory) stimuli (**Chapter 4**). Thus, these data support a mechanism by which earlier stimuli influence osteoblast resilience and responsiveness to subsequent cycles of mechanical stimulation. This might represent the cellular basis for the mechano-adaptive tissue-level behaviours observed in bone, which exhibit a similar memory-like capacity [**Chapter 1** (Carter & Beaupré, 2007; Frost, 1983; Pivonka, 2018; Skerry, 2006; Turner, 1998)]. This hypothesis is especially alluring because ATP is among the first detectable signals following mechanical stimulation, which would enable top-down control of multiple osteo-regulatory pathways, including Wnt, RANKL and OPG (Burnstock, Arnett, & Orriss, 2013; Gartland et al., 2012; Jørgensen, 2018; Sindhavajiva, Sastravaha, Arksornnukit, & Pavasant, 2018). Therefore, our work has provided the mechanism by which membrane disruption-related ATP release is regulated and identified the Ca^{2+}/PLC/PKCμ signalling axis as a regulatory pathway which may provide insights into how mechano-adaptive memory observed in bone is achieved at the cellular level.

8.2.3 Future directions

Composition of the mechanically-induced signal. I have focused on the implications of injury-related ATP release in bone cells, however membrane disruption undoubtedly results in the spillage of other cytosolic contents. Among these cytosolic contents are other purinergic mediators such as ADP, UTP, UDP and UDP-glucose (Traut, 1994). In our mathematical model of ATP

release and signal propagation (**Chapter 7**), we only considered ATP and ADP, assuming the nucleotide species coexist in a 10:1 ratio intracellularly and are released in proportional amounts. However, further work will be needed to characterize the complete profile of nucleotides released and to determine how these nucleotides are metabolized and interact with one another at the level of P2 receptor signalling.

It is also pertinent to understand how the intracellular composition of nucleotides varies under different conditions, since this would directly affect what is released into the extracellular space following mechanical stimulation. During our development of meta-analytic methods (**Chapter 3**), we conducted a rapid review and meta-analysis of intracellular ATP concentrations in osteoblasts that showed that immature osteoblasts contain 2 (95% CI: 1-12) fmol ATP/cell, while mature osteoblast contain 49 (95% CI: 35-68) fmol ATP/cell. This relationship between osteoblast differentiation and change in bioenergetic state is well established (Komarova, Ataullakhanov, & Globus, 2000); however, the association between bioenergetic state and purinergic signalling is less clear. Some insight was gained from our systematic review and meta-analysis, which showed that chronically hypoxic vascular endothelia (i.e., reduced aerobic respiration) released significantly less ATP in response to mechanical stimulation. Therefore, these lines of evidence suggest that there may be an intimate link between cellular bioenergetic state and mechanotransductive purinergic signalling; however, the evolutionary basis and functional implications of coupling these two processes is unclear and further investigation will be needed.

Bone mechano-adaptation in animal models with deficient repair machinery. I have demonstrated that bone cells are routinely and reversibly disrupted *in vivo*, but I did not investigate the tissue-level outcomes of this phenomenon. Nonetheless, mice with cell repair deficiencies consistently have lower bone mass (S. Li et al., 2017; Rufo et al., 2011; Zhao et al., 2008), supporting a role for cell membrane disruption in bone homeostasis and mechano-adaptation.

Duchenne muscular dystrophy (DMD) is a disorder that is in part characterized by cellular membrane instability and increased injury (Cooper & Head, 2015). DMD patients have lower BMD and elevated resorption markers in the serum (Rufo et al., 2011). Similarly, DMD mouse models have lower BMD that is associated with higher resorption and lower mineral apposition rates (Rufo et al., 2011). Synaptotagmin VII (Syt VII) is a Ca^{2+} sensor protein involved in lysosomal exocytosis and membrane repair (Chakrabarti et al., 2003; Martinez et al., 2000). Syt

VII$^{-/-}$ mice are osteopenic due to impaired bone resorption and formation (Zhao et al., 2008). Our studies have additionally implicated PKCμ in mechano-adaptation and membrane repair. PKCμ-deficient mice are osteoporotic (S. Li et al., 2017). Thus, consistent with our hypothesis, these studies strongly suggest that *in vivo* membrane injury and repair are critical in bone for maintaining bone health. However, since these bone phenotypes were characterized in non-loaded mice, there is more to be learned from studying the osteogenic response of these models in response to mechanical loading.

8.3 ATP in the extracellular space

8.3.1 Overview

Upon release into the extracellular space, ATP diffuses and is concurrently metabolized by ecto-nucleotidases before binding to P2 receptors on neighbouring cells and initiating downstream signaling. Since the effective ATP concentration experienced by neighbouring cells depends on the magnitude and geometry of the mechanical injury, as well as the rate of extracellular degradation and distance of neighbouring cells from the site of injury, we developed and validated a mathematical model to investigate how these factors shape the extracellular purinergic signal (**Chapter 7**). We demonstrated that total ATP released, peak extracellular ATP concentration and the ADP-mediated signaling component encode complementary information about the mechanical stimulus, which is subsequently decoded at the level of the P2 receptor response. In this way, we propose that spatiotemporal variations in extracellular ATP concentrations convey information about the severity and relative position of the injury, as well as the mechano-adaptive status of the injured cells.

8.3.2 Discussion

ATP degradation. We found that C2-OB cells predominantly metabolize extracellular ATP through alkaline-phosphate, with a degradation half time of 20 min (95% CI: 17 to 25). This rate of ATP hydrolysis was sufficient to prevent the accumulation of ATP in the extracellular compartment, but not fast enough to transform the purinergic signal released by a *single* osteoblast. For ATP hydrolysis to have a significant impact on the purinergic signal, much higher concentrations of ATP were necessary – this was achieved by mimicking a tissue-level injury through injuring multiple cells. ATP hydrolysis served to attenuate paracrine responses and

promote the ADP-mediated signaling component when multiple cells were stimulated. Since ATP hydrolysis is a first-order reaction, the dependence of ecto-nucleotidase activity on ATP availability explains why the ATP hydrolysis rate scales with the severity of the injury. Our findings position ATP degradation as a signal dampener that is dependent on the extent of the injury, while simultaneously serving to sustain ADP-mediated signals over longer distances.

Our investigation of ATP degradation led us to pinpoint the situations in which ADP plays a significant role as a mechanotransductive paracrine signal. Of the 15 receptors comprising the P2 receptor network, only 3 are exclusively sensitive to ADP: P2Y1, P2Y12 and P2Y13. Since the two major sources of extracellular ADP were the mechanically-stimulated cells and ATP hydrolysis, ADP-mediated P2 signalling was only observed in injured cells (autocrine signal), and in proximal neighbouring cells when there was a severe injury nearby (paracrine signal).

In osteoclasts, ADP is a potent osteolytic agent (Hoebertz, Meghji, Burnstock, & Arnett, 2001). Considering our findings, I postulate that high extracellular ADP concentrations achieved during damage-inducing skeletal loading serves to signal the presence of microscopic fractures – this initiates remodeling by promoting formation of osteoclasts that remove old damaged bone prior to formation of new bone by osteoblasts. Monocyte recruitment during bacterial infection has also been shown to be ADP-dependent (monocytes are precursors to many immune cell types, including macrophages and osteoclasts), and was ablated in P2Y12/13-deficient mice (Zhang et al., 2016). Compared to ATP, we demonstrated that ADP is less potent and concentrations necessary for P2 receptor activation are only achieved over small areas, which would limit non-specific osteoclast activation that could otherwise be pathological. Taken together, these data support a hypothesis in which ADP arising from higher magnitude mechanical loading is involved in initiating micro fracture-related bone remodeling and highlights the importance of ATP degradation in fine-tuning the mechanotransductive purinergic signal.

ATP diffusion. We showed there was an intimate coupling between the dynamics of ATP release from a mechanically-stimulated cell and the spatiotemporal dispersion of ATP by diffusion. By varying the severity of the cell injury and the kinetics of membrane repair, we were able to numerically generate ATP diffusion profiles which varied in peak ATP concentrations and total ATP released. While the severity of the injury dictated peak ATP concentrations, the joint contributions of injury severity and repair rate determined the total amount of ATP released. Thus,

we propose that peak ATP concentrations govern the timing of purinergic responses (e.g., synchronous vs. asynchronous) and activation of low-affinity P2 receptors (e.g., P2X7), while total ATP released determines the total number of cells that respond through activation of high-affinity P2 receptors (e.g., P2Y2).

This biphasic response gating is consistent with earlier work by Xing et al. (2016) who showed that the P2 receptor network exhibits two distinct response thresholds at the level of the calcium response – a sensitivity threshold (at lower ATP concentrations) and an injury threshold [at higher ATP concentrations (Xing, Grol, Grutter, Dixon, & Komarova, 2016)]. These findings are also supported by functional *in vitro* assays which have demonstrated a biphasic response to ATP in osteoblasts and osteoclasts. Low ATP concentrations inhibit mineralization (Hoebertz, Mahendran, Burnstock, & Arnett, 2002; I. Orriss et al., 2007) and promote resorption (Bowler, Littlewood-Evans, Bilbe, Gallagher, & Dixon, 1998), while high ATP concentrations promote mineralization (Ayala-Peña, Scolaro, & Santillán, 2013) and inhibit resorption (Bowler et al., 1998). These data support a model in which information about the mechanical stimulus is encoded within the spatiotemporal variations of ATP released from the stimulated cells, and P2 receptors on neighbouring cells decode the signal, thereby initiating position- and injury-appropriate signalling events, with cell-type specific functional outcomes.

8.3.3 Future directions

Transient and sustained exposures to ATP. In experimental studies, agonist-specific responses are typically studied by bulk application of the agonist to cells. However, in many cases – like ATP signaling – this is a misrepresentation of reality. Extracellular signals are usually transient with temporal and spatial distributions that vary according to the concentration and flux of the signal at the source, and metabolism and diffusion in the extracellular space (Müller & Schier, 2011). Our understanding of how cells perceive such transient signals is remarkably superficial and calls for a long overdue effort to address these important questions.

In a proof-of-principal experiment, investigated the potential difference between signaling induced by transient and sustained applications of ATP. I first stimulated Fura2-loaded C2-OBs with 1 μM ATP for 5 seconds, after which I added either a large volume of physiological solution to effectively dilute the ATP (**Fig 8-2A, B**), or the same volume of 1 μM ATP to mimic sustained ATP exposure (**Fig 8-2A, B**). I found that while the amplitudes of $[Ca^{2+}]_i$ responses to transient

and sustained ATP exposures were identical (**Fig 8-2C**), the number of oscillatory peaks (**Fig 8-2D**) and areas under the response curves (**Fig 8-2E**) were significantly reduced in the transient exposure condition. These findings confirmed my hypothesis – cells can indeed discriminate between sustained and transient exposures to ATP, at least at the level of the calcium response. It remains to be shown whether this translates to a distinct functional outcome, however a recent publication in *Cell* by Nandagopal and colleagues (2018) reported that pulsatile activation of the Notch receptor was able to promote myogenesis while sustained activation of the same receptor inhibited myogenesis (Nandagopal et al., 2018). Although this work was completed in an entirely different signalling system, the principle still holds, and I anticipate future work in this direction will provide invaluable insights into the complexities of the P2 receptor signaling network.

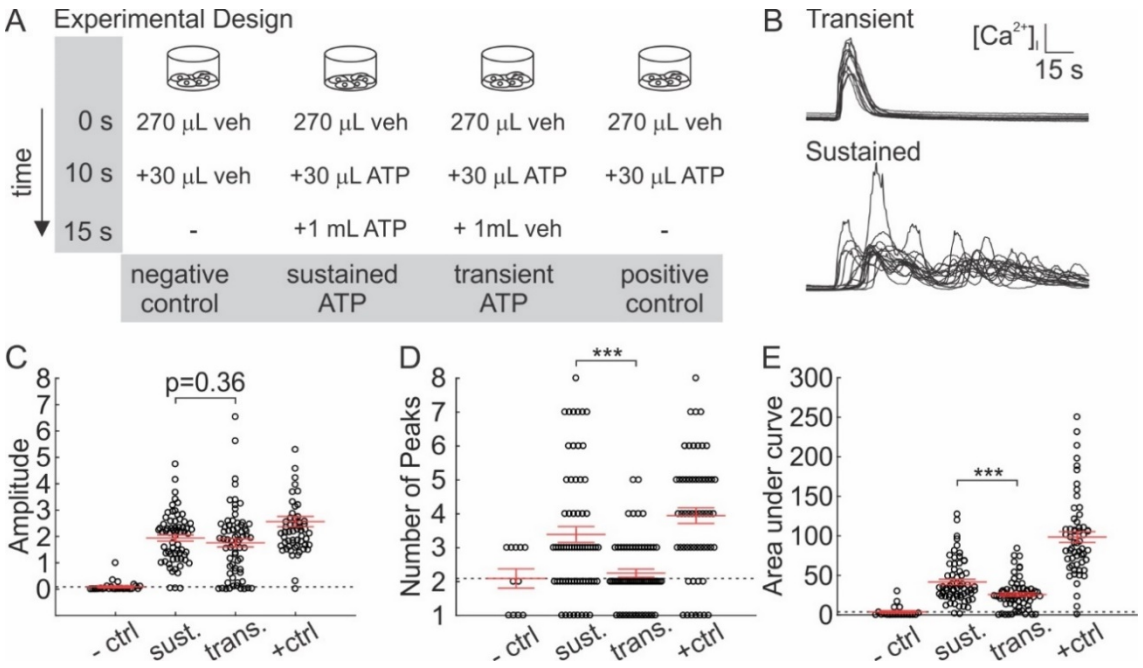

Figure 8-2. **Individual osteoblasts can discriminate between sustained and transient exposures to ATP**. **(A)** Schematic of experimental design: Transient and sustained ATP conditions were achieved by adding 30 µL of 10 µM ATP to Fura2-loaded C2OB cells in 270 µL vehicle (physiological solution) for 5 s, followed by addition of 1 mL vehicle (transient exposure achieved by dilution) or 1 µM ATP (sustained exposure). **(B)** Representative recording of $[Ca^{2+}]_i$ elevations in response to transient (*top*) or sustained (*bottom*) ATP exposure. **(C-E)** Quantification of $[Ca^{2+}]_i$ elevation amplitude (**C**), number of oscillatory peaks (**D**) and area under the curve (**E**). *Round markers*: Individual cell estimates, *red lines*: Means ± standard errors, ***p<0.001 by student t-test.

Other factors influencing purinergic mechanotransduction. We have established that the severity of injury and mechano-adaptive status of the stimulated cells influences purinergic

signaling. However, the basal extracellular environment into which ATP is released can also shape the purinergic signal. Two factors of immediate relevance are cell density and the extracellular compartment volume.

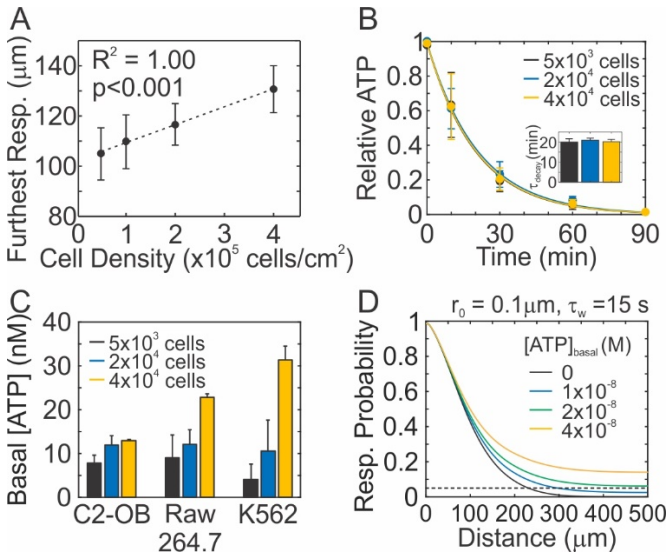

Figure 8-3. **Purinergic mechanotransduction is influenced by cell density**. **(A)** Individual Fura2-loaded CB-OB cell was micropipette-stimulated and the relationship between cell density and the furthest detectable paracrine response was determined. **(B)** 1 μM ATP was added to C2-OB cultures of varying densities and media was sampled and measured at indicated time points by luciferin-luciferase bioluminescence assay. *Inset*: decay time constant τ_{decay}. **(C)** Relationship between basal ATP concentration and cell density in C2-OB, Raw 264.7 and K562 cell cultures. **(D)** Numerically simulated paracrine response probability with different basal ATP concentrations. For A-C, data are means ± SEM.

Bone cell densities vary through proliferation and recruitment during skeletal development and (re)modeling (Kristensen, Andersen, Marcussen, Rolighed, & Delaisse, 2014). To understand how this might affect purinergic mechanotransduction, I conducted a series of exploratory experiments to investigate how differences in cell density affect mechanically-evoked intercellular $[Ca^{2+}]_i$ elevations. C2-OB cells were plated at different densities, and calcium responses were recorded following micropipette stimulation of a single Fura2-loaded C2-OB cell. The signalling range increased as a function of cell density (**Fig 8-3A**). I showed that ATP hydrolysis was independent of cell density (**Fig 8-3B**) but found that basal ATP concentrations positively correlated with cell density (**Fig 8-3C**), which was consistent with what others have reported (Buckley, L Golding, M Rice, P Dillon, & Gallagher, 2003; I. R. Orriss, Key, Hajjawi, & Arnett, 2013). Numerical simulations (using the model developed in **Chapter 7**) showed that increasing basal ATP concentrations could reproduce the observed increases in paracrine signalling radius (**Fig 8-3D**). There remains a distinct possibility that the increase in signalling radius may be explained by increased cell-cell communication via GAP junctions. However, if basal extracellular ATP

concentrations are indeed determined by the surrounding cell density, then our data suggest that purinergic signal is affected by the size of the cellular population.

Since molecular concentration is inversely related to volume, the volume into which ATP is released may also influence purinergic signalling. Volume differences can arise from geometric heterogeneities in trabecular and cortical compartments, as well as structural alterations associated with disease, such as osteoporosis. In support of this hypothesis, I identified a subset of studies from the ATP release meta-analysis (**Chapter 4**) that reported cell densities, culture volumes and basal extracellular ATP concentrations. From 55 datasets, I showed that basal extracellular ATP concentrations were negatively associated with the culture volume (**Table 8-1**, *Model* 1; $p<0.001$), and interestingly, the amount of ATP released per cell was positively associated with volume (**Table 8-1**, *Model* 2; $p<0.001$). Consistent with our cell density-related findings above, these data also showed a positive association between cell count and basal extracellular ATP concentration (**Table 8-1**, *Model* 1; $p<0.001$).

These preliminary data demonstrate that the signalling range of the purinergic signal is affected by factors that regulate basal ATP concentrations, such as cell densities or compartmental volumes. Further work is necessary to further our understanding of how bone cells integrate information about the mechanical stimulus, cellular mechano-adaptive status and environmental factors at the level of the purinergic response.

Table 8-1. Influence of cell density and culture volume (predictors) on basal extracellular ATP concentrations and amount of ATP released per cell under basal conditions (outcomes) was assessed linear regression. N = 55 datasets.

	Coefficient (± 95% CI)	p-value	R^2
Model 1: ATP concentration (log[M])			
Cell Count (log)	0.59 (0.42, 0.77)	<0.001	0.57
Volume (log[mL])	-0.51 (-0.69, -0.32)	<0.001	
Model 2: moles ATP / Cell (log[moles $cell^{-1}$])			
Cell Count (log)	-0.41 (-0.58, -0.23)	<0.001	0.48
Volume (log[mL])	0.49 (0.31, 0.68)	<0.001	

8.4 P2 receptor signalling

8.4.1 Overview

We have learned from our systematic review and meta-analysis that mechanically-stimulated ATP release has been implicated in a variety of musculoskeletal functions (**Chapter 4**), including extracellular matrix synthesis in cartilage (Wann et al., 2012), mechano-sensation in teeth

(Egbuniwe et al., 2014; Liu et al., 2015), and mechanotransduction and remodeling in bone (Romanello, Pani, Bicego, & D'Andrea, 2001; Rumney, Sunters, Reilly, & Gartland, 2012). Furthermore, **Chapter 2** emphasized that P2 receptors are involved in all aspects of bone physiology, including proliferation, differentiation, survival, metabolism and mineralization in osteoblasts, as well as differentiation, survival and resorption in osteoclasts. While our studies have not dwelled on the functional outcomes of P2 receptor signalling per se, they did describe how the mechanical environment shapes the purinergic signal, and the implications of these findings on P2 receptor signalling has been discussed in previous sections. This final section will draw attention to key questions at the level of P2 receptor signalling in bone.

8.4.2 Future directions

Purinergic signalling in osteocytes. I have predominantly focused on purinergic mechanotransduction in osteoblasts, however osteocytes represent a much larger cellular population in bone in which P2 receptors likely play a significant role in bone mechanobiology, metabolism, and homeostasis. The current lack of literature on P2 receptor physiology in osteocytes is largely related to osteocytes being notoriously difficult to study due to their embedment in mineralized tissue. Although, several osteocyte cell lines, including IDG-SW3 (Woo, Rosser, Dusevich, Kalajzic, & Bonewald, 2011), Ocy454 (Spatz et al., 2015), MLO-Y4 (Kato, Windle, Koop, Mundy, & Bonewald, 1997) and MLO-A5 cells (Kato et al., 2001) have been established, thereby enabling *in vitro* study of osteocyte biology, studies of primary *in situ* osteocytes are limited.

As a proof of principle that studies of P2 receptors signaling in bone-embedded osteocytes are feasible, I examined ATP-induced calcium signaling in osteocytes present in freshly isolated bone fragments. Fura2-loaded *in situ* osteocytes responded to ATP with oscillatory $[Ca^{2+}]_i$ elevations, consistent with the presence of functional P2 receptors (**Fig 8-4**). Thus, the most immediate questions that must be addressed are: which P2 receptors and ecto-nucleotidases are expressed by osteocytes? Which nucleotides are released by mechanically-stimulated osteocytes? How does P2 receptor activation influence osteocytic function, such as production of sclerostin and RANKL? Once we begin to understand how P2 receptors function in osteocytes, we will be able to make better sense of the bone phenotypes observed in P2 receptor-deficient animal models. This will

ultimately bring us closer to the development of P2 receptor-targeting therapeutics which may be useful in treating bone disease, such as disuse-related osteoporosis.

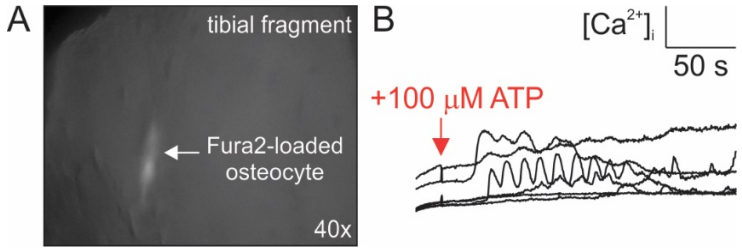

Figure 8-4. *In situ* osteocytes exhibit $[Ca^{2+}]_i$ elevations following application of ATP.
(A) Freshly isolated tibial bone fragments were incubated with Fura2-AM for 30 min and washed, and Fura2-loaded osteocytes were observed *in situ*.
(B) 100 μM ATP was added to *in situ* Fura2-loaded osteocytes and $[Ca^{2+}]_i$ was recorded.

Meta-analysis of purinergic systems. Using the meta-analytic methodology described in **Chapter 3**, future meta-analyses of the basic sciences can further our understanding of the purinergic signalling network. Two relevant parameters of interest in the purinergic system include ecto-nucleotidase activities (e.g., hydrolysis rates) and P2 receptor-mediated signalling (e.g., receptor-specific sensitivities – EC_{50} – determined from calcium mobilization assays, intracellular cAMP generation and IP_3 accumulation). Quantitative synthesis of these functional parameters would also allow us to evaluate how these parameters vary across different model systems and under various experimental conditions.

To demonstrate the value in this approach, I conducted a rapid review and meta-analysis of 31 studies that reported the EC_{50} (concentration of agonist that evoked the half-maximal response) for the P2Y14 receptor, and synthesized outcomes by receptor origin (**Fig 8-5A**), species (**Fig 8-5B**), agonist (**Fig 8-5C**) and secondary messenger (**Fig 8-5D**). The EC_{50} for endogenous P2Y14-mediated $[Ca^{2+}]_i$ responses in murine cells was ~10 μM (**Fig 8-5E**). Of interest, there were two findings that contradicted assumptions that are prevalent in the field of purinergic signalling.

First, it is assumed that characterization of a P2 receptor in heterologous expression system provides a valid approximation of how the receptor behaves in its native environment. However contrary to these assumptions, exogenous P2Y14 was found to be two-orders of magnitude more sensitive to its agonists than endogenous P2Y14 (**Fig 8-5A**). Similar differences in EC_{50} values were previously reported between recombinant (exogenous) and native (endogenous) kainite receptors, in which case it was suggested that regulatory accessory proteins were responsible (Paternain, Rodríguez-Moreno, Villarroel, & Lerma, 1998). Second, P2 receptor activation and sensitivity is thought to be governed at the receptor level, however, meta-analysis revealed that

secondary messengers downstream of P2Y14 had substantially different EC_{50} values (**Fig 8-5D**), which may suggest the existence of a secondary level of regulation that has yet to be explored.

This rapid review together with the systematic review and meta-analysis of mechanically-stimulated ATP release (**Chapter 4**) has provided a glimpse into what meta-analytic efforts in the basic sciences can achieve. Beyond summarizing what is known, consolidation and analysis of such data can reveal non-trivial relationships and generate novel hypotheses. I anticipate that similar meta-analytic efforts will be invaluable in furthering our understanding of purinergic receptor physiology.

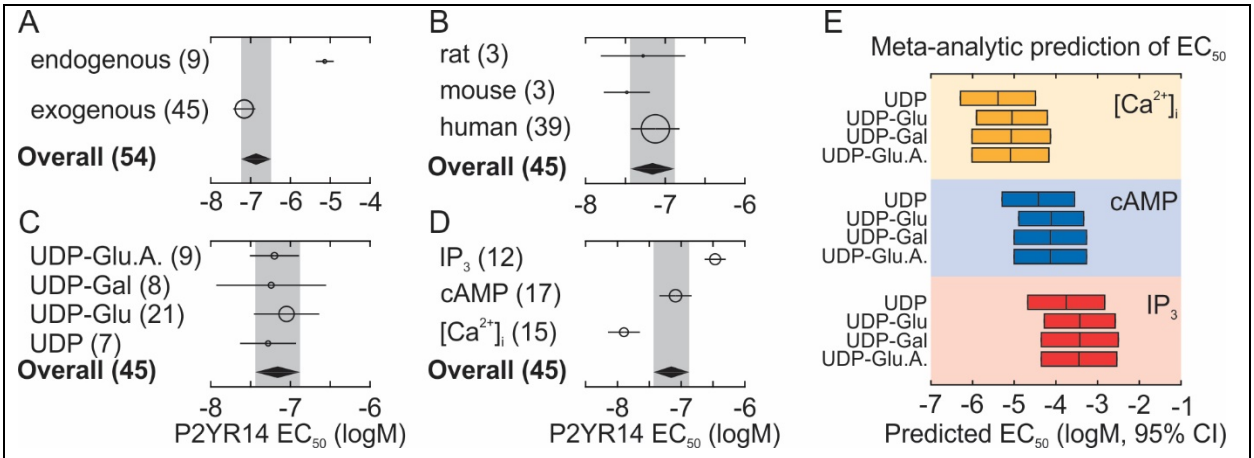

Figure 8-5. Rapid review and meta-analysis of P2Y14 EC_{50}. (A-D) Subgroup analyses of P2Y14 EC50 by receptor origin (**A**), species (**B**), agonist (**C**) and secondary messenger (**D**). *Round markers*: subgroup estimates, *shaded band*: overall estimates. For B-D, only exogenous P2Y14 is assessed. **(E)** Predicted EC_{50} for endogenous P2Y14 in murine cell, by secondary messenger and agonist. Data are means ± 95% CI.

Contribution of P2 receptors to mechanotransductive response. Using P2R antagonists – Suramin and PPADS – we demonstrated that calcium responses following micropipette stimulation of a single osteoblast are mediated by P2 receptors. However, we did not address which P2 receptors mediate this mechanotransductive response. In a series of experiments intended to guide future investigations, we demonstrated that at least seven P2 receptors are expressed in osteoblastic C2-OB cells, including P2Y2, Y4, Y12 and Y14, as well as P2X3, X4 and X7 (**Fig 8-6A**). Surprisingly, we found that by knocking out P2Y2 using a CRISPR-Cas9 approach (**Fig 8-6B**), we were able to abolish nearly all paracrine calcium responses (**Fig 8-6C-E**). These data suggest that the P2Y2 receptor predominates the mechanotransductive calcium response, while the other receptors are either (*i*) silent (i.e., non-functional), (*ii*) their contributions to the mechanical

response cannot be quantified at the level of the calcium response or (*iii*) they are involved in modulating the calcium response that is driven by P2Y2 (e.g., amplitude- and frequency-modulation of oscillatory response). Nonetheless, these findings should first be validated in primary osteoblasts prior to investigating their functional consequences further. Additionally, since the C2-OB cell line is amendable to genetic manipulation, P2 receptor knockout lines for the other P2 receptor subtypes should be established to investigate P2 receptor-specific contributions to osteoblast physiology.

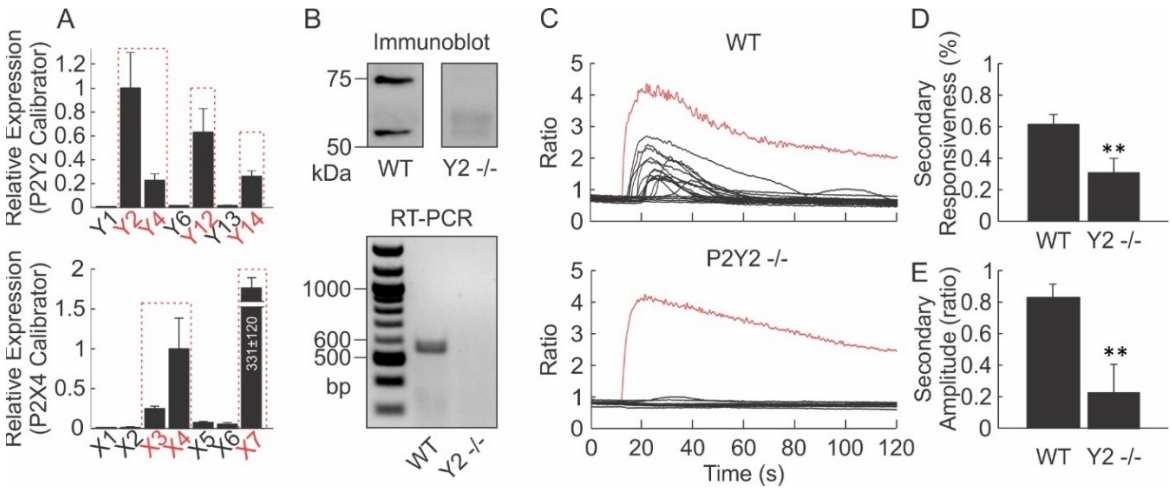

Figure 8-6. **The P2Y2 receptor mediates mechanically-stimulated intercellular calcium responses in osteoblasts. (A)** P2 receptor expression in C2-OB cells assessed by RT-PCR. Highest expressed receptors are indicated (*red*). **(B)** CRISPR-mediated knockout of P2Y2 in C2-OB cells was confirmed by immunoblot (*top*) and RT-PCR (*bottom*). **(C-E)** Single Fura2-loaded WT (*top*) or P2Y2$^{-/-}$ (*bottom*) C2-OB was mechanically stimulated by micropipette and $[Ca^{2+}]_i$ was recorded (**C**), and secondary responsiveness (**D**) and $[Ca^{2+}]_i$ elevation amplitude (**E**) was assessed. Data are means ± standard error, **p<0.01 assessed by students t-test.

8.5 Summary and Conclusions

In the current thesis, we studied the early events that occur following mechanical stimulation of bone cells. Bone cells were mechanically stimulated, ATP was released, and seconds later calcium responses were measured in neighbouring cells – A simple and elegant system to convey information about the mechanical environment. Yet as simple as it may seem, these signals encode complex information that orchestrate the interactions between bone cells that govern how the skeleton adapts to mechanical perturbations, with an astounding memory-like capacity. While the aim of this thesis was to further our understanding of how this is accomplished – which it did –

the insights gained permeate to any paradigm of paracrine signaling. Any signal for which release can be described in terms of its magnitude and kinetics has the capacity to encode information through spatiotemporal variations. Any system capable of metabolizing extracellular signals has the capacity to transform the information transferred between cells. Any responder that has more than two receptors per a signal has the capacity to evoke a multiphasic response. Any response that is modified by prior stimulation can exhibit a memory-like capacity. Thus, the studies of many physiological systems can be informed by the framework developed in this dissertation, which describes how bone cells perceive the mechanical environment, how mechanotransductive signals are generated and transformed, and how they are decoded at the level of the P2 receptor network.

8.6 References

Ayala-Peña, V. B., Scolaro, L. A., & Santillán, G. E. (2013). ATP and UTP stimulate bone morphogenetic protein-2,-4 and -5 gene expression and mineralization by rat primary osteoblasts involving PI3K/AKT pathway. *Exp Cell Res, 319*(13), 2028-2036. doi:10.1016/j.yexcr.2013.05.006

Ayna, G., Krysko, D. V., Kaczmarek, A., Petrovski, G., Vandenabeele, P., & Fésüs, L. (2012). ATP release from dying autophagic cells and their phagocytosis are crucial for inflammasome activation in macrophages. *PLoS ONE, 7*(6), e40069-e40069. doi:10.1371/journal.pone.0040069

Barbee, K. A. (2006). Mechanical Cell Injury. *Ann N Y Acad Sci, 1066*(1), 67-84. doi: 10.1196/annals.1363.006

Bowler, W. B., Littlewood-Evans, A., Bilbe, G., Gallagher, J. A., & Dixon, C. J. (1998). P2Y2 receptors are expressed by human osteoclasts of giant cell tumor but do not mediate ATP-induced bone resorption. *Bone, 22*(3), 195-200. doi: 10.1016/S8756-3282(97)00280-9

Buckley, K. A., L Golding, S., M Rice, J., P Dillon, J., & Gallagher, J. (2003). Release and interconversion of P2 receptor agonists by human osteoblast-like cells. *FASEB K,* 17(11)*,* 10.1096/fj.02-0940

Burnstock, G., Arnett, T. R., & Orriss, I. R. (2013). Purinergic signalling in the musculoskeletal system. *Purinergic Signal, 9*(4), 541-572. doi:10.1007/s11302-013-9381-4

Carter, D. R., & Beaupré, G. S. (2007). *Skeletal function and form: mechanobiology of skeletal development, aging, and regeneration*: Cambridge University Press.

Chakrabarti, S., Kobayashi, K. S., Flavell, R. A., Marks, C. B., Miyake, K., Liston, D. R., . . . Andrews, N. W. (2003). Impaired membrane resealing and autoimmune myositis in synaptotagmin VII-deficient mice. *J Cell Biol, 162*(4), 543-549. doi:10.1083/jcb.200305131

Cooper, S. T., & Head, S. I. (2015). Membrane Injury and Repair in the Muscular Dystrophies. *Neuroscientist, 21*(6), 653-668. doi:10.1177/1073858414558336

Coughlin, T. R., & Niebur, G. L. (2012). Fluid shear stress in trabecular bone marrow due to low-magnitude high-frequency vibration. *J Biomech, 45*(13), 2222-2229. doi:10.1016/j.jbiomech.2012.06.020

Dahl, G. (2015). ATP release through pannexon channels. *Philos Trans R Soc Lond B Biol Sci., 370*(1672), 20140191. doi:10.1098/rstb.2014.0191

Egbuniwe, O., Grover, S., Duggal, A. K., Mavroudis, A., Yazdi, M., Renton, T., . . . Grant, A. D. (2014). TRPA1 and TRPV4 activation in human odontoblasts stimulates ATP release. *J Dent Res, 93*(9), 911-917. doi:10.1177/0022034514544507

Frost, H. M. (1983). A determinant of bone architecture. The minimum effective strain. *Clin Orthop Relat Res*(175), 286-292.

Gartland, A., Orriss, I. R., Rumney, R. M., Bond, A. P., Arnett, T., & Gallagher, J. A. (2012). Purinergic signalling in osteoblasts. *Front Biosci (Landmark Ed), 17*, 16-29.

Genetos, D., Geist, D., Dawei, L., Donahue, H., & Duncan, R. (2005). Fluid Shear-Induced ATP Secretion Mediates Prostaglandin Release in MC3T3-E1 Osteoblasts. *J Bone Miner Res, 20*(1), 41-49. doi:10.1359/JBMR.041009

Hoebertz, A., Mahendran, S., Burnstock, G., & Arnett, T. R. (2002). ATP and UTP at low concentrations strongly inhibit bone formation by osteoblasts: a novel role for the P2Y2 receptor in bone remodeling. *J Cell Biochem, 86*(3), 413-419. doi:10.1002/jcb.10236

Hoebertz, A., Meghji, S., Burnstock, G., & Arnett, T. R. (2001). Extracellular ADP is a powerful osteolytic agent: evidence for signaling through the P2Y(1) receptor on bone cells. *Faseb J, 15*(7), 1139-1148.

Hovater, M. B., Olteanu, D., Hanson, E. L., Cheng, N.-L., Siroky, B., Fintha, A., . . . Schwiebert, E. M. (2008). Loss of apical monocilia on collecting duct principal cells impairs ATP secretion across the apical cell surface and ATP-dependent and flow-induced calcium signals. *Purinergic Signal, 4*(2), 155-170. doi:10.1007/s11302-007-9072-0

Jørgensen, N. R. (2018). The purinergic P2X7 ion channel receptor—a 'repair' receptor in bone. *Current Opinion in Immunology, 52*, 32-38. doi: 10.1016/j.coi.2018.03.016

Kato, Y., Boskey, A., Spevak, L., Dallas, M., Hori, M., & Bonewald, L. F. (2001). Establishment of an osteoid preosteocyte-like cell MLO-A5 that spontaneously mineralizes in culture. *J Bone Miner Res, 16*(9), 1622-1633. doi:10.1359/jbmr.2001.16.9.1622

Kato, Y., Windle, J. J., Koop, B. A., Mundy, G. R., & Bonewald, L. F. (1997). Establishment of an osteocyte-like cell line, MLO-Y4. *J Bone Miner Res, 12*(12), 2014-2023. doi:10.1359/jbmr.1997.12.12.2014

Koizumi, S., Fujishita, K., Tsuda, M., Shigemoto-Mogami, Y., & Inoue, K. (2003). Dynamic inhibition of excitatory synaptic transmission by astrocyte-derived ATP in hippocampal cultures. *Proceedings of the National Academy of Sciences, 100*(19), 11023.

Komarova, S. V., Ataullakhanov, F. I., & Globus, R. K. (2000). Bioenergetics and mitochondrial transmembrane potential during differentiation of cultured osteoblasts. *Am J Physiol Cell Physiol, 279*(4), C1220-1229. doi:10.1152/ajpcell.2000.279.4.C1220

Kringelbach, T. M., Aslan, D., Novak, I., Ellegaard, M., Syberg, S., Andersen, C. K., . . . Jorgensen, N. R. (2015). Fine-tuned ATP signals are acute mediators in osteocyte mechanotransduction. *Cell Signal, 27*(12), 2401-2409. doi:10.1016/j.cellsig.2015.08.016

Kristensen, H. B., Andersen, T. L., Marcussen, N., Rolighed, L., & Delaisse, J.-M. (2014). Osteoblast recruitment routes in human cancellous bone remodeling. *Am J Pathol, 184*(3), 778-789.

Kroemer, G., Galluzzi, L., Vandenabeele, P., Abrams, J., Alnemri, E. S., Baehrecke, E. H., . . . Melino, G. (2008). Classification of cell death: recommendations of the Nomenclature Committee on Cell Death 2009. *Cell Death Differ., 16*, 3. doi:10.1038/cdd.2008.150

Leal Denis, M. F., Alvarez, H. A., Lauri, N., Alvarez, C. L., Chara, O., & Schwarzbaum, P. J. (2016). Dynamic Regulation of Cell Volume and Extracellular ATP of Human Erythrocytes. *PLoS ONE, 11*(6), e0158305. doi:10.1371/journal.pone.0158305

Li, S., Xu, W., Xing, Z., Qian, J., Chen, L., Gu, R., . . . Deng, F. (2017). A Conditional Knockout Mouse Model Reveals a Critical Role of PKD1 in Osteoblast Differentiation and Bone Development. *Scientific Reports, 7*, 40505. doi:10.1038/srep40505

Li, Y., Wang, J., Xing, J., Wang, Y., & Luo, Y. (2016). Surface chemistry regulates the sensitivity and tolerability of osteoblasts to various magnitudes of fluid shear stress. *J Biomed Mater Res A. 104*(12), 2978-2991. doi:10.1002/jbm.a.35848

Liu, X., Wang, C., Fujita, T., Malmstrom, H. S., Nedergaard, M., Ren, Y. F., & Dirksen, R. T. (2015). External Dentin Stimulation Induces ATP Release in Human Teeth. *J Dent Res, 94*(9), 1259-1266. doi:10.1177/0022034515592858

Martinez, I., Chakrabarti, S., Hellevik, T., Morehead, J., Fowler, K., & Andrews, N. W. (2000). Synaptotagmin VII regulates Ca(2+)-dependent exocytosis of lysosomes in fibroblasts. *J Cell Biol, 148*(6), 1141-1149.

McNeil, P. L., & Steinhardt, R. A. (2003). Plasma membrane disruption: repair, prevention, adaptation. *Annu Rev Cell Dev Biol, 19*, 697-731. doi:10.1146/annurev.cellbio.19.111301.140101

Müller, P., & Schier, Alexander F. (2011). Extracellular Movement of Signaling Molecules. *Dev cell, 21*(1), 145-158. doi: 10.1016/j.devcel.2011.06.001

Nandagopal, N., Santat, L. A., LeBon, L., Sprinzak, D., Bronner, M. E., & Elowitz, M. B. (2018). Dynamic Ligand Discrimination in the Notch Signaling Pathway. *Cell, 172*(4), 869-880.e819. doi:10.1016/j.cell.2018.01.002

Orriss, I., Utting, J., Brandao-Burch, A., Colston, K., Grubb, B., Burnstock, G., & Arnett, T. (2007). Extracellular nucleotides block bone mineralization in vitro: evidence for dual inhibitory mechanisms involving both P2Y2 receptors and pyrophosphate. *Endocrinology, 148*(9), 4208-4216. doi:10.1210/en.2007-0066

Orriss, I. R., Key, M. L., Hajjawi, M. O. R., & Arnett, T. R. (2013). Extracellular ATP released by osteoblasts is a key local inhibitor of bone mineralisation. *PLoS ONE, 8*(7), e69057-e69057. doi:10.1371/journal.pone.0069057

Paternain, A. V., Rodríguez-Moreno, A., Villarroel, A., & Lerma, J. (1998). Activation and desensitization properties of native and recombinant kainate receptors. *Neuropharmacology, 37*(10), 1249-1259. doi: 10.1016/S0028-3908(98)00098-7

Pivonka, P. (2018). *Multiscale Mechanobiology of Bone Remodeling and Adaptation*: Springer.

Romanello, M., Codognotto, A., Bicego, M., Pines, A., Tell, G., & D'Andrea, P. (2005). Autocrine/paracrine stimulation of purinergic receptors in osteoblasts: Contribution of vesicular ATP release. *Biochem Biophys Res Commun, 331*(4), 1429-1438. doi:10.1016/j.bbrc.2005.03.246

Romanello, M., Pani, B., Bicego, M., & D'Andrea, P. (2001). Mechanically induced ATP release from human osteoblastic cells. *Biochem Biophys Res Commun, 289*(5), 1275-1281. doi:10.1006/bbrc.2001.6124

Rufo, A., Del Fattore, A., Capulli, M., Carvello, F., De Pasquale, L., Ferrari, S., . . . Teti, A. (2011). Mechanisms Inducing Low Bone Density in Duchenne Muscular Dystrophy in Mice and Humans. *JBMR, 26*(8), 1891-1903. doi:10.1002/jbmr.410

Rumney, R. M. H., Sunters, A., Reilly, G. C., & Gartland, A. (2012). Application of multiple forms of mechanical loading to human osteoblasts reveals increased ATP release in response to fluid flow in 3D cultures and differential regulation of immediate early genes. *J Biomech, 45*(3), 549-554.

Seref-Ferlengez, Z., Maung, S., Schaffler, M. B., Spray, D. C., Suadicani, S. O., & Thi, M. M. (2016). P2X7R-Panx1 Complex Impairs Bone Mechanosignaling under High Glucose Levels Associated with Type-1 Diabetes. *PLoS ONE, 11*(5), e0155107. doi:10.1371/journal.pone.0155107

Sindhavajiva, P. R., Sastravaha, P., Arksornnukit, M., & Pavasant, P. (2018). Intermittent compressive force induces human mandibular-derived osteoblast differentiation via WNT/beta-catenin signaling. *J Cell Biochem, 119*(4), 3474-3485. doi:10.1002/jcb.26519

Skerry, T. (2006). One mechanostat or many? Modifications of the site-specific response of bone to mechanical loading by nature and nurture. *J Musculoskelet Neuronal Interact, 6*(2), 122.

Spatz, J. M., Wein, M. N., Gooi, J. H., Qu, Y., Garr, J. L., Liu, S., . . . Pajevic, P. D. (2015). The Wnt Inhibitor Sclerostin Is Up-regulated by Mechanical Unloading in Osteocytes in Vitro. *J Biol Chem, 290*(27), 16744-16758. doi:10.1074/jbc.M114.628313

Thompson, W. R., Majid, A. S., Czymmek, K. J., Ruff, A. L., Garcia, J., Duncan, R. L., & Farach-Carson, M. C. (2011). Association of the alpha(2)delta(1) subunit with Ca(v)3.2 enhances membrane expression and regulates mechanically induced ATP release in MLO-Y4 osteocytes. *J Bone Miner Res, 26*(9), 2125-2139. doi:10.1002/jbmr.437

Traut, T. W. (1994). Physiological concentrations of purines and pyrimidines. *Molecular and cellular biochemistry, 140*(1), 1-22.

Turner, C. H. (1998). Three rules for bone adaptation to mechanical stimuli. *Bone, 23*(5), 399-407.

Wann, A. K. T., Zuo, N., Haycraft, C. J., Jensen, C. G., Poole, C. A., McGlashan, S. R., & Knight, M. M. (2012). The primary cilium conducts chondrocyte mechanotransduction. *Cilia, 1*(1), P59. doi:10.1186/2046-2530-1-S1-P59

Weinbaum, S., Cowin, S. C., & Zeng, Y. (1994). A model for the excitation of osteocytes by mechanical loading-induced bone fluid shear stresses. *J Biomech, 27*(3), 339-360.

Woo, S. M., Rosser, J., Dusevich, V., Kalajzic, I., & Bonewald, L. F. (2011). Cell line IDG-SW3 replicates osteoblast-to-late-osteocyte differentiation in vitro and accelerates bone formation in vivo. *J Bone Miner Res, 26*(11), 2634-2646. doi:10.1002/jbmr.465

Xing, S., Grol, M. W., Grutter, P. H., Dixon, S. J., & Komarova, S. V. (2016). Modeling Interactions among Individual P2 Receptors to Explain Complex Response Patterns over a Wide Range of ATP Concentrations. *Front Physiol, 7*(294). doi:10.3389/fphys.2016.00294

Yin, J., Xu, K., Zhang, J., Kumar, A., & Yu, F.-S. X. (2007). Wound-induced ATP release and EGF receptor activation in epithelial cells. *J Cell Sci, 120*(5), 815-825. doi:10.1242/jcs.03389

Yu, K., Sellman, D. P., Bahraini, A., Hagan, M. L., Elsherbini, A., Vanpelt, K. T., . . . McGee-Lawrence, M. E. (2017). Mechanical loading disrupts osteocyte plasma membranes which initiates mechanosensation events in bone. *J Orthop Res*. *36*(2) doi:10.1002/jor.23665

Zhang, X., Qin, J., Zou, J., Zhangsheng, L., Binghe, T., Shi, J., . . . Du, B. (2016). Extracellular ADP facilitates monocyte recruitment in bacterial infection via ERK signaling. *Cell Mol Immunol,* 15(1). doi: 10.1038/cmi.2016.56

Zhao, H., Ito, Y., Chappel, J., Andrews, N. W., Teitelbaum, S. L., & Ross, F. P. (2008). Synaptotagmin VII Regulates Bone Remodeling by Modulating Osteoclast and Osteoblast Secretion. *Dev Cell., 14*(6), 914-925. doi:10.1016/j.devcel.2008.03.022

Appendix

A1. MetaLab User Guide

MetaLab is the meta-analytics computational toolbox that implements the methods described in **Chapter 3**. MetaLab can be acquired freely at https://github.com/NMikolajewicz/MetaLab. Here I provide the user guide that describes how MetaLab is used.

A1.1 Introduction

MetaLab is a toolbox for conducting meta-analysis of basic research in MATLAB. It uses a graphical interface, allowing reviewers with minimal prior computation experience to conduct meta-analyses with ease. Data is imported directly from spreadsheet into MATLAB where the analysis is conducted. Conventional meta-analytic techniques have been implemented in MetaLab with extended methods intended to accommodate analysis of basic research studies.

Scope of Guide. This user guide is intended as a guide on how to use MetaLab and not as guide on how to conduct a meta-analysis. The various modules, required (and optional) inputs and generated results are explained in sufficient detail to conduct a meta-analytic project. The underlying equations and meta-analytic techniques are not included in this guide; They can be found described in detail in the corresponding manuscript.

Prerequisites. Users must have MATLAB R2016b or later installed. Spreadsheet formats supported by MetaLab are XLS, XLSX, XLSM, XLTX and XLTM files. All files provided in the MetaLab installation folder must be kept in a designated directory.

Usage. To run MetaLab, open the 'Main.m' file and press 'RUN'. Users can navigate through the tool box using the provided graphical interface and user prompts.

Contact. Please report any problems/bugs to Nicholas.Mikolajewicz@mail.mcgill.ca. Suggestions/improvements are also welcome.

A1.2 Implementation

MetaLab is organized into six modules, each equipped to facilitate different stages of the meta-analytic process. Here we briefly outline the function of each module along with expected inputs and outputs (shown in parentheses are formats) before going into more detail in subsequent sections. The organization and flow of data in MetaLab is illustrated in **Fig A1-1**.

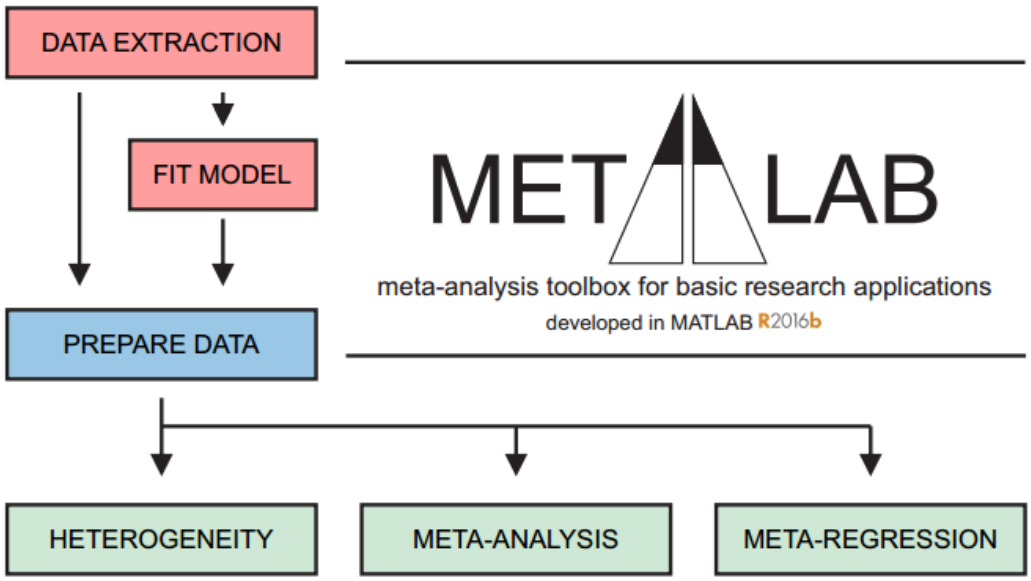

Figure A1-1. MetaLab organization and flow of data.

1. **Data Extraction**: Facilitates systematic and unbiased data extraction. Study figures are used as inputs, axes are then calibrated at reference points specified by the reviewer, and data is extracted.

   Input: Study figures (*.PNG format*)

   Output: Extracted study-level data (*MATLAB structure, spreadsheet*)

2. **Fit Model**: Complex relationships, including response kinetics and dose-dependencies are commonly studied in basic science. This module allows reviewers to fit extracted study-level data with linear, quadratic, exponential, hyperbolic or sigmoidal model and extract parameters of interest for subsequent meta-analysis

   Input: multi-observational data sets (*spreadsheet*)

   Output:

   - Model parameter estimates & statistics (*spreadsheet*)
   - Input data (*plot*)
   - Monte-carlo samples and model fittings (*plot*)
   - Model parameter distributiosn (*plot*)
   - Final model (*plot*)

3. **Prepare Data**: Imports prepared data from spreadsheet into MATLAB and stores data in MATLAB structure for subsequent use and compatibility with heterogeneity, meta-analysis and meta-regression modules.

Input: meta-analytic data set (*spreadsheet*)

Output: Meta-analysis data set (*MATLAB structure*)

4. **Heterogeneity**: Evaluates heterogeneity and bias in meta-analytic data set.

   Input: meta-analysis data set (*MATLAB structure*)

   Output(s):

   - Study-level data distribution: weighted histograms (*plot*) and normal probability (*plot*)
   - Cluster-covariate dependence analysis: k-means clustered distributions (*plot*), independence test of covariate-clusters (*plot*)
   - Funnel plot (*plot*)
   - Variance vs sample size (*plot*)
   - Comparison of weighting schemes: distribution of study-level weights (*plot*), effect sizes compared under different weighting schemes (*plot*)
   - Tau-squared estimator comparison (*plot*)
   - Baujat plot (*plot*)
   - Sensitivity analyses: singly study exclusion analysis (*plot*), cumulative study exclusion analysis (*plot*)

5. **Meta-Analysis**: Synthesis of meta-analysis data set, along with subgroup analyses.

   Input: meta-analysis data set (*MATLAB structure*)

   Output(s):

   - Meta-analysis results and statistics (*spreadsheet*)
   - Subgroup analysis results and statistics (*spreadsheet*)
   - Unweighted data distributions (*plot*)
   - Study-level forest plot (*plot*)

6. **Meta-Regression**: Conducts linear meta-regression analysis with option to validate results through intrastudy (within-study) regression analysis.

   Input: meta-analysis data set (*MATLAB structure*)

   Output(s):

   - Meta-regression results and statistics (*spreadsheet*)
   - Regression diagnostic plot (*plot*)
   - Meta-regression plot (*plot*)

These features are discussed in more detail in the following sections.

A1.2.1 Data Extraction Module

Overview: This module facilitates extraction of quantitative data from graphical or tabular figures. Using a 'point and click' interface, users calibrate graph axes and extract data from figures that are provided as input to this module. Extracted data are subsequently stored in MATLAB structure with option to export to spreadsheet.

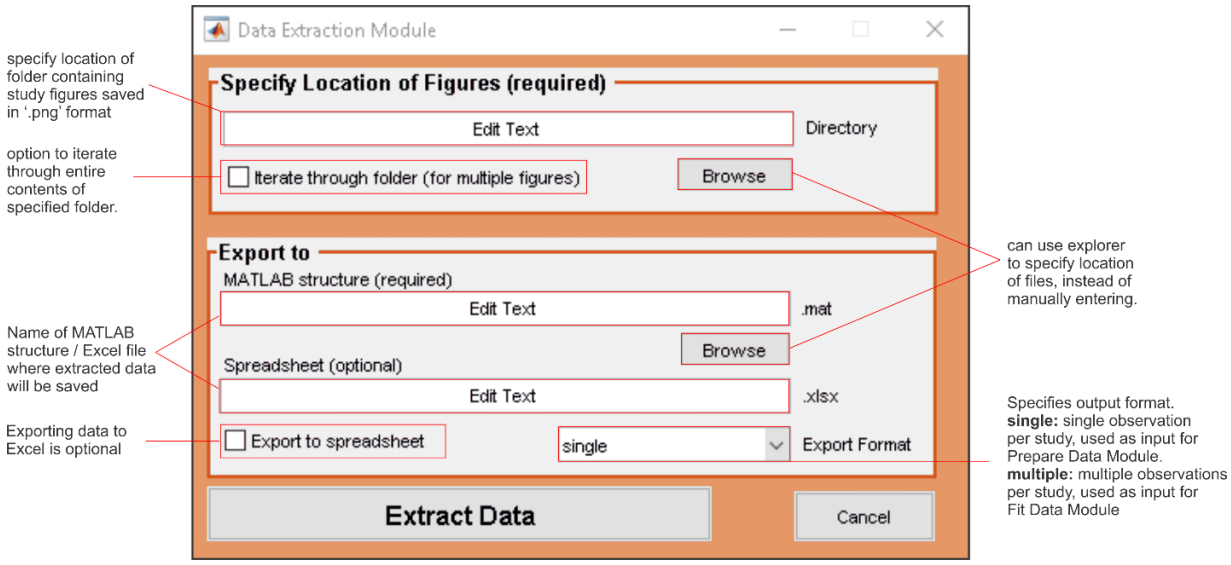

Figure A1-2. Data extraction module user interface

Usage

Input. To begin data extraction, users are *required* to specify the location of figures and name of MATLAB structure to which extracted data are exported (**Fig A1-2**). Study figures must be saved as .PNG format in a designated folder.

> *Tip 1*: Data is extracted from one figure at a time (*default*). To iterate through all figures in saved in folder automatically, select 'iterate' option
>
> *Tip 2*: Save all study figures in designated directory prior to data extraction rather then adding them intermittently.
>
> *Tip 3*: Study figure inputs can be prepared by taking screenshots of graphical data with Print Screen function, pasted into image editor (ex. Microsoft Paint), cropped to size and saved as .PNG file. Saved figures should store in a folder designated for study figures. See for **Fig. 3** for example.

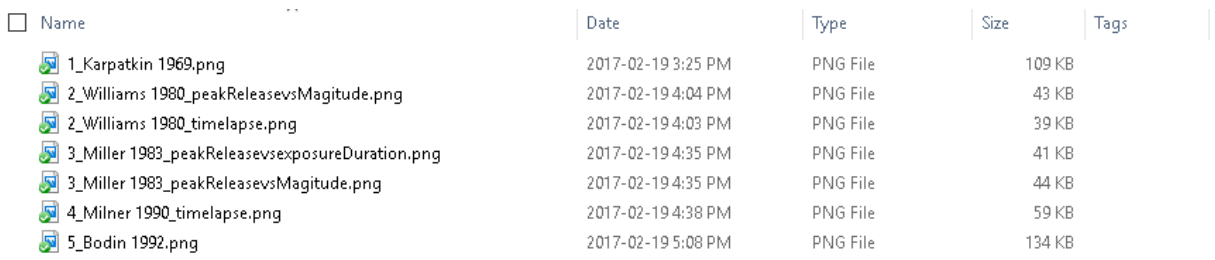

Name	Date	Type	Size	Tags
1_Karpatkin 1969.png	2017-02-19 3:25 PM	PNG File	109 KB	
2_Williams 1980_peakReleasevsMagitude.png	2017-02-19 4:04 PM	PNG File	43 KB	
2_Williams 1980_timelapse.png	2017-02-19 4:03 PM	PNG File	39 KB	
3_Miller 1983_peakReleasevsexposureDuration.png	2017-02-19 4:35 PM	PNG File	41 KB	
3_Miller 1983_peakReleasevsMagitude.png	2017-02-19 4:35 PM	PNG File	44 KB	
4_Milner 1990_timelapse.png	2017-02-19 4:38 PM	PNG File	59 KB	
5_Bodin 1992.png	2017-02-19 5:08 PM	PNG File	134 KB	

Figure A1-3. Study figures saved in designated folder. All figures are saved in .PNG format.

Tracking Extraction Progress. Once data extraction process has started, a progress tracking variable ('currentProgress.mat') will be created which tracks progress within the study figure directory. This ensures continuity across multiple data extraction sessions. If user is starting new set of data extraction, ensure no prior 'currentProgress.mat' variable exists (found in same folder as MetaLab files) otherwise the order of figures retrieved by the module will be wrong.

Axes Calibration & Data Extraction. Data Extraction Module will open study figures. Users will be directed to select figure area of interest with pointer and double click to crop and zoom in. Series of prompts will then enable user to specify key graphical features required to proceed with data extraction. Importantly, the quality of extracted data depends on how precisely the axes are calibrated and data are selected by the user. Not all inputs are required, those that are, are specified.

Extracted data is saved to MATLAB structure by default. To access extracted data, specify spreadsheet name. Export 'single' format assumes single observation per study and is used as input for Prepare Data Module. Export 'multiple' format assumes multiple observations per study and is used as input for Fit Model Module.

> *Tip 4*: If mistake is made during data extraction, users will be presented with option to redo current figure.
>
> *Tip 5*: Make sure to label figures and data during data extraction to be able to map datasets back to original studies!

A1.2.2 Fit Model Module

Overview: Complex relationships are commonly studied in basic science. Fit Model Module allows reviewers to fit study-level data with linear, quadratic, exponential, hyperbolic or sigmoidal model using Monte-Carlo error propagation method. Model parameters and error terms are extracted from fitted model and can then be used for subsequent meta-analysis

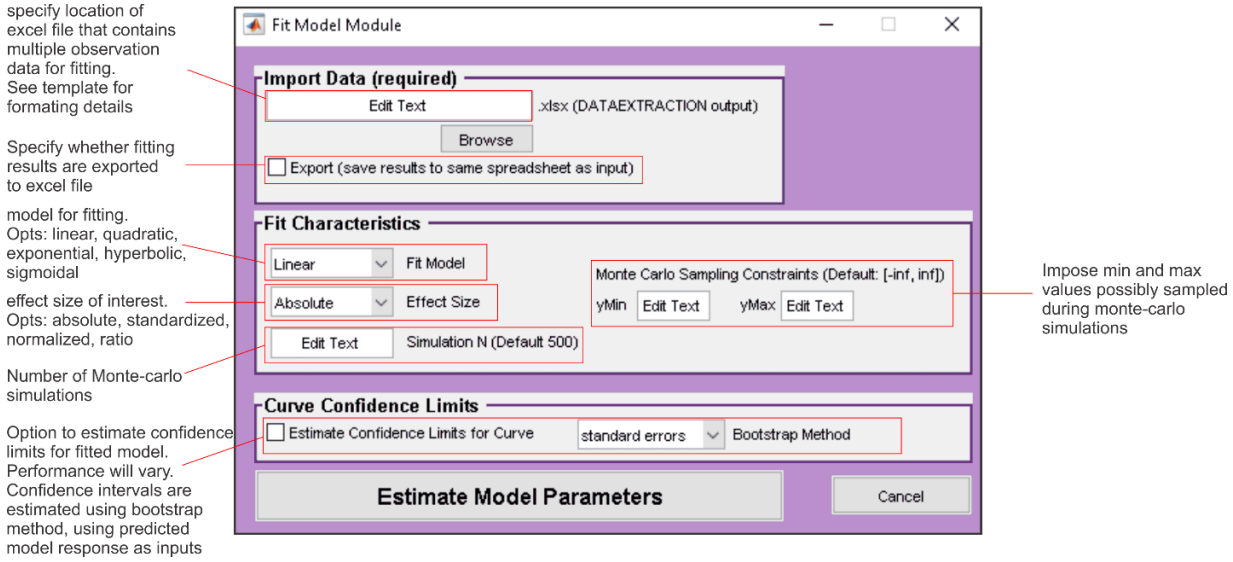

Figure A1-4. Fit model module user interface

Usage

Input. As input, the Fit Model Module requires a spreadsheet where study-level data sets are provided in separate sheets (**Fig A1-4**). Each data set must consist of multiple independent observations organized with the following column headers (headers are case sensitive, see **Fig A1-5** for template):

Required Headers

Study: name of study (string)

exposure: predictor variable (number)

xr: response variable (number)

ser: standard error of xr (number)

nr: sample size of xr (number)

Optional Headers

xc: basal/control variable (number)

sec: standard error of xc (number)

nc: sample size of xc (number)

Tip 6: Data exported in 'multiple' export format from Data Extraction Module (**Fig A1-5)** is compatible as input into Fit Model Module. Otherwise, spreadsheet must be manually prepared by user.

Tip 7: To fit a model to standardized, normalized or ratio data, the optional control variable inputs (i.e., 'xc', 'sec' and 'nc') are necessary to compute the effect size of interest prior to fitting the data.

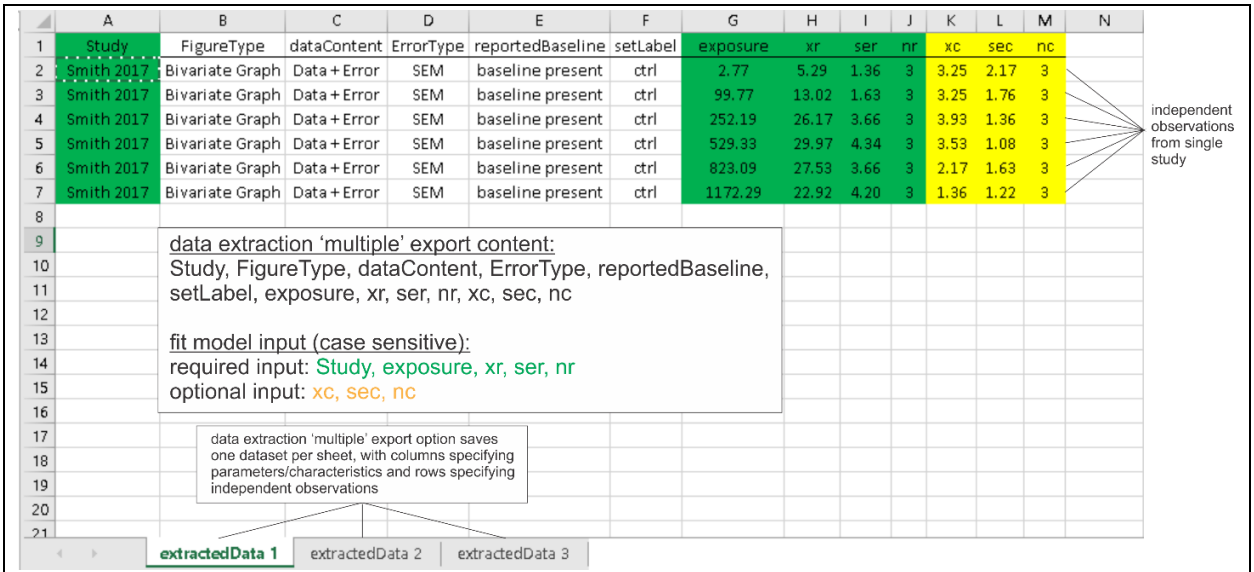

Figure A1-5. Fit model input data format in spreadsheet is shown. The format of exported results from the Data Extraction Module, with 'multiple' export option selected is shown. Manually prepared spreadsheet should follow same format.

Specifying Fit Characteristics: Data can be fit to linear, quadratic, exponential, hyperbolic or sigmoidal model and parameters computed in terms of absolute, normalized, response ratio or Hedges' standardized effect size **(Fig A1-4)**. Parameter estimates will improve as number of simulations N increases (processing time increases with number of simulations, i.e., from seconds to minutes). Restrictions on sampled values can be imposed as yMin and yMax. To generate

confidence intervals, standard errors or 95% percentiles are bootstrapped. Standard error-derived intervals are parametric and will be symmetrical, while percentile-derived intervals are non-parametric and can accommodate non-symmetrical intervals.

> *Tip 8*: Lower bound restriction at 0 (yMin = 0, yMax = inf) is advised if experimental values are known to be non-negative.

***Model Parameter Estimation*.** Upon initiating Fit Model Module, Meta Lab will proceed with Monte-Carlo model fitting. For each set of study-level data, user is prompted to visually evaluate fit.

In cases where fitting algorithm fails to converge to solution, new set of data will be resampled and fitting procedure will be attempted again. This will continue until the desired number of fits (specified by user are attained. Data that is incompatible with the specified model may result in MetaLab running indefinitely. If solutions are not found within ~ 2-5 minutes, cancel the fitting procedure and ensure the input data set is compatible with the specified model, otherwise select a different model or omit data set.

> *Tip 9*: When prompted to evaluate quality of model fit, this is good opportunity to save figures of interest since figures are not automatically saved by MetaLab.

***Output(s)*:** For each data set (i.e., sheet in input spreadsheet), MetaLab will generate figures of (i) initial input data, (ii) Monte-Carlo samples and model fittings, (iii) distributions for estimated parameters and (iv) final model with reported fit results that include model name, function, mean estimates and standard errors.

If export option was specified, results are exported into same spreadsheet file that was initially specified (i.e., spreadsheet with input datasets). Otherwise, only figures are generated.

Example plots are provided as unmodified MetaLab outputs:

(i) Input data

Study-level data means (y) ± standard errors are plotted with respect to exposure (x). Study-level means, and variances are used to approximate distributions from which data are resampled and fit accordingly.

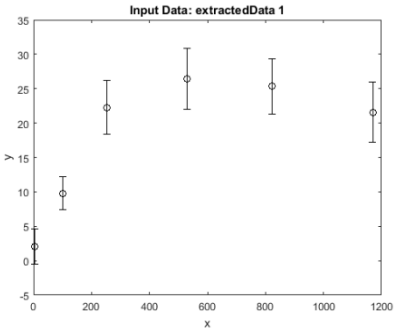

(ii) Monte-Carlo samples and model fits

Monte-Carlo sampled data is plotted along with corresponding model fits (*left*). Outlying fits are omitted (*right*) prior to estimation of final model parameters. Outliers are identified using fitted model parameters. Parameters that exceeded three median absolute deviations away from the median are omitted. See MATLAB isoutlier() function for more details on outlier detection.

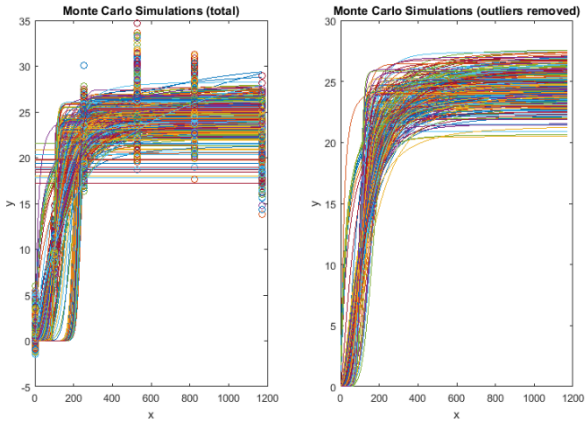

(iii) Model parameter distributions

For each set of Monte-Carlo samples, specified model is fit to data and set of parameters are extracted. Distribution of all fitted parameters are shown. Parameter error terms are derived from these distributions. Normally distributed parameter estimates are typically indicative of reliable parameter estimation.

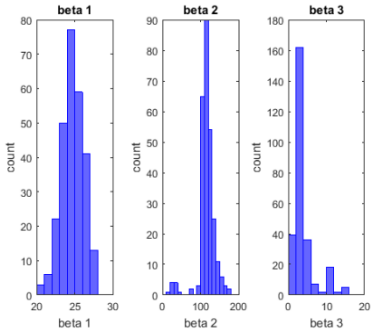

(iv) Final model

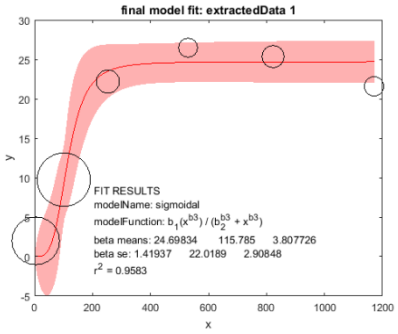

Final model (red curve) and study-level data (black markers) are shown. Optionally, 95% confidence limits are bootstrapped and shown (red bands). Summary of the fit results are displayed, including type of model, model function, parameter means and standard errors along with corresponding R^2 value. Parameters β are numbered as shown in model function and mean and standard errors are listed in order (i.e. means for β_1, β_2, β_3, etc.). These statistics are exported to same spreadsheet as original input if export option was specified.

A1.2.3 Prepare Data Module

Overview: Once study-level data has been extracted and prepared (Data Extraction and/or Fit Model Modules), this module will import the entire meta-analytic data set from a spreadsheet into MATLAB and save it in a standardized MATLAB format that is compatible with Heterogeneity, Meta-analysis and Meta-regression modules. This module also enables optional data stratification for downstream stratified subgroup analysis.

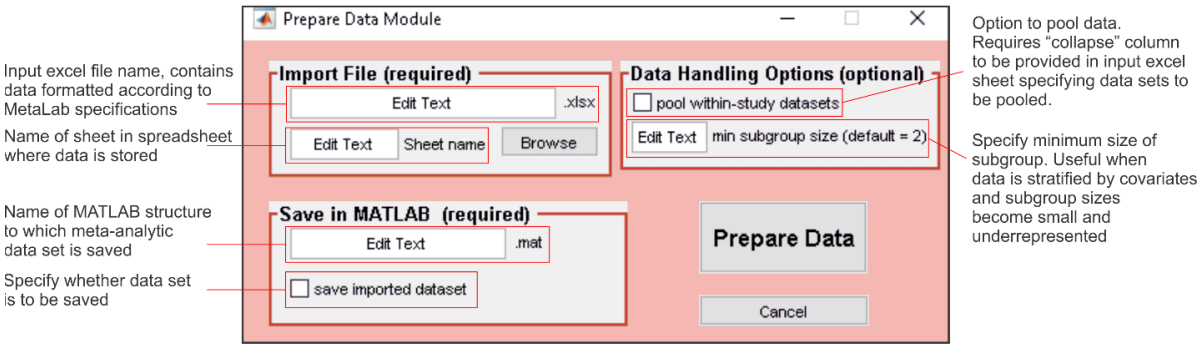

Figure A1-6. Prepare data module user interface

Usage

Input: To import meta-analytic data set into a MATLAB structure (**Fig A1-6**), data must be prepared in a spreadsheet according to MetaLab specifications, as shown in **Fig A1-7**. All data must be stored in a single spreadsheet, with the following column headers (headers are case sensitive):

Required Headers

ID: unique numeric identified for each independent observation

Study: name/label for study (string)

xr: response variable (number)

- Common units of measure must be used for study-level means if the absolute mean/difference is going to be used as effect size. If normalized, standardized or ratio effect sizes will be used, xc, sec and nc are required as inputs as well, however in these cases common units of measure are not required.

ser: standard error of xr (number)

nr: sample size of xr (number)

Optional Headers

xc: basal/control variable (number)

sec: standard error of xc (number)

nc: sample size of xc (number)

collapse: specifies which data sets are to be pooled together

- If the study contains multiple datasets, they can be either pooled together, or treated as independent observations. By default, MetaLab will treat each row as an independent observation. However multiple observations can be pooled together by adding a column in the excel sheet labeled "collapse", where unique numbers are assigned to the datasets that are treated as independent observations, while observations intended to be pooled together receive common values. MetaLab will pool data by calculating weighted means, using sample sizes as weights.

ISR: Specifies which data are grouped together for intrastudy regression (ISR)

- If reviewers wish to perform ISR analysis, additional column titled "ISR" must be included and numbered like the "collapse" column; Data that belong to same data set (i.e., within-study dataset) are designated by common numbers.

Covariates: Additional columns that have not been specified above can be included as covariates

- Categorical covariates must be coded numerically (ex. human – 1; mouse – 2; rat – 3) if reviewers wish to use these in subsequent data stratification or subgroup analysis.
- Current version of MetaLab will treat numerical continuous covariates like numerically-coded categorical covariates for subgroup analysis, however can be used in meta-regression analysis as continuous predictor.

To summarize, the minimum input excel sheet must contain "ID", "Study", "xr", "ser" and "nr" headers with optional columns including "xc", "sec", "nc", "collapse", "ISR", and any additional columns that are to be treated as covariates. Do not include unnecessary columns or rows input. Everything in input spreadsheet will be included part of the meta-analytic data set.

	A	B	C	D	E	F	G	H	I	J
1	ID	Study	xr	ser	nr	collapse	ISR	categorical covariate	continuous covariate	
2	1	Chen2008Fig3C.png	23.03609	0.796768	3	1	1	1	0	
3	2	Chen2008Fig3C.png	19.55603	1.586798	3	1	1	1	1	
4	3	Chen2008Fig3C.png	17.54757	1.952982	3	2	1	1	2	
5	4	Chen2008Fig3C.png	18.71036	1.098552	3	2	1	1	3	
6	5	Chen2008Fig3C.png	35.57895	2.430949	3	2	1	1	4	
7	6	Chen2008Fig3C.png	32.66385	4.028025	3	2	1	1	5	
8	7	Chen2008Fig3C.png	32.55814	3.722872	3	2	1	1	6	
9	8	Chen2008Fig3C.png	36.54661	3.363799	3	3	1	1	14	
10	9	Chen2008Fig3C.png	38.31579	1.64089	3	3	1	1	21	
11	10	Chen2008Fig3C.png	40.90909	2.197105	3	3	1	1	28	
12	11	Choi 2011 Toxicology in Vitro 25 1603–1608	5.82	0.36	3	4	2	3	3	
13	12	Choi 2014 Free Radical Research, 48:7, 729-739	Have	0.04825	3	5	2	3	2	
14	13	Choi 2007	0.103	0.005	3	6	2	3	2	
15	14	Dowd 1990 J Biol Chem 265 34 20833-20838	10.5	2	3	7	3	2	0	
16	15	Esen2013Fig2F.png	3.952381	0.568186	3	8	4	3	1	
17	16	Hsu2013Fig3C.png	30.50093	1.328227	3	9	5	1	21	
18	17	Hsu2013Fig3C.png	34.73098	0.814075	3	9	5	1	21	
19	18	Komarova2000Fig6.png	88.23529	6.417112	4	10	6	2	3	
20	19	Komarova2000Fig6.png	64.28571	12.32143	4	10	6	2	7	

Input format for Prepare Data Module[&]

required input: ID[$], Study, xr, ser, nr
optional input: xc*, sec*, nc*, collapse, ISR
additional inputs: treated as covariates[#]

[&]Header labels are case sensitive
[$]ID must be unique for each row
*omit headers for control variable if not available/required
[#]categorical covariates must be numerically coded, no restrictions imposed on what covariate header labels can be

Figure A1-7. Prepare data input format in spreadsheet. Required and optional headers are shown.

***Data stratification*:** Once Prepare Data Module has been initiated, user will be prompted to optionally stratify data by categorical covariates (**Fig A1-8**). This has been included as option to conduct stratified-subgroup analysis, however is not necessary and users can proceed by selecting "no stratification" option.

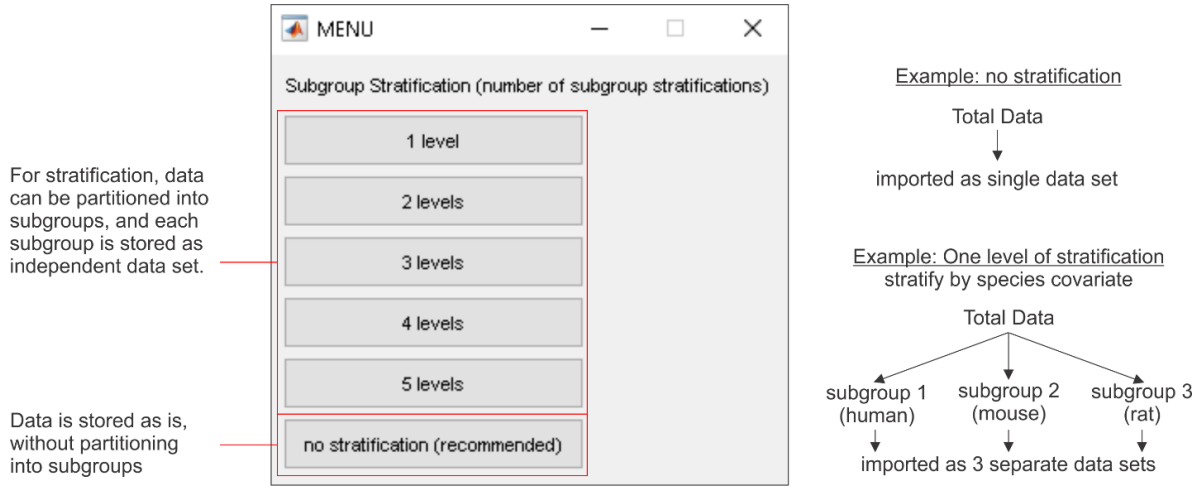

Figure A1-8. Data sets can be stratified according to categorical covariates in Prepare Data Module. Once level of stratification is selected, users can select from list of available covariates to stratify data by.

***Output*:** Imported data will be saved into MATLAB structure and is now ready for analysis in subsequent MetaLab modules. Multiple data sets can be saved to the same MATLAB structure by simply specifying that newly imported data be saved to a pre-existing MATLAB data structure.

When these data structures are used in subsequent analyses (Heterogeneity, Meta-Analysis or Meta-Regression Modules), MetaLab will produce results for each data set independently.

The following prompt will be displayed when data has been successfully imported:

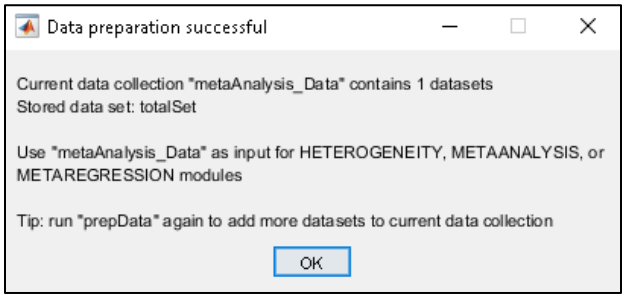

A1.2.4 Heterogeneity Module

Overview: This module is designed to assess the extent of heterogeneity and bias present in a meta-analytic data set. It can be used to generate study-level data distributions, funnel plots and Baujat plots, evaluate variance/sample size assumptions, compare weighting schemes and tau^2 estimates and conduct sensitivity analyses and cluster-covariate dependence analyses.

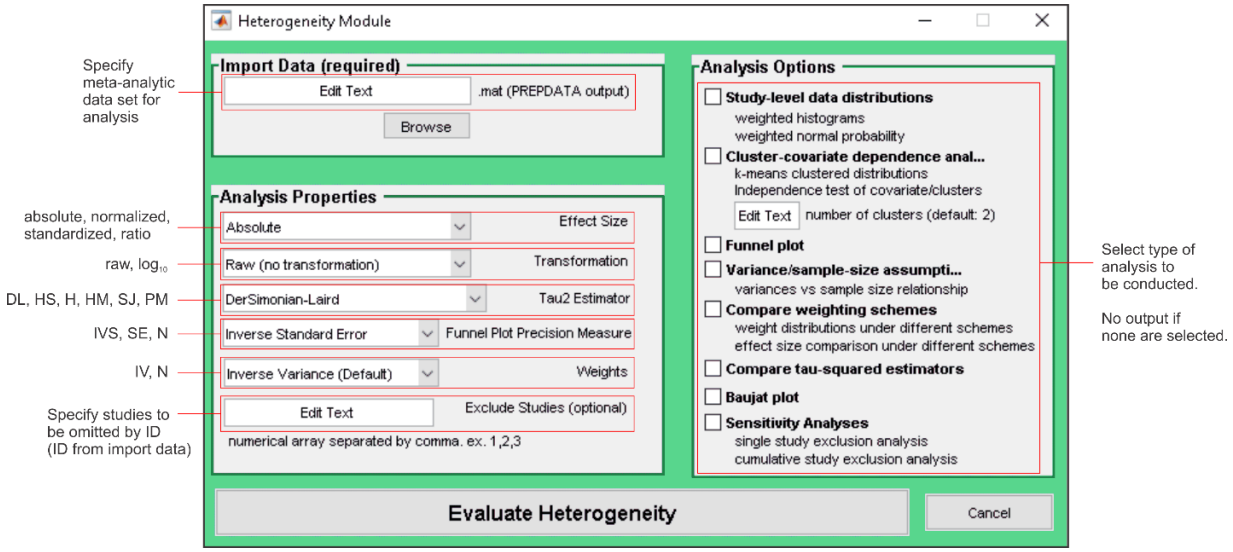

Figure A1-9. **Heterogeneity module user interface**. Tau^2 estimator options are DL: DerSimonian-Laird, HS: Hunter-Schmidt, H: Hedges, HM: Hatung-Makambi, SJ: Sidik-Jonkman, PM: Paule-Mandel. Funnel plot precision measures options are IVS: inverse standard error, SE: standard error and N: sample size. Weighting options are IV: inverse variance and N: sample size.

Usage

Input. Meta-analytic data set(s) that have been imported using the Prepare Data Module can be directly loaded into the Heterogeneity module. Several analysis options are provided along with analysis properties (**Fig A1-9**).

Typical settings used in meta-analyses are set as default. Analyses will be conducted using specified effect size and transformation method.

***Output*:** Heterogeneity module will produce figures for each set of specified analyses, which can then be manually saved. Plots that are provided below are unmodified outputs from MetaLab.

Study-level data distributions

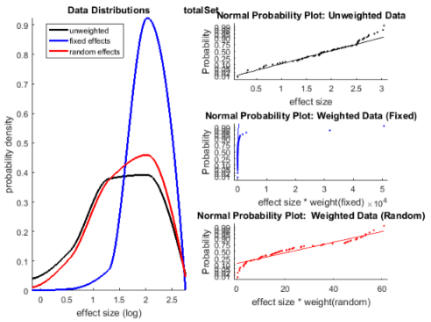

Weighted histograms (unweighted, fixed effects weighted and random effects weighted).

Weighted normal probability plots (unweighted, fixed effects weighted and random effects weighted)

Cluster-covariate dependence analyses

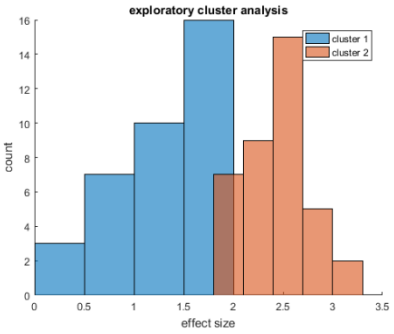

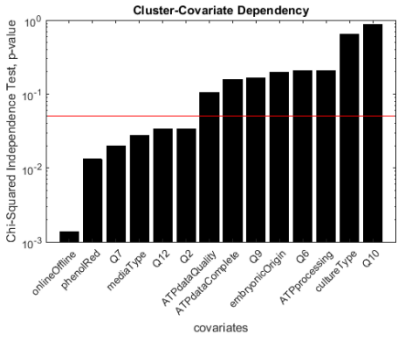

Data are clustered according to k-means algorithm and distributions of clusters are visualized using histograms. Default number of clusters is two however can be modified if more clusters are expected.

p-values for χ^2-test of independence between cluster membership and covariates are plotted (*black bars*) in ascending order with significance threshold (*red*) shown for reference. This analysis is useful for identifying potentiate covariates of interest, which may account for observed heterogeneity.

Funnel plot

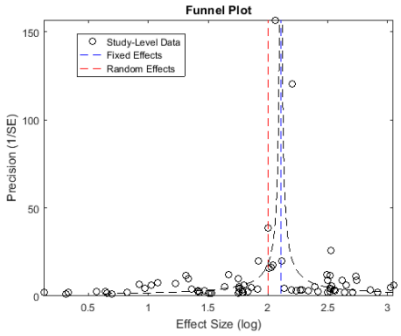

Study-level precisions are plotted with respect to study-level effect sizes (*black markers*). Precision measure (inverse standard error, standard error or sample size) along with transformation (raw or $\log_{10}$) of effect size can be specified. Theoretical 95% confidence intervals *(black curves*) are centered around fixed effects estimate (*blue*), and random effects estimate (*red*) is shown for reference.

Variance/sample size assumption

Study-level variances (squared standard deviation, not squared standard errors) are plotted with respect to sample size, and monotonic relationship is evaluated. Used to test independence assumption between study level variance and sample size. If relationship exists, alternative weighting scheme may be considered (i.e., sample size weighting)

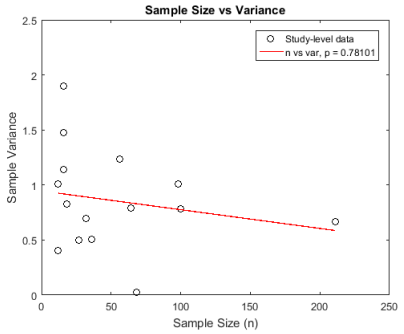

Comparison of weighting schemes

Distribution of weights across studies are visualized, comparing unweighted (UW), fixed effects weighting (FE), random effects weighting (RE) and sample size weighting (N). Proportion of total weight is plotted on Y-axis.

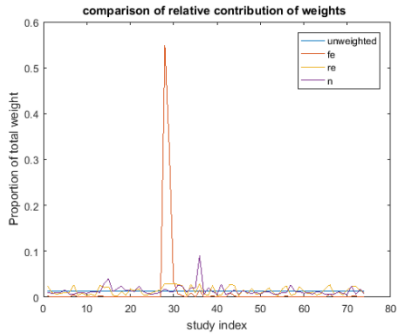

Effect size estimates ± 95% confidence intervals are compared between weighting schemes. If data was synthesized on logarithmic scale, effect size estimates are back-transformed and presented on raw scale.

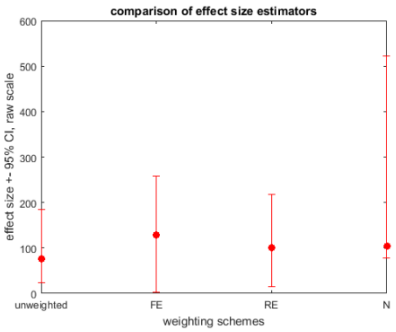

Comparison of τ^2 estimators

τ^2 estimates are computed using different estimators and compared with one another. τ^2 estimators are DL: DerSimonian-Laird, HS: Hunter-Schmidt, H: Hedges, HM: Hatung-Makambi, SJ: Sidik-Jonkman, PM: Paule-Mandel

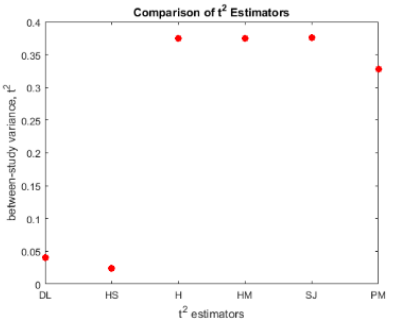

Baujat plot

Extent of influence each study has on heterogeneity (x-axis) and effect size (y-axis) are plotted and outlying studies can be identified in the upper right corner of the plot.

Studies that have significant influence on heterogeneity are plotted in red, as determined by Q-test.

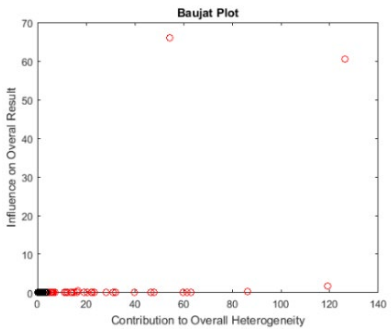

Sensitivity analyses

Single study exclusion plots reveal influential studies, as determined by shift in effect size and Q, H^2 and I^2 heterogeneity statistics after exclusion of single studies. Cumulative study exclusion plots are generated to visualize how effect size and Q, H^2 and I^2 heterogeneity statistics shift with cumulative exclusion of studies according to Q-reduction criteria. Homogeneity threshold T_H is indicated.

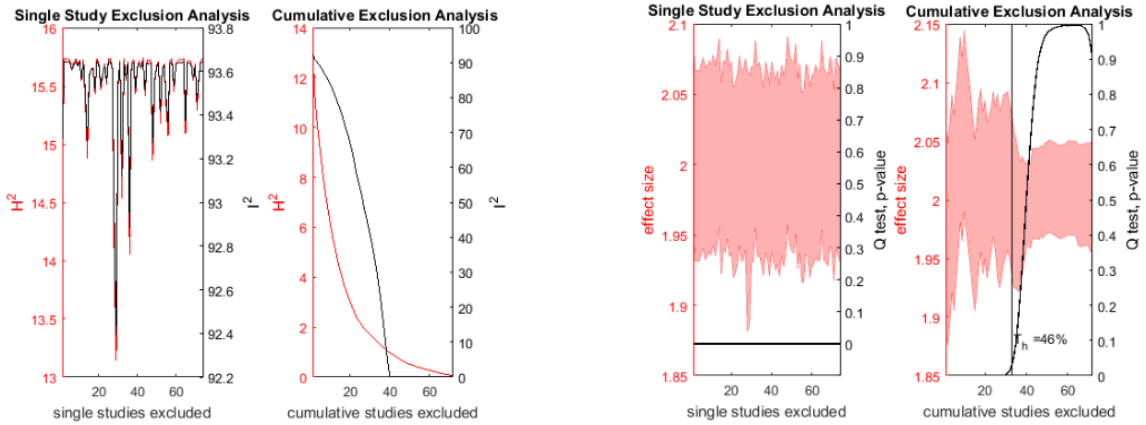

A1.2.5 Meta-Analysis Module

Overview: Synthesize meta-analytic data and conduct subgroup analysis if covariates present.

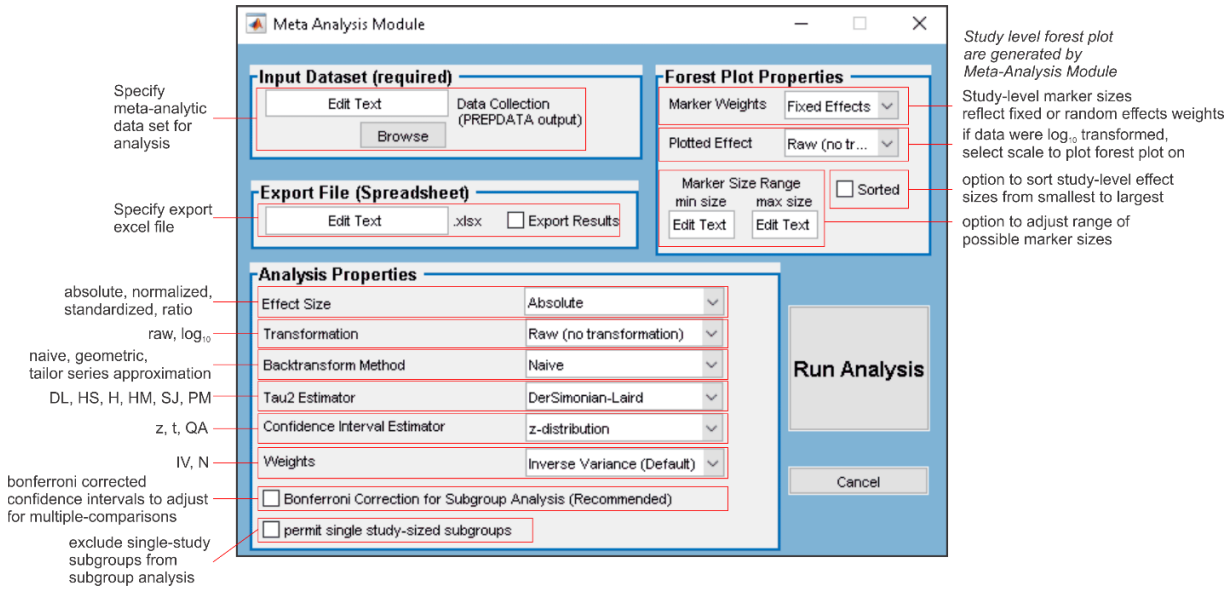

Figure A1-10. **Meta-analysis module user interface**. Tau2 estimator options are DL: DerSimonian-Laird, HS: Hunter-Schmidt, H: Hedges, HM: Hatung-Makambi, SJ: Sidik-Jonkman, PM: Paule-Mandel. Confidence interval estimator options are z: z-distribution, t: t-distribution or QA: quantile approximation method. Weighting options are IV: inverse variance weighting or N: sample size weighting. options are IVS: inverse standard error, SE: standard error and N: sample size.Weighting options are IV: inverse variance and N: sample size. Back-transformation methods are used when data are $\log_{10}$ transformed.

Usage

Input: Meta-analytic data set(s) that have been imported with Prepare Data Module can be directly loaded into the Meta-Analysis module. Several analysis options are provided along with analysis properties (**Fig A1-10**). Typical settings used in meta-analyses are set as default.

Subgroup Analyses: Meta-analysis Module will always proceed to conduct subgroup analysis if covariates are present in data set (see Prepare Data Module for details about including covariates in data set). That is, for a given data set, Meta-Analysis Module will estimate the overall effect size for the total data set (labelled 'totalSet' in output spreadsheet) along with subgroup estimates for each available covariate. This is the simplest form of subgroup analysis which can be extended to accommodate multiple levels of stratification using the stratification option in the Prepare Data Module. For example, if a data set is stratified by 'Species' covariate, the data is partitioned into

human, mouse and rat data subsets which are then saved in a single MATLAB data structure as three independent data sets. When this MATLAB structure loaded into the Meta-Analysis Module, the overall effect size will be estimated for each of the three independent data sets (i.e., human, mouse and rat subsets) along with subgroup estimates nested within these data subsets. Hence, the spreadsheet output will report subgroup estimates nested within each of the species-level data subsets, rather than for the total unpartitioned data set. Note that subgroup estimates are only saved in spreadsheet, and are not represented graphically by the Meta-Analysis Module. Only the 'totalSet' (i.e., overall effect size for given data set) is illustrated in the output study-level forest plot.

> *Tip 10*: While subgroup analysis is useful for identifying sources of heterogeneity, extensive data stratification can result in a diluted data pool, leading to subgroup under-representation and erroneous findings.

Output: Meta-analysis module will produce unweighted distributions (*left*) with specified data transformation and forest plot (*right*) representing study-level effect sizes along with global fixed (*blue band*) and random (*red band*) effects estimates. Y-axis labels correspond with study-level IDs. Example figures are provided as unmodified MetaLab outputs:

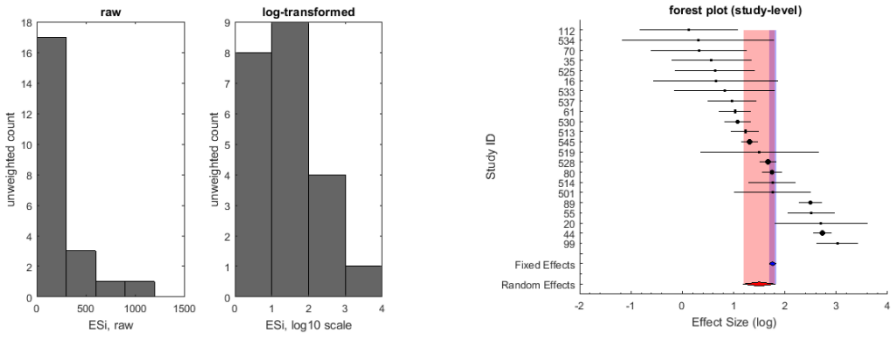

If export option was selected and export file name was specified, results along with input data will be exported to spreadsheet where more detailed statistics are provided, including heterogeneity statistics (I^2, H^2, Q), between-study variance estimate (t^2) and effect size estimates with error terms (**Fig A1-11**).

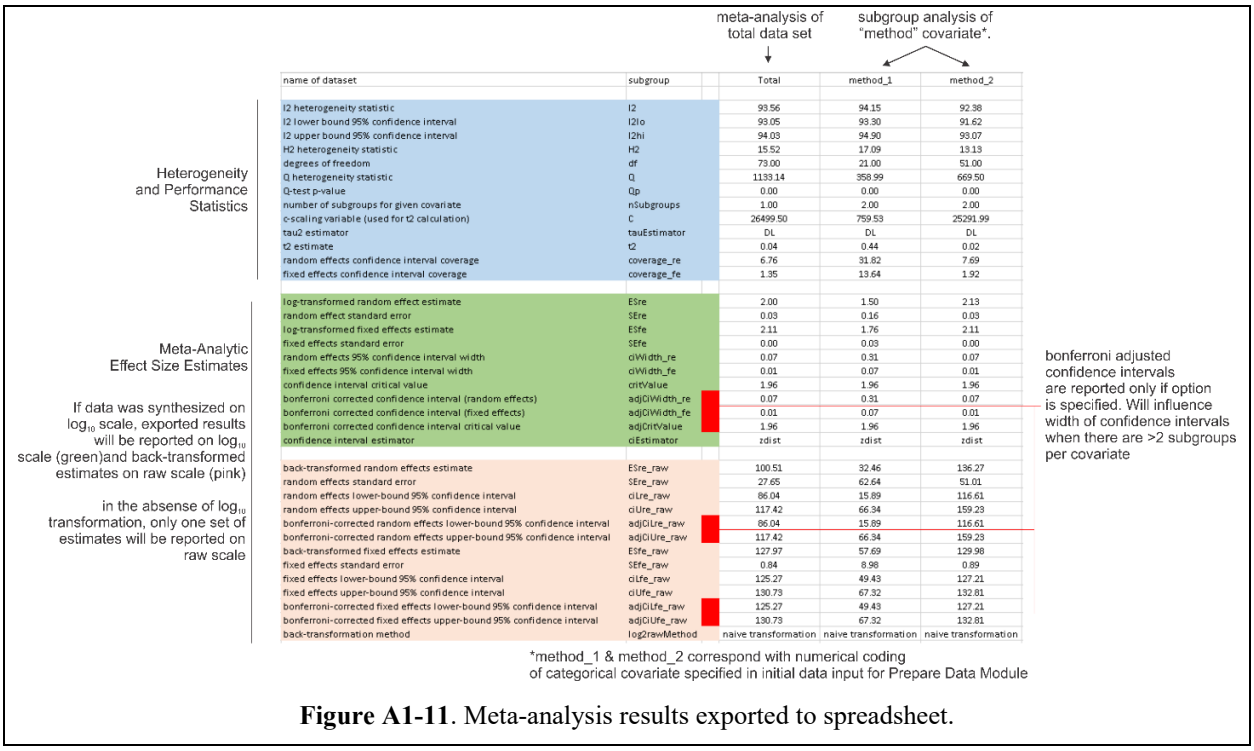

name of dataset	subgroup	Total	method_1	method_2
I2 heterogeneity statistic	I2	93.56	94.15	92.38
I2 lower bound 95% confidence interval	I2lo	93.05	93.30	91.62
I2 upper bound 95% confidence interval	I2hi	94.03	94.90	93.07
H2 heterogeneity statistic	H2	15.52	17.09	13.13
degrees of freedom	df	73.00	21.00	51.00
Q heterogeneity statistic	Q	1133.14	358.99	669.50
Q-test p-value	Qp	0.00	0.00	0.00
number of subgroups for given covariate	nSubgroups	1.00	2.00	2.00
c-scaling variable (used for t2 calculation)	C	26499.50	759.53	25291.99
tau2 estimator	tauEstimator	DL	DL	DL
t2 estimate	t2	0.04	0.44	0.02
random effects confidence interval coverage	coverage_re	6.76	31.82	7.69
fixed effects confidence interval coverage	coverage_fe	1.35	13.64	1.92
log-transformed random effect estimate	ESre	2.00	1.50	2.13
random effect standard error	SEre	0.03	0.16	0.03
log-transformed fixed effects estimate	ESfe	2.11	1.76	2.11
fixed effects standard error	SEfe	0.00	0.03	0.00
random effects 95% confidence interval width	ciWidth_re	0.07	0.31	0.07
fixed effects 95% confidence interval width	ciWidth_fe	0.01	0.07	0.01
confidence interval critical value	critValue	1.96	1.96	1.96
bonferroni corrected confidence interval (random effects)	adjCiWidth_re	0.07	0.31	0.07
bonferroni corrected confidence interval (fixed effects)	adjCiWidth_fe	0.01	0.07	0.01
bonferroni corrected confidence interval critical value	adjCritValue	1.96	1.96	1.96
confidence interval estimator	ciEstimator	zdist	zdist	zdist
back-transformed random effects estimate	ESre_raw	100.51	32.46	136.27
random effects standard error	SEre_raw	27.65	62.64	51.01
random effects lower-bound 95% confidence interval	ciLre_raw	86.04	15.89	116.61
random effects upper-bound 95% confidence interval	ciUre_raw	117.42	66.34	159.23
bonferroni-corrected random effects lower-bound 95% confidence interval	adjCiLre_raw	86.04	15.89	116.61
bonferroni-corrected random effects upper-bound 95% confidence interval	adjCiUre_raw	117.42	66.34	159.23
back-transformed fixed effects estimate	ESfe_raw	127.97	57.69	129.98
fixed effects standard error	SEfe_raw	0.84	8.98	0.89
fixed effects lower-bound 95% confidence interval	ciLfe_raw	125.27	49.43	127.21
fixed effects upper-bound 95% confidence interval	ciUfe_raw	130.73	67.32	132.81
bonferroni-corrected fixed effects lower-bound 95% confidence interval	adjCiLfe_raw	125.27	49.43	127.21
bonferroni-corrected fixed effects upper-bound 95% confidence interval	adjCiUfe_raw	130.73	67.32	132.81
back-transformation method	log2rawMethod	naive transformation	naive transformation	naive transformation

Figure A1-11. Meta-analysis results exported to spreadsheet.

A1.2.6 Meta-Regression Module

Overview: Conducts linear meta-regression analysis. Users can optionally validate between-study (meta)-regression results with intrastudy regression analysis, which conducts linear regression on within-study data sets.

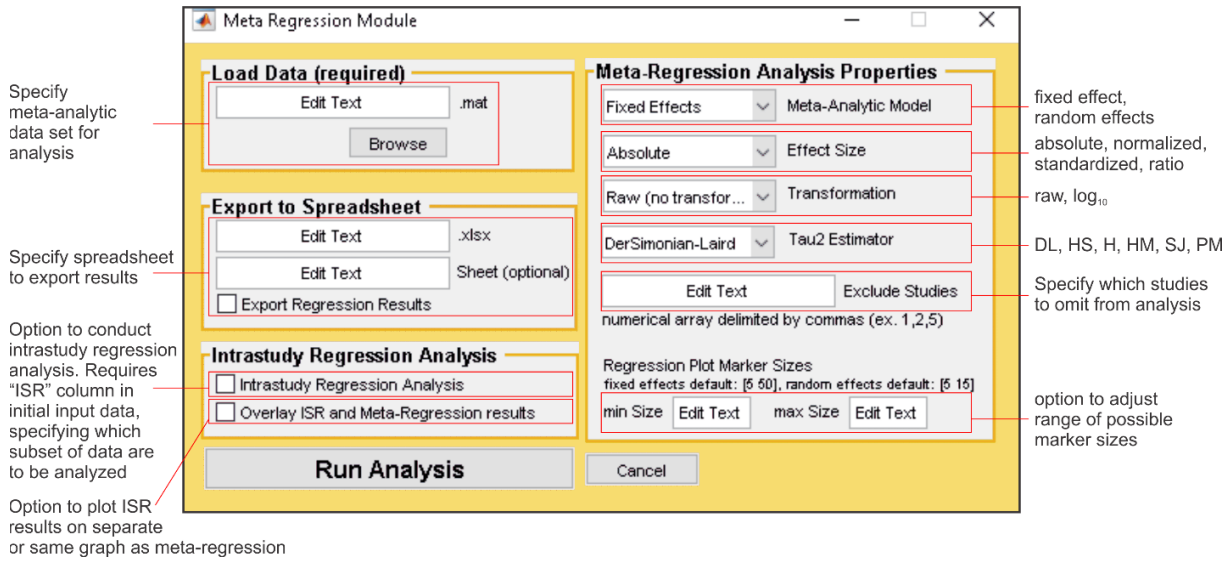

Figure A1-12. Meta-Regression module user interface. Tau2 estimator options are DL: DerSimonian-Laird, HS: Hunter-Schmidt, H: Hedges, HM: Hatung-Makambi, SJ: Sidik-Jonkman, PM: Paule-Mandel

Usage

Input: Meta-analytic data set(s) that have been imported with Prepare Data Module can be directly loaded into the meta-regression module (**Fig A1-12**). Continuous/categorical covariates must be included in dataset to conduct meta-regression analysis. If reviewers wish to perform intrastudy regression analysis (ISR) analysis, additional column titled "ISR" must be included when preparing data set from spreadsheet using Prepare Data Module. The ISR variable specifies which study-level data belong to the same data set such that within-study data sets that differ by level of exposure/predictor are designated by common values (see Prepare Data Module for details/example). Each study must have numerical value assigned in ISR column, those that do not have >2 observations will be automatically omitted from ISR analysis.

Meta-regression analysis: One meta-regression analysis has been started, MetaLab requires users to specify the outcome of interest along with predictor variables (**Fig A1-13**). The effect size of interest will be labeled "Study-level outcome". MetaLab will additionally present all available

covariates that were provided in the initial data input (See Prepare Data Module). Univariate and Multi-variate regression analyses are supported by MetaLab. Linear regression models are created using MATLAB's fitlm() function.

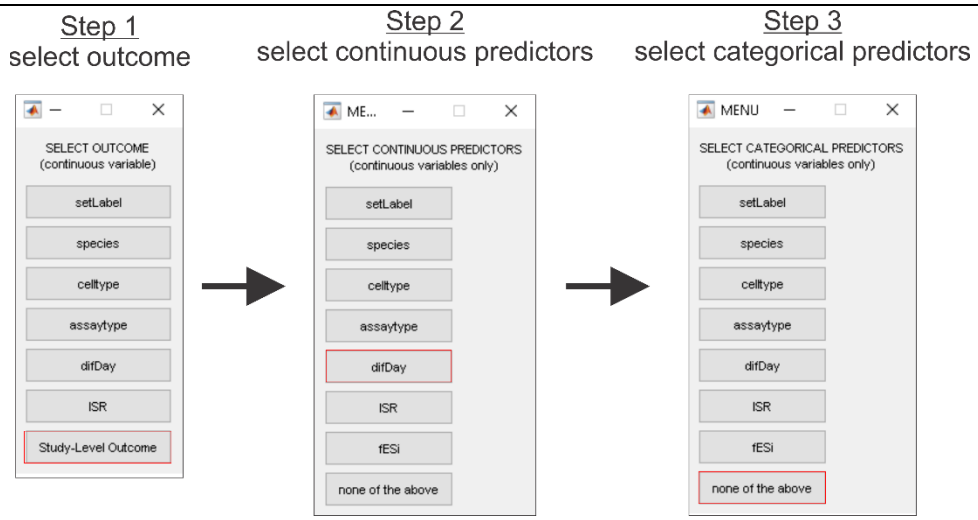

Figure A1-13. Specification of outcome and predictor variables for meta-regression analysis.

Output: Meta-regression module will produce regression diagnostic plots and meta-regression plots. Shown graphs are presented as unmodified MetaLab outputs:

Regression diagnostic plots

The regression diagnostic plot presents the distribution of regression residuals (histograms) and normal probability plots under the assumptions of a fixed (*blue*) and random effects (*red*) model. Moreover, observed outcomes are plotted in relation to model prediction, with the line of equality provided as a reference. Normally distributed residuals and agreement between observed and predicted values are indicative of a decent meta-regression model.

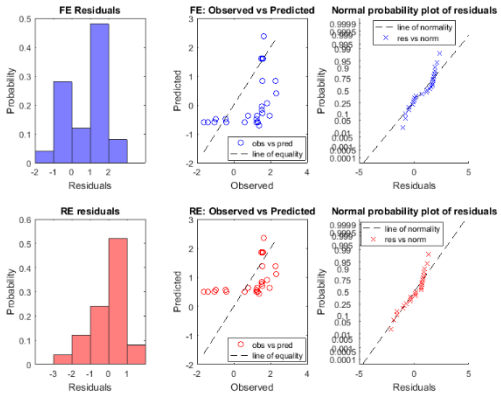

Linear meta-regression plot

The meta-regression plot shows study-level effect sizes (*black markers*), fitted meta-regression curve (*dashed black line*) with associated 95% confidence (dark red band) and prediction (*light red band*) intervals and 95% confidence interval for intercept-only model (*grey band*). Marker sizes are proportional to weights under the respective meta-analytic model (fixed or random effects). Optional ISR analyses are shown (overlaid as *red sold curves*). *difDay*: differentiation day, predictor variable. *fESi*: study-level effect sizes, outcome variable.

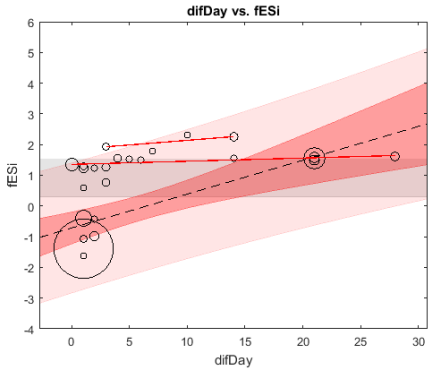

For multivariate meta-regression analyses, MetaLab will plot an adjusted response model for each given predictor variable. The fitted response is then a function of the predictor variable, with all other predictors averaged over the range of data used in the model. See MATLAB plotAdjustedResponse() function for more details.

If export option was selected and export file name was specified, meta-regression results will be exported to spreadsheet where more detailed statistics are provided (**Fig A1-14**). Model specifications are reported along with diagnostic statistics which include analysis of heterogeneity. Intercept only model statistics are shown for reference. Note that intercept-only model estimates may differ from those acquired in Meta-Analysis module due to exclusion of studies where predictor covariates are missing. If ISR analysis was conducted, slopes are compared with those acquired from meta-regression analysis. Validity of results are supported if ISR and meta-regression results are consistent (i.e. p-value > 0.05).

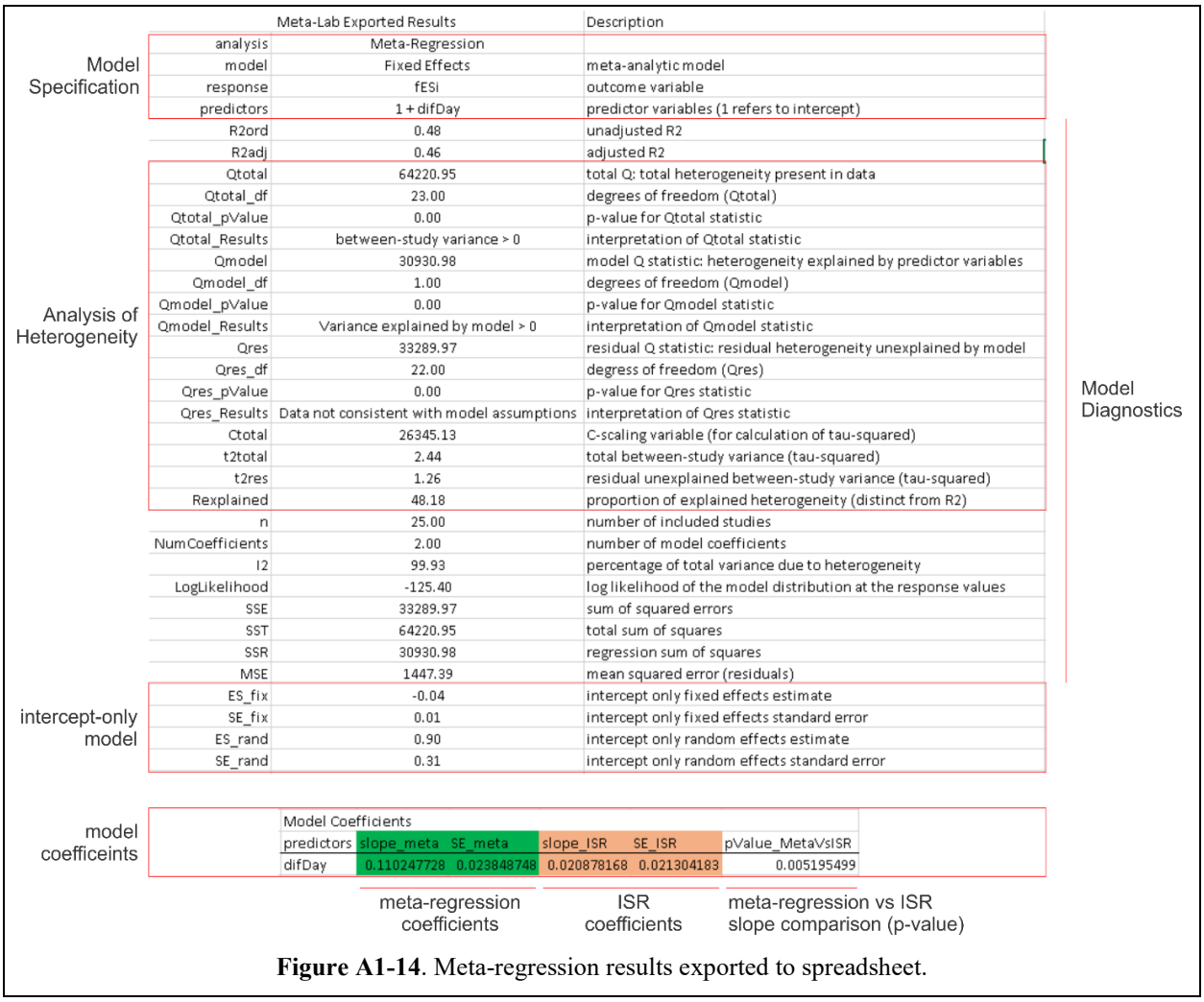

Figure A1-14. Meta-regression results exported to spreadsheet.

A2. Chapter 4 Supplemental Figures and Tables

Supplemental figures and tables referenced in **Chapter 4** are provided here.

A2.1 Supplemental figures

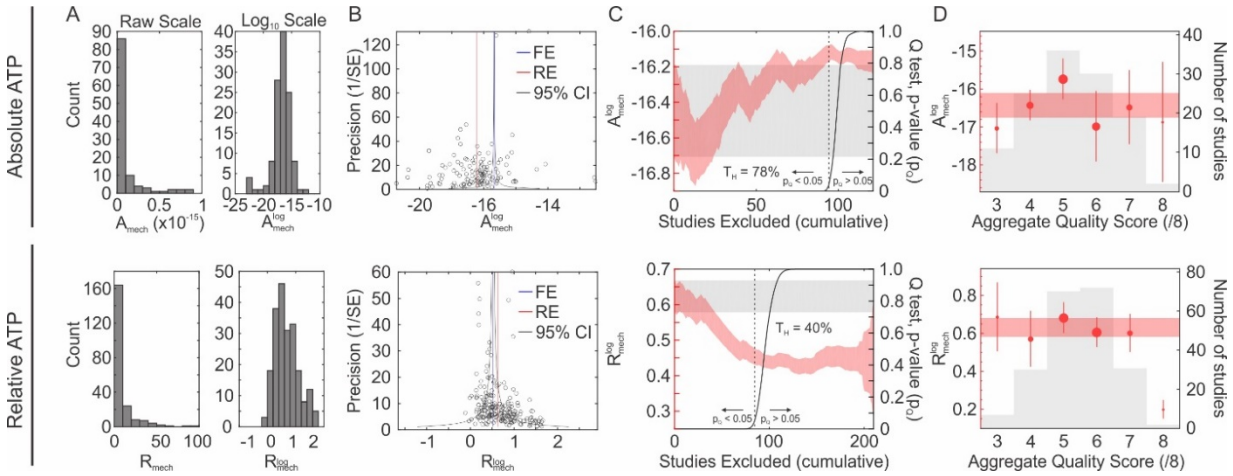

Fig 4-S1. The distribution, bias, extent of heterogeneity and effect of study quality was evaluated for mechanically-stimulated ATP release (A_{mech}, *top row*) and relative ATP release above baseline (R_{mech}, *bottom row*) (A) Study-level outcome distributions on raw scale (*left*) and logarithmic (base 10) scale (*right*). **(B)** Funnel plots for log-transformed study-level effect sizes. *Black markers*: study-level data. *Blue lines*: fixed effect (FE) estimate. *Red lines*: random effects (RE) estimate. *Black lines*: theoretical 95% CI for FE estimate in absence of bias. **(C)** Effect of cumulative study exclusion on RE estimates and heterogeneity of log-transformed effect sizes. *Red band*: 95% CI for studies remaining after exclusion of the most heterogenous. *Grey band*: Overall 95% CI. *Black curve*: p-value p_Q for Q-test. *Dashed black line*: homogeneity threshold T_H. **(D)** Influence of aggregate study quality score on ATP release estimates. *Red band*: 95% CI for overall estimate, *red markers*: score-specific estimate ± 95% CI, *grey bars*: number of studies that received indicated aggregate quality score (also reflected in marker sizes).

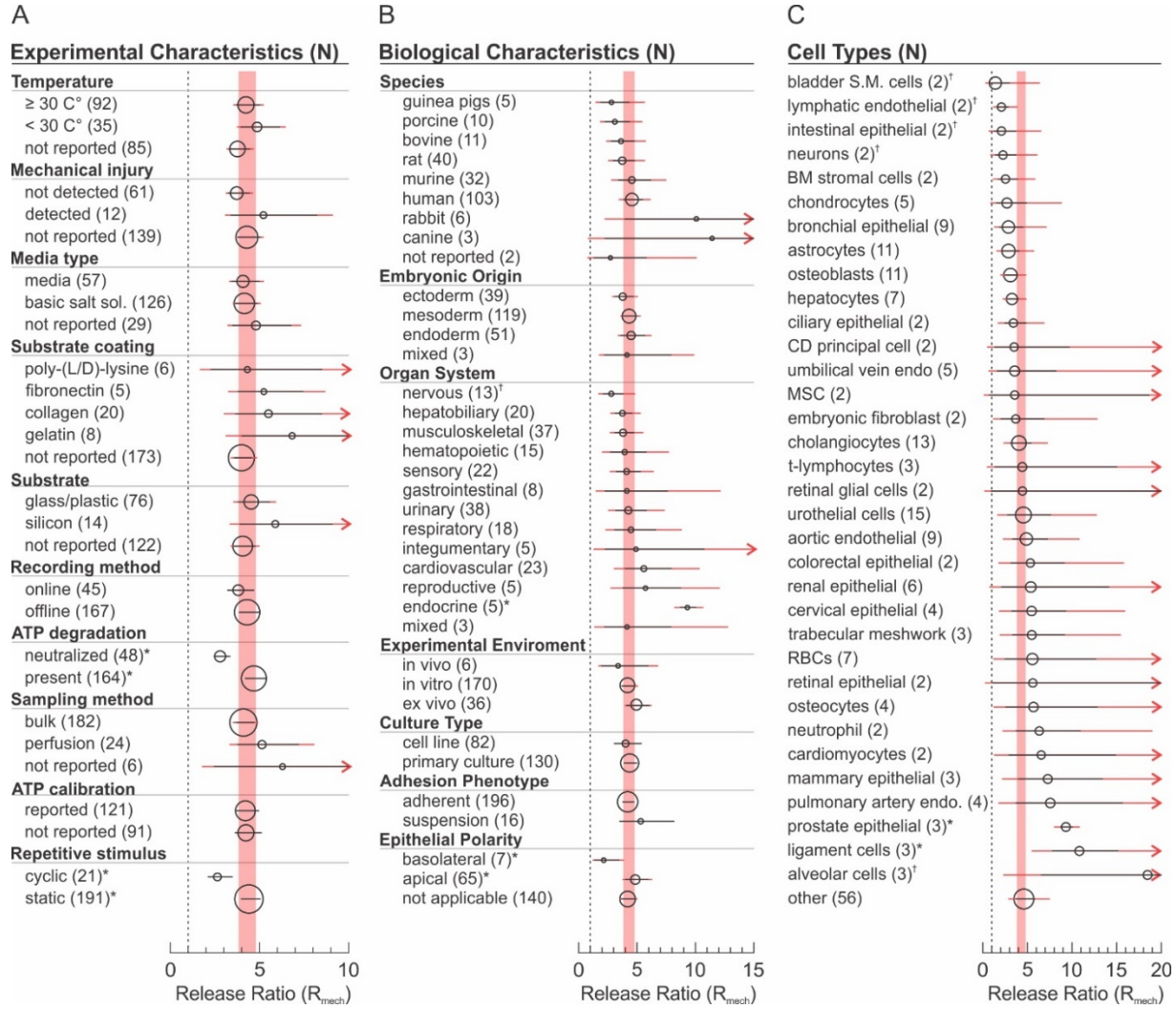

Fig 4-S2. Influence of experimental and biological factors on the amount of ATP released following mechanical stimulation. Shown are estimates of relative ATP release above baseline following mechanical stimulation for different subgroups based on **(A)** experimental characteristics, **(B)** biological characteristics and **(C)** cell-types. *Round markers*: Subgroup-level estimates, markers sizes are proportional to number of datasets N in each subgroup (shown in parentheses), *Horizontal black lines*: ± 95% CI, *Horizontal red lines*: ± Bonferroni-adjusted 95% CI, *Red bands*: overall estimate ± 95% CI. † and * indicate significant differences ($p<0.05$) compared to overall estimate or to other subgroup (in case of two subgroups) before and after Bonferroni adjustment, respectively. Detailed statistics are in **Table 4-S2**.

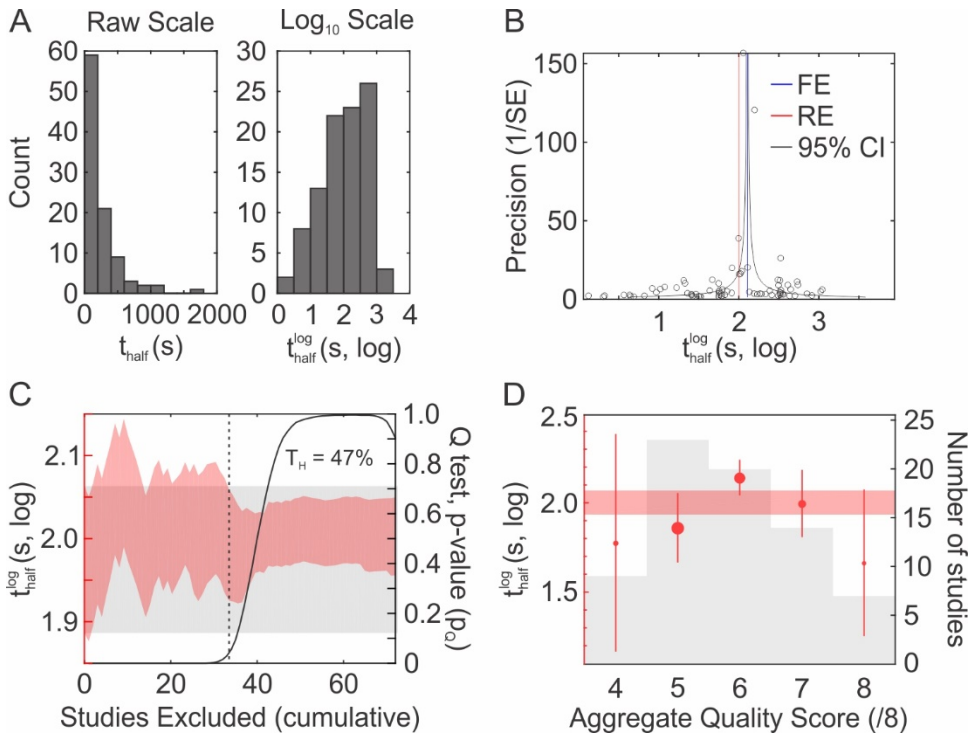

Fig 4-S3. The distribution, bias, extent of heterogeneity and effect of study quality was evaluated for kinetic estimates of ATP release (t_{half}) (A) Study-level effect size distributions on raw scale (*left*) and logarithmic (base 10) scale (*right*). **(B)** Funnel plots for log-transformed study-level estimates. *Black markers*: study-level data. *Blue lines*: fixed effect (FE) estimate. *Red lines*: random effects (RE) estimate. *Black lines*: theoretical 95% CI for FE estimate in absence of bias. **(C)** Effect of cumulative study exclusion on RE estimates and heterogeneity of log-transformed effect sizes. *Red band*: 95% CI for studies remaining after exclusion of most heterogenous. *Grey band*: Overall 95% CI. *Black curve*: p-value p_Q for Q-test. Dashed black line: homogeneity threshold T_H. **(D)** Influence of aggregate study quality score on ATP release kinetic estimates. *Red band*: 95% CI for overall estimate, *red markers*: score-specific estimate ± 95% CI, *grey bars*: number of studies that received indicated aggregate quality score (also reflected in marker sizes).

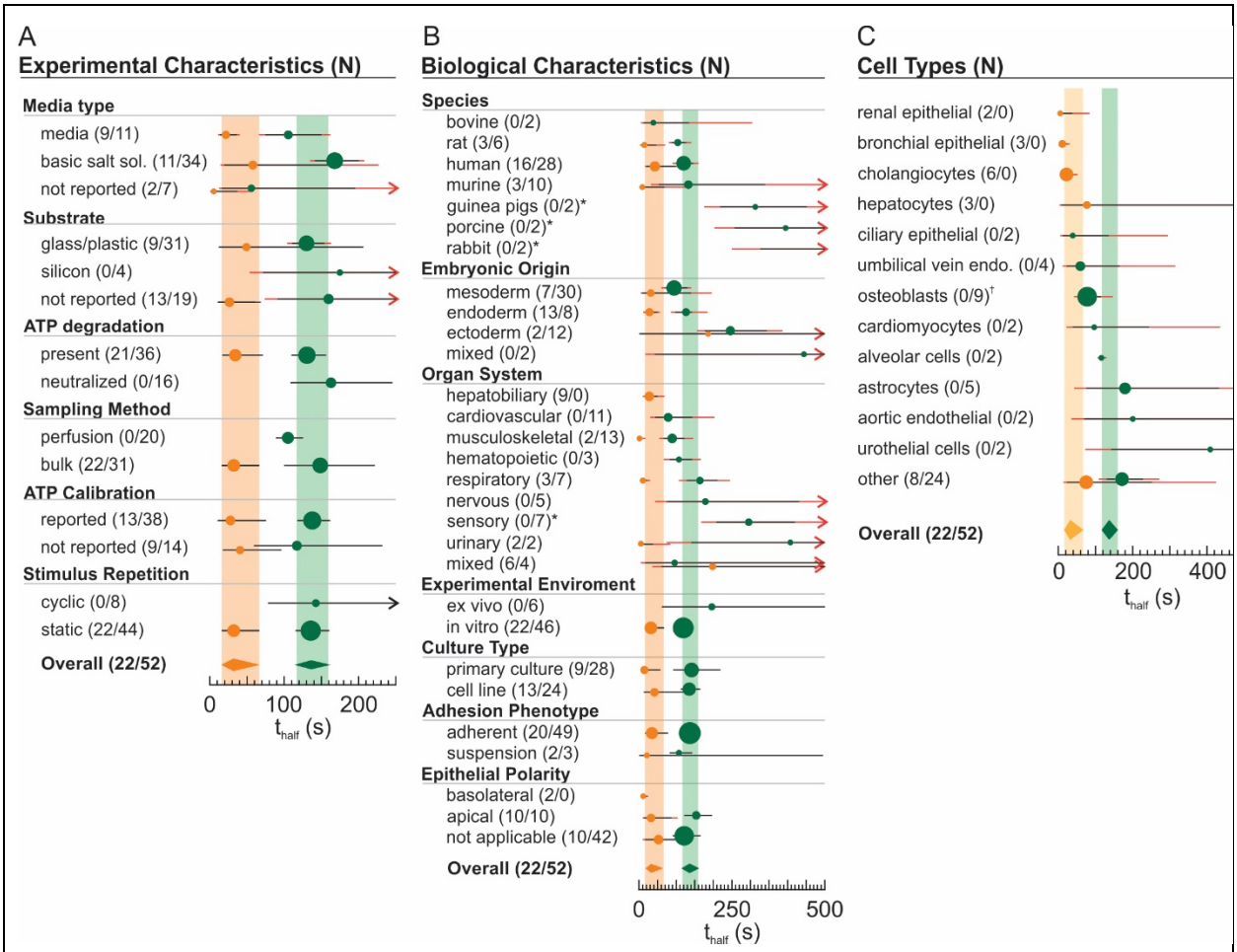

Fig 4-S4. Influence of experimental and biological factors on kinetics of mechanically-stimulated ATP release. (A-E) ATP release kinetic estimates were stratified by online (*orange*) and offline (*green*) recording methods and subgroup analysis was conducted to evaluated influence of experimental **(A)** and biological **(B)** characteristics as well as differences between cell-types **(C)**. *Round markers*: Subgroup-level estimates, *Horizontal black lines*: ± 95% CI, *Horizontal red lines*: ± Bonferroni-adjusted 95% CI, *Bands/diamonds*: overall estimate ± 95% CI. Markers are proportional to number of studies N in each subgroup (shown in parentheses). † and * indicate significant differences (at least 5% level) compared to overall estimate before and after Bonferroni adjustment, respectively. Detailed statistics are in **Table 4-S4**.

A2.2 Supplemental tables

Table 4-S1. Absolute estimates of ATP released from mechanically-stimulated mammalian cells (A_{mech}), intracellular ATP (A_{cell}), and basal extracellular ATP (A_{base}). Shown are meta-analytic outcomes and corresponding heterogeneity statistics I^2, H^2 and Q. CI: Confidence intervals, N: Number of datasets, P_Q: p-value corresponding to Q heterogeneity statistic used to evaluate null hypothesis that all studies reported same effect, Nucleated: Nucleated mammalian cells, RBC: Red blood cells.

	Meta-Analysis Summary Statistics					
	ATP released (± 95% CI), units	N	I^2 (%)	H^2	Q	P_Q
A_{mech}	38.5 (18.2, 81.8) amol cell^{-1}	123	99.9	1695.4	206843.1	<0.001
A_{cell}						
Nucleated	5.0 (2.6, 9.5) fmol cell^{-1}	4	89.2	9.2	27.7	<0.001
RBC	0.14 (0.12, 0.18) fmol cell^{-1}	4	0	0.5	1.6	0.66
A_{base}	8.1 (3.9, 16.6) amol cell^{-1}	84	99.8	657.9	54601.8	<0.001

Table 4-S2. Subgroup analysis of the effects of experimental and biological factors on amount of ATP released following mechanical stimulation. Relative ATP release data were stratified by experimental or biological characteristics, or cell type, and amount of ATP released and heterogeneity was compared between subgroups. R_{mech}: relative ATP release compared to baseline, CI: confidence intervals, P_Q: p-value corresponding to Q heterogeneity statistic used to evaluate null hypothesis that all studies reported same effect, N: number of datasets per group.

	Meta-Analysis Summary Statistics					
Covariates	R_{mech} (±95% CI)	N	I^2 (%)	H^2	Q	P_Q
Influence of experimental characteristics on amount of ATP release						
Temperature						
≥ 30 °C	4.3 (3.7, 5.0)	92	94.4	17.9	1628.6	<0.001
< 30 °C	4.9 (3.9, 6.2)	35	92.4	13.1	444.5	<0.001
Not reported	3.8 (3.3, 4.5)	85	82.5	5.7	479.4	<0.001
Media Type						
Basal/complex media	4.1 (3.4, 5.0)	57	84.5	6.4	361.1	<0.001
Basic salt solution	4.2 (3.6, 4.9)	126	95.6	23.0	2873.2	<0.001
Not reported	4.9 (3.5, 6.8)	29	91.3	11.5	321.9	<0.001
Substrate coating						
Poly-(L/D)-lysine	4.4 (2.3, 8.5)	6	69.1	3.2	16.2	<0.01
Gelatin	6.9 (4.0, 11.9)	8	92.2	12.9	92.2	<0.001
Fibronectin	5.3 (3.8, 7.5)	5	36.6	1.6	6.3	0.18
Collagen	5.6 (3.6, 8.5)	20	89.4	9.4	178.8	<0.001
Not reported	4.0 (3.6, 4.6)	173	94.4	17.8	3055.7	<0.001
Substrate						
Silicon	5.9 (3.9, 9.1)	14	71.6	3.5	45.9	<0.001
Glass/plastic	4.6 (3.8, 5.6)	76	94.3	17.7	1325.8	<0.001
Not reported	4.1 (3.5, 4.8)	121	94.3	17.6	2039.5	<0.001
Repetitive Stimulation						
Cyclic	2.7 (2.1, 3.5)	21	77.3	4.4	88.2	<0.001
Static	4.5 (4.0, 5.0)	191	94.6	18.5	3513.6	<0.001
Mechanical injury						
Detected	5.3 (3.4, 8.2)	12	65.8	2.9	32.2	<0.01
Not detected	3.8 (3.2, 4.4)	61	86.0	7.1	428.0	<0.001
Not reported	4.4 (3.8, 5.0)	139	95.5	22.3	3074.9	<0.001
ATP calibration						
Reported	4.3 (3.7, 5.0)	121	94.3	17.5	2096.5	<0.001
Not reported	4.3 (3.6, 5.1)	91	93.5	15.3	1381.1	<0.001
ATP degradation						
Present	4.7 (4.2, 5.4)	164	92.5	13.3	2161.3	<0.001
Neutralized	2.9 (2.4, 3.3)	48	90.0	10.0	468.4	<0.001
Sampling Method						
Perfusion	5.2 (3.7, 7.2)	24	94.8	19.1	438.7	<0.001

Bulk	4.2 (3.7, 4.7)	182	93.8	16.0	2903.7	<0.001
Not reported	6.4 (2.4, 16.60	5	90.7	10.7	43.0	<0.001
Recording Method						
Offline	4.4 (3.8, 5.0)	167	94.9	19.8	3280.5	<0.001
Online	3.9 (3.2, 4.7)	45	84.3	6.4	280.9	<0.001
Overall	4.3 (3.8, 4.8)	212	94.2	17.4	3667.3	<0.001

Covariates	R_{mech} (±95% CI)	N	I^2 (%)	H^2	Q	P_Q
Influence of biological characteristics on amount of ATP release						
Organ System						
Nervous	2.8 (2.1, 3.8)	13	85.7	7.0	84.0	<0.001
Gastrointestinal	4.1 (2.2, 7.7)	8	98.7	78.6	549.9	<0.001
Sensory	4.1 (3.2, 5.3)	22	74.1	3.9	81.1	<0.001
Musculoskeletal	3.8 (3.1, 4.70	37	86.4	7.3	264.1	<0.001
Hematopoietic	4.0 (2.7, 5.8)	15	93.4	14.1	211.6	<0.001
Respiratory	4.5 (3.1, 6.6)	18	90.8	10.8	183.9	<0.001
Integumentary	4.9 (2.3, 10.8)	5	77.7	4.5	17.9	<0.01
Hepatobiliary	3.8 (3.1, 4.6)	20	59.0	2.4	46.4	<0.001
Urinary	4.3 (3.1, 5.8)	38	92.4	13.1	484.8	<0.001
Reproductive	5.7 (3.8, 8.8)	5	55.0	2.2	8.9	0.06
Cardiovascular	5.6 (3.9, 8.0)	23	92.6	13.4	295.5	<0.001
Endocrine	9.3 (8.7, 10.1)	5	0	0	0.1	1.00
Mixed	4.2 (2.2, 8.0)	3	47.4	1.9	3.8	0.15
Species						
Porcine	3.1 (2.2, 4.4)	10	81.6	5.4	49.0	<0.001
Guinea pig	2.8 (1.9, 4.3)	5	93.7	16.0	63.9	<0.001
Rat	3.8 (2.9, 4.80)	40	94.2	17.2	672.3	<0.001
Bovine	3.6 (2.8, 4.8)	11	67.8	3.1	31.0	<0.01
Murine	4.6 (3.4, 6.2)	32	90.4	10.4	323.5	<0.001
Human	4.6 (3.8, 5.5)	103	95.3	21.4	2178.5	<0.001
Rabbit	10.1 (3.9, 25.9)	6	82.0	5.6	27.8	<0.001
Canine	11.4 (2.2, 59.0)	3	77.7	4.5	9.0	0.01
Not reported	2.7 (1.3, 5.80)	2	0	0.1	0.1	0.81
Embryonic Origin						
Ectoderm	3.8 (3.1, 4.7)	39	85.0	6.7	253.2	<0.001
Mesoderm	4.3 (3.7, 5.0)	119	93.1	14.5	1714.7	<0.001
Endoderm	4.5 (3.6, 5.7)	51	96.1	25.4	1269.8	<0.001
Mixed	4.2 (2.2, 8.0)	3	47.4	1.9	3.8	0.15
Epithelial Polarity						
Basolateral	2.2 (1.3, 3.5)	7	89.1	9.2	55.1	<0.001
Apical	4.9 (4.0, 6.0)	65	94.0	16.6	1063.5	<0.001
Not applicable	4.2 (3.6, 4.9)	140	94.4	18.0	2501.8	<0.001

Adhesion Phenotype						
Adherent	4.2 (3.7, 4.7)	196	93.9	16.4	3198.8	<0.001
Suspension	5.3 (3.5, 8.2)	16	93.9	16.4	246.3	<0.001
Experimental Envirom,						
In vivo	3.4 (1.9, 6.0)	6	58.6	2.4	12.1	0.03
Ex vivo	4.0 (3.0, 5.4)	36	95.9	24.2	848.2	<0.001
In vitro	4.4 (3.9, 5.0)	170	94.0	16.6	2803.5	<0.001
Culture Type						
Primary culture	3.9 (3.4, 4.4)	130	92.6	13.4	1734.9	<0.001
Cell line	5.0 (4.1, 6.1)	82	95.2	20.6	1672.3	<0.001
Overall	4.3 (3.8, 4.8)	212	94.2	17.4	3667.3	<0.001

Covariates	R_{mech} (±95% CI)	N	I^2 (%)	H^2	Q	P_Q
Mechanically-stimulated ATP release by cell type						
Cell types						
Bladder smooth muscle	1.4 (0.7, 3.0)	2	0	0.3	0.3	0.57
Intestinal epithelial	2.1 (1.2, 3.7)	2	97.7	43.8	43.8	<0.001
Lymphatic endothelial	2.1 (1.5, 2.9)	2	0	0	0	0.83
Neurons	2.3 (1.4, 3.7)	2	0	0	0	0.83
Chondrocytes	2.7 (1.5, 4.9)	5	87.6	8.1	32.4	<0.001
Bone marrow stromal	2.6 (1.7, 3.9)	2	59.3	2.5	2.5	0.12
Astrocytes	2.9 (2.1, 4.1)	11	88.1	8.4	83.8	<0.001
Ciliary epithelial	3.5 (2.4, 4.9)	2	0	0.2	0.2	0.65
Mesenchymal stem	3.6 (0.7, 18.7)	2	91.9	12.3	12.3	<0.001
Umbilical vein endo.	3.6 (1.6, 8.2)	5	83.5	6.1	24.3	<0.001
Bronchial epithelial	2.9 (1.8, 4.5)	9	81.3	5.4	42.9	<0.001
Collecting duct princ.	3.5 (1.3, 9.7)	2	50.7	2.0	2.0	0.15
Embryonic fibroblast	3.7 (2.0, 6.9)	2	55.6	2.3	2.3	0.13
Osteoblasts	3.1 (2.5, 3.9)	11	73.1	3.7	37.2	<0.001
Hepatocytes	3.3 (2.7, 4.0)	7	4.4	1.0	6.3	0.39
t-lymphocytes	4.5 (1.3, 15.1)	3	98.0	49.1	98.3	<0.001
Retinal glial cells	4.5 (0.9, 22.1)	2	87.7	8.1	8.1	<0.001
Colorectal epithelial	5.4 (3.1, 9.2)	2	0	0	0	0.90
Cervical epithelial	5.5 (3.2, 9.4)	4	65.6	2.9	8.7	0.03
Neutrophil	6.4 (3.7, 11.0)	2	25.1	1.3	1.3	0.25
Retinal epithelial	5.6 (1.1, 29.1)	2	90.0	10.0	10.0	<0.001
Cholangiocytes	4.1 (3.1, 5.4)	13	69.3	3.3	39.1	<0.001
Urothelial cells	4.6 (2.7, 7.7)	15	80.5	5.1	71.9	<0.001
Mammary epithelial	7.3 (4.0, 13.5)	3	28.5	1.4	2.8	0.25
Renal epithelial	5.4 (2.1, 14.2)	6	89.2	9.3	46.3	<0.001
Aortic endothelial	4.9 (3.3, 7.3)	9	75.0	4.0	32.1	<0.001
Trabecular meshwork	5.5 (3.3, 9.2)	3	51.5	2.1	4.1	0.13

Pulmon. artery endo.	7.6 (3.7, 15.7)	4	97.2	35.8	107.5	<0.001
Cardiomyocytes	6.6 (2.9, 14.9)	2	0	0.5	0.5	0.47
Erythrocytes	5.6 (2.5, 12.7)	7	76.5	4.3	25.5	<0.001
Osteocytes	5.7 (2.5, 12.9)	4	73.6	3.8	11.3	0.01
Prostate epithelial	9.3 (8.7, 10.1)	3	0	0	0	0.98
Ligament cells	10.9 (7.8, 15.2)	3	0	0.5	1.1	0.58
Alveolar type II cells	18.5 (6.5, 52.5)	3	79.4	4.9	9.7	0.01
Other	4.6 (3.7, 5.8)	56	94.7	18.8	1032.4	<0.001
Overall	4.3 (3.8. 4.8)	212	94.2	17.4	3667.3	<0.001

Table 4-S3. Relationship between magnitude of mechanical stimulus and amount of ATP release evaluated by subgroup and meta-regression analyses. *For subgroup analysis*, Relative ATP release data were stratified by type of mechanical stimulus and amount of ATP released and heterogeneity was compared between subgroups. R_{mech}: relative ATP release compared to baseline. P_Q: p-value corresponding to Q heterogeneity statistic used to evaluate null hypothesis that all studies reported same effect. *For meta-regression*, strength of relationship (regression slope, β) was investigated between the magnitude of mechanical stimulus and the amount of relative ATP released on logarithmic scale. Magnitude of stimuli were % stretch for strain, cmH_2O for compression, absolute change in mOsm/L for hypotonic and hypertonic pressures, $dyne/cm^2$ for fluid shear stress (FSS) and μm^{-1} for RBC deformation. Regression slopes were compared between relationships observed within-studies (β_{intra}) and between-studies (β_{inter}). SE(β): standard error of β, P_β: Z-test derived p-value for comparison of β_{inter} and β_{intra}. N: Number of datasets per group.

Covariates	Subgroup-Analysis Summary Statistics					
	R_{mech} (±95% CI)	N	I^2 (%)	H^2	Q	P_Q
Mechanical Stimulus						
Membrane deform.	1.8 (1.1, 2.7)	2	34.5	1.5	1.5	0.22
Strain	3.0 (2.2, 4.1)	22	80.2	5.0	106.0	<0.001
Compression	3.4 (2.1, 5.5)	16	92.7	13.8	206.5	<0.001
Osmotic pressure	4.2 (3.6, 5.0)	98	94.3	17.4	1690.0	<0.001
Fluid shear stress	4.7 (3.8, 5.9)	47	94.2	17.4	799.4	<0.001
Tissue distension	6.9 (5.0, 9.4)	16	83.8	6.2	92.9	<0.001
Injury	7.0 (4.4, 11.0)	4	9.3	1.1	3.3	0.35
RBC deformation	13.0 (2.0, 82.1)	3	81.9	5.5	11.0	<0.01
other	3.1 (1.4, 6.8)	4	90.8	10.9	32.7	<0.001
Overall	4.3 (3.8, 4.8)	212	94.2	17.4	3667.3	<0.001

Covariates	Meta-Regression Summary Statistics					
	β (±95% CI)	SE(β)	P_β	N	I^2 (%)	H^2
Hypotonic (osmotic)						
β_{inter}	0.0042 (0.0031, 0.0053) *	0.0006	0.37	137	82.8	5.9
β_{intra}	0.0035 (0.0024, 0.0046) *	0.0006		17	89.0	9.1
Hypertonic (osmotic)						
β_{inter}	-0.0002 (-0.0028, 0.0025)	0.0014	0.16	11	96.6	32.3
β_{intra}	0.0018 (0.0011, 0.0026) *	0.0004		1	-	-
FSS						
β_{inter}	0.0037 (-0.0106, 0.0074)	0.0073	0.17	46	92.2	13.1
β_{intra}	0.0151 (0.0074, 0.0228) *	0.0039		6	30.9	1.5
Strain						
β_{inter}	-00044 (-0.0121, 0.0033)	0.0039	<0.001	35	75.2	4.2
β_{intra}	0.0526 (0.0339, 0.0713) *	0.0096		3	0	0.1
Compression						

β_{inter}	0.0026 (0.0010, 0.0042) *	0.0008	<0.01	72	89.4	9.6
β_{intra}	0.0094 (0.0057, 0.0133) *	0.0095		10	97.4	38.0
RBC deformation						
β_{inter}	2.08 (-3.70, 7.87)	2.95	0.41	8	61.3	3.1
β_{intra}	4.61 (3.22, 6.00) *	0.71		2	0	0.1

*magnitude of relationship is significant at 95% confidence level.

Table 4-S4. Subgroup analysis of the effects of experimental and biological factors on ATP release kinetics. ATP release kinetics data were stratified by experimental or biological characteristics, cell type, or mechanical stimulus, and kinetics of ATP release and heterogeneity were compared between subgroups. t_{half}: Time to half max release, CI: confidence intervals, P_Q: p-value corresponding to Q heterogeneity statistic used to evaluate null hypothesis that all studies reported same effect, N: number of datasets per group.

Covariates	t_{half}, sec (±95% CI)	N	I^2 (%)	H^2	Q	P_Q
Influence of recording method on kinetic estimates						
Recording Method						
offline	136.3 (116.6, 159.2)	52	92.4	13.1	669.5	<0.001
online	32.5 (15.9, 66.3)	22	94.2	17.1	359.0	<0.001
Overall	100.5 (86.0, 117.4)	74	93.6	15.5	1133.1	<0.001

Covariates	t_{half}, sec (±95% CI)	N	I^2 (%)	H^2	Q	P_Q
Influence of experimental characteristics on kinetic estimates (analysis of offline subgroup)						
Media Type						
Basal/complex	105.8 (74.5, 150.2)	11	57.2	2.3	23.4	<0.01
Basic salt sol.	168.2 (141.0, 200.6)	34	94.0	16.7	551.6	<0.001
Not reported	56.2 (16.1, 195.6)	7	84.3	6.4	38.1	<0.001
Substrate						
silicon	175.1 (71.2, 430.8)	4	75.1	4.0	12.1	<0.01
glass/plastic	130.3 (110.3, 154.0)	31	90.9	11.1	331.5	<0.001
Not reported	160.0 (90.5, 282.8)	17	91.9	12.3	172.9	<0.001
ATP Calibration						
reported	138.0 (115.9, 164.3)	38	93.3	15.0	359.9	<0.001
Not reported	117.3 (59.3, 232.1)	14	94.2	17.3	224.7	<0.001
ATP degradation						
present	130.9 (109.7, 156.2)	36	94.5	18.1	633.6	<0.001
neutralized	163.2 (108.5, 245.6)	16	58.2	2.39	35.9	<0.01
Sampling Method						
perfusion	105.3 (88.6, 125.2)	20	93.8	16.23	308.39	<0.001
bulk	148.8 (99.8, 221.9)	31	87.8	8.2	245.96	<0.001
Stimulus Repetition						
cyclic	142.8 (78.3, 260.6)	8	65.6	2.91	20.4	<0.01
static	135.9 (115.1, 160.6)	44	93.4	15.1	648.5	<0.001
Offline Total	136.3 (116.6, 159.2)	52	92.4	13.1	669.5	<0.001

Covariates	t_{half}, sec (±95% CI)	N	I^2 (%)	H^2	Q	P_Q
Influence of experimental characteristics on kinetic estimates (analysis of online subgroup)						
Media Type						
Basal/complex	21.9 (13.3, 36.1)	9	73.0	3.7	29.6	<0.001

Basic salt sol.	58.3 (19.0, 178.4)	11	94.8	19.1	191.2	<0.001
Not reported	5.7 (0.9, 37.2)	2	0	0.3	0.3	0.57
Substrate						
glass/plastic	49.6 (11.9, 206.4)	9	95.3	21.1	168.4	<0.001
Not reported	26.7 (11.7, 61.0)	13	92.8	13.9	166.3	<0.001
ATP Calibration						
reported	28.1 (10.5, 75.5)	13	95.7	23.3	280.1	<0.001
Not reported	40.9 (17.4, 96.3)	9	80.8	5.2	41.7	<0.001
ATP degradation						
present	34.5 (16.7, 71.3)	21	94.4	17.8	355.8	<0.001
Sampling Method						
bulk	32.5 (15.9, 66.3)	22	94.2	17.1	359.0	<0.001
Stimulus Repetition						
static	32.5 (15.9, 66.3)	22	94.2	17.1	359.0	<0.001
Online Total	32.5 (15.9, 66.3)	22	94.2	17.1	359.0	<0.001

Covariates	t_{half}, sec (±95% CI)	N	I^2 (%)	H^2	Q	P_Q
Influence of biological characteristics on kinetic estimates (analysis of offline subgroup)						
Species						
Bovine	39.2 (11.4, 134.8)	2	0	0.3	0.3	0.60
Rat	104.8 (87.4, 125.7)	6	0	0.4	1.9	0.87
Human	120.6 (99.7, 145.8)	28	93.7	15.9	428.6	<0.001
Murine	133.3 (52.3, 340.1)	10	93.9	16.4	147.3	<0.001
Guinea pigs	313.7 (217.6, 452.2)	2	0	0	0	0.99
Porcine	395.1 (257.3, 606.9)	2	0	0.2	0.2	0.68
Rabbit	529.9 (325.7, 862.1)	2	0	0.6	0.6	0.43
Embryonic Origin						
Mesoderm	95.0 (70.1, 128.7)	30	76.6	4.3	123.8	<0.001
Endoderm	127.0 (97.1, 166.1)	8	97.4	37.9	265.0	<0.001
Ectoderm	246.5 (176.2, 344.9)	12	65.7	2.9	32.1	<0.01
Mixed	444.4 (176.2, 344.9)	2	97.3	37.7	37.7	<0.001
Organ System						
Cardiovascular	79.0 (43.8, 142.7)	11	78.9	4.7	47.5	<0.001
Musculoskeletal	89.8 (65.8, 122.4)	13	40.6	1.7	20.2	0.06
Hematopoietic	108.1 (82.1, 142.4)	3	0	0.9	1.8	0.41
Respiratory	164.4 (127.7, 211.6)	7	97.0	33.6	201.4	<0.001
Nervous	179.3 (74.5, 431.6)	5	75.0	4.2	16.6	<0.01
Sensory	295.8 (208.2, 420.1)	7	55.8	2.3	13.6	0.04
Urinary	408.1 (141.1, 1180.5)	2	53.0	2.1	2.1	0.15
Mixed	96.4 (16.1, 578.0)	4	96.7	30.5	91.4	<0.001
Exp. Environment						
Ex vivo	344.8 (222.2, 534.9)	6	52.4	2.1	10.5	0.06

In vitro	119.6 (101.8, 140.5)	46	92.4	13.2	592.8	<0.001
Culture Type						
Primary culture	142.0 (91.8, 219.5)	28	89.5	9.5	256.8	<0.001
Cell line	135.7 (112.2, 164.1)	24	94.4	17.9	411.9	<0.001
Adhesion Phenotype						
Adherent	137.4 (117.0, 161.3)	49	92.8	13.9	665.9	<0.001
Suspension	108.1 (82.1, 142.4)	3	0	0.9	1.8	0.41
Epithelial polarity						
Apical	154.6 (121.5, 196.6)	10	97.8	46.4	417.6	<0.001
Not applicable	122.1 (90.4, 164.9)	42	83.6	6.1	249.8	<0.001
Offline Total	136.3 (116.6, 159.2)	52	92.4	13.1	669.5	<0.001

Covariates	t_{half}, sec (±95% CI)	N	I^2 (%)	H^2	Q	P_Q
Influence of biological characteristics on kinetic estimates (analysis of online subgroup)						
Species						
Rat	15.0 (4.9, 46.1)	3	54.3	2.2	4.4	0.11
Human	43.3 (19.0, 98.4)	16	94.3	17.7	247.7	<0.001
Murine	9.7 (1.4, 68.8)	3	69.4	6.6	3.3	0.07
Embryonic Origin						
Mesoderm	32.2 (7.4, 140.0)	7	93.0	14.3	85.7	<0.001
Endoderm	28.1 (15.9, 49.5)	13	82.3	5.6	67.7	<0.001
Ectoderm	186.6 (1.4, 24599.3)	2	96.5	28.2	28.2	<0.001
Organ System						
Hepatobiliary	28.6 (15.5, 52.9)	9	84.6	6.5	52.0	<0.001
Musculoskeletal	1.9 (0.4, 9.1)	2	0	0.1	0.1	0.77
Respiratory	11.1 (5.7, 21.7)	3	0	0.5	1.0	0.60
Urinary	5.7 (0.9, 37.2)	2	0	0.3	0.3	0.57
Mixed	196.5 (61.1, 632.1)	6	94.2	17.2	85.9	<0.001
Exp. Environment						
in vivo	32.5 (15.9, 66.3)	22	94.2	17.1	359.0	<0.001
Culture Type						
Primary culture	15.1 (4.0, 56.7)	9	91.3	11.5	91.9	<0.001
Cell line	53.0 (21.4, 131.1)	13	95.3	21.4	257.4	<0.001
Adhesion Phenotype						
Adherent	35.3 (16.1, 77.7)	20	94.5	18.3	347.8	<0.001
Suspension	21.8 (0.6, 840.4)	2	90.5	10.6	10.6	<0.01
Epithelial polarity						
Basolateral	11.8 (6.6, 20.9)	2	0	0.2	0.2	0.62
Apical	33.0 (12.5, 87.1)	10	90.7	10.8	96.8	<0.001
Not applicable	42.1 (12.6, 140.5)	10	95.9	24.5	220.5	<0.001
Online Total	32.5 (15.9, 66.3)	22	94.2	17.1	359.0	<0.001

Covariates	t_{half}, sec (±95% CI)	N	I^2 (%)	H^2	Q	P_Q
Influence of cell type on ATP release kinetics (separated by online/offline subgroups)						
Online Subgroup						
Renal epithelial	5.7 (0.9, 37.2)	2	0	0.3	0.3	0.57
Bronchial epithelial	11.1 (5.7, 21.7)	3	0	0.5	1.0	0.60
cholangiocytes	22.3 (12.7, 39.4)	6	80.4	5.1	25.5	<0.001
hepatocytes	77.0 (7.4, 804.8)	3	90.7	10.7	21.4	<0.001
Other	75.3 (22.6, 251.5)	6	92.9	17.7	124.1	<0.001
Offline Subgroup						
Ciliary epithelial	39.2 (11.4, 134.8)	2	0	0.3	0.3	0.60
Umbilical vein endo.	59.6 (21.5, 165.0)	4	77.1	4.4	13.1	<0.01
osteoblasts	77.9 (53.1, 114.2)	9	22.3	1.3	10.3	0.25
cardiomyocytes	96.8 (38.6, 242.8)	2	23.4	1.3	1.3	0.25
Alveolar cells	115.8 (109.0, 123.1)	2	10.9	1.1	1.1	0.29
astrocytes	179.3 (74.5, 431.6)	5	75.9	4.2	16.6	<0.01
Aortic endothelial cells	200.3 (68.9, 582.3)	2	0	0.2	0.2	0.66
Urothelial cells	408.1 (141.1, 1180.5)	2	53	2.1	2.1	0.15
Other	171.3 (129.2, 227.2)	6	92.7	13.6	313.3	<0.001

Covariates	t_{half}, sec (±95% CI)	N	I^2 (%)	H^2	Q	P_Q
Influence of mechanical stimulus type on ATP release kinetics (separated by online/offline subgroups)						
Online Subgroup						
Osmotic pressure	41.2 (19.9, 85.5)	20	94.4	17.8	338.6	<0.001
Fluid shear stress	2.0 (0.4, 9.1)	2	0	0.1	0.1	0.77
Offline Subgroup						
ultrasound	118.3 (28.1, 497.9)	3	65	2.9	5.7	0.06
Osmotic pressure	166.5 (137.2, 201.9)	21	96	25.2	504.5	0.001
Strain	180.8 (94.4, 346.4)	6	64.1	2.8	13.9	0.02
Fluid shear stress	80.3 (52.8, 122.4)	19	66.4	3.0	53.5	<0.001
Other	218.5 (27.0, 1766.5)	3	86.2	7.3	14.5	<0.01

Table 4-S5. Pharmacological Interventions used to study mechanically-stimulated ATP release. *Bolded interventions* are pharmacological agents that do not overlap with other known mechanisms of MSAR. Uncommon or unverified pharmacological interventions have been omitted.

Target	Pharmacological interventions
Release mechanisms	
Vesicular	**NEM**, **bafilomycin**, **monensin, brefeldin A**
Pannexins	carbenoxolone, 18α/β-glycyrrhetinic acid, probenecid, **10panx1**, NPPB, SITS, **DTT**, mefloquine
Connexins	carbenoxolone, 18 α/β -glycyrrhetinic acid, **octanol**, **heptanol, flufenamic acid** (little activity at Panx1)**,** arachidonic acid, mefloquine, **GAP26**, **GAP27**
VRAC	**tamoxifen**, **fluoxetine**, glybenclamide, **phloretin,** NPPB, SITS, **verapamil**
Maxi-anion	Gd^{3+}, NPPB, SITS, arachidonic acid
Auxiliary mechanisms	
ANK	probenecid
ATP synthase	**angiostatin, piceatannol**
CFTR	glybenclamide, **CFTR-172, Rp-cAMPS, niflumic acid**
ENaC	**amiloride**
L-type VSCC	**nifedipine**
P2X7	**brilliant blue G**, Gd^{3+}, **KN62, A10606120, A438079, A74003**
Piezo1	ruthenium red, Gd^{3+}, **GsMTx4**
TRPV4	**HC067047**, ruthenium red, Gd^{3+}
Regulatory mechanisms	
Intracellular Calcium	**BAPTA-AM, EGTA-AM, thapsigargin**
Extracellular Calcium	Calcium-free (Calcium omitted in solution, optionally chelated)
COX	**etodolac, indomethacin, NS398, ETYA**
PKC	**calphostin C, chelerythrine, myristoylated PKC ζ pseudosubstrate, GF 109203X, Gö6976, Gö6983**
P38 mitogen-activated protein	**SB203590**
Rho kinase	**Y27632, GSK269962, H1152**
MLC kinase	**ML-7**
Tyrosine kinase	**herbimycin A, tyrphostin 46**
PI3K	**wortmannin, LY294002**
f-actin	**cytochalasin B, cytochalasin D**
microtubules	**nocodazole**
cholesterol	**MβCD**
cilia	**chloral hydrate**

Table 4-S6. Mechanisms of mechanically-stimulated ATP release. The effects of pharmacological and genetic interventions on MSAR for studied cell types were calculated as an inhibitory effect (%) ± 95% confidence intervals (CI) compared to vehicle control, according to random effects meta-analysis model. Positive effects (>0%) indicate that MSAR was inhibited and negative effects (<0%) indicate that MSAR was potentiated. Interventions for which 0% was not included in the 95% CI had a significant effect on MSAR. Involvement of studied mechanism in MSAR is indicated by green box (involved) or red box (not involved), and quality of evidence is indicated by dark green/red (finding replicated by separate study/method) or light green/red (not-replicated). Orange boxes: Interventions with inconsistent effects, reasoning for each case is provided in table. P_Q: p-value corresponding to Q heterogeneity statistic used to evaluate null hypothesis that all studies reported same effect, N: number of datasets. *indicates the interventions that were activators or agonists of MSAR, and therefore were not pooled with inhibitory interventions for calculation of overall inhibition.

target	Intervention	inhibition, % (95% CI)	N	P_Q
alveolar type II				
actin	Cytochalasin D (Akopova et al., 2012; Tatur, Groulx, Orlov, & Grygorczyk, 2007)	66.6 (61.9, 71.2)	2	0.82
calcium (intracellular)	2-APB (Tatur et al., 2007)	30.0 (27.6, 32.4)	1	-
	Thapsigargin (Tatur et al., 2007)	56.4 (42.3, 70.4)	1	-
	BAPTA-AM (Ramsingh et al., 2011; Tatur et al., 2007)	59.4 (-4.8, 123.6)	2	<0.001
	Overall	44.0 (20.4, 67.6)	4	<0.01
Calcium (extracellular)	Calcium-free (Ramsingh et al., 2011; Tatur et al., 2007)	6.3 (0.1, 12.5)	2	0.46
microtubules	Nocodazole (Akopova et al., 2012)	58.3 (33.1, 83.5)	1	-
pannexin 1	Panx1 knockdown (Ransford et al., 2009)	60.0 (44.6, 75.4)	1	-
rho kinase	RhoA knockdown (Seminario-Vidal et al., 2011)	62.5 (48.6, 75.4)	1	-
TRPV4	HC067047 (Seminario-Vidal et al., 2011)	44.6 (26.7, 62.6)	1	-
	Ruthenium red (Tatur et al., 2007)	49.1 (44.6, 53.6)	1	-
	TRPV4 knockdown (Seminario-Vidal et al., 2011)	73.5 (59.5, 87.4)	1	-
	Overall	55.6 (39.5, 71.3)	3	<0.01
vesicular	Monensin (Akopova et al., 2012)	81.4 (71.8, 91.0)	1	-
	NEM (Islam, Uramoto, Okada, Sabirov, & Okada, 2012; Ramsingh et al., 2011)	95.1 (91.0, 99.1)	2	0.74
	Bafilomycin (Tatur et al., 2007)	-3.7 (-13.7, 6.4)	1	-
	Brefeldin A (Akopova et al., 2012)	41.1 (33.7, 48.5)	1	-

		Overall	53.6 (11.2, 96.0)	5	<0.001
aortic endothelial					
	actin	Cytochalasin B (Koyama, Oike, & Ito, 2001)	3.8 (-41.9, 49.4)	1	-
	cholesterol/ calveolin	MβCD (Yamamoto et al., 2011)	63.5 (60.7, 66.3)	1	-
		caveolin-1 knockdown (Yamamoto et al., 2011)	58.3 (55.6, 61)	1	-
		Overall	60.9 (55.7, 66)	2	<0.01
	rho kinase	Y27632 (Koyama et al., 2009; Koyama et al., 2001)	85.8 (53.6, 117.9)	2	0.01
		botulinum C3 toxin (Koyama et al., 2001)	54 (29.1, 79)	1	-
		LPA* (Koyama et al., 2001)	-0.8 (-31.5, 30)	2	0.32
		Overall	68.2 (37., 99.1)	3	0.31
	tyrosine kinase	herbimycin A (Koyama et al., 2009; Koyama et al., 2001)	62.8 (52, 73.7)	2	0.82
		tyrphostin 46 (Koyama et al., 2009; Koyama et al., 2001)	75.1 (50.9, 99.3)	2	0.02
		Overall	64.9 (55, 74.8)	4	0.85
	VRAC	Tamoxifen (Hisadome et al., 2002; Koyama et al., 2009)	79.6 (64.4, 94.8)	2	<0.001
		Verapamil (Hisadome et al., 2002; Koyama et al., 2009)	79.9 (66.5, 93.2)	2	<0.001
		Fluoxetine (Hisadome et al., 2002; Koyama et al., 2009)	47.2 (26.7, 67.7)	7	<0.001
		Glybenclamide (Hisadome et al., 2002; H. T. Liu, Toychiev, Takahashi, Sabirov, & Okada, 2008)	48.8 (10.4, 87.3)	6	<0.001
		Overall	67.5 (50.5, 84.5)	17	0.90
Astrocyte					
	actin	clostridial difficile toxin B (Blum, Walsh, & Dubyak, 2010)	-7 (-85.8, 71.9)	2	1.00
	aquaporin4	Aqp4 knockdown (Thrane et al., 2011)	63.7 (24.4, 103.0)	1	-
	calcium (intracellular)	BAPTA-AM (Blum et al., 2010)	5.5 (-37.6, 48.7)	2	0.99
	Calcium (extracellular)	Calcium-free (C. Stout & Charles, 2003; C. E. Stout, Costantin, Naus, & Charles, 2002)	-97.6 (-186.3, -8.8)	2	0.17
	connexin	18α-glycyrrhetinic acid (Beckel et al., 2014)	12.6 (-12.2, 37.4)	1	-
		Octanol (H. T. Liu et al., 2008)	2 (-27.8, 31.8)	1	-

	flufenamic acid (C. E. Stout et al., 2002)	68.5 (32.4, 104.5)	1	-
	Carbenoxolone (H. T. Liu et al., 2008)	31.6 (16.9, 46.3)	9	<0.01
	Overall	27 (4.8, 49.3)	12	0.74

Note: Sensitivity to carbenoxolone and flufenamic acid consistent with connexin involvement, however 18α-glycyrrhetinic acid and octanol were ineffective in blocking ATP release.

CFTR	Glybenclamide (H. T. Liu et al., 2008)	12.9 (-13.4, 39.3)	1	-
maxi-anion	Gd^{3+} (Beckel et al., 2014; Blum et al., 2010; H. T. Liu et al., 2008; C. E. Stout et al., 2002)	36.7 (-5.3, 78.7)	4	<0.001

Note: Gd^{3+} inhibition tends to inhibit, maxi-anion channel possibly involved.

P2RX7	brilliant blue G (H. T. Liu et al., 2008)	-3.7 (-42.9, 35.4)	1	-
	Gd^{3+} (Beckel et al., 2014; Blum et al., 2010; H. T. Liu et al., 2008; C. E. Stout et al., 2002)	36.7 (-5.3, 78.7)	4	<0.001
	Overall	15.7 (-23.8, 55.3)	5	0.75
pannexin	Panx1 knockdown (Beckel et al., 2014)	51.2 (23.3, 79.1)	1	-
	SITS (H. T. Liu et al., 2008)	53.4 (37.1, 69.7)	1	-
	NPPB (H. T. Liu et al., 2008)	49.9 (32.7, 67.1)	1	-
	Probenecid (Beckel et al., 2014; H. T. Liu et al., 2008)	41.4 (-45.9, 128.7)	2	<0.001
	Carbenoxolone (Beckel et al., 2014; Blum et al., 2010)	31.6 (16.9, 46.3)	9	<0.01
	Overall	44.9 (35, 54.7)	14	0.98
piezo1	Gd^{3+} (Beckel et al., 2014; Blum et al., 2010; H. T. Liu et al., 2008; C. E. Stout et al., 2002)	36.7 (-5.3, 78.7)	4	<0.001

Note: Gd^{3+} inhibition tends to inhibit, Piezo1 possibly involved.

rho kinase	GSK269962 (Beckel et al., 2014)	36.2 (28, 44.3)	2	0.52
TRPV4	Gd^{3+} (Beckel et al., 2014; Blum et al., 2010; H. T. Liu et al., 2008; C. E. Stout et al., 2002)	36.7 (-5.3, 78.7)	4	<0.001

Note: Gd^{3+} inhibition tends to inhibit, TRPV4 possibly involved.

VRAC	Phloretin (H. T. Liu et al., 2008)	10.7 (-15.3, 36.7)	1	-
	Verapamil (H. T. Liu et al., 2008)	16.7 (-15.1, 48.4)	1	-
	Glybenclamide (H. T. Liu et al., 2008)	12.9 (-13.4, 39.3)	1	-
	DCPIB (H. T. Liu et al., 2008)	-7.5 (-40.4, 25.4)	1	-
	DIDS (C. E. Stout et al., 2002)	-13.3 (-40.4, 13.8)	1	-
	1,9-dideoxy-forskolin (Blum et al., 2010)	27.4 (5.5, 49.3)	6	<0.001
	Overall	9.4 (-3.3, 22.1)	11	0.77

Bone Marrow Stromal

connexin/ pannexin	18α-glycyrrhetinic acid (Riddle, Taylor, Rogers, & Donahue, 2007)	15.7 (-22.7, 54.1)	1	-
vesicles	NEM (Riddle et al., 2007)	75.7 (41.6, 109.7)	1	-
	Monensin (Riddle et al., 2007)	79.2 (58.6, 99.8)	1	-
	Overall	78.2 (60.6, 95.9)	2	0.86

Bronchial epithelial cells

Calcium (intracellular)	BAPTA-AM (Okada et al., 2013; Ramsingh et al., 2011; Takemura et al., 2003; T. Zhang, Liu, Zhou, Kolosov, & Perelman, 2014)	66.1 (37.3, 94.9)	6	<0.001
Calcium (extracellular)	Calcium-free (T. Zhang et al., 2014)	-16.4 (-61.2, 28.4)	1	-
cAMP	Forskolin (Takemura et al., 2003)	-79 (-129.9, -28.1)	1	-
CFTR	CFTR knockdown (Okada, Nicholas, Kreda, Lazarowski, & Boucher, 2006; Okada et al., 2013)	-23.2 (-61, 14.5)	2	0.20
	CFTR-172 (Okada et al., 2006)	-5.8 (-35.8, 24.2)	1	-
	Overall	-12.6 (-36, 10.9)	4	0.92
connexin	Carbenoxolone (Ransford et al., 2009)	52.7 (-4.4, 109.7)	2	<0.01
	Flufenamic acid (Ransford et al., 2009; Seminario-Vidal et al., 2011)	-35.9 (-129.9, 58.1)	2	0.03
	Overall	16.6 (-68.7, 101.8)	4	0.48
microtubules	Nocodazole (Okada et al., 2013)	28.8 (13.2, 44.3)	1	-
MLC kinase	ML-7 (Seminario-Vidal et al., 2011)	83.5 (71.8, 95.3)	1	-
pannexin	Carbenoxolone (Seminario-Vidal et al., 2011)	52.7 (-4.4, 109.7)	2	<0.01
	Probenecid (Ransford et al., 2009)	45.5 (24.7, 66.3)	1	-
	10panx (Seminario-Vidal et al., 2011)	45.4 (28.6, 62.2)	1	-
	Overall	45.8 (33.1, 58.5)	4	0.09
rho kinase	H1152 (Okada et al., 2013; Seminario-Vidal et al., 2011)	65.4 (54.1, 76.7)	2	0.90
	Y27632 (Okada et al., 2013)	55.5 (41.5, 69.6)	1	
	Overall	61.4 (51.9, 70.9)	3	0.56

	TRPV4	HC067047 (Seminario-Vidal et al., 2011)	64.8 (52, 77.6)	1	-
		ruthenium red (Seminario-Vidal et al., 2011)	54.2 (43.5, 65)	1	-
		Gd^{3+} (Takemura et al., 2003)	33.9 (17.8, 50)	2	0.46
		Overall	51.7 (36, 67.5)	4	0.03
	vesicular	Bafilomycin (Okada et al., 2013)	18.5 (4.8, 32.1)	1	-
		brefeldin A (Okada et al., 2013)	37.6 (22.9, 52.4)	1	-
		NEM(Button, Okada, Frederick, Thelin, & Boucher, 2013)	36.8 (22.6, 51)	1	-
		Overall	30.7 (18.3, 43.2)	3	0.10
	other	H_2O_2 (Krick et al., 2016)	79.3 (67.9, 90.6)	1	-
		IGNγ (Krick et al., 2016)	54.4 (25.5, 83.3)	1	-
		IL-4 (Krick et al., 2016)	13.4 (-50.5, 77.2)	1	-
		TNFα (Krick et al., 2016)	-86.5 (-237.6, 64.7)	1	-
Bronchial Smooth Muscle Cells					
	calcium (intracellular)	BAPTA-AM (Takahara et al., 2014)	62.6 (40.4, 84.8)	1	-
	connexin/ pannexin	Carbenoxolone (Takahara et al., 2014)	4.0 (-97.3, 105.3)	1	-
	piezo1	ruthenium red (Takahara et al., 2014)	-29.6 (-154.5, 95.3)	1	-
	TRPV4	ruthenium red (Takahara et al., 2014)	-29.6 (-154.5, 95.3)	1	-
		TRPV4 knockdown (Takahara et al., 2014)	-4.6 (-95.8, 86.5)	1	-
		Overall	-13.3 (-87, 60.3)	2	0.75
	vesicles	NEM (Takahara et al., 2014)	100.8 (93.1, 108.5)	1	-
		Bafilomycin (Takahara et al., 2014)	79.9 (42.6, 117.1)	1	-
		Monensin (Takahara et al., 2014)	51 (10.5, 91.5)	1	-
		Overall	82.3 (52.6, 112)	3	0.04
Cardiac Fibroblasts					
	Calcium (extracellular)	Calcium free (D. Lu, Soleymani, Madakshire, & Insel, 2012)	-204.8 (-702.1, 292.5)	1	-
	Note: There is tendency to potentiate ATP release which is consistent with connexin involvement				
	connexin 43/45	Carbenoxolone (Krick et al., 2016)	66.1 (34.7, 97.5)	3	0.11

		Cx43/45 knockdown (D. Lu et al., 2012)	48 (28, 68)	2	0.29
		Overall	53.2 (36.3, 70.1)	5	0.92
	pannexin 1	Carbenoxolone (Krick et al., 2016)	66.1 (34.7, 97.5)	3	0.11
		Probenecid (Krick et al., 2016)	43.6 (20.2, 66.9)	4	0.12
		Panx1 knockdown (D. Lu et al., 2012)	17.5 (-68.5, 103.4)	1	-
		Overall	50 (31.7, 68.4)	8	0.97
		Note: Panx1 knockdown inconsistent with pharmacological data			
	vesicular	brefeldin A (D. Lu et al., 2012)	-8.4 (-63.5, 46.7)	2	0.96
Cardiomyocytes					
	CFTR	Glybenclamide (Dutta, Sabirov, Uramoto, & Okada, 2004)	15.7 (-19.7, 51.2)	1	-
	maxi-anion	Gd^{3+} (Dutta et al., 2004)	86.6 (81, 92.3)	1	-
		NPPB (Dutta et al., 2004)	78.6 (71.8, 85.4)	1	-
		SITS (Dutta et al., 2004)	80.3 (70, 90.6)	1	-
		arachidonic acid (Dutta et al., 2004)	76.3 (65.8, 86.7)	1	-
		Overall	81.4 (76.5, 86.4)	3	0.09
	pannexin 2	Carbenoxolone (Oishi et al., 2012)	92 (57.9, 126.1)	1	-
		Panx2 knockdown (Oishi et al., 2012)	85.8 (43.9, 127.7)	1	-
		NPPB (Dutta et al., 2004)	78.6 (71.8, 85.4)	1	-
		SITS (Dutta et al., 2004)	80.3 (70, 90.6)	1	-
		Overall	79.5 (73.9, 85.1)	2	0.44
	VRAC	glybenclamide(Dutta et al., 2004)	15.7 (-19.7, 51.2)	1	-
Cholangiocytes					
	calcium (extracellular)	Calcium free (Gradilone et al., 2007)	75.8 (59.7, 91.9)	1	-
	cilia	Chloral hydrate (Gradilone et al., 2007)	73.4 (46.2, 100.5)	1	-
	CFTR	CFTR knockout (Fiorotto et al., 2007)	61.5 (-47.5, 170.5)	1	-
		Note: Original report concluded CFTR was involved in hypotonic stress induced ATP release, however our analysis shows that there is only tendency to inhibit (significance not achieved)			
	microtubules	Nocodazole (Sathe et al., 2011)	83.3 (72.1, 94.4)	3	0.97

	PI3K	Wortmannin (Feranchak et al., 1999)	85.6 (68.9, 102.4)	1	-
		LY294002 (Feranchak et al., 1999)	90 (75.2, 104.8)	1	-
		Overall	88.1 (77, 99.2)	2	0.70
	PKC	Acute PMA* (Gatof, Kilic, & Fitz, 2004; Sathe et al., 2011; Woo, Dutta, Patel, Kresge, & Feranchak, 2008)	-104.1 (-215.6, 7.4)	4	0.01
		Calphostin C (Gatof et al., 2004; Woo et al., 2008)	42.7 (-43.7, 129.2)	2	0.01
		Chelerythrine (Gatof et al., 2004; Sathe et al., 2011; Woo et al., 2008)	64.5 (58.9, 70)	4	0.95
		Chronic PMA (Woo et al., 2008)	8.6 (-1.8, 19)	1	-
		Myristoylated PKC ζ pseudosubstrate (Woo et al., 2008)	74.4 (67.1, 81.8)	1	-
		Overall	48.8 (18.2, 79.5)	8	<0.001
	TRPV4	TRPV4 knockdown (Gradilone et al., 2007)	64.3 (46.1, 82.4)	1	-
		Gd^{3+} (Roman, Feranchak, Davison, Schwiebert, & Fitz, 1999)	73 (65.3, 80.7)	3	0.29
		TRPV4 overexpression* (Gradilone et al., 2007)	-61.9 (-127.9, 4.1)	1	-
		Overall	71.6 (64.6, 78.7)	4	0.86
	vesicular	Bafilomycin (Sathe et al., 2011)	62.8 (40.4, 85.2)	1	-
		Brefeldin A (Sathe et al., 2011)	85.8 (78.2, 93.4)	3	0.99
		VNUT (SLC17A9) knockdown (Sathe et al., 2011)	42.3 (-5.3, 90)	1	
		Monensin (Woo et al., 2010)	29.5 (-10.7, 69.8)	2	0.98
		Overall	61.2 (35.4, 87)	7	0.05
Chondrocytes					
	ANK	Probenecid (Rosenthal et al., 2013)	51.2 (27.3, 75.1)	3	<0.01
		ANK knockdown (Rosenthal et al., 2013)	80 (32.3, 127.7)	1	-
		Overall	57.9 (34, 81.8)	4	0.77
	calcium (intracellular)	BAPTA-AM (Rosenthal et al., 2013)	89.2 (82.2, 96.1)	1	-
	connexin	Octanol (Graff, Lazarowski, Banes, & Lee, 2000)	42.3 (25.5, 59.1)	2	0.87
		Carbenoxolone (Rosenthal et al., 2013)	-45 (-226.5, 136.5)	1	-
		Flufenamic acid (Rosenthal et al., 2013)	-14 (-59.3, 31.3)	1	-
		Overall	14.4 (-35.7, 64.5)	4	0.11
		Note: Inconsistent findings between octanol and carbenoxolone/flufenamic acid treatments			
	maxi-anion	Gd^{3+} (Rosenthal et al., 2013)	12 (-11.1, 35.1)	1	-

	P2RX4	P2RX4 knockdown (Rosenthal et al., 2013)	-30.7 (-75.9, 14.5)	1	-
	P2RX7	P2RX7 knockdown (Rosenthal et al., 2013)	-18.1 (-142.3, 106.2)	1	-
		AZ10606120 (Rosenthal et al., 2013)	-20 (-179.6, 139.6)	1	-
		A438079 (Rosenthal et al., 2013)	-100 (-196.4, -3.6)	1	-
		Gd^{3+} (Rosenthal et al., 2013)	12 (-11.1, 35.1)	1	-
		Overall	-19.9 (-76.2, 36.3)	4	0.16
	Pannexin 1	Probenecid (Rosenthal et al., 2013)	51.2 (27.3, 75.1)	3	<0.01
		10panx1 (Rosenthal et al., 2013)	-30 (-340.9, 280.9)	1	-
		Carbenoxolone (Rosenthal et al., 2013)	-45 (-226.5, 136.5)	1	-
		Overall	49.1 (25.5, 72.7)	5	0.86
	piezo1	Gd^{3+} (Rosenthal et al., 2013)	12 (-11.1, 35.1)	1	-
	TRPV4	Gd^{3+} (Rosenthal et al., 2013)	12 (-11.1, 35.1)	1	-
	vesicular	Monensin (Rosenthal et al., 2013)	26 (-4.7, 56.7)	1	-
		NEM (Rosenthal et al., 2013)	11 (-313.3, 335.3)	1	-
		Brefeldin (Rosenthal et al., 2013)	12 (-58.6, 82.6)	1	-
		Overall	23.7 (-4.4, 51.7)	3	0.94

Note: Participation of pannexins in MSAR from chondrocyte MSAR may be false finding due to dual effect of probenecid on pannexins and ANK. Moreover, 10panx1 and carbenoxolone did not inhibit ATP release.

Note: There is tendency for vesicular inhibitors to reduce ATP release (nearly significant).

Ciliary Epithelial cells

	CFTR	Glybenclamide (Mitchell, Carre, McGlinn, Stone, & Civan, 1998)	-19.4 (-63, 24.1)	2	0.83
	connexin	Carbenoxolone (A. Li, Leung, Peterson-Yantorno, Mitchell, & Civan, 2010)	38.6 (32.5, 44.8)	1	-
		flufenamic acid (A. Li et al., 2010)	48.8 (37.8, 59.8)	1	-
		Mefloquine (A. Li et al., 2010)	22.7 (2.7, 42.7)	1	-
		Heptanol (A. Li et al., 2010)	48.8 (36.2, 61.4)	1	-
		Overall	41.5 (32.8, 50.3)	4	0.07
	maxi-anion	Gd^{3+} (A. Li et al., 2010)	29.5 (-46.4, 105.3)	1	-

	P2RX7	KN62 (A. Li et al., 2010)	-6.3 (-17.3, 4.7)	1	-
		Gd^{3+} (A. Li et al., 2010)	29.5 (-46.4, 105.3)	1	-
		Overall	-5.5 (-16.4, 5.4)	2	0.36
	pannexin	Mefloquine (A. Li et al., 2010)	22.7 (2.7, 42.7)	1	-
		Probenecid (A. Li et al., 2010)	46.9 (37, 56.7)	1	-
		DTT (A. Li et al., 2010)	28 (18.4, 37.6)	1	-
		NPPB (A. Li et al., 2010; Mitchell et al., 1998)	69.5 (52.8, 86.3)	3	0.01
		Carbenoxolone (A. Li et al., 2010)	38.6 (32.5, 44.8)	1	-
		Overall	41 (29.3, 52.6)	7	<0.01
	piezo1	Gd^{3+} (A. Li et al., 2010)	29.5 (-46.4, 105.3)	1	-
	TRPV4	Gd^{3+} (A. Li et al., 2010)	29.5 (-46.4, 105.3)	1	-
	vesicular	Bafilomycin (A. Li et al., 2010)	25.1 (17.2, 33.1)	1	-
	VRAC	Tamoxifen (Mitchell et al., 1998)	-0.5 (-21.7, 20.6)	2	0.69
		Verapamil (Mitchell et al., 1998)	-6.8 (-48.1, 34.4)	2	0.16
		Glybenclamid e(Mitchell et al., 1998)	-19.4 (-63, 24.1)	2	0.83
		DIDS (Mitchell et al., 1998)	-75.7 (-115.6, -35.8)	2	0.30
		DPC (Mitchell et al., 1998)	12.3 (-10.6, 35.3)	2	0.52
		Overall	-15 (-42.1, 12.1)	10	0.10
Erythrocytes					
	CFTR	Glybenclamide (Moehlenbrock, Price, & Martin, 2006; Sprague, Ellsworth, Stephenson, Kleinhenz, & Lonigro, 1998)	66.6 (62.4, 70.7)	4	0.91
		Rp-cAMPS (Sprague, Ellsworth, Stephenson, & Lonigro, 2001)	54.5 (28.5, 80.6)	3	0.71
		Niflumic acid (Sprague et al., 1998)	57.2 (18.1, 96.3)	3	0.94
		CFTR knockdown (Sprague et al., 1998)	87.6 (79.3, 95.9)	3	0.12
		Overall	70.3 (54.2, 86.4)	13	0.04
	connexin/pannexin	Carbenoxolone (overall) (Locovei, Bao, & Dahl, 2006; Sikora, Orlov, Furuya, & Grygorczyk, 2014)	66.6 (-74.1, 207.3)	2	0.04
		Locovei et. al 2006	126.0 (87.0, 165.1)	1	-
		Sikora et. al 2014	-10.13 (-81.2, 61.0)	1	-

Note: Locovei et. al 2006 and Sikora et. al 2014 report inconsistent MSAR from carbenoxolone-treated erythrocytes. Sikora et al. suggested hemolysis was main MSAR mechanism while Locovei et al. suggested pannexin-mediated ATP release was main MSAR mechanism.

	piezo1	GsMTx4 (Cinar et al., 2015)	41.9 (26.4, 57.3)	1	-
		Piezo1 mutated (Cinar et al., 2015)	61.9 (51.9, 71.9)	1	-
		Ruthenium red(Cinar et al., 2015)	41.5 (26.5, 56.5)	1	-
		Gd^{3+}(Cinar et al., 2015)	30.8 (10.2, 51.5)	1	-
		Overall	45.6 (31.4, 59.7)	4	0.01
	Other	Diamide (Moehlenbrock et al., 2006; Price, Martin, & Spence, 2006; Tolan, Genes, Subasinghe, Raththagala, & Spence, 2009; Wan, Ristenpart, & Stone, 2008)	47.6 (33.8, 61.4)	8	<0.001
		Spermine NONate (Olearczyk, Ellsworth, Stephenson, Lonigro, & Sprague, 2004)	52.2 (0.5, 103.9)	1	-
Glomerular endothelial cells					
	calcium (extracellular)	Calcium free (Toma et al., 2008)	37.7 (20.2, 55.4)	1	-
	connexin 40	Cx40 knockdown (Toma et al., 2008)	80.8 (64.3, 97.3)	1	-
		18α-glycyrrhetinic acid (Toma et al., 2008)	92.7 (89.1, 96.3)	1	-
		Overall	89.6 (79.4, 99.8)	2	
	L-type VSCC	Nifedipine (Toma et al., 2008)	5.1 (-5.1, 15.3)	1	-
Hepatocytes					
	calcium (intracellular)	BAPTA-AM (Feranchak, Fitz, & Roman, 2000)	70.7 (27, 114.5)	1	-
	maxi-anion	Gd^{3+} (Roman, Feranchak, Davison, et al., 1999)	65.9 (52.5, 79.4)	1	-
	Note: Gd^{3+} inhibited ATP release, however insufficient data to resolve maxi-anion involvement.				
	microtubules	Nocodazole (Feranchak et al., 2010)	52.9 (40.9, 65)	1	-
	P2RX7	Gd^{3+} (Roman, Feranchak, Davison, et al., 1999)	65.9 (52.5, 79.4)	1	-
	Note: Gd^{3+} inhibited ATP release, however insufficient data to resolve P2RX7 involvement.				
	pannexin	Carbenoxolone (Dolovcak, Waldrop, Xiao, & Kilic, 2011; Espelt et al., 2013)	20.8 (-35.1, 76.6)	3	<0.01
		Probenecid (Dolovcak et al., 2011)	48.1 (29.6, 66.6)	1	-
		Flufenamic acid (Dolovcak et al., 2011)	35.3 (6.5, 64.2)	1	-
		Mefloquine (Dolovcak et al., 2011)	51.8 (20.5, 83.1)	6	<0.001
		Overall	44.4 (30.8, 57.9)	11	1.00

PI3K	Wortmannin (Dolovcak et al., 2011; Feranchak, Roman, Schwiebert, & Fitz, 1998)	17.3 (-53.1, 87.6)	2	<0001
	LY294002 (Dolovcak et al., 2011; Feranchak et al., 1998)	22.1 (-59.1, 103.3)	2	0.08
	Overall	19.3 (-33.8, 72.5)	4	1.00
	Note: Feranchak 1998 and Dolvcak 2011 reported contradictory effects of PI3K inhibition on ATP release, Dolvcak 2011 suggested that PI3K-independent pool of vesicles may explain discrepancy.			
piezo1	Gd^{3+} (Roman, Feranchak, Davison, et al., 1999)	65.9 (52.5, 79.4)	1	-
	Note: Gd^{3+} inhibited ATP release, however insufficient data to resolve Piezo1 involvement.			
PKC	Acute PMA* (Dolovcak et al., 2011; Feranchak et al., 2010)	-87.6 (-124.2, -51.1)	2	0.45
	Chelerythrine (Dolovcak et al., 2011; Feranchak et al., 2010)	36.9 (-4.6, 78.5)	2	<0.001
	Chronic PMA (Feranchak et al., 2010)	48.1 (30.7, 65.4)	1	-
	Calphostin C (Feranchak et al., 2010)	57.3 (45.6, 69)	1	-
	Overall	53.5 (44.1, 63)	4	0.93
TRPV4	Gd^{3+} (Roman, Feranchak, Davison, et al., 1999)	65.9 (52.5, 79.4)	1	-
	Note: Gd^{3+} inhibited ATP release, however insufficient data to resolve TRPV4 involvement.			
vesicular	Bafilomycin (Dolovcak et al., 2011; Feranchak et al., 2010)	33.4 (-24.7, 91.5)	2	<0.001
	Brefeldin A (Espelt et al., 2013; Feranchak et al., 2010)	69.9 (59.9, 79.8)	2	0.82
	Monensin (Feranchak et al., 2010)	82.6 (70.1, 95.1)	1	-
	Overall	73.5 (59.6, 87.5)	5	0.36
Intestinal epithelial				
actin	Cytochalasin B (Van der Wijk, De Jonge, & Tilly, 1999)	57.6 (25.2, 90)	1	-
calcium (intracellular)	BAPTA-AM (Van der Wijk et al., 1999)	67.4 (37.3, 97.5)	1	-
CFTR	Glybenclamide (Hazama et al., 1999)	-3.8 (-78.4, 70.7)	1	-
connexin	Arachidonic acid (Hazama et al., 1999)	-12.5 (-102, 77)	1	-
maxi-anion	Arachidonic acid (Hazama et al., 1999)	-12.5 (-102, 77)	1	-
	SITS (Hazama et al., 1999)	0.9 (-65.6, 67.5)	1	-
	Overall	-3.9 (-57.3, 49.5)	2	0.81

	P2RX7	Gd^{3+} (Hazama et al., 1999)	60.9 (20.6, 101.2)	3	0.01
		Note: Gd^{3+} inhibited ATP release, however insufficient data to resolve P2RX7 involvement.			
	P2RY1	MRS2179 (B. A. Patel, 2014)	5.7 (-13.4, 24.8)	5	<0.001
	pannexin	NPPB (Hazama et al., 1999)	77.3 (62.3, 92.3)	4	0.05
		SITS (Hazama et al., 1999)	0.9 (-65.6, 67.5)	1	-
		Overall	46.3 (-27.2, 119.8)	5	0.31
		Note: Discrepancies SITS and NPPB are unexplained			
	Piezo 1	Gd^{3+} (Hazama et al., 1999)	60.9 (20.6, 101.2)	3	0.01
		Note: Gd^{3+} inhibited ATP release, however insufficient data to resolve Piezo1 involvement.			
	TRPV4	Gd^{3+} (Hazama et al., 1999)	60.9 (20.6, 101.2)	3	0.01
		Note: Gd^{3+} inhibited ATP release, however insufficient data to resolve TRPV4 involvement.			
	VRAC	Glybenclamide (Hazama et al., 1999)	-3.8 (-78.4, 70.7)	1	-
	other	Mouse IgG (Hazama et al., 1999)	2.4 (-80.2, 84.9)	1	-
		H2D-5 antibody (Hazama et al., 1999)	94.8 (87.2, 102.4)	1	-
		Butanol (Tomassen, van der Wijk, de Jonge, & Tilly, 2004)	78.6 (71.7, 85.6)	1	-
Keratinocytes					
	ATP synthase	oligomycin(Azorin et al., 2011)	35.8 (15.1, 56.5)	1	-
	calcium (intracellular)	thapsigargin(Azorin et al., 2011)	-12.4 (-84, 59.1)	1	-
		thapsigargin, calcium-free(Azorin et al., 2011)	-532.3 (-2023.5, 958.9)	1	-
		EGTA-AM(Azorin et al., 2011)	0 (-98, 98)	1	-
		BAPTA-AM(Azorin et al., 2011)	0 (-98, 98)	1	-
		Overall	-6.6 (-56.3, 43.1)	4	0.91
	CFTR	glybenclamide(Azorin et al., 2011)	13.9 (-56.8, 84.6)	1	-
		niflumic acid(Azorin et al., 2011)	-41.6 (-191.9, 108.6)	1	-
		Overall	3.8 (-60.1, 67.8)	2	0.51
	connexin	18α-glycyrrhetinic acid(Azorin et al., 2011)	20.9 (-38.9, 80.8)	1	-
		carbenoxolone(Azorin et al., 2011)	-6.4 (-62.8, 50.1)	1	-
		octanol(Azorin et al., 2011)	7.4 (-15.6, 30.4)	1	-
		Overall	7.2 (-12.9, 27.2)	3	0.81

	ENaC	amiloride(Azorin et al., 2011)	-32.1 (-102.2, 38)	1	-
	maxi-anion	Gd^{3+}(Azorin et al., 2011)	60.3 (40.8, 79.8)	1	-
		lanthanum(Azorin et al., 2011)	67.4 (51.8, 82.9)	1	-
		NPPB(Azorin et al., 2011)	37.9 (10.4, 65.3)	1	-
		Overall	58.5 (43.4, 73.5)	3	0.19
	P2RX7	Oxidized ATP (Azorin et al., 2011)	1.4 (-20.2, 23.1)	1	-
		Brilliant blue G (Azorin et al., 2011)	-37.7 (-127.2, 51.9)	1	-
		Overall	-0.7 (-21.8, 20.3)	2	0.41
	pannexin	18α-glycyrrhetinic acid (Azorin et al., 2011)	20.9 (-38.9, 80.8)	1	-
		Carbenoxolone (Azorin et al., 2011)	-6.4 (-62.8, 50.1)	1	-
		Overall	6.5 (-34.6, 47.5)	2	0.52
	vesicular	Brefeldin A (Azorin et al., 2011)	6.6 (-64.7, 77.8)	1	-
	VRAC	Glybenclamide (Azorin et al., 2011)	13.9 (-56.8, 84.6)	1	-
Lens epithelial cells					
	pannexin/ connexin	18α-glycyrrhetinic acid (Shahidullah, Mandal, Beimgraben, & Delamere, 2012)	90.9 (71.3, 110.5)	1	-
	vesicular	NEM (Shahidullah, Mandal, Beimgraben, et al., 2012)	-6.3 (-14.9, 2.4)	1	-
Ligament cells					
	calcium (intracellular)	Thapsigargin (Luckprom, Kanjanamekanant, & Pavasant, 2011)	99.8 (95.8, 103.8)	2	0.97
		2-APB (Luckprom et al., 2011)	34.6 (26.4, 42.7)	2	0.42
		Heparin (Luckprom et al., 2011)	55.6 (45.9, 65.3)	2	0.23
		Overall	63.4 (19.3, 107.6)	6	<0.001
	connexin 40	Spermine (Luckprom et al., 2011)	6.0 (-16.7, 28.7)	1	-
	connexin 43	Cx43 knockdown (Luckprom et al., 2011)	73.1 (68.7, 77.4)	1	-
		Carbenoxolone (Luckprom et al., 2011)	70.2 (42.6, 97.9)	2	<0.001
		Meclofenamic acid (Luckprom et al., 2011)	75 (54.8, 95.2)	1	-
		Overall	73.1 (68.0, 77.3)	4	1.00
	pannexin	Carbenoxolone (Luckprom et al., 2011)	70.2 (42.6, 97.9)	2	<0.001
		Panx1 knockdown (Kanjanamekanant, Luckprom, & Pavasant, 2014)	73.6 (69.2, 78)	1	-

	Overall	73.5 (69.1, 77.9)	3	0.97
PKC	TMB-8 (Luckprom et al., 2011)	60.2 (39.1, 81.2)	2	<0.01
Lung fibroblasts				
VDAC-1	VDAC-1 knockout (Okada et al., 2004)	57.1 (16.3, 97.9)	1	-
	VDAC-1 overexpression* (Okada et al., 2004)	-70.9 (-101.6, -40.3)	1	-
	Overall	66.6 (62.4, 70.7)	1	-
Mammary epithelial cells				
ATPase synthase	Angiostatin (Kawai, Kaidoh, Yokoyama, & Ohhashi, 2013)	41.7 (11.6, 71.9)	2	0.10
	Piceatannol (Kawai et al., 2013)	54.6 (36.3, 73)	2	0.50
	Overall	51.2 (35.5, 66.8)	4	0.92
CFTR	Glybenclamid e(Hazama et al., 2000)	-45.6 (-159.5, 68.3)	1	-
	CFTR overexpression* (Hazama et al., 2000)	62.4 (15.2, 109.6)	6	0.38
	Overall	-45.6 (-159.5, 68.3)	1	-
Note: Results are inconclusive. Unclear whether CFTR has role in mammary cells.				
connexin	Carbenoxolone (Furlow et al., 2015)	23.1 (5.6, 40.7)	1	-
	Arachidonic acid (Dutta, Okada, & Sabirov, 2002)	35.6 (25.5, 45.7)	5	<0.001
	Overall	31.5 (20.1, 42.9)	6	0.92
maxi-anion	Arachidonic acid (Dutta et al., 2002)	35.6 (25.5, 45.7)	5	<0.001
	Linoleic acid (Dutta et al., 2002)	33.8 (21.5, 46)	1	-
	Oleic acid (Dutta et al., 2002)	38.4 (28.8, 48.1)	1	-
	Gd^{3+} (Hazama et al., 2000)	81.1 (63.6, 98.5)	1	-
	Overall	45.9 (29.5, 62.3)	8	<0.01
pannexin	Carbenoxolone (Furlow et al., 2015)	23.1 (5.6, 40.7)	1	-
Note: insufficient evidence to discriminate pannexin from connexin.				
vesicular	Bafilomycin (Kawai et al., 2013)	-3.3 (-26.1, 19.6)	1	-
	Omeprazole (Kawai et al., 2013)	1.8 (-23.6, 27.3)	1	-
	Overall	-1 (-18, 16)	2	0.77
VRAC	Glybenclamide (Hazama et al., 2000)	-45.6 (-159.5, 68.3)	1	-
Mesenchymal stem cells				

	MLC kinase	ML-7 (Heo et al., 2016)	88.3 (68.4, 108.2)	1	-
	P38 mitogen-activated protein	SB431642 (Heo et al., 2016)	78.3 (72.1, 84.4)	1	-
	rho kinase	Y27632 (Heo et al., 2016)	75.4 (60.3, 90.6)	1	-
	other	LDN196189 (Heo et al., 2016)	79.1 (72.4, 85.8)	1	-
nasal epithelial cells					
	CFTR	CFTR knockdown (Watt, Lazarowski, & Boucher, 1998)	-0.6 (-34.9, 33.7)	1	-
	connexin	Flufenamic acid (Ohbuchi et al., 2014)	16.3 (-31.1, 63.7)	1	-
	maxi anion	Gd^{3+} (Ohbuchi et al., 2014)	15.4 (-37.9, 68.7)	1	-
	P2RX7	Gd^{3+} (Ohbuchi et al., 2014)	15.4 (-37.9, 68.7)	1	-
	pannexin	Carbenoxolone (Ohbuchi et al., 2014)	51.8 (31.3, 72.4)	1	-
	Note: flufenamic acid dismissed connexin involvement, carbenoxolone likely targets pannexins				
	piezo1	Gd^{3+} (Ohbuchi et al., 2014)	15.4 (-37.9, 68.7)	1	-
	TRPV4	Gd^{3+} (Ohbuchi et al., 2014)	15.4 (-37.9, 68.7)	1	-
Neutrophil					
	connexin				
	Note: connexin/pannexin blocker carbenoxolone had identical inhibitory effect as pannexin blocker 10panx1, thus connexin involvement is unlikely.				
	pannexin 1	10panx1(Chen et al., 2015)	40.2 (36.4, 43.9)	2	0.91
		Carbenoxolone (Chen et al., 2015)	37.3 (19.1, 55.4)	2	0.05
		Overall	40 (36.4, 43.7)	4	0.99
Osteoblast					
	actin	Cytochalasin D (Romanello, Pani, Bicego, & D'Andrea, 2001)	23.8 (-15.1, 62.7)	1	-
	cholesterol	MβCD (Xing et al., 2011)	77.8 (55.3, 100.3)	1	-
	connexin/pannexin	18α-glycyrrhetinic acid (Genetos, Geist, Liu, Donahue, & Duncan, 2005)	-100.1 (-415.7, 215.5)	1	-
		18β-glycyrrhetinic acid (Genetos et al., 2005)	-147.7 (-471, 175.7)	1	-

		Overall	-123.3 (-349.1, 102.5)	2	0.84
	L-type VSCC	Nifedipine (Genetos et al., 2005; Hecht, Liedert, Ignatius, Mizaikoff, & Kranz, 2013)	75.5 (60.4, 90.6)	2	0.54
	maxi-anion	Gd^{3+} (Genetos et al., 2005)	28.2 (-43.7, 100.1)	1	-
	P2RY2	P2RY2 knockout (Xing et al., 2014)	-6.5 (-108.9, 95.9)	1	-
	P2RY13	P2RY13 knockout (N. Wang et al., 2013)	5.7 (-43.5, 54.8)	1	-
	P2RX7	P2RX7 knockout (J. Li, Liu, Ke, Duncan, & Turner, 2005)	19.7 (-42.1, 81.6)	1	-
		Gd^{3+} (Genetos et al., 2005)	28.2 (-43.7, 100.1)	1	-
		Overall	23.3 (-23.6, 70.2)	2	0.86
	piezo1	Gd^{3+} (Genetos et al., 2005)	28.2 (-43.7, 100.1)	1	-
	TRPV4	Gd^{3+} (Genetos et al., 2005)	28.2 (-43.7, 100.1)	1	-
	vesicular	NEM (Genetos et al., 2005)	87.9 (46.9, 128.9)	1	-
		Monensin (Genetos et al., 2005; Romanello et al., 2005)	35.1 (-107.5, 177.8)	2	0.53
		brefeldin A (Genetos et al., 2005)	94.4 (63.8, 125)	1	-
		Overall	90.5 (66.3, 114.6)	4	0.88
Osteocytes					
	connexin	GAP26 (Kringelbach et al., 2015)	-2.7 (-11.9, 6.5)	1	-
		Carbenoxolone (Kringelbach et al., 2015)	35.3 (17.5, 53.2)	1	-
		Mefloquine (Seref-Ferlengez et al., 2016)	82.2 (56.7, 107.6)	1	-
		Cx43 knockdown (Genetos, Kephart, Zhang, Yellowley, & Donahue, 2007)	83.6 (6.8, 160.4)	1	-
		18α-glycyrrhetinic acid (Genetos et al., 2007)	68 (28.8, 107.2)	1	-
		Overall	48.7 (10.4, 87.0)	5	<0.001
	Note: Results for specific inhibitor GAP26 and Cx43 knockdown are inconsistent.				
	P2RX7	A438079 (Seref-Ferlengez et al., 2016)	53.8 (23.5, 84.1)	1	-
		A74003 (Seref-Ferlengez et al., 2016)	45.7 (15, 76.4)	1	-
		Overall	49.8 (28.2, 71.3)	2	0.71

	pannexin 1	Carbenoxolone (Kringelbach et al., 2015)	35.3 (17.5, 53.2)	1	-
		10panx1 (Kringelbach et al., 2015)	1.1 (-11.5, 13.8)	1	-
		Mefloquine (Seref-Ferlengez et al., 2016)	82.2 (56.7, 107.6)	1	-
		18α-glycyrrhetinic acid (Genetos et al., 2007)	68 (28.8, 107.2)	1	-
		Overall	44.7 (7.1, 82.3)	4	<0.001
	Note: Results for specific inhibitor 10panx1 are inconsistent with other blockers.				
	PKC	GF 109203X (Genetos et al., 2007)	77.3 (22.8, 131.8)	1	-
	T-type VSCC	α2β1 VSCC subunit knockdown (Thompson et al., 2011)	99.4 (94.5, 104.3)	1	-
	vesicular	Bafilomycin (Kringelbach et al., 2015)	39.8 (25.1, 54.4)	2	0.18
Pancreatic epithelia					
	calcium (intracellular)	BAPTA-AM (Kowal, Yegutkin, & Novak, 2015)	63.5 (40.2, 86.7)	1	-
	CFTR	CFTR knockdown (Braunstein et al., 2001)	86.2 (80.9, 91.4)	7	0.59
		CFTR overexpression* (Kowal et al., 2015)	-335.9 (-3580.6, 2908.8)	1	-
		Overall	86.2 (80.9, 91.4)	7	0.59
	maxi-anion	Gd^{3+} (Kowal et al., 2015)	82.3 (45.5, 119.2)	1	-
	Note: Gd^{3+} inhibited ATP release, however insufficient data to resolve maxi-anion involvement.				
	P2RX7	Gd^{3+} (Kowal et al., 2015)	82.3 (45.5, 119.2)	1	-
	Note: Gd^{3+} inhibited ATP release, however insufficient data to resolve P2RX7 involvement.				
	pannexin 1	Probenecid (Kowal et al., 2015)	83.3 (70.2, 96.4)	1	-
		10panx1 (Kowal et al., 2015)	82.7 (68.3, 97.1)	1	-
		Overall	83 (73.3, 92.7)	2	0.95
	piezo1	Gd^{3+} (Kowal et al., 2015)	82.3 (45.5, 119.2)	1	-
	Note: Gd^{3+} inhibited ATP release, however insufficient data to resolve Piezo1 involvement.				
	TRPV4	HC067047 (Kowal et al., 2015)	7.5 (-53.7, 68.6)	1	-
	vesicular	NEM (Kowal et al., 2015)	46.4 (-6.1, 98.9)	1	-

		Bafilomycin (Kowal et al., 2015)	88.6 (72.9, 104.4)	1	-
		Glyoxylate (Kowal et al., 2015)	77 (48.8, 105.2)	1	-
		Overall	81.3 (64.4, 98.2)	3	0.28
Platelet					
	calcium (extracellular)	Calcium-free(Oury et al., 2004)	34.8 (31.8, 37.7)	1	-
	integrins	GPIbα Ig (G19H10) (Oury et al., 2004)	49.9 (46.1, 53.7)	1	-
		Tirofiban (Oury et al., 2004)	6.6 (0.6, 12.6)	1	-
		Overall	28.3 (-14.1, 70.8)	2	<0.001
	Note: Not significant after pooling due to heterogeneity				
	MLC kinase	ML-7 (Oury et al., 2004)	27.3 (19.3, 35.3)	1	-
	P2RY1	MRS2179 (Oury et al., 2004)	21.2 (13, 29.3)	1	-
	P2RY12	AR-C69931MX (Oury et al., 2004)	33 (29.8, 36.3)	1	-
	P2RX1	MRS2159 (Oury et al., 2004)	26.7 (22.1, 31.4)	1	-
	PKC	GF 109203X (Oury et al., 2004)	-34.4 (-45.6, -23.2)	1	-
		Gö6976 (Oury et al., 2004)	-24.7 (-33.5, -15.8)	1	-
		Gö6983 (Oury et al., 2004)	-16.6 (-25, -8.2)	1	-
		Overall	-24.6 (-34.3, -15)	3	0.04
	other	anti-VWF Ig (AJVW-2) (Oury et al., 2004)	48.3 (46.3, 50.2)	1	-
Prostate epithelial					
	cAMP	MDL-12330A (Nandigama, Padmasekar, Wartenberg, & Sauer, 2006)	80 (72.4, 87.6)	1	-
	calcium (extracellular)	Calcium-free (Nandigama et al., 2006)	-26.8 (-33.7, -19.9)	1	-
	calcium (intracellular)	BATPA-AM (Nandigama et al., 2006)	71.9 (68.0, 75.9)	1	-
	CFTR	Niflumic acid (Sauer, Hescheler, & Wartenberg, 2000)	49.7 (18.8, 80.6)	1	-
	COX	Etodolac (Nandigama et al., 2006)	60.5 (32.7, 88.4)	1	-

		Indomethacin (Nandigama et al., 2006)	94.2 (83.2, 105.1)	1	-
		NS398 (Nandigama et al., 2006)	76.9 (65.5, 88.4)	1	-
		ETYA (Nandigama et al., 2006)	60.3 (13.9, 106.7)	1	-
		Overall	78.8 (63.4, 94.2)	4	0.04
	fatty acid hydrolase	MAFP (Nandigama et al., 2006)	58.2 (45.1, 71.3)	1	-
	maxi-anion	Gd^{3+} (Sauer et al., 2000)	48.1 (21.2, 75.0)	1	-
	Note: Gd^{3+} inhibited ATP release, however insufficient data to resolve maxi-anion involvement.				
	MEK1/2	U0126 (Nandigama et al., 2006)	47.1 (42.3, 51.8)	1	-
	P2RX7	Gd^{3+} (Sauer et al., 2000)	48.1 (21.2, 75.0)	1	-
	Note: Gd^{3+} inhibited ATP release, however insufficient data to resolve P2RX7 involvement.				
	P2 receptors	PPADS (Nandigama et al., 2006)	80.5 (73.8, 87.2)	1	-
		Suramin (Nandigama et al., 2006)	86.2 (79.8, 92.5)	1	-
		Overall	83.4 (77.9, 89)	2	0.23
	P38 mitogen-activated protein	SB203590 (Nandigama et al., 2006)	39.7 (34.2, 45.2)	1	-
	PI3K	Wortmannin (Nandigama et al., 2006)	56.3 (45.2, 67.4)	1	-
		LY294002 (Nandigama et al., 2006)	51.1 (37, 65.1)	1	-
		Overall	54.3 (45.6, 63)	2	0.57
	piezo1	Gd^{3+} (Sauer et al., 2000)	48.1 (21.2, 75.0)	1	-
	Note: Gd^{3+} inhibited ATP release, however insufficient data to resolve Piezo1 involvement.				
	TRPV4	Gd^{3+} (Sauer et al., 2000)	48.1 (21.2, 75.0)	1	-
	Note: Gd^{3+} inhibited ATP release, however insufficient data to resolve TRPV4 involvement.				
	VRAC	Tamoxifen (Sauer et al., 2000)	79.8 (44, 115.6)	1	-
		NPPB (Sauer et al., 2000)	85 (55.2, 114.9)	1	-
		Overall	82.9 (60.0, 105.8)	2	0.83
	other	DIDS (Sauer et al., 2000)	-27.1 (-179.8, 125.7)	1	-
Pulmonary artery endothelial cells					
	ATP synthase	ATP synthase Ig (Yamamoto et al., 2007)	72.9 (63, 82.9)	1	-
		Angiostatin (Yamamoto et al., 2007)	83.5 (78.4, 88.7)	1	-

		Piceatannol (Yamamoto et al., 2007)	68.4 (61, 75.8)	1	-
		Overall	75.3 (65, 85.6)	3	<0.01
	cholesterol/ calveolin	MβCD (Yamamoto et al., 2007)	60.1 (44, 76.2)	3	0.53
		Cholesterol (Yamamoto & Ando, 2013; Yamamoto et al., 2007)	38.1 (30.2, 46)	3	0.81
		Caveolin-1 knockdown (Yamamoto et al., 2007)	76 (62.4, 89.7)	3	0.78
		Overall	57.6 (32.8, 82.3)	9	<0.01
Renal epithelial					
	BK-β4	BK-β4 knockdown (David Holtzclaw, Cornelius, Hatcher, & Sansom, 2011)	82.5 (61.9, 103.1)	1	-
	calcium (extracellular)	Calcium free (Silva & Garvin, 2008)	90 (50.8, 129.2)	1	-
	CFTR	Niflumic acid (Ostrom et al., 2001)	49.5 (11.8, 87.2)	1	-
	connexin 43	Carbenoxolone (David Holtzclaw et al., 2011)	90.3 (54, 126.5)	1	-
		Heptanol (Chi, Gao, Zhang, Takeda, & Yao, 2014)	51.1 (42.6, 59.6)	1	
		Lindane (Chi et al., 2014)	36.4 (23.2, 49.6)	1	-
		Cx43 knockdown (Chi et al., 2014)	34.3 (25.8, 42.7)	1	-
		Overall	46 (32, 59.9)	4	<0.01
	P2 receptors	Suramin (Chi et al., 2014)	99.3 (96.3, 102.2)	1	-
	pannexin	Carbenoxolone (David Holtzclaw et al., 2011)	90.3 (54, 126.5)	1	-
	Note: Carbenoxolone inhibits MSAR more potently than connexin-specific blockers, suggesting pannexin may also be involved.				
	cilia	Polaris hypomorphic mutation (*Ift88*^{Tg737Rpw}) (Xu et al., 2009)	84.8 (23.3, 146.4)	1	-
	TRPV4	ruthenium red (Silva & Garvin, 2008)	85 (26.2, 143.8)	1	-
		TRPV4 knockdown (Silva & Garvin, 2008)	65 (25.8, 104.2)	1	-
		Gd^{3+} (Chi et al., 2014; Ostrom et al., 2001)	77.2 (36.8, 117.7)	2	<0.001
		Lanthanum (Chi et al., 2014)	99.4 (95.9, 102.8)	1	-
		Overall	90.5 (73.9, 107.1)	4	0.23
	vesicular	Bafilomycin (Bjaelde, Arnadottir, Overgaard, Leipziger, & Praetorius, 2013)	83.9 (5.2, 162.5)	1	-
Retinal epithelial cells					

	calcium (intracellular)	BAPTA-AM (Reigada & Mitchell, 2005)	81.6 (73.4, 89.7)	1	-
	CFTR	CFTR-172 (Reigada & Mitchell, 2005)	53.2 (32.9, 73.4)	5	<0.001
		Glybenclamide (Reigada & Mitchell, 2005)	64.1 (52.9, 75.3)	2	0.78
		Overall	61.5 (51.7, 71.4)	7	0.99
	vesicular	brefeldin A (Reigada & Mitchell, 2005)	69.9 (63, 76.8)	1	-
Retinal glial					
	pannexin 1	10panx1 (Xia et al., 2012)	72.6 (54, 91.1)	1	-
		Carbenoxolone (Xia et al., 2012)	36.4 (21.7, 51)	2	0.86
		Probenecid (Xia et al., 2012)	39.6 (24.2, 55)	2	0.93
		Overall	48.8 (27.8, 69.8)	5	0.04
t-lymphocytes					
	maxi-anion	Gd^{3+} (Woehrle et al., 2010)	30.7 (6, 55.5)	3	0.11
	Note: Gd^{3+} inhibited ATP release, however insufficient data to resolve maxi anion involvement.				
	P2RX7	Gd^{3+} (Woehrle et al., 2010)	30.7 (6, 55.5)	3	0.11
	Note: Gd^{3+} inhibited ATP release, however insufficient data to resolve P2RX7 involvement.				
	pannexin 1	10panx1 (Woehrle et al., 2010)	27.3 (0.6, 54)	3	0.36
		panx1 knockdown (Woehrle et al., 2010)	57.7 (44.9, 70.5)	3	0.04
		Overall	44.9 (15.4, 74.3)	6	0.54
	piezo1	Gd^{3+} (Woehrle et al., 2010)	30.7 (6, 55.5)	3	0.11
	Note: Gd^{3+} inhibited ATP release, however insufficient data to resolve Piezo1 involvement.				
	TRPV4	Gd^{3+} (Woehrle et al., 2010)	30.7 (6, 55.5)	3	0.11
	Note: Gd^{3+} inhibited ATP release, however insufficient data to resolve TRPV4 involvement.				
Trabecular meshwork					
	actin	Cytochalasin D (A. Li, Leung, Peterson-Yantorno, Stamer, & Civan, 2011)	-45.9 (-55.3, -36.5)	1	-
		Dexamethasone* (A. Li, Leung, et al., 2011)	36.4 (24.5, 48.4)	1	-
		Overall	-45.9 (-55.3, -36.5)	1	-
	ATP synthase	Piceatannol (Luna et al., 2009)	-65.6 (-148.8, 17.6)	1	-
	CFTR	Glybenclamide (A. Li, Leung, et al., 2012)	2.9 (1.3, 4.5)	1	-
		Niflumic acid (A. Li, Leung, et al., 2012)	29.3 (-15.3, 73.9)	1	-
		Overall	6.3 (-11, 23.6)	2	0.25

	cholesterol	MβCD (Luna et al., 2009)	-2776.8 (-4126.8, -1426.8)	1	-
	connexin	Heptanol (A. Li, Leung, et al., 2011; A. Li, Leung, et al., 2012)	39.4 (29.8, 49)	3	0.94
		Carbenoxolone (A. Li, Leung, et al., 2012)	37.7 (5.2, 70.1)	2	0.76
		Mefloquine (A. Li et al., 2010)	24.3 (19.6, 29)	1	-
		NFA (A. Li, Leung, et al., 2012)	29.3 (23.2, 35.4)	1	-
		Overall	30.2 (23.3, 37.2)	7	0.21
	maxi-anion	Gd^{3+} (A. Li, Leung, et al., 2012)	3.1 (-3.8, 10)	1	-
		SITS (A. Li, Leung, et al., 2012)	2.4 (-3.7, 8.5)	1	-
		Overall	2.7 (-1.8, 7.3)	2	0.88
	P2RX7	Brilliant blue G (A. Li, Leung, et al., 2012)	31.6 (25.5, 37.7)	1	-
		KN62 (A. Li, Leung, et al., 2011; A. Li, Leung, et al., 2012)	33.9 (24.9, 42.9)	2	0.95
		A438079 (A. Li, Leung, et al., 2012)	29.2 (21.4, 37)	1	-
		Overall	31.4 (27.2, 35.6)	4	0.90
	pannexin	Carbenoxolone (A. Li, Leung, et al., 2012)	37.7 (5.2, 70.1)	2	0.76
		Mefloquine (A. Li, Leung, et al., 2012)	24.3 (19.6, 29)	1	-
		Probenecid (A. Li, Leung, et al., 2011; A. Li, Leung, et al., 2012)	35.6 (30.5, 40.7)	2	0.99
		DTT (A. Li, Leung, et al., 2012)	26.4 (24, 28.8)	1	-
		NPPB (A. Li, Leung, et al., 2011)	32 (23.5, 40.6)	1	-
		Overall	29.2 (24.5, 34.0)	7	0.03
	piezo1	Gd^{3+} (A. Li, Leung, et al., 2012)	3.1 (-3.8, 10)	1	-
	Tyrosine kinase	Lavendustin C (A. Li, Leung, et al., 2012)	5.4 (-5.2, 16)	1	-
	TRPV4	Gd^{3+} (A. Li, Leung, et al., 2012)	3.1 (-3.8, 10)	1	-
	vesicular	Bafilomycin (A. Li, Leung, et al., 2011; A. Li, Leung, et al., 2012)	2.9 (-4.6, 10.3)	2	0.94
		NEM (Luna et al., 2009)	92.1 (72.4, 111.8)	1	-
		Monensin (A. Li, Leung, et al., 2012; Luna et al., 2009)	39.4 (-60.8, 139.6)	2	0.01
		Overall	45.2 (-29.7, 120.2)	5	<0.001
	VRAC	Verapamil (A. Li, Leung, et al., 2012)	0.9 (-4.6, 6.4)	1	-

Note: Luna et al. 2009 reported vesicular-dependent MSAR in response to stretching
Li et al. 2011 reported vesicular-independent MSAR in response to hypotonic stress.

		DCPIB (A. Li, Leung, et al., 2012)	9 (3, 15)	1	-
		Glybenclamide (A. Li, Leung, et al., 2012)	2.9 (1.3, 4.5)	1	-
		DIDS (A. Li, Leung, et al., 2012)	4.1 (-8.8, 17)	1	-
		Overall	3.6 (0.7, 6.5)	3	0.11
Note: Despite involvement in ATP release, relative contribution of VRAC is minimal.					
	other	Orthovanadate (Luna et al., 2009)	13711 (-13162.5, 40584.5)	1	-
Umbilical vein endothelial					
	calcium (extracellular)	Calcium free (Bodin & Burnstock, 2001)	53 (17.9, 88.2)	1	-
	CFTR	Glybenclamide (E. C. Wang et al., 2005)	-13.3 (-54.4, 27.8)	1	-
	piezo1	Piezo1 knockdown (S. Wang et al., 2016)	59.2 (30.2, 88.2)	1	-
	rho kinase	Y27632 (Hirakawa, Oike, Karashima, & Ito, 2004)	89.2 (64.2, 114.1)	1	-
	tyrosine kinase	Tyrphostin 46 (Hirakawa et al., 2004)	86.9 (40.3, 133.5)	1	-
		Herbimycin A (Hirakawa et al., 2004)	77.7 (27.4, 128.1)	1	-
		Overall	82.7 (48.5, 116.9)	2	0.79
	vesicular	Monensin (Bodin & Burnstock, 2001)	75.3 (25.2, 125.5)	1	-
		NEM (Bodin & Burnstock, 2001)	96.7 (73.3, 120.1)	1	-
		Overall	92.9 (71.7, 114.1)	2	0.45
	VRAC	Verapamil (Bodin & Burnstock, 2001; E. C. Wang et al., 2005)	-23.9 (-96.9, 49.2)	1	-
		Glybenclamide (Bodin & Burnstock, 2001)	-13.3 (-54.4, 27.8)	1	-
		Overall	-15.8 (-51.7, 20)	2	0.80
	other	PI-PLC (Yegutkin, Bodin, & Burnstock, 2000)	25.8 (-17.5, 69.1)	1	-
		Lipopolysaccharide (Bodin & Burnstock, 1998)	-153.2 (-337.4, 31.1)	1	-
Urothelial Cells					
	Calcium (intracellular)	BAPTA-AM (Ochodnicky et al., 2013; Olsen, Stover, & Nagatomi, 2011)	30.1 (18.7, 41.4)	2	0.34
		Thapsigargin (Ochodnicky et al., 2013)	25.2 (11.3, 39.1)	1	-

		Overall	34.9 (19.5, 50.3)	4	0.12
	calcium (extracellular)	Calcium free (Miyamoto et al., 2014)	59.2 (34.9, 83.5)	1	-
	CFTR	Glybenclamide (Knight, Bodin, De Groat, & Burnstock, 2002)	36.6 (-0.7, 73.8)	3	0.35
		Note: Sensitivity to glybenclamide possibly due to VRAC involvement			
	connexin	Flufenamic acid (E. C. Wang et al., 2005)	25.4 (-66.5, 117.3)	2	0.04
	ENaC	Amiloride (Birder et al., 2003; Olsen et al., 2011)	84.7 (24.4, 145.1)	2	0.04
	L-Type VSCC	nifedipine(Olsen et al., 2011)	22 (-512.5, 556.5)	1	-
	MEK1/2	U0126 (Ochodnicky et al., 2013)	-7.1 (-29.2, 14.9)	1	-
	P2RX7	P2RX7 knockout (Negoro et al., 2014)	61.1 (13.2, 109.0)	1	-
	pannexin 1	Mefloquine (Negoro et al., 2014)	55.6 (12.0, 99.1)	1	-
		Panx1 knockout (Negoro et al., 2014)	77.8 (16.8, 138.8)	1	-
		Overall	63.1 (27.6, 98.5)	2	0.56
	PKC	Gö6976 (Ochodnicky et al., 2013)	8.2 (-25.8, 42.3)	1	-
	piezo1	Piezo1 knockdown (Miyamoto et al., 2014)	31.4 (6.5, 56.3)	1	-
		Ruthenium red (Olsen et al., 2011)	147.2 (95.1, 199.2)	1	-
		Gd^{3+} (Birder et al., 2003; Knight et al., 2002; Olsen et al., 2011)	72.7 (58.3, 87)	3	0.98
		Overall	77.5 (32, 123)	5	<0.01
	TRPV1/4	Anandamide (E. C. Wang et al., 2005)	95.5 (91.9, 99.1)	2	0.56
		Ruthenium red (Olsen et al., 2011)	147.2 (95.1, 199.2)	1	-
		Gd^{3+} (Birder et al., 2003; Knight et al., 2002; Olsen et al., 2011)	72.7 (58.3, 87)	3	0.98
		TRPV1 knockout (Birder et al., 2002)	92.5 (69, 116)	1	-
		TRPV4 knockout (Gevaert et al., 2007)	90 (50.8, 129.2)	1	-
		Overall	91.6 (76.4, 106.9)	8	0.07
	vesicular	Brefeldin A (Birder et al., 2003; Knight et al., 2002; E. C. Wang et al., 2005)	94.3 (87.8, 100.8)	4	0.03

		Monensin (Birder et al., 2003; Knight et al., 2002)	94.4 (87.4, 101.3)	2	0.40
		Botulinum toxin A (Hanna-Mitchell et al., 2015; Smith, Vemulakonda, Kiss, Boone, & Somogyi, 2005)	95.4 (89.9, 100.8)	2	0.90
		Dipyridamole (E. C. Wang et al., 2005)	90.1 (82.5, 97.8)	2	0.78
		Overall	94 (90.7, 97.2)	10	1.00
	VRAC	Verapamil (E. C. Wang et al., 2005)	88.1 (79.5, 96.7)	2	0.34
		Glybenclamide (Knight et al., 2002)	36.6 (-0.7, 73.8)	3	0.35
		Overall	65.6 (15.6, 115.7)	5	0.14
	other	Cyclophosphamide (Smith et al., 2005)	-518.7 (-7049.2, 6011.8)	1	-
		Histamine (Mansfield & Hughes, 2014)	21.8 (5.2, 38.5)	6	0.10
		Serotonin (Mansfield & Hughes, 2014)	26.2 (16.6, 35.8)	6	0.43
		Silodosin (Matos et al., 2016)	-66.6 (-163.5, 30.3)	1	-

Table 4-S7. ATP release in pathologies. Relative effect (%) of pathology on ATP release compared to unaffected controls. $D_{\downarrow\uparrow}$: specifies direction of effect, CI: confidence intervals, N: number of datasets per condition, I^2 and H^2: heterogeneity statistics, P_Q: p-value corresponding to Q heterogeneity statistic used to evaluate null hypothesis that all studies reported same effect, ADPKD: autosomal dominant polycystic kidney disease, ARPKD: autosomal recessive polycystic kidney disease, CF: cystic fibrosis, Epi.: epithelia, Glaucoma: primary acute angle closure glaucoma, FSS: fluid shear stress, RBC: red blood cells.

Pathologies	Meta-Analysis Summary Statistics					
	$D_{\downarrow\uparrow}$	Rel. Effect, % (±95% CI)	N	I^2 (%)	H^2	P_Q
Cystic fibrosis (Braunstein et al., 2001; Lazarowski, Shea, Boucher, & Harden, 2003; Okada et al., 2006; Okada et al., 2013; Sprague et al., 1998; Watt et al., 1998)	↓	-66.6 (-78.6, -54.5)	14	87.9	37.5	<0.001
RBC, pancreatic epi.	↓	-87.7 (-91.5, -83.8)	10	7.9	1.1	0.37
Airway epi., astrocyte	-	18.1 (-8.5, 44.7)	4	29.1	1.4	0.24
Colitis*(Wynn, Ma, Ruan, & Burnstock, 2004)	↑	248.1 (172.4, 323.8)	9	19.4	1.2	0.27
Diabetes, type II (Carroll et al., 2006)	↓	-49.6 (-75.0, -24.1)	1	-	-	-
Glaucoma (A. Li, Zhang, et al., 2011; W. Lu et al., 2015)	↑	1107.8 (539.0, 1676.6)	2	62.5	2.7	0.10
Hypoxia	-	20.3 (-55.9, 96.5)	8	97.4	37.8	<0.001
*Acute hypoxia** (Bodin & Burnstock, 1995)	↑	60.9 (46.4, 75.4)	7	0	0.8	0.53
Chronic hypoxia (Bodin, Milner, Winter, & Burnstock, 1992)	↓	-91.8 (-103.4, -80.2)	1	-	-	-
Ectopic ossification (Sawada et al., 2008)	-	4.5 (-38.4, 47.5)	1	-	-	-
Interstitial cystitis (Birder et al., 2003; Kumar, Chapple, Surprenant, & Chess-Williams, 2007; Smith et al., 2005; Sun & Chai, 2006; Sun, Keay, De Deyne, & Chai, 2001)	↑	107.7 (53.3, 162.0)	7	0	0.1	0.99
Polycystic kidney disease	-	7.8 (-43.1, 58.8)	7	92.5	13.3	<0.001
FSS – AD/ARPKD (Hovater et al., 2008; Xu et al., 2009)	↓	-72.9 (-98.9, -46.9)	2	0	<0.001	1.00
Hypotonic – ADPKD (E. M. Schwiebert et al., 2002; Wilson, Hovater, Casey, Fortenberry, & Schwiebert, 1999; Xu et al., 2009)	↑	92.9 (15.0, 170.7)	3	75.5	4.1	0.13
Hypotonic – ARPKD (Hovater et al., 2008; E. M. Schwiebert et al., 2002)	↓	-25.2 (-147.8, 97.3)	2	88.2	8.5	<0.01

Pulmonary hypertension*(Sprague, Stephenson, Ellsworth, Keller, & Lonigro, 2001)	↓	-56.6 (-73.0, -40.2)	3	0	0.8	0.43
Spinal cord injury (Smith et al., 2008)	↑	399.2 (-40.3, 838.6)	1	-	-	-
Xerocytosis, hereditary (Cinar et al., 2015)	↓	-61.9 (-71.9, -51.9)	1	-	-	-

*Pooled datasets are from same study

Table 4-S8. Database-specific search strategies

MEDLINE

1. exp Adenosine Triphosphate/
2. (adenosine triphosphate or ATP).ti,ab,kf.
3. 1 or 2
4. (mechanical* adj3 (stimulat* or perturb* or agitat* or compress* or strain* or transduc* or load* or vibrat* or stretch* or press* or displace* or force? or expose? or exposure? or stress* or shear* or deform* or swell* or shock* or shrink* or shrunk or mediat* or sensat* or perfus* or flow* or tension or release? or efflux or secret* or decompress* or stimulus or stimuli)).ti,ab,kf.
5. (fluid? adj3 (stimulat* or perturb* or agitat* or strain* or transduc* or load* or press* or displace* or shear* or shock* or shrink* or shrunk or flow* or tension)).ti,ab,kf.
6. ((osmotic* or hypotonic* or hydrostatic* or hypertonic* or membrane? or centrifug* or gravitatation* or gravity) adj3 (pressure? or compress* or swell* or shrink* or stretch* or shock* or deform* or stress* or stimulat* or challenge? or expose? or exposure?)).ti,ab,kf.
7. ((medium or media) adj3 (displace* or agitat* or perturb*)).ti,ab,kf.
8. (mechanotransduc* or mechanosens* or microgravit* or rotoblat* or ultrasound or ultrasonic* or (bead adj3 displace*) or (centrifug* adj3 force?) or hypotonicity or hypertonicity or (physical* adj3 perturb*)).ti,ab,kf.
9. exp Mechanotransduction, Cellular/
10. exp Mechanical Processes/
11. exp Pressure/
12. exp Biomechanical Phenomena/
13. physical stimulation/ or acoustic stimulation/
14. exp hypertonic solutions/ or exp hypotonic solutions/
15. or/4-14
16. 3 and 15
17. limit 16 to (English)

Embase

1. exp adenosine triphosphate/
2. (adenosine triphosphate or ATP).ti,ab,kw.
3. 1 or 2
4. exp mechanotransduction/
5. exp biomechanics/
6. exp hydrostatic pressure/
7. osmotic pressure/
8. exp osmotic stress/ or exp hyperosmotic stress/ or exp hypoosmotic stress/
9. exp auditory stimulation/

10. exp mechanical stimulation/
11. exp mechanical stress/ or exp contact stress/ or exp contraction stress/ or exp shear stress/ or exp surface stress/
12. (mechanical* adj3 (stimulat* or perturb* or agitat* or compress* or strain* or transduc* or load* or vibrat* or stretch* or press* or displace* or force? or expose? or exposure? or stress* or shear* or deform* or swell* or shock* or shrink* or shrunk or mediat* or sensat* or perfus* or flow* or tension or release? or efflux or secret* or decompress* or stimulus or stimuli)).ti,ab,kw.
13. (fluid? adj3 (stimulat* or perturb* or agitat* or strain* or transduc* or load* or press* or displace* or shear* or shock* or shrink* or shrunk or flow* or tension)).ti,ab,kw.
14. ((osmotic* or hypotonic* or hydrostatic* or hypertonic* or membrane? or centrifug* or gravitatation* or gravity) adj3 (pressure? or compress* or swell* or shrink* or stretch* or shock* or deform* or stress* or stimulat* or challenge? or expose? or exposure?)).ti,ab,kw.
15. ((medium or media) adj3 (displace* or agitat* or perturb*)).ti,ab,kw.
16. (mechanotransduc* or mechanosens* or microgravit* or rotoblat* or ultrasound or ultrasonic* or (bead adj3 displace*) or (centrifug* adj3 force?) or hypotonicity or hypertonicity or (physical* adj3 perturb*)).ti,ab,kw.
17. or/4-16
18. 3 and 17
19. limit 18 to (English)

SCOPUS

(TITLE-ABS-KEY ((adenosine triphosphate OR atp))) AND ((TITLE-ABS-KEY ((mechanical* W/3 (stimulat* OR perturb* OR agitat* OR compress* OR strain* OR transduc* OR load* OR vibrat* OR stretch* OR press* OR displace* OR force? OR expose? OR exposure? OR stress* OR shear* OR deform* OR swell* OR shock* OR shrink* OR shrunk)))) OR (TITLE-ABS-KEY ((mechanical* W/3 (mediate* OR sensate* OR perfuse* OR flow* OR tension* OR release? OR efflux OR secret* OR decompress* OR stimulus OR stimuli)))) OR (TITLE-ABS-KEY ((fluid? W/3 (stimulat* OR perturb* OR agitat* OR strain* OR transduc* OR load* OR press* OR displace* OR shear* OR shock* OR shrink* OR shrunk OR flow* OR tension)))) OR (TITLE-ABS-KEY (((osmotic* OR hypotonic* OR hydrostatic* OR hypertonic* OR membrane? OR centrifuge* OR gravitation* OR gravity) W/3 (pressure? OR compress* OR swell* OR shrink* OR stretch* OR shock* OR deform* OR stress* OR stimulat* OR challenge? OR expose?)))) OR (TITLE-ABS-KEY (((osmotic* OR hypotonic* OR hydrostatic* OR hypertonic* OR membrane? OR centrifuge* OR gravitation* OR gravity) W/3 (exposure?)))) OR (TITLE-ABS-KEY (((medium OR media) W/3 (displace* OR agitat* OR perturb*)))) OR (TITLE-ABS-KEY ((mechanotransduc* OR mechanosens* OR microgravit* OR rotoblat* OR ultrasound OR ultrasonic* OR (bead W/3 displace*) OR (centrifug* W/3 force?) OR hypotonicity OR hypertonicity OR (physical* W/3 perturb*)))))

Biosis

1. (adenosine triphosphate or ATP).ti,ab,kw

2. (mechanical* adj3 (stimulat* or perturb* or agitat* or compress* or strain* or transduc* or load* or vibrat* or stretch* or press* or displace* or force? or expose? or exposure? or stress* or shear* or deform* or swell* or shock* or shrink* or shrunk or mediat* or sensat* or perfus* or flow* or tension or release? or efflux or secret* or decompress* or stimulus or stimuli)).ti,ab,kw
3. (fluid? Adj3 (stimulat* or perturb* or agitat* or strain* or transduc* or load* or press* or displace* or shear* or shock* or shrink* or shrunk or flow* or tension)).ti,ab,kw
4. ((osmotic* or hypotonic* or hydrostatic* or hypertonic* or membrane? or centrifug* or gravitatation* or gravity) adj3 (pressure? or compress* or swell* or shrink* or stretch* or shock* or deform* or stress* or stimulat* or challenge? or expose? or exposure?)).ti,ab,kw
5. ((medium or media) adj3 (displace* or agitat* or perturb*)).ti,ab,kw
6. (mechanotransduc* or mechanosens* or microgravit* or rotoblat* or ultrasound or ultrasonic* or (bead adj3 displace*) or (centrifug* adj3 force?) or hypotonicity or hypertonicity or (physical* adj3 perturb*)).ti,ab,kw
7. 2 or 3 or 4 or 5 or 6
8. 1 and 7
9. Limit 8 to (English)

Table 4-S9. Systematically identified studies and their contributions to meta-analysis. Studies listed with no contributions were identified in the literature search but excluded from quantitative synthesis due to ineligible data reporting.

	A_{mech}	R_{mech}	t_{half}	Interventions	Pathologies
Number of studies	103	169	66	121	25
Number of datasets	123	212	74	681	51
(Karpatkin, 1969)					
(A. R. Williams & Miller, 1980)					
(Miller & Williams, 1983)					
(Milner et al., 1990)	x	x	x		
(Bodin et al., 1992)	x	x	x		x
(Milner, Bodin, Loesch, & Burnstock, 1992)	x	x	x		
(Enomoto, Furuya, Yamagishi, Oka, & Maeno, 1994)					
(Petruzzi et al., 1994)					
(Stuart, Anderson, French, Kirk, & Michell, 1994)					
(Bodin & Burnstock, 1995)	x	x	x		x
(Sprague, Ellsworth, Stephenson, & Lonigro, 1996)	x				
(Stones, Vials, Milner, Beard, & Burnstock, 1996)		x	x		
(Ferguson, Kennedy, & Burton, 1997)					
(Grygorczyk & Hanrahan, 1997)					
(Lazarowski, Homolya, Boucher, & Harden, 1997)	x	x	x		
(Bodin & Burnstock, 1998)	x	x		x	
(Feranchak et al., 1998)		x		x	
(Hamada, Takuwa, Yokoyama, & Takuwa, 1998)	x	x	x		
(Mitchell et al., 1998)		x	x	x	
(Sprague et al., 1998)	x	x		x	x
(Taylor et al., 1998)		x	x		
(Watt et al., 1998)				x	x
(M. S. Williams et al., 1998)					
(Feranchak et al., 1999)		x	x	x	
(Hazama et al., 1999)	x	x	x	x	
(Musante, Zegarra-Moran, Montaldo, Ponzoni, & Galietta, 1999)					
(Pedersen, Pedersen, Nilius, Lambert, & Hoffmann, 1999)					
(Roman, Feranchak, Davison, et al., 1999)		x		x	
(Roman, Feranchak, Salter, Wang, & Fitz, 1999)			x		
(Van der Wijk et al., 1999)	x	x	x	x	
(Wilson et al., 1999)		x	x		x
(Ahmed, Rzigalinski, Willoughby, Sitterding, & Ellis, 2000)	x	x			
(Feranchak et al., 2000)		x	x	x	

Table 4-S9. Systematically identified studies and their contributions to meta-analysis. Studies listed with no contributions were identified in the literature search but excluded from quantitative synthesis due to ineligible data reporting.

	A_{mech}	R_{mech}	t_{half}	Interventions	Pathologies
(Graff et al., 2000)	x	x		x	
(Hazama et al., 2000)		x		x	
(Oike, Kimura, Koyama, Yoshikawa, & Ito, 2000)	x	x			
(Ostrom, Gregorian, & Insel, 2000)	x				
(Salter, Fitz, & Roman, 2000)					
(Sauer et al., 2000)	x	x		x	
(Yegutkin et al., 2000)	x		x	x	
(Bodin & Burnstock, 2001)		x	x	x	
(Braunstein et al., 2001)				x	x
(Harada, Sakamoto, Niwa, & Nakaya, 2001)					
(Koyama et al., 2001)	x	x	x	x	
(Newman, 2001)					
(Ostrom et al., 2001)		x		x	
(Romanello et al., 2001)		x		x	
(Shinozuka et al., 2001)	x	x			
(Sorensen & Novak, 2001)	x	x			
(Sprague, Ellsworth, et al., 2001)	x			x	
(Sprague, Stephenson, et al., 2001)	x				x
(Sun et al., 2001)					x
(Vlaskovska et al., 2001)		x			
(Birder et al., 2002)				x	
(Dutta et al., 2002)	x	x		x	
(Guyot & Hanrahan, 2002)	x	x	x		
(Hisadome et al., 2002)	x	x		x	
(Knight et al., 2002)		x		x	
(Schwiebert, Rice, Kudlow, Taylor, & Schwiebert, 2002)					x
(Sprung, Sprague, & Spence, 2002)	x				
(C. E. Stout et al., 2002)				x	
(Birder et al., 2003)	x			x	x
(Fischer, Torrence, Sprung, & Spence, 2003)					
(Graff & Lee, 2003)	x	x	x		
(Joseph, Buchakjian, & Dubyak, 2003)	x	x			
(Koizumi, Fujishita, Tsuda, Shigemoto-Mogami, & Inoue, 2003)					
(Lazarowski et al., 2003)	x		x		x
(Loomis, Namiki, Ostrom, Insel, & Junger, 2003)	x	x			

Table 4-S9. Systematically identified studies and their contributions to meta-analysis. Studies listed with no contributions were identified in the literature search but excluded from quantitative synthesis due to ineligible data reporting.

	A_{mech}	R_{mech}	t_{half}	Interventions	Pathologies
(Pines et al., 2003)	x	x			
(Rich, Douillet, Mahler, Husain, & Boucher, 2003)		x			
(C. Stout & Charles, 2003)				x	
(Takemura et al., 2003)	x			x	
(Tsuzaki et al., 2003)	x		x		
(van der Wijk, Tomassen, Houtsmuller, de Jonge, & Tilly, 2003)		x			
(Wynn, Rong, Xiang, & Burnstock, 2003)		x			
(Yamamoto et al., 2003)	x	x	x		
(Yamazaki et al., 2003)	x	x			
(Yao et al., 2003)	x	x			
(Boudreault & Grygorczyk, 2004)	x	x	x		
(Chen, Shukla, Namiki, Insel, & Junger, 2004)	x	x			
(Dutta et al., 2004)		x	x	x	
(Gatof et al., 2004)		x	x	x	
(Hirakawa et al., 2004)	x	x		x	
(Koizumi et al., 2004)					
(Kumar, Chapple, & Chess-Williams, 2004)		x			
(Millward-Sadler, Wright, Flatman, & Salter, 2004)		x			
(Okada et al., 2004)	x			x	
(Olearczyk et al., 2004)	x	x		x	
(Oury et al., 2004)	x	x	x	x	
(Price, Fischer, Martin, & Spence, 2004)	x				
(Selzner et al., 2004)	x	x			
(Soto et al., 2004)	x				
(Tomassen et al., 2004)		x		x	
(Wynn et al., 2004)		x			x
(Furuya, Sokabe, & Furuya, 2005)					
(Genetos et al., 2005)	x	x	x	x	
(Godecke, Stumpe, Schiller, Schnittler, & Schrader, 2005)					
(Gomes, Srinivas, Van Driessche, Vereecke, & Himpens, 2005)					
(Hayton et al., 2005)	x		x		
(J. Li et al., 2005)	x	x		x	
(Neary, Kang, Tran, & Feld, 2005)					
(A. S. Patel et al., 2005)					
(Reigada & Mitchell, 2005)		x	x	x	

Table 4-S9. Systematically identified studies and their contributions to meta-analysis. Studies listed with no contributions were identified in the literature search but excluded from quantitative synthesis due to ineligible data reporting.

	A_{mech}	R_{mech}	t_{half}	Interventions	Pathologies
(Romanello et al., 2005)	x	x	x	x	
(Smith et al., 2005)		x		x	x
(Tarran et al., 2005)					
(E. C. Wang et al., 2005)		x		x	
(Zhao, Yu, & Fleming, 2005)		x	x		
(Carroll et al., 2006)	x				x
(Gomes, Srinivas, Vereecke, & Himpens, 2006)					
(Grafe, Schaffer, & Rucker, 2006)					
(Hong, Jaron, Buerk, & Barbee, 2006)	x	x			
(Lewis & Lewis, 2006)		x			
(Locovei et al., 2006)		x		x	
(Moehlenbrock et al., 2006)	x			x	
(Nandigama et al., 2006)	x	x		x	
(Okada et al., 2006)			x	x	x
(Price et al., 2006)				x	
(Sun & Chai, 2006)		x			x
(Ullrich et al., 2006)		x	x		
(Yoshida, Kobayashi, Ohkubo, & Nakahata, 2006)	x	x			
(Zhou, Ferraris, & Burg, 2006)		x			
(Button, Picher, & Boucher, 2007)		x			
(Chow, Liton, Luna, Wong, & Gonzalez, 2007)		x	x		
(Corriden, Insel, & Junger, 2007)					
(Du et al., 2007)		x			
(Fiorotto et al., 2007)		x		x	
(Genetos et al., 2007)	x	x		x	
(Gevaert et al., 2007)		x		x	
(Gradilone et al., 2007)	x	x		x	
(Karczewska, Martyniec, Dzierzko, Stepinski, & Angielski, 2007)		x			
(Kumar et al., 2007)		x			x
(Resta et al., 2007)					
(Riddle et al., 2007)		x		x	
(Salas, Somogyi, Gangitano, Boone, & Smith, 2007)					
(Tatur et al., 2007)	x	x	x	x	
(Yamamoto et al., 2007)		x		x	
(Yin, Xu, Zhang, Kumar, & Yu, 2007)	x	x			
(Yip et al., 2007)					

Table 4-S9. Systematically identified studies and their contributions to meta-analysis. Studies listed with no contributions were identified in the literature search but excluded from quantitative synthesis due to ineligible data reporting.

	A_{mech}	R_{mech}	t_{half}	Interventions	Pathologies
(X. Zhang et al., 2007)		x			
(Calvert, Thompson, & Burnstock, 2008)		x			
(Hovater et al., 2008)		x			x
(Kempson, Edwards, Osborn, & Sturek, 2008)	x	x			
(J. Li et al., 2008)		x			
(H. T. Liu et al., 2008)	x	x	x	x	
(Matsuka et al., 2008)	x	x			
(Reigada, Lu, Zhang, & Mitchell, 2008)		x			
(Riddle, Hippe, & Donahue, 2008)		x			
(Sawada et al., 2008)	x	x			x
(Silva & Garvin, 2008)	x	x		x	
(Smith et al., 2008)		x			x
(Taguchi, Kozaki, Katanosaka, & Mizumura, 2008)					
(Tatur, Kreda, Lazarowski, & Grygorczyk, 2008)					
(Toma et al., 2008)				x	
(Wan et al., 2008)	x			x	
(Woo et al., 2008)				x	
(Y. Zhang, Phillips, Li, & Yeung, 2008)					
(Gardinier, Majumdar, Duncan, & Wang, 2009)					
(Koyama et al., 2009)	x	x		x	
(Luna et al., 2009)				x	
(Matsumoto-Miyai, Kagase, Murakawa, Momota, & Kawatani, 2009)					
(McIlwrath, Davis, & Bielefeldt, 2009)		x			
(Mochizuki, Araki, Yoshiyama, & Takeda, 2009)	x				
(Ransford et al., 2009)				x	
(Tolan et al., 2009)				x	
(Xu et al., 2009)	x	x		x	x
(Alvarenga et al., 2010)		x	x		
(Blum et al., 2010)	x	x	x	x	
(Feranchak et al., 2010)		x	x	x	
(Gonzales et al., 2010)					
(Kawai, Yokoyama, Kaidoh, & Ohhashi, 2010)		x			
(Kumar, Chapple, Rosario, Tophill, & Chess-Williams, 2010)		x			
(A. Li et al., 2010)				x	
(Varela et al., 2010)	x	x			

Table 4-S9. Systematically identified studies and their contributions to meta-analysis. Studies listed with no contributions were identified in the literature search but excluded from quantitative synthesis due to ineligible data reporting.

	A_{mech}	R_{mech}	t_{half}	Interventions	Pathologies
(Woehrle et al., 2010)	x	x		x	
(Woo et al., 2010)		x	x	x	
(Azorin et al., 2011)	x	x	x	x	
(David Holtzclaw et al., 2011)	x	x		x	
(Dolovcak et al., 2011)		x		x	
(A. Li, Leung, et al., 2011)		x		x	x
(A. Li, Zhang, et al., 2011)	x	x			
(Luckprom et al., 2011)		x	x	x	
(Olsen et al., 2011)		x		x	
(Ramsingh et al., 2011)				x	
(Sathe et al., 2011)		x	x	x	
(Seminario-Vidal et al., 2011)		x	x	x	
(Tanaka et al., 2011)					
(Thompson et al., 2011)		x		x	
(Thrane et al., 2011)	x	x		x	
(Xing et al., 2011)	x		x	x	
(Yamamoto et al., 2011)				x	
(Akopova et al., 2012)				x	
(Cabral, Hong, & Garvin, 2012)					
(Islam et al., 2012)	x	x	x	x	
(Kawai, Kaidoh, Yokoyama, & Ohhashi, 2012)		x			
(Kawai, Yoshida, Kaidoh, Yokoyama, & Ohhashi, 2012)		x			
(A. Li, Banerjee, et al., 2012)				x	
(A. Li, Leung, et al., 2012)		x	x		
(D. Lu et al., 2012)		x		x	
(Oishi et al., 2012)	x	x	x	x	
(Rumney, Sunters, Reilly, & Gartland, 2012)		x	x		
(Sadananda, Kao, Liu, Mansfield, & Burcher, 2012)					
(Shahidullah, Mandal, Beimgraben, et al., 2012)		x	x	x	
(Shahidullah, Mandal, & Delamere, 2012)		x			
(Vick & Delay, 2012)		x			
(Wann et al., 2012)		x			
(Xia et al., 2012)		x		x	
(Young, Matharu, Carew, & Fry, 2012)					
(Bjaelde et al., 2013)	x			x	
(Button et al., 2013)		x		x	

Table 4-S9. Systematically identified studies and their contributions to meta-analysis. Studies listed with no contributions were identified in the literature search but excluded from quantitative synthesis due to ineligible data reporting.

	A_{mech}	R_{mech}	t_{half}	Interventions	Pathologies
(Dagenais et al., 2013)	x	x			
(Espelt et al., 2013)		x	x	x	
(Grygorczyk, Furuya, & Sokabe, 2013)					
(Hecht et al., 2013)				x	
(Kawai et al., 2013)		x		x	
(Langevin et al., 2013)		x	x		
(Y. Li et al., 2013)	x	x	x		
(Mairbaurl, Ruppe, & Bartsch, 2013)	x	x	x		
(Noma et al., 2013)					
(Ochodnicky et al., 2013)	x	x	x	x	
(Okada et al., 2013)	x	x	x	x	x
(Rodat-Despoix, Hao, Dandonneau, & Delmas, 2013)					
(Rosenthal et al., 2013)	x	x		x	
(Tong, Zhou, Perelman, & Kolosov, 2013)	x				
(L. Wang et al., 2013)	x		x	x	
(N. Wang et al., 2013)	x	x			
(Yamamoto & Ando, 2013)		x		x	
(Beckel et al., 2014)	x	x		x	
(Chi et al., 2014)				x	
(Egbuniwe et al., 2014)		x			
(Fucikova et al., 2014)		x			
(Furuya, Sokabe, & Grygorczyk, 2014)					
(Gardinier, Gangadharan, Wang, & Duncan, 2014)					
(Haanes et al., 2014)					
(Kanjanamekanant et al., 2014)		x		x	
(Kringelbach, Aslan, Novak, Schwarz, & Jorgensen, 2014)	x				
(Mansfield & Hughes, 2014)	x	x		x	
(McLatchie, Young, & Fry, 2014)	x				
(Miyamoto et al., 2014)				x	
(Murata et al., 2014)					
(Negoro et al., 2014)		x		x	
(Ohbuchi et al., 2014)		x		x	
(B. A. Patel, 2014)		x		x	
(Segawa et al., 2014)		x	x		
(Sikora et al., 2014)	x	x		x	
(Takada, Furuya, & Sokabe, 2014)					

Table 4-S9. Systematically identified studies and their contributions to meta-analysis. Studies listed with no contributions were identified in the literature search but excluded from quantitative synthesis due to ineligible data reporting.

	A_{mech}	R_{mech}	t_{half}	Interventions	Pathologies
(Takahara et al., 2014)		x	x	x	
(Xing et al., 2014)				x	
(T. Zhang et al., 2014)	x			x	
(Chen et al., 2015)	x	x		x	
(Cinar et al., 2015)	x			x	x
(Furlow et al., 2015)				x	
(Govitvattana, Osathanon, Toemthong, & Pavasant, 2015)		x			
(Hanna-Mitchell et al., 2015)		x		x	
(Heo et al., 2015)					
(Kowal et al., 2015)				x	
(Kringelbach et al., 2015)	x	x	x	x	
(X. Liu et al., 2015)		x			
(W. Lu et al., 2015)		x			x
(Manaka et al., 2015)	x		x		
(S. Wang et al., 2015)	x	x			
(Yu, 2015)		x	x		
(Contreras-Sanz et al., 2016)		x			
(Cui, Liu, Qin, Wang, & Huang, 2016)					
(Forst et al., 2016)					
(Furuya et al., 2016)					
(Heo et al., 2016)		x		x	
(Krick et al., 2016)				x	
(Leal Denis et al., 2016)	x	x	x		
(Y. Li, Wang, Xing, Wang, & Luo, 2016)	x	x	x		
(Matos et al., 2016)	x			x	
(Mihara et al., 2016)		x			
(Sano et al., 2016)		x			
(Seref-Ferlengez et al., 2016)		x		x	
(Steward, Kelly, & Wagner, 2016)		x			
(S. Wang et al., 2016)	x		x	x	
(Zappia et al., 2016)					

Table 4-S10. Study level characteristics extracted for each study and used in subgroup analyses.

Characteristic	Description	Subgroups
Experimental Characteristics		
ATP calibration	Specifies whether ATP calibrations were available to convert ATP units to moles/cell.	Reported, not reported
ATP degradation	Specifies whether extracellular ATP degradation was neutralized. Any of the following methods were considered appropriate to neutralize ATP degradation: perchloric acid (acid), TCA (acid), citric acid (acid), centrifuge (cell depletion), heat inactivation (heat), ARL67156 (pharmacological), Ebselen (pharmacological), Levamisole (pharmacological), βγMe-ATP (pharmacological), Suramin (pharmacological), Reactive Blue 2 (pharmacological).	neutralized/inhibited, present
Mechanical injury	Specifies whether cellular injury was detected following mechanical stimulation using any of the following method: dye exclusion, dye retention, reduction potential, cytosolic leakage (i.e., LDH, haemoglobin), functional assay, visual inspection, caspase/annexin V assay.	Detected, not detected, not reported
Mechanical stimulus	Specifies type of mechanical stimulation applied	Compression, fluid shear stress (FSS), injury, membrane deformation, osmotic pressure, tissue distension, red blood cell (RBC) deformation, strain, ultrasound, gravitational, vibrational
Mechanical magnitude	Specifies magnitude of mechanical stimulations. Magnitude of FSS (dynes/cm^2), strain (% stretch), hypotonic pressure (Δ mOsm/L), hypertonic pressure (Δ mOsm/L), compression (cmH_2O), red blood cell deformation (μm^{-1}) were collected.	Numerical.

Table 4-S10. Study level characteristics extracted for each study and used in subgroup analyses.

Characteristic	Description	Subgroups
Media type	Specifies type of media used during experiments. This does not include type of media used for culturing cells prior to experiment	Balanced salt solution (ex. Krebs, Ringer's, HBSS, DPBS), basal/complex media (ex. DMEM, MEM, αMEM), not reported
Recording method	Specifies whether samples were measured directly in real-time (online) or if samples were collected and measured afterwards (offline)	Online, offline
Repetitive stimulus	Specifies whether mechanical stimulus was cyclic or not.	Static, cyclic
Sampling method	Specifies whether bulk or perfusion-based sample collection was used.	Bulk, perfusion, not reported
Substrate	Specifies type of substrate adherent cells were plated on. Data not collected for cells in suspension and ex vivo/in vivo experiments.	Glass/plastic, silicon, not reported
Substrate coating	Specifies coating conditions applied onto culture substrate that adherent cells were plated on. Data not collected for cells in suspension and ex vivo/in vivo experiments.	Collagen, fibronectin, gelatin, poly-(L/D)-lysine, not reported
Temperature	Specifies temperatures at which experiments were conducted. Temperatures were binned.	≥30°C, <30°C, not reported
Biological Characteristics		
Adhesion phenotype	Specifies where cells used were adherent or in suspension	Adherent, suspension
Cell type	Specifies type of cell used	Listed in **Table 4-S2** and **Table 4-S4**

Table 4-S10. Study level characteristics extracted for each study and used in subgroup analyses.

Characteristic	Description	Subgroups
Culture type	Specifies type of cell culture used	Cell line, primary culture
Embryonic origin	Species embryonic origin of cells used	Endoderm, mesoderm, ectoderm
Epithelial polarity	Specifies whether apical or basolateral surface was sampled from polarized epithelial culture	Apical, basolateral, not applicable (ex. non-epithelial cells)
Experimental environment	Specifies whether the experimental setup involved an in vitro (cells in culture), ex vivo (tissue explant in culture) or in vivo (in situ in live animal) system	In vitro, ex vivo, in vivo
Organ system	Specifies organ system from which experimental model is derived	Hematopoietic, cardiovascular, integumentary, endocrine, hepatobiliary, musculoskeletal, nervous, reproductive, respiratory, sensory, urinary, gastrointestinal, other/mixed
Species	Specifies which species the experimental model was derived	Porcine, guinea pigs, rat, bovine, murine, human, rabbit, canine, not reported
<u>Intervention Characteristics</u>		
Pathological condition	Specifies pathological model used in experiments	Autosomal recessive polycystic kidney disease (ARPKD), cystic fibrosis, hereditary xerocytosis, pulmonary hypertension, acute or chronic hypoxia, type II diabetes, autosomal dominant polycystic kidney disease (ADPKD), ossification (of the posterior longitudinal ligament of the spine), interstitial cystitis, colitis, spinal cord injury,

Table 4-S10. Study level characteristics extracted for each study and used in subgroup analyses.

Characteristic	Description	Subgroups
		primary acute angle closure glaucoma (PAACG).
Intervention	Specifies type of pharmacological or genetic intervention used in intervention studies	Listed in **Table 4-S5** and **Table 4-S6**.

Table 4-S11: Experimental parameter assumptions for ATP unit conversion. *Top table* describes how unavailable (output) parameters were calculated based on available (input) parameters and assumed parameter values (assumption). Assumed cell-related parameters are shown in *middle table*, and culture dish-dependent parameters shown in the *bottom table*.

Input parameter(s)	Assumed parameter	Calculation	Output parameter
Cytocrit/hematocrit (CC, %), total volume (TV)	Cell volume (CV)	N = (CC x TV) / CV	Cell number (N)
Protein mass (PM)	Protein / cell (PC)	N = PM / PC	Cell number (N)
DNA mass (DM)	DNA / cell (DC)	N = DM / DC	Cell number (N)
Confluence (C, %), surface area (SA)	Confluent Cell Density (D)	N = SA x C x D	Cell number (N)
Culture Plate	Volume (V)	V	Volume (V)

Assumed parameters	Assumed values
Protein / cell (PC)	320 (pg/cell)
Mammalian cell volume (CV)	2.41 (pL)
RBC volume (CV)	0.10 (pL)
Platelet volume (CV)	0.10 (pL)
Cellular density at confluence (D)	10^5 cells / cm^2

Culture Dish	Surface area	Assumed parameters
	(SA, cm^2)	Volume (V, mL)
10 cm	55	10
6 well (35mm)	9.6	2
48 well	1	1
96 well	0.3	0.2

A3. Chapter 5 Supplemental Methods

Supplemental methods referenced in **Chapter 5** are provided here.

A3.1 Third-order Hermite Polynomials

Two third-order Hermite polynomials have been used in a piecewise-defined manner to form a spline,

$$H_1(x) = \left(2x_1^{\,3} - 3x_1^{\,2} + 1\right)a_0 + \left(x_1^{\,3} - 2x_1^{\,2} + x_1\right)b_0 + \left(-2x_1^{\,3} + 3x_1^{\,2}\right)a_1$$
$$H_2(x) = \left(2x_2^{\,3} - 3x_2^{\,2} + 1\right)a_1 + \left(-2x_2^{\,3} + 3x_2^{\,2}\right)a_2 + \left(x_2^{\,3} - x_2^{\,2}\right)b_2,$$

where $x_1 = \left(t - \rho_{act}\right)/\left(t_{de} - \rho_{act}\right)$ and $x_2 = \left(t - t_{de}\right)/\left(\rho_{de} - t_{de}\right)$. The 6 parameters a_0, a_1, a_2 (the spline values) and b_0, b_1, and b_2 (the spline tangents) are completely defined in terms of the response parameters, as follows:

$$a_0 = A_{act}\frac{\rho_{act}^{\,n_{act}}}{\rho_{act}^{\,n_{act}} + \beta^{\,n_{act}}} + m_{act}\int_0^{\rho_{act}} \frac{x^{\,n_{act}}}{x^{\,n_{act}} + \beta^{\,n_{act}}}dx$$

$$b_0 = A_{act}\frac{n_{act}\beta^{\,n_{act}}\rho_{act}^{\,n_{act}-1}}{\left(\rho_{act}^{\,n_{act}} + \beta^{\,n_{act}}\right)^2} + m_{act}\frac{\rho_{act}^{\,n_{act}}}{\rho_{act}^{\,n_{act}} + \beta^{\,n_{act}}}$$

$$a_1 = A_{act}\frac{\ell_{act}^{\,n_{act}}}{\ell_{act}^{\,n_{act}} + \beta^{\,n_{act}}} + m_{act}\int_0^{\ell_{act}} \frac{x^{\,n_{act}}}{x^{\,n_{act}} + \beta^{\,n_{act}}}dx$$

$$a_2 = A_{de}\frac{\rho_{de}^{\,n_{de}}}{\rho_{de}^{\,n_{de}} + \gamma^{\,n_{de}}} + m_{de}\int_0^{\rho_{de}} \frac{x^{\,n_{de}}}{x^{\,n_{de}} + \gamma^{\,n_{de}}}dx + \left(f_1 - A_{de}\right)$$

$$b_2 = -A_{de}\frac{n_{de}\gamma^{\,n_{de}}\rho_{de}^{\,n_{de}-1}}{\left(\rho_{de}^{\,n_{de}} + \gamma^{\,n_{de}}\right)^2} + m_{de}\frac{\rho_{de}^{\,n_{de}}}{\rho_{de}^{\,n_{de}} + \beta^{\,n_{de}}},$$

where implicit in this formalism that $b_1 = 0$ (to make a_1 correspond to the local maximum of the spline).

A4. Calcium Analyzer User Guide

In this section, the implementation of the calcium signal characterization algorithm developed in **Chapter 5** is described.

Calcium analyzer is freely accessible at:
https://github.com/NMikolajewicz/Calcium-Signal-Analyzer

A4.1 Introduction

Calcium Analyzer is an algorithm for systematic characterization of calcium recordings in cells. It uses a graphical interface, allowing researchers with minimal computation background to characterize their calcium data. Data is imported directly from spreadsheet into MATLAB where the characterization is conducted.

Scope of Guide. This user guide is intended as a guide on how to use the Calcium Analyzer and not as mathematical description of how calcium traces are characterized. The underlying equations and techniques are not included in this guide; They are described in **Chapter 5**.

Prerequisites. Users must have MATLAB R2016b (or later) installed along with the following toolboxes with specified versions or later:

Signal Processing Toolbox v7.3
Image Processing Toolbox v9.5
Statistics and Machine Learning Toolbox v11.0
Curve Fitting Toolbox v3.5.4.

Spreadsheet formats supported by Calcium Analyzer are XLSX and XLS files. All files provided in the Calcium Analyzer installation folder must be kept in a designated directory.

Contact. Please report any problems/bugs to Laurent.Mackay@mail.mcgill.ca or Nicholas.Mikolajewicz@mail.mcgill.ca.

A4.2 Implementation

Step 1. Prepare data input file.

- Input data must be prepared in spreadsheet (.xlsx or .xls)
- Data are organized in columns such that first column represents time vector (**Fig A4-1**; green) and subsequent adjacent columns represent calcium signals (**Fig A4-1**; *yellow*).
    - Length of time vector must equal length of calcium signal.
- Multiple independent recordings can be prepared in single sheet (**Fig A4-1**), and each independent recording can have multiple calcium signals (**Fig A4-2**).
    - Independent recordings organized in common sheet must be separated by blank column (**Fig A4-1**)
    - First row of each sheet must be left blank (**Fig A4-1, A4-2**)

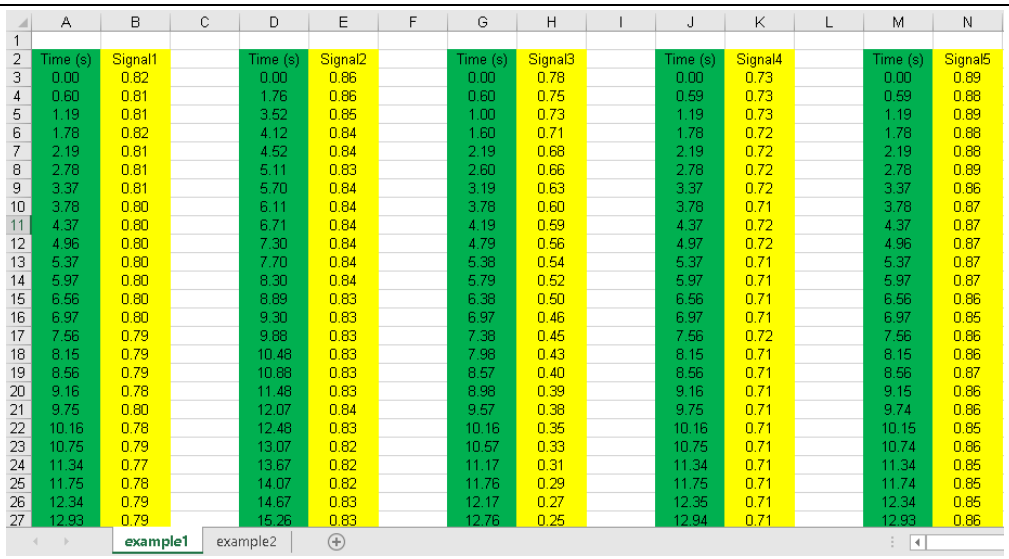

	A	B	C	D	E	F	G	H	I	J	K	L	M	N
1														
2	Time (s)	Signal1		Time (s)	Signal2		Time (s)	Signal3		Time (s)	Signal4		Time (s)	Signal5
3	0.00	0.82		0.00	0.86		0.00	0.78		0.00	0.73		0.00	0.89
4	0.60	0.81		1.76	0.86		0.60	0.75		0.59	0.73		0.59	0.88
5	1.19	0.81		3.52	0.85		1.00	0.73		1.19	0.73		1.19	0.89
6	1.78	0.82		4.12	0.84		1.60	0.71		1.78	0.72		1.78	0.88
7	2.19	0.81		4.52	0.84		2.19	0.68		2.19	0.72		2.19	0.88
8	2.78	0.81		5.11	0.83		2.60	0.66		2.78	0.72		2.78	0.89
9	3.37	0.81		5.70	0.84		3.19	0.63		3.37	0.72		3.37	0.86
10	3.78	0.80		6.11	0.84		3.78	0.60		3.78	0.71		3.78	0.87
11	4.37	0.80		6.71	0.84		4.19	0.59		4.37	0.72		4.37	0.87
12	4.96	0.80		7.30	0.84		4.79	0.56		4.97	0.72		4.96	0.87
13	5.37	0.80		7.70	0.84		5.38	0.54		5.37	0.71		5.37	0.87
14	5.97	0.80		8.30	0.84		5.79	0.52		5.97	0.71		5.97	0.87
15	6.56	0.80		8.89	0.83		6.38	0.50		6.56	0.71		6.56	0.86
16	6.97	0.80		9.30	0.83		6.97	0.46		6.97	0.71		6.97	0.85
17	7.56	0.79		9.88	0.83		7.38	0.45		7.56	0.72		7.56	0.86
18	8.15	0.79		10.48	0.83		7.98	0.43		8.15	0.71		8.15	0.86
19	8.56	0.79		10.88	0.83		8.57	0.40		8.56	0.71		8.56	0.87
20	9.16	0.78		11.48	0.83		8.98	0.39		9.16	0.71		9.15	0.86
21	9.75	0.80		12.07	0.84		9.57	0.38		9.75	0.71		9.74	0.86
22	10.16	0.78		12.48	0.83		10.16	0.35		10.16	0.71		10.15	0.85
23	10.75	0.79		13.07	0.82		10.57	0.33		10.75	0.71		10.74	0.86
24	11.34	0.77		13.67	0.82		11.17	0.31		11.34	0.71		11.34	0.85
25	11.75	0.78		14.07	0.82		11.76	0.29		11.75	0.71		11.74	0.85
26	12.34	0.79		14.67	0.83		12.17	0.27		12.35	0.71		12.34	0.85
27	12.93	0.79		15.26	0.83		12.76	0.25		12.94	0.71		12.93	0.86

example1 example2

Figure A4-1. Example 1: data preparation.

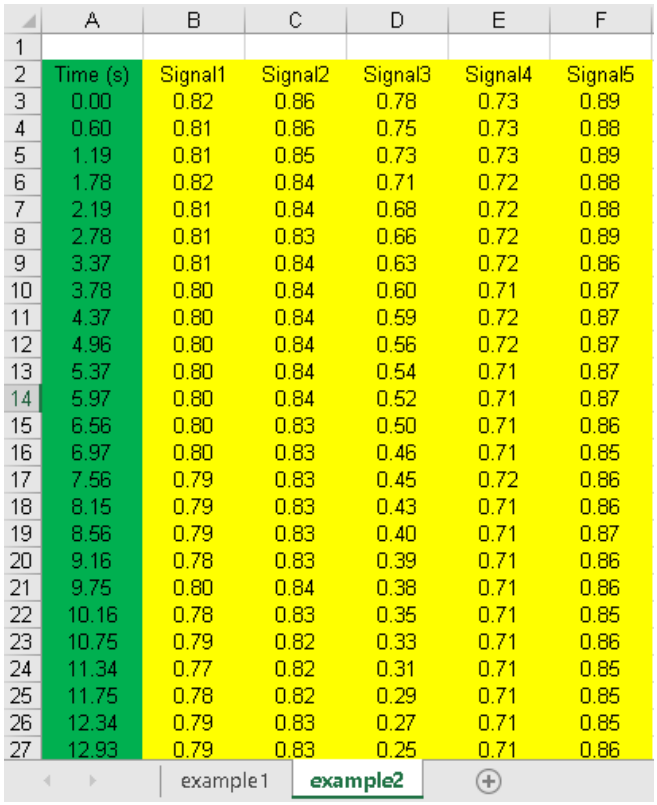

	A	B	C	D	E	F
1						
2	Time (s)	Signal1	Signal2	Signal3	Signal4	Signal5
3	0.00	0.82	0.86	0.78	0.73	0.89
4	0.60	0.81	0.86	0.75	0.73	0.88
5	1.19	0.81	0.85	0.73	0.73	0.89
6	1.78	0.82	0.84	0.71	0.72	0.88
7	2.19	0.81	0.84	0.68	0.72	0.88
8	2.78	0.81	0.83	0.66	0.72	0.89
9	3.37	0.81	0.84	0.63	0.72	0.86
10	3.78	0.80	0.84	0.60	0.71	0.87
11	4.37	0.80	0.84	0.59	0.72	0.87
12	4.96	0.80	0.84	0.56	0.72	0.87
13	5.37	0.80	0.84	0.54	0.71	0.87
14	5.97	0.80	0.84	0.52	0.71	0.87
15	6.56	0.80	0.83	0.50	0.71	0.86
16	6.97	0.80	0.83	0.46	0.71	0.85
17	7.56	0.79	0.83	0.45	0.72	0.86
18	8.15	0.79	0.83	0.43	0.71	0.86
19	8.56	0.79	0.83	0.40	0.71	0.87
20	9.16	0.78	0.83	0.39	0.71	0.86
21	9.75	0.80	0.84	0.38	0.71	0.86
22	10.16	0.78	0.83	0.35	0.71	0.85
23	10.75	0.79	0.82	0.33	0.71	0.86
24	11.34	0.77	0.82	0.31	0.71	0.85
25	11.75	0.78	0.82	0.29	0.71	0.85
26	12.34	0.79	0.83	0.27	0.71	0.85
27	12.93	0.79	0.83	0.25	0.71	0.86

example1 example2

Figure A4-2. Example 2: data preparation.

Step 2. Run Calcium Analyzer

- Open the 'MAIN.m' file in MATLAB and press 'RUN' (**Fig A4-3**). Users can navigate through available characterization options using the provided graphical interface (**Fig A4-4**)
    - Calcium Analyzer performance can be visually evaluated using figures generated throughout the parameter characterization. To plot these, specify "plot", and to save in .PNG format, specify "Save".
    - All Calcium Analyzer MATLAB files along with input spreadsheet must be in a designated directory (**Fig A4-5**)
- Once input data has been specified, press "Characterize Results" and the analysis will proceed.
    - In general, it takes 1-2 seconds to analyze a single calcium signal. A complete calcium signaling experiment typically takes 5-20 minutes to analyze.

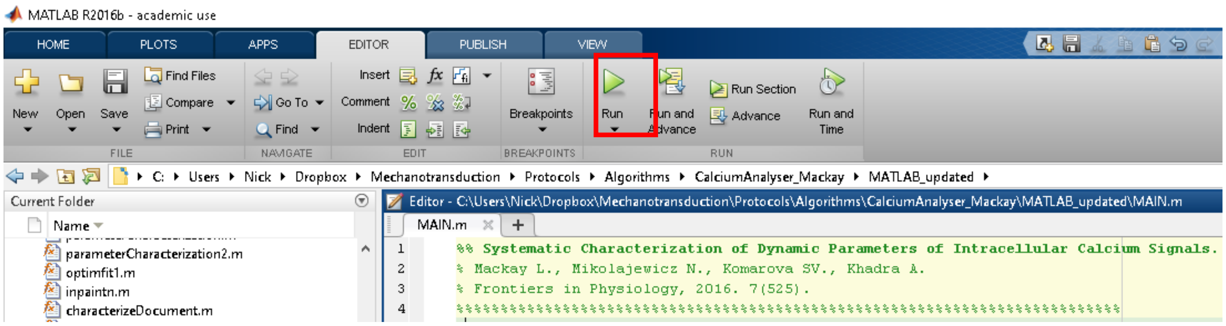

Figure A4-3. Running Calcium Analyzer in MATLAB. Open “Main.m” and press “Run” (*red outline*).

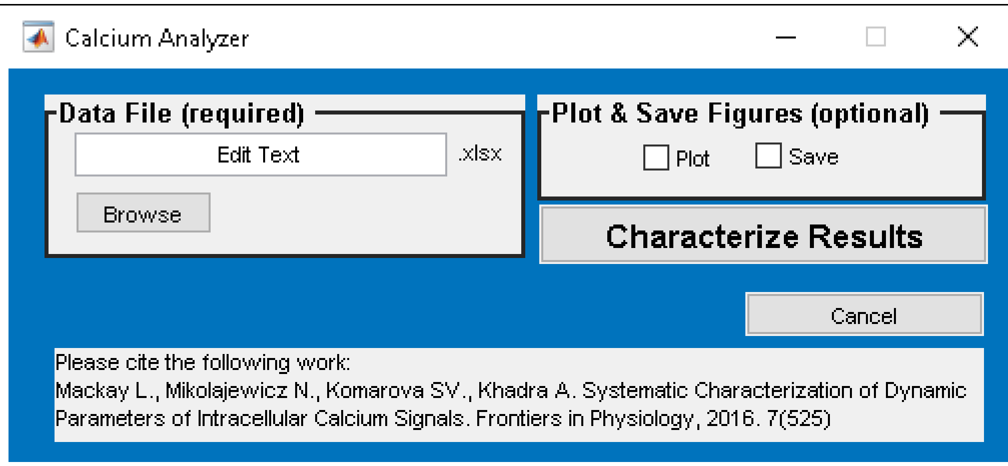

Figure A4-4. Calcium analyzer graphical interface.

Step 3. Calcium Analyzer Output

- Once Calcium Analyzer finished running, a prompt will be presented to the user.
- Calcium Analyzer exports results into a new spreadsheet in the same directory as the data input file (**Fig A4-6**).
    - Results spreadsheet will have same name as input data, followed by “parameterCharacterization” and a time stamp.
- The organization of the results spreadsheet will be consistent with that of the input data (**Fig A4-7**).
- For a complete list and description of the parameters that are characterized, refer to the corresponding manuscript.

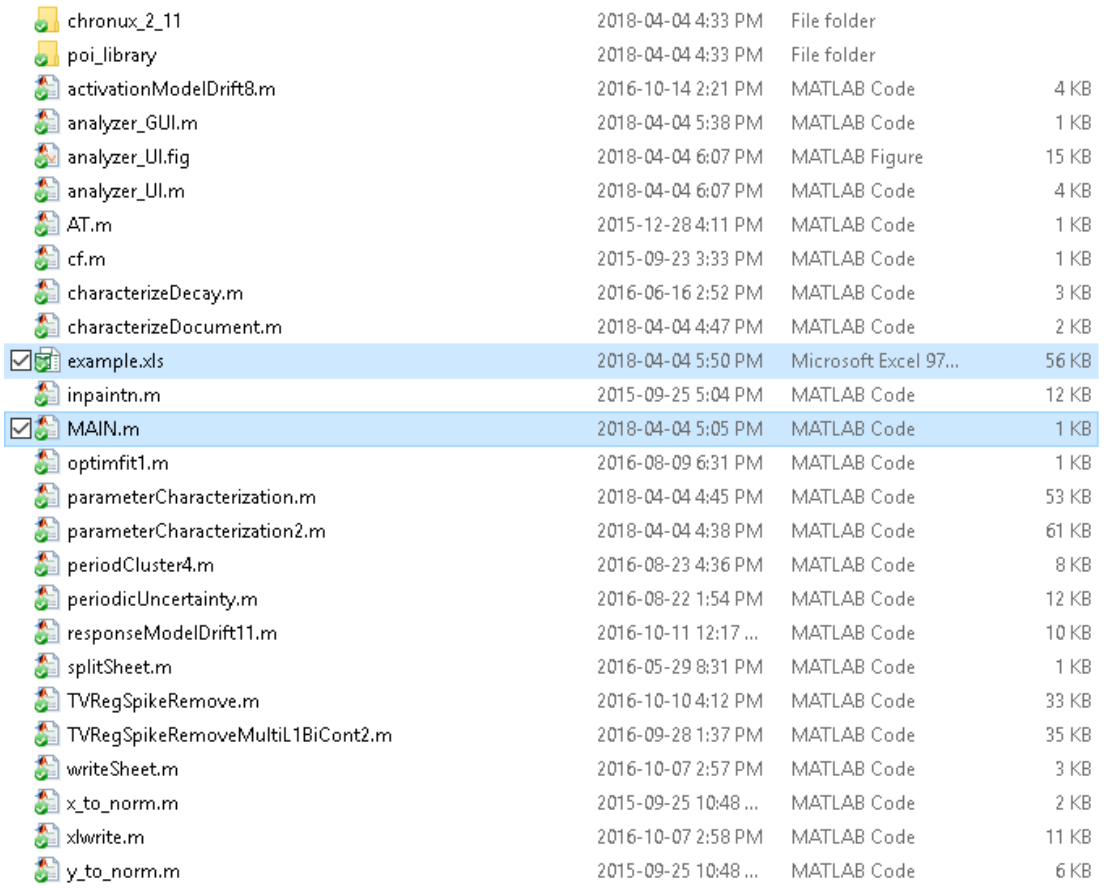

chronux_2_11	2018-04-04 4:33 PM	File folder	
poi_library	2018-04-04 4:33 PM	File folder	
activationModelDrift8.m	2016-10-14 2:21 PM	MATLAB Code	4 KB
analyzer_GUI.m	2018-04-04 5:38 PM	MATLAB Code	1 KB
analyzer_UI.fig	2018-04-04 6:07 PM	MATLAB Figure	15 KB
analyzer_UI.m	2018-04-04 6:07 PM	MATLAB Code	4 KB
AT.m	2015-12-28 4:11 PM	MATLAB Code	1 KB
cf.m	2015-09-23 3:33 PM	MATLAB Code	1 KB
characterizeDecay.m	2016-06-16 2:52 PM	MATLAB Code	3 KB
characterizeDocument.m	2018-04-04 4:47 PM	MATLAB Code	2 KB
example.xls	2018-04-04 5:50 PM	Microsoft Excel 97...	56 KB
inpaintn.m	2015-09-25 5:04 PM	MATLAB Code	12 KB
MAIN.m	2018-04-04 5:05 PM	MATLAB Code	1 KB
optimfit1.m	2016-08-09 6:31 PM	MATLAB Code	1 KB
parameterCharacterization.m	2018-04-04 4:45 PM	MATLAB Code	53 KB
parameterCharacterization2.m	2018-04-04 4:38 PM	MATLAB Code	61 KB
periodCluster4.m	2016-08-23 4:36 PM	MATLAB Code	8 KB
periodicUncertainty.m	2016-08-22 1:54 PM	MATLAB Code	12 KB
responseModelDrift11.m	2016-10-11 12:17 ...	MATLAB Code	10 KB
splitSheet.m	2016-05-29 8:31 PM	MATLAB Code	1 KB
TVRegSpikeRemove.m	2016-10-10 4:12 PM	MATLAB Code	33 KB
TVRegSpikeRemoveMultiL1BiCont2.m	2016-09-28 1:37 PM	MATLAB Code	35 KB
writeSheet.m	2016-10-07 2:57 PM	MATLAB Code	3 KB
x_to_norm.m	2015-09-25 10:48 ...	MATLAB Code	2 KB
xlwrite.m	2016-10-07 2:58 PM	MATLAB Code	11 KB
y_to_norm.m	2015-09-25 10:48 ...	MATLAB Code	6 KB

Figure A4-5. All Calcium Analyzer files and data spreadsheet input files must be stored in same directory. Highlighted is *MAIN.m* used to initiate Calcium Analyzer, and *example.xls* used as an example of a typical input data spreadsheet.

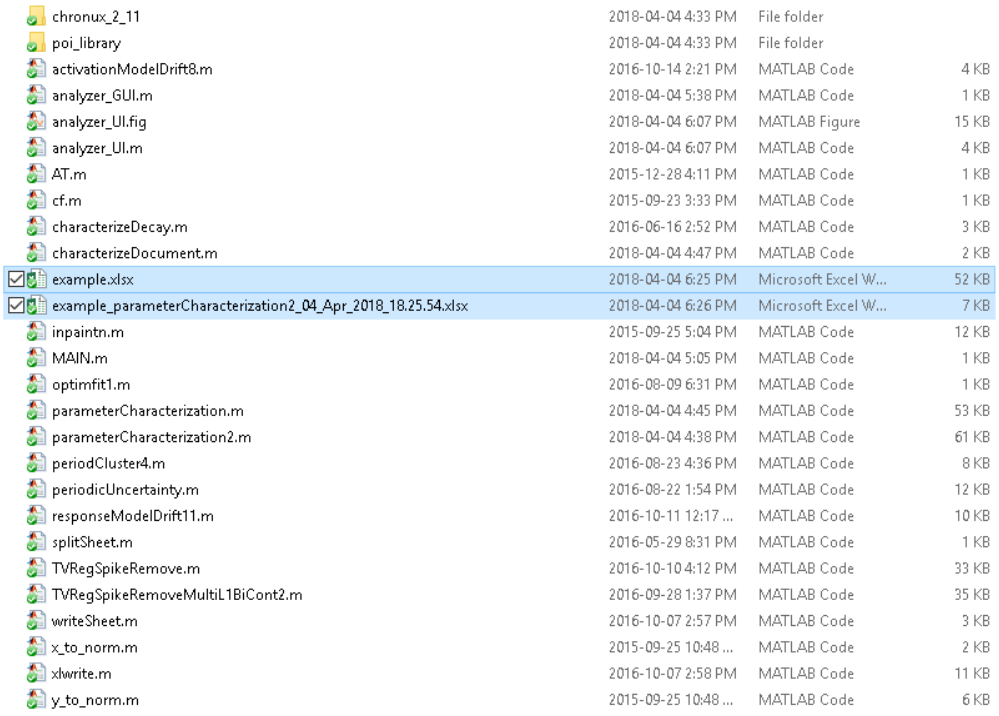

chronux_2_11	2018-04-04 4:33 PM	File folder	
poi_library	2018-04-04 4:33 PM	File folder	
activationModelDrift8.m	2016-10-14 2:21 PM	MATLAB Code	4 KB
analyzer_GUI.m	2018-04-04 5:38 PM	MATLAB Code	1 KB
analyzer_UI.fig	2018-04-04 6:07 PM	MATLAB Figure	15 KB
analyzer_UI.m	2018-04-04 6:07 PM	MATLAB Code	4 KB
AT.m	2015-12-28 4:11 PM	MATLAB Code	1 KB
cf.m	2015-09-23 3:33 PM	MATLAB Code	1 KB
characterizeDecay.m	2016-06-16 2:52 PM	MATLAB Code	3 KB
characterizeDocument.m	2018-04-04 4:47 PM	MATLAB Code	2 KB
example.xlsx	2018-04-04 6:25 PM	Microsoft Excel W...	52 KB
example_parameterCharacterization2_04_Apr_2018_18.25.54.xlsx	2018-04-04 6:26 PM	Microsoft Excel W...	7 KB
inpaintn.m	2015-09-25 5:04 PM	MATLAB Code	12 KB
MAIN.m	2018-04-04 5:05 PM	MATLAB Code	1 KB
optimfit1.m	2016-08-09 6:31 PM	MATLAB Code	1 KB
parameterCharacterization.m	2018-04-04 4:45 PM	MATLAB Code	53 KB
parameterCharacterization2.m	2018-04-04 4:38 PM	MATLAB Code	61 KB
periodCluster4.m	2016-08-23 4:36 PM	MATLAB Code	8 KB
periodicUncertainty.m	2016-08-22 1:54 PM	MATLAB Code	12 KB
responseModelDrift11.m	2016-10-11 12:17 ...	MATLAB Code	10 KB
splitSheet.m	2016-05-29 8:31 PM	MATLAB Code	1 KB
TVRegSpikeRemove.m	2016-10-10 4:12 PM	MATLAB Code	33 KB
TVRegSpikeRemoveMultiL1BiCont2.m	2016-09-28 1:37 PM	MATLAB Code	35 KB
writeSheet.m	2016-10-07 2:57 PM	MATLAB Code	3 KB
x_to_norm.m	2015-09-25 10:48 ...	MATLAB Code	2 KB
xlwrite.m	2016-10-07 2:58 PM	MATLAB Code	11 KB
y_to_norm.m	2015-09-25 10:48 ...	MATLAB Code	6 KB

Figure A4-6. Exported results will be saved in same directory as input data (*highlighted*).

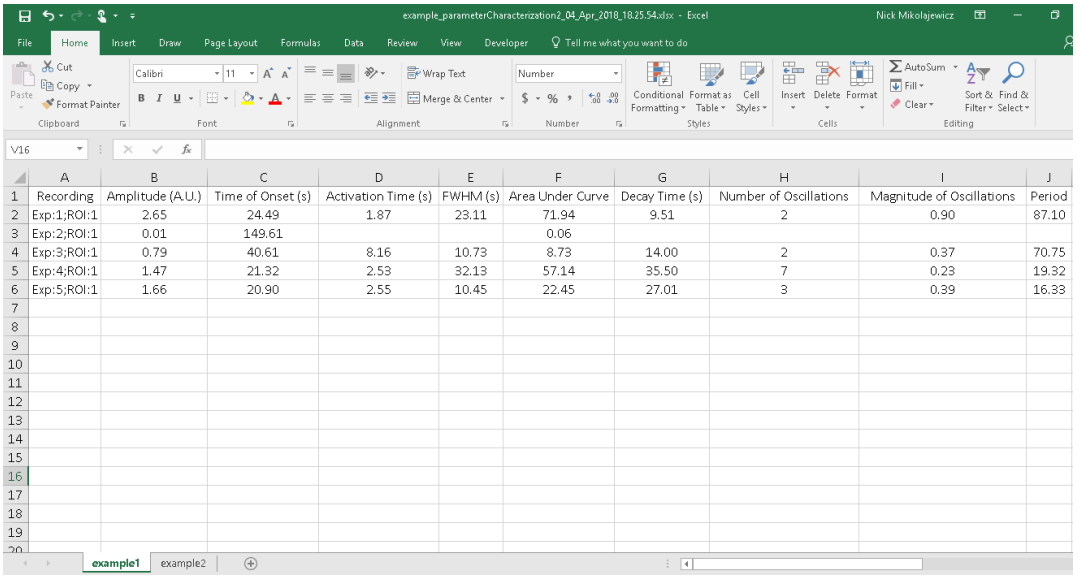

	A	B	C	D	E	F	G	H	I	J
1	Recording	Amplitude (A.U.)	Time of Onset (s)	Activation Time (s)	FWHM (s)	Area Under Curve	Decay Time (s)	Number of Oscillations	Magnitude of Oscillations	Period
2	Exp:1;ROI:1	2.65	24.49	1.87	23.11	71.94	9.51	2	0.90	87.10
3	Exp:2;ROI:1	0.01	149.61			0.06				
4	Exp:3;ROI:1	0.79	40.61	8.16	10.73	8.73	14.00	2	0.37	70.75
5	Exp:4;ROI:1	1.47	21.32	2.53	32.13	57.14	35.50	7	0.23	19.32
6	Exp:5;ROI:1	1.66	20.90	2.55	10.45	22.45	27.01	3	0.39	16.33

Figure A4-7. Results spreadsheet. Parameters are organized by column, and each calcium signal is organized by rows. The Recording labels indicate which recording the signal came from (Experiment; Exp), and which signal (or region of interest; ROI) was analyzed.

A5. Chapter 6 Supplemental Figures

Supplemental figures referenced in **Chapter 6** are provided here.

A5.1 Supplemental Figures

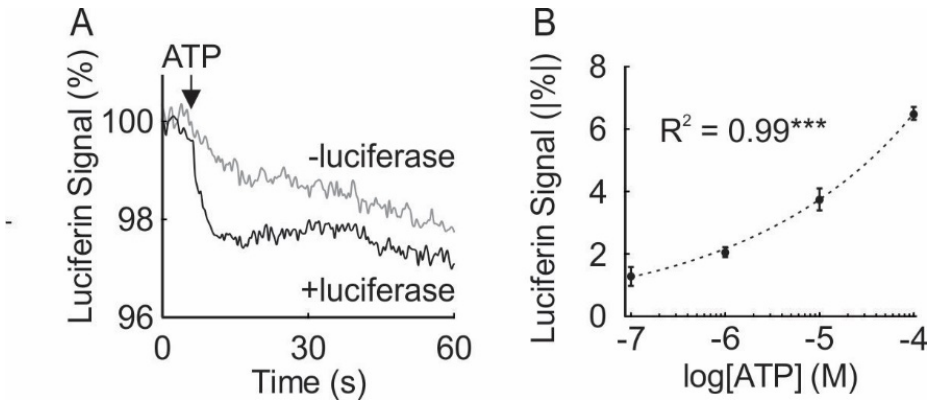

Fig 6-S1. **Real-time ATP measurement assay using fluorescent properties of luciferin-luciferase. (A)** 1 μM ATP was added to luciferin in presence or absence of luciferase and fluorescence was recorded at 380 ex/510 em; normalized to basal luciferin fluorescence. **(B)** $[ATP]_e$ dose dependence of luciferin-luciferase fluorescence change from baseline. Means ± SEM, n = 3 independent recordings, *dashed line*: linear regression, ***p<0.001.

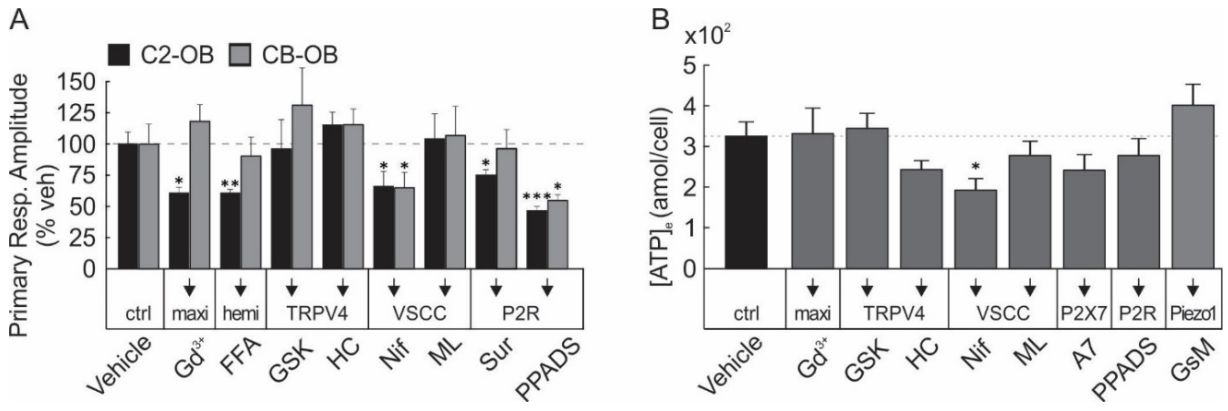

Fig 6-S2. **Involvement of conductive channels in osteoblast response to mechanical stimulation. (A)** Amplitudes of mechanically-evoked $[Ca^{2+}]_i$ transients in osteoblasts pretreated with vehicle, Gd^{3+}, FFA, GSK, HC, Nif, ML, Sur and PPADS. Means ± SEM, n= 5-15 stimulated cells, normalized to vehicle. **(B)** CB-OB cells were stimulated by tFSS (10x) following pre-treatment with conductive channel inhibitors Gd^{3+}, GSK, HC, Nif, ML, A7, PPADs and GsM. Means ± SEM attomoles ATP released per cell over 60 s after stimulation, n = 6-8 separate cultures, compared to vehicle. *p<0.05. **p<0.01 and ***p<0.001 indicate significance of treatment condition compared to vehicle, assessed by ANOVA followed by post-hoc Bonferroni test.

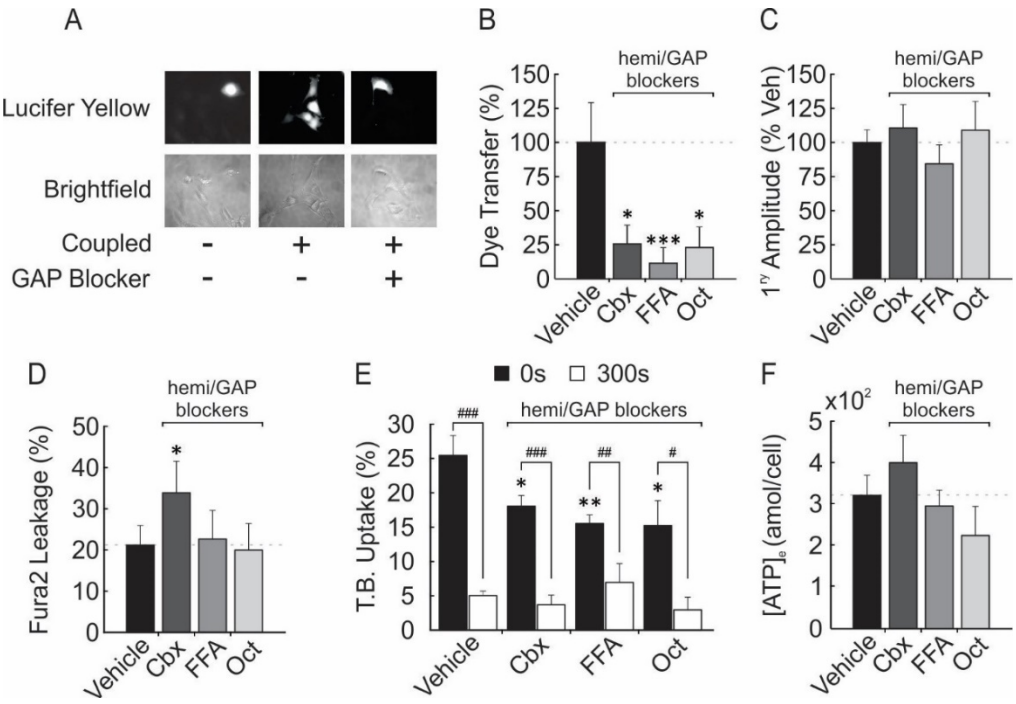

Fig 6-S3. **Involvement of hemichannels in ATP release and membrane resealing in murine osteoblasts (A-B)** To demonstrate the presence of functional GAP-junctions and validate GAP-junction/hemi channel blockers, C2-OB were pretreated (10 min) with vehicle (n = 22), Cbx (n = 11), FFA (n = 6) and Oct (n = 10) and scraped and stained with LY. Sample sizes are regions of interest imaged from 3 independent cultures. Fluorescence (**A**, *top*) and bright field (**A**, *bottom*) images show dye transfer and cell-cell coupling, respectively. Mean ± SEM percentage of cells that were not initially scraped but were coupled and LY-positive following LY staining, normalized to vehicle **(B)**. **(C-D)** Fura2-loaded CB-OB pretreated with GAP-junction/hemi-channel blockers were mechanically stimulated with glass micropipette and $[Ca^{2+}]_i$ elevation amplitude **(C,** mean ± SEM amplitude, normalized to vehicle**)** and percentage of sIn cells (**D,** mean ± SEM percentage**)** was determined (n=6-9 stimulated cells). **(E-F)** Membrane injury of CB-OB following tFSS (10x resuspensions) was assessed by T.B. uptake at 0 and 300s (**E**; n = 5-8 separate cultures, means ± SEM), and ATP release ($[ATP]_e$) was measured using bioluminescence assay (**F**; n = 6 separate cultures, means ± SEM attomoles released per cell over 60 s after simulation) following pre-treatment with GAP-junction/hemichannel blockers. Comparisons to vehicle; *p<0.05, **p<0.01 and ***p<0.001, or as specified; $^{\#}$p<0.05, $^{\#\#}$p<0.01 and $^{\#\#\#}$p<0.001, indicate significance assessed by ANOVA followed by post-hoc Bonferroni test.

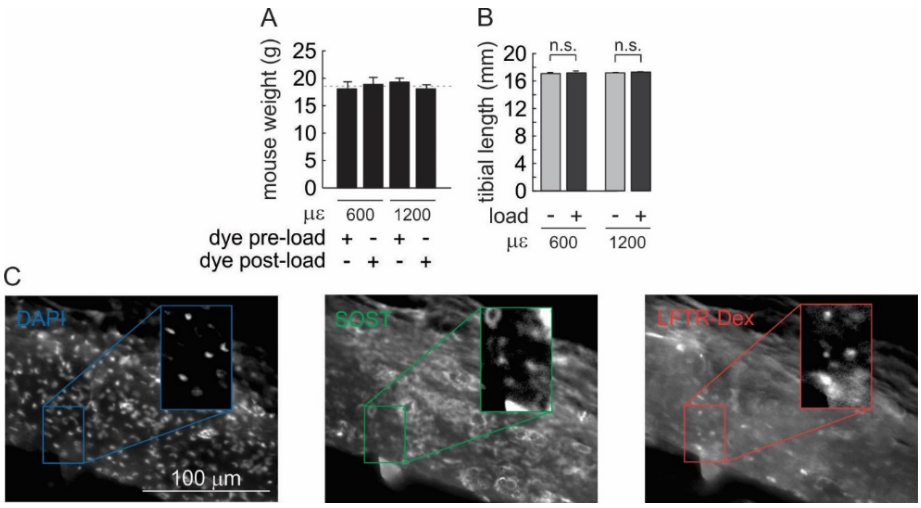

Fig 6-S4. ***in vivo*** **cyclic compressive loading was applied to the left tibia. (A)** Average weights of 10-week-old female C57Bl/6J mice for each experimental cohort. Mean ± SD, n=5 animals per group. **(B)** Impact of loading on tibial length compared to contralateral non-loaded tibia for 600 με (n = 10 animals) and 1200 με (n = 10 animals) loading regime. For (**A**) and (**B**) no significant difference was demonstrated by ANOVA. **(C)** Immunofluorescence images of nuclear DAPI (*left*), anti-sclerostin (*middle*) and LFTR-Dex uptake (*right*) in non-loaded tibia. Magnified regions are contrast-enhanced.

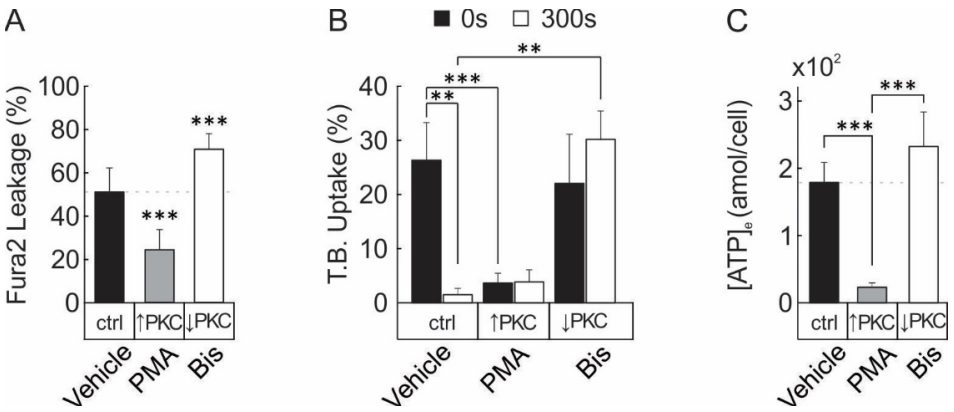

Fig 6-S5. **PKC regulates membrane resealing and ATP release in C2-OB cell line. (A-C)** C2-OB were pre-treated (30 min) with vehicle, PMA or Bis. **(A)** Membrane permeability of micropipette-stimulated Fura2-loaded C2-OB was assessed by dye-leakage. Means ± SEM percentage of sIn cells, n = 11 stimulated cells. **(B)** Membrane permeability of C2-OB stimulated with tFSS (10x resuspensions) was assessed by staining at 0 or 300s with T.B. Means ± SEM percentage of dye-positive cells, n = 7 separate cultures. **(C)** Amount of ATP released ($[ATP]_e$) from tFSS-stimulated (10x resuspensions) C2-OB was assessed by bioluminescence assay. Means ± SEM attomoles ATP release per cell, 60 s after stimulation. Compared to vehicle (unless otherwise specified), **p<0.01 and ***p<0.001 indicate significance assessed by ANOVA followed by post-hoc Bonferroni test.

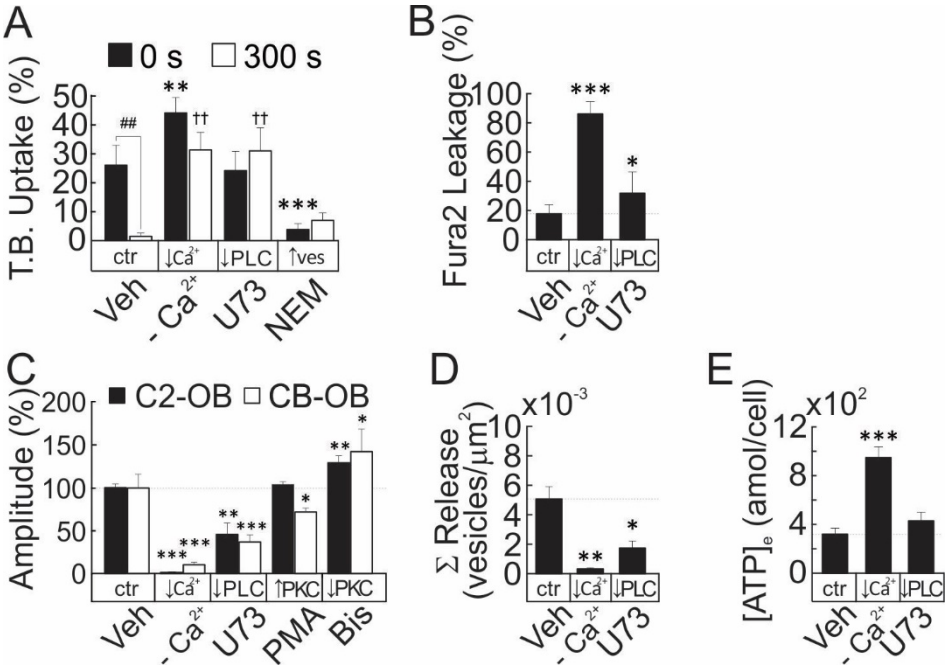

Fig 6-S6. **Membrane resealing, vesicular exocytosis and ATP release are Ca^{2+}/PLC-dependent processes. (A-E)** CB-OB were pretreated with vehicle, calcium-depleted physiological solution (-Ca^{2+}), U73, NEM, PMA or Bis where indicated, and mechanically-induced membrane injury (**A, B**), amplitude of $[Ca^{2+}]_i$ elevations (**C**), vesicular exocytosis (**D**) and ATP release (**E**) were assessed. **(A)** TB uptake at 0 and 300 s after tFSS (10x), n = 5-8 separate cultures. **(B)** Fura2 leakage following micropipette stimulation, determined as percentage of sIn cells after micropipette-stimulation, n = 9-16 stimulated cells. **(C)** Amplitudes of micropipette-stimulated $[Ca^{2+}]_i$ elevations in Fura2-loaded C2-OB and CB-OB cells, n = 9-16 stimulated cells. **(D)** Cumulative vesicular release over 100 s after micropipette-stimulation, n= 6-10 stimulated cells. **(E)** ATP release over 60 s following 10x tFSS stimulation, n = 8 separate cultures. For Fig S6, data are means ± SEM, ***significance compared to vehicle (0 s vehicle for A), ††significance compared to 300 s vehicle (A) and $^{\#\#}$ significance of indicated comparisons (A), by ANOVA or by regression.

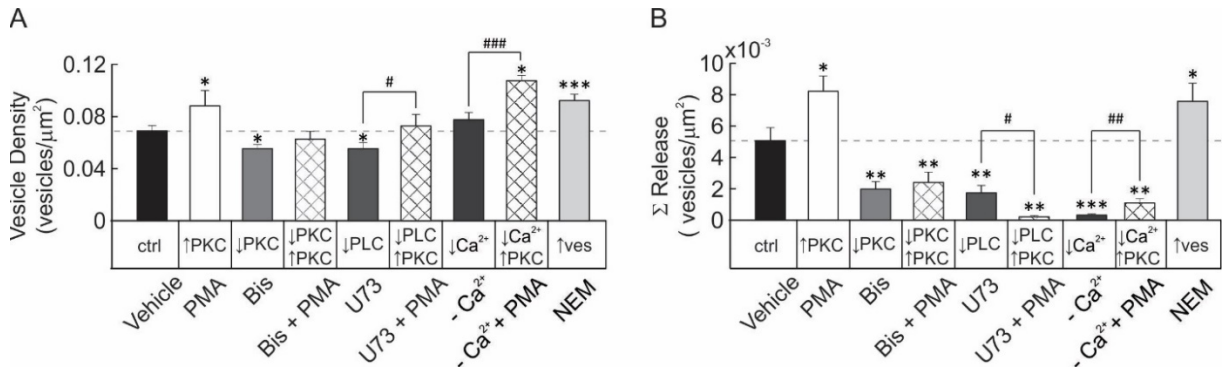

Fig 6-S7. **Basal vesicular density and mechanically-stimulated vesicular release in compact bone-derived osteoblasts. (A-B)** Quinacrine-loaded CB-OB were pretreated (30 min) with PMA, Bis, PMA + Bis, U73, U73 + PMA, $[Ca^{2+}]_e$-free PS, $[Ca^{2+}]_e$-free PS + PMA and NEM. Basal vesicular density **(A)** and cumulative vesicular release in response to stimulation by glass micropipette **(B)** were determined. Mean ± SEM vesicular density or cumulative vesicular release, normalized to unit area (n = 11-16 stimulated cells). Comparisons with vehicle; *p<0.05, **p<0.01 and ***p<0.001, or as specified; #p<0.05, ##p<0.01 and ###p<0.001, indicate significance assessed by ANOVA followed by post-hoc Bonferroni test.

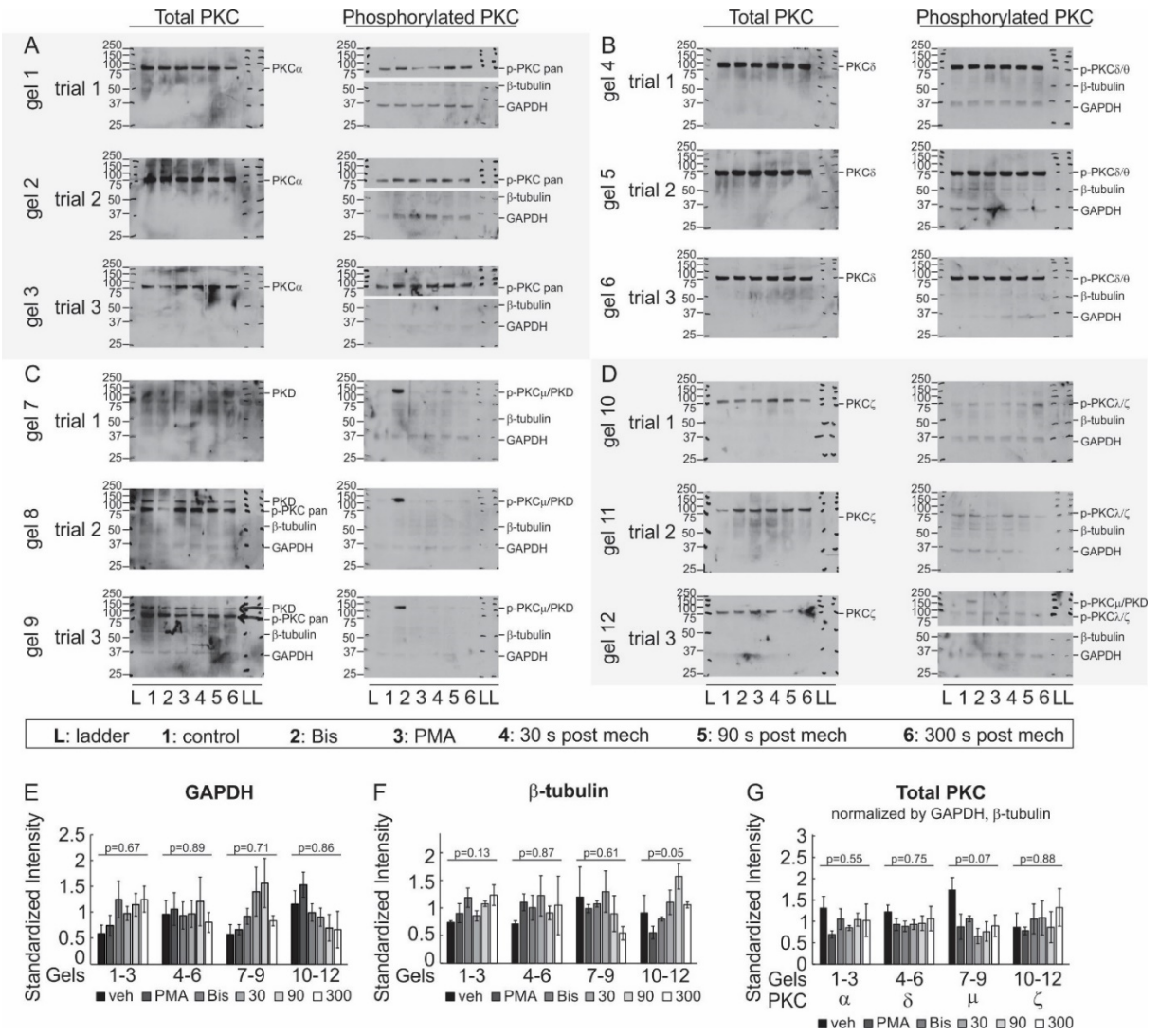

Fig 6-S8. **Immunoblot analysis of PKC isoforms**. **(A-D)** Immunoblots for phospho- and total- conventional PKC (**A**), novel PKC (**B**), PKC/PKCμ (**C**) and atypical PKC (**D**) isoforms, and GAPDH and β-tubulin in cell lysates extracted from CB-OB treated with vehicle, PMA or Bis (30 min); or 30 s, 90 s or 300 s after tFSS (10x). **(E-G)** GAPDH (**E**) and β-tubulin (**F**) band intensities were averaged and used to normalize total PKC levels (**G**). Differences in loading controls and total PKC levels were assessed by ANOVA and p-values are reported, n = 3 cultures isolated from different mice.

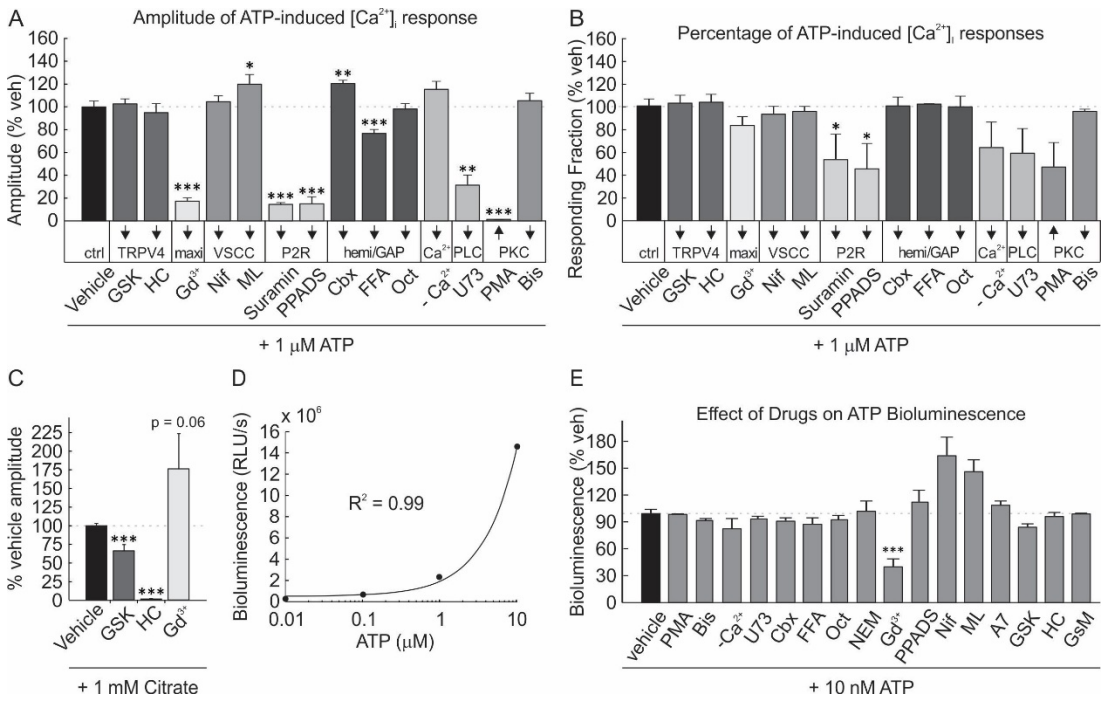

Fig 6-S9. **Effect of drug treatments on $[Ca^{2+}]_i$ elevations and ATP bioluminescence assay. (A, B)** Effect of drugs on P2 receptor-mediated $[Ca^{2+}]_i$ elevation amplitude **(A)** and responsiveness **(B)**. 1 μM ATP was applied to Fura2-loaded C2-OB pre-treated for 10 mins with vehicle (n = 30), GSK (n = 28), HC (n = 30), Gd^{3+} (n = 18), Nif (n = 46), ML (n = 45), Sur (n = 51), PPADS (n = 36), Cbx (n = 47), FFA (n = 45), Oct (n = 39) or 30 mins with $[Ca^{2+}]_e$-free PS (n = 62), U73 (n = 29), PMA (n = 18), or Bis (n = 48). Mean ± SEM response normalized to vehicle. Compared to vehicle, *p<0.05, **p<0.01 and ***p<0.001 indicate significance assessed by ANOVA followed by post-hoc Bonferroni test. **(C)** Effect of drugs on citrate-mediated $[Ca^{2+}]_i$ elevation amplitude. 1 mM citrate was applied as TRP agonist to Fura2-loaded C2-OB pretreated for 10 mins with GSK (n = 48), HC (n = 18) or Gd^{3+} (n = 29). Mean ± SEM amplitude normalized to vehicle condition. For A-C, sample sizes are number of quantified cells from at least 3 independent cultures. **(D)** Calibration curve relating ATP standard concentrations to measured bioluminescence. Mean ± SEM relative light units per sec (RLU/s). Solid line, linear regression. **(E)** Effect of drugs on ATP bioluminescence assay. 10 nM ATP-dependent luciferin/luciferase bioluminescence was measured in the presence of PMA, Bis, $[Ca^{2+}]_e$-free PS, U73, Cbx, FFA, Oct, NEM, Gd^{3+}, PPADS, Nif, ML, A7, GSK, HC, or GsM. Mean ± SEM RLU/s as percentage of vehicle condition. Compared to vehicle, **p<0.01 and ***p<0.001 indicate significance assessed by ANOVA followed by post-hoc Bonferroni test.

A6. Chapter 7 Supplemental Figures and Tables

Supplemental figures and tables referenced in **Chapter 7** are provided here.

A6.1 Supplemental Figures

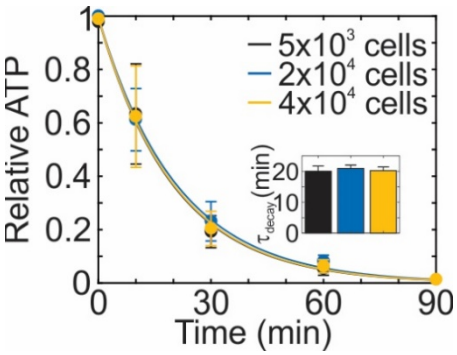

Fig 7-S1. Influence of cell density on ATP degradation. 1 μM ATP was added to C2-OB cultures of varying densities and media was sampled and measured at indicated time points by luciferin-luciferase bioluminescence assay. *Inset*: decay time constant τ_{decay}. Data are means ± SEM, no significant difference by ANOVA.

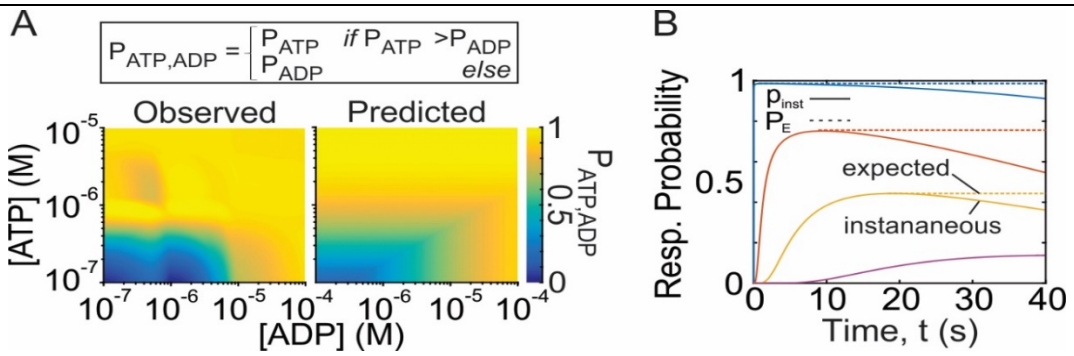

Fig 7-S2. Coupling ATP and ADP diffusion to purinergic response probabilities (A) Surface plot shows the response probabilities of C2-OB stimulated with varying combinations of ATP and ADP. Empirical relationship between ATP and ADP concentrations and the response probability P_i (i denotes ATP only, ADP only, or ATP and ADP in combination) of cells (*top panel*) was established with observed data (*left surface plot*), and used to predict the response probability (*right surface plot*). Pseudo colors represents values of P_i, such that $P_i = 1$ (*yellow*) corresponds to 100% of cells responding to stimulus, while $P_i = 0$ (*dark blue*) corresponds to 0% of cells responding to stimulus. **(B)** ATP and ADP release and diffusion were numerically simulated ($d_0 = 100$ nm, $\tau_{1/2} = 15$ s; Eq. 5, 6) and used to predict instantaneous (p_{inst}) and expected (P_E) response probabilities (Eq. 7).

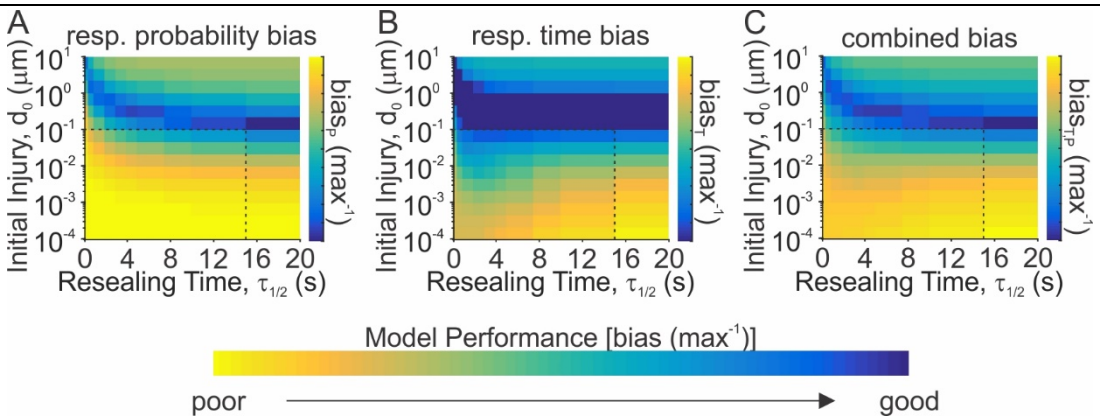

Fig 7-S3. Injury-related parameter estimation. (A, B) Bias between observed and expected response probabilities $Bias_P$ **(A)** and observed and expected response times $Bias_T$ **(B)** was assessed for d_0 and $\tau_{1/2}$ parameter space. **(C)** Combined bias $Bias_{T,P}$ was calculated to identify experimentally consistent parameters. *Dashed black lines*: best-fit parameter set, $d_0 = 100$ nm, $\tau_{1/2} = 15$ s.

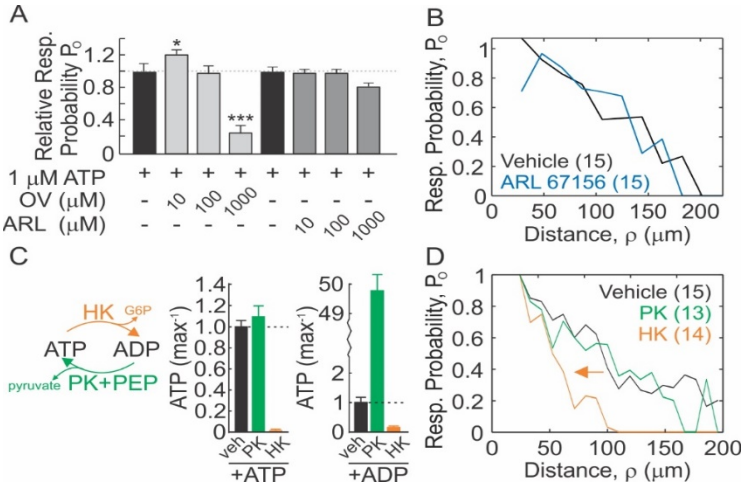

Fig 7-S4. Influence of extracellular ATP degradation on mechanotransductive paracrine responses. (A) 1 μM ATP was applied to Fura2-loaded C2-OB cells in the absence or presence of ecto-nucleotidase inhibitor ARL 67156 (10, 100 or 1000 μM) or alkaline phosphatase inhibitor orthovanadate (10, 100 or 1000 μM) and $[Ca^{2+}]_i$ elevations were recorded. Data are mean response probabilities ± SEM, normalized to 1 μM ATP control, N = 3. *p<0.05 and ***p<0.001 indicate significance compared to 1 μM ATP control, as assessed by ANOVA and Bonferroni test. **(B)** Observed paracrine response probabilities P_O following micropipette stimulation of single Fura2-loaded C2-OB cell in the absence or presence of 10 μM ARL 67156. **(C)** 1 μM ATP (*left bar plot*) or ADP (*right bar plot*) solutions were incubated with vehicle, pyruvate kinase (PK) + PEP or hexokinase (HK) for 5 min and [ATP] was measured. Means ± SEM, N=3. **(D)** Observed paracrine response probabilities P_O following micropipette stimulation of single Fura2-loaded C2-OB cell in the presence of 20 U/mL pyruvate kinase + excess PK or 20 U/mL hexokinase (HK). For B and D, sample sizes N are in parentheses.

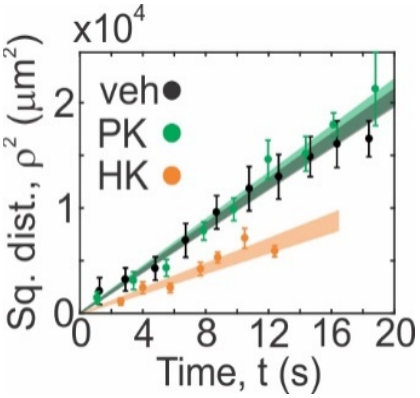

Fig 7-S5. Fura2-loaded C2-OB was mechanically-stimulated by micropipette in presence of vehicle, PK (+PEP) or HK and relationships between secondary response times and squared distance from the source were evaluated. *Shaded bands*: 95% CI, N=10-15

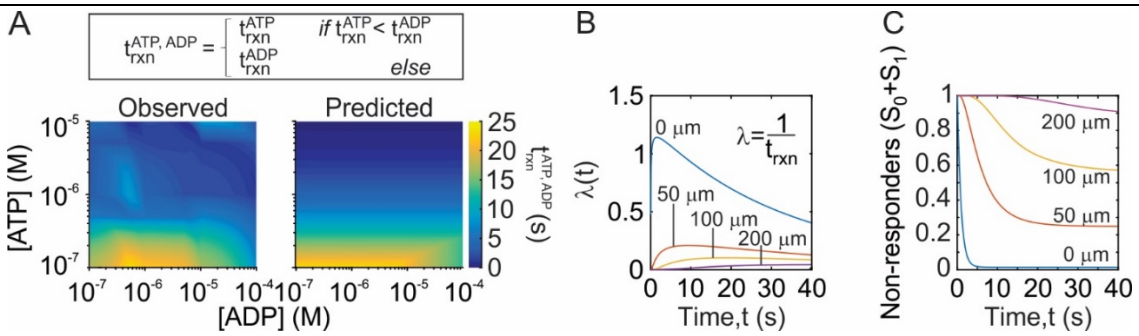

Fig 7-S6. Response-time model parameters. **(A)** Fura2-loaded C2-OB were stimulated by bath application of ATP, ADP, or their combination and the empirical relationship between ATP and ADP concentrations and reaction times t^i_{rxn} (i denotes ATP only, ADP only, or ATP and ADP in combination; *top panel*) was established using observed data (*left surface plot*) and used to predict t^i_{rxn} (*right surface plot*). Pseudo colors represent values of t^i_{rxn} ranging from $t^i_{rxn} = 0\ s$ (*dark blue*) to $t^i_{rxn} = 25\ s$ (*yellow*) and correspond to ATP and ADP concentrations for which responses are observed 0 s to 25 s after stimulation, respectively. **(B, C)** ATP and ADP release and diffusion was numerically simulated ($d_0 = 100$ nm, $\tau_{1/2} = 15$ s; Eq. 5, 6) and used to predict instantaneous reaction rates λ (Eq. 8; **C**) and space- and time-dependent proportion of non-responding neighboring cells $S_0 + S_1$ (**C**).

A6.2 Supplemental Tables

Table 7-S1. Fitted models for ATP and ADP dose-dependencies in C2-OB and ATP degradation kinetics in specified cell types.

Response probabilities, *P*			
Hill function:	$P = \frac{[\text{nucleotide}]^n}{EC_{50}^n + [\text{nucleotide}]^n}$		
Nucleotide species	**EC_{50}, M (95% CI)**	**n (95% CI)**	**R^2**
ATP	1.8e-7 (1.2e-7, 2.4e-7)	1.1 (0.76, 1.4)	0.99
ADP	2.9e-6 (1.3e-6, 4.6e-6)	0.61 (0.44, 0.80)	0.99
Reaction times, t_{rxn}			
Exponential function:	$t_{rxn} = a \cdot \exp(b \cdot \log_{10}[\text{nucleotide}])$		
Nucleotide species	**a (95% CI)**	**b (95% CI)**	**R^2**
ATP	1.3e-5 (-7.0e-5, 9.7e-5)	-2.0 (-2.8, -1.1)	0.96
ADP	0.70 (-0.73, 2.1)	-0.55 (-0.86, -0.23)	0.90
ATP Degradation			
Exponential function:	$\frac{C(t)}{C_0} = \exp(b \cdot t)$		
Cell type (+ condition)		**b (95% CI)**	**R^2**
C2-OB		-0.049 (-0.055, -0.043)	1.00
Raw 264.7		-0.048 (-0.052, -0.044)	1.00
K562		-0.096 (-0.11, -0.085)	1.00
C2-OB + 10 μM ARL 67156		-0.010 (-0.017, -0.0031)	0.93
C2-OB + 10 μM Orthovanadate		-0.0017 (-0.0021, -0.0013)	0.99

C: ATP concentration, C_0: initial ATP concentration, CI: confidence interval, [nucleotide]: nucleotide concentration in molar (M), t: time

A7. Permission for Reproduction from The Company of Biologists

Author Rights

http://www.biologists.com/content/copyright_permissions_content.php#open_permissions

(these rights are retained when publishing an Open Access article)

Authors remain the owners of the copyright to the article and retain the following non-exclusive rights (for further details, please refer to the license agreement that accompanies article proofs):

(1) ***authors may reproduce the article, in whole or in part, in any printed book (including a thesis) of which they are author, provided the original article is properly and fully attributed;***

(2) authors and any academic institution where they are employed may reproduce the article, in whole or in part, for the purpose of teaching students;

(3) authors may post a copy of the article on their website, provided that it has already been published by the journal and is linked to the journal's website.

(4) authors may use data contained in the article in other works they create.

Disclaimer: Responsibility for (1) the accuracy of statements of fact; (2) the authenticity of scientific findings or observations; (3) expressions of scientific or other opinion; (4) any other material published in the journal rests solely with the author(s) of the article in which such statements, etc., appear. No responsibility for such matters is assumed by the journal, its owners, publishers, referees or staff.

A8. Permission for Reproduction from eLife

Author Rights

https://elifesciences.org/terms

Unless otherwise indicated, the articles and journal content published by eLife on the eLife Sites are licensed under a Creative Commons Attribution license (also known as a CC-BY license). This means that you are ***free to use, reproduce and distribute the articles and related content*** (unless otherwise noted), for commercial and non-commercial purposes, subject to citation of the original source in accordance with the CC-BY license.

A9. Permission for Reproduction from Frontiers in Physiology

Author Rights

https://www.frontiersin.org/journals/physiology#about

Open Access funder and institutional mandates: Frontiers is fully compliant with open access mandates, by publishing its articles under the Creative Commons Attribution licence (CC-BY). Funder mandates such as those by the Wellcome Trust (UK), National Institutes of Health (USA) and the Australian Research Council (Australia) are fully compatible with publishing in Frontiers. Authors retain copyright of their work and can deposit their publication in any repository. The work ***can be freely shared and adapted*** provided that appropriate credit is given and any changes specified.

A10. Agreement to use MacKay et al. (2016) in Dissertation

From: Nick Mikolajewicz <nicholas.mikolajewicz@mail.mcgill.ca>
Sent: 04 March 2018 19:00:34
To: Laurent MacKay <laurent.mackay@mail.mcgill.ca>
Subject: Regarding use of manuscript in thesis

Hi Laurent,

I hope all has been well. I wanted to ask whether you were planning on including the calcium parameter characterization paper in your thesis. If you are not planning on using it, I would like to.

Let me know!

Nick

From: Laurent MacKay <laurent.mackay@mail.mcgill.ca>
Sent: March 5, 2018 12:39 PM
To: Nick Mikolajewicz <nicholas.mikolajewicz@mail.mcgill.ca>
Subject: Re: Regarding use of manuscript in thesis

Hi Nick,

I had not planned on using that paper as a thesis chapter, maybe only as a reference in my bibliography. Feel free to use it in your thesis and I will act in accordance to the rule such that you don't have any issues.

Cheers,
Laurent.

From: Nick Mikolajewicz <nicholas.mikolajewicz@mail.mcgill.ca>
Sent: March 5, 2018 12:53 PM
To: Laurent MacKay <laurent.mackay@mail.mcgill.ca>
Subject: RE: Regarding use of manuscript in thesis

Hi Laurent,

Great, thanks a lot.

Best,

Nick

References

Ahmed, S. M., Rzigalinski, B. A., Willoughby, K. A., Sitterding, H. A., & Ellis, E. F. (2000). Stretch-induced injury alters mitochondrial membrane potential and cellular ATP in cultured astrocytes and neurons. *Journal of Neurochemistry, 74*(5), 1951-1960.

Akopova, I., Tatur, S., Grygorczyk, M., Luchowski, R., Gryczynski, I., Gryczynski, Z., . . . Grygorczyk, R. (2012). Imaging exocytosis of ATP-containing vesicles with TIRF microscopy in lung epithelial A549 cells. *Purinergic signalling, 8*(1), 59-70. doi:http://dx.doi.org/10.1007/s11302-011-9259-2

Alvarenga, E. C., Rodrigues, R., Caricati-Neto, A., Silva-Filho, F. C., Paredes-Gamero, E. J., & Ferreira, A. T. (2010). Low-intensity pulsed ultrasound-dependent osteoblast proliferation occurs by via activation of the P2Y receptor: role of the P2Y1 receptor. *Bone, 46*(2), 355-362. doi:http://dx.doi.org/10.1016/j.bone.2009.09.017

Azorin, N., Raoux, M., Rodat-Despoix, L., Merrot, T., Delmas, P., & Crest, M. (2011). ATP signalling is crucial for the response of human keratinocytes to mechanical stimulation by hypo-osmotic shock. *Experimental Dermatology, 20*(5), 401-407. doi:http://dx.doi.org/10.1111/j.1600-0625.2010.01219.x

Beckel, J. M., Argall, A. J., Lim, J. C., Xia, J., Lu, W., Coffey, E. E., . . . Mitchell, C. H. (2014). Mechanosensitive release of adenosine 5'-triphosphate through pannexin channels and mechanosensitive upregulation of pannexin channels in optic nerve head astrocytes: a mechanism for purinergic involvement in chronic strain. *GLIA, 62*(9), 1486-1501. doi:http://dx.doi.org/10.1002/glia.22695

Birder, L. A., Barrick, S. R., Roppolo, J. R., Kanai, A. J., de Groat, W. C., Kiss, S., & Buffington, C. A. (2003). Feline interstitial cystitis results in mechanical hypersensitivity and altered ATP release from bladder urothelium. *American Journal of Physiology - Renal Physiology, 285*(3), F423-429.

Birder, L. A., Nakamura, Y., Kiss, S., Nealen, M. L., Barrick, S., Kanai, A. J., . . . Caterina, M. J. (2002). Altered urinary bladder function in mice lacking the vanilloid receptor TRPV1. *Nature Neuroscience, 5*(9), 856-860.

Bjaelde, R. G., Arnadottir, S. S., Overgaard, M. T., Leipziger, J., & Praetorius, H. A. (2013). Renal epithelial cells can release ATP by vesicular fusion. *Frontiers in Physiology, 4*, 238. doi:http://dx.doi.org/10.3389/fphys.2013.00238

Blum, A. E., Walsh, B. C., & Dubyak, G. R. (2010). Extracellular osmolarity modulates G protein-coupled receptor-dependent ATP release from 1321N1 astrocytoma cells. *American Journal of Physiology - Cell Physiology, 298*(2), C386-396. doi:http://dx.doi.org/10.1152/ajpcell.00430.2009

Bodin, P., & Burnstock, G. (1995). Synergistic effect of acute hypoxia on flow-induced release of ATP from cultured endothelial cells. *Experientia, 51*(3), 256-259. doi:http://dx.doi.org/10.1007/BF01931108

Bodin, P., & Burnstock, G. (1998). Increased release of ATP from endothelial cells during acute inflammation. *Inflammation Research, 47*(8), 351-354.

Bodin, P., & Burnstock, G. (2001). Evidence that release of adenosine triphosphate from endothelial cells during increased shear stress is vesicular. *Journal of Cardiovascular Pharmacology, 38*(6), 900-908.

Bodin, P., Milner, P., Winter, R., & Burnstock, G. (1992). Chronic hypoxia changes the ratio of endothelin to ATP release from rat aortic endothelial cells exposed to high flow. *Proceedings of the Royal Society B: Biological Sciences, 247*(1319), 131-135.

Boudreault, F., & Grygorczyk, R. (2004). Cell swelling-induced ATP release is tightly dependent on intracellular calcium elevations. *Journal of Physiology, 561*(Pt 2), 499-513.

Braunstein, G. M., Roman, R. M., Clancy, J. P., Kudlow, B. A., Taylor, A. L., Shylonsky, V. G., . . . Schwiebert, E. M. (2001). Cystic fibrosis transmembrane conductance regulator facilitates ATP release by stimulating a separate ATP release channel for autocrine control of cell volume regulation. *Journal of Biological Chemistry, 276*(9), 6621-6630.

Button, B., Okada, S. F., Frederick, C. B., Thelin, W. R., & Boucher, R. C. (2013). Mechanosensitive ATP release maintains proper mucus hydration of airways. *Science Signaling [Electronic Resource], 6*(279), ra46. doi:http://dx.doi.org/10.1126/scisignal.2003755

Button, B., Picher, M., & Boucher, R. C. (2007). Differential effects of cyclic and constant stress on ATP release and mucociliary transport by human airway epithelia. *Journal of Physiology, 580*(Pt. 2), 577-592.

Cabral, P. D., Hong, N. J., & Garvin, J. L. (2012). ATP mediates flow-induced NO production in thick ascending limbs. *American Journal of Physiology - Renal Physiology, 303*(2), F194-200. doi:http://dx.doi.org/10.1152/ajprenal.00504.2011

Calvert, R. C., Thompson, C. S., & Burnstock, G. (2008). ATP release from the human ureter on distension and P2X(3) receptor expression on suburothelial sensory nerves. *Purinergic signalling, 4*(4), 377-381. doi:http://dx.doi.org/10.1007/s11302-008-9123-1

Carroll, J., Raththagala, M., Subasinghe, W., Baguzis, S., D'Amico Oblak, T., Root, P., & Spence, D. (2006). An altered oxidant defense system in red blood cells affects their ability to release nitric oxide-stimulating ATP. *Molecular Biosystems, 2*(6-7), 305-311.

Chen, Y., Bao, Y., Zhang, J., Woehrle, T., Sumi, Y., Ledderose, S., . . . Junger, W. G. (2015). Inhibition of Neutrophils by Hypertonic Saline Involves Pannexin-1, CD39, CD73, and Other Ectonucleotidases. *Shock, 44*(3), 221-227. doi:http://dx.doi.org/10.1097/SHK.0000000000000402

Chen, Y., Shukla, A., Namiki, S., Insel, P. A., & Junger, W. G. (2004). A putative osmoreceptor system that controls neutrophil function through the release of ATP, its conversion to adenosine, and activation of A2 adenosine and P2 receptors. *Journal of Leukocyte Biology, 76*(1), 245-253.

Chi, Y., Gao, K., Zhang, H., Takeda, M., & Yao, J. (2014). Suppression of cell membrane permeability by suramin: involvement of its inhibitory actions on connexin 43 hemichannels. *British Journal of Pharmacology, 171*(14), 3448-3462. doi:http://dx.doi.org/10.1111/bph.12693

Chow, J., Liton, P. B., Luna, C., Wong, F., & Gonzalez, P. (2007). Effect of cellular senescence on the P2Y-receptor mediated calcium response in trabecular meshwork cells. *Molecular Vision, 13*, 1926-1933.

Cinar, E., Zhou, S., DeCourcey, J., Wang, Y., Waugh, R. E., & Wan, J. (2015). Piezo1 regulates mechanotransductive release of ATP from human RBCs. *Proceedings of the National Academy of Sciences of the United States of America, 112*(38), 11783-11788. doi:http://dx.doi.org/10.1073/pnas.1507309112

Contreras-Sanz, A., Krska, L., Balachandran, A. A., Curtiss, N. L., Khasriya, R., Kelley, S., . . . Wildman, S. S. (2016). Altered urothelial ATP signaling in a major subset of human overactive bladder patients with pyuria. *American Journal of Physiology - Renal Physiology, 311*(4), F805-F816. doi:http://dx.doi.org/10.1152/ajprenal.00339.2015

Corriden, R., Insel, P. A., & Junger, W. G. (2007). A novel method using fluorescence microscopy for real-time assessment of ATP release from individual cells. *American Journal of Physiology - Cell Physiology, 293*(4), C1420-1425.

Cui, H., Liu, Y., Qin, L., Wang, L., & Huang, Y. (2016). Increased membrane localization of pannexin1 in human corneal synaptosomes causes enhanced stimulated ATP release in chronic diabetes mellitus. *Medicine, 95*(49), e5084.

Dagenais, A., Tessier, M. C., Tatur, S., Brochiero, E., Grygorczyk, R., & Berthiaume, Y. (2013). Hypotonic shock modulates Na(+) current via a Cl(-) and Ca(2+)/calmodulin dependent mechanism in alveolar epithelial cells. *PLoS ONE [Electronic Resource], 8*(9), e74565. doi:http://dx.doi.org/10.1371/journal.pone.0074565

David Holtzclaw, J., Cornelius, R. J., Hatcher, L. I., & Sansom, S. C. (2011). Coupled ATP and potassium efflux from intercalated cells. *American Journal of Physiology - Renal Physiology, 300*(6), F1319-F1326. doi:http://dx.doi.org/10.1152/ajprenal.00112.2011

Dolovcak, S., Waldrop, S. L., Xiao, F., & Kilic, G. (2011). Evidence for sustained ATP release from liver cells that is not mediated by vesicular exocytosis. *Purinergic signalling, 7*(4), 435-446. doi:http://dx.doi.org/10.1007/s11302-011-9240-0

Du, S., Araki, I., Mikami, Y., Zakoji, H., Beppu, M., Yoshiyama, M., & Takeda, M. (2007). Amiloride-sensitive ion channels in urinary bladder epithelium involved in mechanosensory transduction by modulating stretch-evoked adenosine triphosphate release. *Urology, 69*(3), 590-595.

Dutta, A. K., Okada, Y., & Sabirov, R. Z. (2002). Regulation of an ATP-conductive large-conductance anion channel and swelling-induced ATP release by arachidonic acid. *Journal of Physiology, 542*(Pt 3), 803-816.

Dutta, A. K., Sabirov, R. Z., Uramoto, H., & Okada, Y. (2004). Role of ATP-conductive anion channel in ATP release from neonatal rat cardiomyocytes in ischaemic or hypoxic conditions. *Journal of Physiology, 559*(Pt 3), 799-812.

Egbuniwe, O., Grover, S., Duggal, A. K., Mavroudis, A., Yazdi, M., Renton, T., . . . Grant, A. D. (2014). TRPA1 and TRPV4 activation in human odontoblasts stimulates ATP release. *Journal of Dental Research, 93*(9), 911-917. doi:http://dx.doi.org/10.1177/0022034514544507

Enomoto, K., Furuya, K., Yamagishi, S., Oka, T., & Maeno, T. (1994). The increase in the intracellular Ca2+ concentration induced by mechanical stimulation is propagated via release of pyrophosphorylated nucleotides in mammary epithelial cells. *Pflugers Archiv - European Journal of Physiology, 427*(5-6), 533-542.

Espelt, M. V., de Tezanos Pinto, F., Alvarez, C. L., Alberti, G. S., Incicco, J., Leal Denis, M. F., . . . Schwarzbaum, P. J. (2013). On the role of ATP release, ectoATPase activity, and extracellular ADP in the regulatory volume decrease of Huh-7 human hepatoma cells. *American Journal of Physiology - Cell Physiology, 304*(10), C1013-1026. doi:http://dx.doi.org/10.1152/ajpcell.00254.2012

Feranchak, A. P., Fitz, J. G., & Roman, R. M. (2000). Volume-sensitive purinergic signaling in human hepatocytes. *Journal of Hepatology, 33*(2), 174-182.

Feranchak, A. P., Lewis, M. A., Kresge, C., Sathe, M., Bugde, A., Luby-Phelps, K., . . . Fitz, J. G. (2010). Initiation of purinergic signaling by exocytosis of ATP-containing vesicles in liver epithelium. *Journal of Biological Chemistry, 285*(11), 8138-8147. doi:http://dx.doi.org/10.1074/jbc.M109.065482

Feranchak, A. P., Roman, R. M., Doctor, R. B., Salter, K. D., Toker, A., & Fitz, J. G. (1999). The lipid products of phosphoinositide 3-kinase contribute to regulation of cholangiocyte ATP and chloride transport. *Journal of Biological Chemistry, 274*(43), 30979-30986.

Feranchak, A. P., Roman, R. M., Schwiebert, E. M., & Fitz, J. G. (1998). Phosphatidylinositol 3-kinase contributes to cell volume regulation through effects on ATP release. *Journal of Biological Chemistry, 273*(24), 14906-14911.

Ferguson, D. R., Kennedy, I., & Burton, T. J. (1997). ATP is released from rabbit urinary bladder epithelial cells by hydrostatic pressure changes--a possible sensory mechanism? *Journal of Physiology, 505*(Pt 2), 503-511.

Fiorotto, R., Spirli, C., Fabris, L., Cadamuro, M., Okolicsanyi, L., & Strazzabosco, M. (2007). Ursodeoxycholic acid stimulates cholangiocyte fluid secretion in mice via CFTR-dependent ATP secretion. *Gastroenterology, 133*(5), 1603-1613.

Fischer, D. J., Torrence, N. J., Sprung, R. J., & Spence, D. M. (2003). Determination of erythrocyte deformability and its correlation to cellular ATP release using microbore tubing with diameters that approximate resistance vessels in vivo. *Analyst, 128*(9), 1163-1168.

Forst, A. L., Olteanu, V. S., Mollet, G., Wlodkowski, T., Schaefer, F., Dietrich, A., . . . Storch, U. (2016). Podocyte Purinergic P2X4 Channels Are Mechanotransducers That Mediate Cytoskeletal Disorganization. *Journal of the American Society of Nephrology, 27*(3), 848-862. doi:http://dx.doi.org/10.1681/ASN.2014111144

Fucikova, J., Moserova, I., Truxova, I., Hermanova, I., Vancurova, I., Partlova, S., . . . Spisek, R. (2014). High hydrostatic pressure induces immunogenic cell death in human tumor cells. *International Journal of Cancer, 135*(5), 1165-1177. doi:http://dx.doi.org/10.1002/ijc.28766

Furlow, P. W., Zhang, S., Soong, T. D., Halberg, N., Goodarzi, H., Mangrum, C., . . . Tavazoie, S. F. (2015). Mechanosensitive pannexin-1 channels mediate microvascular metastatic cell survival. *Nature Cell Biology, 17*(7), 943-952. doi:http://dx.doi.org/10.1038/ncb3194

Furuya, K., Sokabe, M., & Furuya, S. (2005). Characteristics of subepithelial fibroblasts as a mechano-sensor in the intestine: cell-shape-dependent ATP release and P2Y1 signaling. *Journal of Cell Science, 118*(Pt 15), 3289-3304.

Furuya, K., Sokabe, M., & Grygorczyk, R. (2014). Real-time luminescence imaging of cellular ATP release. *Methods (Duluth), 66*(2), 330-344. doi:http://dx.doi.org/10.1016/j.ymeth.2013.08.007

Furuya, K., Tan, J. J., Boudreault, F., Sokabe, M., Berthiaume, Y., & Grygorczyk, R. (2016). Real-time imaging of inflation-induced ATP release in the ex vivo rat lung. *American Journal of Physiology - Lung Cellular & Molecular Physiology, 311*(5), L956-L969. doi:http://dx.doi.org/10.1152/ajplung.00425.2015

Gardinier, J. D., Gangadharan, V., Wang, L., & Duncan, R. L. (2014). Hydraulic Pressure during Fluid Flow Regulates Purinergic Signaling and Cytoskeleton Organization of Osteoblasts. *Cellular & Molecular Bioengineering, 7*(2), 266-277. doi:http://dx.doi.org/10.1007/s12195-014-0329-8

Gardinier, J. D., Majumdar, S., Duncan, R. L., & Wang, L. (2009). Cyclic Hydraulic Pressure and Fluid Flow Differentially Modulate Cytoskeleton Re-Organization in MC3T3 Osteoblasts. *Cellular & Molecular Bioengineering, 2*(1), 133-143. doi:http://dx.doi.org/10.1007/s12195-008-0038-2

Gatof, D., Kilic, G., & Fitz, J. G. (2004). Vesicular exocytosis contributes to volume-sensitive ATP release in biliary cells. *American Journal of Physiology - Gastrointestinal & Liver Physiology, 286*(4), G538-546.

Genetos, D. C., Geist, D. J., Liu, D., Donahue, H. J., & Duncan, R. L. (2005). Fluid shear-induced ATP secretion mediates prostaglandin release in MC3T3-E1 osteoblasts. *Journal of Bone & Mineral Research, 20*(1), 41-49.

Genetos, D. C., Kephart, C. J., Zhang, Y., Yellowley, C. E., & Donahue, H. J. (2007). Oscillating fluid flow activation of gap junction hemichannels induces ATP release from MLO-Y4 osteocytes. *Journal of Cellular Physiology, 212*(1), 207-214.

Gevaert, T., Vriens, J., Segal, A., Everaerts, W., Roskams, T., Talavera, K., . . . Nilius, B. (2007). Deletion of the transient receptor potential cation channel TRPV4 impairs murine bladder voiding. *Journal of Clinical Investigation, 117*(11), 3453-3462.

Godecke, S., Stumpe, T., Schiller, H., Schnittler, H. J., & Schrader, J. (2005). Do rat cardiac myocytes release ATP on contraction? *American Journal of Physiology - Cell Physiology, 289*(3), C609-616.

Gomes, P., Srinivas, S. P., Van Driessche, W., Vereecke, J., & Himpens, B. (2005). ATP release through connexin hemichannels in corneal endothelial cells. *Investigative Ophthalmology & Visual Science, 46*(4), 1208-1218.

Gomes, P., Srinivas, S. P., Vereecke, J., & Himpens, B. (2006). Gap junctional intercellular communication in bovine corneal endothelial cells. *Experimental Eye Research, 83*(5), 1225-1237.

Gonzales, E., Julien, B., Serriere-Lanneau, V., Nicou, A., Doignon, I., Lagoudakis, L., . . . Tordjmann, T. (2010). ATP release after partial hepatectomy regulates liver regeneration in the rat. *Journal of Hepatology, 52*(1), 54-62. doi:http://dx.doi.org/10.1016/j.jhep.2009.10.005

Govitvattana, N., Osathanon, T., Toemthong, T., & Pavasant, P. (2015). IL-6 regulates stress-induced REX-1 expression via ATP-P2Y1 signalling in stem cells isolated from human exfoliated deciduous teeth. *Archives of Oral Biology, 60*(1), 160-166. doi:http://dx.doi.org/10.1016/j.archoralbio.2014.09.008

Gradilone, S. A., Masyuk, A. I., Splinter, P. L., Banales, J. M., Huang, B. Q., Tietz, P. S., . . . Larusso, N. F. (2007). Cholangiocyte cilia express TRPV4 and detect changes in luminal tonicity inducing bicarbonate secretion. *Proceedings of the National Academy of Sciences of the United States of America, 104*(48), 19138-19143.

Grafe, P., Schaffer, V., & Rucker, F. (2006). Kinetics of ATP release following compression injury of a peripheral nerve trunk. *Purinergic signalling, 2*(3), 527-536. doi:http://dx.doi.org/10.1007/s11302-006-9018-y

Graff, R. D., Lazarowski, E. R., Banes, A. J., & Lee, G. M. (2000). ATP release by mechanically loaded porcine chondrons in pellet culture. *Arthritis & Rheumatism, 43*(7), 1571-1579.

Graff, R. D., & Lee, G. M. (2003). Microplate live cell assay system for early events in mechanotransduction. *Analytical Biochemistry, 318*(2), 181-186.

Grygorczyk, R., Furuya, K., & Sokabe, M. (2013). Imaging and characterization of stretch-induced ATP release from alveolar A549 cells. *Journal of Physiology, 591*(Pt 5), 1195-1215. doi:http://dx.doi.org/10.1113/jphysiol.2012.244145

Grygorczyk, R., & Hanrahan, J. W. (1997). CFTR-independent ATP release from epithelial cells triggered by mechanical stimuli. *American Journal of Physiology, 272*(3 Pt 1), C1058-1066.

Guyot, A., & Hanrahan, J. W. (2002). ATP release from human airway epithelial cells studied using a capillary cell culture system.[Erratum appears in J Physiol. 2003 Feb 1;546(Pt 3):955]. *Journal of Physiology, 545*(Pt 1), 199-206.

Haanes, K. A., Kowal, J. M., Arpino, G., Lange, S. C., Moriyama, Y., Pedersen, P. A., & Novak, I. (2014). Role of vesicular nucleotide transporter VNUT (SLC17A9) in release of ATP from AR42J cells and mouse pancreatic acinar cells. *Purinergic signalling, 10*(3), 431-440. doi:http://dx.doi.org/10.1007/s11302-014-9406-7

Hamada, K., Takuwa, N., Yokoyama, K., & Takuwa, Y. (1998). Stretch activates Jun N-terminal kinase/stress-activated protein kinase in vascular smooth muscle cells through mechanisms involving autocrine ATP stimulation of purinoceptors. *Journal of Biological Chemistry, 273*(11), 6334-6340.

Hanna-Mitchell, A. T., Wolf-Johnston, A. S., Barrick, S. R., Kanai, A. J., Chancellor, M. B., De Groat, W. C., & Birder, L. A. (2015). Effect of botulinum toxin A on urothelial-release of ATP and expression of SNARE targets within the urothelium. *Neurourology and Urodynamics, 34*(1), 79-84. doi:http://dx.doi.org/10.1002/nau.22508

Harada, N., Sakamoto, S., Niwa, Y., & Nakaya, Y. (2001). Involvement of adenosine in vascular contractile preconditioning. *American Journal of Physiology - Heart & Circulatory Physiology, 280*(6), H2911-2919.

Hayton, M. J., Dillon, J. P., Glynn, D., Curran, J. M., Gallagher, J. A., & Buckley, K. A. (2005). Involvement of adenosine 5'-triphosphate in ultrasound-induced fracture repair. *Ultrasound in Medicine & Biology, 31*(8), 1131-1138.

Hazama, A., Fan, H. T., Abdullaev, I., Maeno, E., Tanaka, S., Ando-Akatsuka, Y., & Okada, Y. (2000). Swelling-activated, cystic fibrosis transmembrane conductance regulator-augmented ATP release and Cl- conductances in murine C127 cells. *Journal of Physiology, 523 Pt 1*, 1-11.

Hazama, A., Shimizu, T., Ando-Akatsuka, Y., Hayashi, S., Tanaka, S., Maeno, E., & Okada, Y. (1999). Swelling-induced, CFTR-independent ATP release from a human epithelial cell line: lack of correlation with volume-sensitive cl(-) channels. *Journal of General Physiology, 114*(4), 525-533.

Hecht, E., Liedert, A., Ignatius, A., Mizaikoff, B., & Kranz, C. (2013). Local detection of mechanically induced ATP release from bone cells with ATP microbiosensors. *Biosensors & Bioelectronics, 44*, 27-33. doi:http://dx.doi.org/10.1016/j.bios.2013.01.008

Heo, S. J., Han, W. M., Szczesny, S. E., Cosgrove, B. D., Elliott, D. M., Lee, D. A., . . . Mauck, R. L. (2016). Mechanically Induced Chromatin Condensation Requires Cellular Contractility in Mesenchymal Stem Cells. *Biophysical Journal, 111*(4), 864-874. doi:http://dx.doi.org/10.1016/j.bpj.2016.07.006

Heo, S. J., Thorpe, S. D., Driscoll, T. P., Duncan, R. L., Lee, D. A., & Mauck, R. L. (2015). Biophysical Regulation of Chromatin Architecture Instills a Mechanical Memory in Mesenchymal Stem Cells. *Scientific Reports, 5*, 16895. doi:http://dx.doi.org/10.1038/srep16895

Hirakawa, M., Oike, M., Karashima, Y., & Ito, Y. (2004). Sequential activation of RhoA and FAK/paxillin leads to ATP release and actin reorganization in human endothelium. *Journal of Physiology, 558*(Pt 2), 479-488.

Hisadome, K., Koyama, T., Kimura, C., Droogmans, G., Ito, Y., & Oike, M. (2002). Volume-regulated anion channels serve as an auto/paracrine nucleotide release pathway in aortic endothelial cells. *Journal of General Physiology, 119*(6), 511-520.

Hong, D., Jaron, D., Buerk, D. G., & Barbee, K. A. (2006). Heterogeneous response of microvascular endothelial cells to shear stress. *American Journal of Physiology - Heart & Circulatory Physiology, 290*(6), H2498-2508.

Hovater, M. B., Olteanu, D., Hanson, E. L., Cheng, N. L., Siroky, B., Fintha, A., . . . Schwiebert, E. M. (2008). Loss of apical monocilia on collecting duct principal cells impairs ATP secretion across the apical cell surface and ATP-dependent and flow-induced calcium signals. *Purinergic signalling, 4*(2), 155-170. doi:http://dx.doi.org/10.1007/s11302-007-9072-0

Islam, M. R., Uramoto, H., Okada, T., Sabirov, R. Z., & Okada, Y. (2012). Maxi-anion channel and pannexin 1 hemichannel constitute separate pathways for swelling-induced ATP release in murine L929 fibrosarcoma cells. *American Journal of Physiology - Cell Physiology, 303*(9), C924-935. doi:http://dx.doi.org/10.1152/ajpcell.00459.2011

Joseph, S. M., Buchakjian, M. R., & Dubyak, G. R. (2003). Colocalization of ATP release sites and ecto-ATPase activity at the extracellular surface of human astrocytes. *Journal of Biological Chemistry, 278*(26), 23331-23342.

Kanjanamekanant, K., Luckprom, P., & Pavasant, P. (2014). P2X7 receptor-Pannexin1 interaction mediates stress-induced interleukin-1 beta expression in human periodontal ligament cells. *Journal of Periodontal Research, 49*(5), 595-602. doi:http://dx.doi.org/10.1111/jre.12139

Karczewska, J., Martyniec, L., Dzierzko, G., Stepinski, J., & Angielski, S. (2007). The relationship between constitutive ATP release and its extracellular metabolism in isolated rat kidney glomeruli. *Journal of Physiology & Pharmacology, 58*(2), 321-333.

Karpatkin, S. (1969). Heterogeneity of human platelets. I. Metabolic and kinetic evidence suggestive of young and old platelets. *Journal of Clinical Investigation, 48*(6), 1073-1082.

Kawai, Y., Kaidoh, M., Yokoyama, Y., & Ohhashi, T. (2012). Pivotal roles of shear stress in the microenvironmental changes that occur within sentinel lymph nodes. *Cancer Science, 103*(7), 1245-1252. doi:http://dx.doi.org/10.1111/j.1349-7006.2012.02289.x

Kawai, Y., Kaidoh, M., Yokoyama, Y., & Ohhashi, T. (2013). Cell surface F<inf>1</inf>/F<inf>o</inf> ATP synthase contributes to interstitial flow-mediated development of the acidic microenvironment in tumor tissues. *American Journal of Physiology - Cell Physiology, 305*(11), C1139-C1150. doi:http://dx.doi.org/10.1152/ajpcell.00199.2013

Kawai, Y., Yokoyama, Y., Kaidoh, M., & Ohhashi, T. (2010). Shear stress-induced ATP-mediated endothelial constitutive nitric oxide synthase expression in human lymphatic endothelial cells. *American Journal of Physiology - Cell Physiology, 298*(3), C647-655. doi:http://dx.doi.org/10.1152/ajpcell.00249.2009

Kawai, Y., Yoshida, K., Kaidoh, M., Yokoyama, Y., & Ohhashi, T. (2012). Shear stress-mediated F<inf>1</inf>/F<inf>O</inf> ATP synthase-dependent CO<inf>2</inf> gas excretion from human pulmonary arteriolar endothelial cells. *Journal of Cellular Physiology, 227*(5), 2059-2068. doi:http://dx.doi.org/10.1002/jcp.22937

Kempson, S. A., Edwards, J. M., Osborn, A., & Sturek, M. (2008). Acute inhibition of the betaine transporter by ATP and adenosine in renal MDCK cells. *American Journal of Physiology - Renal Physiology, 295*(1), F108-117. doi:http://dx.doi.org/10.1152/ajprenal.00108.2008

Knight, G. E., Bodin, P., De Groat, W. C., & Burnstock, G. (2002). ATP is released from guinea pig ureter epithelium on distension. *American Journal of Physiology - Renal Physiology, 282*(2), F281-288.

Koizumi, S., Fujishita, K., Inoue, K., Shigemoto-Mogami, Y., Tsuda, M., & Inoue, K. (2004). Ca2+ waves in keratinocytes are transmitted to sensory neurons: the involvement of extracellular ATP and P2Y2 receptor activation. *Biochemical Journal, 380*(Pt 2), 329-338.

Koizumi, S., Fujishita, K., Tsuda, M., Shigemoto-Mogami, Y., & Inoue, K. (2003). Dynamic inhibition of excitatory synaptic transmission by astrocyte-derived ATP in hippocampal cultures. *Proceedings of the National Academy of Sciences of the United States of America, 100*(19), 11023-11028.

Kowal, J. M., Yegutkin, G. G., & Novak, I. (2015). ATP release, generation and hydrolysis in exocrine pancreatic duct cells. *Purinergic signalling, 11*(4), 533-550. doi:http://dx.doi.org/10.1007/s11302-015-9472-5

Koyama, T., Kimura, C., Hayashi, M., Watanabe, M., Karashima, Y., & Oike, M. (2009). Hypergravity induces ATP release and actin reorganization via tyrosine phosphorylation and RhoA activation in bovine endothelial cells. *Pflugers Archiv - European Journal of Physiology, 457*(4), 711-719. doi:http://dx.doi.org/10.1007/s00424-008-0544-z

Koyama, T., Oike, M., & Ito, Y. (2001). Involvement of Rho-kinase and tyrosine kinase in hypotonic stress-induced ATP release in bovine aortic endothelial cells. *Journal of Physiology, 532*(Pt 3), 759-769.

Krick, S., Wang, J., St-Pierre, M., Gonzalez, C., Dahl, G., & Salathe, M. (2016). Dual Oxidase 2 (Duox2) Regulates Pannexin 1-mediated ATP Release in Primary Human Airway Epithelial Cells via Changes in Intracellular pH and Not H2O2 Production. *Journal of Biological Chemistry, 291*(12), 6423-6432. doi:http://dx.doi.org/10.1074/jbc.M115.664854

Kringelbach, T. M., Aslan, D., Novak, I., Ellegaard, M., Syberg, S., Andersen, C. K., . . . Jorgensen, N. R. (2015). Fine-tuned ATP signals are acute mediators in osteocyte mechanotransduction. *Cellular Signalling, 27*(12), 2401-2409. doi:http://dx.doi.org/10.1016/j.cellsig.2015.08.016

Kringelbach, T. M., Aslan, D., Novak, I., Schwarz, P., & Jorgensen, N. R. (2014). UTP-induced ATP release is a fine-tuned signalling pathway in osteocytes. *Purinergic signalling, 10*(2), 337-347. doi:http://dx.doi.org/10.1007/s11302-013-9404-1

Kumar, V., Chapple, C. C., & Chess-Williams, R. (2004). Characteristics of adenosine triphosphate [corrected] release from porcine and human normal bladder.[Erratum appears in J Urol. 2004 Dec;172 (6 Pt 1):2485]. *Journal of Urology, 172*(2), 744-747.

Kumar, V., Chapple, C. R., Rosario, D., Tophill, P. R., & Chess-Williams, R. (2010). In vitro release of adenosine triphosphate from the urothelium of human bladders with detrusor overactivity, both neurogenic and idiopathic. *European Urology, 57*(6), 1087-1092. doi:http://dx.doi.org/10.1016/j.eururo.2009.11.042

Kumar, V., Chapple, C. R., Surprenant, A. M., & Chess-Williams, R. (2007). Enhanced adenosine triphosphate release from the urothelium of patients with painful bladder syndrome: a possible pathophysiological explanation. *Journal of Urology, 178*(4 Pt 1), 1533-1536.

Langevin, H. M., Fujita, T., Bouffard, N. A., Takano, T., Koptiuch, C., Badger, G. J., & Nedergaard, M. (2013). Fibroblast cytoskeletal remodeling induced by tissue stretch involves ATP signaling. *Journal of Cellular Physiology, 228*(9), 1922-1926. doi:http://dx.doi.org/10.1002/jcp.24356

Lazarowski, E. R., Homolya, L., Boucher, R. C., & Harden, T. K. (1997). Direct demonstration of mechanically induced release of cellular UTP and its implication for uridine nucleotide receptor activation. *Journal of Biological Chemistry, 272*(39), 24348-24354.

Lazarowski, E. R., Shea, D. A., Boucher, R. C., & Harden, T. K. (2003). Release of cellular UDP-glucose as a potential extracellular signaling molecule. *Molecular Pharmacology, 63*(5), 1190-1197.

Leal Denis, M. F., Alvarez, H. A., Lauri, N., Alvarez, C. L., Chara, O., & Schwarzbaum, P. J. (2016). Dynamic regulation of cell volume and extracellular ATP of human erythrocytes. *PLoS ONE [Electronic Resource], 11 (6) (no pagination)*(e0158305). doi:http://dx.doi.org/10.1371/journal.pone.0158305

Lewis, S. A., & Lewis, J. R. (2006). Kinetics of urothelial ATP release. *American Journal of Physiology - Renal Physiology, 291*(2), F332-340.

Li, A., Banerjee, J., Peterson-Yantorno, K., Stamer, W. D., Leung, C. T., & Civan, M. M. (2012). Effects of cardiotonic steroids on trabecular meshwork cells: search for mediator of ouabain-enhanced outflow facility. *Experimental Eye Research, 96*(1), 4-12. doi:http://dx.doi.org/10.1016/j.exer.2012.01.009

Li, A., Leung, C. T., Peterson-Yantorno, K., Mitchell, C. H., & Civan, M. M. (2010). Pathways for ATP release by bovine ciliary epithelial cells, the initial step in purinergic regulation of aqueous humor inflow. *American Journal of Physiology - Cell Physiology, 299*(6), C1308-1317. doi:http://dx.doi.org/10.1152/ajpcell.00333.2010

Li, A., Leung, C. T., Peterson-Yantorno, K., Stamer, W. D., & Civan, M. M. (2011). Cytoskeletal dependence of adenosine triphosphate release by human trabecular meshwork cells. *Investigative Ophthalmology & Visual Science, 52*(11), 7996-8005. doi:http://dx.doi.org/10.1167/iovs.11-8170

Li, A., Leung, C. T., Peterson-Yantorno, K., Stamer, W. D., Mitchell, C. H., & Civan, M. M. (2012). Mechanisms of ATP release by human trabecular meshwork cells, the enabling step in purinergic regulation of aqueous humor outflow. *Journal of Cellular Physiology, 227*(1), 172-182. doi:http://dx.doi.org/10.1002/jcp.22715

Li, A., Zhang, X., Zheng, D., Ge, J., Laties, A. M., & Mitchell, C. H. (2011). Sustained elevation of extracellular ATP in aqueous humor from humans with primary chronic angle-closure glaucoma. *Experimental Eye Research, 93*(4), 528-533. doi:http://dx.doi.org/10.1016/j.exer.2011.06.020

Li, J., Gao, Z., Kehoe, V., Xing, J., King, N., & Sinoway, L. (2008). Interstitial adenosine triphosphate modulates muscle afferent nerve-mediated pressor reflex. *Muscle & Nerve, 38*(2), 972-977. doi:http://dx.doi.org/10.1002/mus.21014

Li, J., Liu, D., Ke, H. Z., Duncan, R. L., & Turner, C. H. (2005). The P2X7 nucleotide receptor mediates skeletal mechanotransduction. *Journal of Biological Chemistry, 280*(52), 42952-42959.

Li, Y., Luo, Y., Huang, K., Xing, J., Xie, Z., Lin, M., . . . Wang, Y. (2013). The responses of osteoblasts to fluid shear stress depend on substrate chemistries. *Archives of Biochemistry & Biophysics, 539*(1), 38-50. doi:http://dx.doi.org/10.1016/j.abb.2013.09.005

Li, Y., Wang, J., Xing, J., Wang, Y., & Luo, Y. (2016). Surface chemistry regulates the sensitivity and tolerability of osteoblasts to various magnitudes of fluid shear stress. *Journal of Biomedical Materials Research. Part A, 104*(12), 2978-2991. doi:http://dx.doi.org/10.1002/jbm.a.35848

Liu, H. T., Toychiev, A. H., Takahashi, N., Sabirov, R. Z., & Okada, Y. (2008). Maxi-anion channel as a candidate pathway for osmosensitive ATP release from mouse astrocytes in primary culture. *Cell Research, 18*(5), 558-565. doi:http://dx.doi.org/10.1038/cr.2008.49

Liu, X., Wang, C., Fujita, T., Malmstrom, H. S., Nedergaard, M., Ren, Y. F., & Dirksen, R. T. (2015). External Dentin Stimulation Induces ATP Release in Human Teeth. *Journal of Dental Research, 94*(9), 1259-1266. doi:http://dx.doi.org/10.1177/0022034515592858

Locovei, S., Bao, L., & Dahl, G. (2006). Pannexin 1 in erythrocytes: function without a gap. *Proceedings of the National Academy of Sciences of the United States of America, 103*(20), 7655-7659.

Loomis, W. H., Namiki, S., Ostrom, R. S., Insel, P. A., & Junger, W. G. (2003). Hypertonic stress increases T cell interleukin-2 expression through a mechanism that involves ATP release, P2 receptor, and p38 MAPK activation. *Journal of Biological Chemistry, 278*(7), 4590-4596.

Lu, D., Soleymani, S., Madakshire, R., & Insel, P. A. (2012). ATP released from cardiac fibroblasts via connexin hemichannels activates profibrotic P2Y2 receptors. *FASEB Journal, 26*(6), 2580-2591. doi:http://dx.doi.org/10.1096/fj.12-204677

Lu, W., Hu, H., Sevigny, J., Gabelt, B. T., Kaufman, P. L., Johnson, E. C., . . . Mitchell, C. H. (2015). Rat, mouse, and primate models of chronic glaucoma show sustained elevation of extracellular ATP and altered purinergic signaling in the posterior eye. *Investigative Ophthalmology & Visual Science, 56*(5), 3075-3083. doi:http://dx.doi.org/10.1167/iovs.14-15891

Luckprom, P., Kanjanamekanant, K., & Pavasant, P. (2011). Role of connexin43 hemichannels in mechanical stress-induced ATP release in human periodontal ligament cells. *Journal of Periodontal Research, 46*(5), 607-615. doi:http://dx.doi.org/10.1111/j.1600-0765.2011.01379.x

Luna, C., Li, G., Qiu, J., Challa, P., Epstein, D. L., & Gonzalez, P. (2009). Extracellular release of ATP mediated by cyclic mechanical stress leads to mobilization of AA in trabecular meshwork cells. *Investigative Ophthalmology & Visual Science, 50*(12), 5805-5810. doi:http://dx.doi.org/10.1167/iovs.09-3796

Mairbaurl, H., Ruppe, F. A., & Bartsch, P. (2013). Role of hemolysis in red cell adenosine triphosphate release in simulated exercise conditions in vitro. *Medicine & Science in Sports & Exercise, 45*(10), 1941-1947. doi:http://dx.doi.org/10.1249/MSS.0b013e318296193a

Manaka, S., Tanabe, N., Kariya, T., Naito, M., Takayama, T., Nagao, M., . . . Miyazaki, M. (2015). Low-intensity pulsed ultrasound-induced ATP increases bone formation via the P2X7 receptor in osteoblast-like MC3T3-E1 cells. *FEBS Letters, 589*(3), 310-318. doi:http://dx.doi.org/10.1016/j.febslet.2014.12.013

Mansfield, K. J., & Hughes, J. R. (2014). Effect of inflammatory mediators on ATP release of human urothelial RT4 cells. *BioMed Research International, 2014*, 182862. doi:http://dx.doi.org/10.1155/2014/182862

Matos, R., Cordeiro, J. M., Coelho, A., Ferreira, S., Silva, C., Igawa, Y., . . . Charrua, A. (2016). Bladder pain induced by prolonged peripheral alpha 1A adrenoceptor stimulation involves the enhancement of transient receptor potential vanilloid 1 activity and an increase of urothelial adenosine triphosphate release. *Acta Physiologica, 218*(4), 265-275. doi:http://dx.doi.org/10.1111/apha.12744

Matsuka, Y., Ono, T., Iwase, H., Mitrirattanakul, S., Omoto, K. S., Cho, T., . . . Spigelman, I. (2008). Altered ATP release and metabolism in dorsal root ganglia of neuropathic rats. *Molecular Pain, 4*, 66. doi:http://dx.doi.org/10.1186/1744-8069-4-66

Matsumoto-Miyai, K., Kagase, A., Murakawa, Y., Momota, Y., & Kawatani, M. (2009). Extracellular Ca2+ regulates the stimulus-elicited ATP release from urothelium. *Autonomic Neuroscience-Basic & Clinical, 150*(1-2), 94-99. doi:http://dx.doi.org/10.1016/j.autneu.2009.05.253

McIlwrath, S. L., Davis, B. M., & Bielefeldt, K. (2009). Deletion of P2X3 receptors blunts gastro-oesophageal sensation in mice. *Neurogastroenterology and Motility, 21*(8), 890-e866. doi:http://dx.doi.org/10.1111/j.1365-2982.2009.01292.x

McLatchie, L. M., Young, J. S., & Fry, C. H. (2014). Regulation of ACh release from guinea pig bladder urothelial cells: potential role in bladder filling sensations. *British Journal of Pharmacology, 171*(14), 3394-3403. doi:http://dx.doi.org/10.1111/bph.12682

Mihara, H., Suzuki, N., Boudaka, A. A., Muhammad, J. S., Tominaga, M., Tabuchi, Y., & Sugiyama, T. (2016). Transient receptor potential vanilloid 4-dependent calcium influx and ATP release in mouse and rat gastric epithelia. *World Journal of Gastroenterology, 22*(24), 5512-5519. doi:http://dx.doi.org/10.3748/wjg.v22.i24.5512

Miller, D. L., & Williams, A. R. (1983). Further Investigations of Atp Release from Human Erythrocytes Exposed to Ultrasonically Activated Gas Filled Pores. *Ultrasound in Medicine & Biology, 9*(3), 297-308.

Millward-Sadler, S. J., Wright, M. O., Flatman, P. W., & Salter, D. M. (2004). ATP in the mechanotransduction pathway of normal human chondrocytes. *Biorheology, 41*(3-4), 567-575.

Milner, P., Bodin, P., Loesch, A., & Burnstock, G. (1992). Increased shear stress leads to differential release of endothelin and ATP from isolated endothelial cells from 4- and 12-month-old male rabbit aorta. *Journal of Vascular Research, 29*(6), 420-425.

Milner, P., Kirkpatrick, K. A., Ralevic, V., Toothill, V., Pearson, J., & Burnstock, G. (1990). Endothelial cells cultured from human umbilical vein release ATP, substance P and acetylcholine in response to increased flow. *Proceedings of the Royal Society of London - Series B: Biological Sciences, 241*(1302), 245-248.

Mitchell, C. H., Carre, D. A., McGlinn, A. M., Stone, R. A., & Civan, M. M. (1998). A release mechanism for stored ATP in ocular ciliary epithelial cells. *Proceedings of the National Academy of Sciences of the United States of America, 95*(12), 7174-7178.

Miyamoto, T., Mochizuki, T., Nakagomi, H., Kira, S., Watanabe, M., Takayama, Y., . . . Tominaga, M. (2014). Functional role for Piezo1 in stretch-evoked Ca2+ influx and ATP release in urothelial cell cultures. *Journal of Biological Chemistry, 289*(23), 16565-16575. doi:http://dx.doi.org/10.1074/jbc.M113.528638

Mochizuki, T., Araki, I., Yoshiyama, M., & Takeda, M. (2009). Functional role of the TRPV4 cation channel in stretch-evoked Ca2+ influx and ATP release in mouse urothelial primary cultures. *Neurourology and Urodynamics, 28 (7)*, 706-707. doi:http://dx.doi.org/10.1002/nau.20808

Moehlenbrock, M. J., Price, A. K., & Martin, R. S. (2006). Use of microchip-based hydrodynamic focusing to measure the deformation-induced release of ATP from erythrocytes. *Analyst, 131*(8), 930-937.

Murata, N., Ito, S., Furuya, K., Takahara, N., Naruse, K., Aso, H., . . . Hasegawa, Y. (2014). Ca2+ influx and ATP release mediated by mechanical stretch in human lung fibroblasts. *Biochemical & Biophysical Research Communications, 453*(1), 101-105. doi:http://dx.doi.org/10.1016/j.bbrc.2014.09.063

Musante, L., Zegarra-Moran, O., Montaldo, P. G., Ponzoni, M., & Galietta, L. J. (1999). Autocrine regulation of volume-sensitive anion channels in airway epithelial cells by adenosine. *Journal of Biological Chemistry, 274*(17), 11701-11707.

Nandigama, R., Padmasekar, M., Wartenberg, M., & Sauer, H. (2006). Feed forward cycle of hypotonic stress-induced ATP release, purinergic receptor activation, and growth stimulation of prostate cancer cells. *Journal of Biological Chemistry, 281*(9), 5686-5693.

Neary, J. T., Kang, Y., Tran, M., & Feld, J. (2005). Traumatic injury activates protein kinase B/Akt in cultured astrocytes: role of extracellular ATP and P2 purinergic receptors. *Journal of Neurotrauma, 22*(4), 491-500.

Negoro, H., Urban-Maldonado, M., Liou, L. S., Spray, D. C., Thi, M. M., & Suadicani, S. O. (2014). Pannexin 1 channels play essential roles in urothelial mechanotransduction and intercellular signaling. *PLoS ONE [Electronic Resource], 9*(8), e106269. doi:http://dx.doi.org/10.1371/journal.pone.0106269

Newman, E. A. (2001). Propagation of intercellular calcium waves in retinal astrocytes and Muller cells. *Journal of Neuroscience, 21*(7), 2215-2223.

Noma, N., Shinoda, M., Honda, K., Kiyomoto, M., Dezawa, K., Nakaya, Y., . . . Iwata, K. (2013). Interaction of IL-1beta and P2X(3) receptor in pathologic masseter muscle pain. *Journal of Dental Research, 92*(5), 456-460. doi:http://dx.doi.org/10.1177/0022034513483770

Ochodnicky, P., Michel, M. B., Butter, J. J., Seth, J., Panicker, J. N., & Michel, M. C. (2013). Bradykinin modulates spontaneous nerve growth factor production and stretch-induced ATP release in human urothelium. *Pharmacological Research, 70*(1), 147-154. doi:http://dx.doi.org/10.1016/j.phrs.2013.01.010

Ohbuchi, T., Takenaga, F., Hohchi, N., Wakasugi, T., Ueta, Y., & Suzuki, H. (2014). Possible contribution of pannexin-1 to ATP release in human upper airway epithelia. *Physiological Reports, 2*(2), e00227. doi:http://dx.doi.org/10.1002/phy2.227

Oike, M., Kimura, C., Koyama, T., Yoshikawa, M., & Ito, Y. (2000). Hypotonic stress-induced dual Ca(2+) responses in bovine aortic endothelial cells. *American Journal of Physiology - Heart & Circulatory Physiology, 279*(2), H630-638.

Oishi, S., Sasano, T., Tateishi, Y., Tamura, N., Isobe, M., & Furukawa, T. (2012). Stretch of atrial myocytes stimulates recruitment of macrophages via ATP released through gap-junction channels. *Journal of Pharmacological Sciences, 120*(4), 296-304.

Okada, S. F., Nicholas, R. A., Kreda, S. M., Lazarowski, E. R., & Boucher, R. C. (2006). Physiological regulation of ATP release at the apical surface of human airway epithelia. *Journal of Biological Chemistry, 281*(32), 22992-23002.

Okada, S. F., O'Neal, W. K., Huang, P., Nicholas, R. A., Ostrowski, L. E., Craigen, W. J., . . . Boucher, R. C. (2004). Voltage-dependent anion channel-1 (VDAC-1) contributes to ATP release and cell volume regulation in murine cells. *Journal of General Physiology, 124*(5), 513-526.

Okada, S. F., Ribeiro, C. M., Sesma, J. I., Seminario-Vidal, L., Abdullah, L. H., van Heusden, C., . . . Boucher, R. C. (2013). Inflammation promotes airway epithelial ATP release via calcium-dependent vesicular pathways. *American Journal of Respiratory Cell & Molecular Biology, 49*(5), 814-820. doi:http://dx.doi.org/10.1165/rcmb.2012-0493OC

Olearczyk, J. J., Ellsworth, M. L., Stephenson, A. H., Lonigro, A. J., & Sprague, R. S. (2004). Nitric oxide inhibits ATP release from erythrocytes. *Journal of Pharmacology & Experimental Therapeutics, 309*(3), 1079-1084.

Olsen, S. M., Stover, J. D., & Nagatomi, J. (2011). Examining the role of mechanosensitive ion channels in pressure mechanotransduction in rat bladder urothelial cells. *Annals of Biomedical Engineering, 39*(2), 688-697. doi:http://dx.doi.org/10.1007/s10439-010-0203-3

Ostrom, R. S., Gregorian, C., Drenan, R. M., Gabot, K., Rana, B. K., & Insel, P. A. (2001). Key role for constitutive cyclooxygenase-2 of MDCK cells in basal signaling and response to released ATP. *American Journal of Physiology - Cell Physiology, 281*(2 50-2), C524-C531.

Ostrom, R. S., Gregorian, C., & Insel, P. A. (2000). Cellular release of and response to ATP as key determinants of the set-point of signal transduction pathways. *Journal of Biological Chemistry, 275*(16), 11735-11739.

Oury, C., Sticker, E., Cornelissen, H., De Vos, R., Vermylen, J., & Hoylaerts, M. F. (2004). ATP augments von Willebrand factor-dependent shear-induced platelet aggregation through Ca²⁺-calmodulin and myosin light chain kinase activation. *Journal of Biological Chemistry, 279*(25), 26266-26273. doi:http://dx.doi.org/10.1074/jbc.M402032200

Patel, A. S., Reigada, D., Mitchell, C. H., Bates, S. R., Margulies, S. S., & Koval, M. (2005). Paracrine stimulation of surfactant secretion by extracellular ATP in response to mechanical deformation. *American Journal of Physiology - Lung Cellular & Molecular Physiology, 289*(3), L489-496.

Patel, B. A. (2014). Mucosal adenosine triphosphate mediates serotonin release from ileal but not colonic guinea pig enterochromaffin cells. *Neurogastroenterology & Motility, 26*(2), 237-246. doi:http://dx.doi.org/10.1111/nmo.12254

Pedersen, S., Pedersen, S. F., Nilius, B., Lambert, I. H., & Hoffmann, E. K. (1999). Mechanical stress induces release of ATP from Ehrlich ascites tumor cells. *Biochimica et Biophysica Acta, 1416*(1-2), 271-284.

Petruzzi, E., Orlando, C., Pinzani, P., Sestini, R., Del Rosso, A., Dini, G., . . . Pazzagli, M. (1994). Adenosine triphosphate release by osmotic shock and hemoglobin A1C in diabetic subjects' erythrocytes. *Metabolism: Clinical & Experimental, 43*(4), 435-440.

Pines, A., Romanello, M., Cesaratto, L., Damante, G., Moro, L., D'Andrea, P., & Tell, G. (2003). Extracellular ATP stimulates the early growth response protein 1 (Egr-1) via a protein kinase C-dependent pathway in the human osteoblastic HOBIT cell line. *Biochemical Journal, 373*(Pt 3), 815-824.

Price, A. K., Fischer, D. J., Martin, R. S., & Spence, D. M. (2004). Deformation-induced release of ATP from erythrocytes in a poly(dimethylsiloxane)-based microchip with channels that mimic resistance vessels. *Analytical Chemistry, 76*(16), 4849-4855.

Price, A. K., Martin, R. S., & Spence, D. M. (2006). Monitoring erythrocytes in a microchip channel that narrows uniformly: towards an improved microfluidic-based mimic of the microcirculation. *Journal of Chromatography. A, 1111*(2), 220-227.

Ramsingh, R., Grygorczyk, A., Solecki, A., Cherkaoui, L. S., Berthiaume, Y., & Grygorczyk, R. (2011). Cell deformation at the air-liquid interface induces Ca2+-dependent ATP release from lung epithelial cells. *American Journal of Physiology - Lung Cellular & Molecular Physiology, 300*(4), L587-595. doi:http://dx.doi.org/10.1152/ajplung.00345.2010

Ransford, G. A., Fregien, N., Qiu, F., Dahl, G., Conner, G. E., & Salathe, M. (2009). Pannexin 1 contributes to ATP release in airway epithelia. *American Journal of Respiratory Cell & Molecular Biology, 41*(5), 525-534. doi:http://dx.doi.org/10.1165/rcmb.2008-0367OC

Reigada, D., Lu, W., Zhang, M., & Mitchell, C. H. (2008). Elevated pressure triggers a physiological release of ATP from the retina: Possible role for pannexin hemichannels. *Neuroscience, 157*(2), 396-404. doi:http://dx.doi.org/10.1016/j.neuroscience.2008.08.036

Reigada, D., & Mitchell, C. H. (2005). Release of ATP from retinal pigment epithelial cells involves both CFTR and vesicular transport. *American Journal of Physiology - Cell Physiology, 288*(1), C132-140.

Resta, V., Novelli, E., Vozzi, G., Scarpa, C., Caleo, M., Ahluwalia, A., . . . Galli-Resta, L. (2007). Acute retinal ganglion cell injury caused by intraocular pressure spikes is mediated by endogenous extracellular ATP. *European Journal of Neuroscience, 25*(9), 2741-2754.

Rich, P. B., Douillet, C. D., Mahler, S. A., Husain, S. A., & Boucher, R. C. (2003). Adenosine triphosphate is released during injurious mechanical ventilation and contributes to lung edema. *Journal of Trauma-Injury Infection & Critical Care, 55*(2), 290-297.

Riddle, R. C., Hippe, K. R., & Donahue, H. J. (2008). Chemotransport contributes to the effect of oscillatory fluid flow on human bone marrow stromal cell proliferation. *Journal of Orthopaedic Research, 26*(7), 918-924. doi:http://dx.doi.org/10.1002/jor.20637

Riddle, R. C., Taylor, A. F., Rogers, J. R., & Donahue, H. J. (2007). ATP release mediates fluid flow-induced proliferation of human bone marrow stromal cells. *Journal of Bone & Mineral Research, 22*(4), 589-600.

Rodat-Despoix, L., Hao, J., Dandonneau, M., & Delmas, P. (2013). Shear stress-induced Ca2+ mobilization in MDCK cells is ATP dependent, no matter the primary cilium. *Cell Calcium, 53*(5-6), 327-337. doi:http://dx.doi.org/10.1016/j.ceca.2013.02.002

Roman, R. M., Feranchak, A. P., Davison, A. K., Schwiebert, E. M., & Fitz, J. G. (1999). Evidence for Gd(3+) inhibition of membrane ATP permeability and purinergic signaling. *American Journal of Physiology, 277*(6 Pt 1), G1222-1230.

Roman, R. M., Feranchak, A. P., Salter, K. D., Wang, Y., & Fitz, J. G. (1999). Endogenous ATP release regulates Cl- secretion in cultured human and rat biliary epithelial cells. *American Journal of Physiology, 276*(6 Pt 1), G1391-1400.

Romanello, M., Codognotto, A., Bicego, M., Pines, A., Tell, G., & D'Andrea, P. (2005). Autocrine/paracrine stimulation of purinergic receptors in osteoblasts: contribution of vesicular ATP release. *Biochemical & Biophysical Research Communications, 331*(4), 1429-1438.

Romanello, M., Pani, B., Bicego, M., & D'Andrea, P. (2001). Mechanically induced ATP release from human osteoblastic cells. *Biochemical & Biophysical Research Communications, 289*(5), 1275-1281.

Rosenthal, A. K., Gohr, C. M., Mitton-Fitzgerald, E., Lutz, M. K., Dubyak, G. R., & Ryan, L. M. (2013). The progressive ankylosis gene product ANK regulates extracellular ATP levels in primary articular chondrocytes. *Arthritis Research & Therapy, 15*(5), R154. doi:http://dx.doi.org/10.1186/ar4337

Rumney, R. M., Sunters, A., Reilly, G. C., & Gartland, A. (2012). Application of multiple forms of mechanical loading to human osteoblasts reveals increased ATP release in response to fluid flow in 3D cultures and differential regulation of immediate early genes. *Journal of Biomechanics, 45*(3), 549-554. doi:http://dx.doi.org/10.1016/j.jbiomech.2011.11.036

Sadananda, P., Kao, F. C., Liu, L., Mansfield, K. J., & Burcher, E. (2012). Acid and stretch, but not capsaicin, are effective stimuli for ATP release in the porcine bladder mucosa: Are ASIC and TRPV1 receptors involved? *European Journal of Pharmacology, 683*(1-3), 252-259. doi:http://dx.doi.org/10.1016/j.ejphar.2012.02.041

Salas, N. A., Somogyi, G. T., Gangitano, D. A., Boone, T. B., & Smith, C. P. (2007). Receptor activated bladder and spinal ATP release in neurally intact and chronic spinal cord injured rats. *Neurochemistry International, 50*(2), 345-350.

Salter, K. D., Fitz, J. G., & Roman, R. M. (2000). Domain-specific purinergic signaling in polarized rat cholangiocytes. *American Journal of Physiology - Gastrointestinal & Liver Physiology, 278*(3), G492-500.

Sano, T., Kobayashi, T., Negoro, H., Sengiku, A., Hiratsuka, T., Kamioka, Y., . . . Matsuda, M. (2016). Intravital imaging of mouse urothelium reveals activation of extracellular signal-regulated kinase by stretch-induced intravesical release of ATP. *Physiological Reports, 4*(21).

Sathe, M. N., Woo, K., Kresge, C., Bugde, A., Luby-Phelps, K., Lewis, M. A., & Feranchak, A. P. (2011). Regulation of purinergic signaling in biliary epithelial cells by exocytosis of SLC17A9-dependent ATP-enriched vesicles. *Journal of Biological Chemistry, 286*(28), 25363-25376. doi:http://dx.doi.org/10.1074/jbc.M111.232868

Sauer, H., Hescheler, J., & Wartenberg, M. (2000). Mechanical strain-induced Ca(2+) waves are propagated via ATP release and purinergic receptor activation. *American Journal of Physiology - Cell Physiology, 279*(2), C295-307.

Sawada, T., Kishiya, M., Kanemaru, K., Seya, K., Yokoyama, T., Ueyama, K., . . . Furukawa, K. (2008). Possible role of extracellular nucleotides in ectopic ossification of human spinal ligaments. *Journal of Pharmacological Sciences, 106*(1), 152-161.

Schwiebert, E. M., Wallace, D. P., Braunstein, G. M., King, S. R., Peti-Peterdi, J., Hanaoka, K., . . . Taylor, A. L. (2002). Autocrine extracellular purinergic signaling in epithelial cells derived from polycystic kidneys. *American Journal of Physiology-Renal Physiology, 282*(4), F763-F775. doi:10.1152/ajprenal.0337.2000

Schwiebert, L. M., Rice, W. C., Kudlow, B. A., Taylor, A. L., & Schwiebert, E. M. (2002). Extracellular ATP signaling and P2X nucleotide receptors in monolayers of primary human vascular endothelial cells. *American Journal of Physiology - Cell Physiology, 282*(2), C289-301.

Segawa, S., Nishiura, T., Furuta, T., Ohsato, Y., Tani, M., Nishida, K., & Nagasawa, K. (2014). Zinc is released by cultured astrocytes as a gliotransmitter under hypoosmotic stress-loaded conditions and regulates microglial activity. *Life Sciences, 94*(2), 137-144. doi:http://dx.doi.org/10.1016/j.lfs.2013.11.007

Selzner, N., Selzner, M., Graf, R., Ungethuem, U., Fitz, J. G., & Clavien, P. A. (2004). Water induces autocrine stimulation of tumor cell killing through ATP release and P2 receptor binding. *Cell Death & Differentiation, 11 Suppl 2*, S172-180.

Seminario-Vidal, L., Okada, S. F., Sesma, J. I., Kreda, S. M., van Heusden, C. A., Zhu, Y., . . . Lazarowski, E. R. (2011). Rho signaling regulates pannexin 1-mediated ATP release from airway epithelia. *Journal of Biological Chemistry, 286*(30), 26277-26286. doi:http://dx.doi.org/10.1074/jbc.M111.260562

Seref-Ferlengez, Z., Maung, S., Schaffler, M. B., Spray, D. C., Suadicani, S. O., & Thi, M. M. (2016). P2X7R-Panx1 Complex Impairs Bone Mechanosignaling under High Glucose Levels Associated with Type-1 Diabetes. *PLoS ONE [Electronic Resource], 11*(5), e0155107. doi:http://dx.doi.org/10.1371/journal.pone.0155107

Shahidullah, M., Mandal, A., Beimgraben, C., & Delamere, N. A. (2012). Hyposmotic stress causes ATP release and stimulates Na,K-ATPase activity in porcine lens. *Journal of Cellular Physiology, 227*(4), 1428-1437. doi:http://dx.doi.org/10.1002/jcp.22858

Shahidullah, M., Mandal, A., & Delamere, N. A. (2012). TRPV4 in porcine lens epithelium regulates hemichannel-mediated ATP release and Na-K-ATPase activity. *American Journal of Physiology - Cell Physiology, 302*(12), C1751-1761. doi:http://dx.doi.org/10.1152/ajpcell.00010.2012

Shinozuka, K., Tanaka, N., Kawasaki, K., Mizuno, H., Kubota, Y., Nakamura, K., . . . Kunitomo, M. (2001). Participation of ATP in cell volume regulation in the endothelium after hypotonic stress. *Clinical & Experimental Pharmacology & Physiology, 28*(10), 799-803.

Sikora, J., Orlov, S. N., Furuya, K., & Grygorczyk, R. (2014). Hemolysis is a primary ATP-release mechanism in human erythrocytes. *Blood, 124*(13), 2150-2157. doi:http://dx.doi.org/10.1182/blood-2014-05-572024

Silva, G. B., & Garvin, J. L. (2008). TRPV4 mediates hypotonicity-induced ATP release by the thick ascending limb. *American Journal of Physiology - Renal Physiology, 295*(4), F1090-1095. doi:http://dx.doi.org/10.1152/ajprenal.90365.2008

Smith, C. P., Gangitano, D. A., Munoz, A., Salas, N. A., Boone, T. B., Aoki, K. R., . . . Somogyi, G. T. (2008). Botulinum toxin type A normalizes alterations in urothelial ATP and NO release induced by chronic spinal cord injury. *Neurochemistry International, 52*(6), 1068-1075. doi:http://dx.doi.org/10.1016/j.neuint.2007.11.006

Smith, C. P., Vemulakonda, V. M., Kiss, S., Boone, T. B., & Somogyi, G. T. (2005). Enhanced ATP release from rat bladder urothelium during chronic bladder inflammation: effect of botulinum toxin A. *Neurochemistry International, 47*(4), 291-297.

Sorensen, C. E., & Novak, I. (2001). Visualization of ATP release in pancreatic acini in response to cholinergic stimulus. Use of fluorescent probes and confocal microscopy. *Journal of Biological Chemistry, 276*(35), 32925-32932.

Soto, D., Comes, N., Ferrer, E., Morales, M., Escalada, A., Pales, J., . . . Gasull, X. (2004). Modulation of aqueous humor outflow by ionic mechanisms involved in trabecular meshwork cell volume regulation. *Investigative Ophthalmology & Visual Science, 45*(10), 3650-3661.

Sprague, R. S., Ellsworth, M. L., Stephenson, A. H., Kleinhenz, M. E., & Lonigro, A. J. (1998). Deformation-induced ATP release from red blood cells requires CFTR activity. *American Journal of Physiology, 275*(5 Pt 2), H1726-1732.

Sprague, R. S., Ellsworth, M. L., Stephenson, A. H., & Lonigro, A. J. (1996). ATP: the red blood cell link to NO and local control of the pulmonary circulation. *American Journal of Physiology, 271*(6 Pt 2), H2717-2722.

Sprague, R. S., Ellsworth, M. L., Stephenson, A. H., & Lonigro, A. J. (2001). Participation of cAMP in a signal-transduction pathway relating erythrocyte deformation to ATP release. *American Journal of Physiology - Cell Physiology, 281*(4), C1158-1164.

Sprague, R. S., Stephenson, A. H., Ellsworth, M. L., Keller, C., & Lonigro, A. J. (2001). Impaired release of ATP from red blood cells of humans with primary pulmonary hypertension. *Experimental Biology & Medicine, 226*(5), 434-439.

Sprung, R., Sprague, R., & Spence, D. (2002). Determination of ATP release from erythrocytes using microbore tubing as a model of resistance vessels in vivo. *Analytical Chemistry, 74*(10), 2274-2278.

Steward, A. J., Kelly, D. J., & Wagner, D. R. (2016). Purinergic Signaling Regulates the Transforming Growth Factor-beta3-Induced Chondrogenic Response of Mesenchymal Stem Cells to Hydrostatic Pressure. *Tissue engineering. Part A., 22*(11-12), 831-839. doi:http://dx.doi.org/10.1089/ten.TEA.2015.0047

Stones, R. W., Vials, A., Milner, P., Beard, R. W., & Burnstock, G. (1996). Release of vasoactive agents from the isolated perfused human ovary. *European Journal of Obstetrics Gynecology and Reproductive Biology, 67*(2), 191-196. doi:http://dx.doi.org/10.1016/0301-2115%2896%2902466-9

Stout, C., & Charles, A. (2003). Modulation of intercellular calcium signaling in astrocytes by extracellular calcium and magnesium. *GLIA, 43*(3), 265-273.

Stout, C. E., Costantin, J. L., Naus, C. C., & Charles, A. C. (2002). Intercellular calcium signaling in astrocytes via ATP release through connexin hemichannels. *Journal of Biological Chemistry, 277*(12), 10482-10488.

Stuart, J. A., Anderson, K. L., French, P. J., Kirk, C. J., & Michell, R. H. (1994). The intracellular distribution of inositol polyphosphates in HL60 promyeloid cells. *Biochemical Journal, 303*(Pt 2), 517-525.

Sun, Y., & Chai, T. C. (2006). Augmented extracellular ATP signaling in bladder urothelial cells from patients with interstitial cystitis. *American Journal of Physiology - Cell Physiology, 290*(1), C27-34.

Sun, Y., Keay, S., De Deyne, P. G., & Chai, T. C. (2001). Augmented stretch activated adenosine triphosphate release from bladder uroepithelial cells in patients with interstitial cystitis. *Journal of Urology, 166*(5), 1951-1956.

Taguchi, T., Kozaki, Y., Katanosaka, K., & Mizumura, K. (2008). Compression-induced ATP release from rat skeletal muscle with and without lengthening contraction. *Neuroscience Letters, 434*(3), 277-281. doi:http://dx.doi.org/10.1016/j.neulet.2008.01.068

Takada, H., Furuya, K., & Sokabe, M. (2014). Mechanosensitive ATP release from hemichannels and Ca2+ influx through TRPC6 accelerate wound closure in keratinocytes. *Journal of Cell Science, 127*(Pt 19), 4159-4171. doi:http://dx.doi.org/10.1242/jcs.147314

Takahara, N., Ito, S., Furuya, K., Naruse, K., Aso, H., Kondo, M., . . . Hasegawa, Y. (2014). Real-time imaging of ATP release induced by mechanical stretch in human airway smooth muscle cells. *American Journal of Respiratory Cell & Molecular Biology, 51*(6), 772-782. doi:http://dx.doi.org/10.1165/rcmb.2014-0008OC

Takemura, H., Takamura, Y., Isono, K., Tamaoki, J., Nagai, A., & Kawahara, K. (2003). Hypotonicity-induced ATP release is potentiated by intracellular Ca2+ and cyclic AMP in cultured human bronchial cells. *Japanese Journal of Physiology, 53*(5), 319-326.

Tanaka, I., Nagase, K., Tanase, K., Aoki, Y., Akino, H., & Yokoyama, O. (2011). Modulation of stretch evoked adenosine triphosphate release from bladder epithelium by prostaglandin E2. *Journal of Urology, 185*(1), 341-346. doi:http://dx.doi.org/10.1016/j.juro.2010.09.042

Tarran, R., Button, B., Picher, M., Paradiso, A. M., Ribeiro, C. M., Lazarowski, E. R., . . . Boucher, R. C. (2005). Normal and cystic fibrosis airway surface liquid homeostasis. The effects of phasic shear stress and viral infections. *Journal of Biological Chemistry, 280*(42), 35751-35759.

Tatur, S., Groulx, N., Orlov, S. N., & Grygorczyk, R. (2007). Ca2+-dependent ATP release from A549 cells involves synergistic autocrine stimulation by coreleased uridine nucleotides. *Journal of Physiology, 584*(Pt 2), 419-435.

Tatur, S., Kreda, S., Lazarowski, E., & Grygorczyk, R. (2008). Calcium-dependent release of adenosine and uridine nucleotides from A549 cells. *Purinergic signalling, 4*(2), 139-146. doi:http://dx.doi.org/10.1007/s11302-007-9059-x

Taylor, A. L., Kudlow, B. A., Marrs, K. L., Gruenert, D. C., Guggino, W. B., & Schwiebert, E. M. (1998). Bioluminescence detection of ATP release mechanisms in epithelia. *American Journal of Physiology, 275*(5 Pt 1), C1391-1406.

Thompson, W. R., Majid, A. S., Czymmek, K. J., Ruff, A. L., Garcia, J., Duncan, R. L., & Farach-Carson, M. C. (2011). Association of the alpha(2)delta(1) subunit with Ca(v)3.2 enhances membrane expression and regulates mechanically induced ATP release in MLO-Y4 osteocytes. *Journal of Bone & Mineral Research, 26*(9), 2125-2139. doi:http://dx.doi.org/10.1002/jbmr.437

Thrane, A. S., Rappold, P. M., Fujita, T., Torres, A., Bekar, L. K., Takano, T., . . . Nagelhus, E. A. (2011). Critical role of aquaporin-4 (AQP4) in astrocytic Ca2+ signaling events elicited by cerebral edema. *Proceedings of the National Academy of Sciences of the United States of America, 108*(2), 846-851. doi:http://dx.doi.org/10.1073/pnas.1015217108

Tolan, N. V., Genes, L. I., Subasinghe, W., Raththagala, M., & Spence, D. M. (2009). Personalized metabolic assessment of erythrocytes using microfluidic delivery to an array of luminescent wells. *Analytical Chemistry, 81*(8), 3102-3108. doi:http://dx.doi.org/10.1021/ac900084g

Toma, I., Bansal, E., Meer, E. J., Kang, J. J., Vargas, S. L., & Peti-Peterdi, J. (2008). Connexin 40 and ATP-dependent intercellular calcium wave in renal glomerular endothelial cells. *American Journal of Physiology - Regulatory Integrative & Comparative Physiology, 294*(6), R1769-1776. doi:http://dx.doi.org/10.1152/ajpregu.00489.2007

Tomassen, S. F., van der Wijk, T., de Jonge, H. R., & Tilly, B. C. (2004). Activation of phospholipase D by osmotic cell swelling. *FEBS Letters, 566*(1-3), 287-290.

Tong, J., Zhou, X. D., Perelman, J. M., & Kolosov, V. P. (2013). Effect of epithelium ATP release on cyclic pressure-induced airway mucus secretion. *Bioscience Reports, 16*, 16. doi:http://dx.doi.org/10.1042/BSR20130109

Tsuzaki, M., Bynum, D., Almekinders, L., Yang, X., Faber, J., & Banes, A. J. (2003). ATP modulates load-inducible IL-1beta, COX 2, and MMP-3 gene expression in human tendon cells. *Journal of Cellular Biochemistry, 89*(3), 556-562.

Ullrich, N., Caplanusi, A., Brone, B., Hermans, D., Lariviere, E., Nilius, B., . . . Eggermont, J. (2006). Stimulation by caveolin-1 of the hypotonicity-induced release of taurine and ATP at basolateral, but not apical, membrane of Caco-2 cells. *American Journal of Physiology - Cell Physiology, 290*(5), C1287-1296.

Van der Wijk, T., De Jonge, H. R., & Tilly, B. C. (1999). Osmotic cell swelling-induced ATP release mediates the activation of extracellular signal-regulated protein kinase (Erk)-1/2 but not the activation of osmo-sensitive anion channels. *Biochemical Journal, 343 Pt 3*, 579-586.

van der Wijk, T., Tomassen, S. F., Houtsmuller, A. B., de Jonge, H. R., & Tilly, B. C. (2003). Increased vesicle recycling in response to osmotic cell swelling. Cause and consequence of hypotonicity-provoked ATP release. *Journal of Biological Chemistry, 278*(41), 40020-40025.

Varela, D., Penna, A., Simon, F., Eguiguren, A. L., Leiva-Salcedo, E., Cerda, O., . . . Stutzin, A. (2010). P2X4 activation modulates volume-sensitive outwardly rectifying chloride channels in rat hepatoma cells. *Journal of Biological Chemistry, 285*(10), 7566-7574. doi:http://dx.doi.org/10.1074/jbc.M109.063693

Vick, J. S., & Delay, R. J. (2012). ATP excites mouse vomeronasal sensory neurons through activation of P2X receptors. *Neuroscience, 220*, 341-350. doi:http://dx.doi.org/10.1016/j.neuroscience.2012.06.004

Vlaskovska, M., Kasakov, L., Rong, W., Bodin, P., Bardini, M., Cockayne, D. A., . . . Burnstock, G. (2001). P2X3 knock-out mice reveal a major sensory role for urothelially released ATP. *Journal of Neuroscience, 21*(15), 5670-5677.

Wan, J., Ristenpart, W. D., & Stone, H. A. (2008). Dynamics of shear-induced ATP release from red blood cells. *Proceedings of the National Academy of Sciences of the United States of America, 105*(43), 16432-16437. doi:http://dx.doi.org/10.1073/pnas.0805779105

Wang, E. C., Lee, J. M., Ruiz, W. G., Balestreire, E. M., von Bodungen, M., Barrick, S., . . . Apodaca, G. (2005). ATP and purinergic receptor-dependent membrane traffic in bladder umbrella cells. *Journal of Clinical Investigation, 115*(9), 2412-2422.

Wang, L., Sikora, J., Hu, L., Shen, X., Grygorczyk, R., & Schwarz, W. (2013). ATP release from mast cells by physical stimulation: a putative early step in activation of acupuncture points. *Evidence-Based Complementary & Alternative Medicine: eCAM, 2013*, 350949. doi:http://dx.doi.org/10.1155/2013/350949

Wang, N., Rumney, R. M., Yang, L., Robaye, B., Boeynaems, J. M., Skerry, T. M., & Gartland, A. (2013). The P2Y13 receptor regulates extracellular ATP metabolism and the osteogenic response to mechanical loading. *Journal of Bone & Mineral Research, 28*(6), 1446-1456. doi:http://dx.doi.org/10.1002/jbmr.1877

Wang, S., Chennupati, R., Kaur, H., Iring, A., Wettschureck, N., & Offermanns, S. (2016). Endothelial cation channel PIEZO1 controls blood pressure by mediating flow-induced ATP release. *Journal of Clinical Investigation, 126*(12), 4527-4536. doi:http://dx.doi.org/10.1172/JCI87343

Wang, S., Iring, A., Strilic, B., Albarran Juarez, J., Kaur, H., Troidl, K., . . . Offermanns, S. (2015). P2Y2 and Gq/G11 control blood pressure by mediating endothelial mechanotransduction. *Journal of Clinical Investigation, 125*(8), 3077-3086. doi:http://dx.doi.org/10.1172/JCI81067

Wann, A. K., Zuo, N., Haycraft, C. J., Jensen, C. G., Poole, C. A., McGlashan, S. R., & Knight, M. M. (2012). Primary cilia mediate mechanotransduction through control of ATP-induced Ca2+ signaling in compressed chondrocytes. *FASEB Journal, 26*(4), 1663-1671. doi:http://dx.doi.org/10.1096/fj.11-193649

Watt, W. C., Lazarowski, E. R., & Boucher, R. C. (1998). Cystic fibrosis transmembrane regulator-independent release of ATP. Its implications for the regulation of P2Y2 receptors in airway epithelia. *Journal of Biological Chemistry, 273*(22), 14053-14058.

Williams, A. R., & Miller, D. L. (1980). Photometric Detection of Atp Release from Human Erythrocytes Exposed to Ultrasonically Activated Gas Filled Pores. *Ultrasound in Medicine & Biology, 6*(3), 251-256.

Williams, M. S., Coller, B. S., Vaananen, H. J., Scudder, L. E., Sharma, S. K., & Marmur, J. D. (1998). Activation of platelets in platelet-rich plasma by rotablation is speed-dependent and can be inhibited by abciximab (c7E3 Fab; ReoPro). *Circulation, 98*(8), 742-748.

Wilson, P. D., Hovater, J. S., Casey, C. C., Fortenberry, J. A., & Schwiebert, E. M. (1999). ATP release mechanisms in primary cultures of epithelia derived from the cysts of polycystic kidneys. *Journal of the American Society of Nephrology, 10*(2), 218-229.

Woehrle, T., Yip, L., Manohar, M., Sumi, Y., Yao, Y., Chen, Y., & Junger, W. G. (2010). Hypertonic stress regulates T cell function via pannexin-1 hemichannels and P2X receptors. *Journal of Leukocyte Biology, 88*(6), 1181-1189. doi:http://dx.doi.org/10.1189/jlb.0410211

Woo, K., Dutta, A. K., Patel, V., Kresge, C., & Feranchak, A. P. (2008). Fluid flow induces mechanosensitive ATP release, calcium signalling and Cl- transport in biliary epithelial cells through a PKCzeta-dependent pathway. *Journal of Physiology, 586*(11), 2779-2798. doi:http://dx.doi.org/10.1113/jphysiol.2008.153015

Woo, K., Sathe, M., Kresge, C., Esser, V., Ueno, Y., Venter, J., . . . Feranchak, A. P. (2010). Adenosine triphosphate release and purinergic (P2) receptor-mediated secretion in small and large mouse cholangiocytes. *Hepatology, 52*(5), 1819-1828. doi:http://dx.doi.org/10.1002/hep.23883

Wynn, G., Ma, B., Ruan, H. Z., & Burnstock, G. (2004). Purinergic component of mechanosensory transduction is increased in a rat model of colitis. *American Journal of Physiology - Gastrointestinal & Liver Physiology, 287*(3), G647-657.

Wynn, G., Rong, W., Xiang, Z., & Burnstock, G. (2003). Purinergic mechanisms contribute to mechanosensory transduction in the rat colorectum. *Gastroenterology, 125*(5), 1398-1409.

Xia, J., Lim, J. C., Lu, W., Beckel, J. M., Macarak, E. J., Laties, A. M., & Mitchell, C. H. (2012). Neurons respond directly to mechanical deformation with pannexin-mediated ATP release and autostimulation of P2X7 receptors. *Journal of Physiology, 590*(Pt 10), 2285-2304. doi:http://dx.doi.org/10.1113/jphysiol.2012.227983

Xing, Y., Gu, Y., Bresnahan, J. J., Paul, E. M., Donahue, H. J., & You, J. (2014). The roles of P2Y2 purinergic receptors in osteoblasts and mechanotransduction. *PLoS ONE [Electronic Resource], 9*(9), e108417. doi:http://dx.doi.org/10.1371/journal.pone.0108417

Xing, Y., Gu, Y., Xu, L. C., Siedlecki, C. A., Donahue, H. J., & You, J. (2011). Effects of membrane cholesterol depletion and GPI-anchored protein reduction on osteoblastic mechanotransduction. *Journal of Cellular Physiology, 226*(9), 2350-2359. doi:http://dx.doi.org/10.1002/jcp.22579

Xu, C., Shmukler, B. E., Nishimura, K., Kaczmarek, E., Rossetti, S., Harris, P. C., . . . Alper, S. L. (2009). Attenuated, flow-induced ATP release contributes to absence of flow-sensitive, purinergic Cai2+ signaling in human ADPKD cyst epithelial cells. *American Journal of Physiology - Renal Physiology, 296*(6), F1464-1476. doi:http://dx.doi.org/10.1152/ajprenal.90542.2008

Yamamoto, K., & Ando, J. (2013). Endothelial cell and model membranes respond to shear stress by rapidly decreasing the order of their lipid phases. *Journal of Cell Science, 126*(Pt 5), 1227-1234. doi:http://dx.doi.org/10.1242/jcs.119628

Yamamoto, K., Furuya, K., Nakamura, M., Kobatake, E., Sokabe, M., & Ando, J. (2011). Visualization of flow-induced ATP release and triggering of Ca2+ waves at caveolae in vascular endothelial cells. *Journal of Cell Science, 124*(Pt 20), 3477-3483. doi:http://dx.doi.org/10.1242/jcs.087221

Yamamoto, K., Shimizu, N., Obi, S., Kumagaya, S., Taketani, Y., Kamiya, A., & Ando, J. (2007). Involvement of cell surface ATP synthase in flow-induced ATP release by vascular endothelial cells. *American Journal of Physiology - Heart & Circulatory Physiology, 293*(3), H1646-1653.

Yamamoto, K., Sokabe, T., Ohura, N., Nakatsuka, H., Kamiya, A., & Ando, J. (2003). Endogenously released ATP mediates shear stress-induced Ca2+ influx into pulmonary artery endothelial cells. *American Journal of Physiology - Heart & Circulatory Physiology, 285*(2), H793-803.

Yamazaki, S., Weinhold, P. S., Graff, R. D., Tsuzaki, M., Kawakami, M., Minchew, J. T., & Banes, A. J. (2003). Annulus cells release ATP in response to vibratory loading in vitro. *Journal of Cellular Biochemistry, 90*(4), 812-818.

Yao, J., Suwa, M., Li, B., Kawamura, K., Morioka, T., & Oite, T. (2003). ATP-dependent mechanism for coordination of intercellular Ca2+ signaling and renin secretion in rat juxtaglomerular cells. *Circulation Research, 93*(4), 338-345.

Yegutkin, G., Bodin, P., & Burnstock, G. (2000). Effect of shear stress on the release of soluble ecto-enzymes ATPase and 5'-nucleotidase along with endogenous ATP from vascular endothelial cells. *British Journal of Pharmacology, 129*(5), 921-926.

Yin, J., Xu, K., Zhang, J., Kumar, A., & Yu, F. S. (2007). Wound-induced ATP release and EGF receptor activation in epithelial cells. *Journal of Cell Science, 120*(Pt 5), 815-825.

Yip, L., Cheung, C. W., Corriden, R., Chen, Y., Insel, P. A., & Junger, W. G. (2007). Hypertonic stress regulates T-cell function by the opposing actions of extracellular adenosine triphosphate and adenosine. *Shock, 27*(3), 242-250.

Yoshida, H., Kobayashi, D., Ohkubo, S., & Nakahata, N. (2006). ATP stimulates interleukin-6 production via P2Y receptors in human HaCaT keratinocytes. *European Journal of Pharmacology, 540*(1-3), 1-9.

Young, J. S., Matharu, R., Carew, M. A., & Fry, C. H. (2012). Inhibition of stretching-evoked ATP release from bladder mucosa by anticholinergic agents. *BJU International, 110*(8 Pt B), E397-401. doi:http://dx.doi.org/10.1111/j.1464-410X.2012.10966.x

Yu, W. (2015). Polarized ATP distribution in urothelial mucosal and serosal space is differentially regulated by stretch and ectonucleotidases. *American Journal of Physiology - Renal Physiology, 309*(10), F864-872. doi:http://dx.doi.org/10.1152/ajprenal.00175.2015

Zappia, K. J., Garrison, S. R., Palygin, O., Weyer, A. D., Barabas, M. E., Lawlor, M. W., . . . Stucky, C. L. (2016). Mechanosensory and ATP Release Deficits following Keratin14-Cre-Mediated TRPA1 Deletion Despite Absence of TRPA1 in Murine Keratinocytes. *PLoS ONE [Electronic Resource], 11*(3), e0151602. doi:http://dx.doi.org/10.1371/journal.pone.0151602

Zhang, T., Liu, C., Zhou, X., Kolosov, V. P., & Perelman, J. M. (2014). Effects of ATP release on mucin5AC secretion in airway epithelial cells by mechanical stretching. *Annals of Clinical & Laboratory Science, 44*(4), 425-430.

Zhang, X., Li, A., Ge, J., Reigada, D., Laties, A. M., & Mitchell, C. H. (2007). Acute increase of intraocular pressure releases ATP into the anterior chamber. *Experimental Eye Research, 85*(5), 637-643.

Zhang, Y., Phillips, G. J., Li, Q., & Yeung, E. S. (2008). Imaging localized astrocyte ATP release with firefly luciferase beads attached to the cell surface. *Analytical Chemistry, 80*(23), 9316-9325. doi:http://dx.doi.org/10.1021/ac801701w

Zhao, H. B., Yu, N., & Fleming, C. R. (2005). Gap junctional hemichannel-mediated ATP release and hearing controls in the inner ear. *Proceedings of the National Academy of Sciences of the United States of America, 102*(51), 18724-18729.

Zhou, X., Ferraris, J. D., & Burg, M. B. (2006). Mitochondrial reactive oxygen species contribute to high NaCl-induced activation of the transcription factor TonEBP/OREBP. *American Journal of Physiology - Renal Physiology, 290*(5), F1169-1176.